SOVIET PHYSICS

JETP

A translation of the Journal of Experimental and Theoretical Physics of the USSR.

SOVIET PHYSICS JETP VOL. 34 (7) NO. 2, pp 185-370 August, 1958

EXPLOSION SHOWERS PRODUCED BY HIGH-ENERGY COSMIC RAY PARTICLES

I. I. GUREVICH, A. P. MISHAKOVA, B. A. NIKOL'SKII, and L. V. SURKOVA

Academy of Sciences, U.S.S.R.

Submitted to JETP editor July 6, 1957

J. Exptl. Theoret. Phys. (U.S.S.R.) 34, 265-277 (February, 1958)

Experimental results on 43 showers produced by nucleons of $10^{10}-10^{14}$ ev and on 20 showers produced by particles with $Z \geq 2$ are presented. An asymmetry has been observed in the angular distribution of shower particles with respect to the direction $\pi/2$ in the center-of-mass system in showers produced by nucleons with energy $> 10^{11}$ ev. This fact is not consistent with the concept of shower production on nuclei in nucleon-nucleon collisions and with the predictions of the hydrodynamical theory of multiple particle production proposed by Belen'kii and Landau.

THE present work is devoted to the study of explosion showers produced by high-energy cosmic ray particles by means of an emulsion chamber. Preliminary results obtained for 29 showers were published earlier.[1] The purpose of the present article is to consider the energy dependence of the various characteristics of explosion showers in the region $10^{10}-10^{13}$ ev.

The emulsion chamber consisted of 100 layers 10 cm in diameter. Total thickness of the chamber was equal to 4.5 cm Emulsion NIKFI type R was used. The chamber was irradiated in the stratosphere at 27 km altitude for seven hours in May 1956. Explosion showers with more than five relativistic tracks, concentrated in a sufficiently narrow cone, were found by scanning. There was no discrimination with respect to the number of black and grey tracks in finding the showers. Jets of relativistic particles consisting of more than five tracks were also noted in scanning. Further investigation showed that five of these events represented explosion showers while the remaining 200 jets were identified as electron-photon showers. Charge of the shower producing particle was determined in each case of detected explosion shower (as single, double, or multiple) and the angular distribution of shower particles with respect to the axis was measured.

1. MEASUREMENT OF THE ANGULAR DISTRIBUTION OF SHOWER PARTICLES

For shower particles of the "wide cone," making an angle larger than 5° with shower axis, the angle α in the emulsion plane and the inclination β were measured with an accuracy of 1°. The angular distribution about the shower axis was determined by means of the special device shown in Fig. 1. Each shower particle was marked on an aluminum sphere and the angles α and β were read off the divisions 1 and 2 respectively. The angle ϑ between the particle trajectory and shower axis was found using a plexiglass hemisphere with the latitude (ϑ) and longitude (φ) marked on it, and which could be fitted to the aluminum sphere.

Measurements of the angle ϑ for shower particles with $\vartheta < 5°$ were carried out by means of finding the points of intersection of the tracks with a plane perpendicular to shower axis. An example of such construction for the determination of angular distribution of particles in a shower of 3.7×10^{12} ev is shown in Fig. 2, which represents the

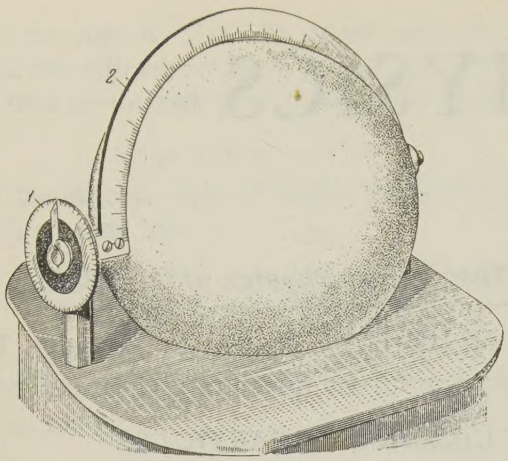

Fig. 1. Apparatus for measurement of the angle between shower axis and direction of emission of shower particles.

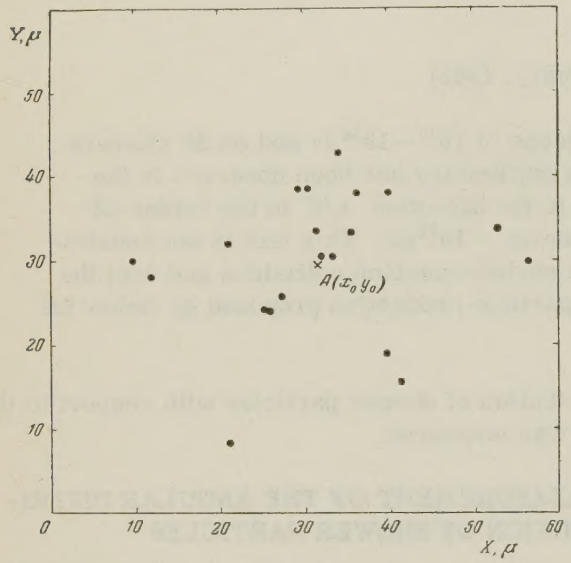

Fig. 2.

plane perpendicular to shower axis at a distance of 200 μ from the shower origin. The point $A(x_0, y_0)$ corresponding to the intersection of the shower axis with the XY plane was determined as

$$x_0 = \sum x_i / n, \quad y_0 = \sum y_i / n,$$

where n is the number of shower particles. The distance between the plane XY and the point of origin of the shower was selected so that the accuracy of angle measurements for most shower particles would not be worse than 5 — 10 percent.

2. DETERMINATION OF SHOWER ENERGY

If we assume that the observed showers were produced as the result of nucleon-nucleon collisions, then it follows from the symmetry of angular distribution of shower particles in the center-of-mass system (c.m.s.) about the direction $\theta = \pi/2$* that the energy of the primary particles in c.m.s., $\gamma_c = 1/\sqrt{1-\beta_c^2}$, can be written in the form

$$\gamma_c = \cot \vartheta_{1/2}, \tag{1}$$

where $\vartheta_{1/2}$ is the angle containing half of the shower particles.

A second method of determination of γ_c, which permits a better use of the data on angular distribution, and makes it possible to determine the statistical error due to the finite number of shower particles, has been proposed by Castagnoli et al.[2] According to their calculations, we have

$$\ln \gamma_c = -\overline{\ln \tan \vartheta} \pm (\sigma / \sqrt{n_s}), \tag{2}$$

where n_s is the number of shower particles and σ is of the order of unity.

The value of γ_c can also be found, for a symmetrical distribution with respect to $\theta = \pi/2$ in the c.m.s., from the integral angular distribution of shower particles. Let us denote the integral angular distribution of shower particles by F. We then have

$$F(\lambda) = \frac{1}{\sum n_s} \int_{-\infty}^{\lambda} \frac{dn_s}{d\lambda} d\lambda, \tag{3}$$

where $\lambda = \ln \tan \vartheta$. $F(\lambda)$ is normalized to unity, i.e.,

$$\int_{-\infty}^{+\infty} F(\lambda)\, d\lambda = 1.$$

It is evident that, for a symmetrical angular distribution, $F/(1-F) = 1$ for $\theta = \pi/2$, i.e., $F/(1-F)$ is such a function of λ that for $\ln [F/(1-F)] = 0$ its argument, according to Eq. (1), is $\lambda_0 = \ln \tan \vartheta_{1/2} = -\ln \gamma_c$. In this way the determination of γ_c is reduced to plotting $\ln [F/(1-F)]$ as a function of $\lambda = \ln \tan \vartheta$ and finding the value λ_0 for which $\ln [F/(1-F)] = 0$.

All these methods of finding γ_c yield results that vary by 20 — 30%, and which are within the statistical accuracy of measurements. It can be seen from Table I that the values of γ_c obtained according to Eq. (2) are lower than those of the two other methods.

It should be noted that the assumption that showers produced on the emulsion nuclei originate in nucleon-nucleon collisions may not correspond to reality. Belen'kii and Landau[3] treated the case of multiple particle production according to the hydrodynamical model, assuming the interaction be-

*Where, as in the following, θ denotes the emission angle of a shower particle in the c.m.s. and ϑ the emission angle of shower particle in the laboratory system.

TABLE I

No.	Primary particle	n_h+n_g	n_s	$\vartheta_{1/2}$, deg.	γ_c			$\bar{\gamma}_c$	E_0, ev	k	l	P_s	E, ev
					$(\vartheta_{1/2})$	$(\bar{\lambda})$	(F)						
1	2	3	4	5	6	7	8	9	10	11	12	13	14
					$E_0=10^{10}$—10^{11} ev								
1	p	14+6	23	11.5	4.9	4.8	6.0	5.2	$5.3\cdot10^{10}$	3.05	8.5	0.05	$4.5\cdot10^{11}$
2	p	15+5	24	10	5.5	4.6	7.6	5.9	$6.9\cdot10^{10}$	3.07	8	0.42	$5.5\cdot10^{11}$
3	p	4+2	8	11	5.1	4.7	—	4.9	$4.7\cdot10^{10}$	0.41	3	0.32	$1.4\cdot10^{11}$
4	n	7+3	13	26	2.0	2.1	2.9	2.3	$1.0\cdot10^{10}$	2.24	6	0.54	$6.0\cdot10^{10}$
5	p	13+5	14	16.5	3.4	2.8	3.6	3.3	$2.1\cdot10^{10}$	1.93	5.5	0.68	$1.2\cdot10^{11}$
6	p	8+8	8	18	2.1	2.0	3.5	2.9	$1.6\cdot10^{10}$	1.13	3.5	0.85	$5.7\cdot10^{10}$
7	p	9+3	12	11	5.1	3.6	5.1	4.6	$4.1\cdot10^{10}$	1.02	4	0.05	$1.6\cdot10^{11}$
8	n	11+2	23	18	3.1	2.5	3.2	2.9	$1.6\cdot10^{10}$	3.68	9.5	0.09	$1.5\cdot10^{11}$
9	p	10+7	25	16.0	3.5				$4.0\cdot10^{10}$	3.42	9	0.68	$3.6\cdot10^{11}$
10	n	6+6	15	16.5	3.4				$2.2\cdot10^{10}$	2.20	6	0.07	$1.3\cdot10^{11}$
11	n	6+9	22	14.5	3.9				$2.9\cdot10^{10}$	2.94	8	0.28	$2.3\cdot10^{11}$
12	n or p	14+6	21	16.5	3.4				$2.2\cdot10^{10}$	2.36	8	0.001	$1.8\cdot10^{11}$
13	p	5+3	22	17	3.3				$2.1\cdot10^{10}$	3.28	9	0.24	$1.9\cdot10^{11}$
14	α	1+2	35	10.7	5.3	4.7	6.4	5.5	$6.0\cdot10^{10}$	3.85		0.67	
15	α	12+3	42	10.6	5.3	5.9	8.3	6.5	$8.4\cdot10^{10}$	3.95		0.14	
16	α	17+9	36	9.0	6.3	5.1	6.5	5.6	$6.2\cdot10^{10}$	4.45		0.50	
17	α	9+4	17	8.0	7.1	5.0	7.9	6.6	$8.6\cdot10^{10}$	2.20		0.42	
18	Z	8+26	87	12.2	4.6					12.3		0.32	
19	α	12+3	20	13.0	4.3	4.3	5.0	4.9	$4.4\cdot10^{10}$	2.35		0.24	
20	α	16+8	45	23.5	2.2	1.9	2.3	2.1	$0.9\cdot10^{10}$	8.40		0.06	
21	α	16+15	35	19.5	2.7	2.4	3.0	2.7	$1.4\cdot10^{10}$	5.85		0.85	
22	Z	17+6	74	10.5	5.3	5.7	7.2	6.0	$7.0\cdot10^{10}$	9.75		0.81	
23	α	16+8	26	23.0	2.3	2.4	2.5	2.4	$1.1\cdot10^{10}$	4.75		0.08	
24	α	10+6	16	15.0	3.7	3.6	4.2	3.8	$2.8\cdot10^{10}$	1.89		0.67	
25	α	15+10	28	9.5	5.9	5.7	6.8	6.1	$7.1\cdot10^{10}$	3.30		0.92	
26	Z	12+8	41	15.0	3.7	3.2	3.8	3.6	$2.4\cdot10^{10}$	6.10		0.54	
27	α	9+3	13	20.0	2.7	3.2	3.6	3.2	$1.9\cdot10^{10}$	1.68		0.081	
28	α	13+5	29	17.0	3.3	3.4	4.0	3.6	$2.4\cdot10^{10}$	4.00		0.42	
					$E_0=10^{11}$—10^{12} ev								
1	p	5+2	23	3.3	17.1	16.6	13.6	15.8	$5.0\cdot10^{11}$	2.50	5	0.32	$2.5\cdot10^{12}$
2	p	3+4	15	3.5	17.1	13.9	20.0	17.0	$5.8\cdot10^{11}$	0.64	3	0.90	$1.7\cdot10^{12}$
3	p	5+3	14	4.7	12.3	10.4	14.1	12.5	$3.1\cdot10^{11}$	0.59	3.5	0.20	$1.1\cdot10^{12}$
4	p	3+2	18	6.5	11.9	11.0	15.1	12.7	$3.2\cdot10^{11}$	1.10	4.5	0.60	$1.4\cdot10^{12}$
5	p	5+3	15	5.5	10.4	7.0	12.6	10.0	$2.0\cdot10^{11}$	1.84	4	0.67	$8.0\cdot10^{11}$
6	p	12+7	24	6.9	8.3	6.1	8.0	7.5	$1.1\cdot10^{11}$	2.57	8	0.60	$9.0\cdot10^{11}$
7	p	9+7	14	5.1	11.2	11.2	15.1	12.5	$3.1\cdot10^{11}$	0.82	3.5	0.01	$1.1\cdot10^{12}$
8	p	13+10	19	2.5	22.9	12.2	15.8	17.0	$5.7\cdot10^{11}$	1.91	4	0.67	$2.3\cdot10^{12}$
9	p	1+2	29	6.5	8.8	7.1	8.7	8.2	$1.3\cdot10^{11}$	3.45	2.5	0.40	$1.2\cdot10^{12}$
10	p	1+1	12	8.1	7.0	5.9	8.3	7.1	$1.0\cdot10^{11}$	1.32	4	0.32	$4.0\cdot10^{11}$
11	p	13+2	30	7.5	7.5	7.6	7.2	7.4	$1.1\cdot10^{11}$	3.70	12	0.60	$1.3\cdot10^{12}$
12	n	10+1	23	7.0	8.1	5.1	8.5	7.2	$1.0\cdot10^{11}$	2.80	8	0.54	$8\cdot10^{11}$
13	p	3+0	8	6.5	8.8	6.9	9.1	7.9	$1.2\cdot10^{11}$	0.80	2.5	0.85	$3\cdot10^{11}$
14	n	4+1	7	3.5	16.3	9.1	12.0	12.3	$3.0\cdot10^{11}$	0.40	1.5	0.94	$4.5\cdot10^{11}$
15	p	10+6	35	6.7	8.3	8.4	15.0	10.6	$2.2\cdot10^{11}$	4.16	10	0.23	$2.2\cdot10^{12}$
16	n	7+5	32	5.4	10.6	9.9	15.0	11.8	$2.8\cdot10^{11}$	3.62	8.5	0.54	$2.4\cdot10^{12}$
17	p	1+1	20	2.0	28.6	15.6	19.5	21.3	$9.1\cdot10^{11}$	1.67	4	0.42	$3.6\cdot10^{12}$
18	n	1+0	10	3.2	17.5	12.6	20.0	16.7	$5.6\cdot10^{11}$	0.40	2	0.80	$1.1\cdot10^{12}$
19	p	1+2	19	6.5	8.8	9.2	11.0	9.7	$1.9\cdot10^{11}$	2.0	5.5	0.80	$1.0\cdot10^{12}$
20	p	10+1	29	5.4	10.5	10.5	13.2	11.4	$2.6\cdot10^{11}$	2.74	8	0.98	$2.1\cdot10^{12}$
21	p	12+3	11	5.7	9.5	6.3	9.6	8.5	$1.4\cdot10^{11}$	0.99	3	0.85	$4.2\cdot10^{11}$
22	Z	1+1	22	6.8	8.4	7.3	10.0	8.6	$1.5\cdot10^{11}$	1.43		0.001	
23	α	3+1	27	4.0	14.3	11.1	12.6	12.5	$3.2\cdot10^{11}$	1.28		0.48	
24	α	0+2	29	6.5	8.8	9.2	10.0	9.2	$1.7\cdot10^{11}$	3.4		0.09	
25	Z	4+0	57	3.7	15.4				$4.7\cdot10^{11}$			0.05	
					$E_0=10^{12}$—10^{13} ev								
1	n	5+8	35	1.0	55	20	53	43	$3.7\cdot10^{12}$	3.95	5	0.5	$1.9\cdot10^{13}$
2	p	2+3	27	2.1	27	32	32	30	$1.8\cdot10^{12}$	2.65	4.5	0.1	$8.1\cdot10^{12}$
3	p	0+0	9	1.7	34	27	37	33	$2.1\cdot10^{12}$	0.14	1.5	0.04	$3.2\cdot10^{12}$
4	p	5+3	27	2.4	24	17	25	22	$9.6\cdot10^{11}$	2.82	5.5	0.8	$5.3\cdot10^{12}$
5	p	2+4	27	1.0	57	36	50	48	$4.6\cdot10^{12}$	1.0	4	0.2	$1.8\cdot10^{13}$
6	p	6+4	20	2.6	22	20	25	22	$9.6\cdot10^{11}$	1.85	4	0.7	$4.0\cdot10^{12}$
7	p	1+2	43	1.3	43	36	40	40	$3.2\cdot10^{12}$	2.48	7	0.75	$2.2\cdot10^{13}$
8	α	7+3	33	2.3	24	21	30	25	$1.3\cdot10^{12}$	2.95		0.03	
					$E_0=10^{13}$—10^{14} ev								
1	p	11+3	16	0.70	81	50	120	84	$1.4\cdot10^{13}$	1.11	1.5	0.40	$2.1\cdot10^{13}$
2	p	5+4	9	0.25	227	141	300	222	$9.9\cdot10^{13}$	0.09	1	0.75	$9\cdot10^{13}$

tween the primary nucleon and the nucleus as a whole, in head-on collisions. They obtained the following formula for the angular distribution of particles in the c.m.s.:

$$dN \sim \exp\left(\sqrt{L^2 - \ln^2 \tan\frac{\theta}{2}}\right) d\left(\ln \tan\frac{\theta}{2}\right). \quad (4)$$

Here $L = \ln[(1+\ell)/4\gamma_c]$, ℓ is the tunnel length, i.e., the number of nucleons on the chord corresponding to the trajectory of the primary particle through the nucleus. According to Eq. (4), $dN/d\theta$ is symmetric about $\theta = \pi/2$. It follows that, if the theory is correct, γ_c can be determined by the same method as for nucleon-nucleon collisions.

In the following we shall ascribe to showers values of γ_c, calculated according to formulae (1) and (2) and from the condition $\ln[F/(1-F)] = 0$, which correspond to the assumption that the distribution of shower particles is symmetric about $\theta = \pi/2$. It should be noted that the experimental data available are not in agreement with this assumption (cf. Sec. 3) and the accuracy of shower energy determination by the above method should not be overestimated.

The shower energy in the laboratory system, E_0, can be determined in a unique way only for the case of nucleon-nucleon collisions:

$$\gamma = 2\gamma_c^2 - 1 \approx 2\gamma_c^2, \quad (5)$$

where $\gamma = E_0/Mc^2$. For collisions between the primary nucleon and nucleons contained in the tunnel, the shower energy in the laboratory system is found from the relation

$$\gamma = 2\gamma_c^2 l, \quad (5')$$

where ℓ is the tunnel length and $\gamma = E/Mc^2$.

3. EXPERIMENTAL RESULTS AND THEIR EVALUATION

Experimental results on 43 showers produced by nucleons and 20 showers generated by α particles and nuclei are summarized in Table I. The showers are divided into three energy groups. Shower energies were calculated according to Eq. (5). Such a procedure is rather arbitrary, since Eq. (5) corresponds to the case of nucleon-nucleon collisions. Energies of nucleon-produced showers, calculated according to Eq. (5′) are shown in Fig. 4. The value of γ_c in Eq. (5′) was found under the assumption that the angular distribution of shower particles in the c.m.s. is, as in the case of nucleon-nucleon collisions, symmetrical with respect to $\theta_{cm} = \pi/2$ (the Belen'kii-Landau theory). It follows, however, from the experimental results of the present work that such an assumption does not conform to reality. It is therefore not clear which method of energy determination is advisable. In the following, dealing with energy dependence of various characteristics of explosion showers, we shall use for that purpose Eq. (5), although the resulting absolute energy values are evidently too low. The nature of primary particles is given in the second column of the table. Singly-charged particles were assumed to be protons, and the neutral ones — neutrons. The number of black and grey tracks ($n_h + n_g$) and the number of shower particles (n_s) are given in the third and fourth columns respectively; the values of γ_c calculated according to Eqs. (1) and (2) and from the condition $\ln[F/(1-F)] = 0$, and also the mean values $\bar{\gamma}_c$ calculated using the above methods are given in columns 6 — 9. k is the coefficient of inelasticity given by the equation[4]

$$k = 1{,}5 n_s \gamma_c \sin\vartheta_{max} / 2\mu(\gamma_c - 1), \quad (6)$$

where ϑ_{max} is the maximum angle between a shower particle and shower axis, and μ is the ratio of the nucleon mass to the π-meson mass. The tunnel length ℓ is a function of γ_c and n_s, according to the relation $n_s = f(\gamma_c, \ell)$ from the statistical theory of multiple particle production. For large γ_c (> 10) the relation is of the form*

$$n_s = 0.9 l^{3/4}(1+l)^{1/4}\sqrt{\gamma_c} + \frac{l+1}{2}, \quad (7)$$

where the coefficient 0.9 is chosen for fit with curves for small values of γ_c, obtained from statistical weight calculations.

A. Angular Distributions of Shower Particles in the C.M.S.

The direction of motion of a relativistic particle in the laboratory system is connected with the direction of motion in the c.m.s. by the following relation:

$$\cot\vartheta = \gamma_c \frac{\cos\theta + (\beta_c/\beta)}{\sin\theta}, \quad (8)$$

where β_c is the velocity of the c.m.s. and β is the particle velocity in the c.m.s. In the extreme relativistic case, $\beta_c \approx \beta \approx 1$, i.e.,

$$\cot\vartheta = \gamma_c \frac{\cos\theta + 1}{\sin\theta} = \gamma_c \cot(\theta/2). \quad (8')$$

*Results of calculations of statistical weights, and formula (7), were kindly communicated by D. S. Chernavskii.

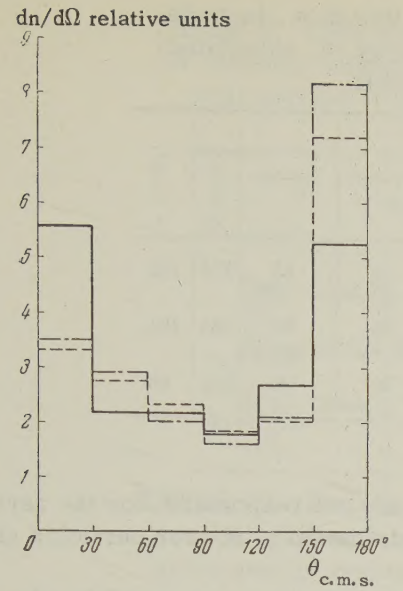

Fig. 3. Angular distributions of shower particles in c.m.s. Solid line – $E_0 = 10^{10} - 10^{11}$ ev, dashed – $E_0 = 10^{11} - 10^{12}$ ev, dot-dash – $E_0 = 10^{12} - 10^{14}$ ev. All distributions pertain to nucleon-produced showers.

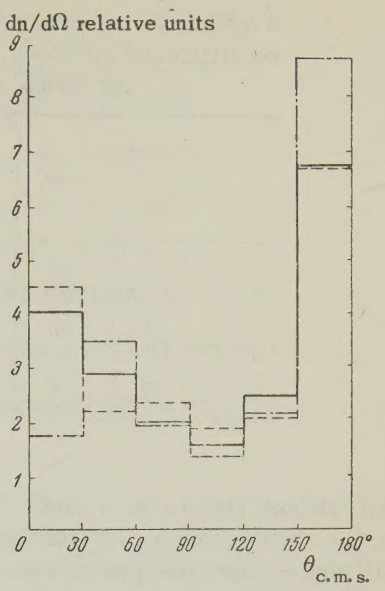

Fig. 4. Angular distributions of shower particles in c.m.s. for nucleon-produced showers. Shower energy calculated according to Eq. (5′). Solid line – $E = 10^{11} - 10^{12}$ ev, dashed – $E = 10^{12} - 10^{13}$ ev, dot-dash – $E = 10^{13} - 10^{14}$ ev.

TABLE II. Angular distribution of particles in c.m.s., in nucleon-produced showers, for three regions of energy E_0 calculated under the assumption of a nucleon-nucleon collision [Eq. (5)].

E_0, ev \ θ c.m.s.	0–30°	30–60°	60–90°	90–120°	120–150°	150–180°	N ($\theta<90°$)	N ($90°<\theta$)
10^{10}–10^{11} N	34	38	50	42	48	31	122	121
10^{10}–10^{11} $dN/d\Omega$	5.4 ±0.92	2.21±0.35	2.13±0.30	1.79±0.27	2.79±0.39	4.92±0.91		
10^{11}–10^{12} N	34	77	91	67	57	75	202	199
10^{11}–10^{12} $dN/d\Omega$	3.28±0.56	2.72±0.3	2.35±0.24	1.73±0.2	2.01±0.26	7.22±0.83		
10^{12}–10^{14} N	19	43	41	33	31	45	103	109
10^{12}–10^{14} $dN/d\Omega$	3.47±0.8	2.87±0.44	2.00±0.31	1.61±0.28	2.07±0.37	8.19±1.2		

TABLE III. Angular distribution of particles in c.m.s., in showers produced by particles with $Z \geq 2$.

E_0, ev \ θ c.m.s.	0–30°	30–60°	60–90°	90–120°	120–150°	150–180°	N ($\theta<90°$)	N ($90°<\theta$)
10^{10}–10^{11} N	47	103	117	107	100	59	267	266
10^{10}–10^{11} $dN/d\Omega$	3.4 ±0.5	2.73±0.27	2.28±0.21	2.0 ±0.2	2.66±0.27	4.29±0.56		
10^{11}–10^{14} N	18	35	30	34	26	25	83	85
10^{11}–10^{14} $dN/d\Omega$	4.13±0.97	2.94±0.50	1.85±0.34	2.09±0.36	2.19±0.43	5.75±1.2		

The angular distribution function $f(\theta)$ in the c.m.s. was found for each shower using Eq. (8′). To obtain better statistical results, summary distributions were constructed for showers of various energy regions. These distributions are given in Tables II, III, and IV and in Figs. 3 and 4. The errors given in the tables represent statistical deviations $\sqrt{N_i}$, where N_i is the number of particles within a given angle interval $\Delta\theta_{c.m.}$. The total number of particles propagating in the forward and

TABLE IV. Angular distribution of particles in c.m.s., in nucleon-produced showers, for three regions of energy E calculated for tunnel-effect interaction [Eq. (5′)].

E, ev \ $\vartheta_{c.m.s.}$		0–30°	30–60°	60–90°	90–120°	120–150°	150–180°	$N(\vartheta<90°)$	$N(\vartheta>90°)$
10^{11}—10^{12}	N	32	63	59	45	54	53	154	152
	$dN/d\Omega$	4.05±0.71	2,92±0,36	2,0 ±0,26	1,54±0,23	2,5 ±0,34	6.7 ±0,91		
10^{12}—10^{13}	N	45	60	88	71	56	67	193	194
	$dN/d\Omega$	4.5 ±0.67	2.2 ±0,28	2.35±0,25	1.9 ±0.22	2.05±0,27	6.7 ±0,81		
10^{13}—10^{14}	N	6	32	25	17	20	29	63	66
	$dN/d\Omega$	1.79±0.73	3.5 ±0.62	2,0 ±0,4	1.36±0,33	2.2 ±0.49	8.7 ±1,61		

backward directions [$N(\vartheta < 90°)$ and $N(\vartheta > 90°)$] is the same for showers with even number of particles and differs by one in showers with odd n_s. The number of particles per steradian in relative units $dN/d\Omega \sim N/\sin\bar{\theta}$, where $\bar{\theta}$ is the mean angle of a given interval $\Delta\theta$ is shown in the figures.

It can be seen from Tables II and III that $f(\theta)$ is substantially anisotropic and for showers generated by nucleons of $10^{11} - 10^{13}$ ev asymmetric with respect to the direction $\theta = \pi/2$. The angular distributions (in the c.m.s.) given in the tables were obtained by means of Eq. (8′), γ_c being defined as $\gamma_c = \cot\vartheta_{1/2}$. For such definition of γ_c the number of particles in angle intervals $0 - \pi/2$ and $\pi/2 - \pi$ was assumed to be equal. It follows therefore, from the asymmetry of the angular distribution for the above definition of γ_c, that $f(\theta)$ cannot be made symmetric for any value of γ_c. It is interesting to note that this asymmetry is absent for showers with $E_0 = 10^{10} - 10^{11}$ ev, and is less marked for showers generated by heavy particles, although the latter conclusion is not sufficiently founded, in view of the small number of observed cases in the region $10^{11} - 10^{1}$ ev. An analogous conclusion about the asymmetry with respect to $\theta = \pi/2$ can be drawn dividing the showers according to energy E (cf. Table IV and Fig. 4). One would expect the observed asymmetry to be caused by secondary interactions of shower particles with nucleons in the nucleus. In the same way, one could explain the fact that the inelasticity coefficients k calculated according to Eq. (6) were found in most cases to be larger than unity. Under this assumption one would expect the asymmetry about $\theta = \pi/2$ to decrease for showers with smaller values of $n_h + n_g$ and with $k < 1$. It follows from Table V, however, that the asymmetry of the angular distribution does not exhibit the expected behavior. This fact indicates that secondary interactions are not responsible for the asymmetric angular distribution of shower particles about $\theta = \pi/2$.

The observed asymmetry could be also due to shower production as the result of several collisions of the primary with nucleons of the nucleus. It is evident that the asymmetry should then increase with the number of shower particles. The results of the experiment, however, contradict this explanation. It can be seen from Table VI that $dN/d\theta$ is independent of the number of particles in the shower n_s. It must be concluded that the asymmetry of $f(\theta)$ with respect to $\theta = \pi/2$ is not due to secondary processes, but is inherent in the process of shower production. This result contradicts the hydrodynamical theory of shower production in head-on collisions, which predicts a symmetrical angular distribution of shower particles about the direction $\pi/2$ in the c.m.s. [cf. Eq. (4)].

D. S. Chernavskii (private communication) proposed a possible explanation of the observed aymmetry of angular distribution in explosion showers, indicating that a part of the shower particles can be produced in interaction between nuclear matter and the π-meson cloud of the incident nucleon. These particles can be associated with additional tunnels in the same nucleus which are characterized by a different value of γ_c (since the mass of a π meson is less than that of a nucleon). It can be easily seen that such mechanism leads to the excess of shower particles propagating backwards in the c.m.s.

Mean values of the angle $\vartheta_{1/2}$, denoted by $\bar{\vartheta}_{1/2}$, for showers with various number of particles n_s and different $n_h + n_g$ are given in Table VII. It can be seen that the mean angle of emission of shower particles does not depend markedly on the above parameter. In other words, possible secondary interactions of shower particles with nucle-

TABLE V. Distribution of shower particles in c.m.s., $dN/d\theta$, for showers with various k and $(n_h + n_g)$. Data refer to the total number of shower particles within a given interval $\Delta\theta$ ($E_0 = 10^{11} - 10^{14}$ ev).

Condition \ θ	0–30°	30–60°	60–90°	90–120°	120–150°	150–180°
$k>1$	51	88	98	77	67	93
$k<1$	2	32	32	23	21	27
$k<0.4$	1	4	12	6	6	4
$n_h+n_g\leqslant 3$ ($\bar{k}=1.9$)	10	23	40	25	30	21
$n_h+n_g<3$ $k<1$	0	3	9	5	6	3

TABLE VI. Distribution of shower particles in c.m.s., for showers with different n_s. $\bar{n}_s$ denotes the mean value of n_s for a given energy region. Data refer to the total number of shower particles within a given interval $\Delta\theta$.

Δθ		0–30°	30–60°	60–90°	90–120°	120–150°	150–180°
$E_0=10^{10}$–10^{11} ev, $\bar{n}_s=18$	$n_s<\bar{n}_s$	5	9	21	18	10	7
	$n_s>\bar{n}_s$	29	28	25	19	34	25
$E_0=10^{11}$–10^{12} ev, $\bar{n}_s=19$	$n_s<\bar{n}_s$	13	33	32	24	21	35
	$n_s>\bar{n}_s$	21	44	57	45	36	40
$E_0=10^{12}$–10^{14} ev, $\bar{n}_s=24$	$n_s<\bar{n}_s$	3	10	13	11	7	10
	$n_s>\bar{n}_s$	16	33	28	22	24	35
$E_0=10^{11}$–10^{14} ev, $\bar{n}_s=21$	$n_s<\bar{n}_s$ $k<1$	1	19	24	18	17	15

TABLE VII. Mean values of the angles of emission of shower particles $\bar{\vartheta}_{1/2}$

E_0, ev	$\bar{n}_s$	$\bar{\vartheta}_{1/2}$	$\bar{\vartheta}_{1/2}(n_s<\bar{n}_s)$	$\bar{\vartheta}_{1/2}(n_s>\bar{n}_s)$	$\bar{\vartheta}_{1/2}(n_h+n_g\leqslant 3)$	$\bar{\vartheta}_{1/2}(n_h+n_g>3)$
10^{10}–10^{11}	17.7	15.3	16.5	14.3	—	—
10^{11}–10^{12}	19.4	5.34	5.12	5.63	5.48	5.29
10^{12}–10^{14}	23.8	1.45	1.30	1.56	1.51	1.43
10^{11}–10^{14}	20.7	4.17	4.04	4.35	4.48	4.06

ons of the nucleus do not change appreciably the value of $\vartheta_{1/2}$.

The anisotropy of the angular distribution of shower particles in the c.m.s. can be characterized by the value Δ defined as follows:

$$\Delta = \left[\sum_i (\bar{\lambda} - \lambda_i)^2 n_i / \sum n_i\right]^{1/2}, \qquad (9)$$

where $\lambda_i = \ln\tan\vartheta_i$, $\bar{\lambda} = \overline{\ln\tan\vartheta_i} = \ln\gamma_c$, and n_i is the number of shower particles in the i-th interval of the variable λ. It is evident that large values of Δ correspond to a larger measure of anisotropy in the angular distribution $f(\theta)$ i.e., to greater emission probability of shower particles at angles close to $\theta = 0$ and $\theta = \pi$ in the c.m.s. It can be easily shown that for a distribution isotropic in the c.m.s. $\Delta_{is} = 0.3$. Table VIII illustrates the variation of Δ for showers with different values of n_s and $n_h + n_g$.

Mean values of Δ for various energy regions calculated according to the hydrodynamical theory of Belen'kii and Landau from distribution (4), $\bar{\Delta}_{theor}$, are also given in the table. In calculating Δ_{theor} it was taken into account that the mean tunnel length for nuclei of the emulsion is $\ell = 3.25$. In addition to Δ_{exp} calculated according to Eq. (9),

TABLE VIII. Mean values of Δ and $\Delta(\lambda < \overline{\lambda})$ [cf. Eq. (9)] for showers of various energies.

E_0, ev	n_s, n_h+n_g	$\overline{\Delta}_{\text{exptl.}}$	$\overline{\Delta}_{\text{exptl.}}$ $(\lambda<\overline{\lambda})$	$\overline{\Delta}_{\text{theoret.}}$
10^{11}—10^{12}	$n_s<\bar{n}_s$	0.52	0.42	0.48
	$n_s>\bar{n}_s$	0.54	0.48	0.47
	$n_h+n_g\leqslant 3$	0.45	0.33	0.47
	$n_h+n_g>3$	0.56	0.49	0.48
10^{12}—10^{14}	$n_s<\bar{n}_s$	0.63	0.50	0.72
	$n_s>\bar{n}_s$	0.73	0.66	0.65
	$n_h+n_g\leqslant 3$	0.39	0.38	0.66
	$n_h+n_g>3$	0.77	0.64	0.69
10^{11}—10^{14}	$n_s<\bar{n}_s$	0.54	0.43	0.55
	$n_s>\bar{n}_s$	0.62	0.56	0.53
	$n_h+n_g\leqslant 3$	0.44	0.34	0.52
	$n_h+n_g>3$	0.62	0.54	0.55
	$n_s<\bar{n}_s$		0.32	
	$n_h+n_g\leqslant 3$			

values of $\Delta(\lambda < \overline{\lambda})$ calculated according to the same formula for values $\lambda < \overline{\lambda}$ are given in Table VIII. These values correspond to small angles of emission of shower particles (if the assumption of a symmetrical distribution of shower particles in the c.m.s. about $\theta = \pi/2$ were correct, then the values $\lambda < \overline{\lambda}$ would correspond to angles of emission $\theta < 90°$ in the c.m.s.). It can be maintained that $\Delta(\lambda < \overline{\lambda})$ characterizes better the anisotropy of the angular distribution of shower particles produced in the primary interaction, since Δ calculated according to Eq. (9), taking into account all values of λ, may be in error due to secondary interactions of shower particles with nucleons of the nucleus.

It can be seen from Table VIII that the anisotropy increases considerably with increasing n_s and, especially, $n_h + n_g$. This cannot be explained by secondary interactions of shower particles, since the increase in Δ with n_s and $n_h + n_g$ should influence $\Delta(\lambda < \overline{\lambda})$ to a larger extent than Δ, calculated for all values of λ.

If we assume that a large value of $n_h + n_g$ indicates, on the average, that the primary particle traversed the center of the nucleus, then it follows from the above results that the anisotropy of shower particles increases with tunnel length ℓ. This result contradicts the predictions of the hydrodynamical theory — a decrease in Δ with increasing ℓ.

B. Inelasticity Coefficient

As it has been shown above [cf. Eq. (6)], data on the angular distribution of shower particles make it possible to calculate the inelasticity coefficient k. The values of k for the observed showers are given in Table I. It should be noted, however, that in defining k in the above manner it is assumed that all particles have the same energy. Since it is very probable that this is not the case, the resulting inelasticity coefficients are only approximate. Since k depends strongly on the maximum angle of emission of shower particles, it can be considerably influenced by secondary interactions of shower particles with nucleons of the nucleus. In the calculation of k according to Eq. (6), it is assumed that showers originate in nucleon-nucleon collisions. For collisions between a nucleon and the nuclear matter of the tunnel, Eq. (6) should be modified by introducing the tunnel length ℓ into the denominator. This would cause a considerable decrease in the values of k. All these factors render the determination of k from Eq. (6) unsatisfactory.

The inelasticity coefficient should, according to its definition, be always less than one. It can be seen from Table I that this is not so for calculations based upon Eq. (6). This fact, as it has been mentioned above, is evidently due to the assumptions made in deriving Eq. (6) and to the influence of secondary interactions of shower particles.

The abnormally high values of k for showers generated by heavy particles are clearly connected with the fact that in those events showers originate in interactions between several pairs of nucleons.

C. Azimuthal Asymmetry of Shower Particles

A marked asymmetry of shower particles with respect to the azimuth φ has been observed for several showers. The values of P_6, given in the

TABLE IX. Mean numbers of shower particles in nucleon-produced showers

E_0, ev	$\bar{\vartheta}_{1/2}$	$\bar{n}_s$	$\bar{n}_s(n_h+n_g<3)$	$\bar{n}_s(n_h+n_g>3)$	$n_s(\vartheta_{1/2}<\bar{\vartheta}_{1/2})$	$n_s(\vartheta_{1/2}>\bar{\vartheta}_{1/2})$	$\delta(\bar{n}_s)$	$\delta(n_h+n_g<3)$	$\delta(\vartheta_{1/2}<\bar{\vartheta}_{1/2})$
10^{10}—10^{11}	15.3	17.7	—	17.7	19.0	16.6	6.1		7.2
10^{11}—10^{12}	5.34	19.4	16.3	20.6	15.3	21.9	8.2		5.3
10^{12}—10^{14}	1.45	23.8	26.0	23.1	26.2	20.8	11.2		13.4
10^{11}—10^{14}	4.17	20.7	18.8	21.4	20.5	20.9	9.2	12.1	10.1

thirteenth column of Table I, represent the Pearson probabilities that a given value of asymmetry in the distribution $f(\varphi)$ will be observed in a given shower, under the assumption that the asymmetry is due to statistical fluctuations. The values $P_6(\chi^2)$ were determined from tables for various values of χ^2 which were found from the formula

$$\chi^2 = \frac{m}{n_s}\left(\sum_{i=1} n_i^2\right) - n_s, \qquad (10)$$

where n_s is the total number of shower particles in a shower, m is the number of intervals of angle φ, and n_i is the number of shower particles in the i-th interval $\Delta\varphi$. The values P_6 given in Table I are calculated for $m = 6$. It should be mentioned that cases of large asymmetry were observed both for showers produced by nucleons and by heavy particles. The results on azimuthal asymmetry are, of course, preliminary and a considerable increase in the number of observed cases is necessary for a final conclusion about the existence of such asymmetry.

D. Relation Between the Number of Shower Particles and the Shower Energy

The mean number of shower particles in nucleon-generated showers of various energy regions are given in Table IX. The values of δ, defined below, are also given in the table.

$$\delta = \left\{\sum_i (\bar{n}_s - n_{si})^2 / \left[\left(\sum_i n_{si}\right) - 1\right]\right\}^{1/2} \qquad (11)$$

δ determines the mean spread in the number of shower particles for individual showers.

It can be seen from Table IX that the number of shower particles n_s depends very little on the angle $\vartheta_{1/2}$. It follows that if the determination of shower energy from the angular distribution of shower particles, by the method described in Sec. 2, yields a correct answer for E_0, then the experimental dependence obtained, $n_s = f(E_0)$, is substantially different from the theoretical prediction* $(\bar{n}_s)_{theor} \sim \sqrt[4]{E_0}$. Table IX illustrates also the weak dependence of $\bar{n}_s$ on $\vartheta_{1/2}$ and on the number of black and grey tracks associated with the shower. This fact indicates that secondary interactions of shower particles with nucleons of the nucleus do not influence greatly the shower production mechanism. It should be noted that the relation $n_s \sim \sqrt[4]{E}$ follows from sufficiently general considerations, and the discrepancy between the experimental and theoretical expressions for $n_s = f(E_0)$ can be regarded, together with the asymmetry of angular distribution (cf. Subsec. A) as a proof against the nucleon-nucleon theory of shower production.

Shower energies calculated under the assumption of interaction between the incident nucleon and nucleons of the tunnel are given in column 14 of Table I. Mean lengths $\bar{l}$ of the tunnel calculated under that assumption for various energy regions are given in Table X. The mean number of shower particles is also given in the table for different energies of the primary particles.

Were the tunnel-effect model of shower production correct, $\bar{l}$ would be the same for all energy regions and equal to the mean tunnel length for emulsion, $\bar{l}_{em} = 3.25$. It can be seen from Table X that $\bar{l}$ does not remain constant for showers of different energies. The small number of observed events, however, does not permit us to draw final conclusions. The difference between the absolute

TABLE X. Mean tunnel lengths for various energies of primary particles.

ΔE, ev	$\bar{E}$, ev	No. of showers	$\bar{n}_s$	$\bar{l}$
10^{11}—10^{12}	$3.7\cdot10^{11}$	18	17.2	6.1
10^{12}—10^{13}	$2.5\cdot10^{12}$	18	21.7	5.5
10^{13}—10^{14}	$3.4\cdot10^{13}$	5	26.0	3.7

*Cf. Ref. 3, for example.

TABLE XI. Angular distributions of shower particles in c.m.s. calculated according to Eq. (8′). Data refer to the number of shower particles within given intervals $\Delta\theta$.

No.	Primary particle	0–30°	30–60°	60–90°	90–120°	120–150°	150–180°
		$E_0=10^{10}$–10^{11} ev					
1	p	8	3	1	2	3	6
2	p	6	4	2	1	5	6
3	p	0	2	2	3	1	0
4	n	2	2	3	4	2	0
5	p	0	2	5	4	2	1
6	p	1	1	2	1	1	2
7	p	0	2	4	2	3	1
8	n	2	7	3	3	5	3
9	p	4	6	3	4	5	3
10	n	2	0	5	4	1	3
11	n	2	3	5	3	6	2
12	n or p	3	3	5	2	7	1
13	p	3	3	5	5	4	2
14	α	2	10	5	7	4	6
15	α	6	12	3	8	10	3
16	α	5	5	8	6	5	7
17	α	1	3	5	3	3	2
18	Z	3	13	27	19	16	8
19	α	1	5	4	4	3	3
20	α	3	11	7	9	5	7
21	α	3	7	7	4	10	3
22	Z	8	17	10	16	14	6
23	α	2	2	9	5	6	2
24	α	2	4	2	1	4	3
25	α	2	0	12	6	6	1
26	Z	3	7	10	10	5	6
27	α	3	2	2	1	4	1
28	α	3	5	6	8	5	1
		$E_0=10^{11}$–10^{12} ev					
1	p	3	2	7	5	2	4
2	p	0	5	2	4	0	4
3	p	0	3	4	2	4	1
4	p	4	2	2	3	3	3
5	p	0	6	2	1	1	6
6	p	0	5	7	3	5	4
7	p	0	4	3	2	3	2
8	p	4	2	3	1	1	8
9	p	1	3	11	4	6	4
10	p	1	4	1	2	1	3
11	p	4	6	5	7	2	5
12	n	1	8	2	2	4	6
13	p	0	1	2	2	1	1
14	n	0	1	2	1	0	1
15	p	0	9	8	13	1	4
16	n	6	5	5	2	8	5
17	p	2	1	7	3	3	4
18	n	0	0	5	1	3	1
19	p	4	2	4	3	4	2
20	p	4	5	6	5	5	4
21	p	0	3	3	1	0	4
22	Z	0	6	5	3	6	2
23	α	2	4	7	4	6	4
24	α	1	8	5	10	2	3
25	Z	9	11	9	12	7	9
		$E_0=10^{12}$–10^{13} ev					
1	n	2	9	6	3	2	12
2	p	8	3	2	3	5	6
3	p	0	2	2	2	2	1
4	p	3	2	8	6	3	5
5	p	1	9	3	3	4	7
6	p	2	4	4	5	1	4
7	p	2	10	9	7	10	5
8	α	6	6	4	5	5	7
		$E_0=10^{13}$–10^{14} ev					
1	p	1	1	5	1	3	4
2	p	0	3	2	3	1	1

value of $\bar{\ell}$ and $\bar{\ell}_{em}$ does not contradict the theory, since the theoretical relation $n_s = f(\bar{\ell}, \gamma_c)$ includes a constant, which has to be determined experimentally.

The values of δ given in Table IX show that the spread in n_s for individual showers is considerably greater than statistical fluctuations $\delta_{fluct} \approx \sqrt{\bar{n}_s}$. A large value of δ can be explained by shower production in interactions of the primary nucleon with tunnels of different lengths.

The number of shower particles in showers generated by particles with $Z \geq 2$ is considerably greater than $\bar{n}_s$ in nucleon-produced showers. This can be explained by assuming that in the former case shower production is due to interaction between several nucleons and the nucleus.

In conclusion, the authors wish to express their gratitude to D. S. Chernavskii for fruitful discussion of results, to V. M. Kutukova and L. A. Smirnova for help in carrying out the work and to D. M. Samoilovich for development of the emulsion chamber.

APPENDIX

Since valid conclusions about showers produced by high-energy cosmic ray particles can be drawn only on the basis of a large statistical material, the authors have thought it useful, for reference purposes, to include data on the angular distribution of shower particles, in the c.m.s., for each observed event. Angular distributions in the c.m.s. were calculated from data on the distribution in the laboratory system according to Eq. (8′), γ_c being determined from the relation $\gamma_c = \cot \vartheta_{1/2}$. The numeration of showers in Table XI corresponds to that of Table I.

It should be noted that for several showers the values n_s given in Table I are slightly larger than the total number of shower particles in Table XI. This is due to the fact that some particles propagate at an angle $\vartheta > 90°$ in the laboratory system, and have not been considered in calculations of the angular distribution according to Eq. (8′).

[1] Alpers, Gurevich, Kutukova, Mishakova, Nikol'skii, and Surkova, Dokl. Akad. Nauk SSSR 112, 33 (1957), Soviet Phys. "Doklady" 2, 1 (1957).
[2] Castagnoli, Cortini, Franzinetti, Manfredini, and Moreno, Nuovo cimento 10, 1539 (1953).
[3] S. Z. Belen'kii and L. D. Landau, Usp. Fiz. Nauk 56, 309 (1955).
[4] G. Bertolino and D. Pescetti, Nuovo cimento 12, 630 (1954).

Translated by H. Kasha
57

SOVIET PHYSICS JETP VOLUME 34 (7), NUMBER 2 AUGUST, 1958

ASYMMETRY IN THE ANGULAR DISTRIBUTION OF $\mu^+ \rightarrow e^+$ DECAY ELECTRONS OBSERVED IN PHOTOGRAPHIC EMULSIONS

I. I. GUREVICH, V. M. KUTUKOVA, A. P. MISHAKOVA, B. A. NIKOL'SKII, and L. V. SURKOVA

Academy of Sciences, U.S.S.R.

Submitted to JETP editor August 14, 1957

J. Exptl. Theoret. Phys. (U.S.S.R.) 34, 280-285 (February, 1958)

Herewith are presented the results of measurements of the angular distribution of $\pi \rightarrow \mu \rightarrow e$ decay electrons observed in a photographic emulsion located either inside a magnetic screen or in a magnetic field $H \sim 1100$ G, longitudinal with respect to the μ-meson motion. The electron angular distributions were found to be describable by a relation of the form $1 + a \cos\theta$. The parameter a was found to be equal to $-(0.092 \pm 0.018)$ and $-(0.16 \pm 0.04)$ for the cases when the emulsion was inside the magnetic screen and the magnetic field respectively.

In the fundamental work of Lee and Yang[1] and Landau,[2] it was shown that a possible method for testing parity nonconservation in weak interactions is to study the asymmetry in the angular distribution of the electrons emitted in the decay of polarized μ mesons. The two-component neutrino theory, developed by the same authors, leads to the conclusion that the μ meson formed in the $\pi \rightarrow \mu$ decay should be fully polarized in the direction of its motion. According to this theory, the electron angular distribution from the $\mu \rightarrow e$ decay is described by the relation

$$f(\theta) = 1 + (\lambda/3)\cos\theta, \qquad (1)$$

where θ is the angle between the electron momentum and the μ-meson spin. The constant λ depends on the relative amount of vector and axial vector coupling in the β decay of the μ meson and can vary between -1 and $+1$.

The first experimental confirmation of parity nonconservation in the $\pi \rightarrow \mu \rightarrow e$ chain came from Garwin et al.[3] Thereafter a rather large number of papers appeared devoted to a more accurate determination of the constant λ, using photoemulsions, counters and bubble chambers. It was established in these experiments that in the $\mu^+ \rightarrow e^+$ decay the positrons are emitted predominantly backwards, i.e., $\lambda < 0$. It also follows from these experiments that the asymmetry in the angular distribution of electrons from $\mu \rightarrow e$ decay depends sensitively on the substance in which the μ meson decays. This indicates the existence of a partial depolarization of the μ mesons and consequently the electron angular distribution from the $\mu \rightarrow e$ decay may be written in the form

$$1 + a\cos\theta, \quad a = (\lambda/3)(1 - \gamma), \qquad (2)$$

where γ is the depolarization coefficient of the μ mesons. The experimentally obtained angular distributions of electrons from $\mu \rightarrow e$ decay agree qualitatively with formula (2) throughout the electron energy spectrum. However, more definite quantitative conclusions can be reached only by substantially increasing the statistical accuracy.

In this work we studied the angular distribution of $\mu^+ \rightarrow e^+$ decay electrons in emulsions. A 7×4×1 cm emulsion chamber consisting of 23 layers of NIKFI type R photoemulsion was irradiated with

slow π^+ mesons from the synchrocyclotron of the Joint Institute for Nuclear Research. The chamber was placed inside a double magnetic screen to avoid precession of the μ-meson spin in the stray magnetic fields of the synchrocyclotron. The emulsion was developed by D. M. Samoilovich. The emulsion was scanned with MBI-2 microscopes at an amplification of 450 X, and the measurements were made at an amplification of 1350 X. In scanning, we selected those cases for which the μ meson from the $\pi \to \mu$ decay was entirely within one emulsion layer and stopped not nearer than 50 μ from the undeveloped surface of the emulsion layer. This method of selection assures the detection of every electron from a stopped μ meson with practically 100% efficiency. Thus, out of 4055 cases of $\pi \to \mu$ decays, only 11 cases were found where the decay electron was not seen. To determine the angle θ between the direction of μ-meson emission in the $\pi \to \mu$ decay and electron emission in the $\mu \to e$ decay, we measured the corresponding angle α in the emulsion plane as well as the inclination angles β_1 and β_2 of the μ meson and electron tracts relative to the emulsion plane. The angle θ is given in terms of α, β_1 and β_2 by

$$\cos\theta = (\tan\beta_1 \tan\beta_2 + \cos\alpha)\cos\beta_1 \cos\beta_2. \qquad (3)$$

In this work the angle θ was determined with the help of a special three-dimensional plotter. The error in θ measured in this way did not exceed $\pm 1°$. The total error in the determination of θ includes the errors in the measurement of the angles α and β as well as the error in determination of the photoemulsion settling. Estimates carried out indicate that the sum of these errors does not have a systematic character and does not exceed 3°. In order to find the angles β_1 and β_2 it is necessary to know with sufficient accuracy the emulsion settling after development. The settling d was determined by a comparison of the thickness of developed and undeveloped emulsion layers as well as from measurements of the track lengths of μ mesons from $\pi \to \mu$ decays parallel and perpendicular to the emulsion plane. To correct the settling coefficient for ambient temperature and humidity variations, the thickness of all emulsion layers was measured twice daily at marked points.

In addition to measuring the angular distribution of the $\mu \to e$ decay electrons for the case when the emulsion was placed inside a magnetic screen, we irradiated with slow π^+ mesons an emulsion chamber of the same dimensions, placed in a magnetic field of intensity $H \sim 1100$ G. In the latter case we selected those μ mesons emitted at an angle of no more than 30° with the magnetic field. The magnetic field here played the role of a magnetic screen in that it confined the stray magnetic fields of the synchrocyclotron and of the earth to one fixed direction. The decrease in μ-meson polarization, resulting from such a selection of $\pi \to \mu$ decays and due to the μ-meson spin precession around the magnetic field H, is not large and amounts to $\sim 7\%$.

Altogether we measured 8990 angles between the directions of electron and μ-meson emissions in the $\pi \to \mu \to e$ chain in the case when the emulsion was inside the magnetic screen, and 2005 angles in the case of $\pi \to \mu \to e$ decays in a magnetic field. The results of these measurements are given in Table I, which shows the number of events in a given interval of $\cos\theta$. The resulting angular distributions are also illustrated in Fig. 1.

It can be seen from Fig. 1 that the angular distributions obtained do not contradict the theoretical relation (2). The best value of a of formula (2) is obtained from the relation

$$a = 3r^2 \sum_{i=1}^{r} n_i \cos_i\theta / (r^2 - 1)\, N, \qquad (4)$$

where N is the total number of cases studied, r the number of intervals, and $\cos_i\theta$ the average value of $\cos\theta$ in the i-th interval. The statistical error in the parameter a obtained in this way is given by

$$\delta a = \sqrt{3r^2 / N (r^2 - 1)}. \qquad (4')$$

TABLE I. Electron angular distribution in $\mu \to e$ decays in emulsions located inside a magnetic screen and in a magnetic field of intensity $H \approx 1100$ G (θ = angle between the directions of emission of the electron and μ meson).

cos θ	Magnetic screen	Magnetic field	cos θ	Magnetic screen	Magnetic field
1.0—0.8	834	181	0 — —0.2	910	188
0.8—0.6	893	187	—0.2— —0.4	928	197
0.6—0.4	836	167	—0.4— —0.6	914	216
0.4—0.2	867	202	—0.6— —0.8	938	229
0.2—0	839	196	—0.8— —1.0	1031	242

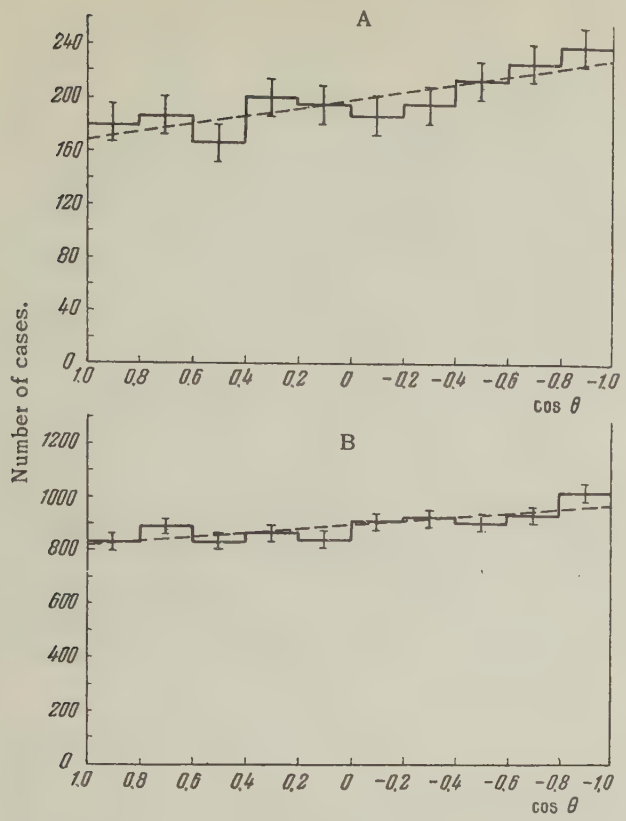

Fig. 1. Electron angular distribution in $\mu \rightarrow e$ decay: A – measurements in a magnetic field $H \approx 1100$ G, $a = -(0.16 \pm 0.04)$; B – measurements inside a magnetic screen, $a = -(0.092 \pm 0.018)$.

The values of the quantity a calculated from these formulae for $r = 10$ were found to be:

1. For emulsion inside magnetic screen,* $a = -(0.092 \pm 0.018)$.

2. For emulsion in magnetic field, $a = -(0.16 \pm 0.04)$. It is seen that the magnetic field ($H \approx 1100$ G) increases the asymmetry somewhat, i.e., decreases the depolarization of μ mesons in emulsion. However this effect is not definitely proven, in view of the small number of $\mu \rightarrow e$ decays found in the magnetic field. It would be interesting to measure the electron angular distribution from $\mu \rightarrow e$ decays in a magnetic field of higher intensity and with better statistics.

After completing this work we became acquainted with the work of Orear et al.[4] dealing with analogous measurements in a magnetic field $H = 9{,}000$ G. In a field of this intensity these authors obtained in emulsion a value $a = -0.25$, which coincides with the maximum value of a observed in any of the substances studied. Inserting $H = 1100$ G into the formula of Orear et al. for the polarization magnitude in an external magnetic field H

$$p = \frac{1}{2}\left(1 + \frac{1}{1 + (1600/H)^2}\right),$$

we obtain $a = 0.13 - 0.16$, in agreement with our measurements.

The value of a for the case of emulsion inside a magnetic screen is in agreement with measurements of other authors as summarized in Table II.

TABLE II. The parameter a of formula (2) for photoemulsion from the data of various authors.

$-a$	Number of cases	Method of observation	Reference
0.222 ± 0.067	1028	In cosmic rays	[5]
0.08 ± 0.05	1562	,,	[6]
0.03 ± 0.04	2117	,,	[7]
0.00 ± 0.07	700	,,	[8]
0.174 ± 0.038	2000	Artificially produced π^+ beams	[9]
0.095 ± 0.04	2003	,,	[10]
0.22 ± 0.12	831	,,	[11]
0.149 ± 0.033	2789	,,	[12]
0.11 ± 0.08	580	,,	[13]

It is interesting to note that in the observations of $\pi \rightarrow \mu \rightarrow e$ decays in cosmic rays, the parameter a is found to be somewhat smaller than in the corresponding observations with accelerators.

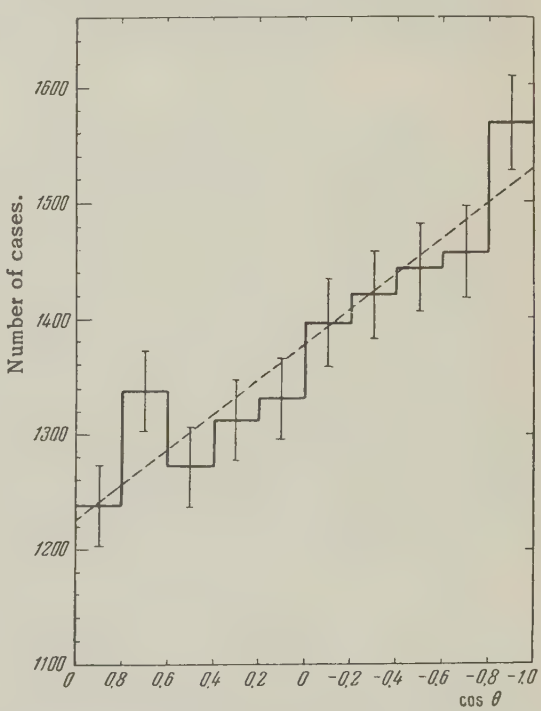

Fig. 2. Electron angular distribution using the combined data of this work and of Ref. 9 and 12; $a = -(0.111 \pm 0.015)$.

*For $r = 2$, the experiment inside the magnetic screen gives $a = -(0.10 \pm 0.021)$.

It is possible that this is to be explained by the absence of special screening in the former case.

The average value of a computed from the data of Table II and from the results of this work is

$$a = -(0.108 \pm 0.0094).$$

The angular distributions of $\mu \rightarrow$ e-decay electrons are given in Refs. 9 and 12. Combining those with our data, yields the angular distribution shown in Fig. 2, which represents 13,770 cases of $\mu \rightarrow$ e decays. It can be seen from Fig. 2 that, within the experimental accuracy, the electron angular distribution is described by $1 + a \cos\theta$ with $a = -(0.111 \pm 0.015)$.

In conclusion, the authors express their gratitude to V. P. Dzhelepov, B. S. Neganov, and V. N. Mekhedov for help in emulsion irradiation, and to N. M. Polievktov-Nikoladze for assistance in the statistical analysis of the results.

[1] T. D. Lee and C. N. Yang, Phys. Rev. **104**, 254 (1956); **105**, 1671 (1957).

[2] L. D. Landau, Nuclear Physics **3**, 127 (1957).

[3] Garwin, Lederman and Weinrich, Phys. Rev. **105**, 1415 (1957).

[4] Orear, Harris and Bierman, Phys. Rev. **107**, 322 (1957).

[5] Castagnoli, Franzinetti and Manfredini, Nuovo cimento **5**, 684 (1957).

[6] Bhowmik, Evans, and Prowse (in press).

[7] Fowler, Freier, Lattes, Ney and St. Lorant, Bull. Am. Phys. Soc. **2**, 191 (1957).

[8] Lattes, Fowler, Freier, Ney and St. Lorant, Bull. Am. Phys. Soc. **2**, 206 (1957).

[9] J. I. Friedman and V. L. Telegdi, Phys. Rev. **106**, 1290 (1957).

[10] Biswas, Ceccarelli and Crussard, Nuovo cimento **5**, 756 (1957).

[11] Heughebaert, Rene, Sacton, and Vanerhaeghe, Nuovo cimento **5**, 1808 (1957).

[12] Chadwick, Durrani, Eisberg, Jones, Wignall, and Wilkinson, Phil. Mag. **2**, 684 (1957).

[13] A. O. Vaisenberg and V. A. Smirnitskii, J. Exptl. Theoret. Phys. (U.S.S.R.) **33**, 621 (1957), Soviet Phys. JETP **6**, 477 (1958).

Translated by A. Bincer
58

SOVIET PHYSICS JETP VOLUME 34 (7), NUMBER 2 AUGUST, 1958

HYPERFRAGMENTS IN NUCLEAR EMULSIONS

B. P. BANNIK, U. G. GULIAMOV, D. K. KOPYLOVA, A. A. NOMOFILOV, M. I. PODGORETSKII, B. G. RAKHIMBAEV, and M. USMANOVA

Joint Nuclear Research Institute and Tashkent Physico-Technical Institute

Submitted to JETP editor July 12, 1957

J. Exptl. Theoret. Phys. (U.S.S.R.) **34**, 286-297 (February, 1958)

The properties and relative frequency of appearance of hyperfragments were investigated. Some effects produced by other types of unstable heavy particles are also mentioned.

THIS investigation was performed with two emulsion stacks which were exposed to cosmic rays in the atmosphere. One stack consisted of 600 μ Ilford G5 emulsions which were exposed at the time of the international expedition in the valley of the Po River, The second stack consisted of NIKFI R-type emulsions 400 μ thick, which were exposed in the Soviet Union. The scanning located all stars with prong numbers $N_h \geq 8-10$ or $n_s \geq 2-3$ as well as σ stars and all double stars regardless of the number of prongs.

The main procedure was area scanning with $10\times10\times1.5$ magnification. In a small number of instances all black prongs were continued until they emerged from the emulsion, and sometimes even up to their termination in other emulsions. But, as a rule, only those double stars were fixed, which were entirely in the field of view of the objective. Altogether there were found six τ mesons, one τ' meson, one Λ^0 particle, four K^- mesons, one Σ^- hyperon and ten hyperfragments, of which five decayed with emission of a π meson.

Not a single case of Σ^+ or of K^+ decay was found, since the method used excluded the possibility of observing such particles. For all primary stars associated with unstable heavy particles, all black and gray tracks were followed until they stopped or emerged from our portion of the pellicle stacks.* Not a single instance of pair production was found in 14 primary stars.

Of the six τ^+ mesons, five were found by area scanning and one by continuing backward the tracks of stopped π mesons. In all cases the tracks of secondary π mesons were observed to be coplanar within $2-3°$. The parent disintegrations were registered in only two cases ($10+0n$ and $11+3n$). The τ' meson[1] was produced in a $3+0n$ star with very small visible energy release. The two black tracks of the parent star (besides the τ' meson) belong to stable particles. After traversing 17 mm the τ' meson stopped inside of the emulsion and decayed. A photomicrograph of this event is shown in Fig. 1.†

The mass of particle 1 was determined to be $(860+50)\,m_e$ from gap length density and the residual range. At the stopping point B the track of a secondary π^+ meson begins, which afterwards undergoes $\pi \to \mu \to e$ decay.‡ The length of the π^+ track is $1930\,\mu$. The photomicrograph reveals the tracks of two relativistic particles 5 and 6 leaving the stopping point of the τ' meson and forming an angle of 1° to 2°. Measurement of multiple scattering gives for track 6

$$p\beta c = (66 \pm 10)\ \text{Mev},$$

whence it follows that this particle is an electron. Track 5 disappears within the emulsion after a range of $\sim 250\,\mu$, which can reasonably be interpreted as the annihilation of a positron in flight. The present event thus evidently represents the decay

$$\tau' \to \pi^+ + \pi^0 + \pi^0$$

followed by

$$\pi^0 \to \gamma + e^+ + e^-.$$

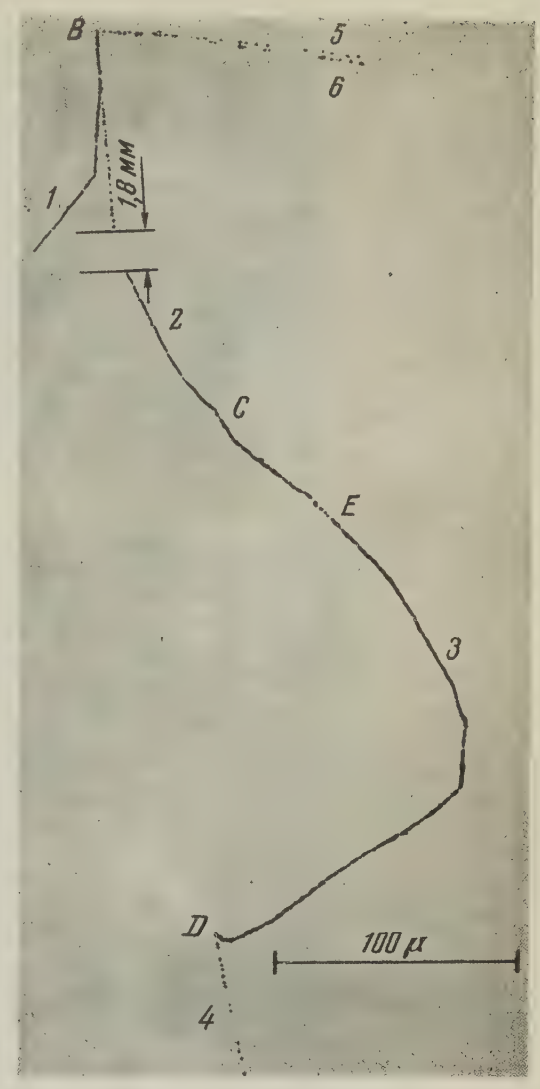

FIG. 1

If this interpretation is correct, then at the present time among K^+ decays leading to π^0 mesons e^+e^- pairs have been observed not only in decays of the type K_{e3}.

Of the four K^- mesons which we found three were detected through systematic scanning and subsequent analysis of the σ stars that possessed a large number of prongs or other unusual characteristics. The parent disintegration was recorded in only one instance ($11+4n$ or $11+3p$).

The K^- meson of the photomicrograph in Fig. 2* had a mass of $(1100+250)\,m_e$ as measured from multiple scattering and the residual range.† One

*In some instances the tracks of the particles of interest were traced in other portions of the pellicle stack which were in laboratories at Budapest, Erevan and Leningrad. The authors wish to thank the staffs of those laboratories for their assistance.

†This event was discovered by L. U. Bannik.

‡The π^+ meson stops and decays at the point C. The apparent reduced ionization at E is associated with the passage of the track from one emulsion to another.

*Discovered by M. I. Tret'iakova.

†Here and hereinafter, except for particle 3 of event No. 2, we used the constant-sagitta method in determining masses from multiple scattering and range.

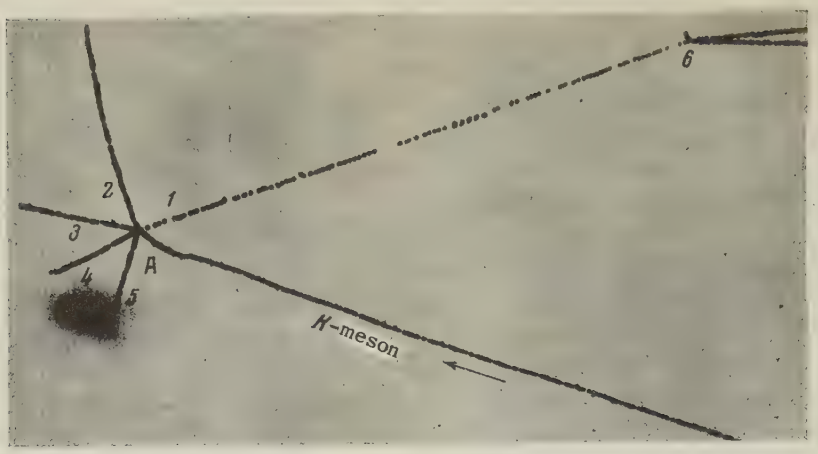

FIG. 2

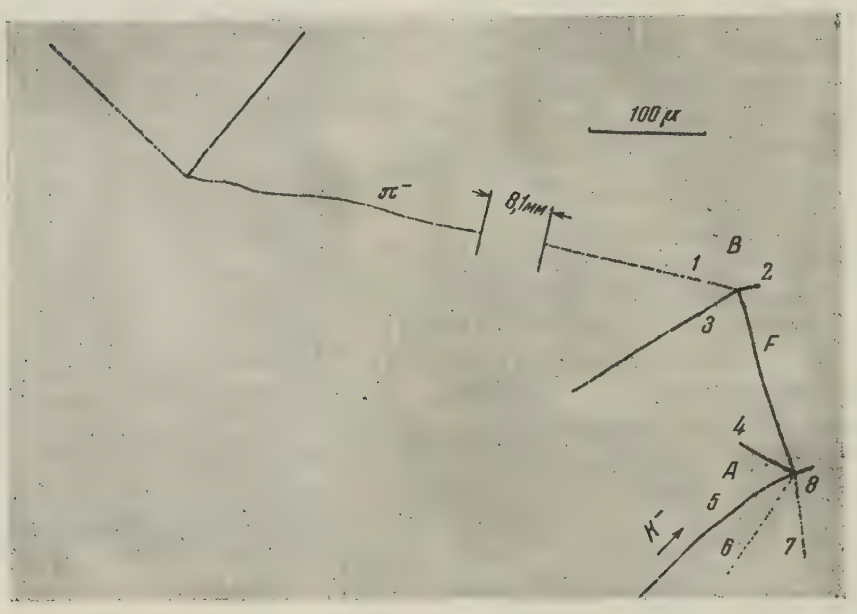

FIG. 3

of the particles (track 1) produced in the five-prong σ star gave rise to a small secondary disintegration at a distance of $\sim 5560\mu$ from the σ star. Multiple scattering and ionization measurements of the connecting track show it to be due to a proton with $E = (103 \pm 13)$ Mev. In a σ star produced by another of the K^- mesons which we observed, a proton possessing the relatively large energy $E \sim 75 - 80$ Mev was also found. It has been noted in the literature that the appearance of high-energy protons can be regarded as an indirect argument for the capture of a stopping K^-, according to the scheme

$$K^- + 2N \rightarrow N + \Sigma$$

(see Ref. 2, for example).

A kinematical analysis of the σ star in Fig. 2 showed that for all possible hypothetical forms of nuclear capture the total energy release considerably exceeds $m_\pi c^2$. The same can be said concerning two of the three other σ_K stars, with four and five secondary prongs, respectively. The third σ_K star also has 5 prongs. It appears that all of the σ_K stars which we discovered were produced through K^- capture in light nuclei of the emulsion. This is completely understandable from our scanning method, whereby preferential selection was made of σ stars that possessed a large number of prongs, large visible energy release or other noteworthy properties. It thus follows that the true number of K^- mesons is a few times greater than the number of those actually found, i.e., it is about the same as the number of τ mesons or even somewhat greater. This result fully agrees with experimental findings regarding the ratio of K^+ and K^- mesons generated in cosmic-ray collisions (see Ref. 3, for example).

TABLE I

Track	4	5	6	7	8	F
Range (μ)*	54.7	>27300	>27500 non-stopping	4880	18	161
Error in range (%)	1.7	—	—	0.1	5.1	0.4
Spread of ranges (%)	1.8	—	—	1.4	2	1.2
Angle β with horizontal plane†	+16.0	—	+7.9	−19.8	+15.8	0
Error in angle β (degrees)	2	—	0.3	1	7	—
Azimuthal angle φ (degrees)‡	44.5	—	126.6	167.8	269.8	0
Error in φ (degrees)	0.7	—	0.7	0.7	1.7	0.7
Number of δ electrons with range $\geq$ four grains**	0	—	—	—	0	0
Charge Z	$\leqslant 2$	−1	± 1	+1	$\leqslant 2$	$\leqslant 2$
Method of measuring mass and its magnitude (m_e)	—	$\langle\alpha\rangle - R$: 914+170 $I - R$: 658±55	$I - \langle\alpha\rangle$: 343^{+94}_{-62}	$\langle\alpha\rangle - R$: 1250+340 $I - R$: 2700±±300	—	—
Identification of particle	p	K^-	π^-	p	He_2^4	$_\Lambda He_2^5$
Energy of particle (Mev)	2.47±0.04	—	66.3±6.5	35.3±0.3	4.6±0.2	21.3±0.3

*All data refer to an unprocessed emulsion.

†All tracks in the direction of the surface bear the plus sign; tracks in the direction of the glass are given with the minus sign.

‡Taken counterclockwise with respect to an arbitrary direction which is the same for all tracks of the star and the track of the hypernucleus.

**1 grain on the track; 3 grains outside of the track.

One of the remaining K^- mesons deserves special mention. The pertinent data are given in Table I and the photomicrograph of this event is shown in Fig. 3.* Particle 5 is a stopping K^- meson, 7 is a proton and 6 is a π meson. There is no sign of thin-down at the ends of tracks 4, 8 and F so that each of these particles must have a charge ≤ 2. From an analysis of the event at B it follows that particle F is the hyperfragment $_\Lambda He_2^5$ (see below, event No. 1).

If 8 were a proton or α particle its energy would be 1.2 or 4.6 Mev, respectively, which is considerably below the height of the Coulomb potential barrier in heavy nuclei of the emulsion. It can therefore be assumed that the K meson was captured in a nucleus of C^{12}, N^{14} or O^{16}. We therefore considered all of the conceivable reactions in C^{12}, N^{14} or O^{16} for all possible masses and charges of particles 4, 6, 7, and 8. It was found that energy and momentum conservation are fulfilled only by

$$K^- + C_6^{12} \rightarrow {}_\Lambda He_2^5 + He_2^4 + 2p + \pi^- + n.$$

The K^- mass is then

$$m_{K^-} = (494.3 \pm 6.8)\ \text{Mev},$$

which is in good agreement with data given in other papers.*

It must be pointed out that conservation of energy and momentum are not fulfilled if F is assumed to be a hyperfragment other than $_\Lambda He_2^5$. We have thus encountered one of the rare cases in which double identification of a hyperfragment is possible, through the phenomena at its decay and from a consideration of the generation process.† The decisive circumstance is the fact that the hyperfragment was produced in a σ_{K^-} star. We can expect that hyperfragments due to K^- capture can generally be identified much more easily and completely than in the usual instances. This may be especially important in studying hyperfragments that undergo nonmesonic decay. Even more favorable conditions are realized in the nuclear capture

*Discovered by N. V. Kirsanova. A detailed analysis is given in Ref. 4.

*For example, Ref. 5 gives $m_{K^+} = (493.66 \pm 0.36)$ Mev. The K^- mass is less accurately known, but we can reasonably assume that $m_{K^-} = m_{K^+}$.

†Ref. 6 describes a similar instance of double identification of a hyperfragment resulting from K^- capture.

of Σ^- hyperons, but, unfortunately, this event is observed much less frequently.

We found only one Σ^- hyperon, produced in a $9+2n$ or $9+1p$ star. One of the gray prongs of the parent star produces in flight a secondary disintegration with small Q (4 black prongs ending in the same emulsion). The length of the Σ^- track is 715μ.

The mass was determined from multiple scattering and residual range, which gave $M = (1.0 \pm 0.4)m_p$ for a gap scheme corresponding to a proton. For gap schemes corresponding to a τ meson and a π meson the mass was $(1.3 \pm 0.3)m_p$ and $(1.4 \pm 0.3)m_p$, respectively. The Σ^- was stopped in producing a three-prong σ star with one gray track (range $> 3800\mu$) and one black track (range 385μ). The third track is very short, being only $\sim 1.5\mu$. Comparison of the ionization and multiple scattering shows that the gray track is probably that of a proton with about 90 Mev.

Although many interesting papers have already been published concerning investigations of hyperfragments there is still no reliable and sufficiently complete information regarding the frequency of their generation and the dependence of this frequency on the character and energy of the generating particles. This results from the difficulty of identifying hyperfragments reliably, especially in the case of nonmesonic decays. Therefore, different investigators use entirely different criteria which are very difficult to correlate; it is thus extremely difficult to compare different data on the frequency of hyperfragment generation. For combining data, it would be important to agree on uniform criteria; for this purpose we believe that the rules suggested in the review article, Ref. 7, are quite suitable. These rules require reliable proof that the event in question is not a σ star and that the kinetic energy of the proposed hyperfragment is small enough to exclude clearly the possibility of the disintegration of some nucleus by collision. Data concerning hyperfragments that undergo mesonic decay are especially reliable and should, we believe, provide the basis for various quantitative comparisons.

In the present work we found ten hyperfragments which satisfy the criteria of Ref. 7. Five of these underwent nonmesonic decay, while the others underwent mesonic decay.* The parent disintegrations were of the types $19+3n$ (or $19+2p$), $17+4n$ (or $17+3p$), $41+7n$ (or $41+6p$), $15+2n$, $13+4n$, $17+4p$, $5+0n$, $27+13n$ and $14+5p$. It is noted that as a rule the very large number N_h of gray and black prongs in the parent disintegrations is considerably larger than in stars containing τ mesons. For the mean number of gray and black prongs we have

$$\bar{N}_h = 18.7 \pm 3.7,$$

which is in good agreement with the data in other papers (see Ref. 8, for example). It would be very interesting to obtain corresponding data for different types of "strange" particles when the nature and energy of the generating particles are known.

In addition to the hyperfragments which have been mentioned ~ 37,000 stars were found with either $N_h \geq 8-10$ or $n_s \geq 2-3$, which corresponds to about 10^5 cosmic-ray stars of all types. Thus from cosmic rays we obtain one mesonic decay of a hyperfragment in about 2.5×10^4 nuclear disintegrations of all kinds. This agrees in general with the results obtained by other investigators. The data are given in Table II.

TABLE II

Primary particles	Reference	Number of Disintegrations	Number of Mesonic Decays
Cosmic rays	[9]	24 000	2
Cosmic rays	[10]	27 000	2
Cosmic rays	[11-12]	119 000	5
Protons with $E_p = 6$ Bev	[11]	10 000	0
π^- mesons with $E_{\pi^-} = 3$ Bev	[11-12]	80 000	3
π^- mesons with $E_{\pi^-} = 4.7$ Bev	[13]	150 000	30
Cosmic rays	Present work	100 000	4

The table shows that for 270,000 cosmic-ray stars there are 13 mesonic decays, i.e., about one decay for 20,000 stars. Also, bombardment with 4.7-Bev π^- mesons yields one mesonic decay for only 5000 disintegrations.* It would not be legitimate to make a direct comparison of these results, because in cosmic rays a large percentage of the disintegrations are produced by particles of relatively low energies. Further work is needed with accelerators that produce particles of various kinds with energies of a few billion electron volts.

In Ref. 7 and elsewhere it is stated that a large

*One of the hyperfragments which underwent mesonic decay was produced in a σ_K star and is therefore excluded from subsequent compilations giving the frequency of generation and the nature of the parent disintegrations.

*A rapid increase of the frequency of hyperfragment generation is noted with increasing π^- energy.

percentage of hyperfragments is found among double-centered stars with very short connecting tracks. In the present work, we observed seven double-centered stars in which the connecting track did not exceed 10μ. In only one of these instances was it possible to prove by means of a detailed kinematical analysis that the secondary disintegration could not have resulted from a stopped π^- meson. In this case the secondary star had five prongs of which one was a proton with the range $11{,}300\mu$ ($E_p \approx 56$ Mev.). In one of the other six cases the secondary star also contains a proton of the relatively high energy ~ 50 Mev, and in a third case the secondary disintegration also has five prongs but the total Q is small. In all of the events that were found, the primary stars have very many black and gray prongs;* the average of these is $\overline{N_h} = 14 \pm 2.7$. However, it must be remembered that this increase of $\overline{N_h}$ above the normal level would have had to occur on the basis of the usual mechanisms for the appearance of the double-centered stars under consideration.

The individual characteristics of the hyperfragments are summarized in Table III. (In calculating the angles the hyperfragment track was assumed to emerge from the center of the secondary star.)

Event No. 1. Fig. 3 is the photomicrograph of this event. Particle 1 is a π^- meson which produces a σ star in stopping. The measured widths of tracks 2, 3, and F showed $Z \leq 2$ for each of these particles. The tracks of 1, 2 and 3 are coplanar to within 3°. This points to the formation of star B by the decay of a stopped hyperfragment to three charged particles. A kinematical analysis of B was carried through for all possible masses of 2 and 3, assuming their charge to be 1 or 2. It appeared that for all of the proposed decay schemes, with one exception, the combined momentum is clearly different from zero. The combined momentum is zero only in the scheme

$$_{\Lambda}He_2^5 \rightarrow He_2^4 + p + \pi^-.$$

Then the combined kinetic energy of all the particles is

$$Q = (34.2 \pm 0.4)\ \text{Mev},$$

and the binding energy of the Λ^0 particle is $B_\Lambda = (2.7 \pm 0.4)$ Mev, which is in good agreement with published data (Ref. 7, for example). The normal to the decay plane and the direction of motion of the hyperfragment form an angle of 82°.

Event No. 2. The mass of the particle F* was determined from multiple scattering and range using the cell schemes for H_1^4, He_2^5 and Li_3^6; the result was $M_F = (6 \pm 2)\, m_p$. Twelve δ electrons were discovered along the F track. Since ~ 5.5 δ electrons are expected along a proton track of this range, the charge of F evidently exceeds unity. On the other hand, the F track shows no sign of thin-down upon stopping as is always observed in Li tracks. Combining these results, we can assume that the charge of F is two. This is also supported by a comparison of the track widths for protons, α particles, and F.

The track of 3 has the character of a light meson. Its mass, from multiple scattering and range, is $(230 \pm 90)\, m_e$. On this basis 3 was identified as a π^- meson which upon stopping produced a nuclear disintegration accompanied by the emission of only neutral particles. Tracks 1, 2, and 3 lie in the same plane within the limits of error. The errors are quite large since track 1 is only 1.6μ long. The combined momentum of 1, 2 and 3 is close to zero only if 2 is a proton. The charge of 1 must then be two. If it is assumed that this event represents the scheme

$$_{\Lambda}He_2^4 \rightarrow He_2^3 + p + \pi^-,$$

the binding energy of Λ^0 is

$$B_\Lambda = (3.1 \pm 0.4)\ \text{Mev},$$

which differs extremely from the results of other investigations. The most probable interpretation apparently is given by

$$_{\Lambda}He_2^5 \rightarrow He_2^4 + p + \pi^-.$$

The decay energy appears to be $B_\Lambda = (3.0 \pm 0.4)$ Mev. The normal to the decay plane and the direction of the hyperfragment track is 56°.

Event No. 3. From measurements of the thickness of the track of F it follows that its charge cannot be more than two. The tracks of 1 and 2 are collinear within the limits of error, from which it follows that 1 decayed after stopping. The mass of 1 from multiple scattering and ionization is $(235 \pm 90)\, m_e$ so that 1 can be regarded as a π meson. In addition, $p\beta c = (89.5 \pm 8)$ Mev, which completely agrees with

$$_{\Lambda}H_1^4 \rightarrow He_2^4 + \pi^-.$$

*The parent stars are of the types 12 + 1n (or 12 + 0p), 9 + 1n (or 9 + 0p), 17 + 2n (or 17 + 1p), 30 + 7n (or 30 + 6p), 14 + 2p, 9 + 2n (or 9 + 1p) and 7 + 1n (or 7 + 0p).

*The letter F everywhere designates a hyperfragment.

TABLE III

hyperfragment	Track	Range (μ)	Error in range (%)	Range spread (%)	Angle β with horizontal plane (degrees)	Error in β (degrees)	Azimuthal angle φ (degrees)	Error in φ (degrees)	Number of δ electrons with range $\geq$ four grains	Charge Z	Method of measuring mass and its magnitude (m_e)	Identification of particle	Energy of particle (Mev)	Parent star
	F	161	0.4	1.2	0		0	0.7	0	$\leqslant 2$		$_{\Lambda}He_2^5$	21.3±0.3	
	1	8481	0.1	3.0	— 9.0	4	232.3	0.7		—1		π^-	21.0±0.4	
1	2	19.3	4.2	2.0	+12.4	7	79.5	1.7	0	$\leqslant 2$		He_2^4	4.8±0.2	
	3	401	0.5	1.6	—18.5	2	278.2	0.7	0	$\leqslant 2$		p	8.4±0.1	
	F	883			—3	0.5	0		12	2	$\langle\alpha\rangle - R$: 11000±3700	$_{\Lambda}He_2^5$		
	1	1.6			—3	2	100	7				He_2^4	0.2±0.1	
2	2	244	1.5	1.6	+8	0.5	233					p	6.2±0.2	13+4 n
	3	13535	0.3	1.2	+9	0.5	37			—1	$\langle\alpha\rangle - R$: 230±90	π^-	27.4±0.3	
	F	88			—1		0	1		$\leqslant 2$		$_{\Lambda}H_1^4$		
3	1	>12350			—34	1	219	1			$\langle\alpha\rangle - I$: 235±30	π^-	51.7±5.5	5+0 n
	2	8.8	~15		+30	7	45	3				He_2^4	2.5±0.4	
	F	450			+2					$2<Z<5$	$\langle\alpha\rangle - R$: 14700±3700	$_{\Lambda}Li_3$ or $_{\Lambda}Be_4$		
4	1	3.2			—40		226					Recoil nucleus		17+4 p
	2	13400			—68		71					π^-	27.2	
	3	280			+70		0					p, d or t	7.4	
	F	82			+48.5		0			3 or 4		$_{\Lambda}Li_3^7$		
	1	10			+13.3		127					He_2^4		
5	2	38			—17.6		24					p		27+13 n
	3	178			— 3.6		311					p		
	4	7476			+ 6.6		214					π^-		
	F	33								$\geqslant 4$		$_{\Lambda}B_5$		
	1	260												17+4 n
	2	1315												or
6	3	14.6												17+3 p
	4	413												
	5	19												
	F	61			—28.7		0			~3		$_{\Lambda}Li_3$		
	1	50			+39.6		299							41+7 n
7	2	612			—72.3		353							or
	3	>19000			+33.5		167					p		41+6 p
	F	55			—31		0			$\geqslant 2$		$_{\Lambda}He_2$ or $_{\Lambda}Li_3$		
	1	1590			—40.7		310							
8	2	3816			+6.6		256				$\langle\alpha\rangle - R$: 1970±330	p		15+2 n
	3	1												
	F	124			+33					$\geqslant 4$		$_{\Lambda}Be_4$		
	1	2660			+22		225				$\langle\alpha\rangle - R$: 2020±550	p		19+3 n
	2	1004			+5.6		143				$\langle\alpha\rangle - R$: 3490±740	d		or 19+2 p
9											$I - R$: 4040±370			
	3	11750			—28.2		4				$\langle\alpha\rangle - R$: 2020±423	p		
	4	202			—18.2		0			1		p, d, t		
	F	92			—8.7					$3<Z<6$	$I - \langle\alpha\rangle$: 725±170	$_{\Lambda}Be_4$		
0	1	>10700			—29	4	0	0.7		±1	700±85	p or K	$\langle\alpha\rangle$: 57±5 if p	14+5 p
	2	8	10	2	+34.8	7	87.6	4		3 or 5	1380±150	Li_3^8 or B_5^8	4.1 (Li) 10.7 (B)	

ne range of 2 is 8.8μ, which also agrees with is decay scheme (see Ref. 14, for example). ne directions of emission of the hyperfragment d the secondary π meson form an angle of 64°.

Event No. 4. The charge of F was measured from the count of δ electrons and track thin-down near stopping. The first method gave Z > 2, while the second method gave Z = 3 to 4 (thinned length

$10 - 20\,\mu$). The mass of F as measured from multiple scattering and range is $(8 \pm 2)\,m_p$. Track 2 stops in a σ star and therefore belongs to π^- meson. The hypothesis of F decay to three charged particles leads to considerable difference from zero for the combined momentum no matter what assumptions are made regarding the nature of 1 and 3. It can thus be concluded that we are dealing with the decay of one of the isotopes of ${}_\Lambda Li$ or ${}_\Lambda Be$ accompanied by the emission of one or more neutral particles. A more detailed analysis was not made because of the great inaccuracy in determining the momentum of 1 and the resulting inaccuracy in determining the neutron momenta.

Event No. 5. The track of F shows thin-down beginning at $10 - 15\,\mu$ from the track end. This is evidence that the decay of the hyperfragment occurred after stopping and that it is triply charged. This last conclusion agrees with the measurement of the F track thickness before the thin-down begins. Track 4 belongs to a π^- meson which gives a σ star after stopping. For any assumptions regarding the nature of 1, 2, and 3 that are compatible with charge conservation, the combined momentum of all the charged secondary particles differs from zero. This result is not changed even if it is assumed that the hyperfragment has charge four. The emission of neutral particles must therefore also be assumed. It appears that for all possible decay schemes with one exception the binding energy B_Λ assumes large negative values. The exception is the decay scheme

$$ {}_\Lambda Li_3^7 \rightarrow He_2^4 + 2p + n + \pi^-, $$

for which $B_\Lambda = (1.9 \pm 1.2)$ Mev. This must be regarded as the most likely interpretation.

Event No. 6. The F track shows thin-down for $20 - 25\,\mu$, which is evidence of stopping of the hyperfragment and corresponds to Z = 4 to 5. Five charged particles resulted from the decay without including a single π meson. F is apparently a ${}_\Lambda B_5$ hyperfragment which underwent nonmesonic decay accompanied by neutron emission.

Event No. 7. The F track shows thin-down for $10 - 15\,\mu$, which corresponds to $Z \sim 3$. Measurements of the track density at large distances from the stopping point lead to the same value. Track 3 leaves our part of the emulsion stack after traversing $\sim 19{,}000\,\mu$. If this track belonged to a π meson its ionization could exceed the minimum by a factor of less than 1.6; in actuality the ionization in track 3 is close to triple the minimum amount,

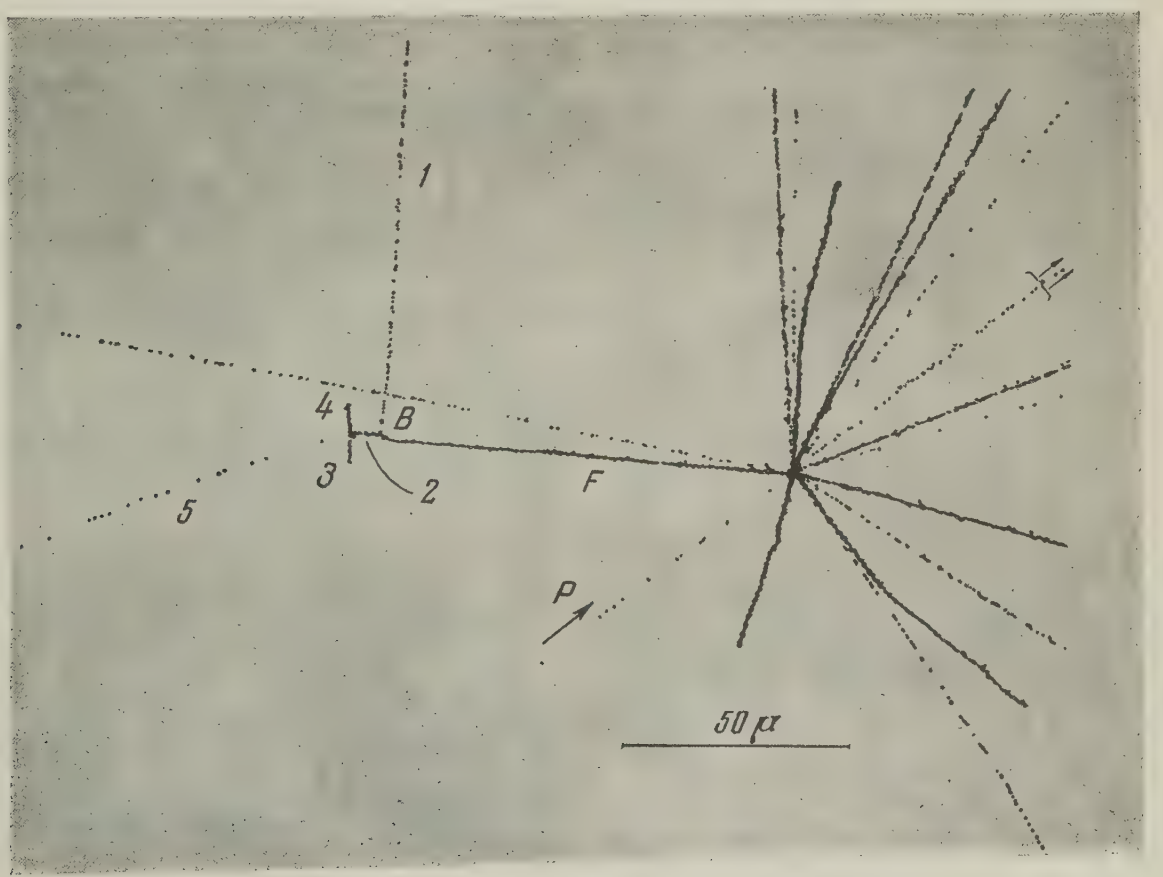

FIG. 4

thus representing a proton with close to 63 ± 14 Mev. The event as a whole is apparently the nonmesonic decay of ${}_{\Lambda}Li_3$ in which neutral particles are also emitted.

Event No. 8. From measurements of track thickness it follows that F has charge $Z \geq 2$. At the very end of the track thinning for a distance of $\sim 5\mu$ is observed, which is less than the usual thinned-down distance for lithium ($\sim 12\mu$). The tracks of α particles as a rule show no thin-down; on this basis, too, it can be concluded that $Z \geq 2$. If the hyperfragment is a lithium isotope there remains the possibility of decay in flight shortly before complete stopping, by which the short thinned length would be accounted for. Of course, this is not a necessary interpretation. 2 must be a proton since its mass, from multiple scattering and residual range, is $(1.1 \pm 0.2)\, m_p$. The nature of 3 is doubtful. We cannot exclude the possibility of a mere chance clustering of grains. The event as a whole must apparently be considered to be the decay of one of the isotopes of ${}_{\Lambda}Li_3$ or ${}_{\Lambda}He_2$.

Event No. 9. The track of F is considerably thinned in its last 20μ, which is evidence of stopping and gives $Z \sim 4$. The mass of 1 was measured from multiple scattering and residual range. Classification of gaps according to the schemes for p and d gives $(1.1 \pm 0.3)\, m_p$ and $(0.9 \pm 0.4)\, m_p$, respectively. 1 is thus a proton. The mass of 3 is $(1.1 \pm 0.2)\, m_p$ and $(1.2 \pm 0.2)\, m_p$ from the proton and τ meson gap schemes, respectively. Thus 3 is also a proton. The mass of 2 is $(1.2 \pm 0.4)\, m_p$, $(1.9 \pm 0.4)\, m_p$ and $(1.7 \pm 0.45)\, m_p$ for the p, d and τ gap schemes, respectively. Therefore we can reasonably assume that 2 is a deuteron. Gap length measurements on the track of 2 are in good agreement with this identification, leading to $(1.1 \pm 0.06)\, m_d$. The thickness of track 4 shows that this particle is singly charged. The combined momentum of 1, 2, 3 and 4 is not zero for the different possible hypotheses concerning the nature of 4. This event can therefore be regarded as nonmesonic decay of an isotope of ${}_{\Lambda}Be_4$ accompanied by the emission of neutral particles.

Event No. 10. Fig. 4 is a photomicrograph of this event.* The parent star is of the type 14 + 5p or 14 + 3p, since the two particles indicated by arrows possibly comprise a (e^+e^-) pair from the decay $\pi^0 \rightarrow e^+ + e^- + \gamma$. Track F has thin-down for $\sim 20\mu$ at its end, so that

$$3 < Z_F < 6.$$

On the other hand, it follows from an analysis of 1 and 2 that $Z_F = 2.4$ or 6. Comparison of the data leads to $Z_F = 4$. Track 2 ends in the characteristic "hammer" whose formation is preceeded by β decay. Therefore 2 is most likely Li_3^8 (or, with smaller probability, B_5^8).

Particle 1 leaves the emulsion stack. Its mass was determined from multiple scattering and ionization, with special attention paid to the reliability of the measurements. Multiple scattering was measured on the portions of the track which were more than 3.5 mm distance from the edge of the emulsion, with a cell length of 112μ. The measurements include a negligible noise effect as is confirmed by measurements with doubly large intervals. Special measurements showed little distortion, which was also excluded by the method of third differences and various other methods. The results obtained with and without elimination of the distortion are in very good agreement. The width of the distribution curve of absolute second differences also agrees with the prediction of multiple scattering theory. The result is $p\beta c = (88 \pm 7)$ Mev.

Ionization was measured by grain counts, by blob counts and from mean gap length. In the first case the number g of grains per unit track length was compared with the grain number g_0 in the tracks of relativistic particles. Measurements were performed by two observers, whose results practically coincided, giving

$$m' = \left(725 \pm {}^{170}_{140}\right) m_e.$$

In the second and third cases results were compared for 1 and the tracks of control π mesons with about the same velocity and dip angle. Prior to that, it was shown especially that in the central portions of the plate and in portions close to the event under consideration (i.e., close to the edge) the ionization characteristics of the particles agree when they have equal velocity. Measurements by the second method yielded

$$m'' = (700 \pm 85)\, m_e,$$

and by the third method,

$$m''' = (1380 \pm 150)\, m_e.$$

It follows that 1 could be regarded as a K meson. Then the event as a whole would be similar to events described in Refs. 15 to 17. However, it must be noted that of the three methods mentioned for measuring ionization the most reliable from a methodological point of view is the last, which gives the largest value for the mass. Therefore 1

*This event was found by U. G. Guliamov.

could possibly be a proton, so that we would have nonmesonic decay of $_{\Lambda}Be_4$ accompanied by neutron emission.

The authors wish to thank Z. P. Golovina and M. I. Filippov for their great assistance with the measurements.

[1] A. A. Nomofilov, Dokl. Akad. Nauk SSSR (in press).

[2] J. Hornbostel and E. O. Salant, Phys. Rev. **102**, 502 (1956).

[3] Dahanayake, Francois, Fujimoto, Iredale, Waddington, and Yasin, Nuovo cimento **1**, 888 (1955).

[4] Bannik, Kopylov, and Nomofilov, Dokl. Akad. Nauk SSSR **116**, 939 (1957), Soviet Physics "Doklady" **2**, 468 (1957).

[5] Birge, Perkins, Peterson, Stork, and Whitehead, Nuovo cimento **4**, 834 (1956).

[6] Gilbert, Violet and White, Phys. Rev. **103**, 248 (1956).

[7] Filipkowski, Gierula and Zielinski, Acta Phys. Polon. **16**, 139 (1957).

[8] Gramenitskii, Zamchalova, Podgoretskii, Tret'iakova, and Shcherbakova, J. Exptl. Theoret. Phys. (U.S.S.R.) **28**, 616 (1955), Soviet Phys. JETP **1**, 562 (1955).

[9] Castagnoli, Cortini and Franzinetti, Nuovo cimento **2**, 550 (1955).

[10] Baldo, Belliboni, Ceccarelli, Grilli, Sechi, Vitale, and Zorn, Nuovo cimento **1**, 1180 (1955).

[11] Fry, Schneps, and Swami, Phys. Rev. **101**, 1526 (1956); **99**, 1561 (1955).

[12] Fry, Schneps and Swami, Phys. Rev. (in press).

[13] Slater, Silverstein, Levi-Setti, and Telegdi, Phys. Rev. (in press).

[14] Haugerud and Sörensen, Phys. Rev. **99**, 1046 (1955).

[15] Varfolomeev, Gerasimova and Karpova, Dokl. Akad. Nauk SSSR **110**, 959 (1956), Soviet Phys. "Doklady" **1**, 594 (1956).

[16] Fry, Schneps and Swami, Phys. Rev. **97**, 1189 (1955).

[17] Fry, Schneps and Swami, Nuovo cimento **2**, 346 (1955).

Translated by I. Emin
59

SOVIET PHYSICS JETP VOLUME 34(7), NUMBER 2 AUGUST, 1958

STUDY OF HIGH-ENERGY NUCLEAR-ACTIVE PARTICLES WITH IONIZATION CHAMBERS

G. T. ZATSEPIN, V. V. KRUGOVYKH, E. A. MURZINA, and S. I. NIKOL'SKII

P. N. Lebedev Physics Institute, Academy of Sciences, U.S.S.R.

Submitted to JETP editor July 20, 1957

J. Exptl. Theoret. Phys. (U.S.S.R.) **34**, 298-300 (February, 1958)

Nuclear-active particles with energy $> 10^{11}$ ev were studied at an altitude of 3860 m above sea level by means of ionization chambers placed under absorbers of various thickness and of a counter hodoscope. Integral spectra of ionization bursts in the chambers are presented, and conclusions are drawn regarding the absorption mean free path in air and in lead of nuclear-active particles with energy $> 10^{11}$ ev.

HIGH-ENERGY nuclear-active particles ($E > 10^{11}$ ev) were studied in Autumn 1955 at 3860 m elevation by means of an array consisting of six pulse ionization chambers placed under lead absorbers of varying thickness (20, 50, and 80 cm, Fig. 1). The ionization chambers were constructed of brass cylinders with walls 3.8 g/cm^2 thick and an internal diameter of 22.5 cm. The effective area of each chamber was 0.22 m^2. The chambers were filled with argon at 4 atmos.

The electronic system made it possible to record the ionization pulse heights in each of the six chambers. The interval of recorded pulses ranged from that due to the passage of a single relativistic particle to that due to 1.5×10^4 particles, assuming the trajectories to lie on the mean chord of the chamber. A hodoscope consisting of 972 counters with total area of ~ 10 m^2 was used in conjunction with the ionization chambers. Alternate triggering was provided: the array was operated whenever

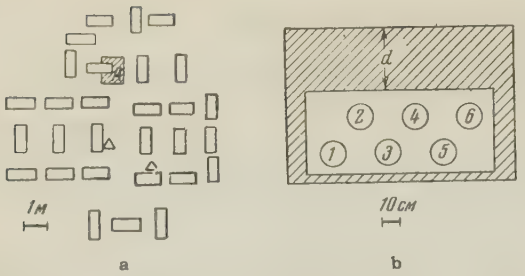

Fig. 1. a – position of the nuclear-active particle detector A with respect to hodoscope counter groups (rectangles). Δ indicates the position of the trigger counters (fourfold coincidence). b – position of the six ionization chambers in the nuclear-active particle detector A. d – variable thickness of lead (20, 50, or 80 cm)

either the total pulse in the ionization chambers was greater than the equivalent of 600 relativistic particles, or the occurrence of an air shower was recorded by a fourfold coincidence of discharges in unscreened counters each 0.05 m^2 in area. The hodoscope made it possible to detect the presence of an air shower associated with an ionization burst, even when the shower was small ($\rho \gtrsim 0.5\,m^2$), and to determine the total number of particles for showers with $n > 10^3$.

Frequency distribution of ionization bursts with respect to their size under different absorbers is shown in Fig. 2, where the x axis represents, in

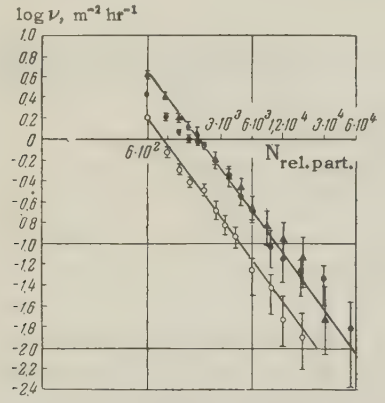

Fig. 2. Frequency distribution of ionization bursts with respect to their size. Absorber thickness: ▲ – 20, ● – 50, ○ – 80 cm Pb.

logarithmic scale, the sum of the bursts in the six chambers, expressed in the corresponding number of relativistic particles N, and the y axis represents the absolute frequency $\nu(>N)$ of bursts greater than N.

Integral spectra of bursts corresponding to $N > 2000$ relativistic particles can be expressed by a power law $\nu(N) = A/N^{\gamma}$, where γ, within statistical accuracy, is the same for all three spectra (20, 50, and 80 cm Pb) and on the average equal $\overline{\gamma} = 1.5 \pm 0.16$. Absolute frequencies of ionization bursts under 20 and 50 cm Pb are, within the accuracy limit, identical. Absorption mean free path for 50 to 80 cm Pb is $\lambda = (340 \pm 60)$ g/cm^2.

Comparison of the frequency of observed ionization bursts with the number of bursts observed at sea-level[1] leads to the conclusion that the absorption mean free path for the nuclear-active component in air amounts to ~ 120 g/cm^2.* Comparison of the absolute intensity of the primary cosmic radiation with the frequency of the observed nuclear-active particles leads also to a value which does not contradict the above result, provided reasonable assumptions concerning the energy are made (an ionization burst due to 10^3 relativistic particles corresponds according to our estimates to a primary particle of 10^{12} ev).

In the study of correlation between ionization bursts and air showers, the events were divided into two groups: (1) ionization bursts accompanied by low-density air showers, when it was not possible to locate the shower axis and to determine the total number of particles in the shower, and (2) ionization bursts accompanied by extensive showers with more than 10^3 particles. The results are given in the table.

Absorber	50 cm Pb			80 cm Pb		
Size of the burst (number of relativistic particles)	600	6000	18000	600	6000	18000
Total number of bursts	360	27	5	266	9	2
Number of bursts accompanied by an air shower	190	18	4	80	7	2
Number of bursts accompanied by an extensive air shower	43	5	3	35	6	2

It can be seen that the probability of the presence of an associated air shower increases with the size of burst.

Bursts which could be interpreted as due to simultaneous incidence of at least two high-energy nuclear-active particles were observed in 25% of cases. Those bursts (> 600 relativistic particles) were accompanied in 70% of cases by air showers.

Just as the spectrum of ionization bursts represents the energy spectrum of all nuclear-active particles at the observation level, so does the spectrum of ionization bursts under more than 20 cm of lead, due to extensive air showers, represent

*It was taken into account in the comparison that the experiments of Ref. 1 were carried out under a thick roof and that a part of the bursts recorded at sea level is due to μ-mesons.

the energy spectrum of the nuclear-active component in extensive air showers when the following three conditions are met: (1) only one nuclear-active particle of the shower falls upon the detector, (2) the shower-detecting system does not introduce any bias for different distances between the core and the nuclear-active particle detector, and (3) the interval of the sizes of observed showers is sufficiently narrow so that the energy spectra of nuclear-active particles in the showers are similar.

We examined showers of $7 \times 10^4 - 7 \times 10^5$ particles. It was found from the measured distribution of axis positions of showers associated with ionization bursts, corresponding to > 600 particles, that in more than 90% of the events the axis was less than 20 m from the detector of nuclear-active particles. For such distances, errors introduced into the shower axis distribution by the four-fold coincidence system were negligible.

The frequency distribution of ionization bursts due to nuclear-active particles of air showers, with respect to their size, is shown in Fig. 3. The frequency of bursts accompanied by extensive air showers decreases with the thickness of absorber, varying from 20 to 80 cm Pb (mean free path $\lambda = (570 \pm 120)$ g/cm^2.

The size distribution of bursts accompanied by extensive air showers can be represented by a power law with an exponent $\gamma = 0.9 \pm 0.2$. If we assume that only a single nuclear-active particle arrives at the detector each time then the spectrum of the nuclear-active component in an extensive air shower of $\sim 10^5$ particles can be expressed as $E^{-0.9 \pm 0.2}$ in the energy region $5 \times 10^{11} - 10^{13}$ ev.

The probability of simultaneous incidence of two

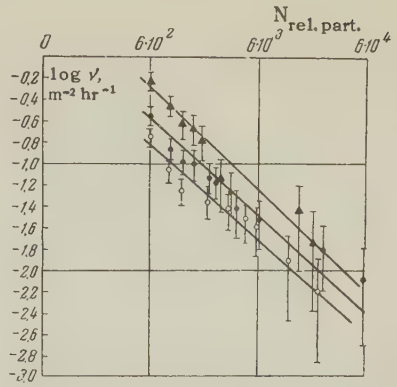

Fig. 3. Frequency distribution of ionization bursts due to nuclear-active particles of extensive air showers with $7 \times 10^4 - 7 \times 10^5$ particles. Absorber thickness: ▲ – 20, ● – 50, ○ – 80 cm Pb.

nuclear-active particles upon a detector may be rather high for extensive showers. The true spectrum of nuclear-active particles in extensive air showers can, therefore, be different from the expression given above. The role of this effect is at present unknown.

The authors wish to express their gratitude to the many workers who took part in carrying out the measurements, especially to V. I. Zatsepin, E. I. Tukish, V. Ia. Markov and B. V. Subbotin, and their appreciation to N. A. Dobrotin for constant interest and help.

[1] D. D. Krasil'nikov and S. I. Nikol'skii, Transactions, Iakutsk Branch, Acad. Sci. U.S.S.R., 1, 1955.

Translated by H. Kasha
60

PRODUCTION OF PIONS BY NEGATIVE PIONS ON HYDROGEN NEAR THE THRESHOLD

V. G. ZINOV and S. M. KORENCHENKO

Joint Institute for Nuclear Research

Submitted to JETP editor October 19, 1957

J. Exptl. Theoret. Phys. (U.S.S.R.) 34, 301-311 (February, 1958)

Production of pions on hydrogen by 307, 333, and 370 Mev negative pions was studied with scintillation counters. In the processes $\pi^- + p \to \pi^- + \pi^+ + n$ and $\pi^- + p \to \pi^- + \pi^0 + p$, the differential cross-section for the formation of a charged meson at an angle of 80° in the laboratory system (106 deg in the c.m.s.) turns out to be $(0.10 \pm 0.06) \times 10^{-27}$, $(0.17 \pm 0.06) \times 10^{-27}$, and $(0.29 \pm 0.05) \times 10^{-7}$ cm^2/sterad for 307, 333, and 370 Mev π^- mesons respectively.

INTRODUCTION

THE production of pions by negative pions on hydrogen, an event that becomes energetically possible when the energy of the incident pion exceeds 170 Mev, has been studied to date only at high energies.[1] The study of the creation of pions by negative pions near the production threshold is of interest not alone from the theoretical point of view. Such measurements are also necessary to estimate the contribution of the creation processes to the experimentally-observed scattering cross-sections of pions.

In addition to causing the scattering processes

$$\pi^- + p \to \pi^- + p \text{ (elastic scattering)} \quad (1)$$
$$\pi^- + p \to \pi^0 + n \text{ (exchange scattering)} \quad (2)$$
$$\pi^0 \to 2\gamma$$

the interaction of negative pions with hydrogen may also result in the following creation processes:

$$\pi^- + p \to \pi^- + \pi^+ + n; \quad (3)$$
$$\pi^- + p \to \pi^- + \pi^0 + p; \quad (4)$$
$$\pi^- + p \to \pi^0 + \pi^0 + n. \quad (5)$$

The work reported here was performed for the purpose of estimating the cross-sections of processes (3) and (4) in the 300 — 370 Mev energy region. It turns out that for 307-Mev negative pions, the negatively charged mesons, produced on hydrogen and recorded at an angle of 80° in the laboratory system, comprise approximately 10% of the number of the elastically scattered negative pions, and the fraction rises to 40% for 370-Mev π^- mesons. Apparently, at 370 Mev, approximately 15% of the total interaction cross-section for the interaction of π^- mesons with hydrogen (i.e., 3.5 to 4 × 10^{-27} cm^2), is due to the creation of mesons by mesons.

BEAMS OF NEGATIVE PIONS, SCINTILLATION COUNTERS, AND ELECTRONIC APPARATUS

Beams of 250, 307, 333, and 370 Mev negative pions, obtained behind the armature of the magnet of the synchrocyclotron of the Joint Institute for Nuclear Research,[2,3] were used. The 250-Mev negative-pion beam was obtained from the 300-Mev beam by means of polyethylene absorbers. The energy of the negative-pion beams were determined from their range in copper. A typical absorption curve is shown in Fig. 1. The muon content in the 300 — 370 Mev beams was 5 ± 1.5%. The muon content of the 250-Mev beam was not determined. The intensities of the various beams were 45, 150, 100, and 45 mesons/cm^2-sec for the 250, 307, 333, and 370 Mev beams respectively.

The intensity distribution over the cross-section of the beam was studied for each beam energy with the aid of a 1×1×1 cm scintillator.

Scintillation counters were used to record the particles. The experimental geometry is shown in Fig. 2. Scintillation counters 1, 3, 4, 7, and 8

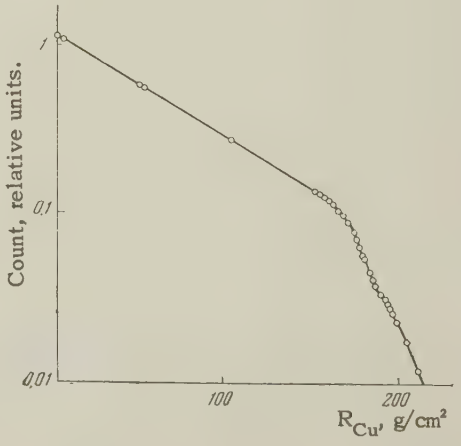

Fig. 1. Typical absorption curve (E_π = 307 Mev).

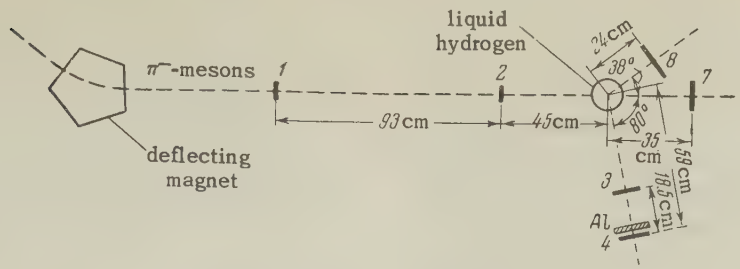

Fig. 2. Geometry of experiment.

are plexiglass containers filled with a solution of terphenyl in phenyl cyclohexane (3 grams per liter). Counters 5 and 6 are not shown on the diagram, for they have been used only in the study of elastic scattering. Counter 1 measures 6×6×1 cm, counters 3, 4, and 7 — 12.6×11.5×1 cm, and counter 8 — 16×17×1.5 cm. To reduce the background due to scattered mesons, counter 2 was made from a tolane crystal measuring 6×6×0.4 cm.

Counters 1, 2, 3, 7, and 8 were connected to photomultipliers by means of plexiglass light pipes. Counter 4 was connected to the photomultiplier with the aid of a hollow light pipe with polished aluminum walls. The need for using a hollow light pipe was dictated by the fact that plexiglass light pipes are sensitive to fast charged particles, although only with an effectiveness of approximately 5% (owing, apparently, to the Cerenkov radiation). The light-gathering effectiveness of such a light pipe is approximately one-half that of a plexiglass light pipe.

The photomultipliers were placed in a double magnetic shield for protection against the stray magnetic field of the synchrocyclotron magnet. Pulses from the photomultiplier were fed to an intermediate shaping cell (Fig. 3). Here the large

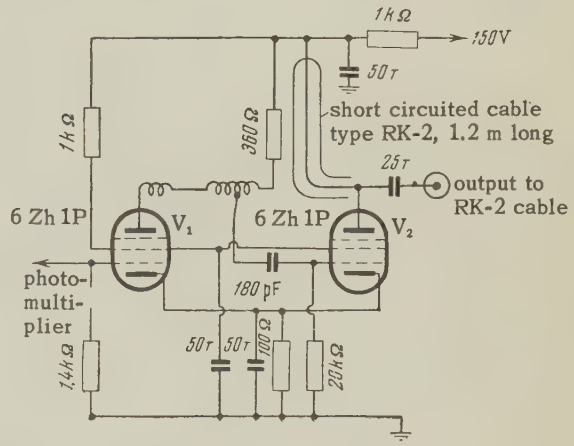

Fig. 3. Diagram of shaping cell (the letter T denotes capacitance in 1,000 μμF).

pulses were limited in amplitude in a simplified "semi-distributed" amplifier stage[4] with tube V_1, while the smaller ones were amplified by a factor of approximately two. The pulses were then shaped in duration by a short-circuited cable stub connected in the plate circuit of tube V_2, and were fed over high frequency coaxial cables approximately 80 m long to the coincidence circuits. The rise time of the pulse front at the output of the intermediate cell amounted to approximately 4×10^{-8}

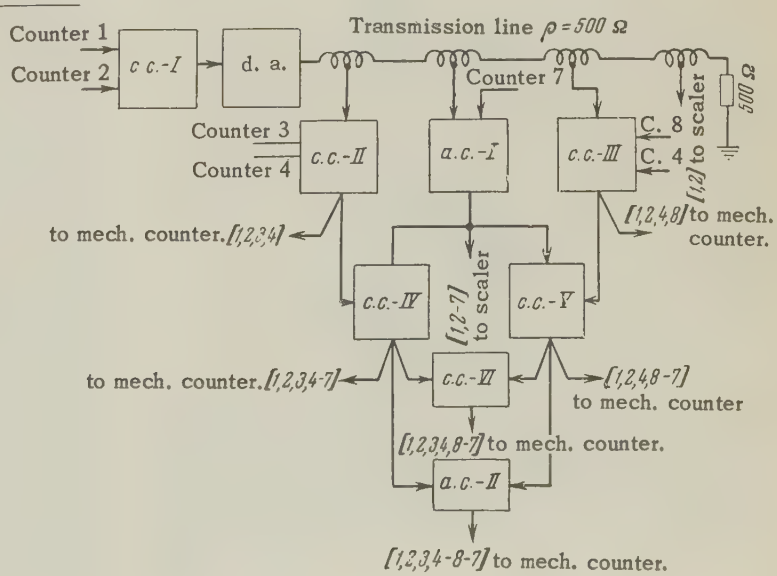

Fig. 4. Block diagram of electronic apparatus. c.c.-I — double coincidence circuit ($\tau \sim 1.2 \times 10^{-8}$ sec.); d.a. — distributed amplifier (f = 50-70 Mc); c.c.-II and c.c.-III — triple coincidence circuits ($\tau \sim 1.2 \times 10^{-8}$ sec.); a.c.-I — anticoincidence circuit ($\tau \sim 2.2 \times 10^{-8}$ sec.); c.c.-IV, c.c.-V, and c.c.-VI — double-coincidence circuits ($\tau \sim 5 \times 10^{-7}$ sec.); a.c.-II — anti-coincidence circuit ($\tau \sim 5 \times 10^{-7}$ sec.).

seconds in response to an input pulse with a front duration on the order of 10^{-9} seconds.

A block diagram of the electronic apparatus is shown in Fig. 4. The fast-coincidence circuits were designed with type DGTs germanium detectors. These circuits give resolution times up to 0.5×10^{-8} seconds at an approximate sensitivity of 0.5 v. The time characteristics of the FEU-19 photomultipliers, however, do not permit operation with a resolution time less than 10^{-8} seconds without loss in efficiency.

The double-coincidence circuit is shown in Fig. 5. It is similar in operating principle to the coincidence circuit described in Ref. 5. In the normal

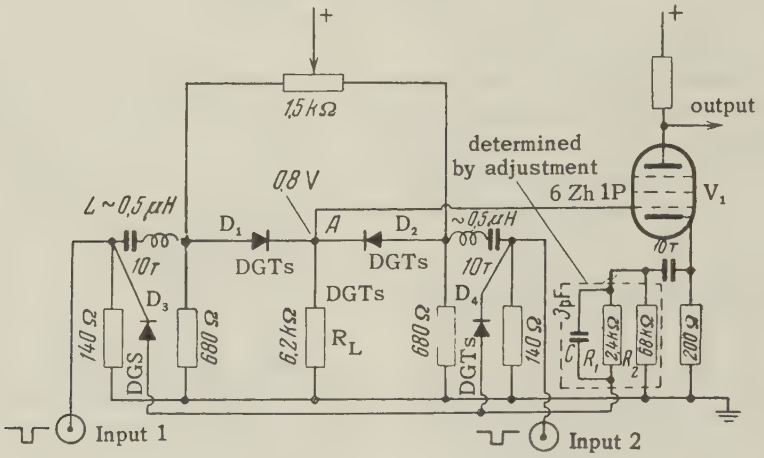

Fig. 5. Double coincidence circuit (monitor).

state, the potential of point A (output of the coincidence circuit) is determined by the currents flowing through detectors D_1 and D_2 and through load resistance R_L. The currents through the detectors are approximately equal in magnitude. If the pulse from the photomultiplier blocks only one of the detectors, for example D_1, the potential of point A changes insignificantly. This is due to the fact that the resistance of detector D_2 is small compared with the load R_L. By virtue of the nonlinearity of the voltage-current characteristic of the detector, doubling the current flowing through the detector produces a proportionately lesser voltage drop across the detector (by a factor 1.2 —1.4). When detectors D_1 and D_2 are blocked simultaneously, the potential of point A tends to zero, and a negative pulse is produced at the output of the coincidence circuit. For satisfactory operation of the circuit it is necessary that the load resistance be many times greater than the high-frequency input impedance.

A distinguishing feature of the double-coincidence circuit employed here is the presence of a system to compensate for "single" pulses; this system comprises detectors D_3 and D_4 together with the RC network consisting of R_1, R_2, and C).

The pulse arriving at the input of the coincidence circuit is applied simultaneously through the compensation network to the cathode of tube V_1. The parameters of the compensation circuit are chosen to neutralize the pulse that appears at the output of the coincidence circuit whenever a pulse arrives from only one of the inputs. Thanks to the nonlinearity of the voltage-current characteristic of the detectors, the addition of the compensation network does not affect noticably the sensitivity of the coincidence circuit, for small pulses do not pass through detectors D_3 or D_4. The use of compensation has made it possible to reduce substantially the magnitude of the "single" pulses from the output of the double-coincidence circuit. This was important for clean operation (without false coincidences) of the triple-coincidence circuit.

The pulse from the output of the double-coincidence circuit is amplified by the distributed amplifier and applied to an artificial line with lumped constants, serving as a natural continuation of the anode line of the amplifier. The capacitances employed in this line are the inputs to four triple-coincidence circuits (of which only two are shown in the block diagram, Fig. 4), and the input to the fast anticoincidence circuit. This method of con-

necting the triple-coincidence circuit makes it possible to isolate the capacitances of the inputs of the individual circuits and to avoid trailing of the pulse from the output of the double-coincidence circuit. If the pulse applied to the input of the line has a front duration approximately 10^{-9} seconds, the rise time of the front of the line-output pulse is approximately 4×10^{-9} seconds.

The triple-coincidence circuit is shown in Fig. 6. It operates on the same principle as the double-coincidence circuit. No compensation circuit is provided. The relatively small pulses at the output of the triple-coincidence circuit, appearing when only one or two of the circuit detectors are blocked, are separated by means of a type DGS detector (D_4).

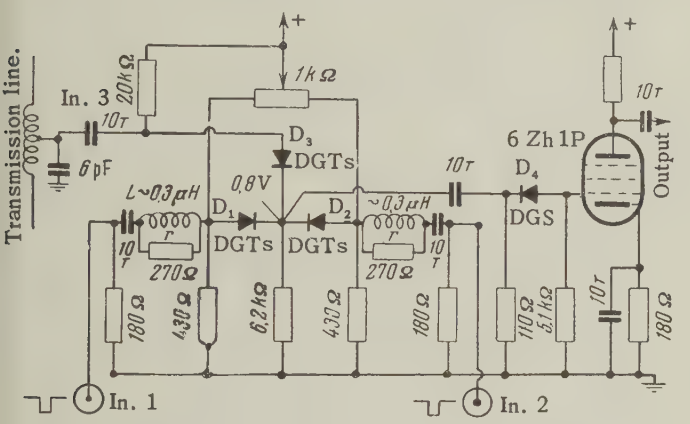

Fig. 6. Triple coincidence circuit (angle telescopes).

The fast anti-coincidence circuit is shown in Fig. 7. It comprises a double-coincidence circuit of the type described above, in which one of the detectors (D_1) is blocked. If a blocking pulse is applied to detector D_2, a pulse will also appear at the output of the anti-coincidence circuit. No pulse can appear at the output of the anti-coincidence circuit if D_2 receives a pulse from the output of the double-coincidence circuit, and simultaneously detector D_1 is unblocked by a positive pulse from tube V_1. The shaped pulses from the anti-coincidence circuit have an approximate duration of 2.2×10^{-8} seconds.

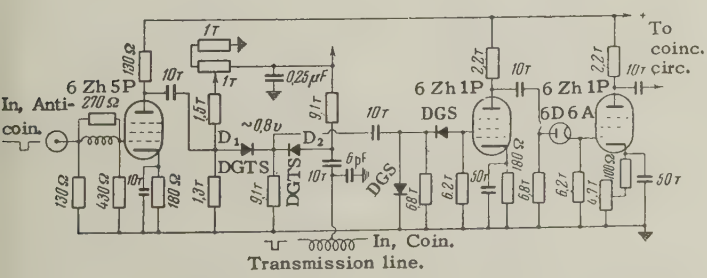

Fig. 7. Fast anticoincidence circuit.

The "slow" ($\tau \sim 5 \times 10^{-7}$ sec) vacuum-tube coincidence and anticoincidence circuits were operated by standard shaped pulses from the output of the "fast" circuits. The efficiencies of the coincidence and anticoincidence circuits were checked by arranging the corresponding counters in a single row in a beam of negative pions of reduced intensity. The efficiency of the coincidence circuit was close to 100%, that of the fast anticoincidences not less than 97%, and that of the slow anticoincidence circuit not less than 99.9%

LIQUID HYDROGEN TARGET

The liquid hydrogen was placed in a vessel made of type PS-4 foamed styrol (density 0.04 g/cm^3). The vessel was attached to the individual blocks with BF-4 glue. The schematic construction of the foamed-styrol target is shown in Fig. 8. The target consists of an inner vessel 1, placed inside an outer vessel 2. The outgoing evaporating hydrogen flows over the walls of the vessels and cools them. To reduce the rate of evaporation of the liquid hydrogen, a jacket 3 of red copper 1 mm

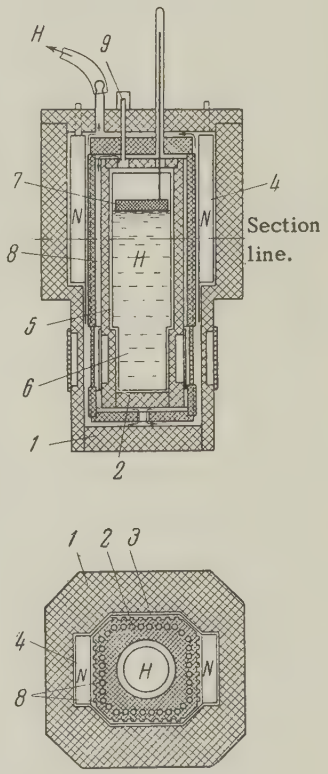

Fig. 8. Diagram of foamy polystyrol vessel for liquid hydrogen. 1 – outer vessel, 2 – inner vessel, 3 – cooling jacket of red copper 1 mm thick, 4 – pockets for liquid nitrogen, 5 – duraluminum cylinder, 6 – working portion of target, 7 – float, 8 – openings for evaporating hydrogen, 9 – filling tube.

thick is placed around the inner vessel and is cooled with liquid nitrogen poured into pockets 4. The walls of the vessel are made thinner at the place where the pion beam passes. The liquid hydrogen is poured into duraluminum cylinder 5. The wall thickness of this cylinder, in the working portion 6, is 0.1 mm. The diameter of the cylinder in the working portion is 11 cm. In the presence of liquid nitrogen in the nitrogen jacket, the rate of evaporation of liquid hydrogen is 0.7 l/hr. The hydrogen reserve (above the working portion) was 6 l. The amount of hydrogen in the target was controlled by means of a float level 7. The float and rod were made of foamed styrol. The wall thickness is 0.35 g/cm^2 across the beam path and 0.34 — 0.38 g/cm^2 in the target of the scattered pion. When the background was measured after evaporation of the liquid hydrogen, gaseous hydrogen was continuously blown through the empty target.

MEASUREMENTS AND CORRECTIONS

The experiment consisted of recording the charged mesons, created on hydrogen in processes (3) and (4), and traveling at an angle of 80° in the laboratory system. Such mesons produce four-fold coincidences in counters 1, 2, 3, and 4. Four-fold coincidences will be produced in counters 1, 2, 3, and 4 (and in greater quantity) also by mesons elastically scattered by hydrogen, along with the created mesons. To prevent counting of elastically-scattered mesons, the coincidences of counters 1, 2, 3, and 4 were connected for anticoincidence with counter 8 (Figs. 2 and 4), which was set at the angle of emergence of the recoil proton in elastic scattering (37.5 — 38°). Thus, the only four-fold coincidences of counters 1, 2, 3, and 4 recorded were those unaccompanied by the passage of a charged particle through counter 8. These will be called henceforth type Q coincidences.

Type Q coincidences can be produced by other than mesons formed on hydrogen. Such coincidences are possible also (a) when the recoil proton in process (1) is scattered by hydrogen and the target walls and does not enter counter 8, while the corresponding negative pion passes through the telescope comprising counters 3 and 4; (b) when the negative pions, previously elastically scattered by hydrogen at an angle other than 80° are secondarily scattered by hydrogen and by the target wall; (c) when the γ quanta from process (2) are converted in the walls of the target and in counter 3; (d) when the π^0 mesons from process (2) disintegrate (in 1.6% of the cases[6]) according to the scheme $\pi^0 \to \gamma + e^+ + e^-$ and the electrons enter into telescope 3, 4; (e) upon scattering of a negative pion with radiation ($\pi^- + p \to \pi^- + p + \gamma$).

Type Q coincidences are also recorded whenever the "slow" anticoincidence circuit does not operate for some reason. The correction for this ineffectiveness in the operation of the anticoincidence circuit does not exceed 0.1% of the elastic cross-section, amounting to approximately 1% of the mesons created by mesons at 307 Mev.

To determine the correction necessitated by (a) it is necessary to know the cross-section of process (1) at the given angle (coincidences of counters 1, 2, 3, 4, and 8). The coincidences of 1, 2, 3, 4, and 8 were recorded during the entire time of the measurement of Q. The number of recoil protons scattered in hydrogen and in the target walls was determined from the total cross-sections of the interaction between the nucleons and hydrogen and carbon.[7] Account was also taken of the multiple and single scattering of protons by the Coulomb field of the nuclei.

An exact determination of the contribution of the secondary scattering of negative pions is almost impossible. It was assumed as a first rough approximation that all the secondary scattered negative pions are isotropically distributed in space. The total number of the secondarily-scattered mesons was determined from the total cross-sections of the elastic scattering of negative pions by hydrogen and of the elastic and inelastic scattering by carbon.[8,9] The resultant number of secondarily-scattered mesons amounted to approximately 1.8% of the number of elastically scattered negative pions. It should be noted that the entire correction amounts to approximately 15% of the observed number of mesons created at 307 Mev, and is even less for higher energies.

To determine the corrections connected with effects (c) and (d), it is necessary to know the number of γ quanta that pass through counter 3. For this purpose, a lead converter 7.35 g/cm^2 thick was placed ahead of counter 3 to increase the efficiency of registration of γ quanta from process (2). Knowing the cross-sections for the conversion of γ quanta in hydrogen, carbon, and lead, it is possible to estimate the correction for conversion of γ quanta in counter 3 and in the target walls. It amounted to 4 ± 1.5% of the effect of lead.

No correction was introduced for pion scattering with radiation. Apparently, the cross-section of this process has a magnitude not more than 1% of the elastic scattering cross-section of negative pions by hydrogen.[10] At 307 Mev this may amount to approximately 10% of the observed creation of

mesons by mesons.

In addition to the above specific corrections, the "usual" corrections were made to account for the following effects: muon impurities in the beam (5 ± 1.5%), counting loss in the monitor (up to 6%) absorption of pions in the target walls and in the hydrogen, absorption of pions in counter 3, and decay of the pions.

To determine the background, not connected with the hydrogen, of mesons scattered in the target wall and in counters 2 and 7, and also the background of the random coincidences, measurements were made with an empty target. Measurements with delayed coincidences showed that the random coincidences were due predominantly to the passage of negative pions through counters 1 and 2, together with simultaneous random passage of some charged particles through counters 3 and 4. Counter 7, connected for anticoincidence with counters 1 and 2 (Figs. 2 and 4), served to reduce the background of random coincidences, so that type Q coincidences were recorded only when a negative pion from the beam was scattered in the target. This made it possible to reduce the background of random coincidences by a factor of approximately 20. The background of random coincidences was further reduced by placing an aluminum filter 5.4 g/cm^2 thick between counters 3 and 4. Thanks to the fact that the intensity of the synchrocyclotron did not vary about the mean level by more than 10% during the time of the measurement, the fluctuations of the background of random coincidences did not exceed ± 0.05 counts per 10^6 monitor counts. This amounted to approximately 7% of the total number of recorded mesons created at 307 Mev.

RESULTS AND CONCLUSION

The experimental quantities obtained at various energies and the corrections introduced into these quantities are listed in the table.

As expected, at a primary-beam energy of 250 Mev, the mesons created on hydrogen are not registered. This is connected with the fact that the created pion should have, under the conditions of our experiment, a kinetic energy in excess of 42 Mev in the laboratory system. Only then would it be registered with a nonzero probability. The high-energy registration threshold is due to a considerable extent to the aluminum filter placed between counters 3 and 4. The influence of the aluminum filter on the efficiency of registration of mesons of various energies was investigaged experimentally.

The presence of an energy threshold for pion registration causes a considerable portion of the mesons created on hydrogen to remain unregistered. To determine the fraction of registered mesons it is necessary to know the energy spectrum of the mesons created. Since no such information is available, it becomes necessary to make certain assumptions concerning the form of the spectrum. If one assumes that in the c.m.s. the energy spectrum is symmetrical about an energy equal to half the maximum energy of the created pions, it turns out that the registration efficiency (i.e., the fraction of registered mesons from the spectrum) does not depend too strongly on the form of the spectrum. Thus, the registration efficiency, for a beam of 307-Mev negative pions, amounts to 44.8, 43.4, and 42.7% for a rectangular, trapezoidal, and triangular energy spectrum

Production of Pions by Negative Pions on Hydrogen

Pion beam energy	Coincidence count 1, 2, 3, 4 – 7, 8 with hydrogen	Coincidence count 1, 2, 3, 4 – 7, 8 without hydrogen	Difference (mean, weighted)	Effect of lead (difference with and without hydrogen)	Effect 1, 2, 3, 4 – 7, 8 (difference with and without hydrogen)	Correction for γ quanta	Correction for elastic scattering	Number of type Q coincidences due to produced mesons, Q_{creat}	Recorded fraction of pions for trapezoidal energy spectrum, ε	Usual corrections, f	Differential cross-section for product of charged meson $(d\sigma/d\omega)$, 105° c.m.s., × 10^{-27} cm^2/sterad	$2\sigma_3 + 0.7\sigma_4 = 4\pi\,(d\sigma/d\omega)$ × 10^{-27} cm^2
250	8.97±0.75 11.86±0.6	7.43±0.52 9.99±0.53	1.73±0.6	23.2±2.1	9.83±0.47	1.31±0.33	0.32±0.15	0.1±0.7	approx. 0	—	—	—
307	10.17±0.32	8.33±0.26	1.84±0.41	14.7±1.7	8.5±0.32	0.81±0.2	0.26±0.13	0.77±0.48	0.44	0.96	0.099±0.062	1.24±0.78
333	10.27±0.37 16.4±0.9	7.50±0.36 14.1±0.8	2.70±0.48	14.3±1.6	8.44±0.32	0.79±0.2	0.25±0.13	1.66±0.54	0.57	0.95	0.166±0.054	2.09±0.68
370	10.89±0.63 11.51±0.59 10.86±0.55	6.60±0.44 6.90±0.53 7.37±0.55	4.13±0.45	11.2±1.9	8.01±0.32	0.62±0.2	0.24±0.12	3.27±0.51	0.67	0.92	0.287±0.047	3.61±0.59

respectively. The table gives the effectivenesses for a spectrum of trapezoidal form.

The differential cross-section for the production of a charged meson at an angle of 80° in the laboratory system was calculated from the formula

$$\left(\frac{d\sigma}{d\omega}\right)_{\text{creat.}} = (Q_{\text{creat.}} / N\omega f\varepsilon)\cdot 10^{-6}, \qquad (6)$$

where Q_{creat} is the number of type Q coincidences, obtained after subtracting the contribution of effects (a), (b), (c), and (d), per 10^6 monitor counts; $N = 0.443 \times 10^{-24}$ is the average number of hydrogen atoms per cm^2; $\omega = 0.0417$ steradians is the solid angle subtended by the telescope consisting of counters 3 and 4; ϵ is the registration efficiency of the produced pions, if the energy spectrum of this pion is trapezoidal in form; and f is a coefficient that accounts for the "usual" corrections. 80° in the laboratory system corresponds on the average to 105 — 107° in the c.m.s. The corresponding transfer coefficient for the differential cross-sections differs from unity, on the average, by not more than 1%.

The differential cross-sections, obtained at various energies, for the production of a charged meson at an angle of 80° in the laboratory system, or approximately 106° in the c.m.s., are given in Fig. 9. It is clear that the differential cross-section increases rapidly with the energy. At 370 Mev the measured cross-section amounts to approximately 60% of the differential elastic-scattering cross-section.

It is interesting to estimate, on the basis of the resultant differential cross-section, the approximate values of the total cross-section for the production of mesons by mesons on hydrogen. If it is assumed that in both processes (3) and (4) the angle of distribution of the mesons is isotropic and the mesons are not correlated, then the quantity $(d\sigma/d\omega)_{\text{creat}} \times 4\pi$ is the sum $2\sigma_{(3)} + 0.7\sigma_{(4)}$ of the total cross-sections of processes (3) and (4) (see table). The coefficient 2 in front of $\sigma_{(3)}$ is caused by the fact that two charged mesons are produced in process (3). The coefficient 0.74 in front of $\sigma_{(4)}$ is due to the fact that, as a rough estimate, approximately 30% of the recoil protons due to process (4) can enter into counter 8, correspondingly reducing the registration efficiency for the negative-pions from process (4).

The total cross-sections obtained under the above assumptions can be compared with recently-published theoretical results.[11,12] Reference 11 treats a charge-symmetrical pseudo-scalar interaction by the Tamm-Dancoff method, neglecting the amplitudes of all states that contain more than two mesons. According to this work, the contribution of meson-meson creation in the energy interval investigated by us is less than 1% of the elastic scattering. This is less than one tenth of our value. It must be noted that the Tamm-Dancoff method gives results that do not agree with experiment even for ordinary scattering of negative pions by protons.

In Ref. 12 the cross-sections of processes (3), (4), and (5) were calculated on the basis of the Chew and Low theory. The dependence of the sum $2\sigma_{(3)} + 0.7\sigma_{(4)}$ on the negative-pion energy, obtained on the basis of the data of that reference, is shown for comparison by the solid line of Fig. 9. From

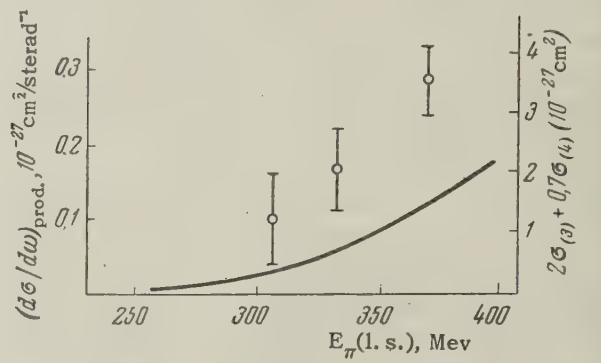

Fig. 9. Differential cross-sections for production of a charged pion at 80° in the laboratory system (106° in the c.m.s.) in processes (3) and (4) (left scale), and sum of total cross-sections $2\sigma_{(3)} + 0.7\sigma_{(4)}$ (right scale). The solid curve represents the sum $2\sigma_{(3)} + 0.7\sigma_{(4)}$, calculated on the basis of the Chew and Low theory.

the methodological point of view, it is interesting to note that there is no great discrepancy between our experimental data and those of Ref. 12.

The authors express their gratitude to Prof. B. M. Pontecorvo for constant attention and aid in the work.

[1] M. Blau and M. Caulton, Phys. Rev. **96**, 150 (1954). W. D. Walker and J. Steinhaber, Sixth Annual Rochester Conference on High-Energy Nuclear Physics, N. Y., 1956. Walker, Hushfar, and Shephard, Phys. Rev. **104**, 526 (1956).

[2] Ignatenko, Krivitskii, Mukhin, Pontecorvo, Reut, and Tarankanov, Атомная энергия (Atomic Energy) May, p 5 (1956).

[3] V. G. Zinov and S. M. Krenchenko, J. Exptl. Theoret. Phys. (U.S.S.R.) **33**, 335 (1957), Soviet Phys. JETP **6**, 260 (1958).

[4] S. T. Kalikhman, Радиотехника (Radio Engineering) June, p 52 (1953).

[5] W. C. Elmore, Rev. Sci. Instr. **21**, 649 (1950).

[6] Lindenfeld, Sachs, and Steinberger, Phys. Rev. **89**, 531 (1953).

[7] Gol' danskii, Liubimov, and Medvedev, Usp. Fiz. Nauk 48, 531 (1952); 49, 3 (1953).
[8] L. M. Barkov and B. A. Nikol' skii, Usp. Fiz. Nauk 61, 341 (1957).
[9] Dzhelepov, Ivanov, Kozodaev, Osipenkov, Petrov, and Rusakov, J. Exptl. Theoret. Phys. (U.S.S.R.) 31, 923 (1956), Soviet Phys. JETP 4, 864 (1957).
[10] V. G. Solov' ev, J. Exptl. Theoret. Phys. (U.S.S.R.) 29, 242 (1955), Soviet Phys. JETP 2, 159 (1956).
[11] M. Nelkin, Phys. Rev. 104, 1150 (1956).
[12] J. Franklin, Phys. Rev. 105, 1101 (1957).

Translated by J. G. Adashko
61

SOVIET PHYSICS JETP VOLUME 34(7), NUMBER 2 AUGUST, 1958

DISTRIBUTION OF MAGNETIC INDUCTION IN THE INTERMEDIATE STATE OF A CURRENT-CARRYING SUPERCONDUCTOR

B. V. MAKEI

Institute of Physics of the Polish Academy of Science, Wroclaw

Submitted to JETP editor July 25, 1957

J. Exptl. Theoret. Phys. (U.S.S.R.) 34, 312-315 (February, 1958)

The distribution of the magnetic field in a slot cut out in the middle part of a tin cylinder carrying a current was measured by the bismuth probe method. The slot was located in a diametral plane of the cylinder. The results obtained are compared with the London and Landau phenomenological theory of the distribution of current density in the intermediate state of a cylindrical superconductor. The existence of a core of intermediate state in a superconducting wire carrying a current above critical is directly demonstrated by the experiments.

INVESTIGATIONS of the breakdown of superconductivity by current are basically devoted to the study of the change of electrical resistivity of a specimen in dependence on temperature and the electric current flowing through it.[1-4] As it appears to us, measurement of the magnetic induction inside a specimen through which an electric current is flowing can also give valuable information on the intermediate state of a superconductor.

In the present work we report the results of measurements of the magnetic induction inside a current-carrying tin specimen 4 mm in diameter and 56 mm long. A 0.2×3.5 mm rectangular slot was cut in the central portion of the cylinder and situated in a diametral plane (with the long side of the slot parallel to the axis of the specimen). The magnetic field was measured by means of a bismuth probe (Fig. 1), such as is used in the study of the microstructure of magnetic fields.[5,6] The

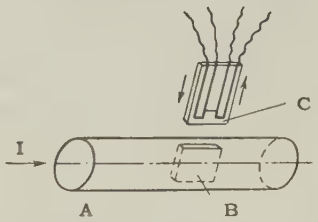

FIG. 1. Diagram of the experiment. A – specimen, B – slot, C – platelet with probe.

probe was a straight segment of bismuth wire 1.5 mm long and 20 μ in diameter, soldered to thin copper strips which served as potential and current leads. To protect the probe against mechanical disturbances, the copper strips were glued between rectangular mica platelets. The probe was moved along the slot (perpendicular to the axis of the specimen) by means of a mechanism with a micrometer screw. The current was fed to the specimen under test by copper tubes tinned with

lead and connected to the specimen by means of special contacts. The electrical resistance of the probe, situated at a known distance from the surface of the specimen, was measured before and after switching on the current in the circuit of the specimen under test. In order to avoid the effect of frozen-in magnetic fields, the specimen was warmed for complete removal of superconductivity before each new measurement. A low resistance type PPTN-1 potentiometer was used to measure the resistance of the probe, the working current of which amounted to 3 ma.

After preliminary compensation of the voltage a FEOU-18 photoelectric amplifier with an automatic recording type EPP-09 potentiometer was connected to the terminals of the probe instead of a galvanometer. The overall voltage sensitivity of the entire apparatus reached 1.3×10^{-9} v/mm of the potentiometer scale. The basic measurements were carried out at a temperature of 3.57°K. At this temperature the critical current for our specimen was 23 amp. The resistance of the specimen at 3.8°K was 7.5×10^{-8} ohm, and at 293°K it was 3.6×10^{-4} ohm.

Before each series of measurements, a calibration of the probe was carried out through the dependence of the magnetic field intensity at the surface of the specimen on the current flowing through the specimen. In order to determine whether or not the method we selected gives correct results, and to measure the edge effect of the slot, measurements of the magnetic induction were carried out along the radius of the specimen at a temperature of 3.80°K, i.e., in the normal state with currents of 23 and 25 amp. The results of the measurements at 23 amp are shown in Fig. 2. For distances of the probe from the surface of the specimen greater than 0.4 mm the experimental points fall on a straight line. Extrapolation of the line to intersection with the axis shows that the presence of the slot decreases the magnetic field intensity at the edge of the slot, on the average, by 11%, while at depths exceeding 0.4 mm the edge effect of the slot is practically unnoticeable. Measurements of the magnetic field intensity outside the specimen showed that it varies, with sufficient accuracy, in inverse proportion to the distance of the probe from the axis of the cylindrical specimen.

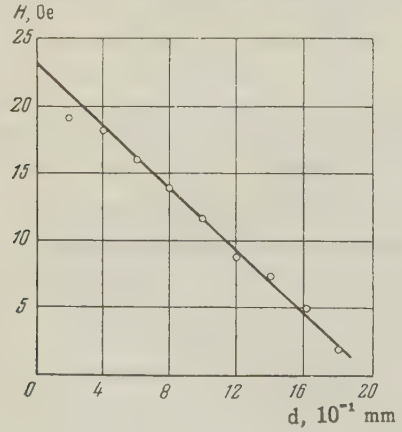

FIG. 2. Dependence of the magnitude of the field inside the slot on distance from the surface of the cylinder; T = 3.80°K.

The results of the measurements of a current-carrying superconductor in the intermediate state at T = 3.57°K are shown in Fig. 3. Also shown in the figure are results of measurements with currents of 19 and 22 amp. With a current of 19 amp, the specimen is in a superconducting state and the magnetic field in the slot arises from the "lingering" of the external field. The magnetic field intensity decreases rapidly with increasing depth beneath the surface of the specimen, and at a depth of 0.4 mm it is no longer detectable. Results of the measurements with a current of 22 amp demonstrate that a transition from the superconducting into the intermediate state has begun, and that the current is no longer constrained to the surface. Since our specimen is not a single crystal, some electrical resistance is observed at currents somewhat below critical. The relatively large scatter of the experimental points is probably due to the instability of the state of the specimen in the region of its transition from the superconducting to the intermediate state and to changes of the current distribution in the specimen with time.

For comparison with the results of the phenomenological theory of the distribution of current density in the intermediate state of a superconductor,

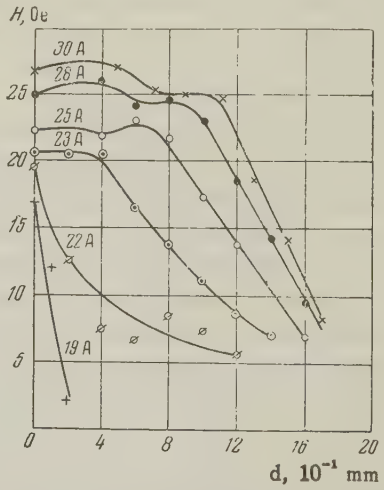

FIG. 3. Dependence of the magnitude of the field inside the slot on distance from the surface of the specimen for different currents in the specimen; T = 3.57°K.

according to London and Landau,[7]* the theoretical curves of the magnetic induction are given in Fig. 4. The slopes of the linear sections of these curves, which determine the quantities H_c/r_0 (H_c is the critical magnetic field intensity and r_0 is the

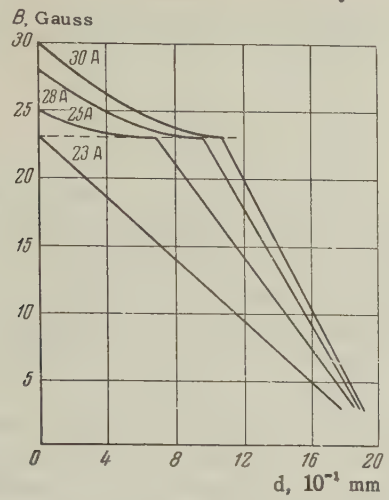

FIG. 4. Dependence of the magnetic induction on distance from the surface of the specimen in the intermediate state, from theoretical data.

radius of the core in the intermediate state), agree, within the limits of experimental error, with the results of the experiments. The existence of a core of intermediate state in a superconducting wire carrying current above critical is thus demonstrated by these experiments. Comparing the experimental curves with the theoretical, we must take it into account that, as a result of the edge effect, the magnetic induction measured in the slot close to the surface of the specimen is less than the actual magnetic induction in a specimen. Therefore, although the course of the experimental curves differs from the theoretical ones in the region of the "crust" of normal conductivity, nothing can be concluded about any incompatibility of the measurement results with the theory, since the maximum deviation of the experimental points from the theoretically expected values exceeds only slightly the mean error of the measurements (±4% of the magnitude of the magnetic field measured in this region). A more exact determination of the course of the curves as functions of the current and of the temperature can render more precise our conceptions on the distribution of current over the entire cross section of a conductor in an intermediate state and, besides, can give some indirect information on the shape of the superconducting regions.

I express sincere thanks to academician P. L. Kapitza for affording me the opportunity to conduct the experimental portion of the work in the Institute of Physical Problems of the Academy of Sciences and for his attention to my work, and to Professor A. I. Shal'nikov and all of his coworkers for valuable advice and aid.

*For valuable hints which turned out to be very useful in the course of the calculations, the author expresses his gratitude to S. S. Gerstein.

[1] L. V. Shubnikov and N. E. Alekseevskii, Nature, 138, 804 (1936).

[2] N. E. Alekseevskii, J. Exptl. Theoret. Phys. (U.S.S.R.) 8, 342 (1938).

[3] R. B. Scott, J. Research Natl. Bur. Standards 581 (1948).

[4] L. Rinderer, Helv. Phys. Acta 29, 339 (1956).

[5] A. Shalnikov, J. of Physics (U.S.S.R.) 9, 202 (1945).

[6] A. G. Meshkovskii and A. I. Shal'nikov, J. Exptl. Theoret. Phys. (U.S.S.R.) 17, 851 (1947).

[7] D. Shoenberg, Superconductivity (Russ. Transl.) IIL, M. 1955, p. 128 [Cambridge, 1952].

Translated by R. Eisner
62

MASS DISTRIBUTION OF FISSION PRODUCTS FROM THE IRRADIATION OF GOLD AND URANIUM BY NITROGEN IONS

N. I. TARANTIN, Iu. B. GERLIT, L. I. GUSEVA, B. F. MIASOEDOV, K. V. FILIPPOVA, and G. N. FLEROV

Submitted to JETP editor August 20, 1957

J. Exptl. Theoret. Phys. (U.S.S.R.) **34**, 316-321 (February, 1958)

A study was made of the mass spectrum of fission fragments produced by irradiating thick gold and uranium targets with 115-Mev nitrogen ions. Fourteen different elements were separated from the irradiated targets. The mass distribution curve for fission fragments produced by irradiating gold has the form of a narrow peak with a half width of about 20 mass units. The maximum of the peak is at $A \sim 100$. The width of the mass distribution curve for fission fragments of irradiated uranium is much larger.

THE study of nuclear fission induced by heavy particles is of great interest because it enables us to obtain much additional information concerning the mechanism of fission at high excitation energies. Irradiation with heavy particles leads to the formation of a compound nucleus whose charge, mass number and excitation energy are determined quite unambiguously, because the capture of an energetic heavy particle, unlike that of a light particle, is not accompanied by the cascade ejection of nucleons. A more definite interpretation of the fission process is therefore possible.

The utilization of heavy particles also permits the investigation of the fission of a greater number of nuclei, including those with atomic numbers from 86 to 89 and from 95 to 100. Very little is known at present about the fission of these nuclei since experiments employing light particles encounter difficulties associated with the necessity for dealing with highly radioactive substances.

The present paper reports an investigation of the mass spectra of fission fragments from radon and einsteinium which were produced by irradiating gold and uranium with nitrogen ions.

EXPERIMENTAL METHOD

Gold and uranium plates 30μ thick and measuring 10×7 mm^2 were irradiated in the internal beam of a 150-cm cyclotron by quintuply charged nitrogen ions from a slit source. The energy of the nitrogen ions was 115 Mev, and the current at the target was $\sim 0.1\,\mu$a. The targets were fastened by means of a copper holder to a water-cooled probe. The current of bombarding particles was measured by using an electrometer to record the ions which passed through the target and entered the collector. In different experiments the time of irradiation varied from 30 min to 2 hrs.

The irradiated targets were dissolved and the different radioactive elements were separated with suitable carriers, which were inactive materials in amounts from 15 to 30 mg. The chemical yield of the carriers was determined by weighing after all purification operations had been performed. The separated radioactive isotopes were identified by their half-lives, energies and β-particle signs.[1] The intensity of β emission was measured by an end-window Geiger counter (type MST-17) with a mica window of 20 mm diameter and $5-6$ mg/cm^2 thickness. In order to avoid back-scattering of β particles the active materials were deposited on 4 mg/cm^2 tracing paper attached to a Plexiglas holder with a central opening. The thickness of the layer of deposited material did not exceed 10 mg/cm^2. The initial β activity of the specimens was $50-15000$ pulses/min from the irradiation of gold and $100-30000$ pulses/min from the irradiation of uranium. The counter background was 20 pulses/min. The β-particle energies were determined by absorption in aluminum, and their maximum energy was calculated by Feather's method. A magnetic analyzer was used to determine the signs of the β particles. The yields of identified nuclei were computed taking into account the time of target irradiation, the time from the termination of irradiation to the beginning of the count, the chemical yield of the element, β-particle absorption in the counter window and self-absorption.

FISSION PRODUCTS FORMED BY THE IRRADIATION OF GOLD WITH NITROGEN IONS

Table I contains a list of the relative yields of nuclei identified among the fission products from a thick gold target irradiated with 115-Mev nitro-

TABLE I

Nucleus	Relative yield	Type	Nucleus	Relative yield	Type
Ga^{72}	0.022±0.005	scr	Nb^{97}	0.29±0.04	scr
Ga^{73}	0.024±0.005	acc	Mo^{99}	1.00±0.25	acc
Rb^{86}	0.060±0.015	scr	Ru^{103}	1.05±0.35	,,
Sr^{89}	0.26±0.06	acc	Ru^{105}	0.62±0.12	,,
Sr^{91}	0.16±0.02	,,	Ag^{111}	0.120±0.025	,,
Sr^{92}	0.12±0.02	,,	Ag^{112}	0.062±0.012	scr
Y^{90}	0.19±0.04	scr	Ag^{113}	0.125±0.025	acc
Y^{91}	0.31±0.09	,,	Cd^{115}	0.045±0.009	,,
Y^{92}	0.26±0.05	,,	Cd^{115M}	0.085±0.025	scr
Y^{93}	0.35±0.05	acc	Sn^{121}	0.020±0.006	acc
Zr^{97}	0.16±0.02	,,	Sn^{123} (T = =40min)	0.085±0.025	,,
Nb^{95}	0.37±0.11	scr	Sb^{122}	0.130±0.025	scr
Nb^{96}	0.37±0.08	,,	Ba^{139}	≤0.001	acc

gen ions. The yield of Mo^{99} is taken as unity. The errors indicated in the tables were obtained by averaging the deviations of several individual experimental values.

Figure 1 presents the yields of the nuclei in the table as a function of the mass number A. It can be seen that most of the yield of fission products is concentrated in a narrow range of mass numbers. The yield of fission products rises quite sharply as the mass number increases from 70 to 100 and then drops off just as sharply for larger masses. This suggests that the yield of fission products of gold irradiated by nitrogen ions describes a curve with a sharp maximum. However such a conclusion requires additional analysis, because the yield curve can only be plotted from knowledge of the total yields of individual mass chains connecting all fission products of the same mass number. In our experiments the individual mass chains were represented by one, or in some instances two, nuclei, including both screened nuclei (scr), i.e., nuclei produced only through fission, and accumulating nuclei (acc), which were produced both directly through fission and by β decay of other nuclei of the same mass chain.

In order to determine how accurately the distribution obtained for the yields of individual nuclei corresponds to the true distribution of fission fragments, an additional calculation was needed to determine the total yields of separate mass chains from the experimental yields of the nuclei which were represented. The yields of the mass chains were calculated on the basis of two different hypotheses concerning the distribution of the charge of a fissioning nucleus between two fragments, that of equal charge displacement for the two fragments[2] and that of proportional distribution of the charge of the fissioning nucleus.[3] In this calculation it was assumed that the average number of neutrons emitted by fission fragments is 1.5 – 2 per fragment. The number of neutrons emitted by a compound nucleus before fission was estimated from the results of Refs. 4 and 5. A comparison of the cross sections for the reactions (N, 4n), (N, 5n) and (N, 6n) in gold and different nitrogen ion energies[4] with the cross section for gold fission,[5] similar to the comparison made in Ref. 6, showed that when a thick gold target is irradiated with 115-Mev nitrogen ions the average number of neutrons emitted by a compound nucleus before fission is 5 to 6 per fission. The total number ν of neutrons emitted in a single fission was taken as nine.

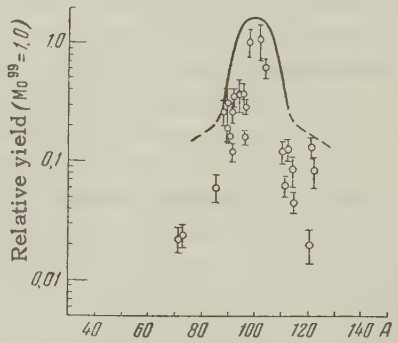

FIG. 1. Mass distribution of fission products produced by irradiating gold with nitrogen ions. o – experimental yields; solid line – curve calculated taking into account the yields of unidentified nuclei.

The expression used for the distribution function of the charges of fragments in a single mass chain was in satisfactory agreement with the experimental yields of the isobars Sr^{91} and Y^{91}, Sr^{92} and Y^{92}, Zr^{97} and Nb^{97}:

$$P(Z) = (1/\sqrt{1.7\pi}) \exp[-(Z - Z_p)^2 / 1.7]$$

$$\text{for } |Z - Z_p| \leqslant 2,$$

where Z_p is the charge of the fission fragment with the greatest yield among the fragments in a single mass chain.

From the experimental yields of individual nuclei we calculated the total yields of the corre-

sponding mass chains. In addition to the experimentally determined yields of identified nuclei we included the yields of short- and long-lived stable fission products which could not be identified in the experiments. The symmetry and smoothness of the calculated curve served as criteria to determine which hypothesis concerning the charge distribution actually applies to gold fission by 115-Mev nitrogen ions. The requirements were satisfied better by the postulate of equal charge displacement.

Fig. 1 shows the yield of gold fission fragments produced by nitrogen ions as a function of mass number, calculated using the postulate of equal charge displacement. It is difficult to estimate the possible error for the calculated values of the yields, but it can be stated that the general character of the curve does not change essentially as ν is varied from 7 to 11. The most reliable data were obtained for the range A = 85 — 115, where the results of the calculation are practically independent of the choice of charge distribution hypothesis. The calculation for A = 121 and 123 gives a lower limit for the yields of these mass chains because the values used for the yields of Sn^{121} and Sn^{123} (T = 40 min) did not take into account the yields of the isomers Sn^{121m} and Sn^{123} (T = 136 days). The calculation for this range of values of A is less unambiguous.

As can be seen from the figure, when the yields of experimentally unidentified nuclides are also taken into account there is no essential change in the character of the experimental distribution. The mass distribution curve of fission fragments in the range A = 85 — 115 has the shape of a narrow peak with a half width of about 20 mass units; the maximum is at A ~ 100. The yields of $Ga^{72,73}$, Se^{123} and Sb^{122}, as well as the yields of the mass chains that correspond to these nuclides, lie off the smooth curve and appear to be somewhat high.

The general character of the mass distribution curve of gold fission fragments produced by nitrogen ions is approximately the same as for the fission of bismuth by 22-Mev deuterons.[7]

FISSION PRODUCTS FORMED BY THE IRRADIATION OF URANIUM WITH NITROGEN IONS

About 20 different isotopes were identified among the fission products of uranium irradiated with nitrogen ions. The yields of accumulating nuclides as a fraction of the yield of Ag^{113} are given in Table II.

If it is assumed that not more than 10 neutrons are emitted by the compound nucleus and fission fragments in one fission of a uranium nucleus by a 115-Mev nitrogen ion, the yield of each of the tabulated nuclides, with the exception of $Sr^{91,92}$, Zr^{97} and $Ba^{139,140}$, is not less than 70% of the total yield of the corresponding mass chain, according to either of the two hypotheses mentioned for the distribution of the charge of the fissioning nucleus between two fission fragments. Therefore the yields in the table must be regarded as lower limits that are quite close to the total yields of the corresponding mass chains. This conclusion is supported by the fact that the yields of screened nuclides Ga^{72} and Ag^{112} are considerably lower than the yields of neighboring accumulating nuclides.

Figure 2 shows the yields of accumulating nuclides as a function of the mass number. The combined yield of Cd^{115} and Cd^{115m} is given for A = 115. It is seen from the figure that the experimental results quite unambiguously determine a curve with a broad maximum. The somewhat reduced yields of $Sr^{91,92}$ and Ba^{140} can be attributed to the fact that these nuclides are more distant than the others from the β-stable range, so that their yields represent only a small part of the total yield of the corresponding mass chains. The yields of the other fission fragments are almost constant for mass numbers from 90 to 145. The half width of the curve is not less than 50 mass units.

An investigation of the fission products from the

TABLE II

Nuclide	Relative yield	Nuclide	Relative yield
Ga^{73}	0.03±0.015	Cd^{115}	0.80±0.15
Sr^{89}	0.65±0.15	Cd^{115m}	0.70±0.25
Sr^{91}	0.40±0.05	Sn^{121}	1.10±0.30
Sr^{92}	0.30±0.05	Ba^{139}	0.65±0.15
Zr^{97}	0.55±0.10	Ba^{140}	0.25±0.06
Mo^{99}	0.80±0.20	Ce^{141}	0.90±0.25
Ag^{111}	0.80±0.15	Ce^{143}	0.70±0.15
Ag^{113}	1.00±0.15		

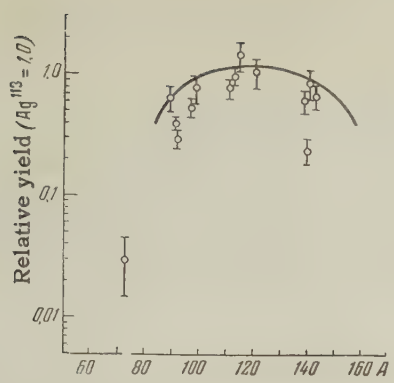

FIG. 2. Mass distribution of fission products from the irradiation of uranium with nitrogen ions.

irradiation of uranium with C^{13} ions[8] also shows the presence of a broad mass spectrum.

DISCUSSION

When elements at the end of the periodic table are bombarded with heavy particles, there is, in most cases, complete fusion of the nuclei that participate in the reactions. The cross sections for reactions which result in the capture of only a part of an incoming particle comprise a small fraction of the total cross section.[9] Therefore fission by heavy particles can be represented by the following scheme: formation of a compound nucleus, neutron emission, and fission. The number of neutrons ejected before fission is determined by the excitation energy of the compound nucleus and by the fissility of the intermediate nucleus.

When Au^{197} is bombarded with 115-Mev ions of N^{14}, excited Rn^{211} compound nuclei are formed which, as already mentioned, fission after the emission of a few, usually 5 or 6, neutrons that carry away a considerable portion of the excitation energy of the compound nucleus. The mass distribution curve of the fission products of gold bombarded with nitrogen ions therefore reflects the character of the fission of $Rn^{206-205}$ at relatively low excitation energies (not above 15 — 20 Mev). In this case, fission yields two fragments of approximately equal masses.

When a thick U^{238} target is bombarded with N^{14} ions compound nuclei of E^{252} are formed, with an excitation energy of 60 — 85 Mev. An investigation of the products of uranium bombardment with energetic heavy particles[9,10] shows that the probability of fission is considerably greater than the probability for the formation of nuclides by neutron evaporation from the compound nucleus. This suggests that the compound nuclei E^{252} fission predominantly without previous emission of neutrons or after emitting only 1 or 2 neutrons, which carry away only a small fraction of the excitation energy of the compound nucleus. Therefore the mass spectrum of fission fragments from uranium bombardment with nitrogen ions is characteristic of the fission of $E^{252-250}$ at high excitation energies (40 — 85 Mev). In this case both symmetric and asymmetric fission occur.

The magnitude of possible fission of uranium by neutrons produced in the bombardment of the target with nitrogen ions was estimated through a control experiment in which the uranium target was covered with 14 mg/cm^2 aluminum foil; in this case fission could be caused only by neutrons. This experiment showed that uranium fission by neutrons does not exceed 5% of fission by nitrogen ions and does not provide an explanation of the broad mass distribution of fragments from uranium fission by nitrogen ions.

Thus the half width of the fragment mass distribution curve is considerably smaller for radon fission than for the fission of einsteinium. It is difficult to determine whether the excitation energy, Z, A or Z^2/A of the fissioned nucleus results in the considerably narrower mass spectrum for the case of radon. However, it is noteworthy that an experiment in which two gold foils placed together were bombarded (with 115-Mev and 85-Mev nitrogen ions striking the first and second foil, respectively) showed that the mass distribution of radon fission fragments is narrower for the lower bombarding energy. The ratio of the yields of fragments at the edges of the peak ($Sr^{89,91,92}$ and $Ag^{111,112,113}$) to the yield of fragments at the center (Mo^{99}) is smaller for the second foil by a factor of 1.5 — 2.5.

The somewhat high yields of Sn^{123} and Sb^{122} from a thick gold target (Fig. 1) are probably associated with the effect of the closed shells of Z = 50 and N = 50. However, the possibility remains that the high yield of these nuclides, as well as of $Ga^{72,73}$, results from asymmetric fission of the lightest radon isotopes produced in the reaction at low excitation energies.

The different ratios of the isotopes Cd^{115} and Cd^{115m} in the fission of radon and einsteinium ($Cd^{115}/Cd^{115m} = 0.5$ for Rn and $Cd^{115}/Cd^{115m} = 1$ for E), are evidently associated with different ratios between the yield of cadmium formed directly through fission and the yield of cadmium which results from the β decay of other fragments.

[1] Seaborg, Perlman, and Hollander; Tables of Isotopes, Revs. of Mod. Phys. 25, 469 (1953).

[2] A. C. Pappas, Proceedings of the International

Conference on the Peaceful Uses of Atomic Energy (United Nations, New York, 1956), Vol. 7, p. 19.

[3] Glendenin, Coryell and Edwards, Radiochemical Studies: The Fission Products, National Nuclear Energy Series, Plutonium Project Record (McGraw-Hill Book Co., Inc. New York, 1951), Vol. 9, Div. IV, p. 449.

[4] Baraboshkin, Karamian, and Flerov, J. Exptl. Theoret. Phys. (U.S.S.R.) **32**, 1294 (1957), Soviet Phys. JETP **5**, 1055 (1957).

[5] Druin, Polikanov and Flerov, J. Exptl. Theoret. Phys. (U.S.S.R.) **32**, 1298 (1957), Soviet Phys. JETP **5**, 1059 (1957).

[6] Glass, Carr, Cobble, and Seaborg, Phys. Rev. **104**, 434 (1957).

[7] A. W. Fairhall, Phys. Rev. **102**, 1335 (1956).

[8] Brown, Price, and Willis, J. Inorg. Nucl. Chem. **3**, 9 (1956).

[9] J. H. Fremlin, Physica **22**, 1091 (1956).

[10] Gerlit, Guseva, Miasoedov, Tarantin, Filippova, and Flerov, J. Exptl. Theoret. Phys. (U.S.S.R.) **33**, 339 (1957), Soviet Phys. JETP **6**, 263 (1958).

Translated by I. Emin
63

SOVIET PHYSICS JETP VOLUME 34(7), NUMBER 2 AUGUST, 1958

THE SCATTERING OF MU MESONS IN BERYLLIUM

V. G. KIRILLOV-UGRIUMOV and A. M. MOSKVICHEV

Moscow Engineering-Physics Institute

Submitted to JETP editor August 30, 1957

J. Exptl. Theoret. Phys. (U.S.S.R.) **34**, 322-326 (February, 1958)

We investigated the scattering of μ mesons in beryllium plates. The momenta of the μ mesons were in the range (130 ± 16) Mev/c. The observed angular distribution agrees within statistical error with the distribution to be expected from a Coulomb interaction between the μ mesons and the atoms of the material.

1. INTRODUCTION

THERE is reliable evidence for the absence of a non-Coulomb interaction between μ mesons and nucleons. It is to be expected, then, that the scattering of μ mesons in matter should be explicable in terms of electromagnetic interactions between the μ mesons and atoms. This question has been investigated experimentally for various momenta of of the μ mesons, and most of the results indicate there are more scattering events than would be expected on the basis of a nuclear model in which the nuclear charge is uniformly distributed in a sphere of finite radius ($R = 1.2 \times 10^{-13} A^{1/3}$ cm.).

According to the latest data from the Manchester group,[1] in the momentum range 600 Mev/c to 100 Bev/c, the experimental distribution of μ mesons scattered from lead differs significantly from what would be expected from a nucleus of finite size, and agrees better with what would be expected from a point nucleus. One might try to explain the increase in the anomalous scattering at high energies by the absorption, in the nucleus, of virtual photons accompanying the moving μ meson. Such calculations have been carried out by Fowler.[2] According to Fowler's data, the anomalous scattering is small or entirely absent at momenta less than 270 Mev/c. The scattering cross section is proportional to A^2 and at large angles is such that the probability of a single scattering with a large momentum transfer is comparable with the corresponding quantity for a point nucleus. It is not yet possible to make a quantitative comparison between Fowler's calculations and the experimental data.

At small momenta, about 100 Mev/c, Alikhanov and Eliseev obtained evidence for anomalous scattering in graphite.[3] The anomalous cross section was about 5×10^{-27} cm^2/nucleon and decreased with increasing energy. Alikhanian and Kirillov-Ugriumov studied the scattering of μ mesons with sharply defined momenta from copper and found an

anomalous cross section of about 10^{-27} cm^2/nucleon. These results cannot be explained by Fowler's mechanism.

We investigated the scattering of cosmic ray μ mesons having a momentum of 130 Mev/c from beryllium. In thin films of light elements, the Coulomb-scattering background is relatively small, so that if there is any anomalous scattering due to a non-Coulomb interaction, one would expect it to show up most clearly in such an experiment.

2. DESCRIPTION OF THE APPARATUS

A schematic diagram of the apparatus is shown in Fig. 1. The large rectangular cloud chamber was triggered by the counter telescope, three rows of which were in coincidence, while the last row was in anticoincidence. We considered the scattering of only those particles which stopped in the two centimeters of lead between the last row of coincidence counters and the row of anticoincidence counters. In order to obtain reliable results, it is very important that the counters, especially those in anticoincidence, be stable. Each counter had its own power supply, and their operation was checked daily. 100 cm of lead were placed above the cloud chamber in order to filter out electrons, protons and π mesons.

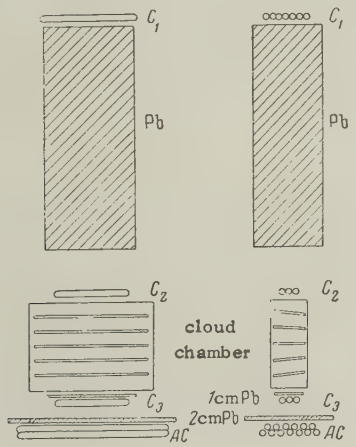

FIG. 1. Schematic diagram of the apparatus. C_1, C_2, C_3 – rows of coincidence counters. AC – row of anticoincidence counters.

The μ mesons were scattered in five beryllium plates one centimeter thick placed in the cloud chamber. The working volume of the cloud chamber was $(40 \times 55 \times 14)$ cm^3, and it was usually operated at a pressure of 0.5 atmos. The cloud chamber was made of aluminum and was illuminated from the sides by two bype IFP-1500 flash bulbs. The stereoscopic pictures were taken 115 cm away. There was negligible error introduced into the measurements of angles by the photography. The expansion was spark-actuated. Spark valves have much less inertia than electromagnetic ones and are more stable over long periods of operation. To minimize track distortion, the cloud chamber was placed in a thermally insulated box which was temperature controlled to 0.5°C.

3. PARTICLE IDENTIFICATION, MEASUREMENT OF MU MESON SCATTERING ANGLES AND MOMENTA

The measurements on the scattering of μ mesons were carried out at sea level. It was estimated that the particle current getting through the meter-thick lead filter consisted almost entirely of μ mesons. No more than 0.1% of the particles we counted could have been π mesons. In 20% of the pictures, there were not one, but two or more particles travelling in the solid angle defined by the apparatus. One of these could have been a δ electron. In finding angular distributions, we did not use pictures containing several particles.

It will be shown below that the average mass of a single particle, as measured from its scattering and range, was 213 electron masses. The residual range of the μ meson was used to find its momentum. It was assumed that the scattering of the μ meson occurred in the middle of the beryllium plate and that the meson stopped in the lead filter between the third row of coincidence counters and the row of anticoincidence ones. In order to decrease the error of the momentum measurement, a lead slab one centimeter thick was placed above the third row of counters. The momentum of those μ mesons counted by this apparatus was (130 ± 16) Mev/c. In computing the range, we took into account the mean angle between the direction at which the μ meson entered the slab and the vertical.

The method described above is not suitable for obtaining the momentum of particles in the "hard" component, i.e., those particles which passed through all the rows of coincidence counters, but which did not stop in the filter and were not rejected by the row in anticoincidence. The number of "hard" particles was obtained by removing the filter over the row of anticoincidence counters. The counting rate decreased to 16% of what it was with the filter in place.

In obtaining the angular distributions, we used the projection of the scattering angle on the plane of the film. A special device was employed to measure the scattering angle. Repeated trials by various observers showed that the root mean square error in measuring angles was 20′.

4. RESULTS AND DISCUSSION

In all, 2250 scattering events of μ mesons on beryllium were observed. Not one of these had a scattering angle with a projection more than 6°. Subtracting the 16% of the events which corresponded to μ mesons of momentum more than 130 Mev/c, the upper limit on the cross section for the scattering of μ mesons with momentum (130 ± 16) Mev/c through angles greater than 6° was 4.5×10^{-28} cm^2/nucleon.

It is possible that some of the μ mesons which were scattered through large angles were not recorded in our apparatus. This would happen if the scattered meson missed the third row of coincidence counters. In particular, the probability of registering a 6° scattering event was 93%. The upper limit on the cross section includes appropriate corrections for this.

Errors in the measured angles could be introduced by gas movement in the cloud chamber, by the finite length of track, etc. In order to minimize such errors, the only cases used in calculating the angular distributions were those satisfying the following conditions: (1) the length of the visible part of the track was not less than 90% of the distance between plates in the cloud chamber; (2) between the plates, the deviation of the track from straightness was not more than half the thickness of the track; (3) the intercept of the track on the cloud chamber axis did not depart by more than 0.5 mm from the point where the scattered particle left the plate. These conditions eliminated cases where the measured angles could have been in error by about a degree, owing to distortions associated with the working of the cloud chamber. The above requirements were satisfied by 1429 scattering events.

Figure 2 shows the angular distribution for μ-meson scattering in each beryllium plate. The dotted curve shows the scattering to be expected from a point nucleus, assuming that all the particles considered were stopped in the filter above the row of anticoincidence counters. It appears that the number of particles scattered into angles between 0 and 1° is larger than predicted by theory. The solid line shows the distribution to be expected upon taking into account the fact that 16% of the μ mesons were "hard" mesons. This curve agrees satisfactorily with the observations at all angles.

In order to estimate the effect an admixture of fast μ mesons, or of other particles, would have on the results, it is interesting to compare the calculated mean-square deviation with the observed

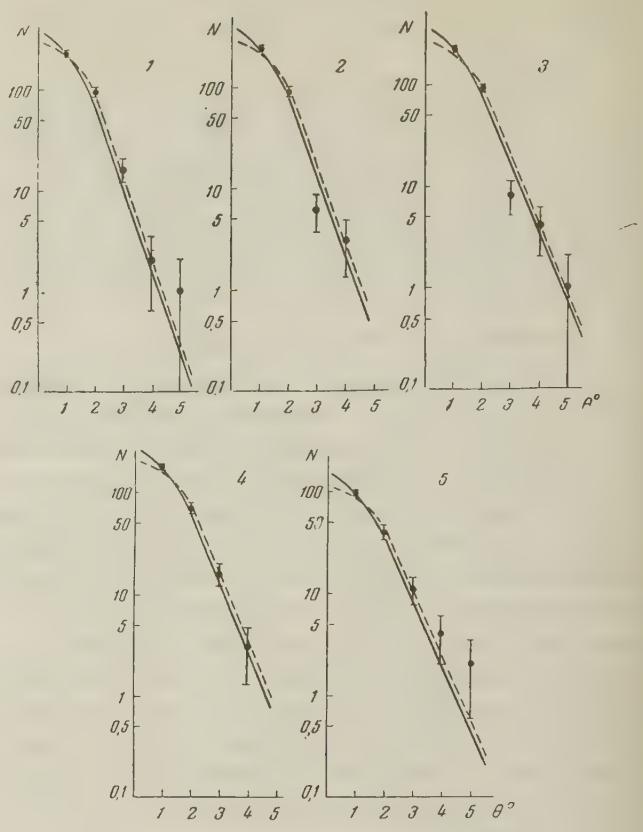

FIG. 2. Angular distributions for the scattering of μ mesons in beryllium plates 1–5. Dashed curve: scattering from a point nucleus, solid curve: expected scattering distribution, taking into account the 16% admixture of "hard" μ mesons. Mean momentum $\bar{p}$ is 140, 135, 131, 127 and 125 Mev/c for plates 1 to 5 respectively.

one. Such data are presented in the table. Knowing the momentum of the meson from its residual range, one can calculate the expected mean square deviation. Since an admixture of fast μ mesons would affect the scattering only at small angles (less than 1°), the data in the table indicate that they have little influence on the mean square deviation of the observed distribution. In particular, if the admixture of fast μ mesons were much greater than we have estimated, then we would not observe a decrease in the mean square deviation with increasing momentum. Analysis shows that the error in measuring angles near the edge of the cloud chamber is somewhat greater than at the center.

Since the range and scattering angle of the particles we observed are known, our data can be used to find their mean mass. This turned out to be 213 ± 10 m_e. This confirms that our apparatus really did record μ mesons which stopped above the row of anticoincidence counters. Figure 3 shows shows the total differential cross section for the

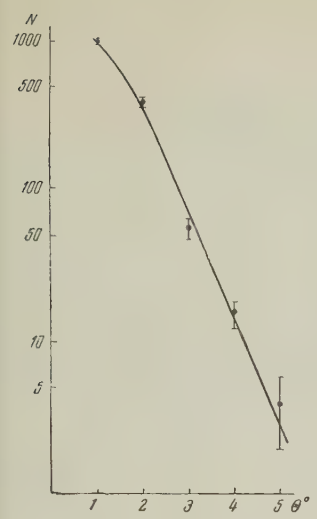

FIG. 3. The total differential cross section for the scattering of μ mesons with momentum (130 ± 16) Mev/c. The solid curve is a theoretical one, and is the sum of the distributions for each of the plates, taking into account the 16% admixture of "hard" μ mesons.

scattering of μ mesons with momentum (130 ± 16) Mev/c. The theoretical curve is the sum of the distributions for each plate, taking into account the 16% admixture of fast μ mesons. It is significant that this admixture has no effect on the scattering through angles greater than 1°. The agreement between the experimental and theoretical angular distributions (estimated by the χ^2 criterion to be 60%) indicates that μ mesons with momentum 130 Mev/c are scattered in beryllium plates 1 cm thick as they should be from a purely Coulomb interaction between the μ mesons and the beryllium atoms.

Since the angles we measured are considerably smaller than λ/R_{Be}, the theoretical scattering from a point charge is practically identical with the scattering from a charge distributed over nuclear dimensions. It should be noted than an angular distribution computed from all 2250 cases observed, i.e., from all events within the solid angle of the apparatus, including those which did not satisfy the requirements imposed above, also agrees well with the calculated distribution. Thus,

Comparison of the calculated with the observed mean square deviations.

Plate number	1	2	3	4	5
$\overline{(p\beta)}$ Mev/c^{-1}	110	106	102	99	96
$\sqrt{\overline{\theta^2}}\cdot 10^{-2}$, calculated	2.02	2.09	2.17	2.25	2.33
$\sqrt{\overline{\theta^2}}\cdot 10^{-2}$, observed	2,20	2,02	2,14	2,47	2,60

for example, the ratio of the number of particles scattered through 3° or more to the expected number is 86/95, while the figure for 4° is 23/18.

Before drawing a final conclusion on the anomalous scattering of μ mesons in this momentum range, it would be desirable to carry out measurements in other materials.

In conclusion, we should like to thank Prof. A. I. Alikhanian for his constant interest in the work and for his help in carrying out the analysis of results. We also would like to thank A. M. Rozhin, L. P. Morozov and S. S. Lomakin for their assistance in making the measurements and in treating the data.

[1] Lloyd, Rössle, and Wolfendale, Proc. Phys. Soc. (London) **A70**, 421 (1957).

[2] G. N. Fowler, Nucl. Phys. **3**, 121 (1957).

[3] A. I. Alikhanov and G. P. Eliseev, Izv. Akad. Nauk SSSR, ser. fiz. **19**, 732 (1955).

[4] A. I. Alikhanian and V. G. Kirillov-Ugriumov, Izv. Akad. Nauk SSSR, ser. fiz. **19**, 737 (1955).

Translated by R. Krotkov
64

ISOTOPE SEPARATION IN NONSTATIONARY MOLECULAR FLOW

K. D. SINEL'NIKOV, V. E. IVANOV, B. G. SAFRONOV, Iu. S. AZOVSKII, and G. G. ASEEV

Submitted to JETP editor August 30, 1957

J. Exptl. Theoret. Phys. (U.S.S.R.) **34**, 327-330 (February, 1958)

A change in the isotopic composition is observed in nonstationary molecular flow of mercury vapor. The data obtained are used to compute the time of adsorption of mercury on the surface of iron ($\tau_e^{198} = 3.4 \times 10^{-2}$ sec for $T = 290°K$) and the ratio of the adsorption times for the isotopes Hg^{198} and Hg^{204} ($\tau_e^{198}/\tau_e^{204} = 1.008$). An estimate is made of the heat of adsorption of mercury on iron (15×10^3 cal/mole).

1. A feature of stationary flow of a gas through a capillary tube is that the current is independent of the lifetime of the molecule in the adsorbed and non-adsorbed states and remains constant in time. To the contrary, as was already shown by Clausing,[1] in nonstationary flow of gas the change in the current depends substantially on the adsorption time of the molecules of the gas on the walls of the capillary tube. Gas diffusion in stationary molecular current, when $\lambda \gg r$, is accompanied by isotope separation (λ is the mean free path and r the radius of the capillary). It is interesting to determine how isotope separation changes in a nonstationary current in the presence of adsorption.

To observe the change in the isotopic composition of gas under the above conditions, it is necessary to admit gas consisting of a mixture of isotopes in one end of the capillary tube (with $\lambda \gg r$) and to measure its composition in the opposite end, from the instant that the gas appears to the instant when stationary flow is established.

Figure 1 shows the experimental setup. The working substance was mercury placed in a steel ampoule that could be cut off from the system by valve 1. Connected to the valve is iron tube 3, wound into a cylindrical coil 160 mm in diameter. The length of the tube L is 4500 mm, and its diameter 2r is 6 mm. The other end of the tube is connected with the ion source of the MS-2 mass spectrometer. Placed inside the coil is oven 2, with which the tube could be heated to 600°C. The temperature was monitored by thermocouple 4. The inner surface of the tube was first treated with hydrochloric and concentrated nitric acid, after which it was washed five times with distilled water at a 100°C.

The tube was trained with the MS-2 vacuum system for several days at $T \sim 450 - 550°C$. The qualitative composition of the separated gas was as follows: CO_2, $CO + M_2$, H_2O (no organic peaks observed). After reducing the separated gas considerably, particularly the H_2O (approximately 4 — 5 times), the training was stopped. The temperature of the tube was reduced to 20°C. The pressure in the ion source was then reduced to $1 - 2 \times 10^{-7}$ mm Hg, and that in the analyzer to $0.7 - 1.0 \times 10^{-7}$ mm Hg, remaining at this value throughout the experiment. The background value of the peak of the isotope 198 amounted to 4 — 5 divisions on the highest-sensitivity scale of the electrometer ($\sim 2 \times 10^{-15}$ amp/division). When these conditions were obtained, the valve was opened and the mercury vapor began to flow into the tube at a pressure of approximately 10^{-5} mm Hg. Within $\Delta t \sim 1$ hr, the electrometer recorded a change of approximately 10^{-15} amp in the I_{198} peak. The ion current I_{198}, which was proportional to the vapor pressure of the mercury in the ion source, was then recorded; simultaneously, the isotopic composition of the mercury was measured until stationary flow was established. The admission of mercury vapor into the tube was then stopped and the composition of the desorbed hydrogen measured. The tube was heated to accelerate the desorption.

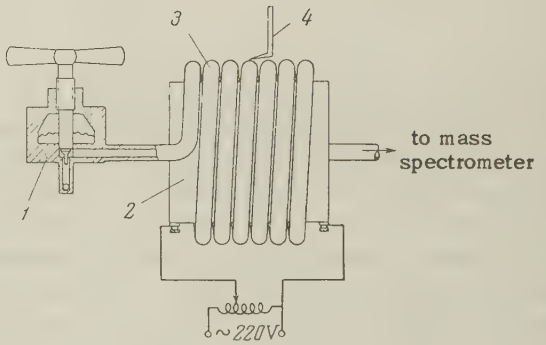

FIG. 1. Diagram of the set-up.

Measurements of the isotopic composition of the mercury were made with the single beam method relative to the extreme isotopes (198 and 204).

The measured currents were used to calculate $\beta = I_{198}/I_{204}$, each value of which was obtained by averaging ten measurements. The time requiring for each series was approximately two minutes. It was shown by means of special measurements that after approximately two days, the standard ratio β_0 remained unchanged. The standard isotopic composition was taken to be the composition of the stationary stream of mercury through the tube. The standard was measured before and after the experiment, and the tube was heated to approximately 300°C to accelerate the establishment of the stationary flow.

Analogous measurements were made with glass and copper tubes. In all cases, the diffusion resistances of the tube were the same.

2. The results obtained with iron and glass tubes are shown in Fig. 2. Curve 1 of the upper graph represents the change in the flow of mercury through an iron tube at T = 20°C, while Curve 2 is for T = 290°C. Curve 3 corresponds to a change in the flow through a glass tube. The lower graph shows the corresponding curves for the variation of the isotopic composition $\Delta = (\beta - \beta_0)/\beta_0$, where $\beta = f(t)$ (a common time axis is used).

It is seen from Curve 1 (lower plot) of Fig. 2 that the initial mercury stream contains an excess of the lighter isotope and approximately eight hours are required to make the composition standard. Section AB of the curve corresponds to the desorption of mercury at T = 20°C, while section BC corresponds to desorption at 300°C. It is seen from the lower plot that the desorbed mercury is enriched with the heavier isotope.

In the case of a glass tube (see Fig. 2), the time to establish the flow and the composition is one tenth that required for an iron tube at T = 20°C. The appearance time was approximately 10 sec in this case. The mercury adsorption on the glass was vanishingly small.

Figure 3 shows the results of the measurements of the flow and of the isotopic composition with a copper tube at T = 20°C. (Curves 1). The curves for copper and for iron are qualitatively the same. Section AB of Curves 1 corresponds to desorption at T = 20°C, while section BC corresponds to desorption at T ~ 150°C, while CD is for T ~ 230° C. The composition of the desorbed mercury in section AB of Fig. 3 can be attributed to the uneven evaporation and to the difference in the isotopic composition of the adsorbed mercury along the length of the tube. Curves 2 of Fig. 3 show the same relations for a copper tube with a diffusion resistance that is one third as large as for the case of Curves 1.

3. P. Clausing[1] solved the diffusion problem for a nonstationary molecular flow, with allowance for the adsorption time. His solution is independent of the degree of jacketing, is subject to the initial and boundary conditions of the present work, and fits very well the experimental Curve 1 (dotted curve of Fig. 2) for a certain value of the parameter α. This indicates that it is proper to employ these calculations for the flow of mercury vapors through an iron tube.

Combining the flow equation[1] for the isotope 198 with the flow equation for the isotope 204, we obtain

$$\Delta = \frac{\beta - \beta_0}{\beta_0} = \frac{1 - 2\left[\exp\left(-t/\alpha_1\right) - \exp\left(-4t/\alpha_1\right) + \exp\left(-9t/\alpha_1\right)\right]}{1 - 2\left[\exp\left(-t/\alpha_2\right) - \exp\left(-4t/\alpha_2\right) - \exp\left(-9t/\alpha_2\right)\right]} - 1, \quad (1)$$

where the indices 1 and 2 refer to the lighter and heavier isotopes, with

$$\alpha = \frac{L^2}{\pi^2 D} = \frac{3}{\pi^2}\left(\frac{L}{2r}\right)^2\left(\frac{2r}{u} + \tau_e\right), \quad (2)$$

where τ_e is the average adsorption time, u the average thermal velocity, and L and r the length and radius of the tube. The value of α_2 is deter-

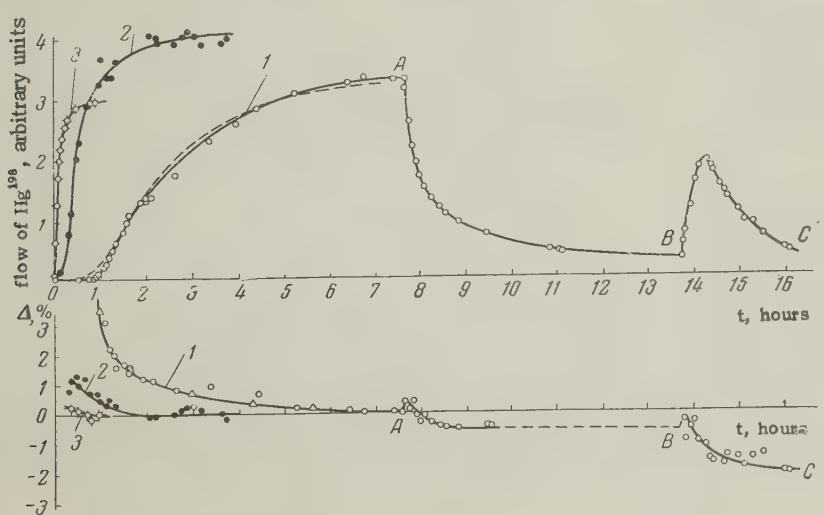

FIG. 2. Variation of stream and of isotopic composition of mercury vapors passing through iron and glass tubes.

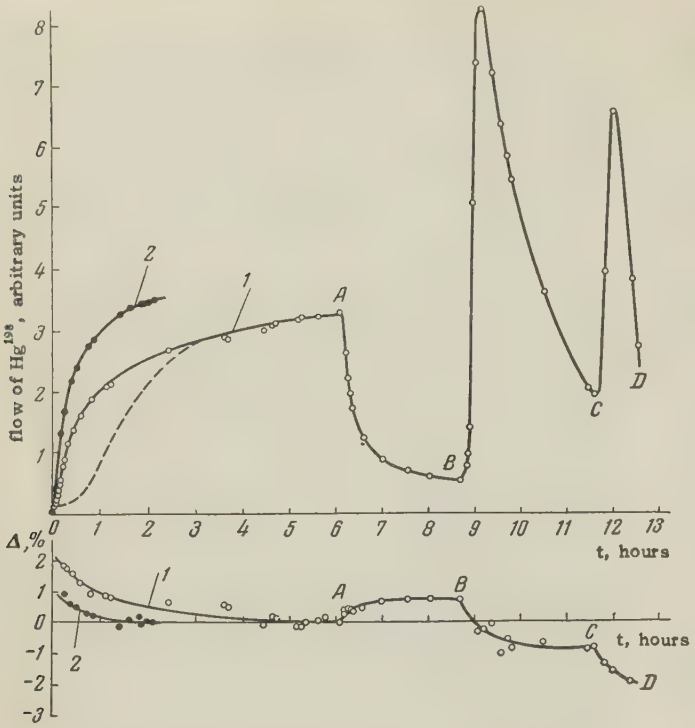

FIG. 3. Variation of flow and isotopic composition of mercury vapors passing through copper tubes.

mined by means of formula (1) from the known values of Δ and α_1, obtained from Curve 1 of Fig. 2. As a check, using the computed values of α_1 and α_2, formula (1) was used to compute points (triangles on Fig. 2), which fit well on the experimental curve.

Analogous calculations for the copper tube have shown that it is possible to describe the variation of the flow and the isotopic composition in terms of the Clausing equations, this being a consequence (see Fig. 3) of the discrepancy between the experimental curve 1 and the calculated one (dotted one). The difference between the curves for the flows through iron and copper tubes can be explained by the presence of dissolution and diffusion of mercury in the wall of the copper tube.

The following values of τ_e were computed from the experimental results with the iron tube:

for $T = 293°K$ $\tau_e^1 = 3.4 \cdot 10^{-2}$ sec, and $\tau_e^2/\tau_e^1 = 1.008$;
for $T = 563°K$ $\tau_e^1 = 1.0 \cdot 10^{-2}$ sec.

Using the values of τ_e^1 for two temperatures, it is possible, after Frenkel',[2] to estimate the heat of adsorption on mercury on iron. It turns to be approximately 15×10^3 cal/mole.

It is thus shown that the different adsorption times of the isotopes, for a nonstationary molecular flow, lead to a separation of the isotopes. The phenomenon described must be taken into account in exact mass-spectrometric measurements, for it is one of the sources of the non-systematic errors.

[1] P. Clausing, Ann. Physik **7**, 489 (1930).
[2] Ia. Frenkel', Z. Physik **26**, 117 (1924).

Translated by J. G. Adashko
65

INVESTIGATION OF GAMMA RAYS EMITTED IN U^{235} FISSION INDUCED BY 2.8 AND 14.7 Mev NEUTRONS

A. N. PROTOPOPOV and B. M. SHIRIAEV

Radium Institute, Academy of Sciences, U.S.S.R.

Submitted to JETP editor August 30, 1957

J. Exptl. Theoret. Phys. (U.S.S.R.) 34, 331-333 (February, 1958)

Gamma rays coinciding in time with fission fragments were recorded with a scintillation counter. It is shown that the γ-ray spectrum is the same for U^{235} fission induced by 2.8 and 14.7 Mev neutrons as for fission induced by thermal neutrons. It is concluded that the total quantum energy per U^{235} fission event induced by 2.8 and 14.7 Mev neutrons is the same to within 15% as that for thermal fission by neutrons.

SEVERAL recent works[1-4] are devoted to a study of the γ rays emitted by fission of heavy nuclei. These works have investigated the spectrum of the γ rays and the average total γ quantum energy per fission event.

The varied values of the residual fragment energy after emission of "prompt" neutrons, and the large number of the fragments themselves, result in a rather complicated γ spectrum, resembling a continuous spectrum whose intensity diminishes rapidly with increasing energy. Individual monochromatic lines have been noted in Refs. 5 and 6, but their intensity is small relative to the background of the main spectrum. It is possible that some of these lines are due to the superposition of γ transitions of nearly-equal energy in different nuclear fragments. The total energy of the γ rays emitted in U^{235} fission induced by thermal neutrons, in accordance with recent investigations,[2,4] is estimated at approximately 7.5 Mev, with approximately eight γ quanta produced per fission.

Leachman[2] calculated the energy emitted by the excited fragments in the form of γ rays and obtained values of 3.8 and 4.1 Mev for fission of U^{235} by thermal and 3-Mev neutrons respectively. The value obtained by Leachman, as can be seen from the above, does not agree with experiments on fission of U^{235} by thermal neutrons. No γ-ray investigation has been made for fission by high-energy neutrons.

In the present work we investigated the emission of γ rays in U^{235} fission by 2.8 and 14.7 Mev neutrons. A coincidence circuit was used to measure the spectrum of the γ quanta that coincide in time with U^{235} fission induced by both fast and the thermal neutrons. By subsequently comparing the experimental spectra it is possible to draw conclusions concerning the γ rays that accompany the fission of U^{235} by fast neutrons.

Figure 1 shows the block diagram of the apparatus employed. The γ quanta were recorded with a scintillation counter with a NaI (Tl) crystal and a FEU-S spectrometric photomultiplier. Two pulses were picked off simultaneously from the photomultiplier, one fed through a linear amplifier to a multi-channel amplitude analyzer, and the second to the coincidence circuit. The operation of the scintillation counter was checked against a Cs^{137} compound with a single-channel analyzer.

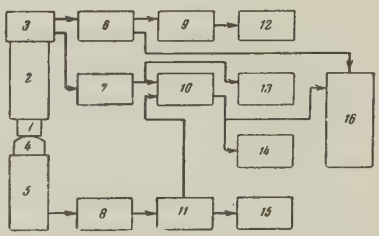

FIG. 1. Block diagram of the apparatus. 1 – NaI(Tl) crystal, 2 – photomultiplier, 3 – cathode follower; 4 – ionization chamber; 5 – preamplifier; 6, 7, 8 – linear amplifiers; 9 – single-channel amplitude analyzer; 10 – coincidence circuit; 11 – pulse-delay regulating network; 12, 13, 14, 15 – counting devices; 16 – multi-channel amplitude analyzer.

The fission fragments were recorded with a multi-layer ionization chamber, filled with a mixture of argon (95%) and carbon dioxide (5%) at a pressure of 760 mm Hg. The layers of the uranium oxide, containing 97.8% U^{225}, were coated on the electrodes of the chamber by electrolysis, to a mean density of 1 mg/cm^2. The total weight of the uranium oxide coated on the electrodes was 100 mg. The chamber pulses were fed through a linear amplifier to the coincidence circuit.

Upon simultaneous receipt of pulses from the scintillation counter and from the fission chamber, the coincidence circuit triggered the multi-channel amplitude analyzer, which photographed the pulses from the cathode ray tube on a moving photofilm. To compensate for the time shifts of the pulses arriving at the coincidence circuit, a network was used to regulate the delay of the pulses from the ionization chamber. The resolving time of the coincidence circuit was 2×10^{-7} sec.

Neutrons of energy 2.8 and 14.7 Mev were produced through $D(d, n)He^3$ and $T(d, n)He^4$ reactions by bombardment with 180-kev deuterons. The fission chamber was placed 10 cm from the neutron source. This made it possible to obtain uniform neutron-flux density on the chamber layers. When operating with fast neutrons, the chamber was covered with a layer of cadmium. The thermal neutrons were obtained by moderating the fast neutrons with lead (10 cm) and paraffin (25 cm). In all measurements, the relative placement of the fission chamber and the crystal with photomultiplier was maintained strictly constant.

The amplitude distributions of the pulses, obtained as a result of the measurements, are shown in Fig. 2 (which shows also the amplitude distribution obtained with γ rays from Cs^{137}). It is seen from the diagram that in all cases the spectra have the same form within the measured range of amplitudes. For fission of U^{235} by thermal neutrons, the amplitude range, fixing the photopeaks up to 1600 kev and the Compton peaks up to 2,000 kev, covers approximately 90% of the total number and 65 — 70% of the total energy of the "prompt" quanta. Considering that the spectrum of the harder γ rays, produced upon fission of U^{235} by fast neutrons, is also similar to the γ-ray spectrum due to fission by thermal neutrons, (as occurs in the case of γ quanta of energy less than 2,000 kev), we can conclude that the total energy of the γ quanta emitted by fission is proportional to their average number per fission.

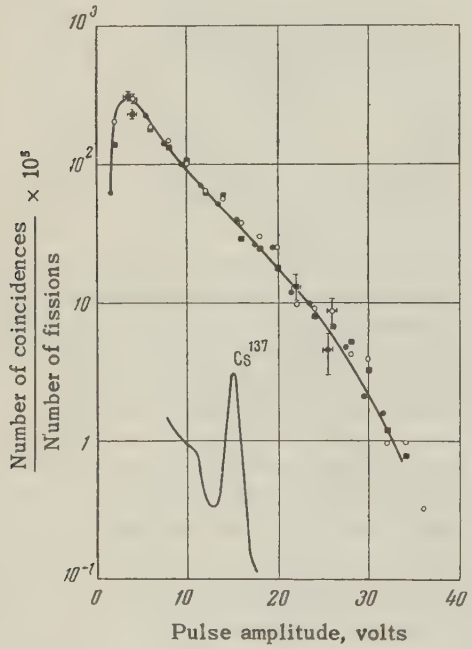

FIG. 2. Amplitude distribution of scintillation-counter pulses accompanying the fission of U^{235}: ● — by thermal neutrons, ○ — by 2.8 Mev neutrons, ■ — by 14.7 Mev neutrons.

After eliminating the background, the ratio of the number of coincidences between the γ quanta and the fragments for U^{235} fission by 2.8 and 14.7 Mev neutrons to the number of coincidences for fission by thermal neutrons is found to be 1.10 ± 0.05 and 1.05 ± 0.05 respectively. It must be noted, that extrapolation of the spectrum introduces a certain indeterminacy in the final results, and that it would be desirable to carry out the measurements for a larger energy interval. However, an estimate of the indeterminacy shows that the error due to extrapolation cannot exceed 10 — 15% of the total γ-ray energy. Taking this indeterminacy into account one can assume that, within the experimental accuracy (on the order of 15%), the total energy of the γ quanta accompanying the fission of U^{235} by 2.8 and 14.7 Mev is the same as obtained in fission by thermal neutrons. This result is not unexpected, considering that the prompt γ rays are emitted essentially by excited fragments after the emission of the neutrons.

The authors thank Iu. M. Artem'ev for great help in the preparation for this investigation.

[1] Kinsey, Hanna, and Van Patter, Can. J. Res. **26A**, 79 (1948).

[2] R. B. Leachman, Phys. Rev. **101**, 1005 (1956).

[3] W. J. Whitehouse, Progress in Nuclear Physics, London, **2**, 1952, pp 150-152.

[4] Artemiev, Protopopov, and Shiriaev, Труды РИАН (Trans. Radium Inst. Acad Sci.) vol. IX (in press).

[5] Skliarevskii, Fomenko, and Stepanov, J. Exptl. Theoret. Phys. (U.S.S.R.) **32**, 256 (1957), Soviet Phys. JETP **5**, 220 (1957).

[6] Voitovetskii, Levin, and Marchenko, J. Exptl. Theoret. Phys. (U.S.S.R.) **32**, 263 (1957), Soviet Phys. JETP **5**, 184 (1957).

Translated by J. G. Adashko
66

ANGULAR DISTRIBUTIONS FOR SOME (d, p) REACTIONS

I. B. TEPLOV and B. A. IUR'EV

Moscow State University

Submitted to JETP editor September 9, 1957

J. Exptl. Theoret. Phys (U.S.S.R.) **34**, 334-340 (February, 1958)

Angular distributions for some of the proton groups from (d, p) reactions on silicon, phosphorus, sulfur, and chlorine were found for 4 Mev deuterons. The results show that when nuetrons with $\ell = 2$ are captured, the maximum in the differential cross section is shifted toward smaller angles from the position of the maximum as given by the Butler theory. A comparison of the angular distributions shows that there is an appreciable effect on the shape of the distribution from the interference between the processes of stripping and compound nucleus formation.

THE angular distribution which was found[1] for the long range protons from the stripping reaction $S^{32}(d, p)S^{33}$ with 4-Mev deuterons was different from the angular distributions of the long range protons from the $P^{31}(d, p)P^{32}$ and $Cl^{35}(d, p)Cl^{36}$ reactions[2,3] for the same deuteron energy. One would have expected that the shapes of the angular distributions would be similar for all three reactions. In the first place, in all three cases the neutron is captured in a $1d_{3/2}$ state, i.e., $\ell = 2$. This follows from the shell model and is confirmed by studies of the stripping reaction for deuteron energies around 8 Mev.[4-6] Secondly, all the fundamental parameters characterizing the three reactions — charge, mass, and nuclear radius, as well as the Q value, are approximately the same (cf. below).

The present paper gives the results of additional studies of these three reactions. In addition we give the angular distributions for two long-range proton groups from the $Si^{28}(d, p)Si^{29}$ reaction with 4-Mev deuterons, as well as the angular distribution of the proton group from $S^{32}(d, p)S^{33}$ in which the final nucleus is left in its ground state. The last group was observed with 1.3 and 2.2 Mev bombarding energy.

EXPERIMENTAL METHOD

The proton angular distributions were studied using NIKFI-Ia2 thick-layered photoplates; all the particulars of the experiment have been previously described.[7] We should add only that the absolute value of the deuteron energy was known to ± 3%, while the energy spread of the beam did not exceed 30 kev.*

PbS, Zn_3P_2, and $BaCl_2$ were used for preparing the targets. These compounds were evaporated onto a gold leaf backing. In the case of sulfur, an additional irradiation at 4 Mev was made after the main irradiations at 4.0, 2.2, and 1.3 Mev. The ratio of the cross sections found in the check series to those in the main series was 0.84, so apparently as a result of deuteron bombardment the number of sulfur atoms in the target had decreased somewhat.

The silicon target was prepared by evaporating coarse-grained silicon from a tungsten helix. In this case the backing was a polystyrene film. Since its thickness was not known, we were unable to determine the absolute value of the $Si^{28}(d, p)Si^{29}$ reaction cross section. Another defect of the polystyrene backing is that the spectrum measurement is made somewhat more difficult because of the presence of a proton group from the $C^{13}(d, p)C^{14}$ reaction.

Purified reagents were used in all cases for preparing targets. No protons were observed from impurities.

EXPERIMENTAL RESULTS

The observed angular distributions are given in Figs. 1 — 8, in which the abscissa gives the angle in the center of mass system, and the ordi-

*This value of the spread comes from measurements by G. F. Timushev, carried out at the same cyclotron using a precision magnetic spectrometer, under conditions similar to ours.

nate is the differential cross section in millibarns per steradian. For the case of silicon, (Figs. 1 and 5), the differential cross sections are given in relative units, with the same scale on both figures. The errors indicated on the figures are statistical errors. (Errors not associated with statistical fluctuations are, in any case, less than 10%, cf. Ref. 7.)

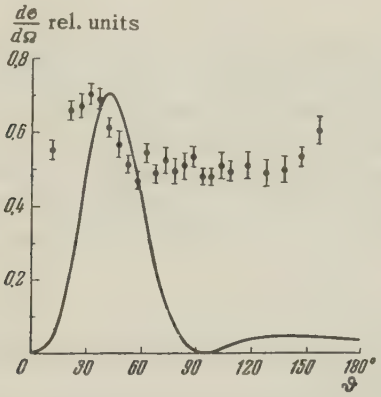

FIG. 1. Silicon reaction. Si^{29} excitation energy = 1.28 Mev; $l = 2$.

The angular distributions for phosphorus and chlorine (Figs. 2 and 4) are based on the same experimental material as in Ref. 3, but the plates were examined again with appreciably greater accuracy. We also checked the calibration of the integrator (by elastic deuteron scattering on gold) and the target thickness. The check showed that the phosphorus reaction cross section is approximately twice as large as that given in Ref. 3.* We should mention that, in the case of phosphorus, at large angles we are able to separate the proton group from the $Zn^{64}(d, p)Zn^{65}$ reaction in which the final nucleus is left in the ground state. At small angles this proton group cannot be separated from the protons from the phosphorus reaction. Thus the results for phosphorus (Fig. 2) at small angles were obtained under the assumption that the distribution of the protons from the $Zn^{64}(d, p)Zn^{65}$ reaction is isotropic and that the differential cross section is 0.25 mbn/sterad.

For chlorine, in addition to the main measurements whose results are given in Fig. 4, we also made some additional measurements. In this case the plates were placed at a smaller number of angles and fewer tracks were measured on each plate than for the main series. However, the shapes of the angular distributions and the absolute total cross sections were practically the same for both cases.

Table I gives the values found for the total cross sections for formation of the various proton groups. The absolute cross sections are determined to 30 — 40% (the uncertainty in the relative cross sections for sulfur is considerably smaller). For silicon we give only the relative cross sections for formation of the two proton groups.

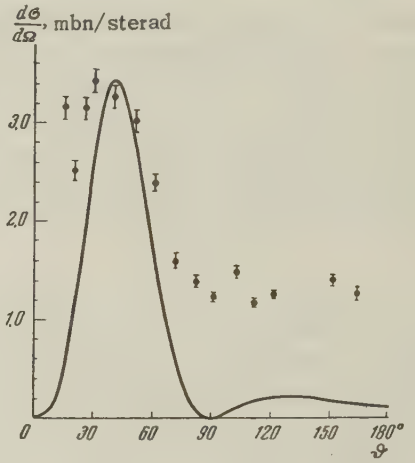

FIG. 2. Phosphorus reaction. P^{32} ground state and first excited state (0.077 Mev); $l = 2$

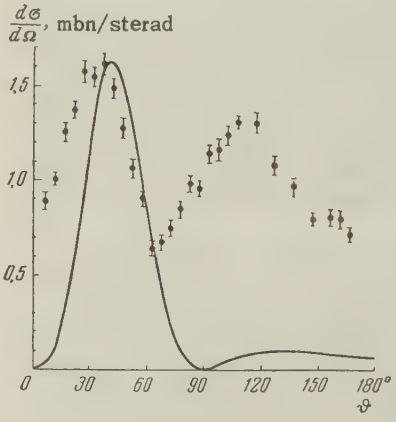

FIG. 3. Sulfur reaction. S^{33} ground state; $l = 2$.

DISCUSSION OF RESULTS

In addition to the experimental results, Figs. 1 — 8 give the angular distributions calculated from the Butler theory;[8] the nuclear radius, in accordance with Holt and Marsham, is taken as $R = (1.7 + 1.22 A^{1/3}) \times 10^{-13}$ cm.

Let us first look at the angular distributions found for the first excited state of Si^{29}, for the close doublet of P^{32} and for the ground states of S^{33} and Cl^{36} (Figs. 1 — 4). In these cases the neutron is captured into a $1d_{3/2}$ state, i.e., with orb-

*The ordinates of all figures in Ref. 3 for phosphorus should therefore be multiplied by 2.

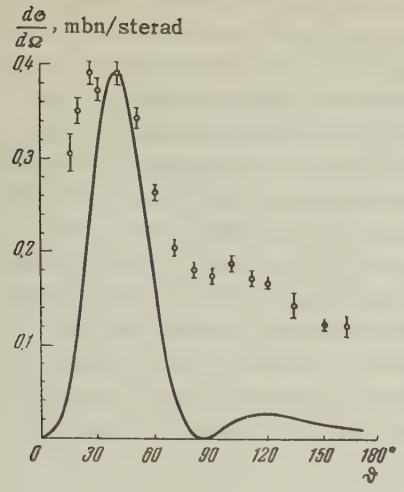

FIG. 4. Chloride reaction. Cl^{36} ground state; $l = 2$.

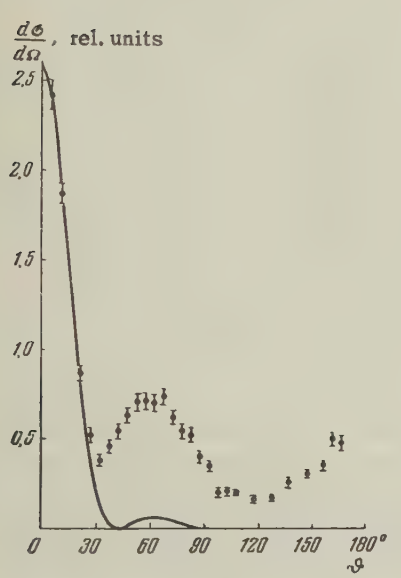

FIG. 5. Silicon reaction. Si^{29} ground state; $l = 0$.

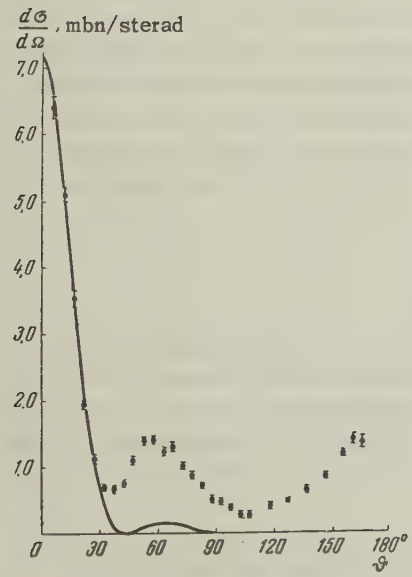

FIG. 6. Sulfur reaction. S^{33} excitation energy = 0.84 Mev; $l = 0$

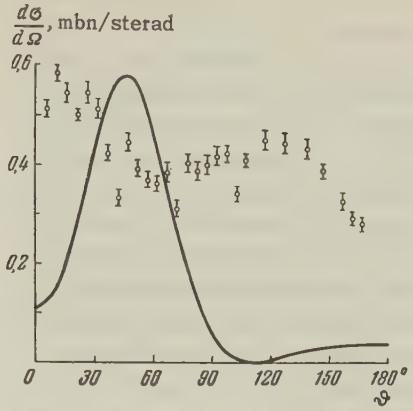

FIG. 7. Sulfur reaction. S^{23} ground state; $l = 2$; deuteron energy = 2.2 Mev.

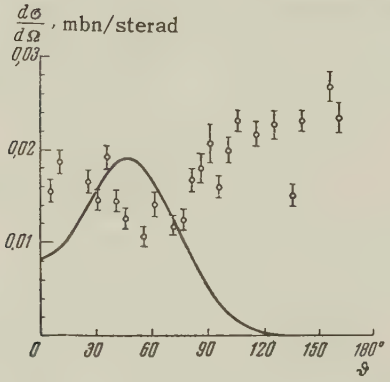

FIG. 8. Sulfur reaction. S^{33} ground state; $l = 2$; deuteron energy = 1.3 Mev

TABLE I

Reaction	Deuteron energy Mev	Excitation energy Mev	l	σ, mbn
$Si^{28}(d, p)Si^{29}$	4.0	0	0	σ_0
$P^{31}(d, p)P^{32}$	4.0	1.28	2	$0.16\sigma_0$
$S^{32}(d, p)S^{33}$	4.0	0+0.077	2	22.6
	4.0	0	2	13.4
	2.2	0	2	5.25
	1.3	0	2	0.23
	4.0	0.84	0	11.0
$Cl^{35}(d, p)Cl^{36}$	4.0	0	2	2.9
$Zn^{64}(d, p)Zn^{65}$	4.0	0	—	3.2

ital angular momentum $l = 2$. All four experimental angular distributions show the main feature of the stripping reaction, the presence of a maximum at small proton angles. But a more detailed comparison shows that there are differences between the experimental and theoretical angular distributions which are common to all four cases. These are, first, the presence of an appreciable "background" (i.e., some differential cross section at the minima of the angular distributions); secondly, there is a shift of the principal maximum toward smaller angles compared with the curve calculated from the Butler theory. The oc-

currence of an appreciable background or, as it is sometimes called, an isotropic part of the angular distribution, is almost always observed with low energy deuterons. It might be attributable to compound nucleus formation. It is entirely possible that it is partially due to the stripping process itself, as is shown by computations of Tobocman and Kalos[10] which include Coulomb and nuclear interactions. As for the shift of the main maximum toward smaller angles, such a shift was already observed in our work[7] in which we studied the potassium and calcium reactions with 4-Mev deuterons. There is also a shift of the maximum in the results of Shapiro[11] for the Na^{23}(d, p)Na^{24} reaction with 3-Mev deuterons.

Thus we may assume that the shift of the characteristic stripping maximum toward smaller angles from the position as computed on the Butler theory is not accidental, at any rate for deuteron energies somewhat below the Coulomb barrier. This result is somewhat unexpected, since the Coulomb interaction should shift the maximum in the opposite direction. Therefore the shift toward 0° shows that nuclear interaction plays an important role in the stripping process. It would seem that the presence of such a shift should be borne in mind when selecting a method of description of the nuclear interaction in calculations of angular distributions according to the formula of Tobocman and Kalos.[10]

TABLE II

Reaction	Excitation energy of final nucleus, Mev	Q, Mev	Target nucleus		Effective Height of Coulomb barrier, Mev	Excitation energy of intermediate nucleus, Mev
			Z	N		
$Si^{28}(d, p)Si^{29}$	1.28	4.97	14	14	4.74	15.5
$P^{31}(d, p)P^{32}$	0+0.077	5.70	15	16	4.88	19.0
$S^{32}(d, p)S^{33}$	0	6.42	16	16	5.14	15.2
$Cl^{35}(d, p)Cl^{36}$	0	6.30	17	18	5.27	19.0

As already remarked, the fundamental parameters describing the reactions are closely equal for silicon, phosphorus, sulfur, and chlorine, which occupy neighboring positions in the periodic table (cf. Table II). Thus, independently of whether we include Coulomb and nuclear interactions in the calculations, the theoretical angular distributions should be alike for all four cases. But it is apparent from Figs. 1 — 4 that only for phosphorus and chlorine are the shapes similar to one another. In the case of sulfur (Fig. 3), a very sizeable secondary maximum is observed (around 115°) in the angular distribution; in the case of the silicon reaction (Fig. 1), the very small height of the main maximum compared to the isotropic part is striking. None of the known theories of the stripping reaction can explain such differences. One can, of course, assume that the nuclear interactions depend essentially on the nucleon configuration in the initial nucleus, but it is more natural to explain the observed differences in terms of the effect of the mechanism of compound nucleus formation. Such an explanation is the more plausible, since Lee and Schiffer[12] recently observed a resonance structure in the excitation curve of the Ca^{40}(d, p)Ca^{41} reaction (in which they found 30 resonances in the range of deuteron energies from 1.50 to 4.22 Mev), and Nemilov and Litvin,[13] in their investigation of the ratio of yield of various proton groups from the reaction Si^{28}(d, p)Si^{29} at fixed angle for the emerging protons, found several sharp resonances separated by about 0.5 Mev. One can try to check whether the resonances found by Nemilov and Litvin are actually caused by the mechanism of formation and breakup of the compound nucleus. The basis of such a test is the fact that, according to stripping theory,* the ratio of the differential cross sections for two neighboring levels should be a function of the quantity

$$k = |\bar{\mathbf{k}}_d - (M_i/M_f)\,\mathbf{k}_p|.$$

Here $\mathbf{k}_d$ and $\mathbf{k}_p$ are the wave vectors of the deuterons and proton in the center of mass system, M_i and M_f are the masses of the initial and final nucleus. The magnitude of k depends on the angle of emergence of the proton and the energy of the

*This holds for the Butler theory and apparently remains approximately true for more complicated theories.

deuteron. Therefore, in the stripping theory there should be a unique relation between the shape of the angular distribution and the shape of the differential excitation curve. This is, of course, not the case for the reaction mechanism associated with compound nucleus formation. The solid curve in Fig. 9 shows the curve obtained by Nemilov and Litvin for the ratio of the yields of the p_1 and p_0 proton groups at an angle of 109° for the emerging protons, as a function of deuteron energy. The dashed curve in the same figure shows the same ratio as found from our measured angular distributions for the p_1 and p_0 proton groups from the $Si^{28}(d, p)Si^{29}$ reaction (Figs. 1 and 5). The shift from angles of emergence of the protons to deuteron energies was made on the assumption that the reaction goes only via stripping.

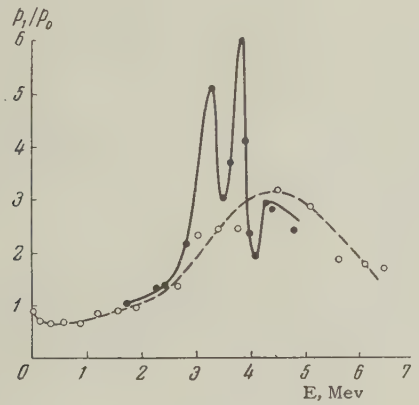

FIG. 9. Energy dependence of the ratio of yields of proton groups p_1 and p_0, at a proton angle of 109°, from the $Si^{28}(d, p)Si^{29}$ reaction. The points are the data of Nemilov and Litvin;[13] the open circles are the results obtained from the angular distributions (Figs. 1 and 5).

Comparison of the two curves of Fig. 9 shows that the sharp peaks cannot be due to the stripping process, since the curve computed from the angular distributions shows no such narrow maxima. Consequently the different shapes of the angular distributions for the cases in which the neutron is captured into a $1d_{3/2}$ state are apparently explained by the effect of the mechanism of compound nucleus formation with subsequent emergence of the proton, in which a change in the interference term obviously plays the principal role. From this point of view, it is easy to explain the marked change in the shape of the angular distribution from the sulfur reaction for decreasing deuteron energy (Figs. 7 and 8, and also Fig. 1 of Ref. 1).

So for target nuclei with charge $Z \leq 20$ and deuteron energies less than or equal to the height of the Coulomb barrier, the angular distributions of protons from (d, p) reactions as computed from the Butler formula may be strongly distorted, first because of nuclear and Coulomb interaction between the particles participating in the reaction and, secondly, because of interference between the stripping process and the process which occurs via compound nucleus formation. The first cause leads to a shift of the main maximum in the angular distribution toward smaller angles, and this shift may be very large [for example, for the case of the $Ca^{40}(d, p)Ca^{41}$ reaction with 2.2-Mev deuterons, cf. Ref. 7]. The second cause apparently produces an increase in the isotropic part of the angular distribution and also affects the relative size of the main and secondary maxima.

The authors express their gratitude to S. S. Vasil'ev for his interest in the work, and to the operating group for the cyclotron, headed by engineer G. V. Kosheliaev.

[1] Teplov, Iur'ev, and Markelova, J. Exptl. Theoret. Phys. (U.S.S.R.) **32**, 165 (1957), Soviet Phys. JETP **5**, 134 (1957).

[2] I. B. Teplov, Dissertation, Moscow State University, 1955.

[3] I. B. Teplov, J. Exptl. Theoret. Phys. (U.S.S.R.) **31**, 25 (1956), Soviet Phys. JETP **4**, 31 (1957).

[4] J. R. Holt and T. N. Marsham, Proc. Phys. Soc. (London) **A66**, 467 (1953).

[5] Parkinson, Beach, and King, Phys. Rev. **87**, 387 (1952).

[6] J. S. King and W. C. Parkinson, Phys. Rev. **88**, 141 (1952).

[7] I. B. Teplov and B. A. Iur'ev, J. Exptl. Theoret. Phys. (U.S.S.R.) **33**, 1313 (1957), Soviet Phys. JETP **6**, 1011 (1958).

[8] S. T. Butler, Proc. Roy. Soc. (London) **A208**, 559 (1951).

[9] J. R. Holt and T. N. Marsham, Proc. Phys. Soc. (London) **A66**, 1032 (1953).

[10] W. Tobocman, Phys. Rev. **94**, 1655 (1954). W. Tobocman and M. H. Kalos, Phys. Rev. **97**, 132 (1955).

[11] P. Shapiro, Phys. Rev. **93**, 290 (1954).

[12] L. L. Lee and J. P. Schiffer, Bull. Am. Phys. Soc. **2**, 208 (1957).

[13] Iu. A. Nemilov and V. F. Litvin, J. Exptl. Theoret. Phys. (U.S.S.R.) **31**, 719 (1956), Soviet Phys. JETP **4**, 606 (1957).

Translated by M. Hamermesh
67

FISSION OF ROTATING NUCLEI

G. A. PIK-PICHAK

Submitted to JETP editor August 2, 1957

J. Exptl. Theoret. Phys. (U.S.S.R.) 34, 341-345 (February, 1958)

An expression is obtained for the fission barrier of a rotating nucleus. The fission cross section is estimated for the reaction of N^{14} ions on heavy nuclei.

DRUIN, Polikanov, and Flerov[1] studied fission induced by heavy particles. Ions of N^{14} with energies ~ 100 Mev were captured by nuclei of U, Bi, Au, and Re, producing a nucleus with high excitation energy and high angular momentum. The maximum angular momentum given to the nucleus is

$$M_{\max} = \sqrt{2\mu (R^* + R_1)^2 (E - B)},$$

where R_1 and R^* are the radii of the ion and the target nucleus, μ is the reduced mass, E is the energy of the ion in the center-of-mass system, and B is the Coulomb barrier. For nuclei with A ~ 200 and ion energies ~ 100 — 200 Mev, the maximum angular momentum is ~ 50 — 120ħ. At such high excitation energy, this angular momentum is almost entirely associated with rotation of the nucleus as a whole. The fraction of the angular momentum associated with the spin of the nucleons is easily estimated for the case of a Fermi gas.[2] The spin of the nucleus turns out to be $\hbar s = M\hbar^2/\Delta I$, where Δ is the spacing between single particle levels ~ 0.1 Mev, and I is the moment of inertia of the nucleus. For excitation energies of the size we are considering, where shell effects can be neglected, the moment of inertia of the nucleus is assumed to be equal to that of a rigid body[3] (for the case of a sphere, $I = I_0 = \frac{2}{5} AmR^2$, where Am and R are the mass and radius of the compound nucleus). On this assumption, $\hbar^2/I \sim 1$ kev and $\hbar s/M \ll 1$.

For $M \sim 50 - 120\hbar$, the rotational energy $E_{rot} = M^2/2I$ is comparable with the height of the fission barrier ($E_{rot} \sim 5 - 20$ Mev), so in this case the rotation of the nucleus must be taken into account in calculating the fission barrier.

The total change in energy of the rotating nucleus upon deformation is

$$\Delta E = \Delta E_s + \Delta E_q + \Delta E_{\text{rot}}, \qquad (1)$$

where ΔE_s, ΔE_q, and ΔE_{rot} are the changes in the surface, Coulomb, and rotational energies. The last change is caused by a change in the momentum of inertia (as a result of deformation of the nucleus) while the angular momentum is kept fixed. The stable shape during rotation of the nucleus is, naturally, that of an axially symmetric oblate ellipsoid with its axis of symmetry along the direction of the angular momentum. Deformations of different types will either favor or hinder fission. For example, deformations corresponding to an elongated ellipsoid with its symmetry axis perpendicular to the angular momentum will favor fission, while the same ellipsoid with its axis along the angular momentum will hinder fission (because of the effect of the centripetal forces).

The transition from the shape of an oblate ellipsoid to that of a prolate ellipsoid with its symmetry axis perpendicular to the angular momentum is accomplished by means of a deformation which is not axially symmetric.

The shape of the nuclear surface is given by the radius vector

$$r(\theta, \varphi) = R_0 \left(1 + \sum_{l,m} \alpha_{lm} D^l_{m0}(\theta, \varphi, 0)\right), \qquad (2)$$

where R_0 is the radius of the sphere of equal volume, $D^{\ell}_{m0}(\theta, \varphi, 0) = D^{m}_{\ell}(\theta, \varphi)$ are the spherical functions with the normalization

$$D^l_m(0, 0) = 1.$$

If we consider a nucleus rotating about one of its axes of inertia and limit ourselves to $\ell = 2$, it is convenient to introduce deformation coordinates in the form[4]

$$\alpha_{21} = \alpha_{2-1} = 0; \quad \alpha_{20} = \alpha \cos\gamma; \quad \alpha_{22} = \alpha_{2-2} = \frac{\alpha}{\sqrt{2}} \sin\gamma.$$

Then the change in the semiaxes of the ellipsoid will be:

$$\delta R_x = \alpha R_0 \cos\left(\gamma - \frac{2\pi}{3}\right); \quad \delta R_y = \alpha R_0 \cos\left(\gamma - \frac{4\pi}{3}\right);$$

$$\delta R_z = \alpha R_0 \cos\gamma.$$

In these variables, we have (dropping terms $\sim \alpha^4$):

$$\Delta E_s + \Delta E_q = 4\pi R^2 O \left\{\frac{2}{5} z\alpha^2 - \frac{4}{105}\alpha^3 \cos^3\gamma\right\}, \qquad z = 1 - x = 1 - (Z^2/A)/(Z^2/A)_{cr}, \tag{3}$$

where $R = r_0 A^{1/3}$; $4\pi r_0^2 O = 15$ Mev is the magnitude of the surface tension, and A and Z are the mass and charge of the nucleus. The value of (3) is triply degenerate in γ, since there is no preferred direction in space, so that it makes no difference along which axis the fission occurs.

But if the nucleus is rotating and the z axis is directed along the angular momentum, the moment of inertia with respect to the z axis is

$$I_z = I_0\left(1 - \alpha_{20} + \frac{3}{7}\alpha_{20}^2 + \frac{22}{7}\alpha_{22}^2 + \ldots\right). \tag{4}$$

Let us calculate the change in energy for a rotating nucleus, limiting ourselves for simplicity to terms of first degree in y in the rotational energy:

$$\Delta E = 4\pi R^2 O\left\{y\alpha_{20} + \frac{2}{5} z\alpha_{20}^2 + \frac{4}{5} z\alpha_{22}^2 - \frac{4}{35}\alpha_{20}^3 + \frac{24}{35}\alpha_{20}\alpha_{22}^2\right\}, \quad y = (M^2/2I_0)/4\pi R^2 O. \tag{5}$$

The condition for an extremal gives four solutions

$$\alpha_{22} = 0, \quad \frac{12}{35}\alpha_{20}^2 - \frac{4}{5} z\alpha_{20} - y = 0, \tag{6}$$

$$\alpha_{20} = -\frac{7}{6} z, \quad \alpha_{22}^2 = \left(\frac{7}{6}\right)^2 \frac{3}{2}\left(z^2 - \frac{5}{7} y\right). \tag{7}$$

Solution (7) gives two saddle points located symmetrically around $\gamma = 0$. At the saddle points the nucleus has a shape close to that of an axially symmetric elongated ellipsoid with its axis of symmetry perpendicular to the angular momentum.

Solution (6) corresponds to an axially symmetric shape of the nucleus with its symmetry axis along the angular momentum. The first solution of (6) with $\alpha_{20} > 0$ gives a saddle shape, while the second solution of (6) with $\alpha_{20} < 0$ requires additional investigation. In the neighborhood of the second solution (6), the energy has the form:

$$\Delta E = \text{const} + \frac{2}{5} z\sqrt{1 + 15y/7z^2}\,\Delta^2 + \frac{4}{5} z\left(2 - \sqrt{1 + 15y/7z^2}\right)\gamma^2,$$

where Δ and γ are small deviations from the values of α_{20} and α_{22}, respectively, in (6). It is easy to see that for $y < y_{cr} = 7z^2/5$, the solution gives an absolute minimum, while for $y > y_{cr}$ we get a saddle, since the coefficient of γ^2 becomes negative. [We also note that for $y = y_{cr}$ the solutions (7) and the solution of (6) for $\alpha_{20} < 0$ coincide.] Thus for $y \geq y_{cr}$ there is no stable state of the nucleus and, consequently, the fission barrier for such a nucleus is equal to zero.

Inclusion of quadratic terms in α in ΔE_{rot} does not change the qualitative results, but for a more exact calculation these terms cannot be neglected. This gives an essential change not only in the value of y_{cr}, but also in the dependence of the fission barrier on angular momentum. Inclusion of further terms ($\sim \alpha^4$ and $\alpha_{\ell m}$ with $\ell > 2$) produces little change in the result. Naturally these terms become important for y close to y_{cr}. If we limit ourselves to 15% accuracy in the dependence of the fission barrier on angular momentum for $z \leq 0.3$, we may drop terms $\sim \alpha^4$ and $\alpha_{\ell m}$ with $\ell > 2$, and neglect terms of third degree in α in ΔE_{rot}. As a result of long-winded but straightforward computations, the height of the fission barrier E_f, corresponding to fission through the saddles (7) is equal in this approximation to

$$E_f = 4\pi R^2 O\,[0.73 z^3 - (1.2z + 5.6z^2)y + (4.6 + 11z)y^2] = 4\pi R^2 O f(z, y), \tag{8}$$

and the quantity y_{cr} (neglecting y^2) is

$$y_{cr} = 7z^2/5\,(1 + 6z). \tag{9}$$

The deformation at the position of the minimum (6) is

$$\alpha_{20} = -1.25y/z + (0.58 + 1.8z)\,y^2/z^3; \quad \alpha_{22} = 0, \tag{10}$$

and the energy corresponding to (10),

$$\Delta E_{min} = -0.625y^2/z + \cdots.$$

Strictly speaking, the fission barrier is the quantity $E_f - \Delta E_{min}$, but since for $y < y_{cr}$, $\Delta E_{min} \ll E_f$, and $|\Delta E_{min}| \sim |E_f|$ only for $y \approx y_{cr}$, we can neglect ΔE_{min} in this case. The quantity f(x, y) is shown in Fig. 1. The solid curves give f(x, y) according to (8).

We note that an axially symmetric deformation with symmetry axis perpendicular to the angular momentum gives a position of the saddle only slightly different from (8). The barrier height for such a "relative" saddle actually is the same as for (8). The value of f(x, y) for axially symmetric deformations is shown by the dashed line in Fig. 1.

Now we find the magnitude of the fission cross section. For high excitation energy, two main processes are possible: neutron evaporation and

fission of the nucleus. We use the statistical formulas for the neutron and fission widths[5]*

$$\Gamma_n = (T^2 A^{2/3}/\pi K)\exp(-E_n/T),$$
$$\Gamma_f = (T/2\pi)\exp(-E_f/T), \qquad (11)$$

where $T = (10U/A)^{1/2} \approx 2$ Mev for $A \sim 200$ and $U \sim 100$ Mev is the excitation energy of the nucleus, $K = 10$ Mev, E_n is the neutron binding energy.

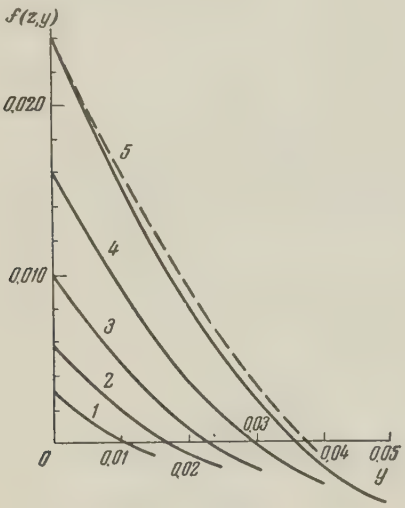

FIG. 1. 1 – z = 0.16; 2 – z = 0.20; 3 – z = 0.24; 4 – z = 0.28; 5 – z = 0.32.

We shall assume that the temperature and angular momentum of the compound nucleus do not change when a neutron is boiled off (this is valid, at least, for the first stage of the evaporation process, in which half the number of neutrons emerge of those which can be boiled off at the given excitation energy). In this case the probability of fission with emission of a number of neutrons equal to or less than m is

$$W_f(y) = 1 - (\Gamma_n/\Gamma)^{m+1}, \qquad (12)$$

where $\Gamma = \Gamma_n + \Gamma_f$. The total fission cross section for $M_{max}/\hbar \gg 1$ is

$$\sigma_f = \pi(R^* + R_1)^2\left(1 - \frac{B}{E}\right)\frac{1}{y_{max}}\int_0^{y_{max}} W_f(y)\,dy,$$
$$y_{max} = \frac{\mu(R^* + R_1)^2}{I_0}\,\frac{E - B}{4\pi R^2 O}. \qquad (13)$$

*Γ_f depends on the angular momentum M not only via the dependence of the fission barrier E_f on M, but also through the M dependence of the factor in front of the exponential, which comes from integration of the angular distribution of the fission fragments. (For $M \neq 0$, the fission probability depends on the direction of fission.) But because of the weak dependence of this factor on M, we shall use formula (11) which was derived for the case of isotropic fission.

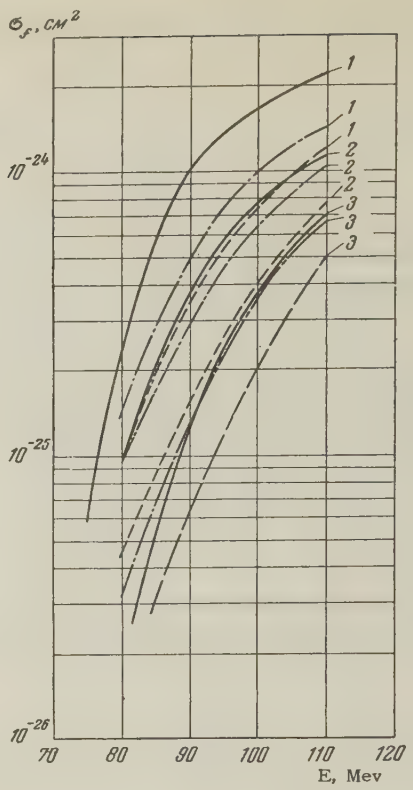

FIG. 2. Curve 1 – Bi, 2 – Au, 3 – Re.

The number of emerging neutrons as a function of energy of the ions was determined[6] for the reaction on Au^{197}. The same dependence is assumed for the reactions on Bi^{209} and Re^{187}. The solid curves of Fig. 2 show the experimental curves for the fission cross section as a function of energy of incident ions in the laboratory system. The behavior of the fission cross section calculated from (13) with $r_0 = 1.5 \times 10^{-13}$ cm [the dashed curve is for $(Z^2/A)_{cr} = 52$, the dot-dash curve for $(Z^2/A)_{cr} = 51$], are in qualitatively good agreement with experiment. The best agreement is obtained for $(Z^2/A)_{cr} = 51$. This number is somewhat greater than that found from the value of the fission barrier in U^{238} (Ref. 7). This difference is apparently explained by the fact that, first of all, the value of the fission barrier for Au and Re in the approximate expression (8) is lowered relative to the exact calculation[8] for zero angular momentum (and also for angular momenta different from zero) and secondly, the fission barrier of U^{238} apparently depends essentially on shell effects. [Thus, for example, from the fission barrier of Am^{242}, $E_f \cong 6.1$ Mev,[9,10] we get $(Z^2/A)_{cr} = 49$.]

For higher energies of the ions than those used in Refs. 1 and 6, the fission cross section on nu-

clei lighter than Au will increase, while for energies for which $y_{max} \sim y_{cr}$, the fission cross section will actually coincide with the total reaction cross section. Since the value of z will be greater than 0.3 for target nuclei lighter than Au, expression (8) will contain a large error, so we can only approximately give the region of ion energies for which the fission cross section will equal the total cross section. Thus, for example, for Yb and Dy, this region is around 150 Mev. The fission cross section, naturally, also increases with increasing mass of the bombarding particles.

In conclusion I thank B. T. Geilikman and V. M. Strutinskii for discussion of this work and for valuable comments.

[1] Druin, Polikanov, and Flerov, J. Exptl. Theoret. Phys. (U.S.S.R.) **32**, 1298 (1957), Soviet Phys. JETP **5**, 1059 (1957).

[2] W. Heisenberg, Nuclear Physics, London, Methuen, 1953.

[3] H. A. Bethe, Revs. Mod. Phys. **9**, 69 (1937).

[4] A. Bohr, Kgl. Danske Videnskab. Selskab, Mat.-fys. Medd. **26**, #14 (1952).

[5] Y. Fujimoto and Y. Yamaguchi, Progr. Theoret. Phys. (Japan) **5**, 76 (1950).

[6] Baraboshkin, Karamian, and Flerov, J. Exptl. Theoret. Phys. (U.S.S.R.) **32**, 1294 (1957), Soviet Phys. JETP **5**, 1055 (1957).

[7] D. Hill and J. Wheeler, Phys. Rev. **89**, 1102 (1953).

[8] W. J. Swiatecki, Phys. Rev. **104**, 993 (1956).

[9] D. J. Hughes and R. B. Schwartz, Neutron Cross Sections, Suppl. 1, 1957.

[10] Experimental Nuclear Physics, ed. E. Segre, Vol. 1, article by K. T. Bainbridge, "Atomic Masses," Wiley, New York, 1953.

Translated by M. Hamermesh
68

SOVIET PHYSICS JETP VOLUME 34 (7), NUMBER 2 AUGUST, 1958

ON THE THEORY OF THERMAL EXCITATION OF POLARONS

V. A. MOSKALENKO

Kishinev State University

Submitted to JETP editor February 25, 1957; resubmitted November 29, 1957

J. Exptl. Theoret. Phys. (U.S.S.R.) **34**, 346-354 (February, 1958)

The probability of a quantum transition of a polaron from the 1s to the 2p state caused by thermal vibrations of the lattice is computed. The adiabatic form of perturbation theory is used in the calculations. At room and higher temperatures transition to the 2p state occurs during $10^{-8} - 10^{-9}$ sec.

1. INTRODUCTION

POLARONS are the principal carriers of current in ionic crystals.[1] As is well known, in crystals which have large cohesive energies polarons are characterized by larged effective masses, and also by the existence of a fluctuation movement of the electron with respect to the center of gravity of the polaron. There exists a series of bound states, between which quantum transitions are possible. In this paper we shall consider such a transition between a 1s ground state and a 2p final state.

During the transition, the momentum of the polaron is conserved and changes in its kinetic energy occur at the expense of changes in its effective mass. The process under consideration turns out to be a multiphonon process. Frenkel[2] was the first to show that such transitions are possible in crystals. He pointed out that the equilibrium configuration of the field oscillators changes during such a transition. A quantitative theory of nonradiative transitions at F centers, based on this idea, was presented by a number of authors.[3-6] Another mechanism for thermal transitions was suggested by Kubo.[7]

In this paper the basic idea and method of the

theory of nonradiative transitions at F centers, proposed by Lax,[4] is used.

In the present work by a thermal transition is meant a transition induced by thermal vibrations of the lattice, and described by the terms in the initial Hamiltonian for the quantitative description of the polaron as proposed by Bogoliubov and Tiablikov. These terms are caused by departures from adiabaticity, and equal weight is given to all terms, which have the same order of smallness (ϵ^3). By formulating the problem in this way, we shall obtain information about the duration of the ground state (1s).

Anticipating the results somewhat, it can be said, that in the case under consideration the most important part of the transition matrix element is that part which is related to the dependence of the electronic wave function on the oscillator coordinates. This agrees with previously cited work.[3-6]

Finally it should be noted, that for a more consistent treatment, in the theory of F centers there must arise a question about changes of frequency of the field oscillators in the presence of an electron. This question is considered in Sec. 2 of this paper.

2. TRANSFORMATION OF THE HAMILTONIAN OF THE SYSTEM

The Hamiltonian of the polaron problem has the form

$$H=\frac{p^2}{2m}+\sum_{\mathbf{f}}A_f e^{i\mathbf{f}\mathbf{r}}q_{\mathbf{f}}+\frac{1}{2}\sum_{\mathbf{f}}E(\mathbf{f})\,(q_{\mathbf{f}}q_{-\mathbf{f}}+\varepsilon^4 p_{\mathbf{f}}p_{-\mathbf{f}}). \quad (1)$$

Here $\mathbf{p}$ and $\mathbf{r}$ are the momentum and coordinate of the electron; $\mathbf{p_f}$ and $\mathbf{q_f}$ are analogous quantities for the field oscillators; $E(\mathbf{f})=\hbar\omega_{\mathbf{f}}$ with $\omega_{\mathbf{f}}\approx\omega$, the limiting frequency of optical vibrations,

$$A_f=-(e/f)\,(4\pi\hbar\omega c/V)^{1/2},$$

where $c=1/n^2-1/\epsilon_0$, n^2 and ϵ_0 are the square of the index of refraction and the dielectric constant of the material respectively, and V is the volume of the crystal.

According to Bogoliubov and Tiablikov,[8-10] to separate the translational invariance of Eq. (1) one must write

$$\mathbf{r}=\boldsymbol{\lambda}+\mathbf{q},\quad q_{\mathbf{f}}=(r_{\mathbf{f}}+\varepsilon Q_{\mathbf{f}})\,e^{-i\mathbf{f}\mathbf{q}}; \quad (2)$$

$\boldsymbol{\lambda}$ and $\mathbf{q}$ describe the fluctuational and translational motion of the electron, respectively.

For nonspherically symmetrical states, the limitations on the new coordinates $\mathbf{Q_f}$ should be written thus

$$\sum_{\alpha}\sum_{\mathbf{f}}f^{\alpha}v^{*}_{\alpha\beta}(\mathbf{f})\,Q_{\mathbf{f}}=0,\quad \beta=1,2,3, \quad (3)$$

where

$$\sum_{\beta}\sum_{\mathbf{f}}f^{\alpha}f^{\beta}v^{*}_{\gamma\beta}(\mathbf{f})\,r_{\mathbf{f}}=\delta_{\alpha\gamma}. \quad (4)$$

In terms of the new variables the Hamiltonian (1) takes the form

$$H=H_0+\varepsilon H_1+\varepsilon^2 H_2 \quad (5)$$

where

$$H_0=\frac{p_\lambda^2}{2m}+\sum_{\mathbf{f}}A_f e^{i\mathbf{f}\boldsymbol{\lambda}}r_{\mathbf{f}}+\frac{1}{2}\sum_{\mathbf{f}}E(\mathbf{f})\,|\,r_{\mathbf{f}}\,|^2,$$

$$H_1=\sum_{\mathbf{f}}\{A_{\mathbf{f}}e^{i\mathbf{f}\boldsymbol{\lambda}}+E(\mathbf{f})\,r_{-\mathbf{f}}\}\,Q_{\mathbf{f}};$$

$$H_2=\frac{1}{2}\sum_{\mathbf{f}}E(\mathbf{f})\,Q_{\mathbf{f}}Q_{-\mathbf{f}}+\frac{1}{2}\sum E(f)\{P'_{-\mathbf{f}}-\frac{i}{\hbar}v_{\alpha\beta}(\mathbf{f})\,f^{\beta}J_{\alpha}\}$$
$$\times\{P'_{\mathbf{f}}+\frac{i}{\hbar}v^{*}_{\alpha\beta}(\mathbf{f})\,f^{\beta}J_{\alpha}\};$$

$$H_3=-\frac{1}{2}\sum_{\mathbf{f}}E(\mathbf{f})\left\{P'_{-\mathbf{f}}-\frac{iv_{\alpha\beta}(\mathbf{f})}{\hbar}f^{\beta}J_{\alpha}\right\}v^{*}_{\gamma\delta}(\mathbf{f})\{f^{\delta}\partial/\partial\lambda_{\gamma}$$
$$+\sum_{\mathbf{k}}k^{\delta}f^{\gamma}Q_{\mathbf{k}}P'_{\mathbf{k}}+\frac{i}{\hbar}\sum_{\mathbf{k}}f^{\delta}k^{\gamma}k^{\sigma}J_{\rho}v^{*}_{\sigma\rho}(\mathbf{k})\,Q_{\mathbf{k}}\}- \quad (6)$$
$$-\frac{1}{2}\sum_{\mathbf{f}}E(\mathbf{f})\,v^{*}_{\alpha\beta}(\mathbf{f})\left\{f^{\beta}\partial/\partial\lambda_{\alpha}+\frac{1}{\hbar}\sum_{\mathbf{k}}f^{\beta}k^{\alpha}k^{\sigma}J_{\rho}v^{*}_{\sigma\rho}(\mathbf{k})\,Q_{\mathbf{k}}\right.$$
$$\left.+\sum_{\mathbf{k}}k^{\alpha}f^{\beta}Q_{\mathbf{k}}P'_{\mathbf{k}}\right\}\left\{P'_{-\mathbf{k}}-\frac{i}{\hbar}v_{\varepsilon\delta}(\mathbf{f})\,f^{\varepsilon}J_{\delta}\right\}.$$

Here the following notation is used:

$$\mathbf{P}_{\lambda}=-i\hbar\partial/\partial\boldsymbol{\lambda},\quad P_{\mathbf{f}}=-i\partial/\partial Q_{\mathbf{f}},\quad \mathbf{J}=-i\hbar\partial/\partial\,\mathbf{q},$$

$$P'_{\mathbf{f}}=P_{\mathbf{f}}-\sum_{\alpha\beta}v^{*}_{\alpha\beta}(\mathbf{f})\,f^{\alpha}\sum_{\mathbf{k}}k^{\beta}r_{\mathbf{k}}P_{\mathbf{k}}. \quad (7)$$

The quantity $\mathbf{J}$ is the momentum of the whole system, and is an integral of the motion.

In the first approximation in ϵ, we obtain for the electronic function the expression

$$\varphi_n(\lambda,\ldots,Q_f\ldots)=\varphi_n(\lambda)+\varepsilon\sum_{m}{}'\frac{(H_1)_{mn}}{W_n^0-W_m^0}\varphi_m(\lambda), \quad (8)$$

where $\varphi_n(\lambda)$ and W_n^0 are non-self-consistent quantities of the zeroth approximation. The symbols $\psi_n(\lambda)$ and G_n will be used to denote self-consistent quantities.

The energy of the electron $W_n(\ldots Q_{\mathbf{f}}\ldots)$ depends on $Q_{\mathbf{f}}$ through perturbation theory corrections of the first, second, and third order, i.e., through ϵ, ϵ^2, and ϵ^3, it being obvious that the first-order correction $\epsilon(H_1)_{nn}$ vanishes. This leads to the definition

$$r_{\mathbf{f}}=-\frac{A_f}{E(\mathbf{f})}J_{\mathbf{f}}^{nn}, \quad (9)$$

where

$$J_{\mathbf{f}}^{nm}=(\varphi_n(\lambda),\ e^{i\mathbf{f}\boldsymbol{\lambda}}\varphi_m(\lambda)).$$

The motion of the oscillators is described by the equation

$$[\varepsilon^2\tilde{H}_2+\varepsilon^3\tilde{H}_3-(E'_{nN}-G_n)]\,\Phi'_{nN}=0, \tag{10}$$

where

$$\tilde{H}_2=(H_2)_{nn}+\sum{}'_m\frac{(H_1)_{nm}(H_1)_{mn}}{G_n-W^0_m}, \tag{11}$$

$$\tilde{H}_3=(H_3)_{nn}+\sum{}'_p\sum{}'_m\frac{(H_1)_{nm}(H_1)_{mp}(H_1)_{pn}}{(G_n-W^0_m)(G_n-W^0_p)}. \tag{12}$$

The last terms in (11) and (12) we denote by

$$\sum B_{fg}Q_fQ_g \text{ and } \sum B_{fgh}Q_fQ_gQ_h.$$

respectively.

In determining the energy E'_{nN} of the whole system and the corresponding wave function, we shall neglect the term of order ϵ^3, considering it to be one of the causes of quantum transitions between the states that are obtained. In this way we obtain

$$\varepsilon^2H_2\Phi_{nN}\,(\ldots Q_f\ldots)=(E_{nN}-G_n)\,\Phi_{nN}(\ldots Q_f\ldots), \tag{13}$$

where N is the set of quantum numbers of the oscillators. The first index in Φ_{nN} indicates that the motion of the oscillators occurs under the action of average field of an electron in the state n.

The unknown quantities, $v_{\alpha\beta}$ are determined from the following relationship:[9,10]

$$\sum_\alpha k^\alpha v_{\alpha\beta}(k)=\hbar^2r_kk^\beta/E(k)\,\mu^\beta, \tag{14}$$

where μ is the diagonalized effective mass tensor of the polaron

$$\mu^\alpha=\hbar^2\sum k^{\alpha2}|r_k|^2/E(k). \tag{15}$$

Taking (14) and (15) into account, we have

$$\tilde{H}_2=\tfrac{1}{2}\sum_\alpha J^2_\alpha/\mu^\alpha+\tfrac{1}{2}\sum_f E(f)(Q_fQ_{-f}+P'_fP'_{-f})+\sum_{f,g}B_{fg}Q_fQ_g, \tag{16}$$

$$\tilde{H}_3=i\hbar\,(\mathbf{V}\partial/\partial\boldsymbol{\lambda})_{nn}-\sum_f(\mathbf{V}f)\,v^*_{\alpha\beta}(f)\,f^\alpha J_\beta Q_f+i\hbar\sum_f(fV)\,Q_fP'_f+\sum_{fgh}B_{fgh}Q_fQ_gQ_h, \tag{17}$$

where

$$V^\alpha=J_\alpha/\mu^\alpha.$$

According to Tiablikov,[10] diagonalization of Eq. (16) is accomplished by a single orthogonal transformation by the matrix $a_{f,\nu}$:

$$Q_f=\sqrt{E(f)}\sum_\nu a_{f\nu}q_\nu,\quad P_f=\frac{1}{\sqrt{E(f)}}\sum_\nu a^*_{f\nu}P_\nu; \tag{18}$$

$$p_\nu=-i\partial/\partial q_\nu.$$

The matrix $a_{f\nu}$ is determined from the condition

$$E^2(f)\,a_{f\nu}+\sum_g\overline{B}_{-f,g}\,a_{g\nu}=\lambda^2_\nu a_{f\nu}, \tag{19}$$

where

$$\overline{B}_{fg}=\sqrt{E(f)\,E(g)}\;(B_{fg}+B_{gf});$$

q_ν and λ_ν are the new coordinates and frequencies of the field oscillators. Equation (19) has three eigenvalues λ_α (α = 1, 2, 3) which are equal to zero; thus

$$a_{f\alpha}=-i\hbar f^\alpha r_f/\sqrt{E(f)\,\mu^\alpha}. \tag{20}$$

It should be noted that the coordinates q_α corresponding to λ_α, are equal to zero. This means, that as a result of condition (3), three degrees of freedom of the field are transferred to the polaron and they are found in the translational motion of the latter.

After diagonalization, $\tilde{H}_2$ has the form

$$\tilde{H}_2=\tfrac{1}{2}\sum_\alpha J^2_\alpha/\mu^\alpha+\tfrac{1}{2}\sum{}'_\nu(p_\nu p_\nu+\lambda^2_\nu q_\nu q_{-\nu}). \tag{21}$$

The primes on the summation sign signify that terms with $\nu=\alpha$ are to be left out of the sum. It should be noted that μ^α, λ_ν and q_ν depend on the state of the electron and therefore should bear indices which correspond to the appropriate electronic state. We shall introduce the Bose operators ζ_ν and ζ^+_ν as follows:

$$q_\nu=\frac{1}{\sqrt{2\lambda_\nu}}(\zeta_\nu+\zeta^+_{-\nu}),\quad p_\nu=-i\sqrt{\frac{\lambda_\nu}{2}}(\zeta_{-\nu}-\zeta^+_\nu). \tag{22}$$

Then

$$\tilde{H}_2=\tfrac{1}{2}\sum_\alpha J^2_\alpha/\mu^\alpha+\sum{}'_\nu\lambda_\nu(\zeta^+_\nu\zeta_\nu+\tfrac{1}{2}) \tag{23}$$

The eigenfunctions and eigenvalues of Eq. (13) assume the form:

$$\Phi_{nNJ}=V^{-1/2}e^{iJq/\hbar}\prod_{\nu\neq\alpha}\Phi_{nn_\nu}(q_\nu), \tag{24}$$

$$E_{nNJ}=G_n+\varepsilon^2\sum_\alpha J^2_\alpha/2\mu^\alpha_n+\varepsilon^2\sum{}'_\nu\lambda^n_\nu(n_\nu+\tfrac{1}{2}). \tag{25}$$

For the wave function of the complete system we have

$$\psi_{nNJ}=\psi_n(\ldots,q_\nu\ldots)\,\Phi_{nNJ}. \tag{25'}$$

3. PROBABILITY OF A NONRADIATIVE TRANSITION

Quantum transitions will occur between the states given by Eq. (25′). These transitions come about because of the inaccuracy of the function (25′) and omission of the terms $\epsilon^3\widetilde{H}_3$ from the Hamiltonian.

The probability $P_{nn'}$ of a quantum transition per unit time between the initial state of the system nN and its final state n′N′ has the form:

$$P_{nn'} = \frac{2\pi}{\hbar}\,\mathrm{Av}_N \sum_{N'}\int d\Gamma\,|(n'N'|H - E_{nN}|nN)|^2\,\delta(E_{n'N'} - E_{nN}), \tag{26}$$

Here $d\Gamma$ is the number of states, in the energy interval $dE_{n'N'}$ of the final states. Summation over N′ is performed over all final oscillator states. Av_N denotes an average over the initial quantum states of the oscillators, N. The matrix element in (26), to an accuracy of quantities of the order ϵ^3, has the form:

$$\begin{aligned}(n', \ldots, n'_\nu \ldots |H - E_{nN}| n, \ldots, n_\nu \ldots) &= \varepsilon^3 \int \prod_\sigma{}' \Phi_{n'n_\sigma'} \Big\{ \sum_\nu{}' \lambda_\nu^n M_\nu^{n'n} (\zeta_{-\nu}^+ - \zeta_\nu) \\ &+ N^{nn'} \widetilde{H}_3 \Big\} \prod_\sigma{}' \Phi_{nn_\sigma} \prod_\sigma{}' dq_\sigma,\end{aligned} \tag{27}$$

$$\begin{aligned}M_\nu^{n'n} &= \int \psi_{n'}^*(\lambda)\, L_\nu^n(\lambda)\, d\lambda\,, \\ L_\nu^n(\lambda) &= \sum_p{}' \sum_f \frac{a_{f\nu} A_f \sqrt{E(f)}\, J_f^{pn}}{\sqrt{2\lambda_\nu^n}\,(G_n - W_p^0)}\,\varphi_p(\lambda)\,,\end{aligned} \tag{28}$$

where λ_ν^n is the lattice vibration frequency, $N^{nn'} = (\psi_{n'}, \psi_n)$ is the non-orthogonality integral of the self-consistent functions. To evaluate the sum (26) over all final oscillator states we make use of the integral form of the Dirac δ-function.

To simplify the calculation, let us change $a_{f\nu}$ into $\delta_{f\nu}$ and λ_ν into $\hbar\omega$. Let us also take it into account that in our case $N^{nn'} = 0$. Then after a series of simple transformations, we obtain:

$$\begin{aligned}P_{nn'} = -\frac{\varepsilon^6}{\hbar^2}\int d\Gamma \int_{-\infty}^{\infty} \exp\{(2\pi i\nu_0 + i\omega_a)\,u\}\,du\,\mathrm{Av}_N\,(N|V^{-1/2} \\ \times \sum_f (m_f^{n'n^*}\zeta_f^+ - m_{-f}^{n'n^*}\zeta_f) \prod_r \exp_{[-]}\Big\{\frac{i}{\hbar\sqrt{V}}\int_0^u (R_{r\zeta_r} e^{-i\omega s} \\ + R_{-r}\zeta_r^+ e^{i\omega s})_s ds\Big\} \times V^{-1/2} \sum_g (m_{-g}^{n'n_r}\zeta_g^+ e^{i\omega u} \\ - m_g^{n'n}\zeta_g e^{-i\omega u})|N),\end{aligned} \tag{29}$$

where

$$\begin{aligned}m_f^{n'n}/\sqrt{V} &= \frac{1}{\sqrt{2}}\,A_f E(f)\,(G_n - W_p^0)_{\mathrm{av}}^{-1} J_f^{n'n}, \\ R_f/\sqrt{V} &= \frac{E(f)}{\sqrt{2}}\,(r_{-f}^n - r_{-f}^{n'}), \\ \hbar\omega_a &= {}^1\!/_2 \sum_f E(f)\,|r_f^n - r_f^{n'}|^2, \\ h\nu_0 &= G_{n'} - G_n + {}^1\!/_2 \sum_\alpha J_\alpha^2\,(1/\mu_{n'}^\alpha - 1/\mu_n^\alpha).\end{aligned} \tag{30}$$

A quantity with the index "av" is a certain average value of the denominator in Eq. (28). The sign [−] indicates a reordering of the operators in the product, so that they are arranged, reckoning from right to left, in order of decreasing value of the index s.[4,11] In computing the average over the initial states N, the only terms retained in Eq. (29) are those which remain finite as $V \to \infty$.

Let us introduce the symbols

$$S = {}^1\!/_2 \sum_f A_f^2\,|J_f^{nn} - J_f^{n'n'}|^2 / E^2(f); \tag{31}$$

$$Z^2 = [(G_n - W_p^0)_{\mathrm{av}}^{-1}]^2 \sum_f A_f^2 E^2(f)\, J_f^{n'n} J_{-f}^{nn'}; \tag{32}$$

$$Y = (G_n - W_p^0)_{\mathrm{av}}^{-1} \sum_f A_f^2 J_{-f}^{n'n}\,(J_f^{n'n'} - J_f^{nn}). \tag{33}$$

The index n corresponds to the self-consistent state 1s, n′ to the self-consistent state 2p.

In terms of these new symbols one is led to the following result of averaging:

$$\begin{aligned}P_{nn'} = \Big(\frac{2\pi\epsilon^6}{\hbar^2\omega}\Big) \exp[-S(2\bar{n}+1) \mp il\varphi] \times \\ \times \Big\{\frac{Z^2}{2}\sqrt{\bar{n}(\bar{n}+1)}\,(I_{l-1}(z) + I_{l+1}(z)) + \frac{|Y|^2}{4}\,\bar{n}(\bar{n}+1) \times \\ \times (I_{l+2}(z) + I_{l-2}(z)) + |Y|^2[(\bar{n}+{}^1\!/_2)^2 + {}^1\!/_2\bar{n}(\bar{n}+1)]\,I_l(z) \\ - (\bar{n}+{}^1\!/_2)\sqrt{\bar{n}(\bar{n}+1)}\,|Y|^2\,(I_{l-1}(z) + I_{l+1}(z))\Big\},\end{aligned} \tag{34}$$

where

$$\begin{aligned}\bar{n} &= [\exp(\hbar\omega/kT) - 1]^{-1} l = 2\pi\nu_0/\omega, \\ \varphi &= \frac{i}{2}\ln\frac{\bar{n}+1}{\bar{n}}, \quad z = 2s\sqrt{\bar{n}(n+1)};\end{aligned} \tag{35}$$

$I_l(z)$ is Bessel's function with an imaginary argument. The probability depends on the momentum of the polaron through the quantity l.

Polarons obey the Maxwellian velocity distribution law; therefore the probability, averaged over the initial kinetic energy of the polaron, can be calculated from the equation:

$$\bar{P}_{nn'} = (2\pi\mu_n kT)^{-3/2} \int P_{nn'} \exp(-J^2/2\mu_n kT)\,d\mathbf{J}. \tag{36}$$

It can be evaluated approximately at low and high temperatures.

It should be noted that for the transition considered here Y = 0, and therefore Eq. (34) is simplified. Furthermore, it turns out that in the

state 2p differences among components in the effective mass tensor of the polaron are not large. To simplify the calculation of the integral (36), we introduce an average effective mass of the polaron in the excited state, representing it by the symbol $\mu_{n'}$.

At low temperatures, $I_{\ell-1}(z)$ turns out to be the larger of the two Bessel functions in Eq. (34). A simple calculation leads to the following expression:

$$\bar{P}_{nn'} = \omega K \exp\left(-\frac{\Delta G}{kT}\right) \times \left\{1 + \frac{3}{2}\frac{kT}{\hbar\omega}\frac{\mu_n - \mu_{n'}}{\mu_n}[\ln S - \psi(\gamma - 1)] + \ldots\right\}, \quad (37)$$

where

$$K = \frac{\pi}{(\hbar\omega)^2} Z^2 \frac{e^{-S} S^{\gamma-1}}{\Gamma(\gamma)} (\mu_{n'}/\mu_n)^{3/2};$$

$$\gamma = \frac{\Delta G}{\hbar\omega}; \quad \Delta G = G_{2p} - G_{1s}; \quad (38)$$

$\psi(\gamma)$ is the logarithmic derivative for Γ.

For the high temperature region, but at the same time with the restrictive condition:

$$1 \ll kT/\hbar\omega < S,$$

one can obtain an approximate expression for (36), by the method of steepest descent.[12] Let us take account of the fact that in this temperature range one can write

$$\bar{n} \approx kT/\hbar\omega, \quad z = 2S(\bar{n} + 1/2).$$

We then obtain

$$\bar{P}_{nn'} = \frac{\sqrt{\pi}}{\hbar^2\omega} Z^2 \sqrt{\frac{kT}{\hbar\omega}} \left(\frac{2\mu_{n'}}{\mu_n + \mu_n'}\right)^{3/2} S^{-1/2} \times \exp\left[-\frac{\Delta G}{2kT}\left(1 + \frac{\gamma}{2S}\right)\right] \quad (37')$$

$$\times \cosh\left(\frac{\gamma\hbar\omega}{2SkT}\right) \sigma^{-3/2}\left(1 - \frac{15}{4}\frac{kT}{\hbar\omega}\frac{1}{S}\left(\frac{\mu_n - \mu_{n'}}{\mu_n + \mu_{n'}}\right)^2 \sigma^{-2}\right),$$

where

$$\sigma = 1 + (\gamma/S)(\mu_n - \mu_{n'})/(\mu_n + \mu_{n'}).$$

4. CALCULATION OF THE PARAMETERS OF THE THEORY AND EVALUATION OF THE TRANSITION PROBABILITIES

For the ground state of the polaron, following Ref. 1, we have

$$\psi_{1s} = \frac{\alpha_1^{3/2}}{\sqrt{7\pi}}(1 + \alpha_1 r)\, e^{-\alpha_1 r}, \quad \alpha_1 = me^2c/2\hbar^2,$$
$$G_{1s} = -0.0535\ me^4c^2/\hbar^2, \quad (39)$$
$$\mu_{1s} = 5{,}8 \cdot 10^{-3}(me^2c/\hbar^2)^3 e^2c/\omega^2.$$

For the 2p state of the polaron, consistent with 1s, we have

$$\varphi_{2p} = (4!)^{-1/2}(2\alpha)^{3/2}(2\beta)^{4/2}(2\alpha r)\, e^{-2\beta\alpha r} Y_{10}(\theta),$$

where

$$\alpha = 0.6585me^2c/\hbar^2, \ 2\beta = 0{,}5146. \ W^0_{2p} = 0{,}0153me^4c^2/\hbar^2. \quad (40)$$

In the self-consistent 2p state, we have

$$\psi_{2p} = \frac{\alpha_2^{3/2}}{2\sqrt{6}} e^{-\alpha_2 r/2}(2\alpha_2 r)\, Y_{10}(\theta),$$
$$\alpha_2 = 0.3914me^2c/\hbar^2, \ G_{2p} = -0.0191me^4c^2/\hbar^2. \quad (41)$$

For the effective mass of the polaron in the excited states we can write:

$$\mu^1_{2p} = \mu^2_{2p} = 6{,}30 \cdot 2^{-10}(e^2c/\omega^2)\alpha_2^3;$$
$$\mu^3_{2p} = 2{,}69 \cdot 2^{-9}(e^2c/\omega^2)\alpha_2^3. \quad (42)$$

In view of the above, the average effective mass of the polaron in this state is equal to:

$$\mu_{2p} = (2\mu^1_{2p} + \mu^3_{2p})/3. \quad (42')$$

The ratio of the polaron effective masses in the two states is the same in all crystals and is equal to:

$$\mu_{1s}/\mu_{2p} = 16.51. \quad (43)$$

Calculations of Eqs. (31), (32), and (33) yield the following expressions:

$$S = \frac{e^2c\alpha_1}{\hbar\omega}\left\{0.2142 + 0.1957\tau - \frac{\tau}{14}\left[\frac{7 + 9\tau}{(1+\tau)^2} + \frac{11\tau^2 + 5\tau}{(1+\tau)^4} + \frac{6\tau^2 + 16\tau^3}{(1+\tau)^6} + \frac{15\tau^3}{(1+\tau)^7}\right]\right\}, \quad (44)$$

$$Z^2 = \frac{4}{3}\frac{e^2c\alpha_1(\hbar\omega)^3}{(1+\tau)^7}\left[\left(\frac{1}{G_{1s} - W^0_p}\right)_{\text{av}}\right]^2 \times \left(1 + \frac{7}{1+\tau} + \frac{185}{14(1+\tau)^2}\right), \quad (45)$$

where $\tau = \alpha_2/2\alpha_1$.

From Eqs. (44) and (45) we obtain

$$S = 0.0508\ me^4c^2/\hbar^3\omega, \quad (44')$$
$$Z^2 = 0.0156(\hbar\omega)^3 e^2c\alpha_1[(G_{1s} - W^0_p)^{-1}_{\text{av}}]^2. \quad (45')$$

To calculate the average indicated here, one can make use of Kessler's method.[13] This average value is of the order

$$(G_{1s} - W_{2p})^{-1},$$

if the energy of the states 2s, 2p, and 3s, consistent with 1s, are approximately equal to each other. Then one can write

$$Z^2 = 0.0567(\hbar\omega)^2/\gamma. \quad (45'')$$

For Eq. (37) we obtain

$$\bar{P}_{nn'} = \frac{1.917\cdot 10^{-3}\omega}{\gamma\sqrt{S}}\sqrt{\frac{kT}{\hbar\omega}}\left(1-\frac{1.148}{S}\frac{kT}{\hbar\omega}\right)$$
$$\times \cosh\left(\frac{0.338\hbar\omega}{kT}\right)\exp\left(-0.668\,\frac{\Delta G}{kT}\right). \qquad (37'')$$

Table I lists the values of the coefficient K of Eq. (38) for certain alkali-halide crystals.

Values of the probabilities of thermal excitation $\bar{P}_{nn'}$, arrived at from Eq. (37''), are presented in Table II (the probability is given in sec^{-1}).

TABLE I

	NaCl	KCl	KBr	KJ
K	$3.40\cdot 10^{-5}$	$7.42\cdot 10^{-5}$	$7.76\cdot 10^{-5}$	$8.39\cdot 10^{-5}$
$K\omega$	$1.66\cdot 10^{9}$	$2.96\cdot 10^{9}$	$2.37\cdot 10^{9}$	$2.15\cdot 10^{9}$

In Table II, the last two values ($T = 700°$ K) are less precise, since the criterion $kT/\hbar\omega < S$ does not hold very well.

TABLE II

T °K	NaCl	KCl	KBr	KJ
293	$5.39\cdot 10^{7}$	$3.38\cdot 10^{8}$	$5.78\cdot 10^{8}$	$7.60\cdot 10^{8}$
500	$4.19\cdot 10^{8}$	$1.22\cdot 10^{9}$	$1.44\cdot 10^{9}$	$1.45\cdot 10^{9}$
700	$0.94\cdot 10^{9}$	$1.91\cdot 10^{9}$	$1.74\cdot 10^{9}$	$1.40\cdot 10^{9}$

These tables show that at room temperature and at higher temperatures, the probability of thermal excitation of the polaron $1s \rightarrow 2p$ is significant. The transition into an excited state occurs approximately in a time $10^{-8} - 10^{-9}$ sec.

The author takes this opportunity to express his deep gratitude to S. V. Tiablikov for his interest in the work and valuable discussions during its course, and he also wishes to thank Iu. E. Perlin for discussion of the work and valuable criticism.

[1] S. I. Pekar, Исследования по электронной теории кристаллов (Investigations on the Electron Theory of Crystals), Moscow, 1951.

[2] J. Frenkel, Phys. Rev. **37**, 17; 1276 (1931).

[3] K. Huang and A. Rhys, Proc. Roy. Soc. **A204**, 406 (1950).

[4] M. Lax, Jour. Chem. Phys. **20**, 1752 (1952).

[5] M. A. Krivoglaz, J. Exptl. Theoret. Phys. (U.S.S.R.) **25**, 191 (1953).

[6] Iu. E. Perlin and M. M. Sharand, Уч. зап. Кишиневского ун-та (Science Notes, Kishinev State Univ.) **24**, 41 (1956).

[7] R. Kubo, Phys. Rev. **86**, 929 (1952).

[8] N. N. Bogoliubov, Укр. математич. журнал (Ukrainian Math. Jour.) **2**, 3 (1950).

[9] S. V. Tiablikov, J. Exptl. Theoret. Phys. (U.S.S.R.) **21**, 377 (1951).

[10] S. V. Tiablikov, Doctoral Dissertation, Moscow (1954).

[11] R. P. Feynman, Phys. Rev. **84**, 108 (1951).

[12] V. I. Smirnov, Курс высшей математики (A Course in Higher Mathematics), Vol. 3, p. 286 (1955).

[13] P. Kessler, Compt. rend. **240**, 1058 (1955).

Translated by J. J. Loferski
69

EFFECT OF INHOMOGENEITIES OF THE CRYSTAL LATTICE ON THE THERMODYNAMICS OF A GAS OF QUASI PARTICLES IN THE CRYSTAL

M. A. KRIVOGLAZ

Institute of Metal Physics, Academy of Sciences, Ukrainian S.S.R.

Submitted to JETP editor March 28, 1957

J. Exptl. Theoret. Phys. (U.S.S.R.) **34**, 355-370 (February, 1958)

Various types of quasi particles interacting among themselves or with static inhomogeneities of the crystal are considered. General formulas for the thermodynamic potential, valid for any type of particle and for an arbitrary law of interaction, are obtained by perturbation theory methods under the assumption that the interaction energy is not large. As an example an almost-degenerate Fermi gas of quasi particles (metal electrons) interacting with the crystal defects is considered. Interaction of the conductivity electrons with composition fluctuations leads in the case of alloys to a dependence of the electron part of the free energy, the electron chemical potential, the thermoelectron emission current, etc. on the long and short range order parameters. The ordering energies associated with the electron part of the free energy are of the same order of magnitude as the experimentally observed ordering energies. The vibrational part of the free energy has been determined for solid solutions in which both the masses of the atoms and their interaction energies are different.

As is well known (see, for example, Landau and Lifshitz[1]) the weakly excited states of a solid may be regarded as a superposition of elementary excitations which form a "gas" of weakly interacting quasi particles. The existence in the crystal of various inhomogeneities alters the properties of the elementary excitations (for example, their energy spectrum). The introduction of elementary excitations in a system which does not have translational symmetry is a much more complicated problem than their introduction in the case of an ideal crystal. Therefore for the investigation of a non-ideal crystal if the degree of inhomogeneity occurring in it is not great, it often turns out to be more convenient to introduce elementary excitations in an ideal crystal which serves as a "zero-order approximation" for the inhomogeneous crystal under discussion, and to take into account the effect of the inhomogeneities by means of a potential energy acting on them. In this case the problem of finding the partition function for the crystal is reduced to the problem of finding the partition function for the gas of quasi particles moving in an external potential field.

The inhomogeneities of the crystal are often practically stationary. Static inhomogeneities of such a type occur, for example, in solid solutions where they are associated with composition fluctuations, in piezoelectric crystals where they are associated with polarization fluctuations, etc. The potential energy of the quasi particles in such cases depends on the magnitude of the corresponding fluctuations. In other cases fields produced by the inhomogeneities of the lattice vary rapidly in time and it is necessary to take their dynamic character into account explicitly. Dynamic inhomogeneities occur, for example, as a result of vibrations of the atoms of the lattice, or as a result of the excitation of spin waves in ferromagnetics. The effect of such inhomogeneities on the quasi particles could be described in a number of cases by considering the action of a variable field on a system of particles. However, since in such cases time averaging must be performed, and often the reaction of the quasi particles on the inhomogeneities is important, such a method of treatment is usually inconvenient. It is much more convenient to consider that to each type of dynamic inhomogeneities there corresponds its own kind of quasi particles (phonons, ferromagnons, etc.) and their effect on the thermodynamics of the system of quasi particles under discussion can be determined by evaluating the partition function for the interacting quasi particles of different kinds.

Thus, in order to determine the effect of the inhomogeneities of the lattice on the thermodynamic quantities it is necessary to obtain the partition function for the gas of quasi particles subjected to the field of the static fluctuation inhomogeneities of the crystal, or interacting with another

system of quasi particles. In practice, it is more convenient to evaluate not the ordinary but the grand partition function which, as is well known, may be represented in the form

$$Z = \sum_{\ldots N_\alpha \ldots} \exp\left(\lambda \sum_\alpha \mu_\alpha N_\alpha\right) \mathrm{Sp}\, e^{-\lambda H}. \tag{1}$$

Here $\lambda = 1/kT$, N_α is the number of particles of type α, μ_α is their chemical potential, $H = H_0 + H_1$ is the Hamiltonian of the system (dependent on N_α), H_0 is the Hamiltonian of the system in the absence of static inhomogeneities and of interactions between the quasi particles, and H_1 is the interaction Hamiltonian. In the evaluation of the trace the summation is taken over the complete system of functions possessing the required symmetry (depending on the type of quasi particles). If the interaction energy is not great, one can use for the evaluation of Z the thermodynamic perturbation theory treating H_1 as a small perturbation. In so doing it is convenient to make use of Schwinger's expansion[2] for the trace of the exponential operator:

$$\mathrm{Sp}\exp[-\lambda(H_0 + H_1)] = \mathrm{Sp}\, e^{-\lambda H_0} - \lambda\, \mathrm{Sp}\, H_1 e^{-\lambda H_0} + \frac{\lambda^2}{2}\int_0^1 du\, \mathrm{Sp}\, H_1 e^{-\lambda H_0 u} H_1 e^{-\lambda H_0 (1-u)} + \cdots \tag{2}$$

Formula (2) has been used previously for the determination of the partition function of conduction electrons interacting with lattice vibrations[3] or with static inhomogeneities[4] in semiconductors. In the present paper we shall determine with the aid of formulas (1) and (2) the grand partition function (and the thermodynamic potential corresponding to it) for a system which is described by a Hamiltonian of quite a general form.

As an example we shall consider the interaction of metal conduction electrons with static inhomogeneities arising as a result of composition fluctuations in solid solutions or of fluctuations in magnetization of ferromagnetics near the Curie point. As a second example we shall consider the interaction of lattice vibrations with composition fluctuations.

1. GENERAL EXPRESSION FOR THE THERMODYNAMIC POTENTIAL

For the zero-order Hamiltonian H_0 we shall take the Hamiltonian of non-interacting particles consisting of the sum of terms corresponding to the individual particles. Then $H_1 = H - H_0$ will describe the interaction between the particles and also their interaction with the static inhomogeneities. It is convenient to solve the above many-body problem by making use of the second quantization representation obtained with the aid of single particle functions which are eigenfunctions of the Hamiltonians of the individual particles. In this representation the energy operator H_0 (defined up to a constant term) has the form

$$H_0 = \sum_\alpha \sum_k \varepsilon_{\alpha k} a^+_{\alpha k} a_{\alpha k}, \tag{3}$$

where α denotes the kind of particles, k is the set of quantum numbers characterizing the states of the individual particles, $\epsilon_{\alpha k}$ is the energy of the particle in the k-th state, and $a^+_{\alpha k}$ and $a_{\alpha k}$ are the particle creation and annihilation operators. These operators satisfy the commuation relation

$$a_{\alpha k} a^+_{\alpha' k'} \mp a^+_{\alpha k} a_{\alpha' k'} = \delta_{\alpha\alpha'}\delta_{kk'}. \tag{4}$$

Both here and below the upper sign should be taken in the case of Fermi statistics, and the lower sign in the case of Bose statistics.

The perturbation energy operator H_1 in the case of particles interacting with static inhomogeneities, or of particles of one kind interacting among themselves, may be written in the form

$$H_1 = \sum_{\alpha k} \sum_{i=1}^{l} [V_{\alpha k i}\, a^+_{\alpha k_1} \ldots a^+_{\alpha k_i} a_{\alpha k_{i+1}} \ldots a_{\alpha k_l} + V^*_{\alpha k i}\, a_{\alpha k_1} \ldots a_{\alpha k_i} a^+_{\alpha k_{i+1}} \ldots a_{\alpha k_l}], \tag{5}$$

where the constants $V_{k\ell i} = V_{\alpha k_1 \ldots k_\ell i}$ are determined by the nature of the quasi particles and of the static inhomogeneities and satisfy the conditions

$$V_{\alpha \ldots k_a \ldots k_b \ldots i} = V^*_{\alpha \ldots k_b \ldots k_a \ldots i} \quad \text{for} \quad 1 \leqslant a \leqslant i, \quad i < b \leqslant l.$$

The summation over αk is taken over all $k_1 \ldots k_\ell$ and over all α. In special cases expressions (5) may be considerably simplified since the $V_{\alpha k i}$ differ from zero only for special values of i satisfying certain conditions. In a number of cases H_1 may be a sum of expressions (5) corresponding to different ℓ. However, since in the evaluation of Z up to the second order inclusively the individual terms of H_1 enter additively, we shall restrict ourselves to a consideration of H_1 of type (5) [or (6)], bearing in mind that corrections corresponding to terms with different ℓ may be simply added.

In the case of interaction of quasi particles of different kinds with each other (and also in the case of interaction with static inhomogeneities if

quasi particles of one kind can transform into quasi particles of a different kind), H_1 has the form

$$H_1 = \sum_{\alpha<\beta} \sum_{k\varkappa} \sum_{i=1}^{l} \sum_{j=1}^{m} [V_{\alpha k i \beta \varkappa j} a^+_{\alpha k_1} \ldots a^+_{\alpha k_i} a_{\alpha k_{i+1}} \ldots a_{\alpha k_l} a^+_{\beta \varkappa_1} \ldots a^+_{\beta \varkappa_j} a_{\beta \varkappa_{j+1}} \ldots a^+_{\beta \varkappa_m} + V^*_{\alpha k i \beta \varkappa j} a_{\alpha k_1} \ldots a_{\alpha k_i} a^+_{\alpha k_{i+1}} \ldots a^+_{\alpha k_l} a_{\beta \varkappa_1} \ldots a_{\beta \varkappa_j} a^+_{\beta \varkappa_{j+1}} \ldots a^+_{\beta \varkappa_m}, \tag{6}$$

where κ_a denote quantum numbers of quasi particles of type β

$$V_{\alpha k i \beta \varkappa j} = V_{\alpha k_1 \ldots k_l i, \beta \varkappa_1 \ldots \varkappa_m j},$$

$$V_{\alpha_a \ldots k_a \ldots k_b \ldots i, \beta \ldots \varkappa_c \ldots \varkappa_d \ldots j} = V^*_{\alpha \ldots k_b \ldots k_a \ldots i, \beta \ldots \varkappa_d \ldots \varkappa_c \ldots j}$$

with $1 \le a \le i$, $i < b \le l$, $1 \le c \le j$, $j < d \le m$. Summation over $k\kappa$ is taken over all $k_1 \ldots k_l$, $\kappa_1 \ldots \kappa_m$.

Let us now evaluate by means of formulas (1) and (2) the grand partition function up to the second order perturbation theory terms inclusively, and also the corresponding thermodynamic potential

$$\Omega = \Omega_0 + \Omega_1 + \Omega_2 + \ldots = -kT \ln Z = -kT \ln Z^{(0)} - kT \frac{Z^{(1)}}{Z^{(0)}} - kT \left[\frac{Z^{(2)}}{Z^{(0)}} - \frac{1}{2} \left(\frac{Z^{(1)}}{Z^{(0)}} \right)^2 \right] - \ldots \tag{7}$$

In carrying out the above calculation we shall evaluate the traces with the aid of the complete system of eigenfunctions of the operator H_0 in the second quantization representation. These functions are specified by the occupation numbers

$$n_{\alpha k} = a^+_{\alpha k} a_{\alpha k}; \quad N_\alpha = \sum_k n_{\alpha k}. \tag{8}$$

It is convenient to use the grand partition function and the second quantization representation because in this case the evaluation of the trace in (1) and the summation over N_α reduces to an elementary summation over all possible values of $n_{\alpha k}$. Thus for $Z^{(0)}$ one immediately obtains from (1), (3), and (8) the well-known expression (see, for example, Landau and Lifshitz[1]):

$$Z^{(0)} = \prod_\alpha \prod_k [1 \pm \exp \lambda (\mu_\alpha - \varepsilon_{\alpha k})]^{\pm 1}. \tag{9}$$

In evaluating the first order corrections in the case of interaction with static inhomogeneities, it should be taken into account that the diagonal matrix elements in (5) differ from zero only if to each annihilation operator there corresponds a creation operator with the same α and k, i.e., only those terms are important for which $i = l/2$ (l should be even), and which have the same sets of numbers $k_1 \ldots k_i$ and $k_{i+1} \ldots k_l$. Evaluating Ω_1 by means of formulas (7), (1) — (3), (5), and (8) we obtain

$$\Omega_{1\,st} = -kT \frac{Z^{(1)}_{st}}{Z^{(0)}} = \frac{1}{Z^{(0)}} \times \sum_{\ldots N_\alpha \ldots} \exp \left(\lambda \sum_\alpha \mu_\alpha N_\alpha \right) \mathrm{Sp} [H_1 \exp (-\lambda H_0)] = i! \sum_{\alpha k}{}' V'_{\alpha k i} [\bar{n}_{\alpha k_1} \ldots \bar{n}_{\alpha k_i} + (1 \mp \bar{n}_{\alpha k_1}) \ldots (1 \mp \bar{n}_{\alpha k_i})], \tag{10}$$

where $i = l/2$, $V'_{\alpha k l} = V_{\alpha k_1 \ldots k_i k_1 \ldots k_i}$ and $\bar{n}_{\alpha k}$ are the mean occupation numbers

$$\bar{n}_{\alpha k} = [\exp \lambda (\varepsilon_{\alpha k} - \mu_\alpha) \pm 1]^{-1}. \tag{11}$$

If H_1 is given by formula (6) then Ω_1 is determined in a similar manner:

$$\Omega_{1d} = i!j! \sum_{\alpha<\beta} \sum_{k\varkappa}{}' V'_{\alpha k i \beta \varkappa j} [\bar{n}_{\alpha k_1} \ldots \bar{n}_{\alpha k_i} \bar{n}_{\beta \varkappa_1} \ldots \bar{n}_{\beta \varkappa_j} + (1 \mp \bar{n}_{\alpha k_1}) \ldots (1 \mp \bar{n}_{\alpha k_i}) (1 \mp \bar{n}_{\beta \varkappa_1}) \ldots (1 \mp \bar{n}_{\beta \varkappa_j})], \tag{12}$$

where

$$i = l/2, \; j = m/2, \; V'_{\alpha k i \beta \varkappa j} = V_{\alpha k_1 \ldots k_i k_1 \ldots k_i i, \alpha \varkappa_1 \ldots \varkappa_j \varkappa_1 \ldots \varkappa_j j}.$$

Determining further on the correction Ω_2 to the operators (5) and (6) we obtain

$$\Omega_{2\,st} = -\lambda \sum_{\alpha k} \sum_{i=1}^{l} (1 + \delta_{i,l/2})\, i!\, (l-i)!\, |V_{\alpha k i}|^2 \times \int_0^1 du\, (1 \mp \bar{n}_{\alpha k_1}) \ldots (1 \mp \bar{n}_{\alpha k_i}) \times \bar{n}_{\alpha k_{i+1}} \ldots \bar{n}_{\alpha k_l} \exp [-\lambda (\varepsilon_{\alpha k_1} + \ldots + \varepsilon_{\alpha k_i} - \varepsilon_{\alpha k_{i+1}} - \ldots - \varepsilon_{\alpha k_l}) u]; \tag{13}$$

$$\Omega_{2st} = -\lambda \sum_{\alpha<\beta} \sum_{k\varkappa} \sum_{i=1}^{l} \sum_{j=1}^{m} (1 + \delta_{i,l/2})(1 + \delta_{j,m/2})\, i!\, (l-i)!\, j!\, (m-j)! \times |V_{\alpha k l \beta \varkappa j}|^2 \int_0^1 du\, (1 \mp \bar{n}_{\alpha k_1}) \ldots (1 \mp \bar{n}_{\alpha k_i}) \bar{n}_{\alpha k_{i+1}} \ldots \bar{n}_{\alpha k_l} (1 \mp \bar{n}_{\beta \varkappa_1}) \ldots (1 \mp \bar{n}_{\beta \varkappa_j}) \bar{n}_{\beta \varkappa_{j+1}} \ldots \bar{n}_{\beta \varkappa_m} \exp [-\lambda (\varepsilon_{\alpha k_1} + \ldots + \varepsilon_{\alpha k_i} - \varepsilon_{\alpha k_{i+1}} \ldots - \varepsilon_{\alpha k_l} + \varepsilon_{\beta \varkappa_1} + \ldots \varepsilon_{\beta \varkappa_j} - \varepsilon_{\beta \varkappa_{j+1}} - \ldots - \varepsilon_{\beta \varkappa_m}) u]. \tag{14}$$

In summing over $\ldots k_a \ldots k_b \ldots$ ($1 \leq a \leq i$, $i < b \leq \ell$) in formulas (13) and (14), the terms with $k_a = k_b$ (or $\kappa_a = \kappa_b$) should be excluded.

The above general formulas for the corrections to Ω will be applied below to various physical systems. In addition to the examples considered below they may be employed for the investigation of the effect on the thermodynamics of spin waves in ferromagnetics of their interaction with fluctuations in composition and in order parameters, with conduction electrons and with lattice vibrations. They can also be used for the investigation of the effect of anharmonicity on the thermodynamics of the phonon gas, for the determination of corrections to the thermodynamic potential associated with the interaction of atoms in a mixture of different gases (for example, He^3-He^4), etc.

2. INTERACTION OF A STRONGLY DEGENERATE GAS OF FERMI QUASI PARTICLES WITH CRYSTAL INHOMOGENEITIES

As the first example, we consider a system of Fermi quasi particles interacting with static crystal inhomogeneities. We suppose that the interaction of the particles with each other may be neglected and that the gas is in a nearly completely degenerate state. The results obtained on solving such a problem may be applied to the investigation of the effect on the thermodynamics of the crystal of the interaction of metal conduction electrons with static inhomogeneities. In this case one can consider either the conduction electrons in a single-electron approximation, or (more accurately) the Fermi quasi particles obtained after eliminating the Coulomb interaction between the electrons. The screened Coulomb interaction of such particles with one another, and their interaction with the collective oscillations of the electron plasma, are both small and their effect on the thermodynamics of the electrons may be taken into account separately by means of formulas (13) and (14).

We expand the potential energy of interaction of a particle with the static inhomogeneities into a Fourier series:

$$V(r) = \sum_{\varkappa} (V_\varkappa e^{i\varkappa r} + V_\varkappa^* e^{-i\varkappa r}); \quad V_{-\varkappa} = V_\varkappa^*, \qquad (15)$$

where the vector κ takes on values determined by the conditions at the crystal boundary. (Terms corresponding to κ and to $-\kappa$ are obviously the same.) We shall choose the potential energy in the zero-order approximation in such a way that $V_K = 0$ for $\kappa = 0$. Going over to the second-quantization representation we find that the Hamiltonian of the system in the case under discussion has the form

$$H = H_0 + H_1 = \sum_{\mathbf{k}} \varepsilon_{\mathbf{k}} a_{\mathbf{k}}^+ a_{\mathbf{k}} + \sum_{\varkappa} \sum_{\mathbf{k}} [V_{\varkappa \mathbf{k}} a_{\mathbf{k}}^+ a_{\mathbf{k}-\varkappa'} + V_{\varkappa \mathbf{k}}^* a_{\mathbf{k}} a_{\mathbf{k}-\varkappa'}^+]. \qquad (16)$$

Here $\mathbf{k}$ is the propagation vector (not in reduced form) of the quasi particle; $\epsilon_{\mathbf{k}}$ is its energy; $V_{\kappa \mathbf{k}} = V_\kappa p_{\kappa \mathbf{k}}$ where $p_{\kappa \mathbf{k}}$ is the matrix element of the function $\exp(i\kappa \cdot \mathbf{r})$ formed using the single-particle wave functions corresponding to the propagation vectors $\mathbf{k}$ and $\mathbf{k} - \kappa'$ ($p_{\kappa \mathbf{k}} \sim 1$), $\kappa' = \kappa - 2\pi \mathbf{K}_\delta$ where the reciprocal lattice vector $\mathbf{K}_\delta$ is chosen in such a way as to make the vectors $\mathbf{k}$ and $\mathbf{k} - \kappa'$ lie in one cell. For the sake of simplicity in the Hamiltonian (16) terms are omitted which correspond to virtual transitions between different energy zones. This approximation holds if the separation between the zones is considerably larger than the Fermi energy. We note that taking into account the terms mentioned above does not alter the qualitative conclusions reached below.

Since for $\kappa = 0$, $V_K = 0$ and $V_{\kappa \mathbf{k}} = 0$ (i.e., in the notation of the preceding section, $V_{\alpha \mathbf{k}_1 \mathbf{k}_2} = 0$), then it follows from (10) that the first order correction Ω_1 reduces to zero. Evaluating the second order correction by means of formulas (13), (16) and taking into account the fact that in the new notation $\mathbf{k}_1 \to \mathbf{k}$, $\mathbf{k}_2 \to \mathbf{k} - \kappa'$, $V_{\alpha \mathbf{k}_1 \mathbf{k}_2} \to V_{\kappa \mathbf{k}}$ we obtain

$$\Omega \approx \Omega_0 + \Omega_2 = \Omega_0 - 2g\lambda \sum_{\varkappa} \sum_{\mathbf{k}} |V_{\varkappa \mathbf{k}}|^2 \bar{n}_{\mathbf{k}} (1 - \bar{n}_{\mathbf{k}-\varkappa'}) \times \int_0^1 \exp[\lambda (\varepsilon_{\mathbf{k}} - \varepsilon_{\mathbf{k}-\varkappa'}) u] du. \qquad (17)$$

Here Ω_0 is the thermodynamic potential (expressed in terms of the variables v, T, μ) of the system of Fermi quasi particles in an ideal crystal, while the factor g takes into account the spin of the particles and in the case of electrons is equal to 2. The sum over $\mathbf{k}$ in the second term of formula (17) may be replaced by integration over $(v/8\pi^3)d\mathbf{k}$, where v is the volume of the crystal, and similarly in the case of the summation over κ. The integration over $\mathbf{k}$ may be carried out in the limiting cases of weak and strong degeneracy of the Fermi gas. In the case of weak degeneracy one gets a result which had been obtained earlier by Krivoglaz and Rybak.[4] In the case of almost complete degeneracy when $\mu/kT \gg 1$ in the evaluation of the sum over $\mathbf{k}$ and of the integral over u

$$J(\varkappa) = \lambda \sum_{\mathbf{k}} |p_{\varkappa \mathbf{k}}|^2 \bar{n}_{\mathbf{k}} (1 - \bar{n}_{\mathbf{k}-\varkappa'}) \int_0^1 \exp[\lambda (\varepsilon_{\mathbf{k}} - \varepsilon_{\mathbf{k}-\varkappa'}) u] du = \frac{v}{8\pi^3} \int d\mathbf{k} |p_{\varkappa \mathbf{k}}|^2 \frac{\bar{n}_{\mathbf{k}} - \bar{n}_{\mathbf{k}-\varkappa'}}{\varepsilon_{\mathbf{k}-\varkappa'} - \varepsilon_{\mathbf{k}}} \qquad (18)$$

one may expand asymptotically in powers of kT/μ and limit oneself to the first non-vanishing term of the expansion.

It is not difficult to obtain an explicit expression for $J(\varkappa)$ in the case when the dependence of $|p_{\varkappa\mathbf{k}}|^2$ on $\mathbf{k}$ may be neglected ($|p_{\varkappa\mathbf{k}}|^2 = |p_{\varkappa\mathbf{k}}|^2$) and when, moreoever, $\epsilon_{\mathbf{k}}$ depends quadratically on $\mathbf{k}$: $\epsilon_{\mathbf{k}} = \hbar^2k^2/2m$ where m is the effective mass of the Fermi quasi particles. Carrying out a simple calculation, we find that in this case

$$J(\varkappa) = \frac{v}{4\pi^2}\frac{mk_0}{\hbar^2}|p_\varkappa|^2\left(1 + \frac{4k_0^2 - \varkappa'^2}{4k_0\varkappa'}\ln\frac{2k_0+\varkappa'}{|2k_0-\varkappa'|}\right), \quad (19)$$

$$k_0 = \sqrt{2\mu m}/\hbar = \sqrt{6\pi^2 N_e/gv};$$

k_0 is the boundary propagation vector of the degenerate Fermi gas, N_e is the number of Fermi quasi particles. The derivative of the function (19) with respect to $\varkappa$ has a discontinuity at the point $\varkappa = 2k_0$. This singularity, as well as the singularity of the function $\bar{n}_{\mathbf{k}}$ at absolute zero, is associated with the asymptotic nature of the expression obtained above and disappears in the exact expression.

In the general case of arbitrary dependence of $\epsilon_{\mathbf{k}}$ on $\mathbf{k}$ it is impossible to carry out the evaluation of $J(\varkappa)$ for arbitrary $\varkappa$. One can only note that in the adopted approximation $J(\varkappa)$ does not depend on λ, and one can also find the expression in the limiting case of small $|\varkappa'|$:

$$J(\varkappa) = \frac{v}{8\pi^3}S(\mu)\overline{|p_{\varkappa\mathbf{k}}|^2}. \quad (20)$$

Here $S(\epsilon) = d\omega(\epsilon)/d\epsilon$ where $\omega(\epsilon)$ is the volume of $\mathbf{k}$ space contained inside the surface $\epsilon_{\mathbf{k}} = \epsilon$ while the bar denotes averaging over the surface $\epsilon_{\mathbf{k}} = \mu$.

As is well known, small changes in the thermodynamic potentials, expressed in appropriate variables, are all the same (see, for example, Landau and Lifshitz[1]). This means that the correction Ω_2 expressed in terms of the variables T, v, and μ_α coincides with the correction to the free energy F_2 expressed in terms of the variables T, v, N_α. Therefore, it follows from formulas (17) and (18) that the expression for the free energy may be written in the form

$$F_\phi \approx F_0 + F_2 = F_0 - (gv/4\pi^3)\int J(\varkappa)|V_\varkappa|^2\,d\varkappa. \quad (21)$$

Here one should replace $|V_\kappa|^2$ in (21) by its average over the statistical ensemble.

Static inhomogeneities should play an essential role in alloys. In this case the inhomogeneities are caused by fluctuations in the concentrations of the components of the alloy. Let us consider a binary alloy AB which in the general case may be in an ordered state. Let us suppose that the atomic sizes are almost the same so that the geometric distortions of the crystal lattice can be neglected. It is convenient to choose for the zero-order approximation the completely ordered alloy composed of effective atoms whose potential energy of interaction with the Fermi quasi particles is equal to the average potential energy of interaction of atoms situated at lattice points of a given kind. Then the potential energy of the perturbation associated with the inhomogeneities of concentrations may be written in the following form:

$$V(\mathbf{r}) = \sum_{s=1}^{N/\nu}\sum_{\gamma=1}^{\nu}[c_{s\gamma}V_A(\mathbf{r}-\mathbf{R}_{s\gamma}) + (1-c_{s\gamma})V_B(\mathbf{r}-\mathbf{R}_{s\gamma}) - \bar{c}_\gamma V_A(\mathbf{r}-\mathbf{R}_{s\gamma}) - (1-\bar{c}_\gamma)V_B(\mathbf{r}-\mathbf{R}_{s\gamma})]. \quad (22)$$

Here s is the index of the crystal cell; γ is the index of the lattice point in the cell; N is the number of atoms in the crystal, ν is the number of lattice points in the cell; $\mathbf{R}_{s\gamma}$ is the vector drawn from the origin to the lattice point γ in the s-th cell; $c_{s\gamma} = 1$ if an atom A is situated at the lattice point $s\gamma$, and $c_{s\gamma} = 0$ if an atom B is situated there; $\bar{c}_\gamma$ and $1 - \bar{c}_\gamma$ are atomic concentrations of atoms A and B at lattice points of type γ; V_A and V_B are potential energies of interaction with atoms A and B respectively.

It follows from (22) that the Fourier component of the potential energy V_κ is equal to

$$V_\varkappa = \frac{1}{2v}\int V(\mathbf{r})\exp(-i\varkappa\mathbf{r})\,d\tau = \frac{1}{v_a}(f_A - f_B)c_\varkappa, \quad (23)$$

where

$$c_\varkappa = c_{\varkappa'} = \frac{1}{2N}\sum_s\sum_\gamma(c_{s\gamma} - \bar{c}_\gamma)\exp(-i\varkappa'\mathbf{R}_{s\gamma});\ c_{s\gamma} - \bar{c}_\gamma = \sum_{\varkappa'}[c_{\varkappa'}\exp(i\varkappa'\mathbf{R}_{s\gamma}) + c^*_{\varkappa'}\exp(-i\varkappa'\mathbf{R}_{s\gamma})]; \quad (24)$$

$$f_A = \int V_A(\mathbf{r})\exp(-i\varkappa\mathbf{r})\,d\tau;\ f_B = \int V_B(\mathbf{r})\exp(-i\varkappa\mathbf{r})\,d\tau, \quad (25)$$

$v_a = v/N$ is the atomic volume. The quantities c_κ obviously satisfy the condition

$$\sum_{\varkappa'}|c_\varkappa|^2 = \frac{1}{4N}\sum_s\sum_\gamma(c_{s\gamma} - \bar{c}_\gamma)^2 = \frac{1}{4\nu}\sum_{\gamma=1}^{\nu}\bar{c}_\gamma(1-\bar{c}_\gamma). \quad (26)$$

It may be seen from formulas (21) and (23) that the correction to the free energy is determined by the magnitude of the mean values of the squares of the Fourier components of the concentration fluctuations. Multiplying the expression (24) for c_κ by the complex conjugate expression we obtain

$$\overline{|c_{\varkappa}|^2} = \frac{1}{4\nu N}\sum_{\gamma=1}^{\nu}\bar{c}_{\gamma}(1-\bar{c}_{\gamma}) - \frac{1}{4N}\sum_{\rho\neq 0}\cos(\varkappa'\rho)\,\varepsilon(\rho), \qquad (27)$$

where the vectors $\rho = \mathbf{R}_{s'\gamma'} - \mathbf{R}_{s\gamma}$ take on the values of all the radius vectors of the lattice points and

$$\varepsilon(\rho) = -\frac{1}{\nu}\sum_{\gamma=1}^{\nu}{}^{(\rho)}\overline{(c_{s\gamma}c_{s'\gamma'} - \bar{c}_{\gamma}\bar{c}_{\gamma'})}. \qquad (28)$$

The quantities $\epsilon(\rho)$ are the parameters of correlation between the occupancy by atoms A of lattice points separated from one another by a distance ρ (more accurately they are the average values of these parameters over different kinds of lattice points separated by a distance ρ). These quantities may be determined on the basis of x-ray or neutron data.[5] We note that if we can neglect the scattering associated with geometric distortions of the lattice and with thermal vibrations then the quantity $|\overline{c_{\kappa}}|^2$ is proportional to the intensity of diffuse scattering of x-rays or of neutrons divided by the square of the difference between the atomic scattering factors for atoms A and B.

Substituting (23) into (27) and (21) we find that the electron part of the free energy of the alloy up to the second order perturbation theory terms may be written in the form

$$F_{\Phi} = F_0 - a_0\frac{1}{\nu}\sum_{\gamma=1}^{\nu}\bar{c}_{\gamma}(1-\bar{c}_{\gamma}) + \sum_{\rho\neq 0}a_{\rho}\varepsilon(\rho), \qquad (29)$$

where

$$a_0 = \frac{g}{16\pi^3 v_a}\int |f_A - f_B|^2 J(\varkappa)\,d\varkappa;$$
$$a_{\rho} = \frac{g}{16\pi^3 v_a}\int |f_A - f_B|^2 J(\varkappa)\cos\varkappa'\rho\,d\varkappa. \qquad (30)$$

The electron part of the zero-order free energy F_0 is defined as the free energy of the electron gas in an ideal periodic crystal made up of effective atoms, and depends only on the long-range parameters (on the quantities $\bar{c}_{\gamma}$), but not on the correlation parameters. In the case of absence of long-range order (disordered alloys), F_0 may be considered to be independent of the temperature (if one neglects a small term proportional to T^2 which provides a linear term in the heat capacity of the metal). However, in this case the last term in (29) still depends on the temperature due to the correlation parameters $\epsilon(\rho)$. For the same reason the electron chemical potential $\mu = dF/dN_e$ also depends on the temperature (in defining F and μ, we adopt as zero energy the energy of the electron at the bottom of the conduction band of a disordered crystal composed of effective atoms). The dependence of μ on the correlation parameters must lead to a change in alloy properties such as contact potential, thermoelectron emission current, etc., when the short-range order is changed. Thus, the magnitude of the thermoelectron emission current J from a metal is given, as is well known,[6] by the formula

$$J = D\frac{m_e k^2 |e|}{2\pi^2\hbar^3}T^2\exp\frac{\mu-\chi}{kT}. \qquad (31)$$

Here m_e is the electron mass (in vacuo), D is the transmission coefficient of electrons from vacuum into the metal, χ is the energy difference between an electron at rest in vacuo and at the bottom of the conduction band.

In order to estimate the change in J when short-range order is established, one may set $|\partial F'/\partial N_e| \sim |F/N_e|$ and evaluate the constants a_0 and a_{ρ} by making use of data on the residual electrical resistance of alloys. Thus, for example, by utilizing the estimate of the matrix element of the perturbing energy for Au Ag alloys (see Bethe and Sommerfeld,[7] §43) we shall find that $|f_A - f_B|^2 \sim 10^{-2}\mu^2 v_a^2$ for $\kappa \sim k_0$. Carrying out the integration in formula (30) for a_0 over the volume of the first cell of the reciprocal lattice (this will give an underestimate of the result), and ultilizing expression (19) for $J(\kappa)$, we obtain $a_0 \sim 10^{-2}\mu N_e$, i.e., $a_0/N_e \sim 0.1$ ev. Because of the factors $\cos(\kappa'\cdot\rho)$ in the integrand of formula (30), the quantities a_{ρ} must be somewhat smaller and may be negative. For a number of disordered alloys the correlation parameters $\epsilon(\rho)$ for the first few coordinative spheres are $\sim 10^{-12}$. Since kT $\sim$ 0.1 ev, and the coordination number is $\sim$ 10, it can be seen from (31) that, if the change in $\epsilon(\rho)$ is of the same order as $\epsilon(\rho)$ itself, the change in J, in establishing or destroying short-range order in the solution, may amount to $\sim$ 0.1J. The change in the contact potential, which is equal to the change in the chemical potential, may in this case amount to $\sim 10^{-2}$ ev. For the same change in $\epsilon(\rho)$, greater effects can be expected, generally speaking, in the case of alloys with a large residual resistance. A particularly large change in μ in disordered solutions can be expected during the early stages of decay (during aging) when large regions appear in the crystal with a very high degree of short-range order.

In the commonly employed theory of alloys, which is based on the approximation of pair interactions, and which does not take into account collective degrees of freedom, the coefficient Nzw/2, (where w is the energy of ordering and z is the

coordination number), appears in the expression for the total energy in front of the correlation parameter for the first coordinative sphere. For the majority of alloys $w \sim 0.01 - 0.1$ ev, i.e., zw is of the same order of magnitude as the corresponding coefficient $za_{\rho 1}/N_e$ in the electron part of the free energy. Thus, contrary to the rather widely held opinion,[6] the change in the electron part of the free energy may play a very essential role in the appearance of short-range (and also of long-range) order in the alloy.

The change in the long-range order in the alloy may affect the electron part of the free energy and the properties of the alloy discussed above considerably more than a change in the short-range order. In this case the concentrations are different for lattice points of different kinds, and the potential energy of the electrons in the zero-order approximation, and consequently also F_0, depend on the degree of long-range order. In the approximation of strongly-bound and weakly-bound electrons, the dependence of the energy spectrum of the zero-order approximation on the degree of long-range order (which enables us to determine F_0) has been obtained by Smirnov.[8] The terms in F_0 containing the degree of long-range order are proportional to the square of the difference $V_A - V_B$ (and not to the difference itself), so that in order to investigate the effect of order, even for small $V_A - V_B$, it is necessary to take into account not only F_0, but also the second term in (29).

A particularly sharp change in the electron part of the free energy can be expected near the temperature of the transition of the second kind into the ordered state, and also near the critical point on the decay curve. In such cases the second derivatives of the free energy with respect to the degree of long-range order, or with respect to the concentration, vanish, and anomalously large fluctuations occur in the degree of long-range order or in the composition, respectively.[9,10] For the sake of simplicity let us consider a binary solid solution undergoing ordering, which contains in an elementary cell of the ordered crystal one lattice point of the first kind and one of the second kind (for example, crystals of the type NaCl or of the type of β-brass). In this case the quantities $c_{s\gamma}$ can be written in the form $c_{s1} = c_s + \eta_s/2$, $c_{s2} = c_s - \eta_s/2$. The average values of the quantities c_s and η_s, taken over a large number of cells, evidently coincide with the concentration of atoms A and with the long-range order η, which are related to the concentrations $\bar{c}_\gamma$ by the equations: $\bar{c}_1 = c + \eta/2$, $\bar{c}_2 = c - \eta/2$. For small $\kappa' = \kappa - 2\pi \times K_\delta$ (K_δ is a vector of the reciprocal lattice of the disordered alloy) the quantities $c_{s\gamma}$ in formula (24) for c_κ can be approximately replaced by the quantities c_s, since $\exp(-i\kappa' \cdot R_{s\gamma})$ changes appreciably only over distances which extend over a large number of lattice constants, while the quantities $\pm \eta_s/2$ mutually cancel within the boundaries of a cell. On the other hand, for values of κ close to $2\pi K'_\delta$ (K'_δ is the vector of the reciprocal lattice which appears in the ordered alloy), the quantities c_s compensate each other [since the factors $\exp(-2\pi i K'_\delta \cdot R_{s\gamma})$ have different signs for lattice points of different kinds in a cell], and one must substitute $\eta_s/2$ in place of $c_{s\gamma}$ in (24). Thus, for small $\kappa' = \kappa - 2\pi K_\delta$ or $\kappa'' = \kappa - 2\pi K'_\delta$, the average values of $|c_\kappa|^2$ can be evaluated as average values of the squares of the moduli of the Fourier components of the fluctuations in the composition or in the degree of long-range order. The latter have been evaluated by the author[10] for solid solutions in connection with the problem of the diffuse scattering of x-rays or of neutrons. Making use of the results given in that paper we find that in the case of cubic crystals in the neighborhood of a point of phase transition of the second kind for $|\kappa''| \ll 1/d_0$:

$$\overline{|c_\kappa|^2} = {}^1/_4 \overline{|\eta_\kappa|^2} = (kT/16v)\,[\varphi_{\eta\eta} - \varphi^2_{c\eta}/\varphi_{cc} + \alpha\kappa''^2]^{-1}; \quad (32)$$

where φ_{cc}, $\varphi_{\eta\eta}$, and $\varphi_{c\eta}$ are the second derivatives of the free energy (and not only of its electron part) per unit volume with respect to c and η; α may be taken as constant in the neighborhood of the transition point and on the order of[9] $N_0 k T_0 d_0^2$, where N_0 is Avogadro's number, T_0 is the temperature of ordering, and d_0 is the lattice constant. The derivative $\varphi_{c\eta}$ is always equal to zero for disordered solutions, and vanishes near the point at which ordering occurs for ordered solutions whose composition corresponds to the maximum temperature of ordering. Similarly, for $|\kappa'| \ll 1/d_0$, one can obtain for disordered solutions

$$\overline{|c_\kappa|^2} = (kT/4v)\,[\varphi_{cc} + \beta\kappa'^2]^{-1}, \quad (33)$$

where β is a constant of the same order of magnitude as α.

At the point of phase transition of the second kind, $\varphi_{\eta\eta}$ and $\varphi_{c\eta}$ vanish and $\overline{|c_\kappa|^2} \to \infty$ as $\kappa'' \to 0$. As a result of this, the electron part of the free energy must vary sharply near the temperature T_0. We consider first the case when $\varphi_{c\eta} = 0$. In order to separate out that term in F_Φ which depends most strongly on the temperature, we separate in the integral (21), in the neighborhood of the points $\kappa = 2\pi K'_\delta$ (in which $\overline{|c_\kappa|^2}$ reaches a maximum), spheres of small radius

$R \ll 1/d_0$ and carry out a change of variables $\kappa = x\sqrt{\varphi_{\eta\eta}/\alpha}$. In accordance with (21), (23), and (22) integration over these spheres will lead to the appearance in F_Φ of the term

$$-g\frac{kT}{16\pi^2 v_a^2}\frac{\sqrt{\varphi_{\eta\eta}}}{\alpha^{3/2}}\sqrt{\alpha/\varphi_{\eta\eta}}\int_0^R \frac{x^2+1-1}{x^2+1}dx\sum_\delta J(2\pi K'_\delta)|f_{A\delta}-f_{B\delta}|^2 = -g\frac{kT}{16\pi^2\alpha v_a^2}R\sum_\delta J(2\pi K'_\delta)|f_{A\delta}-f_{B\delta}|^2$$
$$+g\frac{kT}{32\pi v_a^2}\frac{\sqrt{\varphi_{\eta\eta}}}{\alpha^{3/2}}\sum_\delta J(2\pi K'_\delta)|f_{A\delta}-f_{B\delta}|^2, \qquad (34)$$

where $f_{A\delta}$ and $f_{B\delta}$ are the values of the functions f_A and f_B at the points $\kappa = 2\pi K_\delta$.

The last term in (34) proportional to $\sqrt{\varphi_{\eta\eta}}$ leads to the most pronounced dependence of F_Φ on the temperature in the neighborhood of the temperature T_0. However, one should keep in mind that the integration in the integral (21) over the remainder of κ-space outside the selected spheres also contains a term proportional to $\sqrt{\varphi_{\eta\eta}}$ which, however, cannot be evaluated without making use of a specific model of the alloy which permits one to evaluate the correlation parameters $\epsilon(\rho)$. We shall therefore take these terms into account by means of the factors L_δ (where $L_\delta \lesssim 1$) under the summation sign in formula (34). Thus, near the point of phase transition of the second kind, the expression for the electron part of the free energy may be written in the form

$$F_\Phi = F_0 + F'_2 + A'\sqrt{\varphi_{\eta\eta}}, \qquad (35)$$

where

$$A' = (gkT_0/32\pi v_a^2\alpha^{3/2})\sum_\delta L_\delta J(2\pi K'_\delta)|f_{A\delta}-f_{B\delta}|^2, \qquad (36)$$

while F'_2 contains higher powers of $\varphi_{\eta\eta}$ (for example, the first). For small η, F_0 contains a term $\sim\eta^2$ which leads to a less pronounced temperature dependence of F_Φ near T_0 than the term with $\sqrt{\varphi_{\eta\eta}}$. In the general case when for a given composition the temperature T_0 is not a maximum and in the ordered state $\varphi_{c\eta} \neq 0$, one should replace $\varphi_{\eta\eta}$ in (35) by the expression $\varphi_{\eta\eta} - \varphi_{c\eta}^2/\varphi_{cc}$ (which also vanishes when $T = T_0$).

Similarly, near the critical point on the decay curve in which φ_{cc} vanishes,

$$F_\Phi = F_0 + F''_2 + A''\sqrt{\varphi_{cc}}, \qquad (37)$$

where A'' differs from A' by the replacement of α by β and by summation over the points $2\pi K_\delta$, which correspond to vectors of the reciprocal lattice of the disordered alloy.

One can similarly determine the form of the expression for the electron part of the free energy near the point of phase transition into the ferromagnetic state in pure metals (the Curie point). In this case an interaction, associated with exchange interaction,[11] takes place between the conduction electrons and the fluctuations of magnetization. The Hamiltonian of such an interaction has the form

$$H_1 = Cs\Delta\mathfrak{M}(r), \qquad (38)$$

where s is the spin operator of a conduction electron, $\Delta\mathfrak{M}(\mathbf{r})$ is the fluctuation change in the distribution of magnetic moments at the point $\mathbf{r}$ [$\mathfrak{M}(\mathbf{r})$ is a periodic function with the periods of the lattice], while C is a constant. Since near the Curie point the relaxation processes become extremely slow, the fluctuations may be regarded as static ones (see, for example, Krivoglaz and Rybak[4]). Since in the case under consideration the electron energy in the zero-order approximation depends on the spin direction (in the ferromagnetic state), taking the spin into account does not reduce simply to multiplication by g, and the expression for $J(\kappa)$ will be somewhat altered. However, near the Curie temperature, when the terms proportional to the square of the magnetization M^2 are negligibly small (see Krivoglaz and Rybak[4]), one may, as before, use formulas (21) and (18) in the calculation of F_0, after replacing $|V_{\kappa k}|^2$ by

$$\tfrac{1}{2}\sum_{\sigma,\sigma'}|V_{\varkappa k\sigma\sigma'}|^2 = \tfrac{1}{4}C^2|p_{\varkappa k}|^2|f_\varkappa|^2\overline{|M_\varkappa|^2}. \qquad (39)$$

Here σ and σ' are the spin components ($\pm\frac{1}{2}$), $\mathbf{M}_\kappa$ are the Fourier components of the magnetization vector, while f_κ is a factor which appears in the transition from the Fourier component of a rapidly oscillating function $\mathfrak{M}(\mathbf{r})$ to the smooth function $\mathbf{M}(\mathbf{r})$ ($f_\kappa < 1$ and $f_\kappa \to 1$ as $\kappa \to 0$). Applying the same considerations to the case of a cubic ferromagnetic in which the spontaneous magnetization is directed along the cubic axis (z axis), as in the case of solid solutions, and utilizing the expressions for $\overline{|M_{\kappa i}|^2}$ ($i = x, y, z$) given by Krivoglaz and Rybak,[4] we find that near the Curie point the expression for the electron part of the free energy has the form

$$F = F_0 + F'''_2 + A'''[2\sqrt{\partial^2\varphi/\partial M_x^2} + \sqrt{\partial^2\varphi/\partial M_z^2}], \qquad (40)$$

where A''' is a constant, while the derivatives of φ vanish at the Curie point.

One can make a rough estimate of the constants A', A'', A'''. Assuming, as we have done before on the basis of data on the residual resistance of alloys, that $|f_A - f_B|^2 \sim 10^{-2}\mu^2 v_a^2$, we obtain with the aid of formulas (36) and (19)

$$\sqrt{N_0 kT_0}A'/N_e \sim \sqrt{N_0 kT_0}A''/N_e \sim 10^{-3} \text{ ev}.$$

In order to evaluate the constant A''', we set $CM_s \sim kT_0 \sim 10^{-3}\mu$, where M_s is the saturation magnetization. Then

$$\sqrt{N_0 kT_0}A'''/N_e M_s \sim 10^{-5} \text{ ev}.$$

It should be noted that the expressions for the free energy given above cease to be valid at the transition point itself, since on approaching it the higher order terms in the expansion in powers of the interaction constant of the quasi particles with the inhomogeneities of the crystal lattice begin to play an ever increasing role.

The interaction between the electrons and the lattice vibrations may be treated with the aid of formula (14) in the same way as was done above in the case of the interaction of electrons with static inhomogeneities. Such an interaction leads to a renormalization of the velocities of propagation of elastic vibrations and to the appearance of a certain correction to the electron part of the free energy. The solution of this problem has already been obtained[13] by means of perturbation theory.*

*We note the free energy must contain terms associated with the interaction not only for superconductivity, but also for certain other phenomena. Thus, the term in the free energy of the conduction electrons (proportional to T), which appears because of frequency renormalization at high temperatures ($T \gg \theta$, where θ is the Debye temperature), must lead to the appearance of a term proportional to T in the contact potential of the metal, and also to appearance of an additional factor in front the exponential in the thermoelectron emission current [see formula (31)]. An additional factor in front of the exponential also appears owing to thermal expansion, but this effect may be separated out by studying the dependence of J on the pressure. The interaction of conduction electrons with lattice vibrations leads to the dependence of the chemical potential of the conduction electrons on the isotopic composition. This means that the contact potential difference, the thermoelectromotive force, the factor in front of the exponential in the thermo-electron emission current (but not the work function) etc., must also depend on the isotopic composition. From this it follows, in particular, that a contact potential difference (which is almost independent of T at low temperatures and is proportional to T at high temperatures) and a thermoelectromotive force (smaller by 2 or 3 orders of magnitude than in the case of different elements) must arise between different isotopes of the same metal. The isotope effects noted above must occur not only in metals but also in semiconductors, where they are a consequence of the "polaron" or the "condenson" effect.[14]

3. INTERACTION OF LATTICE VIBRATIONS WITH INHOMOGENEITIES OF COMPOSITION

In the investigation of the vibrations of the crystal lattice the inhomogeneities may consist either of a difference in the atomic masses or of a difference in the potential energy of interaction of different atoms. In the case when only the masses are different (solution of isotopes) the lattice vibrations have been treated in a number of papers.[15] In the present article we shall investigate with the aid of the perturbation theory formulas derived above (on the assumption that no local vibrations appear) the more general case of a binary solid solution of atoms of different kinds in which not only the masses of the atoms, but also their interaction energies, are different. The solution may be either in a disordered state with one atom per unit cell, or in an ordered state.

The Hamiltonian of the lattice vibrations has in the harmonic approximation the form

$$H = -\frac{\hbar^2}{2}\sum_{s\gamma}\sum_{i=1}^{3}\frac{1}{m_{s\gamma}}\frac{\partial^2}{\partial r_{s\gamma i}^2} + \frac{1}{2}\sum_{s\gamma}\sum_{s'\gamma'}\sum_{i,j=1}^{3}V_{s\gamma s'\gamma'}^{ij} r_{s\gamma i} r_{s'\gamma' j}. \quad (41)$$

Here i and j are indices of the Cartesian coordinates, and $r_{s\gamma i}$ is the deflection of the atom situated at the lattice point γ of the s-th cell from its equilibrium position (in a solid solution these positions do not form an ideal lattice). The atomic masses $m_{s\gamma}$ may take on two values, m_1 and m_2, depending on whether atom A or B occupies the lattice point $s\gamma$.

We suppose that the coefficients V in (41) depend only on the kind of atoms situated at the lattice points $s\gamma$ and $s'\gamma'$, and do not depend on the kind of neighboring atoms. Then for the pairs AA, AB, and BB these quantities may take on respectively the values

$$V(1,1),\ V(1,2),\ V(2,2).$$

For the zero-order Hamiltonian we choose the Hamiltonian for the vibrations of an ideal ordered crystal with masses $\overline{m}_\gamma$ and constants $\overline{V}$ which are the average values of the corresponding quantities

$$\overline{m}_\gamma = \overline{c}_\gamma m_1 + (1-\overline{c}_\gamma)m_2,$$
$$\overline{V}_{s\gamma s'\gamma'}^{ij} = p_{s\gamma s'\gamma'}(1,1)V_{s\gamma s'\gamma'}^{ij}(1,1) + [p_{s\gamma s'\gamma'}(1,2) + p_{s\gamma s'\gamma'}(2,1)]V_{s\gamma s'\gamma'}^{ij}(1,2) + p_{s\gamma s'\gamma'}(2,2)V_{s\gamma s'\gamma'}^{ij}(2,2). \quad (42)$$

Here, for example, $p_{s\gamma s'\gamma'}(1,2)$ is the probability that the lattice point $s\gamma$ is occupied by atom A, while the lattice point $s'\gamma'$, separated from it

by the distance $\mathbf{R}_{s'\gamma'} - \mathbf{R}_{s\gamma}$, is occupied by atom B. Then the Hamiltonian (41) takes on the form

$$H = H_0 + H_1 = -\frac{\hbar^2}{2}\sum_{\gamma}\frac{1}{\bar{m}_\gamma}\sum_{s}\sum_{i=1}^{3}\frac{\partial^2}{\partial r_{s\gamma i}^2} + \frac{1}{2}\sum_{s\gamma}\sum_{s'\gamma'}\sum_{i,j=1}^{3}\bar{V}^{ij}_{s\gamma s'\gamma'} r_{s\gamma i} r_{s'\gamma' j} - \frac{\hbar^2}{2}\sum_{\gamma}\frac{1}{\bar{m}_\gamma}\sum_{s}\sum_{i=1}^{3}\mu_{s\gamma}\frac{\partial^2}{\partial r_{s\gamma i}^2} + \frac{1}{2}\sum_{s\gamma}\sum_{s'\gamma'}\sum_{i,j=1}^{3}\Delta V^{ij}_{s\gamma s'\gamma'} r_{s\gamma i} r_{s'\gamma' j}, \tag{43}$$

where

$$\mu_{s\gamma} = (\bar{m}_\gamma - m_{s\gamma})/m_{s\gamma}; \quad \Delta V = V - \bar{V}. \tag{44}$$

We express the coordinates of the atomic deflections in terms of creation and annihilation operators for Bose particles corresponding to different normal coordinates:

$$\mathbf{r}_{s\gamma} = \sum_{kt}(\hbar/2N\bar{m}_\gamma\omega_{kt})^{1/2}\mathbf{e}_{kt\gamma}(\cos k\mathbf{R}_{s\gamma} - \sin k\mathbf{R}_{s\gamma})(a_{kt} + a_{kt}^{+}),$$
$$\partial/\partial\mathbf{r}_{s\gamma} = \frac{1}{2N}\sum_{kt}(2N\bar{m}_\gamma\omega_{kt}/\hbar)^{1/2}\frac{\mathbf{e}_{kt\gamma}}{|\mathbf{e}_{kt\gamma}|^2}(\cos k\mathbf{R}_{s\gamma} - \sin k\mathbf{R}_{s\gamma})(a_{kt} - a_{kt}^{+}). \tag{45}$$

Here t indicates the branches of the vibration frequencies, ω_{kt} are the eigen-frequencies in the zero-order approximation, $\mathbf{e}_{kt\gamma}$ are the polarization vectors satisfying the condition

$$\sum_{\gamma=1}^{\nu}|e_{kt\gamma}|^2\bar{m}_\gamma = \sum_{\gamma=1}^{\nu}\bar{m}_\gamma.$$

Substituting (45) into (44) we shall find the expression for H in the second-quantization representation:

$$H = H_0 + H_1 = \sum_{kt}\hbar\omega_{kt}\left(a_{kt}^{+}a_{kt} + \frac{1}{2}\right) + \frac{1}{4}\sum_{kt}\sum_{k't'}\hbar\sqrt{\omega_{kt}\omega_{k't'}}\,(V'_{ktk't'} + V''_{-ktk't'} - \mu'_{ktk't'} + \mu''_{-ktk't'})(a_{kt}a_{k't'} + a_{kt}^{+}a_{k't'}^{+} + a_{kt}a_{k't'}^{+} + a_{kt}^{+}a_{k't'}), \tag{46}$$

where

$$\mu_{ktk't'} = \frac{1}{N}\sum_{s\gamma}\mu_{s\gamma}(\mathbf{e}_{kt\gamma}\mathbf{e}_{k't'\gamma})\exp[i(k - k', \mathbf{R}_{s\gamma})],$$
$$V_{ktk't'} = \frac{1}{N\omega_{kt}\omega_{k't'}}\sum_{i,j=1}^{3}\sum_{ss'\gamma\gamma'}(\bar{m}_\gamma\bar{m}_{\gamma'})^{-1/2}\Delta V^{ij}_{s\gamma s'\gamma'}e_{kt\gamma i}e_{k't'\gamma' j} \times \exp[i(k\mathbf{R}_{s\gamma} - k'\mathbf{R}_{s'\gamma'})], \tag{47}$$

while $'$ and $''$ denote the real and the imaginary parts of the quantities μ and V.

We note that for $k = k'$, $t = t'$ in accordance with (47), (44), and (42)

$$V_{ktkt} = 0, \quad \mu_{ktkt} = \frac{1}{N}\sum_{s\gamma}\mu_{s\gamma} = \frac{(m_1 - m_2)^2}{m_1 m_2}\frac{1}{\nu}\sum_{\gamma=1}^{\nu}\bar{c}_\gamma(1 - \bar{c}_\gamma). \tag{48}$$

The quantities $\mu_{ktk't'}$ and $V_{ktk't'}$ may be expressed in terms of c_κ [see (24)] and of the Fourier components of $p_q(\rho)$ defined by the formula

$$p_q(\rho) = \frac{1}{2N}\sum_{s\gamma}(c_{s\gamma}c_{s'\gamma'} - \overline{c_{s\gamma}c_{s'\gamma'}})\exp\left(-\frac{1}{2}iq,\ \mathbf{R}_{s\gamma} + \mathbf{R}_{s'\gamma'}\right), \tag{49}$$

where the summation is carried out keeping $\mathbf{R}_{s'\gamma'} = \mathbf{R}_{s\gamma} + \rho$. The free energy may then be calculated up to the second order inclusively with the aid of formulae (12) and (14) (in which one should set $l = 2$). Taking into account (48) and (26) and the fact that a small change in Ω is equivalent to a small change in F expressed in terms of appropriate variables we obtain

$$F_\kappa = F_0 + \frac{2(m_1 - m_2)^2}{m_1 m_2}\sum_{kt}\sum_{k't'}\varphi_{ktk't'}(e_{kt}e_{k't'})^2\overline{|c_{k-k'}|^2} - 2\sum_{kt}\sum_{k't'}\left[\hbar\omega_{kt}\left(\bar{n}_{kt} + \frac{1}{2}\right) - \varphi_{ktk't'}\right] \times \overline{\left|\sum_{\rho\neq 0}u_{ktk't'}(\rho)\,c_{k-k'} - w_{ktk't'}(\rho)\,p_{k-k'}(\rho)\right|^2}, \tag{50}$$

where F_0 is the free energy of the vibrations of a completely ordered crystal consisting of effective atoms corresponding to the zero-order approximation, and

$$u_{ktk't'}(\rho) = \frac{4}{m\omega_{kt}\omega_{k't'}}\sin\frac{k\rho}{2}\sin\frac{k'\rho}{2}\cos\frac{k - k'}{2}\rho \times \sum_{i,j=1}^{3}e_{kti}e_{k't'j}[\Delta V_\rho^{ij}(1,2) - \Delta V_\rho^{ij}(2,2)],$$
$$w_{ktk't'}(\rho) = \frac{2}{m\omega_{kt}\omega_{k't'}}\sin\frac{k\rho}{2}\sin\frac{k'\rho}{2}\sum_{i,j=1}^{3}e_{kti}e_{k't'j}[2\Delta V_\rho^{ij}(1,2) - \Delta V_\rho^{ij}(1,1) - \Delta V_\rho^{ij}(2,2)]; \tag{51}$$

$$\varphi_{ktk't'} = \hbar[\omega_{kt}^3(\bar{n}_{kt} + 1/2) - \omega_{k't'}^3(\bar{n}_{k't'} + 1/2)]/2(\omega_{kt}^2 - \omega_{k't'}^2). \tag{52}$$

For ideal solutions in which all the lattice points are equivalent and there is no correlation the expression for F_K simplifies to

$$F_K = F_0 + \frac{(m_1 - m_2)^2}{2Nm_1m_2} c(1-c) \sum_{kt} \sum_{k't'} \varphi_{ktk't'} (e_{kt}e_{k't'})^2 - \frac{c(1-c)}{2N} \sum_{kt} \sum_{k't'} \left[\hbar\omega_{kt} \left(\bar{n}_{kt} + \frac{1}{2} \right) - \varphi_{ktk't'} \right] \left\{ 2c(1-c) \sum_{\rho \neq 0} w^2_{ktk't'}(\rho) + \left[\sum_{\rho \neq 0} \left(u_{ktk't'}(\rho) - 2c \cos\left(\frac{k-k'}{2} \rho \right) w_{ktk't'}(\rho) \right) \right]^2 \right\}. \quad (53)$$

Formulas (50) and (53) enable us to compute F_K without determining the frequency spectrum of the vibrations of the solution, but using only the frequency spectrum of the ideal crystal corresponding to the zero-order approximation and the values of the constants u and w for different ρ.

[1] L. D. Landau and E. M. Lifshitz, Статистическая физика (Statistical Physics), GITTL, 1951.

[2] J. Schwinger, Phys. Rev. **82**, 664 (1951).

[3] M. A. Krivoglaz and S. I. Pekar, Izv. Akad. Nauk SSSR, ser. fiz. **21**, 3 (1957).

[4] M. A. Krivoglaz and S. A. Rybak, J. Tech. Phys. (U.S.S.R.) (in press).

[5] J. M. Cowley, J. Appl. Phys. **21**, 24 (1950); Danilenko, Krivoglaz, Matysina, and Smirnov, Физика металлов и металловедение (Physics of Metals and Metal Research) **4**, 28 (1957).

[6] R. H. Fowler and E. A. Guggenheim, Statistical Thermodynamics, Cambridge, 1939.

[7] H. Bethe and A. Sommerfeld, Electron Theory of Metals Handb. Phys. 24/2, 2d Ed., 1933.

[8] A. A. Smirnov, J. Exptl. Theoret. Phys. (U.S.S.R.) **17**, 730 (1947); Dokl. Akad. Nauk Ukr. S.S.R. **1**, 67 (1955).

[9] L. D. Landau, J. Exptl. Theoret. Phys. (U.S.S.R.) **7**, 1232 (1937).

[10] M. A. Krivoglaz, J. Exptl. Theoret. Phys. (U.S.S.R.) **31**, 625 (1956), Soviet Phys. JETP **4**, 293 (1957).

[11] S. V. Vonsovskii, J. Exptl. Theoret. Phys. (U.S.S.R.) **16**, 981 (1946).

[12] L. D. Landau, J. Exptl. Theoret. Phys. (U.S.S.R.) **7**, 19 (1937).

[13] M. J. Buckingham and M. R. Schafroth, Proc. Phys. Soc. **A67**, 828 (1954); F. Kaschluhn, Ann. Physik **16**, 257 (1955); **19**, 94 (1956); H. Ichimura, Prog. Theoret. Phys. **15**, 151 (1956).

[14] S. I. Pekar, Исследования по электронной теории кристаллов (Investigations on the Electron Theory of Crystals), GITTL, 1951. M. F. Deigen and S. I. Pekar, J. Exptl. Theoret. Phys. (U.S.S.R.) **21**, 803 (1951).

[15] I. M. Lifshitz, Usp. Mat. Nauk **7**, 171 (1952); Nuovo cimento (Suppl.) **3**, 716 (1956). Prigogine, Bingen, and Jeener, Physica **20**, 383 (1954). J. Prigogine and J. Jeener, Physica **20**, 516 (1954). G. V. Chester, Phys. Rev. **100**, 446 (1955). I. M. Lifshitz and G. I. Stepanova, J. Exptl. Theoret. Phys. (U.S.S.R.) **30**, 938 (1956), **31**, 156 (1956); Soviet Phys. JETP **3**, 656 (1956), **4**, 151 (1957).

Translated by G. Volkoff
70

ROLE OF LATTICE THERMAL CONDUCTIVITY IN THE PHENOMENOLOGICAL THEORY OF PARAMAGNETIC RELAXATION

N. K. BELOUSOVA

Groznyi Petroleum Institute

Submitted to JETP editor April 19, 1957; resubmitted September 30, 1957

J. Exptl. Theoret. Phys. (U.S.S.R.) 34, 371-378 (February, 1958)

The thermal conductivity of the lattice is introduced into the phenomenological theory of paramagnetic relaxation[1] in parallel fields. It is assumed that the surface of the spherical sample is isothermal. Lattice thermal conductivity is found to be important at low temperatures (helium temperatures and below).

1. The first phenomenological theory of paramagnetic relaxation in parallel fields, developed by Casimir and Du Pré,[2] in which only spin-lattice relaxation was considered, was extended by Eisenstein[3] to take account of lattice relaxation due to the finite thermal conductivity of the lattice; it was assumed that the surface of the paramagnetic sample is isothermal. In the present work we consider lattice relaxation in conjunction with spin-lattice relaxation and spin relaxation. The spin relaxation is considered only within the framework of the Shaposhnikov analysis,[1] i.e., spin relaxation is considered without taking account of the modifications which have been introduced recently in Ref. 4. Thus, we are extending the Shaposhnikov analysis in the same way as Eisenstein extended the Casimir-Du Pré theory. This extension and the evaluation of the roles played by all three of the above-mentioned relaxation processes at various field strengths, frequencies, and temperatures are of interest for two reasons: on the one hand, at helium temperatures and low frequencies, where the Casimir-Du Pré theory does not agree with experiment, relaxation within the lattice is important (cf. Ref. 3); on the other hand, at high temperatures and frequencies the spin relaxation becomes important, assuming a decisive influence at room temperatures and ultrahigh frequencies (cf. Refs. 5 — 7).

2. Before turning to the analysis indicated above, we shall consider the question of whether or not a complete theory of paramagnetic relaxation should take account of still one other relaxation process — relaxation within the spin system, due to the finite thermal conductivity of this system.

The relaxation times θ_l and θ_s, which characterize the rate of dissipation of temperature inhomogeneities in the lattice and in the spin system, are proportional respectively to the ratios c_l/λ and c/λ_s where c_l is the heat capacity of the lattice, c is the heat capacity of the spin system, and λ and λ_s are the thermal conductivities of the lattice and spin system. Thus the ratio of relaxation times θ_s and θ_l is given by:

$$\theta_s / \theta_l \sim c\lambda / c_l\lambda_s. \quad (1)$$

To make a rough estimate it is sufficient to consider the behavior of $\theta_s\omega$ at frequencies for which $\theta_l\omega \sim 1$; in the indicated frequency region, from the relation in (1) we have

$$\theta_s\omega \sim c\lambda / c_l\lambda_s. \quad (2)$$

Information as to c, c_l, and λ for various materials can be determined over a rather wide temperature range. As far as λ_s, however, we are familiar only with the work of Akhiezer and Pomeranchuk,[8] who obtained results for thermal conductivity of paramagnetic materials at very low temperatures; at these temperatures the small-excitation method can be used. At temperatures of 0.14 — 0.3° K and for $H = 0$, λ_s in potassium chrome alum was found to be approximately 5×10^3 times smaller than λ.[8,9] At these same temperatures and in the absence of a magnetic field it is found that $c/c_l > 10^3$ (Ref. 10). In the frequency region in which the relation in (2) applies, we have $\theta_s\omega > 10^6$; consequently, the thermal conductivity of the spin system is not important in the indicated temperature region in the absence of an external magnetic field at frequencies for which lattice relaxation is of importance. These frequencies are approximately 10^4 sec^{-1} because for the temperatures being considered $\theta_l \sim 10^{-4}$ sec, as is shown by estimates carried out for a number of salts of elements of the iron group (cf. below, Sec. 7). However, there is a factor of 10^6 in the

right-hand part of the inequality given above. Hence our conclusion that the thermal conductivity of the spin system can be neglected holds for the entire frequency region used in studying paramagnetic relaxation. Obviously this conclusion is all the more justified when an external magnetic field is applied or at higher temperatures since c_l and λ do not change as the field is increased, c does not change or changes slowly, and λ_S falls off very rapidly as the temperature is increased. The rapid decrease in λ_S predominates over the variation of the other quantities which appear in (2). It is therefore reasonable to assume that the thermal conducitivity of the spin system is not of any great importance in paramagnetic relaxation (it should be noted, however, that the data on λ_S used in the present estimates refer only to the very low temperatures considered in Ref. 8).

3. Following Eisenstein,[3] we consider the problem of a spherical paramagnetic sample at the surface of which a constant temperature is maintained. The choice of a spherical geometry is occasioned by the fact that of all the simple shapes the sphere is the one which most closely approximates the shape of the samples used in experiments (cf. Ref. 11, for example). As far as the constant temperature at the surface of the sample is concerned it must be noted that an analysis of the degree to which this situation corresponds to the experimental conditions is not a simple one and requires individual attention in each different experimental case. There is always, however, some exchange of heat between the surface of the sample and the medium which surrounds it. Hence, in any case, it may be assumed that an analysis of paramagnetic relaxation under the assumption of isothermal conditions at the surface of the sample, such as used by Eisenstein,[3] is closer to reality than earlier analyses in which the temperature of the lattice (hence, the spin system) was assumed to be uniform over the entire sample.

We consider a solid non-conducting paramagnetic material with pure spin magnetism which is magnetically isotropic. The paramagnetic material is placed in an external magnetic field of fixed direction and magnitude which depends on the time t as follows:

$$H(t<0)=H_0, \quad H(t\geqslant 0)=H_0+\eta_0 e^{i\omega t}. \tag{3}$$

4. In a phenomenological theory of paramagnetic relaxation which treats both the spin-lattice relaxation and the spin relaxation attention must be paid to the fact that when the paramagnetic material is placed in an alternating magnetic field its spin system passes through non-equilibrium states (cf. Refs. 1 and 4). Applying non-equilibrium thermodynamics (the justification for applying this analysis in paramagnetic relaxation is discussed in Refs. 1 and 12) in the general scheme used earlier[1,4] and taking account of the thermal conductivity of the lattice the following equations are obtained:

$$\Phi_{TM}\Phi_{MM}\tau_l\dot{\xi}+\Phi_{TT}\Phi_{MM}\tau_l(\dot{\vartheta}+\dot{\vartheta}_l)$$
$$-(\Phi_{TM}^2-\Phi_{TT}\Phi_{MM})\vartheta=\Phi_{TH}\Phi_{MM}\tau_l\dot{\eta}, \tag{4}$$

$$\Phi_{MM}\tau_s\dot{\xi}+\Phi_{MM}\xi+\Phi_{TM}(\vartheta+\vartheta_l)=-\Phi_{HM}\eta, \tag{5}$$

$$c_l\dot{\vartheta}_l=\lambda\Delta\vartheta_l+\alpha\vartheta, \tag{6}$$

where

$$\tau_l\equiv T_0\alpha^{-1}\Phi_{MM}^{-1}(\Phi_{TM}^2-\Phi_{TT}\Phi_{MM}), \tag{7}$$

$$\tau_s\equiv\varkappa^{-1}\Phi_{MM}^{-1}. \tag{8}$$

Here ξ is the variable part of the magnetization M, ϑ is the difference between the temperature of the spin system T and the lattice temperature, ϑ_l is the difference in the temperature of the lattice and the fixed temperature T_0 at the surface of the sample, the Φ indices are the partial derivatives of the non-equilibrium thermodynamic potential of the spin system $\Phi(H, T, M)$ taken at $H=H_0$, $T=T_0$, and $M=M_0$ where M_0 is the equilibrium value of the magnetization, corresponding to $T=T_0$ and $H=H_0$, $\alpha(H_0, T_0)$ is the coefficient of heat conduction between the spin system and the lattice, $\varkappa(H_0, T_0)$ characterizes the rate of change of ξ due to the interaction within the spin system (cf. Refs. 1 and 4), τ_l is the spin-lattice relaxation time, which characterizes the rate of equalization of the temperatures of the spin system and the lattice under the assumption that the spin system and the lattice each pass through their own states of internal equilibrium without coming to equilibrium with each other, and T_S is the spin relaxation time, which characterizes the rate at which the magnetization M approaches its equilibrium value M_0 for an isothermal spin system at $T=T_0$ [by virtue of internal interactions in the spin system (cf. Ref. 13)].

It will be assumed that up to $t=0$, at which time the variable external magnetic field is switched on, the system has been in an equilibrium state corresponding to a magnetic field H_0 and temperature T_0; in this case the initial conditions are that ϑ, ϑ_l, and ξ are zero. The boundary conditions are obviously $\vartheta_l=0$ at the surface of the sphere and $d\vartheta_l/dr=0$ at the center of the sphere. Thus, the initial conditions and boundary conditions for the problem are

$$t=0: \quad \vartheta=0, \quad \vartheta_l=0, \quad \xi=0;$$
$$r=R: \quad \vartheta_l=0; \quad r=0: \quad (\partial\vartheta_l/\partial r)=0. \tag{9}$$

5. The system of equations given in (4) — (6) and (9) is solved by means of a Laplace transform. The steady-state solution is used to find the complex magnetic susceptibility as a function of the radial coordinate. In order to obtain the general characteristics of the entire paramagnetic sample this expression must be averaged over the entire sample. The following expression is obtained for the susceptibility χ:

$$\frac{\chi}{\chi_0}=\frac{1+i(1-F)\tau_l\omega+(F^*/G)[3\coth(G^{1/2}R)/G^{1/2}R-3/GR^2-1]}{1+i(\tau_l+\tau_s)\omega-(1-F)\tau_l\tau_s\omega^2}; \tag{10}$$

$$F^*\equiv iFc_H\lambda^{-1}\omega[1-(1-F)\tau_l\tau_s\omega^2+i(\tau_l+\tau_s)\omega]^{-1}, \tag{11}$$

$$G\equiv ic_l\lambda^{-1}\omega\{1+(c_H/c_l)[1+i(1-F)\tau_s\omega][1-(1-F)\tau_l\tau_s\omega^2+i(\tau_l+\tau_s)\omega]^{-1}\}, \tag{12}$$

$$F\equiv 1-\Phi_{TT}\Phi_{MM}(\Phi_{TT}\Phi_{MM}-\Phi_{TM}^2)^{-1}, \tag{13}$$

$$\chi_0=-\Phi_{HM}/\Phi_{MM}. \tag{14}$$

The quantity χ_0 is the equilibrium magnetic susceptibility; the quantity F is equal to $1-c_M/c_H$ where c_M and c_H are the specific heats of the spin system for constant magnetization and for constant field.

6. The general expression given in (10) for χ, the complex magnetic susceptibility, is rather complicated. Hence we consider the two limiting cases in which the argument of the hyperbolic cotangent in (10) is either very small or very large. In the first case

$$\theta_l\omega\ll 1, \quad \theta_l\omega\ll c_l/c_H, \tag{15}$$

where

$$\theta_l=c_lR^2/15\lambda \tag{16}$$

[cf. Eq. (12)] and the following approximate expressions are obtained for the real part χ' and the imaginary part χ'' of the susceptibility

$$\frac{\chi'}{\chi_0}=\frac{1+(1-F)\tau_l^2\omega^2}{[1-(1-F)\tau_l\tau_s\omega^2]^2+(\tau_l+\tau_s)^2\omega^2}-\frac{2F(\tau_l+\tau_s)\omega[1-(1-F)\tau_l\tau_s\omega^2]}{\{[1-(1-F)\tau_l\tau_s\omega^2]^2+(\tau_l+\tau_s)^2\omega^2\}^2}\frac{c_H}{c_l}\theta_l\omega, \tag{17}$$

$$\frac{\chi''}{\chi_0}=\frac{(F\tau_l+\tau_s)\omega+(1-F)^2\tau_l^2\tau_s\omega^3}{[1-(1-F)\tau_l\tau_s\omega^2]^2+(\tau_l+\tau_s)^2\omega^2}+\frac{F[1-(\tau_l+\tau_s)^2\omega^2]+(1-F)^2\tau_l^2\tau_s^2\omega^4}{\{[1-(1-F)\tau_l\tau_s\omega^2]^2+(\tau_l+\tau_s)^2\omega^2\}^2}\frac{c_H}{c_l}\theta_l\omega. \tag{18}$$

In the second case:

$$\theta_l\omega\gg 1/15 \quad \text{or} \quad \theta_l\omega\gg c_l/15c_H, \tag{19}$$

and an approximate expression for the complex susceptibility may be written as follows:

$$\frac{\chi}{\chi_0}=\frac{1+i(1-F)\tau_l\omega+(F^*/G)[3/\sqrt{G}R-1]}{1-(1-F)\tau_l\tau_s\omega^2+i(\tau_l+\tau_s)\omega}. \tag{20}$$

The quantity θ_ℓ given in (16) may be considered the lattice relaxation time which determines the rate of dissipation of spatial inhomogeneities in the lattice temperature.

Below we shall examine the approximate expressions given in (17), (18), and (20) to determine the role of lattice relaxation at various temperatures and to investigate the frequency region $\tau_\ell\omega\sim 1$ at low (helium) temperatures; the latter is of interest in connection with our analysis of various experiments (cf. below, Sec. 9).

7. To delineate the role of lattice relaxation at various temperatures we consider the temperature dependence of the quantities θ_ℓ, τ_ℓ, and c_ℓ/c_H which determine the temperature variation of the magnetic susceptibility. In a large number of cases the spin-lattice relaxation time, τ_ℓ, (for example, almost all investigated compounds of elements of the iron group) at temperatures which are not too low, lies within the limits $10^{-6}-10^{-8}$ sec;[14] as the temperature is reduced the spin-lattice relaxation time reaches values close to $10^{-2}-10^{-3}$ sec at helium temperatures.[15,11] The quantity θ_ℓ depends on temperature through the heat capacity of the lattice c_ℓ and through the coefficient of heat conductivity λ. At temperatures which are appreciably above the Debye temperature of the material c_ℓ is temperature independent (cf. Ref. 16 for example). At these temperatures the heat conductivity of dielectric crystals[16] is proportional to T^{-1} so that $\theta_\ell\sim T$. At lower temperatures c_ℓ diminishes as the temperature is reduced whereas λ exhibits approximately the same temperature dependence ($\lambda\sim T^{-1}$) so that θ_ℓ increases with increasing temperature at a still higher rate. At helium temperatures the thermal conductivity falls off rapidly as the tempera-

ture is reduced, approximately as T^3, (Refs. 9, 17), while c_ℓ and θ_ℓ remain constant at temperatures below the Debye temperature. In potassium chrome alums in the form of single crystals $\lambda = 5.3 \times 10^5 T^3$ erg-sec^{-1}-deg^{-1} for $T = 0.14 - 0.3°$ K,[9] $\rho = 1.8$ g-cm^{-3} (Ref. 3), $c_\ell = 100\ T^3$ erg-g^{-1} (Ref. 10). Whence, from Eq. (16), $\theta_\ell = 2 \times 10^{-5}$ sec; in a powder θ_ℓ becomes longer because of the reduction in λ (Ref. 18). Hence it is clear that for a wide range of temperatures $\theta_\ell/\tau_\ell \gg 1$ and $\theta_\ell/\tau_\ell \sim 1$ and only at helium temperatures does $\theta_\ell/\tau_\ell \ll 1$. Finally, in many salts of elements of the iron group we have $c_\ell/c_H \gg 1$ down to very low temperatures; it is only as the helium temperature is approached that the heat capacity of the lattice becomes comparable with the heat capacity of the spin system. The lattice heat capacity falls off rapidly as the temperature is reduced further. Thus, in a number of salts of the iron group $c_\ell/c_H \sim 10^3$ in a field of 5,000 oersted at 15° K whereas a field of 1,000 oersted is required to obtain this value at 10° K.[10]

We now consider the effect of the lattice heat conductivity on the magnetic susceptibility at various temperatures. We have shown above that a wide temperature region, aside from extremely low temperatures, $\theta_\ell/\tau_\ell > 1$. At all these temperatures, in accordance with our approximation, it is meaningful to consider only the case $\theta_\ell\omega \gg 1/15$ since $\theta_\ell\omega \ll 1$ is realized at frequencies which are small in the sense $\tau_\ell\omega \ll 1$, when the susceptibility is essentially equal to its static value. In the appropriate approximate expression (20) terms proportional to F^*/G and $F^*/G^{3/2}R$ take account of the effect of lattice heat capacity and heat conductivity respectively [cf. Eqs. (11) and (12)]. Because of the ratio F^*/G, these terms are proportional to the quantity c_H/c_ℓ which, as we have seen, is small down to very low temperatures. Moreover, the second of these terms falls off still more rapidly as the temperature increases because of the factor $(G^{1/2}/R)^{-1}$ which, in accordance with Eqs. (12) and (16) is proportional to $(\theta_\ell\omega)^{-1/2}$ (cf. the temperature dependence for θ_ℓ indicated above). Thus we may conclude that the lattice heat conductivity, being considered in the present work, is important only at extremely low temperatures (helium temperatures and below).

8. In accordance with this conclusion, we now consider the helium temperature region; this is the region which is of interest from the point of view of experimental results (cf. Sec. 9). At helium temperatures $\theta_\ell/\tau_\ell \ll 1$, hence in our approximation it is necessary to take the case $\theta_\ell\omega \ll 1$ since when $\theta_\ell\omega \gg 1$ and $\theta_\ell\omega \sim 1$, the condition that $\theta_\ell/\tau_\ell \ll 1$ corresponds to frequencies such that $\tau_\ell\omega \gg 1$; at these frequencies lattice relaxation processes become unimportant. Having in mind a discussion of experiments at helium temperatures, we apply Eqs. (16) and (17) for frequencies such that $\tau_\ell\omega \sim 1$. Inasmuch as $\tau_\ell \sim 10^{-2} - 10^{-3}$ sec at helium temperatures while the spin relaxation time τ_S, as has been shown by many experiments,[14] is temperature independent and of the order of 10^{-9} sec, $\tau_\ell \gg \tau_S$. Hence we may expand Eqs. (17) and (18) in a power series in $\tau_S\omega$ and consider only the linear terms; this procedure yields:

$$\frac{\chi'}{\chi_0} = \left(1 - \frac{F\tau_l^2\omega^2}{1+\tau_l^2\omega^2}\right)\left(1 - \frac{2F\tau_l^2\omega^2}{1+\tau_l^2\omega^2}\,\frac{\tau_s}{\tau_l} - \frac{2F\tau_l^2\omega^2}{[1+(1-F)\tau_l^2\omega^2](1+\tau_l^2\omega^2)}\,\frac{c_H}{c_l}\,\frac{\theta_l}{\tau_l}\right); \tag{21}$$

$$\frac{\chi''}{\chi_0} = \frac{F\tau_l\omega}{1+\tau_l^2\omega^2}\left[1 + \frac{1}{F} + \frac{1+(2(1-F)-F^2)\tau_l^2\omega^2+(1-F)^2\tau_l^4\omega^4}{1+\tau_l^2\omega^2}\,\frac{\tau_s}{\tau_l} + \frac{1-\tau_l^2\omega^2}{1+\tau_l^2\omega^2}\,\frac{c_H}{c_l}\,\frac{\theta_l}{\tau_l}\right]. \tag{22}$$

It is obvious from the expressions obtained that at the frequencies being considered the spin-lattice relaxation, which is governed by the Casimir-Du Pré formula,[2] plays an important role; the second and third terms reflect the effect of spin relaxation and lattice relaxation repsectively. Since the coefficients for τ_S/τ_ℓ and $\theta_\ell c_H/\tau_\ell c_\ell$ are of the order of unity at average fields regardless of temperature, the effect of both of the above-indicated relaxation processes on magnetic susceptibility is determined by the quantities τ_S/τ_ℓ and $\theta_\ell c_H/\tau_\ell c_\ell$. At helium temperatures $\tau_S/\tau_\ell \sim 10^{-7} - 10^{-5}$ while $\theta_\ell c_H/\tau_\ell c_\ell$, as has been indicated by estimates for a number of materials (cf. below, Sec. 9), is of the order of $10^{-2} - 10^{-1}$; whence it is clear that spin relaxation is not important at the temperatures and frequencies being considered. However, at higher temperatures and these same frequencies the spin relaxation process becomes more important whereas the lattice relaxation becomes less important. Thus, at some temperature the effect of both of these processes on magnetic susceptibility should be the same. To determine this temperature and to evaluate the spin relaxation and lattice relaxation as compared with spin-lattice relaxation, we consider the expression in (20). This relation, as has been mentioned above, is of interest

at relatively high temperatures for which $c_\ell/c_H \gg 1$ in the frequency region for which $\tau_\ell\omega \sim 1$ (and $\tau_S\omega \ll 1$). Expanding the expression in (20) with $\tau_S\omega \ll 1$ and $c_H/c_\ell \ll 1$ we obtain the following expressions for χ' and χ'':

$$\frac{\chi'}{\chi_0} = \left[1 - \frac{F\tau_l^2\omega^2}{1+\tau_l^2\omega^2} - \frac{1-\tau_l^2\omega^2}{(1+\tau_l^2\omega^2)^2} F\frac{c_H}{c_l}\right]\left[1 - \frac{2F\tau_l^2\omega^2}{1+\tau_l^2\omega^2}\frac{\tau_s}{\tau_l} + \sqrt{0.3}\,\frac{1-\tau_l^2\omega^2-2\tau_l\omega}{(1+\tau_l^2\omega^2)(1+(1-F)\tau_l^2\omega^2)(\tau_l\omega)^{1/2}} F\frac{c_H}{c_l}\left(\frac{\tau_l}{\theta_l}\right)^{1/2}\right]; \quad (23)$$

$$\frac{\chi''}{\chi_0} = \left[\frac{F\tau_l\omega}{1+\tau_l^2\omega^2} - \frac{2F\tau_l\omega}{(1+\tau_l^2\omega^2)^2}\frac{c_H}{c_l}\right]\left[1 + \frac{1+(2(1-F)-F^2)\tau_l^2\omega^2+(1-F)^2\tau_l^4\omega^4}{F(1+\tau_l^2\omega^2)}\frac{\tau_s}{\tau_l} + \sqrt{0.3}\,\frac{1-\tau_l^2\omega^2+2\tau_l\omega}{(1+\tau_l^2\omega^2)(\tau_l\omega)^{3/2}}\frac{c_H}{c_l}\left(\frac{\tau_l}{\theta_l}\right)^{1/2}\right]. \quad (24)$$

The second and third terms, which are proportional to τ_S/τ_ℓ and $(c_H/c_\ell)(\tau_\ell/T_\ell)^{1/2}$ characterize the effect of spin relaxation and lattice relaxation on the susceptibility. If we estimate these effects for potassium chrome alum on the basis of the data in Refs. 3 and 14, at average fields ($F \sim 1$) these quantities become of the same order of magnitude at $T \sim 13°$ K, namely $10^{-4} - 10^{-5}$. Thus, when the effects of both relaxation processes on the complex susceptibility becomes equal they are no longer important.

9. In conlusion we shall use the results obtained in the present work for a qualitative discussion of a number of experiments carried out at helium temperatures[11,15,20,21] which have not been explained satisfactorily by the Casimir-Du Pré theory.[2] All these experiments were carried out in the frequency region for which $\tau_\ell\omega \sim 1$ and for average constant magnetic fields in the range ($10^3 - 10^4$ oersted). In this region of frequency and field strength relaxation effects are described by Eqs. (21) and (24). It is apparent from these equations that the role of lattice relaxation and spin relaxation are characterized respectively by the quantities $\theta_\ell c_H/\tau_\ell c_\ell$ and τ_S/τ_ℓ which we now evaluate.

As an example we consider iron ammonium alums. The quantity c_H is found from the formula[14] $c(b/c + H^2)T^{-2}$ where c and b are the constants in the Curie susceptibility relation and the specific heat of the spin system; $c = 8.8\times10^{-3}$ deg-g^{-1} (Ref. 22), $b/c = 0.24 \times 10^6$ gauss^2 (Ref. 14). We take λ to be $1.31 \times 10^5 T^3$ erg-sec^{-1}-deg^{-1} (Ref. 23) iron aommonium alum in the form of a pressed powder. The results given below for powder and crystal samples may differ from the true values but are correct within an order of magnitude.[18] Further, $\tau_\ell = (0.2 - 0.4) \times 10^{-3}$ sec for $H_0 = 285 - 968$ oersted and $T_0 = 2.13°$ K for the powder while $\tau_\ell = 7.5 \times 10^{-3}$ sec for $T_0 = 0.94°$ K in a field $H_0 = 748$ oersted for a single crystal;[11] $\rho = 1.7$ g-cm^{-3} (Ref. 22), and $\tau_S = 0.7 \times 10^{-9}$ sec (Ref. 14). Starting from these data, for a powder sample in the form of a sphere of radius 1 cm we obtain the following values for $\theta_\ell c_H/\tau_\ell c_\ell$: for $T_0 = 2.13°$ K and $H_0 = 285$ and 968 oersted, 0.32 and 0.53 respectively; for $T_0 = 0.93°$ K and $H_0 = 285$ and 968 oersted, 2.1 and 3.3 respectively. For a sample in the form of a single crystal an estimate gives the following values of $\theta_\ell c_H/\tau_\ell c_\ell$ for $H_0 = 748$ oersted: 0.02 for $T_0 = 2.16°$ K and 0.11 for $T_0 = 0.94°$ K. In the case of the single crystal with $T_0 = 2.16°$ K and $H_0 = 748$ oersted we have $\tau_S/\tau_\ell = 10^{-7}$. Thus the role of lattice relaxation is important in the materials being considered whereas spin relaxation is completely negligible.

A similar qualitative evaluation of experiments has been carried out for potassium chrome alums, cesium titanium alums, and manganese ammonium sulphate (of these materials the potassium chrome and cesium titanium alums have also been considered by Eisenstein[3,24]); the same qualitative results were obtained.

In conclusion we wish to express our gratitude to I. G. Shaposhnikov for proposing this work and for his guidance in the course of its execution.

[1] I. G. Shaposhnikov, Doctoral dissertation, Perm State University (1949); J. Exptl. Theoret. Phys. (U.S.S.R.) **18**, 533 (1948).

[2] H. B. G. Casimir and F. K. Du Pré, Physica **5**, 507 (1938).

[3] J. Eisenstein, Phys. Rev. **84**, 548 (1951).

[4] N. K. Belousova and I. G. Shaposhnikov, J. Exptl. Theoret. Phys. (U.S.S.R.) **33**, 238 (1957); Soviet Phys. JETP **6**, 183 (1958).
[5] N. S. Garif'ianov, J. Exptl. Theoret. Phys. (U.S.S.R.) **25**, 359 (1953).
[6] K. P. Sitnikov, Dissertation, Kazan' State University (1954).
[7] A. I. Kurushin, Izv. Akad. Nauk SSSR, ser. fiz. **20**, 1232 (1956).
[8] A. I. Akhiezer and I. Ia. Pomeranchuk, Sov. Phys. **8**, 216 (1944).
[9] C. G. B. Carrett, Phil. Mag. **41**, 621 (1950).
[10] H. B. G. Casimir, Magnetism and Very Low Temperatures, Cambridge 1940.
[11] R. J. Benzie and A. H. Cooke, Proc. Phys. Soc. **A63**, 201 (1950).
[12] G. R. Khutsishvili, J. Exptl. Theoret. Phys. (U.S.S.R.) **29**, 329 (1955), Soviet Phys. JETP **2**, 187 (1956).
[13] I. G. Shaposhnikov, Izv. Akad. Nauk SSSR, ser. fiz. **20**, 1255 (1956).
[14] C. J. Gorter, Paramagnetic Relaxation Amsterdam, 1947.
[15] Kramers, Bijl, and Gorter, Physica **16**, 65 (1950).
[16] M. Born and M. Goeppert Mayer, Dinam. Gittertheor. d. Kristalle, Handb. Phys. 24/2, 2d Ed., 1933.
[17] D. Bijl, Physica **14**, 684 (1949).
[18] Kürti, Rollin, and Simon, Physica **3**, 266 (1936).
[19] H. B. G. Casimir, Physica **6**, 156 (1939).
[20] D. Bijl, Physica **16**, 269 (1950).
[21] D. Bijl and A. H. Cooke, Proc. Roy. Soc. **A209**, 269 (1951).
[22] International Critical Tables, Vol. I, p. 106; Vol. VI, p. 351.
[23] H. Van Dijk and W. H. Keesom, Physica **7**, 970 (1940).
[24] J. Eisenstein, Phys. Rev. **87**, 522 (1952).

Translated by H. Lashinsky
71

SOVIET PHYSICS JETP VOLUME 34 (7), NUMBER 2 AUGUST, 1958

USE OF COLLECTIVE VARIABLES AND TREATMENT OF SHORT-RANGE FORCES IN THE THEORY OF A SYSTEM OF CHARGED PARTICLES

I. R. IUKHNOVSKII

L'vov State University

Submitted to JETP editor June 15, 1957

J. Exptl. Theoret. Phys. (U.S.S.R.) **34**, 379-389 (February, 1958)

The free energy and the distribution functions (binary and ternary) of a system of charged particles are calculated with effects of short-range forces included. Expressions for these quantities are written in terms of series of group integrals (correlations). It is shown that for an electron plasma in a compensating field the Coulomb potential does not give divergences in the expressions for the free energy and the distribution functions. The total free energy of a system of particles with a Coulomb interaction potential is also calculated. The "transition function" for such systems is constructed.

1. STATEMENT OF THE PROBLEM

UNTIL recently the determination of the thermodyanamic characteristics of ionic systems has been carried out by the use of partial distribution functions — single-particle and binary functions. The calculations involved cumbersome computations and the solution of complicated systems of integro-differential equations. In these calculations for systems of charged particles short-range forces could be taken into account only with special forms of force law; for example, with the choice of the mutual potential in the form[1]

$$\Phi = (e^2/r)[1 - A(r)e^{-\alpha r}].$$

The construction of the exact binary function of a system by the method of the Bogoliubov equations, independent of the actual form of the short-range part of the total interaction potential, remained an unsolved problem.

Since 1949 there have been appearing papers by Bogoliubov, Zubarev, Bohm, Gross, Pines and others in which a new and original method of collective variables is presented, which makes it possible to find at once the partition functions of systems of interacting particles. In this method the behavior of the system is described from the point of view of the collective vibrations that occur owing to the interaction and motion of the particles. For the appearance of vibrations that include whole groups of particles it is naturally necessary that the sphere of effective action of the field of one particle must extend to many other particles. Langmuir and Tonks have shown[2] that the wavelength of the oscillations in an ionic system is not smaller than the Debye radius r_d, which is of the order $c^{-1/2} \times 10^{-8}$ cm, where c is the concentration in moles per liter. On the other hand, r_d can be regarded as the radius of the sphere of effective action of the Coulomb forces.

From this it follows that for systems with a Coulomb interaction potential the coordinate space can be replaced by a space of collective variables $\rho_{\mathbf{k}}$, each of which describes a certain monochromatic vibration in the system, with the wave vector $\mathbf{k}$.

The van der Waals forces and the repulsive forces act at distances considerably smaller than r_d. The action of these forces does not give rise to collective vibrations, and consequently, they cannot be described in the space of the $\rho_{\mathbf{k}}$.

Bogoliubov has suggested the study of the "mixed" problem: the calculation of the integral over states (partition function) of an ionic system, in which the short-range forces are described in the coordinate space and the long-range forces are described by means of collective variables. The present paper is devoted to the solution of this problem.

Let us consider a system in equilibrium, which is neutral as a whole and consists of M kinds of ions, containing N_a particles of type a. The interaction is described by the "exact" potential[3]

$$U = \frac{1}{2} \sum_{\substack{1 \leqslant a,b \leqslant M \\ 1 \leqslant i \neq j \leqslant N_a, N_b}} \left(\frac{e_a e_b}{\varepsilon r_{ij}} + \frac{A_{ab}}{r_{ij}^6} + b_{ab} e^{-r_{ij}/\rho} \right). \quad (1.0)$$

Let us calculate the free energy of this system

$$F = -kT \ln Z_{id} Z, \quad (1.1)$$

where Z_{id} is the ideal part of the statistical integral (omitted in what follows).

We introduce the collective variable

$$\rho_{\mathbf{k}} = \sum_{a=1}^{M} \lambda_a N^{-1/2} \sum_{1 \leqslant i \leqslant N_a} e^{i\mathbf{k}\mathbf{r}_i}$$

which is the Fourier transform of the function

$$f(\mathbf{r}) = \sum_{i,a} \lambda_a N^{-1/2} \delta(\mathbf{r} - \mathbf{r}_i),$$

$$\lambda_a = e_a \left(\sum e_c^2 n_c \right)^{-1/2}, \quad n_c = N_c / N, \quad \mathbf{k} \neq 0.$$

and by its use we write the configuration integral in the form[4]

$$Z = \exp\left(\frac{1}{2} \sum_{\mathbf{k}} \alpha(\mathbf{k}) \right) \int \exp\left(-\frac{1}{2} \sum_{\mathbf{k}} \alpha(\mathbf{k}) \rho_{\mathbf{k}} \rho_{-\mathbf{k}} \right) J(\rho_{\mathbf{k}}) (d\rho_{\mathbf{k}}),$$

$$\alpha(\mathbf{k}) = \sum e_c^2 n_c \nu(k) / v\Theta, \quad v = \frac{V}{N}, \quad (1.2)$$

where $\nu(\mathbf{k})$ is the Fourier transform of the Coulomb potential. $J(\rho_{\mathbf{k}})$ is the "transition function"[4] providing for the transition from Eq. (1.2) to the usual form

$$Z = \int \exp\{-U(r_1, \ldots, r_N)/\Theta\} \, dq_1 \ldots dq_N. \quad (1.3)$$

From $\rho_{\mathbf{k}} \rho_{-\mathbf{k}} = \rho_{\mathbf{k}}^{C2} + \rho_{\mathbf{k}}^{S2}$ it follows that the potential energy of the Coulomb interaction of the ions is replaced by the potential energy of a system of harmonic oscillators, over whose amplitudes the integration is to be taken. The sum over k has an upper limit at some value k_{max} depending on the concentration, which corresponds to the existence of a value λ_{min}.

We do not expand the short-range potentials in Fourier series. They remain in the coordinate representation and can enter, for example, into the make-up of the transition function $J(\rho_{\mathbf{k}})$, which is given by

$$J(\rho_{\mathbf{k}}) = \int \exp\left\{ -\frac{1}{2\Theta} \sum_{a,b,i,j} \varphi_{ab}(r_{ij}) \right\}$$

$$\times \prod_{k \neq 0}{}' \delta\left(\rho_{\mathbf{k}}^c - \sum_{a,i} \lambda_a N^{-1/2} \cos \mathbf{k}\mathbf{r}_i \right) \quad (1.4)$$

$$\times \delta\left(\rho_{\mathbf{k}}^s - \sum_{a,i} \lambda_a N^{-1/2} \sin \mathbf{k}\mathbf{r}_i \right) dq_1 \ldots dq_N,$$

where

$$\varphi_{ab}(r_{ij}) = A_{ab} / r_{ij} + b_{ab} \exp\{-r_{ij}/\rho\}.$$

Taking $\varphi_{ab}(\mathbf{r}) = 0$, we get the transition function for the Coulomb potential. Since this case is of great importance for the further work, we shall examine it in more detail.

2. THE CONFIGURATION INTEGRAL IN THE CASE OF THE COULOMB INTERACTION POTENTIAL

As in Ref. 4, we substitute into Eq. (1.4) the integral representation of the δ function

$$\delta\left(\rho_{\mathbf{k}} - N^{-1/2}\sum_{a=1}^{M}\lambda_a\sum_{i=1}^{N_a}e^{i\mathbf{k}\mathbf{r}_i}\right) = \int\exp\left\{i\pi\left(\rho_{\mathbf{k}} - \sum_{ai}\lambda_a N^{-1/2}e^{i\mathbf{k}\mathbf{r}_i}\right)\omega_{\mathbf{k}}\right\}d\omega_{\mathbf{k}}.$$

On integrating over the coordinates and over $\omega_{\mathbf{k}}$ we get the transition function in an operator form that is convenient for calculation:

$$J^k(\rho_{\mathbf{k}}) = V^N\exp\left\{\sum_{i\geqslant 3}(-1)^i D_i\right\}\left\{1 - \sum_a N_a\left(\frac{1}{2\cdot 3!}\frac{\lambda_a^6}{N^3}\times\sum_{\mathbf{k}_1+\mathbf{k}_2+\mathbf{k}_3=0}\frac{\partial^6}{\partial\rho_{\mathbf{k}_1}\partial\rho_{-\mathbf{k}_1}\dots\partial\rho_{-\mathbf{k}_3}} + \dots\right)\times\exp\left\{-\frac{1}{N}\sum_{i\geqslant 2}(-1)^i D_i^a\right\} - \sum_{a,b}N_aN_b\dots\right\}\exp\left\{-\frac{1}{2}\sum(\rho_{\mathbf{k}}\rho_{-\mathbf{k}} + \ln\pi)\right\}, \tag{2.1}$$

where the operators are defined by

$$D_n^a = \frac{\lambda_a^n N^{-(n-2)/2}}{n!}\sum_{\mathbf{k}_1+\dots+\mathbf{k}_n=0}\partial^n/\partial\rho_{\mathbf{k}_1}\dots\partial\rho_{\mathbf{k}_n},$$

$$D_n = \sum_{a=1}^{M}n_aD_n^a.$$

In the sum $\mathbf{k}_1 + \mathbf{k}_2 + \dots + \mathbf{k}_n = 0$ no sum of order less than n is equal to zero.

We confine ourselves to calculations carried out with only the first two terms in the braces of Eq. (2.1).

We shall show that the first term

$$J_0^k = V^N\exp\left\{\sum_{i\geqslant 3}(1)^i D_i\right\}\exp\left\{-\frac{1}{2}\sum_{\mathbf{k}}(\rho_{\mathbf{k}}\rho_{-\mathbf{k}} + \ln\pi)\right\}, \tag{2.2}$$

gives the main part of the transition function, and the second

$$J_1^k = -V^N\exp\left\{\sum_{i\geqslant 3}(-1)^i D_i\right\}\sum_a N_a\left(\frac{1}{2\cdot 3!}\frac{\lambda_a^6}{N^3}\times\sum_{\mathbf{k}_1+\mathbf{k}_2+\mathbf{k}_3=0}\frac{\partial^6}{\partial\rho_{\mathbf{k}_1}\partial\rho_{-\mathbf{k}_1}\dots\partial\rho_{\mathbf{k}_3}\partial\rho_{-\mathbf{k}_3}} + \frac{1}{2\cdot 4!}\frac{\lambda_a^8}{N^4}\sum_{\mathbf{k}_1+\dots+\mathbf{k}_4=0}\frac{\partial^8}{\partial\rho_{\mathbf{k}_1}\dots\partial\rho_{-\mathbf{k}_4}} + \dots\right)\times\exp\left\{-\frac{1}{N}\sum_{i\geqslant 2}(-1)^i D_i^a\right\}\exp\left\{-\frac{1}{2}\sum_{\mathbf{k}}(\rho_{\mathbf{k}}\rho_{-\mathbf{k}} + \ln\pi)\right\} \tag{2.3}$$

(and subsequent terms) lead to quantities proportional to 1/V, which can be neglected. For this purpose we substitute Eq. (2.1) into (1.2) and expand the exponentials of operators in series. Under the integral sign there remains the exponential function

$$\exp\left\{-\frac{1}{2}\sum_{\mathbf{k}}(\alpha(\mathbf{k}) + 1)\rho_{\mathbf{k}}\rho_{-\mathbf{k}}\right\},$$

which is an even function of $\rho_{\mathbf{k}}$. Therefore on integration over the collective variables the expressions different from zero will be those in which the differentiation is an "even" one of the type

$$\partial^{2n}/\partial\rho_{\mathbf{k}_1}\partial\rho_{-\mathbf{k}_1}\dots\partial\rho_{\mathbf{k}_n}\partial\rho_{-\mathbf{k}_n}.$$

Let us consider first the main contribution to the statistical integral, in which one takes for the transition function the expression (2.2):

$$Z_0^k = \exp\left(\frac{1}{2}\sum_{\mathbf{k}}\alpha(\mathbf{k})\right)\int\exp\left(-\frac{1}{2}\sum_{\mathbf{k}}\alpha(\mathbf{k})\rho_{\mathbf{k}}\rho_{-\mathbf{k}}\right)J_0^k(\rho_{\mathbf{k}})(d\rho_{\mathbf{k}}). \tag{2.4}$$

The expansions in $J_0^k(\rho_{\mathbf{k}})$ can be written out in the form

$$(1 - D_3 + D_4 - D_5 + \dots + D_3D_3 - D_3D_4 + \dots + D_4D_4 - D_4D_5 + \dots - D_3D_3D_3 + D_3D_3D_4 - \dots)\exp\left(-\frac{1}{2}\sum_{\mathbf{k}}(\rho_{\mathbf{k}}\rho_{-\mathbf{k}} + \ln\pi)\right). \tag{2.5}$$

According to the definition of the $\rho_{\mathbf{k}}$, all $\mathbf{k} \neq 0$; moreover, in the sums $\mathbf{k}_1 + \mathbf{k}_2 + \dots + \mathbf{k}_n = 0$ there is nowhere a $\mathbf{k}_i$ equal to $-\mathbf{k}_j$; therefore the linear terms in Eq. (2.5) (except for the 1) can be dropped, since they give zero when one carries out the integration in Eq. (2.4). The same is true of many of the products of the D_i by twos, threes, and so on.

In the sum in Eq. (2.5) we must consider the terms containing even derivatives. The factors $\rho_{\mathbf{k}}\rho_{-\mathbf{k}}$ obtained after the differentiations in the expression (2.4) for J_0^k can conveniently be replaced by operators $[1 + \partial/\partial\alpha(\mathbf{k})]$, which can be taken outside the sign of integration over $\rho_{\mathbf{k}}$.

Expanding, finally, the combination of operators $[1 + \partial/\partial\alpha(\mathbf{k})]$, we get as the result of the inverse Fourier transformation the main contribution to the configuration integral in the following form:

$$Z_0^k = \prod_k{}' \frac{e^{\alpha(k)}}{\alpha(k)+1}\left\{1 + N\left[\frac{N}{V}\sum_{a,b}\frac{n_an_b}{2!}\int\left(e^{-g_{ab}} - 1 + g_{ab} - \frac{g_{ab}^2}{2}\right)dq + \frac{N^2}{V^2}\sum_{a,b,c}\frac{n_an_bn_c}{3!}\int\left(e^{-g_{ac}} - 1 + g_{ac}\right)\times\left(e^{-g_{cb}} - 1 + g_{cb}\right)3g_{ab}\,dq_1dq_2 + \int(e^{-g_{ab}} - 1 + g_{ab})(e^{-g_{ac}} - 1 + g_{ac})(e^{-g_{cb}} - 1 + g_{cb})\,dq_1dq_2 + \frac{N^3}{V^3}\sum_{a,b,c,d}n_an_bn_cn_d\dots\right] + \dots\right\}, \tag{2.6}$$

where $\Theta g_{ab}(r)$ is the self-consistent Debye potential*

$g_{ab}(r) = (e_a e_b / \varepsilon\Theta) e^{-\varkappa r} / r$ for the Coulomb potential (2.7a)

$$g_{ab}(r) = \frac{e_a e_b}{\varepsilon\Theta} \frac{1}{\sqrt{1 - 4\beta^2\varkappa^2}} \frac{e^{-qr} - e^{-pr}}{r},$$

for the potential $\frac{e_a e_b}{\varepsilon r}(1 - e^{-\alpha r})$, (2.7b)

$$p = \frac{1}{2}\alpha(\sqrt{1 + 2\beta\varkappa} + \sqrt{1 - 2\beta\varkappa}),$$

$$q = \frac{1}{2}\alpha(\sqrt{1 + 2\beta\varkappa} - \sqrt{1 - 2\beta\varkappa}),$$

$$\alpha = 1/\beta \sim 10^8 \text{ cm}^{-1}, \varkappa = 1/r_a.$$

For a system of ions of different signs interacting according to the Coulomb law the integral $\int e^{-g_{ab}(r)} dq$ diverges at zero.† Therefore in the case of a system of ions of different signs we shall use a cut off Coulomb potential and substitute the expression (2.7b) for g_{ab}.

In order to get the terms in Eq. (2.6) proportional to $(N/V)^3$ it is necessary to examine products of four operators in Eq. (2.5). For example, the calculation of the operator $D_3D_3D_3D_3$ leads to three integrals

$$N\frac{N^3}{V^3}\int g_{ab}g_{bc}g_{cd}g_{da}g_{ac}g_{bd}dq_1dq_2dq_3,$$

$$N\frac{N^3}{V^3}\int \frac{g_{ab}^2}{2}\frac{g_{cd}^2}{2} g_{ac}g_{bd}dq_1dq_2dq_3,\ N^2\frac{N^2}{2V^2}\left(\int \frac{g_{ab}^3}{3!}dq\right)^2.$$

The first two are the beginning of a series of complicated correlation expressions. The last is the third term of the series expansion of the expression

$$\exp\left(N\frac{N}{V}\int\frac{1}{3!}g_{ab}^3 dq\right).$$

Developing the higher products of operators in Eq. (2.5) we get on one hand, new correlation terms proportional to N, and on the other hand, powers of these terms, corresponding to the expansion of the exponential.

Thus the whole expression for the main part of the statistical integral in an exponential function of the terms proportional to the first power of N. On the other hand, the free energy is the logarithm of the statistical integral. The additivity properties require that

$$F = -kT\ln Z = Nf(T, V/N).$$

Therefore in the expansion for ln Z we must confine ourselves to terms proportional to the first power of N. This combination corresponds to the logarithm of the whole expression for the statistical integral (cf. also Ref. 5, p. 239).

In calculating the expression (2.6) we were examining only the main part of the statistical integral. We shall now show that in the calculation of F the operator J_1^k leads to infinitely small quantities of the order 1/V which can be neglected.

To do this we substitute J_1^k into Eq. (2.4) instead of J_0^k and calculate the integral

$$Z_1^k = \exp\left(\frac{1}{2}\sum_k \alpha(k)\right)\int\exp\left(-\frac{1}{2}\sum_k \alpha(k)\rho_k\rho_{-k}\right)J_1^k(\rho_k)(d\rho_k). \quad (2.8)$$

Comparing Eqs. (2.2) and (2.3), we find it useful to write J_1^k in the form

$$J_1^k = -\sum_a N_a \exp\{-D_2^a/N\}(1 + D_3^a/N - D_a^4/N + \cdots)$$

$$\times\left(\frac{1}{2\cdot 3!}\frac{\lambda_a^6}{N^3}\sum_{k_1+k_2+k_3=0}\partial^6/\partial\rho_{k_1}\cdots\partial\rho_{-k_3} + \cdots\right)J_0^k. \quad (2.3a)$$

After Eq. (2.3a) is substituted into Eq. (2.8), the further calculations are analogous to Eqs. (2.4) — (2.6) and lead to the following result:

$$Z_1^k = -Z_0^k\sum_a\frac{n_a}{2}e^{-g_{aa}(0)}$$

$$\times\frac{N}{V}\int\left(e^{-g_{aa}(r)} - 1 + g_{aa}(r) - \frac{g_{aa}^2}{2}\right)dq \quad (2.9)$$

$$\times\left[1 + \frac{N}{3!V}\frac{1}{Z_0^k}\sum_b n_b\int g_{ab}^3 dq + \cdots\right] = -Z_0^k\frac{N}{V}\varphi\left(\frac{N}{V}\right),$$

where $\varphi(N/V)$ is a finite function of the concentration.

The general expression for the statistical integral of a system of charged particles (without inclusion of short-range forces) is

$$Z^k = Z_0^k + Z_1^k = Z_0^k(1 + N\varphi/V). \quad (2.10)$$

3. THE FREE ENERGY OF A COULOMB SYSTEM

In the formula

$$F^k = -kT\ln Z^k \quad (3.1)$$

we substitute Z_0^k from Eq. (2.6) and expand the logarithms in powers of N. Taking into account the considerations presented above, we confine ourselves to expressions proportional to the first power of N. Then

*After the inverse Fourier transformation one puts

$$\int\left(g_{ab} - \frac{1}{V}\int g_{ab}dq\right)^i dq \approx \int g_{ab}^i dq,\ i \geqslant 3.$$

†For oppositely charged particles $g_{ab}(r) < 0$.

$$F = -NkT\left\{\ln V + \frac{1}{N}\sum_k{}' [\alpha(k) - \ln(\alpha(k)+1)]\right. + \frac{N}{V}\sum_{a,b}\frac{n_a n_b}{2}\int\left(e^{-g_{ab}} - 1 + g_{ab} - \frac{1}{2}g_{ab}^2\right)dq$$

$$+ \frac{N^2}{V^2}\sum_{a,b,c}\frac{n_a n_b n_c}{3!}\left[\int\left(e^{-g_{ac}} - 1 + g_{ac}\right)(e^{-g_{cb}} - 1 + g_{cb}) 3\, g_{ab}\, dq_1\, dq_2 + \cdots\right] \tag{3.2}$$

$$\left. + \frac{N^3}{V^3}\sum_{a,b,c,d}\cdots - \frac{1}{V}\sum_a \frac{n_a}{2} e^{-g_{aa}(0)} \frac{N}{V}\int\left(e^{-g_{aa}(r)} - 1 + g_{aa}(r) - \frac{1}{2}g_{aa}^2(r)\right)dq\left[1 + \frac{N}{3!V}\frac{1}{Z_0^k}\sum_b n_b\int g_{ab}^3\, dq + \cdots\right]\right\},$$

where

$$\alpha(k) = \sum(e_c^2 n_c N / V\Theta)\,\nu(k), \quad \nu(k) = \int \Phi^k(r)\, e^{i\mathbf{kr}}\, dq = 4\pi\alpha^2/k^2(\alpha^2+k^2), \quad \Phi^k(r) = (1 - e^{-\alpha r})/r.$$

The last terms of Eq. (3.2) are smaller than the other terms by a factor 1/V and can be neglected.*

Thus it is established that for the calculation of the free energy of a system of charged particles the transition function is given, apart from terms proportional to 1/V, by the expression

$$J^k = J_0^k = \exp\left(\sum_{i\geqslant 3}(-1)^i D_i\right)\exp\left(-\frac{1}{2}\sum_{\mathbf{k}}\rho_{\mathbf{k}}\rho_{-\mathbf{k}} + \ln\pi\right). \tag{3.3}$$

Terms whose application would result in infinitely small quantities of the order $e^{-g_{aa}(0)}/V$ have been dropped.

We now proceed to substitute into Eq. (3.2) the value of $\alpha(k)$ and to sum over k.

The free energy of a neutral system of ions with (cut off) Coulomb interaction potential is given by the following final formula:

$$F = -NkT\left\{\ln V + \frac{1}{4\pi\beta}\frac{V}{N}\left(\frac{\varkappa^2}{2} - \frac{1}{3\beta^2}[1 - (1-\beta\varkappa)\sqrt{1+2\beta\varkappa}]\right)\right\} + \frac{N}{V}\sum_{a,b}\frac{n_a n_b}{2}\int\left(e^{-g_{ab}(r)} - 1 + g_{ab} - \frac{1}{2}g_{ab}^2\right)dq$$

$$+ \frac{N^2}{V^2}\sum_{a,b,c}\frac{n_a n_b n_c}{3!}\left\{\int\left(e^{-g_{ac}} - 1 + g_{ac}\right)(e^{-g_{cb}} - 1 + g_{cb})\, 3 g_{ab} dq_1\, dq_2\right.$$

$$\left. + \int(e^{-g_{ab}} - 1 + g_{ab})(e^{-g_{ac}} - 1 + g_{ac})(e^{-g_{cb}} - 1 + g_{cb})\, dq_1\, dq_2\right\} + \frac{N^3}{V^3}\cdot\cdots. \tag{3.4}$$

For small concentrations this goes over into the relation

$$F = -NkT\left[\ln V + \frac{1}{4\pi\beta}\frac{V}{N}\left\{\frac{\varkappa^2}{2} - \frac{1}{3\beta^2}\left(1 - (1-\beta\varkappa)\sqrt{1+2\beta\varkappa}\right)\right\}\right], \tag{3.5}$$

which can be obtained by means of the zeroth approximation to the binary distribution function.†

It is now easy to go on to treat the problem of constructing the distribution functions and the thermodynamic functions for the case in which one includes in the interaction energy all the central forces, of both long and short ranges. One can also deal with a system of ions in external fields. For the case of an external field potential that possesses a Fourier transform the transition function remains the same as in the absence of the field, and is given by Eq. (3.3).

4. THE DISTRIBUTION FUNCTIONS AND FREE ENERGY OF A SYSTEM OF CHARGED PARTICLES WITH INCLUSION OF EFFECTS OF SHORT-RANGE FORCES

By using the results of Secs. 2 and 3 one can carry out the study of systems of charged particles with the exact interaction law of Eq. (1.0) in two ways, which lead to identical results.

In the first place, one can replace the configuration integral of the system,

$$Z = \int\exp\left\{-\sum_{a,b,i,j}\frac{1}{\Theta}(\Phi_{ab}^k(r_{ij}) + \varphi_{ab}(r_{ij}))\right\}dq_1 \ldots dq_N, \tag{4.1}$$

*In the case of the Coulomb potential $\Phi^k(r) = 1/r$, $g_{aa}(0) = \infty$, and these terms are simply equal to zero.

†In the limit $\beta \to 0$ Eq. (3.5) goes over into Debye's result, which Zubarev[4] has obtained by the method of collective variables.

where

$$\Phi^k_{ab}(r_{ij}) = e_a e_b / \varepsilon r_{ij}, \quad \varphi_{ab}(r_{ij}) = A_{ab}/r^6_{ij} + b_{ab}e^{-r_{ij}/\rho}, \; r_{ij} = |\mathbf{r}_i - \mathbf{r}_j|,$$

by the expression (1.2), in which the Coulomb energy is represented by the energy of the harmonic vibrations, and the short-range part of the force law (1.0) affects the structure of the transition function, given by

$$J(\rho_{\mathbf{k}}) = V^N \Big\{1 + \sum_{a,b} \frac{N_a N_b}{2V} \int f_{ab}(r) \Big(1 - \frac{\lambda_a \lambda_b}{N} \exp\Big\{\sum_{i\geqslant 2} (-1)^i D^{ab}_i / N\Big\} \sum_{\mathbf{k}} \frac{\partial^2}{\partial\rho_{\mathbf{k}}\partial\rho_{-\mathbf{k}}} + \cdots\Big) dq$$

$$+ \sum_{a,b,c} \frac{N_a N_b N_c}{3!V^2} \int [3 f_{ab} f_{bc} + f_{ab} f_{bc} f_{ca}] \Big[1 + \frac{1}{N} \exp\Big\{\sum_{i\geqslant 2} (-1)^i D^{abc}_i / N\Big\} \sum_{\mathbf{k}} \frac{\partial^2}{\partial\rho_{\mathbf{k}}\partial\rho_{-\mathbf{k}}} (\lambda_a\lambda_b e^{i\mathbf{k}\mathbf{r}_1} + \lambda_a\lambda_c e^{i\mathbf{k}\mathbf{r}_2} \tag{4.2}$$

$$+ \lambda_b\lambda_c e^{i\mathbf{k}(\mathbf{r}_1 - \mathbf{r}_2)}) + \cdots\Big] dq_1\, dq_2 + \sum_{abcd} \cdots\Big\} J^k(\rho_{\mathbf{k}}),$$

Here

$$f_{ab} = e^{-\varphi_{ab}/\Theta} - 1, \quad D^{ab}_i = \sum_{\mathbf{k}_1 + \cdots + \mathbf{k}_i = 0} \frac{\lambda^i_a + \lambda^i_b}{i!\, N^{(i-2)/2}} \partial^i / \partial\rho_{\mathbf{k}_1} \cdots \partial\rho_{\mathbf{k}_i}, \; D^{abc}_i = \sum_{\mathbf{k}_1 + \cdots + \mathbf{k}_i = 0} \frac{\lambda^i_a + \lambda^i_b + \lambda^i_c}{i!\, N^{(i-2)/2}} \partial^i / \partial\rho_{\mathbf{k}_1} \cdots \partial\rho_{\mathbf{k}_i};$$

and in the sum $\mathbf{k}_1 + \ldots + \mathbf{k}_i$ no sum of order less than i is equal to zero. J^k is the transition function for the Coulomb potential, given by Eq. (3.3). After Eq. (4.2) has been substituted into Eq. (1.2) the further developments are analogous to the treatment for the Coulomb problem. Here one again has to group the operators D_i and to sum complicated series.

This procedure is perhaps the more cumbersome. In this paper the calculation will be carried out by the second method, in which one uses the properties of the free energy as a generating functional.

Let us introduce a functional of the $\psi_{ab}(r_{ij})$, which are an arbitrary system of regular rapidly decreasing radially symmetrical functions:

$$L(\psi) = -\Theta \ln Z(\psi) = -\Theta \ln \int \exp\Big\{-\sum \frac{1}{\Theta} (\Phi^k_{ab}(r_{ij}) + \varphi_{ab}(r_{ij}) + \psi_{ab}(r_{ij})\Big\} dq_1 \cdots dq_N. \tag{4.3a}$$

The integrand can be transformed into a sum by the substitution

$$f^x_{ab}(r_{ij}) = \exp\{-[\varphi_{ab}(r_{ij}) + \psi_{ab}(r_{ij})]/\Theta\} - 1.$$

The result is the following way of writing the generating functional $L(\psi)$:

$$L(\psi) = -\Theta \ln \int \exp\Big(-\frac{1}{\Theta} \sum \Phi^k_{ab}(r_{ij})\Big)\Big\{1 + \sum f^x_{ab}(r_{ij}) + \sum (f^x_{ab}(r_{ij}) f^x_{bc}(r_{jk}) + f^x_{ab} f^x_{bc} f^x_{ca}) + \cdots\Big\} dq_1 \ldots dq_N. \tag{4.3b}$$

Carrying out the integration, we use the sequence of Bogoliubov distribution functions of Coulomb systems

$$Z^{-k} \int \exp\Big(-\sum \frac{1}{\Theta} \Phi^k_{ab}(r_{ij})\Big) dq_{s+1} \ldots dq_N = V^{-s} F^k_{a_1 \ldots a_s}(r_1 \ldots r_s). \tag{4.4}$$

Then we get from Eqs. (4.3)

$$L(\psi) = -\Theta \ln Z^k - \Theta \ln \Big\{1 + \frac{1}{V^2} \sum \int f^x_{ab}(r_{ij})\, F^k_{ab}(r_{ij})\, dq_i dq_j + \frac{1}{V^3} \sum \int (f^x_{ab}(r_{ij})\, f^x_{bc}(r_{jk}) + f_{ab} f_{bc} f_{ca})$$

$$\times F^k_{abc}(r_i, r_j, r_k) \quad dq_i\, dq_j dq_k + \sum_{a,b,c,d} \cdots\Big\}, \tag{4.5}$$

where Z^k is the statistical integral of the Coulomb system and $F^k_{ab}(r_{12})$ and F^k_{abc} are the binary and ternary distribution functions of the Coulomb system.[4] The expression (4.5) is the starting point for the solution of the stated problem.

Let us begin with the distribution functions. By the definition of functional differentiation the binary function is given by

$$F_{ab}(r_{12}) = V^2 (\delta L(\psi)/\delta\psi_{ab}(r_{12}))_{\psi=0}$$

or by Eq. (4.5):

$$F_{ab}(r_{12}) = \exp\{-\varphi_{ab}(r_{12})/\Theta\}\left\{F^k_{ab}(r_{12}) + \sum_c \frac{N_c}{V}\int (f_{ac}+f_{bc}+f_{ac}f_{bc})\,F^k_{abc}(r_1r_2r_3)\,dq_3 + \cdots\right\}. \tag{4.6}$$

The triple functional derivative leads us to the ternary distribution function

$$F_{abc}(r_1r_2r_3) = \exp\left[-\frac{1}{\Theta}(\varphi_{ab}+\varphi_{bc}+\varphi_{ca})\right]\left\{F^k_{abc}\right.$$
$$\left. + \sum_x \frac{N_x}{V}\int (f_{ax}+f_{bx}+f_{cx}+f_{ax}f_{bx}+\cdots+f_{ax}f_{bx}f_{cx})\,F^k_{abcx}\,dq_x + \cdots\right\}. \tag{4.7}$$

Substituting into Eqs. (4.6) and (4.7) the values of F^k_{ab} and F^k_{abc} from Ref. 1,

$$F^k_{ab}(r_{12}) = e^{-g_{ab}(r_{12})}\left\{1 + \frac{N}{V}\sum_c n_c\int[(e^{-g_{ac}}-1)(e^{-g_{cb}}-1) - g_{ac}g_{cb}]\,dq_c\right.$$
$$\left. + \frac{N^2}{V^2}\sum_{cd} n_c n_d\int(e^{-g_{ac}}-1)(e^{-g_{cd}}-1+g_{cd})\times(e^{-g_{db}}-1)\,dq_c dq_d + \frac{N^3}{V^3}\sum_{cde}\cdots\right\}; \tag{4.8}$$

$$F^k_{abc}(r_1r_2r_3) = F^k_{ab}F^k_{bc}F^k_{ca} + \frac{N}{V}\sum_x n_x\int(e^{-g_{ax}}-1)(e^{-g_{bx}}-1)(e^{-g_{cx}}-1)\,dq_x + \cdots, \tag{4.9}$$

and collecting the terms with equal powers of N/V we get the binary function

$$F_{ab} = \exp\left[-\frac{1}{\Theta}(\varphi_{ab}+g_{ab})\right]\left\{1 + \frac{N}{V}\sum_c n_c\left[\int[(e^{-g_{ac}}-1)(e^{-g_{cb}}-1)\right.\right.$$
$$\left.\left. - g_{ac}g_{cb}]\,dq_c + \int(f_{ac}+f_{bc}+f_{ac}f_{bc})\,e^{-(g_{ac}+g_{bc})}\,dq_c\right] + \frac{N^2}{V^2}\sum_{c,\,d}\cdots\right\}. \tag{4.10}$$

The first term in the expression (4.10) is the product of the Boltzmann and Debye probabilities for the distribution of two particles. The subsequent terms involve group integrals of Coulomb and mixed types.

In order to get the free energy of the system, we set $\psi = 0$ in Eq. (4.5). Then

$$F = F^k - \Theta\sum_{a,\,b}\frac{N_aN_b}{2V}\int f_{ab}F^k_{ab}(r)\,dq - \Theta\sum_{a,\,b,\,c}\frac{N_aN_bN_c}{3!V^2}\int(3f_{ab}f_{bc}+f_{ab}f_{bc}f_{ca})\,F^k_{abc}dq_1\,dq_2 + \cdots, \tag{4.11}$$

where $F^k = -\Theta\ln Z^k$ is the free energy of the Coulomb system, given by Eq. (3.4).

Substituting Eqs. (4.8), (4.9), and (3.4) into Eq. (1.11), we find finally

$$F = -\Theta\left(\ln V + \frac{V}{N}\frac{1}{4\pi\beta}\left(\frac{\varkappa^2}{2} - \frac{1}{3\beta^2}(1-(1-\beta\varkappa)\sqrt{1+2\beta\varkappa})\right) + \frac{N}{2V}\sum_{a,\,b} n_an_b\left[\int f_{ab}e^{-g_{ab}}dq\right.\right.$$
$$\left.\left. + \int\left(e^{-g_{ab}} - 1 + g_{ab} - \frac{1}{2}g^2_{ab}\right)dq\right] + \frac{N^2}{2V^2}\sum_{a,\,b,\,c} n_an_bn_c\left[\int f_{ab}e^{-g_{ab}}\{(e^{-g_{ac}}-1)(e^{-g_{cb}}-1) - g_{ac}g_{cb}\}\,dq_1\,dq_2\right.$$
$$+\int\left\{f_{ac}f_{cb} + \frac{1}{3}f_{ac}f_{bc}f_{ca}\right\}e^{-(g_{ab}+g_{ac}+g_{bc})}\,dq_1\,dq_2 + \frac{1}{3}\int(e^{-g_{ac}}-1+g_{ac})(e^{-g_{cb}}-1+g_{cb})(e^{-g_{ab}}-1+g_{ab})\,dq_1\,dq_2$$
$$\left.\left. - \int g_{ab}(e^{-g_{cb}}-1+g_{cb})(e^{-g_{ac}}-1+g_{ac})\,dq_1dq_2\right] + \frac{N^3}{V^3}\cdots\right) \tag{4.12}$$

In Eqs. (4.10) and (4.12) expressions for the binary function and the free energy of a neutral system of ions are written in the form of series of group integrals. The first terms of these series correspond to the self-consistent (Debye) interaction between the ions. The second terms, arising from combinations of pairs of operators D_i, characterize the binary correlation between the particles. After these come triple, quadruple, and still higher correlations.

Each group correlation consists of integrals of Coulomb and mixed types. The integrals corresponding to pure Coulomb (or "cut off" Coulomb) interaction are made up of exponential functions of the type $e^{-g_{ab}} - 1$, where $g_{ab} \cong e^{-r_{ab}/r_d}$ is the self-consistent Debye potential. Thus the integrands go to zero very rapidly with increasing r. Furthermore, the group integrals decrease rapidly with increase of the order of the correlation.

The mixed group correlations involve the usual functions of the van der Waals theory, $\exp(-\varphi_{ab}/\Theta) - 1$, and functions $e^{-g_{ab}} - 1$. Such group integrals also decrease rapidly with

increasing order of correlation.

The expressions for the free energy and the distribution functions also have the form of power series in N/V. These are not, however, expansions in powers of the concentration. In the first place, such expansions lose their meaning when $N/V > 1$; in the second place, the group integrals depend on N/V.

The expressions for the binary distribution function and the free energy are series expressions in the correlations. Because the Coulomb forces occur in the integrals in the form of the screened self-consistent potential, for which the screening radius (r_d) decreases with increasing concnetration, these expansions are obviously valid for high concentrations.

Let us consider further a special case of Eqs. (4.6) and (4.12) — a system of electrons in a compensating external field, for which $\int \Phi^k dq = \nu(0) = 0$. Since in this case $f_{ab}(0) = 0$, the quantities $F_{ab} = F^k_{ab}$ and $F = F^k$ are given by Eqs. (4.8) and (3.4), respectively. The binary and ternary distribution functions do not diverge at zero, and the integrands in the correlation terms of Eqs. (4.8), (4.9), and (3.4) are also free from singularities. This indicates that for electrons in a compensating field there is no need to "cut off" the Coulomb potential.

In a subsequent paper the thermodynamic functions of ionic systems will be calculated and compared with experiment.

In conclusion I express my sincere gratitude to N. N. Bogoliubov for suggesting this problem and to A. E. Glauberman for a discussion of the paper.

Note (September 3, 1957). The remark in the recently published paper of Bazarov[6] about the incorrectness of the formula (2.4) for the free energy in the paper of Glauberman and Iukhnovskii[7] is without foundation. The divergence of F and the departure from the Debye formula for $\beta \to 0$ are avoided by the choice of the arbitrary constant of integration (to the accuracy with which F is defined), after which Eq. (2.4) takes the form

$$F_e = -\frac{T}{2\varepsilon}\sum_a N_a e_a^2 \left\{\frac{1}{2ac^3}\left[\frac{1}{5}(x-1)^5 - \frac{2}{3}(x-1)^3 + (x-1) + \frac{1}{20}(x-2)^5 - \frac{1}{4}(x-2)^4 x - \frac{8}{15}\right]\right\}.$$

[1] I. R. Iukhnovskii, J. Exptl. Theoret. Phys. (U.S.S.R.) **27**, 690 (1954).

[2] I. Langmuir and L. Tonks, Phys. Rev. **33**, 195 (1929).

[3] M. Born and J. Mayer, Z. Phys. **75**, 1 (1932).

[4] D. I. Zubarev, Dokl. Akad. Nauk SSSR **95**, 757 (1954).

[5] L. Landau and E. Lifshitz, Статистическая физика (Statistical Physics), M.-L., 1951.

[6] I. P. Bazarov, J. Exptl. Theoret. Phys. (U.S.S.R.) **32**, 1065 (1957), Soviet Phys. JETP **5**, 872 (1957).

[7] A. E. Glauberman and I. R. Iukhnovskii, J. Exptl. Theoret. Phys. (U.S.S.R.) **22**, 563 (1952).

Translated by W. H. Furry
72

THEORY OF THE MASER AND MASER FLUCTUATIONS

V. S. TROITSKII

Gor'kii State University

Submitted to JETP editor July 5, 1957

J. Exptl. Theoret. Phys. (U.S.S.R.) **34**, 390-393 (February, 1958)

The maser is considered as an oscillating system with one degree of freedom, the steady-state oscillations of which are described by the Basov-Prokhorov equations. It is shown that there is a "soft" mode and an analog of the "hard" mode which is preceded by a region of noise generation. The natural line width due to thermal noise is determined and found to be 10^{-4} cps for an ammonia maser at room temperature.

1. The general form of the oscillating equation for a maser is represented by the system:

$$L_k(E + 4\pi\sigma) = 0;\ L_m(E) = \sigma,$$

where E is the field in the oscillator circuit and σ is the molecular polarization. The first equation is the usual differential circuit equation while the second applies to the system of molecules. The analysis of the second equation is extremely difficult and has not been carried out at the present time. However, certain problems in the theory of maser oscillations can be solved by means of the Basov-Prokhorov equation[1] which describes the steady-state oscillations and is a circuit equation with a complex dielectric constant ϵ associated with the beam of molecules

$$\frac{d^2V}{dt} + \frac{\omega_0}{Q}\frac{dV}{dt} + \frac{\omega_0^2}{\varepsilon}V = 0.$$

This equation can be obtained from the system written above if the well-known relation $E(\epsilon - 1)/4\pi = \sigma$ is applied in the second equation; in the present case this relation applies only in the case of sinusoidal oscillations because of saturation effects.

Fluctuations in amplitude and frequency in a maser are a result of thermal noise $\xi(t)$ with a spectral density

$$w_\xi = 4r\Theta;\ \Theta = \hbar\omega/2 + [e^{\hbar\omega/kT} - 1]^{-1}\hbar\omega$$

and the "shot" effect associated with the dielectric constant of the gas, i.e., fluctuations in ϵ. When these fluctuations are taken into account the equation is written in the form

$$\frac{d^2(V\varepsilon)}{dt^2} + \frac{\omega_0}{Q}\frac{d(V\varepsilon)}{dt} + \omega_0^2 V = \omega_0^2\xi(t).$$

It can be shown that the random dependence of ξ on t gives rise to a fluctuating emf (containing the derivatives $d\xi/dt$ and $d^2\xi/dt^2$) which is negligibly small compared with $\xi(t)$ even when $T = 0$. However, the parametric effect of the fluctuations in ϵ are important and are considered below. The final equation is

$$\frac{d^2V}{dt^2} + \omega_0^2 V = \mu\left[\omega_0 Q\left(1 - \frac{\varepsilon_1}{|\varepsilon|^2}\right)V - Q\left(\frac{\omega_0}{Q} + \frac{\omega_0^2}{\omega}\frac{\varepsilon_2}{|\varepsilon|^2}\right)\frac{dV}{dt}\right] + \omega_0^2\frac{\varepsilon_1}{|\varepsilon|^2}\xi(t), \tag{1}$$

where $V = A_0 \exp i\omega t$ is the steady-state sinusoidal voltage across the condenser, Q is the quality factor of the circuit, ω_0 is the natural resonant frequency of the circuit in the absence of molecules, $\epsilon = \epsilon_1(\omega, E_0, t) - i\epsilon_2(\omega, E_0, t)$ is the dielectric constant of the gas averaged over the volume, which is time dependent because of the shot effect, $E_0 = A/d$ is the field in the condenser, and $\mu = 1/Q$.

Equation (1) can be used only when V changes in a quasi-static way. Consequently the application of Eq. (1) for finding fluctuations in V is valid if $\xi(t)$ is characterized by a narrow spectrum $\Delta\omega_\xi \ll \Delta\omega_e$ (where $\Delta\omega_e$ is the width of the absorption line of the gas) centered about the frequency of the steady-state oscillations. As is shown by the theory,[2] this spectrum determines completely the spectral line width of the maser.

The solution of Eq. (1) is written in the form $V = A\cos\vartheta$ and the fluctuations are analyzed in accordance with the Bershtein method.[3] The usual transformations[3,4] yield the following equations:

$$\begin{aligned}
&\frac{d\vartheta}{dt} = \Psi(A,\dot\vartheta) - \frac{\omega_1}{A}\xi(t)\cos\omega_1 t;\\
&\frac{dA}{dt} = \Phi(A,\dot\vartheta) - \omega_1\xi(t)\sin\omega_1 t,\\
&\Psi(A,\dot\vartheta) = \omega_0 - \frac{\omega_0}{2}\left(1 - \frac{\varepsilon_1}{|\varepsilon|^2}\right);\\
&\Phi(A,\dot\vartheta) = -\frac{A}{2}\left[\frac{\omega_0}{Q} + \frac{\omega_0^2}{\omega}\frac{\varepsilon_2}{|\varepsilon|^2}\right],
\end{aligned} \tag{2}$$

where $\omega = \dot{\vartheta}$ and ω_1 are respectively the instantaneous and mean statistical frequencies of the steady-state oscillations.

2. Using the well-known expression[1] for the polarizability $\kappa_1(\omega, t)$ and $\kappa_2(\omega, t)$ and the distribution over time of flight $P(\tau) = (\tau/\tau_0^2) \times \exp(-\tau/\tau_0)$, the dielectric constant of the beam of gas molecules in the circuit, averaged over the volume, can be written

$$\varepsilon_2(\omega, E_0, t) = \frac{4\pi M(t)}{Sl} \int_0^\infty P(\tau) \frac{d\tau}{\tau} \int_0^\tau \varkappa_2(\omega, t)\, dt$$
$$= -\frac{4\pi\hbar^3\beta\tau_0}{d^2 Sl} \frac{M(t)}{u^2+1+\Delta^2}, \qquad \varepsilon_1(\omega, E_0, t) = 1 - u\,|\varepsilon_2|, \tag{3}$$

where $u = (\omega_2 - \omega)\tau_0$, ω_2 is the frequency of the photon, $\Delta^2 = E_0^2\beta\tau_0^2$, d is the dipole moment of the molecules, S and ℓ are the cross section and length of the beam of molecules and M(t) is the number of molecules in the condenser at any given instant of time.

The fluctuations in M(t) are determined by the shot effect in the dielectric constant. For a beam with the distribution denoted above by $P(\tau)$, the spectral density in the fluctuations of the number of particles $m(t) = M(t) - \overline{M}$ is

$$W_m(F) = 2\overline{M}\tau_0 (3 + \Omega^2\tau_0^2)/(1 + \Omega^2\tau_0^2), \quad \Omega = 2\pi F. \tag{4}$$

3. The mean values of the amplitude A_0 and the frequency $\vartheta_1 = \omega_1$ are found from the conditions $\Phi(A_0, \omega_1) = 0$ and $\omega_1 = \Psi(A_0, \omega_1)$. From the first of these, to an accuracy of μ^2, we find the equation for power as a function of tuning and oscillation frequency

$$\Delta^2 = \eta - 1 - u^2. \tag{5}$$

The second equation yields an equation for the circuit frequency (or oscillation frequency if the maser is excited)

$$u^3 - u^2 v + u(1 + \Delta^2 + R\eta) - v(1 + \Delta^2) = 0, \tag{6}$$

where $\eta = (8\pi\hbar^3/Sld^2)\tau_0^2\overline{N}Q$ is a dimensionless parameter which characterizes the excitation of the maser ($\overline{N}$ is the mean flux of molecules per unit time), $V = (\omega_2 - \omega_0)\tau_0$, $R = \omega_2\tau/2Q$ is the ratio of the quality factor of the absorption line of the gas $Q_\ell = \omega_2\tau_0/2$ to the figure of merit of the circuit; usually R is approximately $10^3 - 10^4$.

The mean amplitude and frequency are determined from the solution which satisfies Eqs. (5) and (6). From Eq. (5) we obtain the values at which self-excitation is achieved $|u| \leq \sqrt{\eta - 1}$. To determine the stability of these oscillations we write Eq. (2) with $\xi(t) = 0$ in the form

$$\omega_1 = \Psi_1(A_0), \quad dA_0/dt = \Phi_1(A_0, \Psi(A_0)). \tag{7}$$

In accordance with the general rule the oscillations are stable when

$$\frac{d\Phi_1}{dA_0} = p_0 = \left(p + \frac{p_1 q}{1 - q_1}\right) < 0, \tag{7}$$

where $p = \partial\Phi/\partial A$, $p_1 = \partial\Phi/\partial\omega$, $q = \partial\Psi/\partial A$, $q_1 = \partial\Psi/\partial\omega$ for $\omega = \omega_1$ and $A = A_0$. An examination of this equation indicates that when $\eta \leq 2$ the region of stable oscillations coincides with the excitation region $|u| \leq \sqrt{\eta - 1}$; when $\eta > 2$ the region of stable sinusoidal oscillations is smaller than the region of self-excitation and is equal to $|u| \leq \sqrt{\eta/2}$. In the unstable region $\sqrt{\eta/2} \leq |u| \leq \sqrt{\eta - 1}$ one expects noise oscillations with a spectrum of absorption lines or relaxation oscillations in which both frequency and amplitude change. When $\eta \leq 2$ there is a "soft" mode of production of harmonic oscillations depending on u or η while for $\eta \geq 2$ there is an analog to a "hard" model.

4. To determine the fluctuations in amplitude and phase we set $\dot{\vartheta} = \omega = \omega_1 + \nu(t)$; $A = A_0 + A_0 \times \alpha(t)$, where $\nu(t)$ and $A_0\alpha(t)$ are the fluctuations in frequency and amplitude. Substituting these in Eq. (2) and taking $M(t) = \overline{M} + m(t)$, after making a series expansion and separation of variables, limiting ourselves to linear terms we have

$$\frac{d\nu}{dt} = p_0\nu + \frac{p_2 q - p q_2}{1 - q_1} m + \frac{q_2}{1 - q_1}\frac{dm}{dt} + \frac{1}{1 - q_1}\left[\frac{p}{A_0}\xi\omega_1\cos\omega_1 t - q\xi\omega_1\sin\omega_1 t - \frac{d}{dt}\left(\xi\frac{\omega_1}{A_0}\cos\omega_1 t\right)\right],$$
$$\frac{d\alpha}{dt} = p_0\alpha + \frac{p_m}{A_0} m - \frac{p_1}{1 - q_1}\xi\frac{\omega_1}{A_0}\cos\omega_2 t - \xi\frac{\omega_1}{A_0}\sin\omega_1 t, \qquad p_2 = \partial\Phi/\partial M; \quad q_2 = \partial\Psi/\partial M; \quad p_m = p_2 + p_1 q_2/(1 - q_1). \tag{8}$$

It can be shown that the factor $p_2 q - p q_2$ is identically equal to zero, i.e., fluctuations in the number of particles do not produce fluctuations in the frequency of oscillation [assuming that Eq. (3) applies for ϵ]. This is easily explained by the effect of saturation more precisely by the dependence of the frequency of oscillation (by virtue of ϵ_1) not only on M but also on E_0. From Eq. (8) we obtain an expression for the spectral densities $\nu(t)$ and $\alpha(t)$ (for $u \approx 0$; $\eta > 1$)

$$W_\alpha(F) = \frac{\eta^2}{\overline{N}(\eta - 1)^2} + \frac{\Theta\eta^2}{P(\eta - 1)^2}; \quad W_\nu(F) = \frac{\Theta\omega_2^2}{R^2 PQ^2}, \tag{9}$$

where P is the oscillation power of the maser. The amplitude fluctuations are produced by the shot effect in the flux of molecules (first term) as well as thermal fluctuations (second term). The frequency fluctuations are produced only by thermal effects. In an ammonia maser with the circuit at room temperature $kT \gg \hbar\omega$ and $\Theta = kT$; setting $\tau_0 = 10^{-4}$ sec, $P = 10^{-9}$ watts, from Eq. (9) the spectral line width is found to be[5]

$$\Delta F = W_\nu(0)/4\pi = (kT/\hbar\omega_2)(1/\pi\bar{N})\tau_0^{-2} \simeq 10^{-4} \text{ cps}.$$

At low circuit temperatures, if millimeter waves are considered (or absolute zero for any wavelength) $\hbar\omega_1 \gg kT$ and $\Theta = \hbar\omega_2/2$, yielding $\Delta F = \omega_2^2/8\pi Q_1^2$ for the line width due to "zero field" fluctuations.

Equation (9) shows that the fluctuations in the frequency of a maser are $R^2 \sim 10^6 - 10^8$ times smaller than the fluctuations associated with the thermal noise in an equivalent vacuum tube oscillator. The monochromaticity and stability of maser oscillations are explained by the automatic frequency-regulating effect which results from the dependence of ϵ on the frequency of oscillation. In accordance with Eq. (3), an increase in frequency by an amount ν_0 leads to an increase in ϵ_1, thereby producing a compensating reduction of frequency by an amount ν_1; the resulting frequency displacement is

$$\nu = \nu_0 + \nu_1, \quad \nu_1 = \frac{d}{d\varepsilon_1}\left(\frac{\omega_0}{V\bar{\varepsilon}_1}\right)\frac{d\varepsilon_1}{d\omega}\nu \simeq q_1\nu.$$

Thus $\nu = \nu_0/(1 - q_1) \approx \nu_0/R$ (it can be shown that $1 - q_1 \cong q_2 \approx R$). If ν_0 is the fluctuation in frequency which takes place without self-compensation (fluctuations in an ordinary oscillator), Eq. (9) is easily obtained from the expression $\overline{\nu^2} = \overline{\nu_0^2}/R^2$.

If the frequency of the fluctuations is such that $2\pi F > \tau_0^{-1}$ the self-regulating effect of ϵ_1 does not operate (ϵ_1 cannot "follow" variations in ω and A) and one expects that at these frequencies W(F) will be R^2 times larger than indicated by Eq. (9). However, this situation does not lead to a broadening of the line but merely increases the intensity in the wings. The spectral line width has been considered in Ref. 6 by another method but the results obtained there differ somewhat from those described here.

A detailed description of the present work is given in Ref. 7.

[1] N. G. Bosov and A. M. Prokhorov, J. Exptl. Theoret. Phys. (U.S.S.R.) **27**, 431 (1954); Dokl. Akad. Nauk SSSR **101**, 47 (1955); Usp. Fiz. Nauk **57**, 485 (1955); J. Exptl. Theoret. Phys. (U.S.S.R.) **30**, 560 (1956), Soviet Phys. JETP **3**, 426 (1956).

[2] S. M. Rytov, J. Exptl. Theoret. Phys. (U.S.S.R.) **29**, 304, 315 (1955), Soviet Phys. JETP **2**, 217, 225 (1956).

[3] I. L. Bershtein, Dokl. Akad. Nauk SSSR **20**, 11 (1938); Izv. Akad. Nauk SSSR, ser. fiz. **14**, 145 (1950).

[4] A. A. Andronov and S. E. Khaikin, Theory of Oscillations, Princeton Univ. Press, 1949.

[5] V. S. Troitskii, Радиотехника и электроника (Radio Engineering and Electronics) **1**, 818 (1956).

[6] Shimoda, Wang, and Townes, Phys. Rev. **102**, 1308 (1956).

[7] V. S. Troitskii, Радиотехника и электроника (Radio Engineering and Electronics), June (1958).

Translated by H. Lashinsky
73

HOLE BANDS IN NaCl TYPE CRYSTALS

T. I. KUCHER

Zhitomir Pedagogical Institute

Submitted to JETP editor July 11, 1957

J. Exptl. Theoret. Phys. (U.S.S.R.) 34, 394-404 (February, 1958)

The energy and state function of a NaCl type cubic crystal with a single electron removed (with a hole) are considered in the Fock many-electron approximation assuming tight binding. It is shown that three hole bands exist which are contiguous for $K = 0$, corresponding to a stationary (but not minimal) value of the crystal energy. The dependence of the energy E on K in the vicinity of $K = 0$ is anisotropic and is not of a tensor nature. The band of the lightest holes is important for conduction. This band has four absolute minima for values of $K\{\pm \pi/d; \pm \pi/d; \pm \pi/d\}$ and three relative minima for $K\{\pm 2\pi/d; 0; 0\}$, $\{0; \pm 2\pi/d; 0\}$ and $\{0; 0; \pm 2\pi/d\}$.

Values of the effective masses when $K = 0$ are given for various directions of K and the effective mass tensor for the afore-mentioned extremal values is written out. Numerical results are given for KCl.

1. STATEMENT OF THE PROBLEM AND BASIC ASSUMPTIONS

We shall consider a binary cubic ionic crystal of the NaCl type with one electron removed. We shall assume tight binding, i.e., the hole will be regarded as localized close to halogen sites. This is permissible because of the large energy required for double ionization of alkali metal atoms by comparison with halogen atoms.

As in other papers by the author[1,2] we shall use $\mathbf{r}_s^l$ to denote the equilibrium position of an s-type ion in the l-th cell ($s = 1, 2$ for + and − ions). $\rho_s^{l\lambda}$ will denote the set of $3N_s$ coordinates of the N_s electrons of ion s, l (λ is the permutation index of the electrons in the crystal), and $\rho_{n_s}^l$ will denote the radius vector of the n_s-th electron ($n_s = 1, 2, \ldots N_s$) with respect to the nucleus at $\mathbf{r}_s^l$. Because of the translational symmetry of the crystal and the corresponding degeneracy the Ψ function of the crystal is taken in the form

$$\Psi_\kappa = A\sum_{l=1}^{M} e^{i\kappa r_s^l}\Psi_s^l, \qquad (1)$$

where Ψ_s^l is an auxiliary many-electron function which is the antisymmetrized product of the functions of all ions $\psi_{s'}^{l'}$ including the function φ_s^l of the ion which lacks a single electron (see Ref. 1). The wave functions $\psi_{s'}^{l'}$ and φ_s^l, of individual ions as well as of ions and the atom, will be considered as orthogonal in the same sense as in Ref. 1.

The Hamiltonian of the system will consist of the sum of the Hamiltonians of the individual ions and of interactions between different ions. Since the hole moves only about the halogen ions (the tight binding assumption) its energy will be determined by the exchange integrals of neighboring halogen ions. In calculating these integrals we have neglected the exchange of electrons in the p valence shell with inner electrons, i.e., we have considered[3] only 6 (or 5) of the outermost electrons for nuclear charge $Z = 5$. Since the Hamiltonian is independent of spin the wave functions of atom and ion which we use are those of Fock[4] for many-electron atoms. We thus have

$$\psi_s^l(\rho_s^l) = \frac{1}{\sqrt{720}}\sum_1^{20}(-1)^\nu \alpha(i)\,\alpha(j)\,\alpha(k)\,\beta(l)\,\beta(m)\,\beta(n) \times \begin{vmatrix} \psi_x(i) & \psi_y(i) & \psi_z(i) \\ \psi_x(j) & \psi_y(j) & \psi_z(j) \\ \psi_x(k) & \psi_y(k) & \psi_z(k) \end{vmatrix} \begin{vmatrix} \psi_x(l) & \psi_y(l) & \psi_z(l) \\ \psi_x(m) & \psi_y(m) & \psi_z(m) \\ \psi_x(n) & \psi_y(n) & \psi_z(n) \end{vmatrix}. \qquad (2)$$

Here

$$\psi_x(n) = R(\rho_{n_s}^l)\sin\vartheta_{n_s}^l\cos\varphi_{n_s}^l, \qquad (3)$$

$$\psi_y(n) = R(\rho_{n_s}^l)\sin\vartheta_{n_s}^l\sin\varphi_{n_s}^l, \quad \psi_z(n) = R(\rho_{n_s}^l)\cos\vartheta_{n_s}^l$$

are the normalized one-electron functions of the p state of the n_s-th electron of ion s,l in the coordinate system whose center is as the corresponding nucleus. As the functions in (3) are spatially asymmetrical, the directions of the axes must be specified. We shall assume hereinafter

that function (1) is given in the coordinate system where the axes of all ions are parallel to each other and to the edges of the crystal, as shown in Fig. 1.

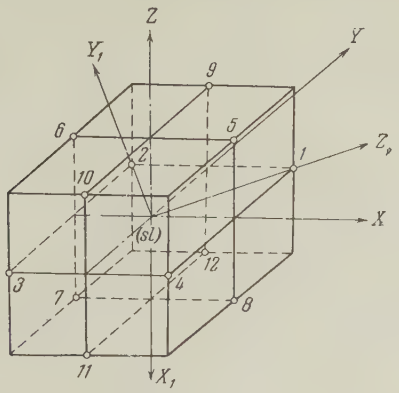

FIG. 1

The form of the radial part R(r) of (3) depends on the crystal and in first approximation on the halogen. For KCl, R(r) in the region that is important for exchange between ions is taken to agree with Hartree's results[5] for the 3p shell of Cl. For lack of other information we assume that the radial function is identical for the atom and ions in the crystal and for chlorides is given by

$$R(r) = (3\alpha^3/\pi)\, e^{-\alpha r} \text{ with } \alpha d/2 = 4.835; \tag{4}$$

where $d/2 = 3.145 \times 10^{-8}$ cm is the lattice constant of KCl. For fluorides Eq. (4) can also be used, with $\alpha = 1.481 \times 10^8\,\text{cm}^{-1}$, but with less accuracy; in this case it is better to use

$$H_\kappa = \frac{2e^2}{d}\left[B - \sum_{l'=1}^{12} I^{ll'} \exp\{i\kappa(\mathbf{r}_s^l - \mathbf{r}_s^{l'})\}\right]. \tag{5}$$

In (2) $\alpha(n)$ and $\beta(n)$ denote the usual one-electron spin eigenfunctions of the corresponding electrons[6] (of different orientations). The number of these functions corresponds to the total zero (saturated) spin of a halogen ion. The summation in (2) is performed over all permutations of six electrons i, j, ... with two spins α, β, of which 20 are possible. The factor $(-1)^\nu$ is +1 or −1 depending upon whether the given term is obtained by an even or odd number of electron permutations from some initial order such as 1, 2, ..., 6.

In the atom one electron of the p shell is absent, so that its electron functions are triply degenerate and their linear combination must be used. The total spin of the crystal is unchanged (and is assumed to be negative). Then for the atom, using the previous notation,

$$\psi_{am} \equiv \varphi_s^l(\boldsymbol{\rho}_s^l) = \frac{1}{\sqrt{120}} \sum_1^{10} (-1)^\nu \alpha(j)\,\alpha(k)\,\beta(l)\,\beta(m)\,\beta(n) \times \begin{vmatrix} b & c & a \\ \psi_x(j) & \psi_y(j) & \psi_z(j) \\ \psi_x(k) & \psi_y(k) & \psi_z(k) \end{vmatrix} \begin{vmatrix} \psi_x(l) & \psi_y(l) & \psi_z(l) \\ \psi_x(m) & \psi_y(m) & \psi_z(m) \\ \psi_x(n) & \psi_y(n) & \psi_z(n) \end{vmatrix}; \tag{6}$$

here b, c, a are coefficients, so far unknown, of the linear combination of mutually-orthogonal functions (minors of the determinant) which satisfy the normalization condition

$$|a|^2 + |b|^2 + |c|^2 = 1. \tag{7}$$

They will be determined subsequently by minimizing the total energy of the system.

A check of the orthogonality of (4) and (6) for KCl shows that $I_{\text{orth}} = 5.2 \times 10^{-4}$ for two ions and $\leq 5 \times 10^{-3}$ for an atom and an ion.

2. TOTAL ENERGY AND EXCHANGE INTEGRALS

The average energy, using the function (1), is

$$\overline{H}_\kappa = \sum_{\sigma_1} \cdots \sum_{\sigma_N} \int \Psi_\kappa^* \hat{H} \Psi_\kappa d\tau = \frac{1}{M} \sum_l \sum_{l'} \exp\{i\kappa(\mathbf{r}_s^l - \mathbf{r}_s^{l'})\}\, \overline{H}_{ss}^{ll'}. \tag{8}$$

The diagonal term is

$$\overline{H}_{ss}^{ll} = \int \Psi_s^{l*} \hat{H} \Psi_s^l d\tau = \frac{2e^2}{d} B = 2\frac{\alpha e^2}{d} + V_{\text{Cl}}^- + U_+, \tag{9}$$

where $\alpha = 1.747$ is the Madelung constant, $V_{\text{Cl}}^- = 3.72$ ev is the electron affinity of Cl (Ref. 7), and U_+ is the eigenvalue of the energy of a hole in the field of the ions which it has polarized. As shown in Ref. 2, $U_+ = -1.352$ ev for KCl. Hence we obtain for (9) 10.4 ev.

The offdiagonal terms $\overline{H}_{ss}^{ll'}$ differ from zero only when sℓ and sℓ′ are nearest neighbors. We denote

$$\overline{H}_{ss}^{ll'} = \int \Psi_s^{l*} \hat{H} \Psi_s^{l'} d\tau = -\frac{2e^2}{d} I^{ll'} \delta_{l'; l\pm 1}, \tag{10}$$

where $\delta_{\ell'; \ell\pm1} \neq 0$ only for the 12 ℓ′ of the nearest like neighbors of the site sℓ. Then

$$\overline{H}_\kappa = \frac{2e^2}{d}\left[B - \sum_{l'=1}^{12} I^{ll'} \exp\{i\kappa(\mathbf{r}_s^l - \mathbf{r}_s^{l'})\}\right]. \tag{11}$$

Substituting (1) into (10) and taking into account the orthogonality of the ψ functions,[1] we obtain

$$I^{ll'} = -\frac{d^2}{2} \sum_{\sigma_1} \cdots \sum_{\sigma_{11}} \int \psi_s^{l'*} \varphi_s^{l*} \Big\{ -\frac{\hbar^2}{2me^2} \Delta_\rho - \sum_{s'', l''} V_{s''}(\boldsymbol{\rho} - \mathbf{r}_{s''}^{l''}) - Z_s/|\boldsymbol{\rho} - \mathbf{r}_s^l| - Z_s/|\boldsymbol{\rho} - \mathbf{r}_s^{l'}| + \sum_{n_s=1}^{5} 1/|\boldsymbol{\rho} - \boldsymbol{\rho}_{ns}^l| + \sum_{n_s=1}^{5} 1/|\boldsymbol{\rho} - \boldsymbol{\rho}_{n_s}^{l'}| \Big\} \psi_s^l \varphi_s^{l'} d\tau. \tag{12}$$

In (12) the electron whose radius vector is denoted by $\boldsymbol{\rho}$ passes from site sℓ to site sℓ′. The first term in the braces is its kinetic energy operator, the second term is the potential of all ions of the crystal except sℓ and sℓ′ at $\boldsymbol{\rho}$, and the last

four terms describe the interaction of the indicated electron with nuclei and with the other five electrons at sites $s\ell$ and $s\ell'$. Here $Z_S = 5$ is the effective charge of the halogen nucleus, since part of the charge is screened by inner electrons, the interaction with which we are neglecting in the exchange integral.

We shall add a second term to the Madelung potential in the brace of Eq. (12). For this purpose we must add inside the braces terms which are the average quantum mechanical potentials at the point ρ of ordinary halogen ions at the sites $s\ell$ and $s\ell'$. The exchange integral of the Madelung potential is zero, by virtue of the latter's constancy within the important region of integration between ions and from the orthogonality condition. Since the ionic functions ψ_s^ℓ have been antisymmetrized, all ions are equivalent and all components of their average quantum mechanical potentials are respectively equal. On the other hand, the integrals of the exact electron potentials depend on whether the spins at ρ and $\rho^\ell_{n_s}$ (or $\rho^{\ell'}_{n_s}$) are equal or different.

There are two of the first kind in each ion and three of the second kind. Therefore

$$I^{ll'} = \frac{d}{2}\sum_{\sigma_1}\cdots\sum_{\sigma_{11}}\int \psi_s^{l'*}\varphi_s^{l*}\Big\{\frac{\hbar^2}{2me^2}\Delta_\rho + 12\Big[\frac{|\psi_s^l|^2}{|\rho-\rho^l_{n_s}|}\,d\tau - \frac{4}{|\rho-\rho^l_{n_s}|}\Big|_{\text{same spin}} - \frac{6}{|\rho-\rho^l_{n_s}|}\Big|_{\substack{\text{different}\\ \text{spin}}}\Big]\psi_s^l\varphi_s^{l'}\,d\tau \equiv T^{ll'} + 12V_s^{ll'} - 4E_s^{ll'} - 6E_2^{ll'}. \tag{13}$$

To obtain the energy we must substitute into (11) the 12 exchange integrals of (12), and for this purpose (13) must be calculated.

The functions ψ and φ under the integral sign in (13) are the 3rd order determinants (2) and (6), whose elements (3) in each row are three "projections" of certain "vectors" on the coordinate axes. These "vectors" are of equal "length" $R(r)$ with the exception of the "vector" $a\{b; c; a\}$, which is of "length" 1. The determinants are then analogous to "volumes." When the coordinate system is rotated the lengths of the vectors and magnitudes of the volumes are unchanged, and the projections of the vectors change in magnitude but not in form. Therefore in integrating (13) we can rotate the coordinate axes at will without changing the form of the integrands nor the magnitudes of the integrals. However, b, c, a then are transformed into b', c', a', which are linear combinations of the original quantities depending on the angles of rotation. We now rotate the coordinate axes in (13) so that the polar axis $Z^{\ell\ell'}$ passes through the sites $s\ell$ and $s\ell'$ (Fig. 1). The new coefficients, which differ for different sites, are denoted by $b^{\ell\ell'}$, $c^{\ell\ell'}$, $a^{\ell\ell'}$. The $I^{\ell\ell'}$ will be identical quadratic forms of their coefficients.

Simple calculations show that the terms $V_S^{\ell\ell'}$ and $E_2^{\ell\ell'}$ in (13) are identical (exchange with electrons of different spin is forbidden). The remaining term $6V_S^{\ell\ell'}$ is also reduced by the Coulomb part $4E^{\ell\ell'}$. The general result[3] is

$$I^{ll'} = T^{ll'} + (6V_s^{ll'} - 4E_1^{ll'}) = D(|b^{ll'}|^2 + |c^{ll'}|^2) - E|a^{ll'}|^2 = D - (D+E)|a^{ll'}|^2, \tag{14}$$

where D and E are exchange integrals, i.e., constants of the crystal. In the case of crystals for which the radial part can be given in the form of (4), such as all chlorides, we have

$$E = -\frac{d}{6}\int\{Q(r_s^{l'}) + P(r_s^{l'})\}\,\psi_3^*(\mathbf{r}_s^l)\,\psi_3(\mathbf{r}_s^{l'})\,d\tau,$$
$$D = \frac{d}{6}\int\{Q(r_s^{l'}) + P(r_s^{l'})\}\,\psi_1^*(\mathbf{r}_s^l)\,\psi_1(\mathbf{r}_s^{l'})\,d\tau; \tag{15}$$

where

$$\psi_{1,2}(r) = \frac{R(r)}{\sqrt{2}}\sin\vartheta e^{\pm i\varphi};\quad \psi_3(\mathbf{r}) = \psi_z(\mathbf{r}); \tag{16}$$

$$Q(r) + P(r) = \frac{\hbar^2}{2me^2}\Big(\alpha - \frac{2\alpha}{r} - \frac{2}{r^2}\Big) + \frac{2\alpha}{5}\Big[\frac{5}{\rho} + \frac{6}{\rho^3} - e^{-2\rho}\Big(4\rho + 13 + \frac{17}{\rho} + \frac{12}{\rho^2} + \frac{6}{\rho^3}\Big) - 8\rho^2\,\mathrm{Ei}(-2\rho)\Big]. \tag{17}$$

Here $\rho = \alpha r$ and $\mathrm{Ei}(-x)$ is the familiar tabulated function.[8]

For KCl with the already indicated values of α and d we obtain

$$D = 0{,}9\cdot10^{-2};\quad E = 4{,}6\cdot10^{-2};$$
$$2e^2D/d = 0{,}041\,\text{ev};\quad 2e^2E/d = 0{,}211\,\text{ev}. \tag{18}$$

For the other crystals which contain Cl the numerical difference from (18) should not be very large since their lattice constants are approximately the same.

Substituting (14) in (11), we obtain

$$\frac{d}{2e^2}\overline{H}_\kappa = B - D\sum_{l'=1}^{12}\exp\{i\kappa(\mathbf{r}_s^l - \mathbf{r}_s^{l'})\} + (E+D)\sum_{l'=1}^{12}|a^{ll'}|^2\exp\{i\kappa(\mathbf{r}_s^l - \mathbf{r}_s^{l'})\}. \tag{19}$$

For the determination of $\overline{H}_K$ it is necessary to replace $a^{\ell\ell'}$ by $\{b; c; a\}$ for all sites. (The lat-

TABLE I. Coefficients of a{b, c, a}

No. of site	Coordinates of site l', in units d/2			$\sqrt{2}\cdot b^{l'}$	$\sqrt{2}\cdot c^{l'}$	$\sqrt{2}\cdot a^{l'}$	No. of site	Coordinates of site l', in units d/2			$\sqrt{2}\cdot b^{l'}$	$\sqrt{2}\cdot c^{l'}$	$\sqrt{2}\cdot a^{l'}$
	x	y	z					x	y	z			
1	1	1	0	$-a$	$(-b+c)$	$(b+c)$	7	−1	0	−1	$(-b+a)$	c	$-(b+a)$
2	−1	1	0	$-a$	$-(b+c)$	$(-b+c)$	8	1	0	−1	$(b+a)$	c	$(-b+a)$
3	−1	−1	0	$-a$	$(b-c)$	$-(b+c)$	9	0	1	1	$(c-a)$	$-b$	$(c+a)$
4	1	−1	0	$-a$	$(b+c)$	$(b-c)$	10	0	−1	1	$-(c+a)$	b	$(-c+a)$
5	1	0	1	$(b-a)$	c	$(b+a)$	11	0	−1	−1	$-(c+a)$	$-b$	$(c-a)$
6	−1	0	1	$-(b+a)$	c	$(b-a)$	12	0	1	−1	$(c-a)$	b	$-(c+a)$

ter are determined from Fig. 1 and are listed in Table I.) When this has been done, using $\mathbf{k} = \mathrm{K}d/2$, we obtain, in the original coordinate system,

$$\frac{d}{2e^2}\overline{H}_{\mathrm{K}} = B - 4D\sum_{x\neq y}\cos k_x \cos k_y + 2(E+D)\{\sum_{x\neq y} b^2 \cos k_x(\cos k_y + \cos k_z) - 2\sum_{x\neq y} bc \sin k_x \sin k_y\}. \quad (20)$$

3. DETERMINATION OF THE COEFFICIENTS b, c, a AND OF THE ENERGY AS A FUNCTION OF K

From the minimum of (20), taking into account the normalization of **a** (7), we obtain for **a** three linear homogeneous equations which can be solved if their determinant is zero:

$$\Delta_{\mathrm{K}} = \begin{vmatrix} 2\cos k_x(\cos k_x+\cos k_z)-\lambda & -2\sin k_x \sin k_y & -2\sin k_x \sin k_z \\ -2\sin k_x \sin k_y & 2\cos k_y(\cos k_x+\cos k_z)-\lambda & -2\sin k_y \sin k_z \\ -2\sin k_x \sin k_z & -2\sin k_y \sin k_z & 2\cos k_z(\cos k_x+\cos k_y)-\lambda \end{vmatrix} = 0 \quad (21)$$

There are three real roots $\lambda_{1,2,3}$ of (21), giving three hole bands that do not generally coincide. The roots λ and the coefficients b, c, a depend essentially on **K** and are independent of the crystal parameters D and E; they are identical for all cubically symmetrical crystals with p electrons.*

In the general case the energy can be expressed in terms of the exchange integrals D and E [Eqs. (14) and (15)]. The values of E and D vary with the crystal but are always positive with E > D, because E (15) is derived from $\psi_3 = \psi_2$, which contains $\cos\vartheta$, while D is derived from ψ_1 and ψ_2, which contain $\sin\vartheta$ and therefore overlap much less. In KCl, for example, E/D = 5. Therefore for alkali-halide cubic crystals it is possible to establish the general approximate character of the dependence of the energy on the wave vector **K** in hole bands by assuming $D \approx 0$. Such "reduced" curves for one direction of the wave vector **K** in units of 10 E are plotted with discontinuous lines in Fig. 2. **K** is taken along the diagonal of the coordinate cube. The same figure shows corresponding curves of the energy for KCl, in ev by continuous lines. The usual notation[9] is used to indicate points on the boundary of the first Brillouin zone, namely the points $\Gamma(0, 0, 0)$ and $L(\pi/d, \pi/d, \pi/d)$.

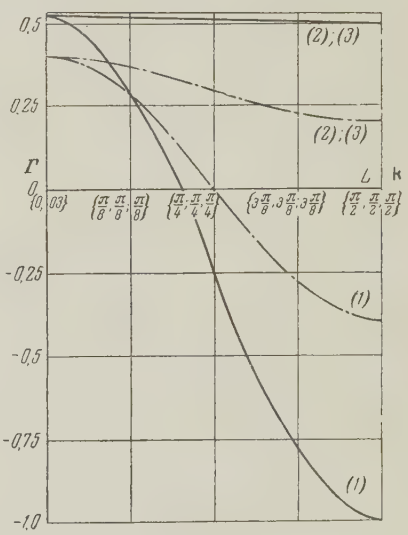

FIG. 2

Table II contains analytic expressions for the branches of $\overline{H}(\mathrm{K})$. It can be seen that the curves in the figure essentially provide a qualitative description of the energy variation for all three branches. It can be regarded as established that

*Nothing is changed when the integer vectors of the reciprocal lattice are added to K. When the sign of a component of K is reversed, the sign of the corresponding component of a is reversed. λ and $\overline{H}_{\mathrm{K}}$ remain unchanged.

TABLE II. The energy $\overline{H}_K$ as a function of the modulus of **k**, for the directions of k(0; 0; 1), (0; 1; 1), and (1; 1; 1)

Vector k			No. of branches	λ	Vector a			Energy $\frac{d}{2e^2}\overline{H}_K - B$	μ in the given wave vector direction			
									At (0; 0; 0)		For α = π	
k_x	k_y	k_z			b	c	a		General form	For KCl	General form	For KCl
0	0	$k \equiv \alpha$	1	$4\cos k$	0	0	1	$4[E\cos k - D(1+\cos k)]$	$-C(E-D)^{-1}\cdot 0.5$	—1.14	$0.5C(E-D)^{-1}$	1.14
			2;3	$2(1+\cos k)$	$b^2+c^2=1$		0	$2[E(1+\cos k) - D(1+3\cos k)]$	$-C(E-3D)^{-1}$	—4.45	$C(E-3D)^{-1}$	4.45
0	$\frac{k}{\sqrt{2}} \equiv \alpha$	$\frac{k}{\sqrt{2}} \equiv \alpha$	1	$4\cos\alpha$	1	0	0	$4\cos\alpha[E - D(1+\cos\alpha)]$	$-C(E-3D)^{-1}$	—4.45	$C(E+D)^{-1}$	1.55
			2	$2[\cos\alpha + 1]$	0	$\frac{1}{\sqrt{2}}$	$-\frac{1}{\sqrt{2}}$	$2[E(1+\cos\alpha) - D(2\cos^2\alpha - 1 + 3\cos\alpha)]$	$2C(7D-E)^{-1}$	10.0	$2C(E+D)^{-1}$	3.1
			3	$2[\cos\alpha + \cos 2\alpha]$	0	$\frac{1}{\sqrt{2}}$	$\frac{1}{\sqrt{2}}$	$2[E(\cos\alpha + \cos 2\alpha) - D(1+3\cos\alpha)]$	$-2C(5E-3D)^{-1}$	—0.84	$-\frac{2}{3}C(E+D)^{-1}$	—1.0
$\frac{k}{\sqrt{3}} \equiv \alpha$	$\frac{k}{\sqrt{3}} \equiv \alpha$	$\frac{k}{\sqrt{3}} \equiv \alpha$	1	$4\cos^2 2\alpha$	$\frac{1}{\sqrt{3}}$	$\frac{1}{\sqrt{3}}$	$\frac{1}{\sqrt{3}}$	$4[E\cos 2\alpha - D(1+\cos^2\alpha)]$	$-\frac{3}{4}C(2E-D)^{-1}$	—0.77	for $\alpha = \pi/2$ $\frac{3}{4}C(2E-D)^{-1}$	0.77
			2;3	$2(1+\cos^2\alpha)$	$a+b+c=0$ $ac+ab+ac=\frac{-1}{2}$			$2[E(1+\cos^2\alpha) - D(4\cos^2\alpha - \sin^2\alpha)]$	$-\frac{3}{2}C(E-5D)^{-1}$	—128	$\frac{3}{2}C(E-5D)^{-1}$ for $\alpha = \pi/2$	128

in the crystals under consideration* the energy minimum corresponds to $\mathbf{k}\{\pi/2, \pi/2, \pi/2\}$ rather than to $\mathbf{K} = 0$. In the vicinity of $\mathbf{k}\{\pi/2, \pi/2, \pi/2\}$ branch 1, which is important in all processes, lies $6(E + D)$ (corresponding to 1.5 ev for KCl) below the other two branches. Therefore in crystal calculations involving holes, for which the present theory is employed, it is not essential to take the spin-orbit interaction into account, because the degeneracy at the unimportant minima of the 2nd and 3rd branches is thus removed while the main branch is only slightly shifted. The absolute minimum of the energy $\overline{H}_K$ is that required for transferring an electron from the valence band to the vacuum. In our case this is $\overline{H}_{K\min} = 10.4 - 1 = 9.4$ ev. This is in fair agreement with data on the fundamental absorption bands of alkali halides,[10] which for KCl give $\lambda = 1320$ A or 10.4 ev.

Since the minimum energy corresponds to the edge of the Brillouin zone it is not unlikely that for localized hole states (such as hole F center) with ψ functions which, according to Ref. 1, can be written as linear combinations $\Psi_S = \sum_\ell b_S^\ell \Psi_S^\ell$, the minimum energy state will be similar to a p state, with coefficients b_S^ℓ of opposite signs on the two sides of the defect. Indeed, this state will possess a minimum number of nodal surfaces.

*The energy of the hole in all cases means the energy of the crystal. We have not used the concept of an "almost filled" valence band.

4. EFFECTIVE MASS IN A HOLE BAND

We shall now expand the energy (21) in powers of $\Delta\mathbf{k} = \mathbf{k} - \mathbf{k}_0$ in the vicinity of the stationary point $\mathbf{k} = 0$ and the minima $\mathbf{k}_0\{\pi/2; 0; 0\}$ and $\mathbf{k}_0\{\pi/2; \pi/2; \pi/2\}$, where **k** is the dimensionless wave vector $\mathbf{k} = d\mathbf{K}/2$. As E. I. Rashba has noted, the existence of the stationary condition for $\mathbf{K} = 0$ and of the extremals at $\mathbf{k}_0\{\pi; 0; 0\}$ and $\mathbf{k}_0\{\pi/2; \pi/2; \pi/2\}$ can be derived through group theory from considerations of symmetry.

1. About the point $\mathbf{k}_0\{0; 0; 0\}$ (for small **K**), λ is given by

$$\varepsilon^3 + 4\varepsilon^2 + (5-3u)\varepsilon + (2-3u+5v) = 0, \qquad (22)$$

where

$$\lambda = \lambda_0 + \varepsilon = 4 + \varepsilon;$$

$$u = \sum_{x\neq y} \xi^2\eta^2, \quad v = \xi^2\eta^2\zeta^2; \quad \xi = \Delta k_x/|\Delta\mathbf{k}|.$$

Since (22) is a cubic equation, the energy cannot be expressed as an analytic function of **K**. This results from the fact that for $\mathbf{K} = 0$ all three bands are contiguous, i.e., this is a case of degeneracy. But here also we can introduce the effective hole mass m_+ and the dimensionless mass $\mu = m_+/m$ (which is not a tensor) depending on the direction of **K** through the equation $\hbar^2/m_+ = \partial^2|E(K)|/\partial|K|^2$. The values of μ for a number of directions of **k** in KCl are given at the end of Table III.

2. Near the point $\mathbf{k}_0\{\pi; 0; 0\}$ in the branches of light holes, for which $\overline{H}_{K_0} - (2e^2/d)B = -4E$,

TABLE III. Variation of the energy in the vicinity of extremals inside of the Brillouin zone

Direction of K			No. of branches	Energy $\frac{d}{2e^2}\bar{H}_K - B$ in the vicinity of the extremal	μ for KCl	Kind of extremal
k_x	k_y	k_z				
0	α	α	2	$2\left[E(1+C_2) - D\left(2C_2^2 - 1 + 3C_2\right)\right]$	−6.3	max
			3	$2\left[E(C_3 + \cos 2\alpha_3) - D(3C_3 + 1)\right]$	0.16	min
0	$\alpha - k$	$\alpha + k$	2	$\bar{H}_0 - k^2\left[3.5E + 1.5D(1 - C_2)\right]$	−6.08	max
			3	$\bar{H}_0 + k^2\left[4D(1 + C_3) + (E + D)\left(3 - C_3^2\right)\right]$	10.12	min
$\delta \neq 0$	α	α	2	$\bar{H}_0 - \delta^2 C_2(E - 3D)$	−193	max
			3	$\bar{H}_0 - \delta^2\left[-4C_3D + \frac{B}{A}(E + D)\right]$	−7.6	max

Here $\alpha_2 = \arccos\frac{1}{4}\left(-3 + \frac{E}{D}\right)$; $\alpha_3 = \arccos -\frac{1}{4}\left(1 - 3\frac{D}{E}\right)$; $C = \cos\alpha$; $A = 1 + C - 2C^2$, $B = (AC + 4 - 4C^2)$

$$\bar{H}_K - H_{K_0} = (\Delta k)^2\{E + D + (E - 3D)\xi^2\}. \quad (23)$$

Thus the constant energy surface is an ellipsoid of revolution which is oblate along the x axis of rotation. The effective mass is a tensor; for KCl

$$\mu_{xx} = C/(2E - D) = 1.15; \quad \mu_{yy} = \mu_{zz} = C/(E + D) = 1.55; \quad C = 8.51\cdot 10^{-2}. \quad (24)$$

An analogous expansion with respect to Δk at the same point for the other two (degenerate) branches gives, in virtue of the non-analyticity,

$$\Delta\bar{H}_K = (\Delta k)^2\{-4D\xi^2 + (E + D) \times [(\xi^2 - \zeta^2)c_0^2 + (\xi^2 - \eta^2)a_0^2 - 4a_0c_0\zeta\eta]\}, \quad (25)$$

where

$$a_0^2 = \left[1 + \frac{\xi^2 - \eta^2 - \varepsilon}{\xi^2 - \zeta^2 - \varepsilon}\right]^{-1}; \quad c_0^2 = \left[1 + \frac{\xi^2 - \zeta^2 - \varepsilon}{\xi^2 - \eta^2 - \varepsilon}\right]^{-1};$$

$$2\varepsilon = 2\xi^2 - \zeta^2 - \eta^2 \pm \sqrt{\zeta^4 + \eta^4 + 14\eta^2\zeta^2}.$$

The numerical values of $\Delta\bar{H}_k$ and μ for these branches can be obtained only for specific values of Δk, i.e., when ξ, η and ζ are given. For example, with $\Delta k\{0; \Delta k; 0\}$, i.e., $\xi = \zeta = 0$, $\Delta\bar{H}_K$ has the two values 0 and $-(E + D)(\Delta k)^2$, which in KCl correspond to the effective masses $\mu_1 = \infty$; $\mu_2 = -1.55$. In the direction (1; 0; 0)

$$\mu_1 = \mu_2 = C/(E - 3D) = 4.45.$$

3. In the vicinity of the most important point $k_0\{\pi/2; \pi/2; \pi/2\}$ for which $\bar{H}_{K_0} - (2e^2/d)B = -4(E + D)$, similar calculations lead to

$$\bar{H}_K - \bar{H}_{K_0} = (\Delta k)^2\frac{4}{3}\{D + E + (E + 4D)\sum_{x\neq y}\xi\eta\}. \quad (26)$$

The constant energy surface is again an ellipsoid of revolution, which is more oblate than the preceeding one and has its axis along the diagonal of the coordinate cube; μ is again a tensor. Along the diagonal of the coordinate cube, with $\xi = \eta = \zeta$,

$$\mu = \mu_{\min} = \frac{6.38\cdot 10^{-2}}{(2E + 5D)} = 0.47,$$

while perpendicular to the diagonal, with $\xi + \eta + \zeta = 0$, $\mu = 4.56$.

Thus in the principal hole band there exists strong anisotropy of the hole effective masses, which are positive. The principal role in conduction and in other effects is played by light holes.

In addition to these three points extremals were also found at two points on the less important branches of Table III. The locations and character of these extremals depend on E and D, but they were not investigated in detail. In Table IV, which gives the band widths, these extremals provide the top of band 2 and the bottom of band 3.

A simplified calculation of the hole bands was also carried through in which $I^{ll'}$ was calculated[10] not by means of the functions (2), (3), and (6), but using linear combinations of simplified, spherically symmetrical one-electron functions of the form

$$\psi_s^l(\rho_s^l) = \varphi(\rho_s'^l)\chi(\rho_{n_s}^l), \quad (27)$$

TABLE IV. Locations and magnitudes of the absolute extremals in each band and the widths of the bands

No. of band	Location of maximum*			Maximum energy		Location of minimum*			Minimum energy		Width of band	
	k_x	k_y	k_z	General form	in KCl	k_x	k_y	k_z	General form	in KCl	General form	in KCl
1	0	0	0	$4(E-2D)$	0.52	$\frac{\pi}{2}$	$\frac{\pi}{2}$	$\frac{\pi}{2}$	$4(E+D)$	−1.0	$4(2E-D)$	1.52
2	0	α_2	α_2	$\frac{1}{4}\left\{2E\left(\frac{E}{D}+1\right)-D\left(\frac{E^2}{D^2}-17\right)\right\}$	0.551	0	0	π	$4D$	0.16	$\frac{1}{4}\left\{2E\left(\frac{E}{D}+1\right)-D\left(\frac{E^2}{D^2}-1\right)\right\}$	0.391
3	0	0	0	$4(E-2D)$	0.52	0	0	α_3	$-\frac{1}{4}\left\{9E\left(1-\frac{D^2}{E^2}\right)+2D\left(1+9\frac{D}{E}\right)\right\}$	−0.513	$\frac{1}{4}\left\{E\left(25-9\frac{D^2}{E^2}\right)-2D\left(15-9\frac{D}{E}\right)\right\}$	1.038
Sph. Sym.	$\frac{\pi}{8}$	$\frac{\pi}{8}$	$\frac{\pi}{8}$	-14.4811	1.159	0	0	π	41	−0.32	-18.41	1.472
						$\frac{\pi}{2}$	0	π				

*The notation α_2 and α_3 is the same as in Table III.

where φ is the ψ function of the five electrons of the halogen ion, which function is left undetermined, and χ is the ψ function of the sixth electron of the Cl atom, given by

$$\chi(\rho^l_{n_s}) = R(\rho^l_{n_s}) + \gamma \sum_{l'=1}^{12} R(\rho^{l'}_{n_s}); \qquad (28)$$

here $R(\rho)$ is given by (4) and γ was chosen to satisfy orthogonality.[1]

For KCl the result was $I^{ll'} = I = -0.08$. The nondegenerate energy obtained in this approximation has a minimum at $K\{0, 0, 2\pi/d\}$, and the band width in the last line of Table IV is in good agreement with the width of the important band in the foregoing stricter approximation.

The present paper presents a relatively simple method of calculating the hole bands of all halogenous crystals as well as of others, such as oxides, with NaCl type lattices. The author is preparing to calculate the bands for LiCl, NaCl, RbCl and AgCl as well as for the fluorides.

In conclusion, it is a pleasure for the author to thank K. B. Tolpygo for suggesting this research and for his continued interest, and E. I. Rashba for a discussion of the results.

[1] T. I. Kucher and K. B. Tolpygo, J. Exptl. Theoret. Phys. (U.S.S.R.) **31**, 1002 (1956), Soviet Phys. JETP **4**, 883 (1957).

[2] T. I. Kucher, J. Exptl. Theoret. Phys. (U.S.S.R.) **30**, 724 (1956), Soviet Phys. JETP **3**, 580 (1956).

[3] S. I. Pekar, J. Exptl. Theoret. Phys. (U.S.S.R.) **18**, 525 (1948).

[4] V. A. Fock, (Jubilee Volume for the 30th Anniversary of the Great Socialist October Revolution) Acad. Sci. Press, M.—L., 1947, Ch. 1, p. 255.

[5] D. R. Hartree and W. Hartree, Proc. Roy. Soc. (London) **A156**, 45 (1936).

[6] A. Sommerfeld and H. Bethe, Elektronentheorie der Metalle, Handb. Phys. 24/2, 2d Ed., Berlin, 1933.

[7] M. Born and K. Huang, Dynamical Theory of Crystal Lattices, Oxford, 1954, p. 3.

[8] G. G. Gell-Mann, Quantum Chemistry (Russ. Transl.) ONTI, NKTP SSSR, M.—L., 1937.

[9] Bouckaert, Smoluchowski, and Wigner, Phys. Rev. **50**, 58 (1936).

[10] N. F. Mott and R. W. Gurney, Electronic Processes in Ionic Crystals, Oxford, 1950.

Translated by I. Emin
74

ON THE SCATTERING OF X-RAYS AND THERMAL NEUTRONS BY SINGLE-COMPONENT CRYSTALS NEAR PHASE-TRANSITION POINTS OF THE SECOND KIND

M. A. KRIVOGLAZ

Institute of Metal Physics, Academy of Sciences, Ukrainian S.S.R.

Submitted to JETP editor July 11, 1957; resubmitted October 29, 1957

J. Exptl. Theoret. Phys. (U.S.S.R.) 34, 405-411 (February, 1958)

A study is made of peculiarities of the scattering of x-rays and thermal neutrons by single-component crystals near phase-transition points of the second kind. Explicit account is taken of geometric distortions of the crystal lattice owing to fluctuations of the internal parameters characterizing long-range order. The general case is considered, in which the long-range order is characterized not by just one parameter, but by several. Inclusion of the geometrical distortions can lead to a decided change of the qualitative pattern of intensity distribution of the diffuse scattering in the reciprocal lattice space, and in particular to the appearance of components that are inversely proportional to the distance from a point of the reciprocal lattice, i.e., that become infinite with approach to such points. Near a phase-transition point of the second kind peculiarities can be observed in the distribution of the diffuse scattering both near superlattice reflections and also near the main regular reflections. The type of temperature dependence shown by the scattering and its position in the reciprocal lattice space depend in an essential way on the symmetry of the crystal. Ferroelectric crystals are discussed in greater detail. In this case the parameters that determine the intensity of the diffuse scattering near reciprocal lattice points can be found by means of independent experiments.

In the preceding paper[1] (cited hereafter as I) the discussion of the geometrical distortions of the crystal lattice of a solid solution was based on a method in which the distortions were related to waves of variation of composition or of the long-range order parameters. Important lattice distortions can also arise from fluctuations of the internal parameters that characterize the long-range order in single-component crystals (ferroelectric, ferromagnetic, antiferroelectric, and antiferromagnetic substances, quartz, etc.). As Landau has shown,[2] particularly large fluctuations of the long-range order parameters, giving rise to anomalously large scattering of x-rays, must occur near a phase-transition point of the second kind. In Ref. 2 the calculation of the scattering was carried out without including the geometrical distortions of the lattice, and the case considered was that in which the long-range order can be characterized by only one parameter. In a number of cases, however, as can be seen from the results obtained for solid solutions (cf. I), the presence of geometrical distortions leads to the appearance of qualitatively new effects. Therefore the purpose of the present paper is to discuss the scattering of x-rays and thermal neutrons near phase-transition points of the second kind, including the effects of geometrical distortions of the crystal lattice. In addition, the results of Landau will be extended to the case in which the change of the long-range order in the crystal is characterized not by just one, but by several parameters. The scattering by ferroelectric crystals is considered in greater detail.

We consider the case of scattering of monochromatic radiation by a single crystal, and take into account neither scattering by thermal vibrations, nor Compton scattering of x-rays and magnetic scattering of neutrons by the electron shells of atoms. The calculation is carried out in the framework of the kinematic theory of scattering. For definiteness the formulas given will be written in terms appropriate to the scattering of x-rays. Formulas for the scattering of neutrons can be obtained from them essentially by just a simple change of notation.

Let us first consider the case in which the values of the long-range order parameters that are subject to anomalously large fluctuations can be uniquely specified by giving the values of the components of the spontaneous polarization, P_i. This is the case, for example, in $BaTiO_3$. In addition to the long-range order parameters, there can also be fluctuations in the internal parameters that characterize the local order in the distribution of

atoms at the lattice points. But in the cases considered with below, in which the fluctuations of the P_i lead to anomalously large scattering, fluctuations of the local-order parameters evidently play a relatively small part and will not be taken into account.

The fluctuations $P_i - \overline{P}_i$ of the polarization components can be expanded in Fourier series:

$$P_{it} - \overline{P}_i = \sum_{\mathbf{k}}{}' [P_{\mathbf{k}i} \exp(-i\mathbf{k}\mathbf{R}_t) + P^*_{\mathbf{k}i} \exp(i\mathbf{k}\mathbf{R}_t)]. \quad (1)$$

Here $\overline{P}_i$ is the average equilibrium value of the i-th component of the polarization vector, P_{it} is the value of P_i corresponding to cell number t, $\mathbf{R}_t$ is the radius vector of this cell, and the prime on the summation sign means that the summation is taken over values of the vector $\mathbf{k}/2\pi$ that lie in a half-cell of the reciprocal lattice and satisfy cyclic conditions, the term with $\mathbf{k} = 0$ being excluded. The polarization wave for each value of $\mathbf{k}$ corresponds to a wave of displacements of the atoms. In what follows we shall study the diffuse scattering only in the neighborhood of the regular Laue reflections (where this scattering is anomalously large). Because of this we can restrict ourselves to the consideration of long waves of fluctuation. For these waves the displacements of lattice points of different types are almost identical (cf. Sec. 2 in I), so that the displacements of the various atoms of cell number t corresponding to the $\mathbf{k}$-th polarization wave are practically the same and can be written in the form:

$$\delta\mathbf{R}_{t\mathbf{k}} = i \sum_{i=1}^{3} a_{\mathbf{k}i} \mathbf{k}' k^{-2} [P_{\mathbf{k}i} \exp(-i\mathbf{k}\mathbf{R}_t) - P^*_{\mathbf{k}i} \exp(i\mathbf{k}\mathbf{R}_t)], \quad (2)$$

where $\mathbf{k}'$ is a vector along the displacement of the atoms in the $\mathbf{k}$-th wave, with $k' = k$.

The intensity of the x-ray scattering in the neighborhood of the Laue reflections, expressed in electronic units, can be represented in the following form:

$$I = \overline{\left| \sum_t f_{lt} \exp(i\mathbf{q}_1 \cdot \mathbf{R}_t + \delta\mathbf{R}_t) \right|^2}. \quad (3)$$

Here $\mathbf{q}_1$ is the difference of the wave vectors of the scattered and incident waves, the averaging is taken over all possible configurations of the atoms, and $f_{\ell t}$ is the structure factor of cell number t corresponding to the ℓ-th Laue reflection and calculated with inclusion of effects of geometrical distortions. The quantity $f_{\ell t}$ can be written as the sum of the average value of the structure factor corresponding to the ℓ-th reflection, $\overline{f}_\ell$, and the departure from the average value, $\Delta f_{\ell t}$, corresponding to cell number t. In the calculation of $f_{\ell t}$ the atomic factors for the individual lattice points must be multiplied by factors $\exp(-L_\gamma/2)$ for each type γ of lattice point, to take account of the weakening of the amplitude because of the geometrical distortions (cf. Sec. 2 in I). Since in the determination of the L_γ one must include not only the long but also the short waves, we shall not give formulas for these quantities, recalling that the structure factor $\overline{f}_\ell$ can be determined directly from x-ray data on the intensities of the regular reflections.

When the components of the polarization vector are changed by amounts ΔP_i the average structure factor $\overline{f}_\ell$ is changed by the amount $d_{\ell i}\Delta P_i$, where $d_{\ell i}$ depends on the number of the reflection (for some reflections $d_{\ell i} = 0$). Here and in what follows, summation over repeated indices i is understood. The deviation of the atomic factor of cell number t from the average value is $(P_{it} - \overline{P}_i) d_{\ell i}$. (Some difference is possible between the values of $d_{\ell i}$ that are involved in the change of the $f_{\ell t}$ by fluctuations and are defined for unchanged values of the short-range order parameters and the values of $d_{\ell i}$ that correspond to the equilibrium values $\overline{f}_\ell$ and are defined for values of the short-range order parameters that do not vary with changes of the $\overline{P}_i$.) For the neighborhood of a regular reflection, where we can use for the calculation of the diffuse reflection the $d_{\ell i}$ corresponding to that reflection and the displacements of the atoms can be determined according to Eq. (2) without taking account of the atomic structure, by Eqs. (3) and (2) the contribution to the scattering amplitude from elementary cell number t is given by

$$\left[\bar{f}_l + \sum_{\mathbf{k}}{}' (d_{li} - \bar{f}_l a_{\mathbf{k}i} \mathbf{k}'\mathbf{q}_1/k^2) P_{\mathbf{k}i} \exp(-i\,\mathbf{k}\mathbf{R}_t) + \sum_{\mathbf{k}}{}' (d_{li} + \bar{f}_l a_{\mathbf{k}i}\, \mathbf{k}'\mathbf{q}_1/k^2) P^*_{\mathbf{k}i} \exp(i\,\mathbf{k}\mathbf{R}_t) \right] \exp(i\,\mathbf{q}_1\mathbf{R}_t). \quad (4)$$

In the summation of the expression (4) over the elementary cells (over t) near regular reflections (where a condition of the type of Eq. (9) of I is satisfied), the most important part in the sum over $\mathbf{k}$ is played by the term with $\mathbf{k} = \mathbf{q}$ or $\mathbf{k} = -\mathbf{q}$, where $\mathbf{q} = \mathbf{q}_1 - 2\pi\mathbf{K}_\ell$, and $\mathbf{K}_\ell$ is the vector of the reciprocal lattice lying closest to the end of the vector $\mathbf{q}_1/2\pi$ and corresponding to the ℓ-th reflection (the "reduced" vector $\mathbf{q}/2\pi$ lies in the first cell of the reciprocal lattice). Therefore, squaring the indicated sum in accordance with Eq. (3), we find that the intensity of the scattering is given by

$$I = 8\pi^3 \frac{N_0}{\Delta'} \overline{|f_l|^2}\, \delta(\mathbf{q}_l) + N_0^2 \overline{\left| (\bar{f}_l \frac{\mathbf{q}_1\mathbf{q}'}{\mathbf{q}^2} a_{\mathbf{q}i} - d_{li})\, P_{\mathbf{q}i} \right|^2}, \quad (5)$$

where N_0 is the number of elementary cells in the crystal and Δ' is the volume of a cell. The

first term, involving the δ function, gives the intensity of the regular reflection, and the second term gives the intensity I_F of the diffuse scattering.

To carry out the averaging in Eq. (5) one can use the probability distribution for the Fourier components P_{ki} of the polarization fluctuations for small k:

$$w \sim \exp\left[-\frac{V}{kT}\sum_{k}'\left(\frac{\partial^2\varphi}{\partial P_i \partial P_j} + A_{ijmn}k_m k_n\right)P_{ki}P_{kj}^*\right]. \quad (6)$$

Here φ is the thermodynamic potential per unit volume, and A_{ijmn} is a tensor of the fourth order. Using the fact that $\partial^2\varphi/\partial P_i \partial P_j = \kappa_{ij}^{-1}$, where κ_{ij}^{-1} is a tensor, the reciprocal of the electric susceptibility tensor,[3] we get from Eqs. (5) and (6):

$$I = 8\pi^3 \frac{N_0}{\Delta'}|\bar{f}_l|^2 \delta(q_l) + \frac{N_0 kT}{\Delta'}\left(\bar{f}_l a_{qi}\frac{q_l q'}{q^2} - d_{li}\right)\left(\bar{f}_l a_{qj}\frac{q_l q'}{q^2} - d_{lj}\right) \times (\kappa^{-1} + A_{mn}q_m q_n)_{ij}^{-1}. \quad (7)$$

Here $(\kappa^{-1} + A_{mn}q_m q_n)_{ij}^{-1}$ are the components of a tensor, the reciprocal of the tensor $\kappa_{ij}^{-1} + A_{ihmn}q_m q_n$. For sufficiently small values of q the last factor in Eq. (7) is just the electric susceptibility κ_{ij}.

The quantities d_{li} appearing in Eq. (7) can be determined from the dependence of the structure factors (i.e., the intensities of the regular reflections) on the polarization (or on the intensity of the external electric field). One can find the quantities a_{qi} by considering the expression for the stress tensor in an inhomogeneously polarized crystal. If we note that in the presence of fluctuations δP the expression for the free energy of the deformed crystal contains the term $-\epsilon_{ijm}u_{ij}\delta P_m$, we get for the components σ_{ij} of the stress tensor the expression

$$\sigma_{lj} = \lambda_{ijmn}u_{mn} - \varepsilon_{ijm}\delta P_m, \quad (8)$$

where u_{mn} are the components of the deformation tensor and λ_{ijmn} are the components of the elastic modulus tensor. In order to get the formula for a_{qm} we must insert in Eq. (8) instead of δP_m a periodic function corresponding to the k-th fluctuation wave, and instead of u_{mn} the components of the deformation tensor corresponding to the wave of geometrical distortion produced by the fluctuation wave in question when the boundaries of the crystal are kept motionless. Then, noting that $\partial\sigma_{ij}/\partial x_j = 0$, and carrying out the same argument as for the derivation of Eq. (16) of I, we get three equations for $a_{km}k_r'$:

$$\lambda_{ijpr}n_i n_p a_{km}k_r'/k = \varepsilon_{ijm}n_j \qquad (i = 1,2,3), \quad (9)$$

where n_i are the direction cosines of the wave vector k. Here it is clear that the third-order tensor ϵ_{ijm} is to be determined from the dependence of the stresses (or deformations) on the polarization (i.e., on the external electric field). Thus, just as in the case of scattering by solid solutions, all the parameters appearing in the expression for the diffuse scattering, with the exception of A_{ijmn}, can be determined from independent experiments.

As follows from the thermodynamic theory of ferroelectricity,[4] at a phase transition point of the second kind the components of the reciprocal dielectric susceptibility tensor κ_{ij}^{-1} go to zero, and by Eq. (7) this has the consequence that an anomalously large diffuse scattering should appear near this point. In this connection the nature of the dependences of I_F on the temperature and on q depends on the symmetry of the crystal. Near the temperature T_0 of a phase transition of the second kind the tensor ϵ_{ijm} can be written in the form

$$\varepsilon_{ijm} = \varepsilon_{ijm}^0 + \delta_{ijmn}P_n.$$

Let us first consider the case in which the tensor components ϵ_{ijm}^0 are different from zero (i.e., in which there is a piezoelectric effect in the non-ferroelectric phase). For this case Eqs. (7) and (9) show that for reflections for which $\bar{f}_l \neq 0$ in the non-ferroelectric phase, both above and below the temperature T_0 there is a term in the expression for I_F that has the factor q^{-2} and thus goes to infinity as we approach a point of the reciprocal lattice. For sufficiently small q the coefficient of this term contains κ_{ij}, i.e., it becomes anomalously large for $T \to T_0$ (this coefficient is, of course, decidedly dependent on the quantity ϵ_{ijm}^0). The terms containing the factor q^{-2} must lead to a strong anisotropy of the intensity distribution of the diffuse scattering, regarded as a function of position in the space in the reciprocal lattice, since they are proportional to $\cos^2\varphi$, where φ is the angle between the vectors q' and q_l. Since according to Eq. (9) the a_{qm} can also depend strongly on the orientation of the vector q, this anisotropy does not reduce to just a proportionality to $\cos^2\varphi$, and the pattern of the intensity distribution of the diffuse scattering will be different in the neighborhoods of different reciprocal lattice points. The term proportional to q^{-2} is absent for small scattering angles, when $q = q_l$, and the coefficient of this term increases with increase of the order of the reflection (with increase of $|q_l|$).

Besides the terms containing factors q^{-2} and q^{-1}, for reflections with $d_{\ell i}$ different from zero there is also a sharp increase near the temperature T_0 in a term proportional to $d_{\ell i}^2$, which plays an important role for somewhat larger values of q. If $\bar{f}_\ell = 0$ for $T > T_0$, only this term remains in the non-ferroelectric phase, and near such regular reflections the intensity of the diffuse scattering does not go to infinity for $q \to 0$, but reaches its maximum value (which increases rapidly as $T \to T_0$) at the point $\mathbf{q} = 0$. For $T < T_0$ the quantity $\bar{f}_\ell$ in this case is small near the temperature T_0, so that the terms proportional to q^{-2} have a small proportionality coefficient. Along with the sharp increase of I_F, near the temperature T_0 there must be an increase of the quantities L_γ that determine the intensities of the regular reflections. It can be shown that near the temperature T_0 these quantities contain terms proportional to $\kappa^{1/2}$. This sort of qualitative picture of the intensity distribution should be found, for example, in scattering by crystals of the type of Rochelle salt, KH_2PO_4, etc.

The qualitative picture of the temperature dependence of I_F is changed if the ϵ^0_{ijm} vanish identically because of requirements imposed by the symmetry of the crystal. This occurs if the crystal in the non-ferroelectric phase has a center of symmetry. In this case in the non-ferroelectric phase Eqs. (7) and (9) indicate that even in the neighborhoods of reflections at which $\bar{f}_\ell \neq 0$ the coefficients of q^{-2} and q^{-1} arising from the polarization fluctuations considered here are equal to zero (there can be some nonvanishing contributions to these coefficients, arising from fluctuations in the short-range order). In the ferroelectric phase the coefficient in question is proportional to $\bar{P}^2$ (since $a_{qm} \sim \bar{P}$), where $\bar{P}$ is the spontaneous polarization, and because of this for small values of $\bar{P}$, near an ordinary phase transition point of the second kind, the term proportional to q^{-2} does not become as large as in the case considered above. The term proportional to $d_{\ell i}^2$ here gives the anomalously large scattering at the transition point. But near the critical point at which the curve of points of phase transition of the second kind goes over into a curve of phase transition of the first kind, the product $\bar{P}^2\kappa_{ij}$ is very large, so that just as in the case considered above ($\epsilon^0_{ijm} \neq 0$) the term containing the factor q^{-2} becomes anomalously large for the ferroelectric phase as we approach the critical point (the same thing happens for phase transitions of the first kind, near the critical point). In the non-ferroelectric phase the coefficient of q^{-2} must be considerably smaller. The scattering proportional to q^{-2} should appear particularly strongly in crystals with a large discontinuity of the coefficient of thermal broadening. Crystals with $\epsilon^0_{ijm} = 0$ include, for example, ferroelectrics of the type of $BaTiO_3$. In these crystals the polarization is directed along the cubic axis (the z axis), and the only nonvanishing components of the electric susceptibility tensor are $\kappa_{11} = \kappa_{22}$ and κ_{33}. In this case the explicit form of the temperature dependence of I_F can be found if we substitute for κ_{ij} and $\bar{P}$ (involved in a_{qm}) in Eq. (7) the expressions for these quantities obtained in the theory of ferroelectricity [for example, Eqs. (19) and (20) of Ref. 3].

One can deal in the same way with the general case of crystals observed near phase transition points of the second kind. Here the inhomogeneity of the crystal is characterized by the fluctuations of the quantities c_i which determine the change of the symmetry of the crystal in the phase transition. These quantities can be taken to be the coefficients in the expansion of the change $\delta\rho$ of the density function of the crystal in the transition: $\delta\rho = \sum c_i\varphi_i$, where the φ_i form the basis of the irreducible representation of the symmetry group of the more symmetrical phase which is manifested in the transition to the less symmetrical phase.[5] It is clear that the intensity of the scattering arising from the fluctuations of the c_i can be determined in the same way as the intensity of the scattering arising from the fluctuations of the P_i, i.e., by a formula analogous to Eq. (7):

$$I = 8\pi^3 \frac{N_0}{\Delta'} |\bar{f}_l|^2 \delta(\mathbf{q}_l) + \frac{N_0 kT}{\Delta'} \left(\bar{f}_l a_{qi} \frac{q_l q'}{q^2} - d_{li}\right)\left(\bar{f}_l a_{qj} \frac{q_l q'}{q^2} - d_{lj}\right) \varphi^{-1}_{qij}. \qquad (10)$$

The summations over i and j are here taken from 1 to p, where p is the number of functions forming the basis of the irreducible representation in question. The $\varphi^{-1}_{\mathbf{q}ij}$ are the elements of the matrix reciprocal to the matrix $\partial^2\varphi/\partial c_i \partial c_j + A_{ijmn}q_m q_n$. The quantities $d_{\ell i}$ are the coefficients in the expansion of the $\bar{f}_\ell$ in terms of the c_i, so that they can be determined from the change of the $\bar{f}_\ell$ (the intensities of the regular reflections) below the transition temperature. The coefficients a_{qi} can be found from Eq. (9) if we substitute instead of the ϵ_{ijm} the quantities ϵ'_{ijm} that give the dependence of the stress tensor components on the c_i:

$$\sigma_{ij} = \lambda_{ijmn}u_{mn} - \varepsilon'_{ijm}c_m. \qquad (11)$$

The application of these formulas to various systems (antiferroelectrics, ferromagnetic sub-

stances, antiferromagnetics, quartz near the point of the $\alpha - \beta$ transition, and so on) and the determination of the connections between the c_i and the macroscopic parameters of the crystal require special considerations involving the concrete changes of symmetry in the various transitions. A qualitative picture of the dependence of the intensity of the scattering on the temperature and on $\mathbf{q}$ can, however, be obtained from the general formulas given here. As is well known,[5] the derivatives $\partial^2\varphi/\partial c_i \partial c_j$ go to zero at a phase transition point of the second kind. Because of this an anomalously large scattering should be observed near the temperature T_0. As in the case of ferroelectric crystals considered above, the type of dependence of I_F on T and $\mathbf{q}$ depends essentially on whether or not there is a term of degree zero in the expansion of ϵ'_{ijm} in powers of the c_i. Depending on this, one gets a qualitative picture of the intensity distribution of the scattering which is of some one of the types discussed above. In particular, in the neighborhoods of those regular reflections at which $d_{\ell i} = 0$ (in the case of x-ray scattering by ferromagnetic and antiferromagnetic crystals $d_{\ell i} = 0$ for all reflections), there must be characteristic peculiarities of I_F near the temperature T_0 in crystals for which $\epsilon'^{0}_{ijm} \neq 0$, and also in those for which $\epsilon'^{0}_{ijm} = 0$ but at the transition point there is a large change of the thermal expansion coefficient (neighborhood of the critical point). In the neighborhoods of reflections for which $d_{\ell i} \neq 0$ the expressions for I_F always contain large terms not proportional to q^{-2}. In particular, characteristic peculiarities in the intensity distribution of the diffuse scattering should be found in quartz near the point of the $\alpha - \beta$ transition.

In conclusion we remark that near a phase transition point of the second kind there should also be characteristic peculiarities in the intensity distribution of the diffuse scattering by the thermal vibrations. This problem will be dealt with elsewhere.

[1] M. A. Krivoglaz, J. Exptl. Theoret. Phys. (U.S.S.R.) **34**, 204 (1958), Soviet Phys. JETP **7**, 139 (1958).

[2] L. D. Landau, J. Exptl. Theoret. Phys. (U.S.S.R.) **7**, 1232 (1937).

[3] M. A. Krivoglaz and S. A. Rybak, J. Exptl. Theoret. Phys. (U.S.S.R.) **33**, 139 (1957), Soviet Phys. JETP **6**, 107 (1958).

[4] V. L. Ginzburg, J. Exptl. Theoret. Phys. (U.S.S.R.) **15**, 739 (1945); **19**, 36 (1949); Usp. Fiz. Nauk **38**, 490 (1949); A. F. Devonshire, Phil. Mag. **40**, 1040 (1949); **42**, 1065 (1951).

[5] L. D. Landau, J. Exptl. Theoret. Phys. (U.S.S.R.) **7**, 19 (1937); L. Landau and E. Lifshitz Статистическая физика (Statistical Physics), GITTL 1951.

Translated by W. H. Furry
75

ON THE THEORY OF FERROMAGNETIC SUPERCONDUCTORS

G. F. ZHARKOV

P. N. Lebedev Physics Institute, Academy of Sciences, U.S.S.R.

Submitted to JETP editor July 19, 1957

J. Exptl. Theoret. Phys. (U.S.S.R.) 34, 412-416 (February, 1958)

We obtain the conditions for the existence of a superconducting state in bulk, single-domain ferromagnetic samples in the shape of an ellipsoid of revolution. The direction of the spontaneous magnetization is assumed to make an arbitrary angle θ_0 with the direction of the external field, which is parallel to the axis of the ellipsoid. We give estimates from which it follows that the superconducting state can occur only if the angle $\theta_0 \lesssim 10^{-2}$. If this condition is satisfied, the use of oblate samples with a large demagnetization factor should formally favor the possibility of detecting the superconductivity.

1. The problem of a possible observation of superconductivity in ferromagnetics was considered in a paper by Ginzburg.[1] It was shown that in the case of a bulk cylindrical specimen, magnetized along the axis of the cylinder, the possibility of a transition to a superconducting state was hampered because of the presence inside the specimen of the magnetic induction $B_0 = 4\pi M_0$, which is connected with the spontaneous magnetization M_0 of the ferromagnetic. For specimens with a large demagnetization factor (for instance, for thin disks magnetized perpendicularly to their plane) the induction B in the sample in the normal state turns out to be very small compared to $4\pi M_0$ which can assist the onset of superconductivity. Ginzburg, when considering this, pointed out at the same time the necessity of a special analysis of that case, taking boundary effects into account. In the present paper we elucidate the conditions for the existence of a superconducting phase in ferromagnetics of finite dimensions and ellipsoidal shape with a spontaneous magnetization at an arbitrary angle with the direction of the external field.

2. It is well-known[2,3] that if the processes considered take place at constant temperature T and everywhere constant and uniform magnetic field H_0, the following function is extremal in the equilibrium state,

$$\Phi(T, H_0) = \int F_H\, dv - \frac{1}{4\pi}\int \mathbf{H}_0\mathbf{B}\, dv + \frac{1}{8\pi}\int H_0^2\, dv. \quad (1)$$

Here F_H is the internal free energy density of the system under consideration, taking the total magnetic field H into account, B is the induction field, and the integration is over the whole of space.

For a solid in the normal state the free energy is of the form

$$\int F_{nH}\, dv = \int F_{n0}\, dv + \int w_m\, dv, \quad (2)$$

where F_{n0} is the free energy density when no magnetic field is present and w_m the free energy density connected with the field. For a ferromagnetic we must take

$$w_m = \frac{1}{4\pi}\int_0^{\mathrm{B}} \mathbf{H}d\mathbf{B} = \frac{H^2}{8\pi} - 2\pi M_0^2 = \frac{B^2}{8\pi} - \mathbf{M}_0\mathbf{B}, \quad (3)$$

where we have used in (3) the expression $B = H + 4\pi M_0$ for the induction inside an "ideal" ferromagnetic (the magnetic permeability μ is put equal to unity, which corresponds to the saturated case). We shall assume that the specimen consists of one domain and that at liquid helium temperatures M_0 is constant and does not depend on the temperature.

From (1) to (3) we get for a specimen in the normal state

$$\Phi_n(T, H_0) = \int F_{n0}\, dv^- + \frac{1}{8\pi}\int (\mathbf{H} - \mathbf{H}_0)^2\, dv - \mathbf{M}_0\mathbf{H}_0 v^- - 2\pi M_0^2 v^-, \quad (4)$$

where v^- is the volume of the specimen.

We shall consider specimens which are sufficiently large so that we can neglect surface effects. For a ferromagnetic in the superconducting state the free energy is equal to

$$\int F_{sH}\, dv = \int F_{s0}\, dv + \int \left(\frac{B^2}{8\pi} - \mathbf{M}_0\mathbf{B}\right) dv = \int F_{s0}\, dv + \frac{1}{8\pi}\int (H^+)^2\, dv^+,$$

inasmuch as within a superconductor $B = 0$ and outside the specimen $B = H^+$ (H^+ is the field outside the specimen and v^+ the volume outside the

specimen). For the thermodynamic potential (1) we get

$$\Phi_s(T, H_0) = \int F_{s0}\, dv^- + \frac{1}{8\pi}\int H_0^2\, dv^- + \frac{1}{8\pi}\int (\mathbf{H}^+ - \mathbf{H}_0)^2\, dv^+. \quad (5)$$

Equilibrium between the normal and the superconducting phases is possible only if the potentials are equal,

$$\Phi_n(T, H_0) = \Phi_s(T, H_0). \quad (6)$$

Below we evaluate the quantities (4) and (5) for the case of samples having the shape of ellipsoids of revolution with the axis of revolution parallel to the external field.

3. First we find the magnetic field outside and inside a prolate ellipsoid of revolution, the spontaneous magnetization of which is in the direction which makes an angle θ_0 with the direction of the external field. Introducing spheroidal coordinates ξ, η, ϕ (see, for instance, Ref. 4) and solving the usual magnetostatic problem in the case of a specimen in the normal state, we get for the scalar potential of the magnetic field the expression

$$\varphi^+ = c\xi\eta\,[H_0 + A_1 I_1(\xi)] + c\sqrt{\xi^2-1}\sqrt{1-\eta^2}\,A_2 I_2(\xi)\cos\phi,$$
$$\varphi^- = c\xi\eta\,[H_0 + A_1 I_1(\xi_0)] + c\sqrt{\xi^2-1}\sqrt{1-\eta^2}\,A_2 I_2(\xi_0)\cos\phi; \quad (7)$$

$$A_1 = -4\pi M_0 \xi_0 (\xi_0^2 - 1)\cos\theta_0,\quad A_2 = 4\pi M_0 \xi_0 (\xi_0^2-1)\sin\theta_0,$$
$$I_1(\xi) = \int_\xi^\infty d\xi/\xi^2(\xi^2-1),\quad I_2(\xi) = \int_\xi^\infty d\xi/(\xi^2-1)^2. \quad (7a)$$

The coordinate surface $\xi = \xi_0$ coincides with the surface of the ellipsoid considered, the equation of which is of the form

$$(x^2+y^2)/(\xi_0^2-1) + z^2/\xi_0^2 = c^2,$$

where $2c$ is the interfocal distance.

In the case of a superconducting ellipsoid (inside the specimen $B^- = 0$) we find

$$\varphi^+ = c\xi\eta H_0 + \frac{H_0\xi_0(\xi_0^2-1)}{1 - I_1(\xi_0)\,\xi_0(\xi_0^2-1)}\, c\xi\eta I_1(\xi). \quad (8)$$

For the case of an oblate ellipsoid of revolution we obtain similar expressions.

Evaluating the field $\mathbf{H} = -\operatorname{grad}\varphi$ and performing the integrations indicated in (4) and (5), we obtain equations which are correct both for a prolate and for an oblate ellipsoid of revolution.*

$$\Phi_n = \int F_{n0}\, dv - \frac{v^-}{8\pi}(4\pi M_0)^2\,[(1-n_1)\cos^2\theta_0 + (1-n_2)\sin^2\theta_0] - v^- M_0 H_0 \cos\theta_0,$$
$$\Phi_s = \int F_{s0}\, dv + \frac{v^-}{8\pi}\frac{H_0^2}{1-n_1}. \quad (9)$$

In the case of a prolate ellipsoid of revolution the quantities n_1 and n_2 entering into (9) have the form

$$n_1 = \xi_0(\xi_0^2-1)\left[\frac{1}{2}\ln\frac{\xi_0+1}{\xi_0-1} - \frac{1}{\xi_0}\right],$$
$$n_2 = \xi_0(\xi_0^2-1)\left[\frac{\xi_0}{2(\xi_0^2-1)} - \frac{1}{4}\ln\frac{\xi_0+1}{\xi_0-1}\right]. \quad (10)$$

In the case of an oblate ellipsoid of revolution, the equation of which is

$$(x^2+y^2)/\xi_0^2 + z^2/(\xi_0^2-1) = c^2,$$

the quantities n_1 and n_2 have the form ($\rho_0 = \sqrt{\xi_0^2 - 1}$),

$$n_1 = \rho_0(\rho_0^2+1)\left[\tan^{-1}\rho_0 + \frac{1}{\rho_0} - \frac{\pi}{2}\right],$$
$$n_2 = \rho_0(\rho_0^2+1)\left[\frac{\pi}{4} - \frac{\rho_0}{2(\rho_0^2+1)} - \frac{1}{2}\tan^{-1}\rho_0\right]. \quad (11)$$

4. Equating the thermodynamic potentials (9) we find the critical external magnetic field H_{cr} for which the normal and the superconducting phase can exist in equilibrium with one another,

$$H_{cr} = -4\pi M_0\cos\theta_0 \pm R;$$
$$R = \{8\pi\Delta(1-n_1) - (4\pi M_0)^2(1-n_1)(1-n_2)\sin^2\theta_0\}^{1/2},$$
$$\Delta = \frac{1}{v^-}\int (F_{n0} - F_{s0})\, dv^-. \quad (12)$$

We note that for $\theta_0 = 0$ the expression for H_{cr} coincides with the one obtained by Ginzburg.[1]

The direction of the external field $\mathbf{H}_0$ will always be taken as positive so that we must have $H_{cr} \geq 0$. As far as the spontaneous magnetization $\mathbf{M}_0$ is concerned, two cases are possible.

(1) The case where $\cos\theta_0 \geq 0$. Then

$$H_{cr} = -4\pi M_0\cos\theta_0 + R. \quad (13)$$

In order that H_{cr} be real and positive, the following inequality must be satisfied

$$8\pi\Delta \geqslant (4\pi M_0)^2\,[(1-n_1)\cos^2\theta_0 + (1-n_2)\sin^2\theta_0]. \quad (14)$$

*Since at infinity the field $H - H_0$ is the field of a dipole with moment μ, the same result for Φ_s can be obtained by using the equation (see Ref. 3).

$$\Phi_s = \int F_{s0}\, dv - \frac{v^-}{2}\mu H_0.$$

To violate this inequality we must have $\Phi_n - \Phi_S < 0$, i.e., the superconducting phase must be thermodynamically unfavorable. If Eq. (14) is satisfied the superconducting state is possible* for $H_0 < H_{cr}$, and for $H > H_{cr}$ the normal state.

(2) The case where $\cos\theta_0 \leq 0$. Then there are, generally speaking, two critical fields possible,

$$H_{cr1} = 4M_0|\cos\theta_0| - R, \quad H_{cr2} = 4\pi M_0|\cos\theta_0| + R. \quad (15)$$

In order that such critical fields can exist it is necessary that the following conditions be fulfilled

$$(4\pi M_0)^2(1-n_2)\sin^2\theta_0 \leqslant 8\pi\Delta; \quad (16)$$

$$(4\pi M_0)^2[(1-n_1)\cos^2\theta_0 + (1-n_2)\sin^2\theta_0] \geqslant 8\pi\Delta. \quad (17)$$

Condition (16) is necessary for the possibility of the existence of superconductivity. If it is violated, we get $\Phi_n - \Phi_S < 0$, i.e., the normal state will be more favorable. If (16) is satisfied, but condition (17) is violated, H_{cr1} turns out to be negative, but $\Phi_n - \Phi_S > 0$ for $H_0 < H_{cr2}$. This means that the critical field H_{cr1} does not exist and superconductivity is possible in a field $H_0 \leq H_{cr2}$. If both conditions (16) and (17) are fulfilled, the superconducting state is possible only in the range of fields $H_{cr1} \leq H_0 \leq H_{cr2}$. In the last case it is clearly necessary that the field H_{cr1} directed against the spontaneous magnetization M_0 is less than the coercive force of the sample H_c, that is, we must have

$$\{8\pi\Delta(1-n_1) - (4\pi M_0)^2(1-n_1)(1-n_2)\sin^2\theta_0\}^{1/2} > 4\pi M_0(1-n_1)|\cos\theta_0| - H_c. \quad (18)$$

5. Let us now go over to a discussion of the conconditions which we have obtained for the existence of a superconducting state in ferromagnetic specimens. The quantity $8\pi\Delta \equiv (H^0_{crM})^2$ which occurs in Eqs. (14), (16), and (17) is clearly the square of the critical magnetic field, as it was in a non-ferromagnetic metal with the same difference $\Delta = F_{n0} - F_{s0}$, as also for the ferromagnetic considered. For the known superconducting elements the value of H^0_{crM} at $T = 0$ varies from several tens to several thousands of oersteds. Below we shall assume $H^0_{crM} \sim 100$ oersted and $B_0 = 4\pi M_0 \sim 10^4$ gauss to obtain some estimates. The quantity n_1 varies from zero for a cylindrical specimen to unity for a specimen in the shape of a thin disk. The quantity n_2 varies from zero (disk) to $1/2$ (cylinder).

Let us consider the case $\cos\theta_0 > 0$ and condition (14). It is easily seen that for the values of H^0_{crM} and B_0 chosen by us, it is necessary for the possible existence of a superconducting state to take a disk-shaped specimen with $1 - n_1 \lesssim 10^{-4}$, magnetized perpendicularly to the plane of the disk, while the angle θ_0 of the deflection of M_0 from the direction of H_0 may not exceed $\theta_0 \sim 10^{-2}$. In the case of prolate specimens or for angles $\theta_0 > 10^{-2}$, the superconducting state is possible only for elements with an anomalously large value of $\Delta = F_{n0} - F_{s0}$ or else with an anomalously small value of $B_0 = 4\pi M_0$ which strongly decreases the probability of observing the superconductivity of ferromagnetics.

In the case $\cos\theta_0 < 0$ the necessary condition (16) also requires that the angles are small, $\theta_0 \lesssim 10^{-2}$. Condition (17), i.e., the condition for the existence of the critical field H_{cr1}, can be satisfied only for not too oblate specimens (or for anomalous values of Δ and B_0). In that case it is necessary to take also into consideration condition (18) which in several cases apparently can be realized.

In the case of prolate specimens the known values of M_0 and H_c for ferromagnetic elements do not allow any hope for the observation of superconductivity in bulk specimens.

For very oblate specimens with $1 - n_1 \sim 10^{-4}$ superconductivity is possible in an arbitrarily small external field, limited by the requirement $H_0 < H_c$.

Thus we can summarize and say that the possibility to observe a superconducting state in bulk ferromagnetic samples is formally facilitated by using specimens with a large demagnetization factor.

In practice, however, it is impossible to obtain a single-domain sample with the quantity $1 - n_1 \sim 10^{-4}$, or in other words with the ratio of the transverse dimensions of the specimen to its thickness equal to 10^4. In view of this it is necessary to analyze further the problem taking into account the role of domain structure, the energy of magnetic anisotropy, and so on.

In conclusion I want to use the opportunity to thank V. L. Ginzburg for valuable hints and for his interest in this paper.

*Indeed, as in the case of ordinary superconductors a pure superconducting state is possible only if the maximum field at the equator of the ellipsoid of revolution does not exceed the critical field, that is, in a field $H_0 < H_{crM}(1-n_1)$. In the range of fields $H_{crM}(1-n_1) < H_0 < H_{crM}$ the intermediate state is realized

[1] V. L. Ginzburg, J. Exptl. Theoret. Phys. (U.S.S.R.) 31, 202 (1956), Soviet Phys. JETP 4, 153 (1957).

[2] V. P. Silin, J. Exptl. Theoret. Phys. (U.S.S.R.)

21, 1330 (1951).

[3] V. L. Ginzburg, J. Exptl. Theoret. Phys. (U.S.S.R.) 34, 113 (1958), Soviet Phys. JETP 7, 78 (1958).

[4] J. A. Stratton, Electromagnetic Theory, Mc-Graw-Hill, 1941.

Translated by D. ter Haar
76

SOVIET PHYSICS JETP VOLUME 34 (7), NUMBER 2 AUGUST, 1958

APPLICATION OF THE METHODS OF QUANTUM FIELD THEORY TO A SYSTEM OF BOSONS

S. T. BELIAEV

Academy of Sciences, U.S.S.R.

Submitted to JETP editor August 2, 1957

J. Exptl. Theoret. Phys. (U.S.S.R.), 34, 417-432 (February, 1958)

It is shown that the techniques of quantum field theory can be applied to a system of many bosons. The Dyson equation for the one-particle Green's function is derived. Properties of the condensed phase in a system of interacting bosons are investigated.

1. INTRODUCTION

In recent years Green's functions have been widely used[1] in quantum field theory, and in particular in quantum electrodynamics. This has made possible the development of methods[2] which escape from ordinary perturbation theory. The method of Green's functions has also been shown* to be applicable to many-body problems. In such problems the one-particle Green's function determines the essential characteristics of the system, the energy spectrum, the momentum distribution of particles in the ground state, etc.[3]

The present paper develops the method of Green's functions for a system consisting of a large number N of interacting bosons. The special feature of this system is the presence in the ground state of a large number of particles with momentum $\mathbf{p} = 0$ (condensed phase), which prevent the usual methods of quantum field theory from being applied. We find that for large N the usual technique of Feynman graphs can be used for the particles with $\mathbf{p} \neq 0$, while the condensed phase (we show that it does not disappear when interactions are introduced) can be considered as a kind of external field.

The Green's function is expressed in terms of three effective potentials Σ_{ik}, describing pair-production, pair-annihilation and scattering, and in terms of a chemical potential μ. This is the analog of Dyson's equation in electrodynamics.[4,1] Some approximation must be made in the calculation of Σ_{ik} and μ. If these quantities are computed by perturbation theory, the quasi-particle spectrum of Bogoliubov[5] is obtained. In the following paper[6] we evaluate Σ_{ik} and μ in the limit of low density.

*Private communication from A. B. Migdal.

2. STATEMENT OF THE PROBLEM. FEYNMAN GRAPHS

We consider a system of N spinless bosons with mass $m = 1$, enclosed in a volume V. We suppose N and V become infinite, the density $N/V = n$ remaining finite. A summation over discrete momenta is then replaced by an integral according to the rule

$$\sum_{\mathbf{p}} \to (2\pi)^{-3} V \int d\mathbf{p}.$$

The Hamiltonian of the system is $H = H_0 + H_1$, where

$$H_0 = \frac{1}{2}\int \nabla\Psi^+(x)\,\nabla\Psi(x)\,dx = \sum_{\mathbf{p}} \varepsilon_{\mathbf{p}}^0 a_{\mathbf{p}}^+ a_{\mathbf{p}}; \quad \varepsilon_{\mathbf{p}}^0 = \frac{p^2}{2}, \tag{2.1}$$

$$H_1 = \frac{1}{2}\int \Psi^+(x)\,\Psi^+(x')\,U(x-x')\,\Psi(x')\,\Psi(x)\,dx\,dx' = \frac{1}{2V}\sum_{\mathbf{pp'q}} U_{\mathbf{q}} a_{\mathbf{p}}^+ a_{\mathbf{p'}}^+ a_{\mathbf{p'}-\mathbf{q}} a_{\mathbf{p}+\mathbf{q}}. \tag{2.2}$$

The units are chosen so that $\hbar = 1$. $U(\mathbf{x}-\mathbf{x}')$ is the interaction between a pair of particles, $U_{\mathbf{q}} = \int e^{-i\mathbf{q}\mathbf{x}} U(\mathbf{x})\, d\mathbf{x}$ is its Fourier transform, and

$$\Psi = V^{-1/2} \sum_{\mathbf{p}} e^{ipx} a_p, \quad \Psi^+ = V^{-1/2} \sum_{\mathbf{p}} e^{-ipx} a_{\mathbf{p}}^+,$$

where $a_{\mathbf{p}}$ and $a_{\mathbf{p}}^+$ are the usual boson operators with the commutation law $[a_{\mathbf{p}}, a_{\mathbf{p}'}^+] = \delta_{\mathbf{p}\mathbf{p}'}$.

The one-particle Green's function may be defined in two equivalent ways. In terms of Heisenberg-representation operators we may write

$$iG(x-x') = \langle \Phi_0^N,\ T\{\Psi(x)\Psi^+(x')\}\Phi_0^N\rangle, \tag{2.3}$$

with the expectation value taken in the ground-state of the N interacting particles. In terms of interaction-representation operators we may write

$$iG(x-x') = \langle T\{\Psi(x)\Psi^+(x')S\}\rangle / \langle S\rangle, \tag{2.4}$$

with the expectation value taken in the ground-state of the non-interacting particles, which has all the particles in the condensed phase so that $N_{\mathbf{p}\neq 0} = 0$, $N_0 = N$. The S-matrix for this system has the form

$$S = T\left\{\exp\left(-\frac{i}{2}\int d^4x_1 d^4x_2 U\right.\right.$$
$$\left.\left.(1-2)\Psi^+(1)\Psi^+(2)\Psi(2)\Psi(1)\right)\right\}, \tag{2.5}$$

where we have written for convenience $U(1-2) = U(\mathbf{x}_1-\mathbf{x}_2)\delta(t_1-t_2)$. Here and henceforth $x, \ldots, p$ are four-vectors, and $px = \mathbf{p}\mathbf{x} - p_0x_0$. The definition (2.3) is convenient for relating G to physical quantities, while Eq. (2.4) is convenient for calculations.

In the numerator of Eq. (2.4) we expand the S-matrix in a series, each term of which is a T-product of a certain number of factors Ψ and Ψ^+. A T-product can be expressed by standard methods[7] as a sum of normal products in which some of the factors Ψ and Ψ^+ have been paired. In quantum electrodynamics the vacuum expectation value of every term which contains an unpaired annihilation operator vanishes from this sum. The surviving terms, which contain only pairs of Ψ and Ψ^+, are represented by certain Feynman graphs. In our case the expectation value is taken in a state containing N particles with momentum $\mathbf{p} = 0$. The expectation value of an N-product containing a_0 does not vanish, and the usual method of constructing graphs is not applicable.

Because of the special role of the state with $\mathbf{p} = 0$, it is convenient to separate the operators a_0 and a_0^+ from Ψ and Ψ^+. Thus we write

$$\Psi = \Psi' + a_0/\sqrt{V}; \quad \Psi^+ = \Psi'^+ + a_0^+/\sqrt{V}. \tag{2.6}$$

The Green's function (2.4) is also divided into two parts. The uncondensed particles give

$$iG'(x-x') = \langle T\{\Psi'(x)\Psi'^+(x')S\}\rangle / \langle S\rangle \tag{2.7}$$

while the Green's function of the condensed phase, a function of $(t-t')$ only, is

$$iG_0(t-t') = \langle T\{a_0(t)a_0^+(t')S\}\rangle / V\langle S\rangle. \tag{2.8}$$

The two functions are not independently determined, since the S-matrix appears in the definition of both and itself contains both Ψ' and a_0 operators. We shall prove later that when N is large the usual method of Feynman graphs can be adapted to the calculation of G', the condensed phase behaving just like an external field.

We divide the operations T and $\langle \ldots \rangle$ into two successive operations, the first acting only upon Ψ' and Ψ'^+, the second acting only upon a_0 and a_0^+. Thus

$$T = T^0T', \quad \langle \ldots \rangle = \langle\langle \ldots \rangle'\rangle^0,$$

where T^0 and $\langle \ldots \rangle^0$ act on a_0 and a_0^+.

We now drop the prime from G' and write Eq. (2.7) in the form

$$iG(x-x') = \langle T^0\{\mathfrak{G}(x-x')\}\rangle^0 / \langle S\rangle, \tag{2.9}$$

with

$$\mathfrak{G}(x-x') = \langle T'\{\Psi'(x)\Psi'^+(x')S\}\rangle'. \tag{2.10}$$

Eq. (2.10) has the same structure as the numerator of Eq. (2.7), but the operators a_0, a_0^+ occurring in S are now to be treated as parameters. The expectation value in Eq. (2.10) is taken in the ground state of the operators Ψ', Ψ'^+. This equivalent to a vacuum expectation value, and so the usual formalism of Feynman graphs can be used for calculating $\mathfrak{G}$.

We represent the potential $-iU(1-2)$ by a dotted line joining the points 1 and 2. The pair of operators $\dot{\Psi}'(1)\ \dot{\Psi}'^+(2) = iG^{(0)}(1-2)$ is represented by a continuous line directed from 2 to 1. From the form of the interaction Hamiltonian (2.2) it follows that every graph contributing to Eq. (2.10) is a combination of the eight elementary graphs shown in Fig. 1. These correspond to the various terms which appear in Eq. (2.2) after the substitution (2.6). A missing continuous line (incomplete vertex) corresponds to a factor $(a_0/\sqrt{V})$ or $(a_0^+/\sqrt{V})$. Fig. 2 shows an example of one graph which appears in $\mathfrak{G}(x_1-x_2)$, corresponding to the integral

$$\mathfrak{M}_2(x_1;\ x_2) = i^2 \int G^{(0)}(1-3)U$$
$$\times (3-4)\, G^{(0)}(3-5)\, G^{(0)}(4-6)\, U(5-6) \tag{2.11}$$
$$\times G^{(0)}(6-2)\, V^{-1} a_0^+(t_4)\, a_0(t_5)\, d^4x_3 d^4x_4 d^4x_5 d^4x_6.$$

Let $\mathfrak{M}(x; x')$ be any graph contributing to Eq. (2.10) and not containing disconnected parts or vacuum loops. Together with $\mathfrak{M}$ we may consider all graphs differing from $\mathfrak{M}$ by the addition of vacuum loops. The totality of such graphs gives $\mathfrak{M}$ multiplied by a factor which is just the vacuum expectation value of the S matrix, namely $\langle S\rangle'$ in this case, since we are taking matrix elements only of Ψ' and Ψ'^{+}. Thus the inclusion of vacuum loops changes $\mathfrak{M}$ into

$$\mathfrak{M}(x; x')\langle S\rangle'. \tag{2.12}$$

In quantum electrodynamics the factor $\langle S\rangle$ cancels the denominator of Eq. (2.4), so that we can ignore the vacuum loops and merely omit this denominator. In our case, as we shall see later, the factor $\langle S\rangle'$ has a real significance.

Eq. (2.12) substituted into Eq. (2.9) gives

$$\langle T^0\{\mathfrak{M}(x; x')\langle S\rangle'\}\rangle^0/\langle S\rangle, \tag{2.13}$$

where the operation T^0 acts on the factors a_0, a_0^+ occurring in $\mathfrak{M}$ and in $\langle S\rangle'$. Suppose that $\mathfrak{M}$ contains m pairs of operators a_0, a_0^+. Then

$$\mathfrak{M}(x; x') = V^{-m}\int M(x; x'; t_1 \dots t_m; t_1' \dots t_m')\, a_0(t_1)\dots$$

$$\dots a_0(t_m)\, a_0^+(t_1')\dots a_0^+(t_m')\,(dt)\,(dt'),$$

and Eq. (2.13) becomes

$$\int MiG_0(t_1 \dots t_m; t_1' \dots t_m')\,(dt)\,(dt'), \tag{2.14}$$

where

$$iG_0(t_1 \dots t_m; t_1' \dots t_m')$$

$$= \langle T\{a_0(t_1)\dots a_0^+(t_m')\,S\}\rangle / V^m\langle S\rangle \tag{2.15}$$

is the m-particle Green's function of the condensed phase, Eq. (2.8) being the special case m = 1.

The graphs for the Green's function (2.9) thus coincide with the graphs for $\mathfrak{G}$, only the factors $(a_0a_0^+/V)$ in the integrals are replaced by the corresponding Green's function of the condensed phase. For example, in the integral (2.11), the factor $(a_0^+(t_4)\, a_0(t_5)/V)$ is replaced by $iG_0(t_5 - t_4)$. We need not consider graphs with disconnected parts, since these are already included in G_0. The problem is therefore reduced to the determination of the Green's functions G_0 of the condensed phase.

3. THE GREEN'S FUNCTIONS OF THE CONDENSED PHASE

We write the m-particle Green's function (2.15) of the condensed phase in the form

$$iG_0(t_1 \dots t_m; t_1' \dots t_m')$$

$$= \frac{1}{V^m\langle S\rangle}\langle T^0\{a_0(t_1)\dots a_0(t_m)\, a_0^+(t_1')\dots$$

$$\dots a_0^+(t_m')\langle S\rangle'\}\rangle^0. \tag{3.1}$$

The quantity $\langle S\rangle'$ is the sum of contributions from all vacuum loops. If λ is the sum of contributions from all connected vacuum loops, then[8] the sum of contributions from all pairs of connected loops is $(\lambda^2/2!)$, the sum of contributions from all triples is $(\lambda^3/3!)$, and so on. Therefore $\langle S\rangle' = e^{\lambda}$. In our case λ is a functional of $a_0a_0^+$, and is proportional to the volume V if we take $(a_0a_0^+/V)$ to be finite. This can be seen by considering any vacuum loop as obtained from a graph with two free ends, carrying momenta $\mathbf{p}$ and $\mathbf{p}'$, by setting $\mathbf{p} = \mathbf{p}' = 0$. The graph with free ends gives a contribution proportional to $\delta(\mathbf{p}-\mathbf{p}') \sim (2\pi)^{-3}\, V\delta_{\mathbf{p}\mathbf{p}'}$, and so the vacuum loop becomes proportional to V. Therefore $\lambda = V\sigma$, where σ is a finite functional of $(a_0a_0^+/V)$, and

$$\langle S\rangle' = e^{V\sigma}. \tag{3.2}$$

The commutator of a_0 and a_0^+ is unity, and is small compared with their product which is of order N. At first glance it would seem that the order of factors a_0, a_0^+ was unimportant, and that the T-product in Eq. (3.1) could be omitted. But one must remember that the T^0 in Eq. (3.1) links the product $a_0 \dots a_0^+$ with the quantity $e^{V\sigma}$, which contains all powers of the volume and hence may compensate for the smallness of the commutator of a_0 with a_0^+. Only after disentangling $a_0 \dots a_0^+$ from the T-product may we neglect the commutators. We observe that a_0 and a_0^+ commute with H_0 given by Eq. (2.1), so these operators are independent of time in the interaction representation. The arguments of the $a_0(t)$ and $a_0^+(t')$ in Eq. (3.1) are only ordering symbols for the operation of T^0. After carrying out the T-ordering we may consider a_0 and a_0^+ as time-independent.

The disentangling of $a_0 \dots a_0^+$ from the T-product is done by means of the following theorem. Let $B(a_0a_0^+/V)$ and $\sigma(a_0a_0^+/V)$ be any functionals of $(a_0a_0^+/V)$, which is considered as a finite quantity. The "disentangling rule"

$$T^0\{B(a_0a_0^+/V)\, e^{V\sigma}\} = B(AA^+)\, T^0\{e^{V\sigma}\}. \tag{3.3}$$

holds with an error of order $(1/V)$. The quantities A and A^+ are defined by the integral equations

$$A(t) = C(AA^+) + \int dt'\, \theta(t-t')\,\delta\sigma(AA^+)/\delta A^+(t'),$$

$$A^+(t) = C^+(AA^+) + \int dt'\, \theta(t'-t)\,\delta\sigma(AA^+)/\delta A(t'), \tag{3.4}$$

where $\theta(t-t')$ is the contribution from a factor-pair (a_0, a_0^+),

$$\theta(t-t') = \dot{a}_0(t)\dot{a}_0^+(t') = \begin{cases} 1 & \text{for } t > t' \\ 0 & \text{for } t < t', \end{cases} \quad (3.5)$$

and C, C^+ are time-independent functionals defined by the quadratic equations

$$C^2 + C\int \frac{\delta\sigma(AA^+)}{\delta A^+(t)}\,dt = \frac{a_0^2}{V};$$

$$C^{+2} + C^+\int \frac{\delta\sigma(AA^+)}{\delta A(t)}\,dt = \frac{a_0^{+2}}{V}. \quad (3.6)$$

A proof of this theorem is given in the Appendix.

Applying Eq. (3.3) to (3.1), we obtain

$$iG_0(t_1 \ldots; \ldots t_m) = \langle A(t_1)\ldots A^+(t'_m)\rangle^0.$$

The denominator of Eq. (3.1) cancels against $\langle T^0\langle S\rangle'\rangle^0 = \langle S\rangle$. When the expectation value of the product $(A\ldots A^+)$ is taken, we may with an error of order $(1/V)$ replace all factors a_0, a_0^+ by $\sqrt{N}$. Let K and K^+ denote the result of making this replacement in A and A^+. Then

$$iG_0(t_1\ldots t_m; t'_1\ldots t'_m)$$
$$= K(t_1)\ldots K(t_m)K^+(t'_1)\ldots K(t'_m), \quad (3.7)$$

holds, with K and K′ given according to Eq. (3.4) by the integral equations

$$K(t) = \bar{C} + \int dt'\theta(t-t')\frac{\delta\sigma(KK^+)}{\delta K^+(t')},$$

$$K^+(t) = \bar{C}^+ + \int dt'\theta(t'-t)\frac{\delta\sigma(KK^+)}{\delta K(t')}, \quad (3.8)$$

and with $\bar{C}$ and $\bar{C}^+$ defined by

$$\bar{C}^2 + \bar{C}\int \frac{\delta\sigma(KK^+)}{\delta K^+(t)}\,dt = \frac{N}{V};$$

$$\bar{C}^{+2} + \bar{C}^+\int \frac{\delta\sigma(KK^+)}{\delta K(t)}\,dt = \frac{N}{V}. \quad (3.9)$$

Eq. (3.7) shows that the Green's functions of the condensed phase are products of factors, each factor being a function of one time variable. The physical meaning of this result may be clarified by the following qualitative argument. For simplicity we consider the one-particle function for non-interacting particles $iG_0^{(0)}(t-t') = \langle a_0(t)\,a_0^+(t')\rangle/V$. It describes the propagation of a particle from t′ to t. If there was originally a vacuum, then this process can proceed only by creating a particle at time t′ and annihilating it at the later time t, which is represented by the factor-pairing $\mathring{a}_0\mathring{a}_0^+ = \theta$. In this case $G^{(0)}$ coincides with the factor-pairing, as is the case in electrodynamics. But if the process occurs in the presence of N particles of the same type, the created and absorbed particles may be different. In this case the propagation of a particle from t′ to t is composed of two processes, the creation of an extra particle in the condensed phase at time t′, and the absorption of one particle from the condensed phase at time t. The time sequence of these two events is immaterial, to order N^{-1}, if N is large. The processes are therefore independent. These arguments are valid also for the exact function G_0. It is also a product of two factors K(t) and $K^+(t')$, describing the two independent processes of emission and absorption of a particle at the two corresponding times.

We consider in greater detail the one-particle function of the condensed phase

$$iG_0(t-t') = K(t)K^+(t'). \quad (3.10)$$

The left side is a function of the difference $(t-t')$. The right side is a product of functions of t and t′. Therefore K(t) and $K^+(t')$ must be exponentials

$$K(t) = \sqrt{n_0}\,e^{-i\mu t}; \quad K^+(t) = \sqrt{n_0}\,e^{i\mu t} \quad (3.11)$$

so that

$$iG_0(t-t') = n_0 e^{-i\mu(t-t')}. \quad (3.12)$$

To understand the physical meaning of the quantities n_0 and μ, we go back to the definition (2.3) of G_0

$$iG_0(t-t') = \langle\Phi_0^N,\, T\{a_0(t)\,a_0^+(t')\}\,\Phi_0^N\rangle/V. \quad (3.13)$$

Putting $t' = t$ in Eq. (3.13) we find

$$iG_0(0) = \langle\Phi_0^N,\, a_0^+a_0\Phi_0^N\rangle/V = \bar{N}_0/V. \quad (3.14)$$

Comparing Eq. (3.14) with (3.12), we see that $n_0 = (\bar{N}_0/V)$ is the mean density of particles in the condensed phase.

Next, suppose for definiteness $t > t'$, and write Eq. (3.13) in the form

$$iG_0(t-t') = \frac{1}{V}\langle\Phi_0^N a_0(t)\,\Phi_0^{N+1}\rangle\langle\Phi_0^{N+1}a_0^+(t')\,\Phi_0^N\rangle$$
$$+ \frac{1}{V}\sum_{s\neq 0}\langle\Phi_0^N a_0(t)\,\Phi_s^{N+1}\rangle\langle\Phi_s^{N+1}a_0^+(t')\,\Phi_0^N\rangle,$$

Separating out the time dependence of the Heisenberg operators, this expression becomes

$$iG_0(t-t') = \frac{1}{V}\exp\{-i(E_0^{N+1}-E_0^N)(t-t')\}\langle\Phi_0^N a_0\Phi_0^{N+1}\rangle\langle\Phi_0^{N+1}a_0^+\Phi_0^N\rangle$$
$$+\frac{1}{V}\sum_{s\neq 0}\exp\{-i(E_s^{N+1}-E_0^N)(t-t')\}\langle\Phi_0^N a_0\Phi_s^{N+1}\rangle\langle\Phi_s^{N+1}a_0^+\Phi_0^N\rangle. \quad (3.15)$$

We compare the exact Eq. (3.15) with the approximation (3.12) which is valid as $N\to\infty$, and conclude that the second term in Eq. (3.15) must vanish as $N\to\infty$. Comparison of the time dependence of the first term in Eq. (3.15) with that of Eq. (3.12) then shows that μ is the chemical potential of the system,

$$\mu = E_0^{N+1} - E_0^N \approx \partial E_0^N/\partial N. \quad (3.16)$$

The parameters n_0 and μ which appear in K and K^+ can be calculated in principle by solving Eq. (3.8). In practice this is very difficult. The trouble is that, in calculating the vacuum loops which contribute to σ, one has first to integrate over a finite time interval $(-T, T)$, so that the parameter T appears in Eq. (3.8). One may pass to the limit $T\to\infty$ in the solutions, but not in the equations. Thus it is incorrect to use in $\sigma(KK^+)$ the limiting expressions (3.11) for K and K^+. One has instead to solve the nonlinear equations (3.8) directly.

We can obtain from Eq. (3.8) one relation between the quantities n_0 and μ. Differentiating Eq. (3.8) with respect to t, and remembering that $d\theta(t-t')/dt = \delta(t-t')$, we obtain the differential equations

$$dK/dt = \delta\sigma(KK^+)/\delta K^+(t);$$
$$dK^+/dt = -\delta\sigma(KK^+)/\delta K(t). \quad (3.17)$$

Let σ be expanded in a series

$$\sigma(KK^+) = -i\sum_{(W)}\frac{1}{m}\int W_m(t_1'\ldots t_m'; t_1\ldots t_m)K^+(t_1')\ldots$$
$$\ldots K^+(t_m')K(t_1)\ldots K(t_m)(dt)(dt'), \quad (3.18)$$

in which each term corresponds to a certain vacuum loop with m pairs of incomplete vertices, and the sum is taken over all such loops. The "vacuum amplitudes" W_m are functions of only $(2m-1)$ variables (time differences), so that the limiting values of K and K^+ would give an infinite result when substituted into Eq. (3.18). If Eq. (3.18) is varied with respect to K^+, one integration disappears, and the result becomes finite. The Fourier transform of $W_m(t'; t)$ may be written

$$W_m(\omega_1'\ldots;\ldots\omega_m)\,\delta\left(\sum\omega - \sum\omega'\right)$$
$$= \int W_m(t'; t)\,e^{i(\omega' t' - i(\omega t)}(dt)(dt'),$$

Then Eq. (3.11) and (3.18) give

$$\frac{\delta\sigma(KK^+)}{\delta K^+(t)}$$
$$= -i\sqrt{n_0}\sum_{(W)}n_0^{m-1}W_m(\mu\ldots;\ldots\mu)e^{-i\mu t}. \quad (3.19)$$

Substituting Eq. (3.19) into (3.17) and using Eq. (3.11), we obtain the desired relation

$$\mu = \sum_{(W)}n_0^{m-1}W_m(\mu\ldots\mu;\mu\ldots\mu). \quad (3.20)$$

The summation here extends over the various vacuum loops which contribute to the quantity $(\delta\sigma/\delta K^+(t))$ according to Eq. (3.19). Each such loop is to be taken with unit weight, remembering that there is one special incomplete vertex t, at which the variation with respect to K^+ was taken. Two loops are to be counted as different if they have the same geometrical structure and differ only in the position of the special vertex.

Equation (3.20) may be considered as an equation for $\mu(n_0)$. There is one free parameter in the problem, the total particle number N or the density n. Thus μ and n_0 ought to be expressible in terms of n. However n does not appear explicitly in the equation. It is thus convenient to consider n_0 instead of n as the free parameter, and to express all other quantities as functions of n_0. The connection between n_0 and n can be found after the problem is solved. From this standpoint, Eq. (3.20) completely determines K and K^+ and consequently all the Green's functions of the condensed phase. We might also solve the problem with two free parameters μ and n_0, and only consider the connection between them in the final result.[6] But this procedure would considerably increase the mathematical difficulties.

4. PROPERTIES OF THE CONDENSED PHASE

The form of the functions G_0 of the condensed phase leads to some deductions concerning the properties of the condensed phase in a system of interacting particles.

In the absence of interaction, the momentum distribution of particles in the ground state is $\delta(\mathbf{p}) = (2\pi)^{-3}V\delta_{\mathbf{p}0}$. When interactions are introduced the distribution is smeared out. In principle two possibilities are open. Either the term in $\delta(\mathbf{p})$ completely disappears and the distribution

becomes continuous (there is no condensed phase), or a term in $\delta(\mathbf{p})$ remains and the state $\mathbf{p} = 0$ is still exceptional (there is a condensed phase). In the first case all average occupation numbers $\overline{N}_{\mathbf{p}}$ are finite, and $\overline{N}_{\mathbf{p}} \to \overline{N}_0$ as $\mathbf{p} \to 0$. In the second case $\overline{N}_{\mathbf{p}\neq 0}$ is finite but $\overline{N}_0 \sim V$.

The neglect of the second term in Eq. (3.15) is equivalent to the assumption that a_0, operating on the ground state Φ_0^N, does not excite the system, or in symbols

$$a_0\Phi_0^N \approx (N_0)^{1/2}\Phi_0^{N-1}. \tag{4.1}$$

This assumption seems at first glance strange. A change in the number of particles with $\mathbf{p} = 0$, disturbing the stationary relation between the occupation numbers, must excite the system. If N_0 were finite, a change of it by one unit would change the state appreciably, but if $N_0 \sim V$ this change will practically not disturb the ground state. Equation (4.1) supports the second alternative. Therefore the introduction of interactions never causes the condensed phase to disappear entirely.

We next examine the problem of the fluctuation of the number of particles in the condensed phase. The quantity N_0 does not have an exact value in the state Φ_0^N. We expand Φ_0^N into eigenstates of the operator N_0. The expansion may be written

$$\Phi_0^N = \sum_{m=0}^{N} C_{N-m}^N \varphi_0^{N-m} \chi_m^N, \tag{4.2}$$

where $\varphi_0^{N_0}$ is a function only of the occupation number of the condensed phase, while χ_m^N depends on the other variables. χ_m^N describes a state of m particles with momenta distributed over all values $\mathbf{p} \neq 0$. It is a superposition of states with definite occupation numbers for the momenta $\mathbf{p} \neq 0$. The coefficients in this superposition depend on the upper index N. The normalization of χ_m^N is given by $\langle \chi_m^N \chi_{m'}^N \rangle = \delta_{mm'}$.

Equation (4.1), with the orthogonality of $\varphi_0^{N_0}$ and $\varphi_0^{N_0'}$ for $N_0 \neq N_0'$, now gives the result

$$\langle \Phi_0^{N-1} a_0 \Phi_0^N \rangle = \sum_{m=0}^{N-1} \sqrt{N-m}\,(C_{N-m-1}^{N-1})^* C_{N-m}^N \langle \chi_m^{N-1} \chi_m^N \rangle \tag{4.3}$$

We assume that C_{N-m}^N and χ_m^N are smooth functions of N, so that

$$C_{N-m-1}^{N-1} \approx C_{N-m}^N - \partial C_{N-m}^N/\partial N = C_{N-m}^N \{1 + O(N^{-1})\};$$
$$\chi_m^{N-1} \approx \chi_m^N - \partial \chi_m^N/\partial N = \chi_m^N \{1 + O(N^{-1})\}.$$

Then Eq. (4.3) becomes

$$\langle \Phi_0^{N-1} a_0 \Phi_0^N \rangle = \sum_{m=0}^{N-1} \sqrt{N-m}\,|C_{N-m}^N|^2 \{1 + O(N^{-1})\}.$$

The sum here is simply $N_0^{1/2}$, so that

$$\langle \Phi_0^{N-1} a_0 \Phi_0^N \rangle = \overline{N_0^{1/2}} \{1 + O(N^{-1})\}. \tag{4.4}$$

A similar expression naturally holds also for $\langle \Phi_0^{N+1} a_0^+ \Phi_0^N \rangle$.

We estimate the sum in Eq. (3.15) after setting $t = t'$. Using Eq. (4.4) and (3.14), we find

$$\sum_{s\neq 0} \langle \Phi_0^N a_0 \Phi_s^{N+1} \rangle \langle \Phi_s^{N+1} a_0^+ \Phi_0^N \rangle \approx \overline{N}_0 - (\overline{N_0^{1/2}})^2, \tag{4.5}$$

from which it is clear that the sum is connected with the magnitude of the fluctuations in the number of particles in the condensed phase. From the fact that the sum is negligible as $N \to \infty$, we conclude

$$[\overline{N}_0 - (\overline{N_0^{1/2}})^2] / \overline{N}_0 \to \infty \text{ for } N \to \infty, \tag{4.6}$$

Thus the fluctuations in the number of particles in the condensed phase are relatively small.

5. GREEN'S FUNCTION FOR A PARTICLE WITH $\mathbf{p} \neq 0$

The expressions obtained in Sec. 3 for the functions of the condensed phase allow us to reformulate the rules which were described in Sec. 2 for the construction of graphs.

Every graph is a combination of eight elementary graphs (Fig. 1). Every incomplete vertex carries a factor $K(t) = \sqrt{n_0}\, e^{-i\mu t}$ corresponding to a missing incoming continuous line, or a factor $K^+(t) = \sqrt{n_0}\, e^{i\mu t}$ corresponding to a missing outgoing line. These factors mean that the interaction

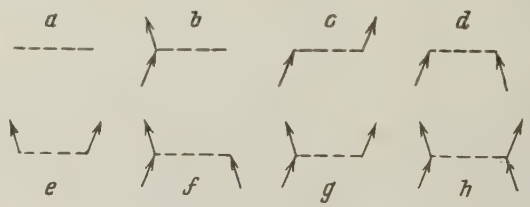

FIG. 1

involves the absorption or the emission of a particle of energy μ in the condensed phase. We may draw a wavy line corresponding to every incoming or outgoing particle of the condensed phase. All such lines have free ends. In analogy with quantum electrodynamics, we may say that the condensed phase behaves like an external field with frequency μ.

Consider the general structure of a graph which contributes to the Green's function (2.7). Every

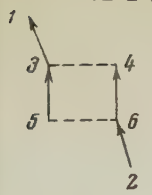

FIG. 2

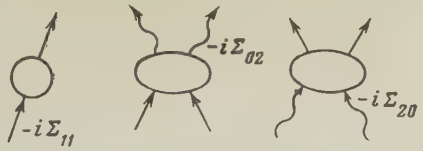

FIG. 3

graph contributing to G has the form of a chain consisting of separate irreducible parts connected to each other by only one continuous line. There are only three types of irreducible parts (i.e., parts which cannot be separated into pieces joined by only one continuous line). The three types differ in the number of outgoing and incoming continuous lines (Fig. 3). The sums of the contributions from all irreducible parts of each type we call respectively $-i\Sigma_{11}$, $-i\Sigma_{02}$, $-i\Sigma_{20}$. Σ_{11} describes processes in which the number of particles out of the condensed phase is conserved. Σ_{02} and Σ_{20} describe the absorption and emission of two particles out of the condensed phase; in these processes two particles in the condensed phase must be simultaneously emitted or absorbed, and their energy 2μ must be taken into account. In the momentum representation, $\Sigma_{11}(p_1; p_2)$ contains a factor $\delta(p_1 - p_2)$, while $\Sigma_{02}(p_1 p_2)$ and $\Sigma_{20}(p_1 p_2)$ contain* $\delta(p_1 + p_2 - 2\mu)$. Henceforth we shall assume momentum conservation in the arguments of the functions Σ_{ik}, representing the quantities which multiply the δ-functions by the notations

$$\Sigma_{11}(p;\ p) \equiv \Sigma_{11}(p);\ \Sigma_{02}(p + \mu, -p + \mu) \equiv \Sigma_{02}(p + \mu);$$
$$\Sigma_{20}(p + \mu, -p + \mu) \equiv \Sigma_{20}(p + \mu). \qquad (5.1)$$

The functions Σ_{ik} are characteristic of the particle interactions, and we may call them the effective potentials of the pair interaction.

Besides the Green's function G we introduce an auxiliary quantity $\hat{G}$, consisting of the sum of contributions from graphs with two ingoing lines. Graphs contributing to G have one ingoing and one outgoing. Figure 4 shows some of the graphs which contribute to $\hat{G}$. The quantity $\hat{G}$ describes the transition of two particles into the condensed phase. In momentum representation we write $\hat{G}(p + \mu)$ when the ingoing lines carry momenta $(p + \mu)$ and $(-p + \mu)$.

There are two equations, analogous to the Dyson equation in electrodynamics,[5,1] for the functions G and $\hat{G}$,

$$G(p+\mu) = G^{(0)}(p+\mu) + G^{(0)}(p+\mu)\Sigma_{11}(p+\mu)G(p+\mu) + G^{(0)}(p+\mu)\Sigma_{20}(p+\mu)\hat{G}(p+\mu),$$
$$\hat{G}(p+\mu) = G^{(0)}(-p+\mu)\Sigma_{11}(-p+\mu)\hat{G}(p+\mu) + G^{(0)}(-p+\mu)\Sigma_{02}(p+\mu)G(p+\mu). \qquad (5.2)$$

The structure of these equations is illustrated graphically by Fig. 5 and does not need any further explanation. Solving the system (5.2) for G and $\hat{G}$, we find

$$G(p+\mu) = (G^{(0)-1} - \Sigma_{11})^{-}\{(G^{(0)-1} - \Sigma_{11})^{+}(G^{(0)-1} - \Sigma_{11})^{-} - \Sigma_{20}\Sigma_{02}\}^{-1},$$
$$\hat{G}(p+\mu) = \Sigma_{02}\{(G^{(0)-1} - \Sigma_{11})^{+}(G^{(0)-1} - \Sigma_{11})^{-} - \Sigma_{20}\Sigma_{02}\}^{-1}, \qquad (5.3)$$

where the suffixes $\pm$ indicate the values $(\pm p + \mu)$ of the arguments. Equation (5.3) for G may be written in the usual form of a Dyson equation

$$G^{-1} = G^{(0)-1} - \Sigma,$$
$$\Sigma(p+\mu) = \Sigma_{11}(p+\mu) + \Sigma_{20}\Sigma_{02}/[G^{(0)-1}(-p+\mu) - \Sigma_{11}(-p+\mu)]. \qquad (5.4)$$

Into Eq. (5.3) we substitute the explicit form of the free-particle Green's function,

$$G^{(0)-1}(p) = p^0 - \varepsilon_p^0 + i\delta; \qquad (\varepsilon_p^0 = p^2/2;\ \ \delta \to +0), \qquad (5.5)$$

and obtain for G and $\hat{G}$ the expressions

$$G(p+\mu) = \frac{p^0 + \varepsilon_p^0 + \Sigma_{11}^{-} - \mu}{[p^0 - (\Sigma_{11}^{+} - \Sigma_{11}^{-})/2]^2 - [\varepsilon_p^0 + (\Sigma_{11}^{+} + \Sigma_{11}^{-})/2 - \mu]^2 + \Sigma_{20}\Sigma_{02}}, \qquad (5.6)$$

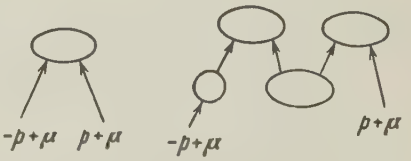

FIG. 4

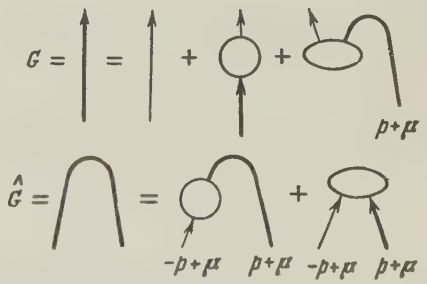

FIG. 5

*Here μ represents a 4-vector having only its fourth component non-zero.

$$\hat{G}(p+\mu) = \frac{-\Sigma_{02}}{[p^0-(\Sigma_{11}^+-\Sigma_{11}^-)/2]^2-[\varepsilon_p^0+(\Sigma_{11}^++\Sigma_{11}^-)/2-\mu]^2+\Sigma_{20}\Sigma_{02}}. \quad (5.7)$$

Equation (5.6) determines the Green's function in terms of the effective potentials Σ_{ik} and the chemical potential μ of the system. Equations for Σ_{ik} and μ cannot be obtained in so general a form. To calculate these quantities we have to use approximate methods to sum over series of graphs. In Sec. 7 we shall calculate Σ_{ik} and μ by perturbation theory. In the following paper[6] we develop an approximation in which the density is considered as a small parameter.

6. CONNECTION BETWEEN THE GREEN'S FUNCTION AND PROPERTIES OF THE SYSTEM

The energy E_0 of the ground state is the expectation value of the Hamiltonian (2.1), (2.2) in the state Φ_0^N,

$$E_0 = \langle \Phi_0^N H \Phi_0^N \rangle = \sum_p \varepsilon_p^0 \langle a_p^+ a_p \rangle + \frac{1}{2V} \sum_{pp'q} U_q \langle a_p^+ a_{p'}^+ a_{p'-q} a_{p+q} \rangle. \quad (6.1)$$

The last term in Eq. (6.1) is connected with the Green's function G. Consider G in the $(\mathbf{p}, t)$ representation, i.e., in the momentum representation for the space-components only. Taking the expectation value in the state Φ_0^N, Eq. (2.3) becomes

$$iG(\mathbf{p};\ t-t') = \langle T\{a_p(t)\, a_p^+(t')\}\rangle, \qquad (\mathbf{p}\neq 0), \quad (6.2)$$

from which it is easy to deduce

$$(i\partial/\partial t - \varepsilon_p^0)\, G(\mathbf{p};\ t-t') = \delta(t-t') + R(\mathbf{p};\ t-t'), \quad (6.3)$$

with

$$R(\mathbf{p};\ t-t') = -\frac{i}{V}\sum_{p'q} U_q \langle T\{a_{p'}^+(t)\, a_{p'-q}(t)\, a_{p+q}(t) a_p^+(t')\}\rangle. \quad (6.4)$$

We multiply Eq. (6.3) by $e^{ip^0(t-t')}$ and integrate with respect to t. Then using Eq. (5.5) we obtain

$$G^{(0)-1}(p)\, G(p) = 1 + R(p),$$

This, with the definition (5.4) of Σ, gives immediately

$$R(p) = \Sigma(p)\, G(p), \qquad (\mathbf{p}\neq 0). \quad (6.5)$$

On the other hand, Eq. (6.4) shows that $R(\mathbf{p}; -0)$ is related to the last sum in Eq. (6.1), namely

$$\frac{1}{2V}\sum_{pp'q} U_q \langle a_p^+ a_{p'}^+ a_{p'-q} a_{p+q}\rangle = \frac{i}{2}\sum_p R(\mathbf{p};\ -0). \quad (6.6)$$

The expression (6.5) for R holds only when $\mathbf{p}\neq 0$. For $\mathbf{p}=0$ the left side of Eq. (6.2) is $iVG_0(t-t')$ according to Eq. (3.13). Instead of Eq. (6.3) we have in this case

$$i\frac{\partial}{\partial t} G_0(t-t') = \frac{1}{V}\delta(t-t') + \frac{1}{V} R(0;\ t-t'). \quad (6.7)$$

We neglect the δ-function since it is of order V^{-1}, and use Eq. (3.12) for G_0. This gives

$$R(0;\ -0) = i\left[\frac{\partial}{\partial\tau} G_0(\tau)\right]_{\tau=-0} = -i\mu n_0. \quad (6.8)$$

Equations (6.6) and (6.8) bring the expression (6.1) for E_0 into the form

$$E_0 = \sum_p \varepsilon_p^0 \langle a_p^+ a_p\rangle + \frac{i}{2}\sum_{p\neq 0} R(\mathbf{p};\ -0) + \frac{1}{2}\mu n_0. \quad (6.9)$$

From Eq. (6.2) we find

$$\overline{N}_p = \langle a_p^+ a_p\rangle = iG(\mathbf{p};\ -0) = i\int G(p)\, dp^0/2\pi \quad (6.10)$$

Using Eq. (6.5) and (6.10), and passing from summation to integration in Eq. (6.9), we obtain the following expression* for the ground-state energy E_0,

$$E_0/V = i\int [\varepsilon_p^0 + {}^1/_2\Sigma(p)]\, G(p)\, d^4p/(2\pi)^4 + \mu n_0/2 \quad (6.11)$$

The p_0-integration is to be taken with a small detour into the upper half-plane.

The quantities Σ and G depend parametrically upon μ and n_0, supposing that Eq. (3.20) has not been used in order to eliminate one of these parameters. Therefore Eq. (6.11) gives a relation between (E_0/V), μ, and n_0. There are two further relations between these quantities. First there is the definition of the chemical potential μ,

$$\mu = \frac{\partial E_0}{\partial N} = \frac{\partial}{\partial n}\left(\frac{E_0}{V}\right), \quad (6.12)$$

and second there is the condition that the total number of particles is conserved, which by Eq. (6.10) can be written in the form

$$n = n_0 + i\int G(p)\, d^4p/(2\pi)^4. \quad (6.13)$$

Equations (6.11), (6.12), and (6.13) determine (E_0/V), μ, and n_0 in terms of the density n, or determine any three of these quantities in terms of the fourth. The relation (3.20) which we found earlier does not give any new information; it is

*V. M. Galitskii informed me that a similar relation exists for Fermi systems.

satisfied identically when Eq. (6.11), (6.12), and (6.13) hold.

7. PERTURBATION THEORY APPROXIMATION TO Σ_{ik} AND μ

In the first order of perturbation theory, the graphs which contribute to Σ_{ik} are the elementary graphs shown in Fig. 1. Graphs b and c refer to Σ_{11}, d to Σ_{02} and e to Σ_{20}. These graphs give the contributions

$$\Sigma_{02} = \Sigma_{20} = n_0 U_p; \qquad \Sigma_{11}^{+} = n_0 (U_0 + U_p). \tag{7.1}$$

In first approximation the only vacuum loop is the elementary graph a of Fig. 1. Thus Eq. (3.20) gives for μ the value

$$\mu = n_0 U_0. \tag{7.2}$$

Inserting Eq. (7.1) and (7.2) into the expression (5.6) for the Green's function, we find

$$G(p + \mu) = p^0 + \varepsilon_p^0 + n_0 U_p / (p^{0\,2} - \varepsilon_p^{0\,2} - 2n_0 U_p \varepsilon_p^0 + i\delta). \tag{7.3}$$

The Green's function $G(p + \mu)$ has a pole at a value $p_0(\mathbf{p})$ which defines the energy of an elementary excitation of the system[3] (quasi-particle). Equation (7.3) gives for the quasi-particle energy

$$\varepsilon_p = \sqrt{\varepsilon_p^{0\,2} + 2n_0 U_p \varepsilon_p^0}. \tag{7.4}$$

Substituting Eq. (7.3) into (6.10), we obtain the mean occupation number of the ground state,

$$\begin{aligned} \bar{N}_p &= (-\varepsilon_p + \varepsilon_p^0 + n_0 U_p) / 2\varepsilon_p \\ &= (n_0 U_p)^2 / 2\varepsilon_p (\varepsilon_p + \varepsilon_p^0 + n_0 U_p). \end{aligned} \tag{7.5}$$

Equations (7.4) and (7.5) coincide with the results of the well-known work of Bogoliubov.[5]

APPENDIX. PROOF OF THEOREM (3.3)

We use the method of Wick[9] to transform the T-product in Eq. (3.3), which may be written symbolically

$$T\{Be^{V\sigma}\} = N\{e^{\Delta} Be^{V\sigma}\}, \tag{A.1}$$

where Δ is an operator which changes a pair $a_0 a_0^{+}$ into its replacement (3.5),

$$\begin{aligned} \Delta &= \frac{1}{V} \int dt dt' \theta(t - t') \frac{\delta^2}{\delta\alpha(t)\, \delta\alpha^{+}(t')}; \\ (\alpha &= a_0 / \sqrt{V}; \quad \alpha^{+} = a_0^{+} / \sqrt{V}). \end{aligned} \tag{A.2}$$

The proof of the theorem proceeds in two stages: (1) pulling B out across the operator e^{Δ}, and (2) a final disentangling of the N-product.

(1) The result of the first stage can be formulated as follows. With an error of order V^{-1} we have

$$e^{\Delta}\{B(\alpha;\ \alpha^{+}) e^{V\sigma}\} = B(\beta;\ \beta^{+})\, e^{\Delta}\{e^{V\sigma}\}, \tag{A.3}$$

where β and β^{+} are defined by the equations

$$\begin{aligned} \beta(t) &= \alpha + \int dt' \theta(t - t')\, \delta\sigma(\beta\beta^{+}) / \delta\beta^{+}(t'); \\ \beta^{+}(t) &= \alpha^{+} + \int dt' \theta(t' - t)\, \delta\sigma(\beta\beta^{+}) / \delta\beta(t'). \end{aligned} \tag{A.4}$$

Proof. The factor V^{-1} in Δ can be compensated on the left side of Eq. (A.3) only if $e^{V\sigma}$ is involved in at least one operation of Δ. We write $\Delta = \Delta_{\sigma\sigma} + \Delta_{B\sigma} + \Delta_{\sigma B}$, where the first suffix indicates the object upon which the variation with respect to α operates, and the second suffix refers to the variation with respect to α^{+}. The result of operating with $e^{\Delta\sigma\sigma}$ can be written

$$e^{\Delta_{\sigma\sigma}}\{e^{V\sigma}\} = e^{V\sigma'} \tag{A.5}$$

It will be shown later that σ' is independent of V. Equation (A.5) gives

$$e^{\Delta}\{Be^{V\sigma}\} = \exp(\Delta_{B\sigma} + \Delta_{\sigma B})\{Be^{V\sigma'}\}. \tag{A.6}$$

We let $e^{\Delta B\sigma}$ operate first on $e^{V\sigma'}$. From Eq. (A.2) we obtain

$$\Delta_{B\sigma} e^{V\sigma'} = e^{V\sigma'} \int dt dt' \theta(t - t') \frac{\delta\sigma'}{\delta\alpha^{+}(t')} \left[\frac{\delta}{\delta\alpha(t)}\right]_B \equiv e^{V\sigma'} D_B. \tag{A.7}$$

Successive application of Eq. (A.7) gives $(\Delta_{B\sigma})^k \times e^{V\sigma'} = e^{V\sigma'} (D_B)^k$, since the operators $\Delta_{B\sigma}$ produce variations only in the exponential. Therefore

$$e^{\Delta_{B\sigma}} e^{V\sigma'} = e^{V\sigma'} e^{D_B}. \tag{A.8}$$

From (A.7) it is clear that e^{D_B} is a displacement operator, displacing $\alpha(t)$ by the quantity

$$\alpha_1(t) = \int dt' \theta(t - t')\, \delta\sigma' / \delta\alpha^{+}(t'),$$

Therefore

$$\begin{aligned} e^{\Delta_{B\sigma}}\{B(\alpha;\ \alpha^{+}) e^{V\sigma'}\} &= e^{V\sigma'} e^{D_B} B(\alpha;\ \alpha^{+}) \\ &= e^{V\sigma'} B(\alpha + \alpha_1;\ \alpha^{+}). \end{aligned} \tag{A.9}$$

An analogous result holds for the operator $e^{\Delta\sigma B}$, which displaces $\alpha^{+}(t)$. We obtain finally from Eq. (A.6)

$$e^{\Delta}\{B(\alpha;\ \alpha^{+}) e^{V\sigma}\} = B(\beta;\ \beta^{+}) e^{V\sigma'} = B(\beta;\ \beta^{+})\, e^{\Delta}\{e^{V\sigma}\}, \tag{A.10}$$

where

$$\begin{aligned} \beta(t) &= \alpha + \int dt' \theta(t - t')\, \delta\sigma' / \delta\alpha^{+}(t'); \quad \beta^{+}(t) \\ &= \alpha^{+} + \int dt' \theta(t' - t) \delta\sigma' / \delta\alpha(t'); \end{aligned} \tag{A.11}$$

Equation (A.10) is identical with (A.3). It remains to show that Eq. (A.11) and (A.4) are identical. Varying both sides of Eq. (A.5) with respect to

$\alpha(t)$ and $\alpha^+(t)$, and using Eq. (A.10), we obtain

$$\delta\sigma'(\alpha\alpha^+)/\delta\alpha(t) = \delta\sigma(\beta\beta^+)/\delta\beta(t);$$
$$\delta\sigma'(\alpha\alpha^+)/\delta\alpha^+(t) = \delta\sigma(\beta\beta^+)/\delta\beta^+(t); \quad (A.12)$$

Equations (A.12) and (A.11) define σ'. When Eq. (A.12) is substituted into (A.11), the result is Eq. (A.4).

(2) In the second stage of the proof we may consider α and α^+ to be constant operators (see the beginning of Sec. 3). Then σ' and $B(\beta\beta^+) = B'(\alpha\alpha^+)$ are functions of α, α^+ instead of functionals. By integrating Eq. (A.12) with respect to time we obtain the connection between the functions $\sigma'(\alpha\alpha^+)$ and σ,

$$\int \frac{\delta\sigma(\beta\beta^+)}{\delta\beta(t)}\,dt = \int \frac{\delta\sigma'(\alpha\alpha^+)}{\delta\alpha(t)}\,dt = \frac{\partial\sigma'}{\partial\alpha}; \quad \int \frac{\delta\sigma(\beta\beta^+)}{\delta\beta^+(t)}\,dt = \frac{\partial\sigma'}{\partial\alpha^+}. \quad (A.13)$$

For the following argument it is important that σ' and β' depend only on $\nu = \alpha^+\alpha$. This being so, the disentangling proceeds according to the rule

$$N\{B'(\nu)\,e^{V\sigma'(\nu)}\} = B'(\bar{\nu})\,N\{e^{V\sigma'}\}, \quad (A.14)$$

with $\bar{\nu}$ obtained from ν by the relation

$$\nu = \bar{\nu}[1 + \partial\sigma'(\bar{\nu})/\partial\bar{\nu}] \equiv \bar{\nu}X^2 \quad (A.15)$$

We defer the proof of Eq. (A.14), and show first that Eq. (A.3) and (A.14) imply the truth of the theorem (3.3). After the infinite factor $e^{V\sigma'}$ is removed, the lack of commutativity of α and α^+ can be neglected. The substitution $\nu \to \bar{\nu}$ which appears in Eq. (A.14), can therefore be divided into the two substitutions $\alpha \to \bar{\alpha}$, $\alpha^+ \to \bar{\alpha}^+$, where $\alpha = \bar{\alpha}X$ and $\alpha^+ = \bar{\alpha}^+X$ according to Eq. (A.15). After some algebra we find

$$\alpha^2 = \bar{\alpha}^2 + \bar{\alpha}\partial\sigma'(\bar{\nu})/\partial\bar{\alpha}^+; \quad \alpha^{+2} = \bar{\alpha}^{+2} + \bar{\alpha}^+\partial\sigma'(\bar{\nu})/\partial\bar{\alpha}. \quad (A.16)$$

We denote by A, A^+ the quantities into which β, β^+ are transformed under the substitution α, $\alpha^+ \to \bar{\alpha}$, $\bar{\alpha}^+$. The equations for A and A^+ are obtained from Eq. (A.4) by changing the terms outside the integrals into $\bar{\alpha}$ and $\bar{\alpha}^+$, thus

$$A(t) = \bar{\alpha} + \int dt'\theta(t-t')\,\delta\sigma(AA^+)/\delta A^+(t');$$
$$A^+(t) = \bar{\alpha}^+ + \int dt'\theta(t'-t)\,\delta\sigma(AA^+)/\delta A(t'), \quad (A.17)$$

By the definition of $B'(\nu)$, $B'(\bar{\nu}) = B(AA^+)$, and so Eq. (A.3) and (A.14) imply (3.3). To complete the proof of the theorem it remains to show the equivalence of Eq. (A.17) and (3.4). To do this, we substitute α, $\alpha^+ \to \bar{\alpha}$, $\bar{\alpha}^+$ in Eq. (A.13), and find the result

$$\frac{\partial\sigma'(\bar{\nu})}{\partial\bar{\alpha}} = \int \frac{\delta\sigma(AA^+)}{\delta A(t)}\,dt; \quad \frac{\partial\sigma'(\bar{\nu})}{\partial\bar{\alpha}^+} = \int \frac{\delta\sigma(AA^+)}{\delta A^+(t)}\,dt. \quad (A.18)$$

Equation (A.16) for $\bar{\alpha}$ and $\bar{\alpha}^+$ are identical with Eq. (3.6) by virtue of Eq. (A.18). Therefore $\bar{\alpha}$, $\bar{\alpha}^+$ are identical with C, C^+, and the theorem is proved.

We now return to the proof of Eq. (A.14). Let L be a quantity related to σ' by the equation

$$N\{e^{V\sigma'}\} = e^{VL}. \quad (A.19)$$

We shall later express L explicitly in terms of σ' and shall verify that L is independent of V. Suppose that $B'(\nu)$ has the form

$$B'(\nu) = \sum_k b_k\nu^k, \quad (A.20)$$

Then Eq. (A.19) implies

$$N\{B'e^{V\sigma'}\} = \sum_k b_k\alpha^{+k}N\{e^{V\sigma'}\}\alpha^k = \sum_k b_k\alpha^{+k}e^{VL}\alpha^k. \quad (A.21)$$

The commutation relation $\alpha y(\nu) = (y + \frac{1}{V}\frac{\partial y}{\partial\nu})\alpha$ holds for any function $y(\nu)$. Applying it repeatedly, we find

$$\alpha^k e^y = \exp\left\{\left(1 + \frac{1}{V}\frac{\partial}{\partial\nu}\right)^k y\right\}\alpha^k. \quad (A.22)$$

We choose y to satisfy $(1 + \frac{1}{V}\frac{\partial}{\partial\nu})^k y = VL$. Then Eq. (A.22) gives the rule for pulling α^k through e^{VL},

$$\exp\{VL\}\alpha^k = \alpha^k \exp\left\{\left(1 + \frac{1}{V}\frac{\partial}{\partial\nu}\right)^{-k} VL\right\}$$
$$\approx \alpha^k \exp\left(-k\frac{\partial L}{\partial\nu}\right)\exp\{VL\}. \quad (A.23)$$

Applying Eq. (A.23) to Eq. (A.21), we obtain

$$N\{B'e^{V\sigma'}\} = \sum_k b_k(\nu e^{-\partial L/\partial\nu})^k e^{VL} = B'(\tilde{\nu})e^{VL}, \quad (A.24)$$

with

$$\tilde{\nu} = \nu e^{-\partial L/\partial\nu}. \quad (A.25)$$

L can be determined by differentiating both sides of Eq. (A.19) with respect to α. On the left side we find

$$\frac{1}{V}\frac{\partial}{\partial\alpha}N\{e^{V\sigma'}\} = N\left\{\frac{\partial\sigma'}{\partial\alpha}e^{V\sigma'}\right\} = \alpha^+N\left\{\frac{\partial\sigma'}{\partial\nu}e^{V\sigma'}\right\}$$

which with Eq. (A.24) and (A.19) gives

$$\frac{1}{V}\frac{\partial}{\partial\alpha}N\{e^{V\sigma'}\} = \alpha^+\frac{\partial\sigma'(\tilde{\nu})}{\partial\tilde{\nu}}e^{VL}. \quad (A.26)$$

In differentiating the right side of Eq. (A.19) with respect to α, we must remember that $(\partial L/\partial\alpha)$ and L do not commute. Since $(\partial L/\partial\alpha) = \alpha^+(\partial L/\partial\nu)$, the commutation rule $L\alpha^+ = \alpha^+(L + \frac{1}{V}\frac{\partial L}{\partial\nu})$ implies

$$\frac{1}{V}\frac{\partial}{\partial\alpha}L^k = \alpha^+\left\{\left(L + \frac{1}{V}\frac{\partial L}{\partial\nu}\right)^k - L^k\right\}, \quad (A.27)$$

and hence

$$\frac{1}{V}\frac{\partial}{\partial\alpha}e^{VL}=\alpha^{+}(e^{\partial L/\partial\nu}-1)e^{VL}. \qquad (A.28)$$

By comparing Eq. (A.28) with (A.26), we obtain the desired relation between L and σ',

$$\partial\sigma'(\bar{\nu})/\partial\bar{\nu}=e^{\partial L/\partial\nu}-1. \qquad (A.29)$$

Equations (A.29) and (A.25) imply Eq. (A.15), and by Eq. (A.24) this proves Eq. (A.14).

[1] V. B. Berestetskii and A. D. Galanin, Проблемы современной физики (Problems of Modern Physics), No. 3 (1955), (introductory paper).

[2] Abrikosov, Landau, and Khalatnikov, Dokl. Akad. Akad. Nauk SSSR **95**, 497, 773 and 1177; **96**, 261 (1954).

[3] V. M. Galitskii and A. B. Migdal, J. Exptl. Theoret. Phys. (U.S.S.R.) **34**, 139 (1958); Soviet Phys. JETP **7**, 96 (1958).

[4] F. J. Dyson, Phys. Rev. **75**, 1736 (1949).

[5] N. N. Bogoliubov, Izv. Akad. Nauk SSSR, ser. fiz. **11**, 77 (1947).

[6] S. T. Beliaev, J. Exptl. Theoret. Phys. (U.S.S.R.) **34**, 433 (1958); Soviet Phys. JETP **7**, 289 (1958) (this issue).

[7] G. C. Wick, Phys. Rev. **80**, 268 (1950).

[8] R. P. Feynman, Phys. Rev. **76**, 749 (1949).

[9] S. Hori, Prog. Theoret. Phys. **7**, 578 (1952).

Translated by F. J. Dyson
77

SOVIET PHYSICS JETP VOLUME 34(7), NUMBER 2 AUGUST, 1958

ENERGY-SPECTRUM OF A NON-IDEAL BOSE GAS

S. T. BELIAEV

Academy of Sciences, U.S.S.R.

Submitted to JETP editor August 2, 1957

J. Exptl. Theoret. Phys. (U.S.S.R.) **34**, 433-446 (February, 1958)

The one-particle Green's function is calculated in a low-density approximation for a system of interacting bosons. The energy spectrum of states near to the ground state (quasi-particle spectrum is derived.

1. INTRODUCTION

In the preceding paper[1] the method of Green's functions was developed for a system consisting of a large number of bosons. The one-particle Green's function was expressed in terms of the effective potentials Σ_{ik} of pair interactions and the chemical potential μ of the system. Approximate methods must be used to determine Σ_{ik} and μ. In the present paper we study a "gaseous" approximation, in which the density n, or the ratio between the volume occupied by particles and the total volume, is treated as a small parameter. The interaction between particles is assumed to be central and short-range, but not necessarily weak. The first two orders of approximation involve only the scattering amplitude f of a two-particle system. But in the next order (proportional to $(\sqrt{nf^3})^2$) the effects of three-particle interaction amplitudes appear, which means that practical calculations to this order are hardly possible.

From the Green's function which we calculate, we derive the energy spectrum of excitations or quasi-particles, the energy of the ground state, and also the momentum distribution of particles in the ground state.

2. ESTIMATE OF THE GRAPHS CONTRIBUTING TO THE EFFECTIVE POTENTIALS

The definition of the potentials Σ_{ik}, and the rules for constructing Feynman graphs, were described in our earlier paper,[1] which we shall call I.

We shall estimate by perturbation theory the various graphs contributing to Σ_{ik} and μ. For the Fourier transform of the potential $U(p)=U_p$,

we assume for simplicity* $U_p = U_0$ for $p < 1/a$, and $U_p = 0$ for $p > 1/a$. Then a is of the order of magnitude of the particle radius.

For definiteness we examine Σ_{20}. The graphs for Σ_{02}, Σ_{11} and μ are essentially similar. The first order of perturbation theory, as we saw in Sec. (I, 7), gives $\Sigma_{20}^{(1)} = n_0 U_p$; $\mu = n_0 U_0$.

In the estimate of any graph there may appear three parameters — U_0 and a, characterizing the interaction, and n_0, characterizing the density of particles in the condensed phase. The three parameters can be combined into two dimensionless ratios,

$$\xi = U_0 / a; \qquad \beta = \sqrt{n_0 a^3}. \tag{2.1}$$

The quantity ξ is the usual parameter which appears in perturbation theory (in ordinary units $\xi \sim mU(r)a^2/\hbar^2$), while β is a parameter of gas-density.

FIG. 1

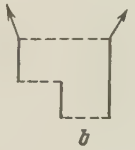

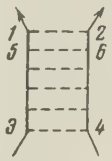

FIG. 2

The only non-vanishing graph in second order is the one shown in Fig. 1a. This gives a contribution

$$M_a \sim n_0 \int G^0(q+\mu)\, G^0(-q+\mu)\, U_0 U_{p+q} d^4q$$

Substituting for G^0 from

$$G^0(p) = (p^0 - \varepsilon_p^0 + i\delta)^{-1}, \qquad \varepsilon_p^0 = p^2/2, \qquad \delta \to +0 \tag{2.2}$$

and carrying out the q^0-integration, we find

$$M_a \sim n_0 U_0^2 \int\limits_{qa<1} d\mathbf{q} \int \frac{dq^0}{(q^0 + \mu - \varepsilon_q^0 + i\delta)(-q^0 + \mu - \varepsilon_q^0 + i\delta)}$$

$$\sim n_0 U_0^2 \int\limits_{qa<1} d\mathbf{q}\, \frac{1}{\mu - \varepsilon_q^0 + i\delta}.$$

In the last integral the main contribution comes from $q \sim 1/a$, where $\mu/\epsilon^0 \sim n_0 U_0 a^2 = \xi\beta^2 \ll 1$. Therefore

$$M_a \sim n_0 U_0^2 / a = \Sigma^{(1)}_{20} \xi. \tag{2.3}$$

We consider next the third-order graph (1b). This gives a contribution

$$M_b \sim n_0^2 \int G^0(q+\mu)\,[G^0(-q+\mu)]^2\, U_0 U_q U_{p+q} d^4q$$

$$\sim n_0^2 U_0^3 \int d\mathbf{q}\,/(\mu - \varepsilon_q^0 + i\delta)^2.$$

The last integral, unlike the previous one, converges at the upper limit, and the main contribution now comes from the range $q \sim \sqrt{\mu} = \sqrt{n_0 U_0}$. Therefore

$$M_b \sim n_0^2 U_0^3 / \sqrt{\mu} = \Sigma^{(1)}_{20} \xi^{3/2} \beta. \tag{2.4}$$

From Eqs. (2.3) and (2.4) we see that $M_b/M_a \sim \xi^{1/2}\beta$. This is a consequence of the fact that M_a contains an integral of a product of two factors G^0, formally diverging at the upper limit, while M_b contains an integral of a product of three factors G^0 and converges without any cut-off. In the graphs this difference is indicated by the number of continuous lines in the closed circuit formed by the continuous and dotted lines. The same result holds when the circuits form part of a more complicated graph.

Thus every circuit containing more than two continuous lines introduces the small parameter β, while circuits with two continuous lines do not involve β. In the lowest order we need consider only graphs whose circuits are all of the two-line type. All such graphs are of the "ladder" construction shown in Fig. 2. We denote by $-i\Gamma(12; 34)$ the total contribution from all such graphs. The first-order approximation in β then differs from the first-order approximation in perturbation theory by changing the potential U (arising from a ladder with one rung) into Γ (arising from ladders of all lengths). Similar conclusions hold also for the higher approximations. A summation over a set of graphs, differing only by the insertion of ladder circuits into a fixed skeleton, produces a change of U into Γ. If we represent Γ by a rectangle, all graphs can be constructed by means of rectangles and continuous lines only. In this way the potential U is eliminated from the problem. The effective potential is Γ.

3.* EQUATION FOR THE EFFECTIVE POTENTIAL Γ

We can write down an integral equation

$$\Gamma(12;34) = U(1-2)\,\delta(1-3)\,\delta(2-4)$$
$$+ i\int U(1-2)\, G^0(1-5)\, G^0(2-6)\, \Gamma(56;34)\, d^4x_5 d^4x_6. \tag{3.1}$$

for the sum of contributions from all graphs of the ladder type (see Fig. 2). The notations are the

*The letters p, q, ... are used to denote the lengths of 3-vectors, or to denote 4-vectors. There can be no confusion, because they denote 4-vectors only when they appear as arguments in G(p), Σ(p), etc.

*The problems connected with Γ were solved in collaboration with V. M. Galitskii, who was working simultaneously on the analogous problems in Fermion systems.

same as in I. We next transform Eq. (3.1) into momentum representation. In order to relieve the equations of factors of 2π, we shall use the conventions

$$d^4p = (2\pi)^{-4} dp^1 dp^2 dp^3 dp^0;$$
$$\delta(p) = (2\pi)^4 \delta(p^1)\delta(p^2)\delta(p^3)\delta(p^0),$$

and similarly we understand $d\mathbf{p}$ and $\delta(\mathbf{p})$ to carry factors of $(2\pi)^3$. We write

$$\Gamma(p_1p_2;\ p_3p_4)\,\delta(p_1+p_2-p_3-p_4) = \int \exp\{-ip_1x_1 - ip_2x_2 + ip_3x_3 + ip_4x_4\}\,\Gamma(12;34)\,d^4x_1 d^4x_2 d^4x_3 d^4x_4, \tag{3.2}$$

and introduce the relative and total momenta by

$$p_1 + p_2 = P';\ p_3 + p_4 = P;$$
$$p_1 - p_2 = 2p',\ p_3 - p_4 = 2p, \tag{3.3}$$

Then, by Eq. (3.1), $\Gamma(p';\,p;\,P) \equiv \Gamma(p_1p_2;\,p_3p_4)$ satisfies the equation

$$\Gamma(p';p;P) = U(p'-p) + i\int d^4q\, U(p'-q)\,G^0(P/2+q) \times G^0(P/2-q)\,\Gamma(q;p;P). \tag{3.4}$$

Since the interaction U is instantaneous, $U(1-2) = U(\mathbf{x}_1 - \mathbf{x}_2)\,\delta(t_1 - t_2)$, and therefore the points 1, 2 and 3, 4 in $\Gamma(12;34)$ must be simultaneous. In momentum representation this means that $\Gamma(p_1p_2;\,p_3p_4)$ depends on the fourth components only in the combination $p_1^0 + p_2^0 = p_3^0 + p_4^0 = P^0$. Therefore $\Gamma(p';\,p;\,P)$ is independent of the fourth components of its first two arguments (the relative momenta). The q^0-integration in Eq. (3.4) can thus be carried out, giving

$$\int dq^0 G^0\left(\tfrac{1}{2}P + q\right) G^0\left(\tfrac{1}{2}P - q\right) = -i\left(P^0 - \tfrac{1}{4}\mathbf{P}^2 - \mathbf{q}^2 + i\delta\right)^{-1}, \tag{3.5}$$

and then Eq. (3.4) takes the form

$$\Gamma(\mathbf{p}';\mathbf{p};P) = U(\mathbf{p}'-\mathbf{p}) + \int d\mathbf{q}\,\frac{U(\mathbf{p}'-\mathbf{q})\,\Gamma(\mathbf{q};\mathbf{p};P)}{k_0^2 - q^2 + i\delta};$$
$$k_0^2 = P^0 - \tfrac{1}{4}\mathbf{P}^2. \tag{3.6}$$

Equation (3.6) cannot be solved explicitly, but its solution can be expressed in terms of the scattering amplitude of two particles in a vacuum. We write $\chi(\mathbf{q}) = (k_0^2 - q^2 + i\delta)^{-1}\ \Gamma(\mathbf{q};\,\mathbf{p};\,P)$. Then Eq. (3.6) becomes

$$(k_0^2 - p'^2)\,\chi(\mathbf{p}') - \int U(\mathbf{p}'-\mathbf{q})\,\chi(\mathbf{q})\,d\mathbf{q} = U(\mathbf{p}'-\mathbf{p}). \tag{3.7}$$

Let $\Psi_{\mathbf{k}}(\mathbf{p}')$ be the normalized wave-function which satisfies the equation

$$(k^2 - p'^2)\,\Psi_{\mathbf{k}}(\mathbf{p}') - \int U(\mathbf{p}'-\mathbf{q})\,\Psi_{\mathbf{k}}(\mathbf{q})\,d\mathbf{q} = 0, \tag{3.8}$$

Then the solution of Eq. (3.7) may be written

$$\chi(\mathbf{p}') = \int \frac{\Psi_{\mathbf{k}}(\mathbf{p}')\,\Psi_{\mathbf{k}}^*(\mathbf{q})}{k_0^2 - k^2 + i\delta}\,U(\mathbf{q}-\mathbf{p})\,d\mathbf{q},$$

and so $\Gamma(\mathbf{p}';\,\mathbf{p};\,P)$ becomes

$$\Gamma(\mathbf{p}';\mathbf{p};P) = (k_0^2 - p'^2)\int \frac{\Psi_{\mathbf{k}}(\mathbf{p}')\,\Psi_{\mathbf{k}}^*(\mathbf{q})}{k_0^2 - k^2 + i\delta}\,U(\mathbf{q}-\mathbf{p})\,d\mathbf{q}. \tag{3.9}$$

We observe now that Eq. (3.8) is the Schrödinger equation in momentum representation. Thus $\Psi_{\mathbf{k}}(\mathbf{p})$ is the wave-function for a scattering problem with potential U. The scattering amplitude* $f(\mathbf{p}'\,\mathbf{p})$ is related to the Ψ-function by

$$f(\mathbf{p}'\mathbf{p}) = \int e^{-i\mathbf{p}'\mathbf{r}}\,U(\mathbf{r})\,\Psi_{\mathbf{p}}(\mathbf{r})\,d\mathbf{r} = \int U(\mathbf{p}'-\mathbf{q})\,\Psi_{\mathbf{p}}(\mathbf{q})\,d\mathbf{q}, \tag{3.10}$$

or by

$$\Psi_{\mathbf{p}}(\mathbf{p}') = \delta(\mathbf{p}-\mathbf{p}') + f(\mathbf{p}'\mathbf{p})/(p^2 - p'^2 + i\delta). \tag{3.11}$$

In the first Eq. (3.10), $\Psi_{\mathbf{p}}(\mathbf{r})$ is the wave-function in coordinate space which behaves at infinity like a plane wave with momentum $\mathbf{p}$ and an outgoing spherical wave. The usual scattering amplitude is the value of $f(\mathbf{p}'\,\mathbf{p})$ at $\mathbf{p}' = \mathbf{p}$. We consider arbitrary values of the arguments, so that $f(\mathbf{p}'\,\mathbf{p})$ is in general defined by Eq. (3.10).

Because $\Psi_{\mathbf{p}}(\mathbf{p}')$ satisfies orthogonality conditions in both its arguments, $f(\mathbf{p}'\,\mathbf{p})$ satisfies the unitarity conditions

$$f(\mathbf{p}'\mathbf{p}) - f^*(\mathbf{p}'\mathbf{p}) = \int d\mathbf{q} f(\mathbf{p}'\mathbf{q})\,f^*(\mathbf{p}\mathbf{q})\left[\frac{1}{q^2 - p'^2 + i\delta} - \frac{1}{q^2 - p^2 - i\delta}\right] = \int d\mathbf{q} f^*(\mathbf{q}\mathbf{p}')\,f(\mathbf{q}\mathbf{p})\left[\frac{1}{q^2 - p'^2 + i\delta} - \frac{1}{q^2 - p^2 - i\delta}\right]. \tag{3.12}$$

When $\mathbf{p}' = \pm\mathbf{p}$, Eq. (3.12) gives the imaginary part of the forward and backward scattering amplitudes. Since $f(-\mathbf{p}'-\mathbf{p}) = f(\mathbf{p}'\,\mathbf{p})$, Eq. (3.12) implies

$$\mathrm{Im}\, f(\pm\mathbf{p}\mathbf{p}) = -i\pi\int d\mathbf{q} f(\mathbf{p}\mathbf{q})\,f^*(\pm\mathbf{p}\mathbf{q})\,\delta(q^2 - p^2). \tag{3.13}$$

For the forward scattering amplitude, Eq. (3.13) gives just the well-known relation between the imaginary part of the amplitude and the total cross-section σ, $\mathrm{Im}\, f(\mathbf{p}\,\mathbf{p}) = -ip\sigma$.

We substitute Eq. (3.11) into (3.9) and use Eq. (3.12). This gives two equivalent expressions for $\Gamma(\mathbf{p}';\,\mathbf{p};\,P)$,

$$\Gamma(\mathbf{p}';\mathbf{p};P) = f(\mathbf{p}'\mathbf{p}) + \int d\mathbf{q} f(\mathbf{p}'\mathbf{q})\,f^*(\mathbf{p}\mathbf{q})\left[\frac{1}{k_0^2 - q^2 + i\delta} + \frac{1}{|q^2 - p^2 - i\delta}\right] \tag{3.14}$$
$$= f^*(\mathbf{p}\mathbf{p}') + \int d\mathbf{q} f(\mathbf{p}'\mathbf{q})\,f^*(\mathbf{p}\mathbf{q})\left[\frac{1}{k_0^2 - q^2 + i\delta} + \frac{1}{q^2 - p'^2 + i\delta}\right].$$

*The quantity $f(\mathbf{p}'\,\mathbf{p})$ differs by a numerical factor from the usual amplitude $a(\mathbf{p}'\,\mathbf{p})$, in fact $f = -4\pi a$.

expressing the effective potential $\Gamma(\mathbf{p}'; \mathbf{p}; \mathrm{P})$ in terms of the scattering amplitudes of a two-particle system.

4. FIRST-ORDER GREEN'S FUNCTION

The effective potentials Σ_{ik} are determined by special values which Γ takes when two out of the four particles involved in a process belong to the condensed phase. Thus two of the four particles must have $\mathbf{p} = 0$, $p^0 = \mu$. Each particle of the condensed phase also carries a factor $\sqrt{n_0}$. Therefore we find

$$\Sigma_{20}(p+\mu) = n_0\Gamma(\mathbf{p}; 0; 2\mu);\ \Sigma_{02}(p+\mu) = n_0\Gamma(0; \mathbf{p}; 2\mu),$$
$$\Sigma_{11}(p+\mu) = n_0\Gamma(\mathbf{p}/2; \mathbf{p}/2; p+2\mu) + n_0\Gamma(-\mathbf{p}/2; \mathbf{p}/2; p+2\mu). \quad (4.1)$$

To obtain the chemical potential we must let all four particles in Γ belong to the condensed phase, and divide by one power of n_0 [see Eq. (I, 3.20)]. We then have

$$\mu = n_0\Gamma(0; 0; 2\mu). \quad (4.2)$$

Substituting into Eqs. (4.1) and (4.2) the value of Γ from Eq. (3.14), we find

$$\mu = n_0 f(00) + n_0\int d\mathbf{q}\,|f(0q)|^2\left[\frac{1}{2\mu - q^2 + i\delta} + \frac{1}{q^2}\right],$$
$$\Sigma_{20}(p+\mu) = n_0 f(\mathbf{p}0) + n_0\int d\mathbf{q} f(\mathbf{pq}) f^*(0\mathbf{q})\left[\frac{1}{2\mu - q^2 + i\delta} + \frac{1}{q^2}\right],$$
$$\Sigma_{02}(p+\mu) = n_0 f^*(\mathbf{p}0) + n_0\int d\mathbf{q} f(0\mathbf{q}) f^*(\mathbf{pq})\left[\frac{1}{2\mu - q^2 + i\delta} + \frac{1}{q^2}\right],$$
$$\Sigma_{11}(p+\mu) = 2n_0 f_s\left(\frac{\mathbf{p}}{2}\,\frac{\mathbf{p}}{2}\right) + 2n_0\int d\mathbf{q}\left|f_s\left(\frac{\mathbf{p}}{2}\,\mathbf{q}\right)\right|^2\left[\frac{1}{p^0 + 2\mu - p^2/4 - q^2 + i\delta} + \frac{1}{q^2 - p^2/4 - i\delta}\right]. \quad (4.3)$$

In the last equation we have introduced the symmetrized amplitude

$$f_s(\mathbf{p}'\mathbf{p}) = [f(\mathbf{p}'\mathbf{p}) + f(-\mathbf{p}'\mathbf{p})]/2.$$

All the integrals in Eq. (4.3) converge at high momentum, even if the amplitudes are taken to be constant. For dimensional reasons these terms are of order $n_0 f^2\sqrt{\mu}$. Compared with the first terms in Eq. (4.3), these terms contain an extra factor $\sqrt{n_0 f^3}$, which is just the gas-density parameter (2.1) obtained by substituting the amplitude f for the particle radius. In first approximation we neglect the integral terms in Eq. (4.3) and obtain

$$\mu = n_0 f(00);\ \Sigma_{20}(p+\mu) = \Sigma^*_{02}(p+\mu) = n_0 f(\mathbf{p}0);$$
$$\Sigma^{\pm}_{11} \equiv \Sigma_{11}(\pm p + \mu) = 2n_0 f_s\left(\frac{\mathbf{p}}{2}\,\frac{\mathbf{p}}{2}\right). \quad (4.4)$$

The Green's function G is given by Eq. (I, 5.6),

$$G(p+\mu) = \frac{p^0 + \varepsilon^0_{\mathbf{p}} + \Sigma^-_{11} - \mu}{[p^0 - (\Sigma^+_{11} - \Sigma^-_{11})/2]^2 - [\varepsilon^0_{\mathbf{p}} + (\Sigma^+_{11} + \Sigma^-_{11})/2 - \mu]^2 + \Sigma_{20}\Sigma_{02} + i\delta} \quad (4.5)$$

and after substituting from Eq. (4.4) this becomes

$$G(p+\mu) = \frac{p^0 + \varepsilon^0_{\mathbf{p}} + 2n_0 f_s\left(\frac{\mathbf{p}}{2}\,\frac{\mathbf{p}}{2}\right) - n_0 f(00)}{p^{02} - \varepsilon^2_{\mathbf{p}} + i\delta}, \quad (4.6)$$

with

$$\varepsilon_{\mathbf{p}} = \sqrt{\left[\varepsilon^0_{\mathbf{p}} + 2n_0 f_s\left(\frac{\mathbf{p}}{2}\,\frac{\mathbf{p}}{2}\right) - n_0 f(00)\right]^2 - n_0^2 |f(\mathbf{p}0)|^2}. \quad (4.7)$$

The point $p_0(\mathbf{p})$, at which the Green's function $G(\mathbf{p} + \mu)$ has a pole, determines the energy $\epsilon_{\mathbf{p}}$ of elementary excitations or quasi-particles[2] carrying momentum $\mathbf{p}$. To calculate $\epsilon_{\mathbf{p}}$ we must know three distinct amplitudes. $f_s(\mathbf{p}/2\ \mathbf{p}/2)$ is the ordinary symmetrized amplitude for forward scattering, and $f(0\ 0)$ is a special value of the same amplitude. However, $f(\mathbf{p}\ 0)$ does not have any obvious meaning in the two-particle problem, since it refers to a process which is forbidden for two particles in a vacuum.

At small momenta, we may neglect the momentum dependence of $f_s(\mathbf{p}/2\ \mathbf{p}/2)$ and of $f(\mathbf{p}\ 0)$, setting $f_s(\mathbf{p}/2\ \mathbf{p}/2) \approx f(\mathbf{p}\ 0) \approx f(0\ 0) \equiv f_0$. This approximation is allowed when the wavelength is long compared with the characteristic size of the interaction region, which has an order of magnitude given by the scattering amplitude f_0. Therefore when $p < f_0^{-1}$ we may consider all the amplitudes in Eq. (4.6) and (4.7) to be constant. For higher excitations with $p \gtrsim f_0^{-1}$, the momentum dependence of the amplitude becomes important, and the problem cannot be treated in full generality. We shall examine the higher excitations (in Sec. 8) for the special example of a hard-sphere gas.

Confining ourselves to the case $pf_0 < 1$, we deduce from Eq. (4.6) and (4.7)

$$G(p+\mu) = (p^0 + \varepsilon^0_{\mathbf{p}} + n_0 f_0)/(p^{02} - \varepsilon^2_{\mathbf{p}} + i\delta), \quad (4.8)$$

with

$$\varepsilon_{\mathbf{p}} = \sqrt{\varepsilon^{02}_{\mathbf{p}} + 2n_0 f_0 \varepsilon^0_{\mathbf{p}}}. \quad (4.9)$$

Equations (4.8) and (4.9) are formally identical with the results obtained from perturbation theory in Eq. (I, 7.3) and (I, 7.4). Only the scattering amplitude f_0 now appears instead of the Fourier transform $U_{\mathbf{p}}$ of the potential.

Equation (4.9) shows that quasi-particles with $p \ll \sqrt{n_0 f_0}$ have a sound-wave type of dispersion law $\epsilon_{\mathbf{p}} \approx p\sqrt{n_0 f_0}$. When $p \gg \sqrt{n_0 f_0}$ they go over into almost free particles with $\epsilon_{\mathbf{p}} \approx \epsilon^0_{\mathbf{p}} + n_0 f_0$.

This sort of energy spectrum appears also when one considers particles moving in a continuous medium with a refractive index. The transition from phonon to free particle behavior occurs at $p \sim \sqrt{n_0 f_0} \ll 1/f_0$, so that the approximation of constant amplitudes is valid in both ranges.

The conditions $\sqrt{n_0 f_0^3} \ll 1$ and $pf_0 \ll 1$ are not independent. If we look at momenta p not greatly exceeding $\sqrt{n_0 f_0}$, then the second condition is a consequence of the first. If we are then neglecting quantities of order $\sqrt{n_0 f_0^3}$, we must also treat the amplitudes as constant.

In Sec. (I, 5) we introduced the quantity $\hat{G}(p+\mu)$, the analog of the Green's function G but constructed from graphs with two ingoing ends instead of one ingoing and one outgoing. The analogous quantity with two outgoing ends will be denoted by $\check{G}(p+\mu)$. It is obtained from $\hat{G}(p+\mu)$ when Σ_{02} is replaced by Σ_{20}. In the constant-amplitude approximation, Eq. (I, 5.7) and (4.4) give

$$\hat{G}(p+\mu) = \check{G}(p+\mu) = -n_0 f_0/(p^{02} - \varepsilon_p^2 + i\delta). \quad (4.10)$$

5. SECOND APPROXIMATION FOR THE GREEN'S FUNCTION

For the second approximation to Σ_{ik} and μ, we must retain quantities of order $\sqrt{n_0 f_0^3}$. As we saw at the end of the preceding section, we must then also retain terms of order pf_0 in the amplitudes. The real part of the amplitude involves only even powers of p, and the imaginary part only odd powers. Terms of order pf_0 arise only from the lowest approximation to the imaginary part of the amplitudes. The imaginary part of $f_S(\mathbf{p}/2\ \mathbf{p}/2)$ is given by Eq. (3.13), and from Eq. (3.10) we see that the amplitude $f(\mathbf{p}\ 0)$ is real [and anyway in this approximation we need only the square of the modulus of $f(\mathbf{p}\ 0)$].

The graphs of the first approximation give terms of order $\sqrt{n_0 f_0^3}$, namely the integral terms in Eq. (4.3). In these terms, as in Eq. (3.13), we may take the amplitudes to be constant. We have seen in Sec. 2 that graphs containing one circuit with three or more continuous lines give contributions of the same order. The summation over sets of graphs, which differ only in the number of continuous lines in a circuit, is automatically performed if one replaces the zero-order Green's function G^0 by the first-order functions G, $\hat{G}$ and $\check{G}$. We therefore consider immediately the circuits which can be built out of G, $\hat{G}$, $\check{G}$ and Γ. There are altogether ten essentially different circuits (see Fig. 3). A rectangle with a cross denotes a sum of two rectangles, one being a direct interaction and the other an exchange interaction. The two differ only by an

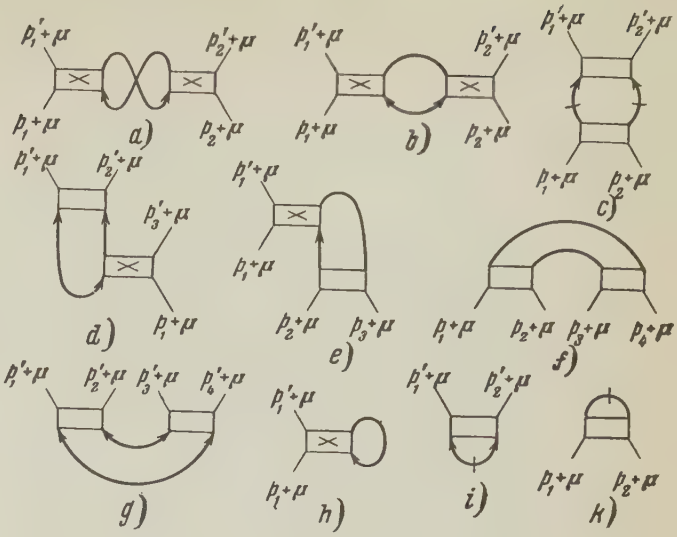

FIG. 3

interchange of the upper or the lower ends. The sum of the two rectangles introduces a factor $-i[\Gamma(12;34) + \Gamma(12;43)]$, or in momentum representation $-i[\Gamma(\mathbf{p}';\mathbf{p};P) + \Gamma(-\mathbf{p}';\mathbf{p};P)]$. If G, $\hat{G}$ and $\check{G}$ are expanded in powers of the effective potential Γ, then in the lowest approximation the graphs (3c, 3i, 3k) become circuits with two continuous lines. But all such circuits are already included in Γ and must therefore be omitted. This omission is represented in Fig. 3 by the strokes across the continuous lines. Let $-iF_{a,b\ldots}(p'_1,\ldots,p_1\ldots)$ denote the contributions from the graphs of Fig. 3. In the constant-amplitude approximation these contributions are:

$$\begin{aligned}
F_a(p'_1p'_2;\ p_1p_2) &= i4f_0^2\int G(q+\mu)\,G(p_1-p'_1+q+\mu)\,d^4q;\\
F_b &= i4f_0^2\int \hat{G}(q+\mu)\,\check{G}(p_1-p'_1+q+\mu)\,d^4q;\\
F_c &= if_0^2\int\{G(q+\mu)\,G(p_1+p_2-q+\mu)\\
&\quad - G^0(q+\mu)\,G^0(p_1+p_2-q+\mu)\}\,d^4q;\\
F_d &= i2f_0^2\int \hat{G}(q+\mu)\,G(p'_2+p'_3-q+\mu)\,d^4q,\\
F_e &= i2f_0^2\int \check{G}(q+\mu)\,G(p'_1+p'_2-q+\mu)\,d^4q;\\
F_f &= if_0^2\int \hat{G}(q+\mu)\,\hat{G}(p_1+p_2-q+\mu)\,d^4q;\\
F_g &= if_0^2\int \check{G}(q+\mu)\,\check{G}(p'_1+p'_2-q+\mu)\,d^4q;\\
F_h &= i2f_0\int G(q+\mu)\,d^4q;\\
F_i &= if_0\int\{\check{G}(q+\mu) - n_0f_0G^0(q+\mu)\,G^0(-q+\mu)\}\,d^4q;\\
F_k &= if_0\int\{\hat{G}(q+\mu) - n_0f_0G^0(q+\mu)\,G^0(-q+\mu)\}\,d^4q.
\end{aligned} \quad (5.1)$$

Momentum conservation $\Sigma p = \Sigma p'$ is assumed to hold everywhere. The q^0-integration in F_h is performed with a detour into the upper half-plane, since this contribution must vanish as $G \to G^0$. Everywhere on the right of Eq. (5.1) the first-

approximation value $\mu^{(1)} = n_0 f_0$ should be substituted for μ.

The Σ_{ik} involve special values of the F, together with a factor $\sqrt{n_0}$ for each particle of the condensed phase:

$$\Sigma'_{20}(p+\mu) = n_0 F_a(p-p;\ 00) + n_0 F_b(p-p;\ 00) + n_0 F_e(p0-p;\ 0) + n_0 F_e(0p-p;\ 0) + n_0 F_e(-p0p;\ 0) + n_0 F_e(0-pp;\ 0) + n_0 F_g(p0-p0;) + n_0 F_g(p00-p;) + F_i(p-p;);$$

$$\Sigma'_{02}(p+\mu) = n_0 F_a(00;\ p-p) + n_0 F_b(00;\ p-p) + n_0 F_d(0;\ p-p0) + n_0 F_d(0;\ p0-p) + n_0 F_d(0;\ -pp0) + n_0 F_d(0;\ -p0p) + n_0 F_f(;\ p0-p0) + n_0 F_f(;\ p00-p) + F_k(;\ p-p); \qquad (5.2)$$

$$\Sigma'_{11}(p+\mu) = n_0 F_a(p0;\ 0p) + n_0 F_b(p0;\ 0p) + n_0 F_c(p0;\ p0) + n_0 F_c(p0;\ 0p) + n_0 F_d(p;\ 0p0) + n_0 F_d(p;\ 00p) + n_0 F_e(p00;\ p) + n_0 F_e(0p0;\ p) + F_h(p;\ p).$$

To enumerate the vacuum loops which contribute to μ, we must first distinguish one incoming or outgoing particle of the condensed phase (see Section (I, 4)). After this we must sum the loops, counting separately all possible geometric structures and all possible positions of the distinguished particle. The vacuum loops include three types of rectangle, differing in the numbers of incoming and outgoing continuous lines, and corresponding to factors $\Sigma_{11}^{(1)}$, $\Sigma_{02}^{(1)}$ and $\Sigma_{20}^{(1)}$. The distinguished particle of the condensed phase may come out from $\Sigma_{11}^{(1)}$ or from $\Sigma_{02}^{(1)}$. The sums of contributions from graphs of these two types are respectively $-iF_h(0;0)$ and $-iF_i(0\,0;)$. The term in μ arising from all these vacuum loops is thus

$$\mu' = F_h(0;\ 0) + F_i(00;). \qquad (5.3)$$

To carry out the q^0-integration in Eq. (5.1), it is convenient to represent G and $\hat{G} = \check{G}$ in the following form,

$$G(q+\mu) = \frac{A_q}{q^0 - \varepsilon_q + i\delta} - \frac{B_q}{q^0 + \varepsilon_q - i\delta};$$

$$\hat{G} = \check{G}(q+\mu) = -C_q\left[\frac{1}{q^0 - \varepsilon_q + i\delta} - \frac{1}{q^0 + \varepsilon_q - i\delta}\right], \qquad (5.4)$$

with

$$A_q = (\varepsilon_q + \varepsilon_q^0 + n_0 f_0)/2\varepsilon_q;$$

$$B_q = (-\varepsilon_q + \varepsilon_q^0 + n_0 f_0)/2\varepsilon_q$$

$$= n_0^2 f_0^2/2\varepsilon_q(\varepsilon_q + \varepsilon_q^0 + n_0 f_0);\ C_q = n_0 f_0/2\varepsilon_q \qquad (5.5)$$

depending only on $|\mathbf{q}|$. The q^0-integrations are now performed and the results substituted into Eq. (5.2) and (5.3). After some manipulations we obtain

$$\Sigma'_{02\,(20)}(p+\mu) = 2n_0 f_0^2 \int d\mathbf{q}\,[(A_q;\ B_k) - (A_q + B_q;\ C_k) + 3C_q C_k] \times \left(\frac{1}{p^0 - \varepsilon_q - \varepsilon_k + i\delta} - \frac{1}{p^0 + \varepsilon_q + \varepsilon_k - i\delta}\right) - f_0 \int d\mathbf{q}\left\{C_q + \frac{n_0 f_0}{2n_0 f_0 - 2\varepsilon_q^0 + i\delta}\right\},$$

$$\Sigma'_{11}(p+\mu) = 2n_0 f_0^2 \int d\mathbf{q}\left\{\frac{(A_q;\ B_k) + 2C_q C_k + A_q A_k - 2(A_q;\ C_k)}{p^0 - \varepsilon_q - \varepsilon_k + i\delta} - \frac{(A_q;\ B_k) + 2C_q C_k + B_q B_k - 2(B_q;\ C_k)}{p^0 + \varepsilon_q + \varepsilon_k - i\delta} - \frac{1}{p^0 + 2n_0 f_0 - \varepsilon_q^0 - \varepsilon_k^0 + i\delta}\right\} + 2f_0 \int d\mathbf{q}\, B_q, \qquad (5.6)$$

$$\mu' = 2f_0 \int d\mathbf{q}\, B_q - f_0 \int d\mathbf{q}\left\{C_q + \frac{n_0 f_0}{2n_0 f_0 - 2\varepsilon_q^0 + i\delta}\right\},$$

Here $\mathbf{k} = \mathbf{p} - \mathbf{q}$, and the symbol (;) denotes a symmetrized product, $(A_\mathbf{q};\ B_\mathbf{k}) = A_\mathbf{q} B_\mathbf{k} + B_\mathbf{q} A_\mathbf{k}$. The integrands are all symmetrical in $\mathbf{q}$ and $\mathbf{k}$.

Before we add to Eq. (5.6) the second-order terms from Eq. (4.2), we transform the expression (4.3) for Σ_{11}. Remembering that

$$q^2 + p^2/4 = \varepsilon^0_{\mathbf{p}/2+\mathbf{q}} + \varepsilon^0_{\mathbf{p}/2-\mathbf{q}}$$

and introducing the new integration variable $\mathbf{q}' = \mathbf{q} + \mathbf{p}/2$, we find that Eq. (4.3) gives to the required approximation

$$\Sigma_{11}(p+\mu) = 2n_0 f_0 + 2n_0 \operatorname{Im} f_s\left(\frac{\mathbf{p}}{2}\frac{\mathbf{p}}{2}\right) + 2n_0 f_0^2 \int d\mathbf{q}\left[\frac{1}{p^0 + 2n_0 f_0 - \varepsilon_q^0 - \varepsilon_k^0 + i\delta} - \frac{1}{\varepsilon_p^0 - \varepsilon_q^0 - \varepsilon_k^0 + i\delta}\right]. \qquad (5.7)$$

The total of all second-order terms in now obtained from Eq. (5.6), (4.3), and (5.7), and after some algebra becomes

$$\mu^{(2)} = 2f_0\int d\mathbf{q}\, B_{\mathbf{q}} + \frac{1}{2}\, n_0 f_0^2 \int d\mathbf{q}\left(\frac{1}{\varepsilon_{\mathbf{q}}^0} - \frac{1}{\varepsilon_{\mathbf{q}}}\right),$$

$$\Sigma_{20\,(02)}^{(2)}(p+\mu) = 2n_0 f_0^2 \int d\mathbf{q}\,[(A_{\mathbf{q}};\ B_{\mathbf{k}}) -$$

$$-(A_{\mathbf{q}} + B_{\mathbf{q}};\ C_{\mathbf{k}}) + 3C_{\mathbf{q}}C_{\mathbf{k}}]$$

$$\times\left(\frac{1}{p^0 - \varepsilon_{\mathbf{q}} - \varepsilon_{\mathbf{k}} + i\delta} - \frac{1}{p^0 + \varepsilon_{\mathbf{q}} + \varepsilon_{\mathbf{k}} - i\delta}\right)$$

$$+\frac{1}{2}\, n_0 f_0^2 \int d\mathbf{q}\left(\frac{1}{\varepsilon_{\mathbf{q}}^0} - \frac{1}{\varepsilon_{\mathbf{q}}}\right);$$

$$\Sigma_{11}^{(2)}(p+\mu)$$

$$= 2n_0 f_0^2 \int d\mathbf{q}\left\{\frac{(A_{\mathbf{q}};\ B_{\mathbf{k}}) + 2C_{\mathbf{q}}C_{\mathbf{k}} + A_{\mathbf{q}}A_{\mathbf{k}} - 2(A_{\mathbf{q}};\ C_{\mathbf{k}})}{p^0 - \varepsilon_{\mathbf{q}} - \varepsilon_{\mathbf{k}} + i\delta}\right.$$

$$-\frac{(A_{\mathbf{q}};\ B_{\mathbf{k}}) + 2C_{\mathbf{q}}C_{\mathbf{k}} + B_{\mathbf{q}}B_{\mathbf{k}} - 2(B_{\mathbf{q}};\ C_{\mathbf{k}})}{p^0 + \varepsilon_{\mathbf{q}} + \varepsilon_{\mathbf{k}} - i\delta}$$

$$\left.+\frac{1}{4}\left(\frac{1}{\varepsilon_{\mathbf{q}}} + \frac{1}{\varepsilon_{\mathbf{k}}}\right)\right\} + 2f_0\int d\mathbf{q}\, B_{\mathbf{q}} \qquad (5.8)$$

$$+2n_0\,\mathrm{Im}\, f_s\left(\frac{\mathbf{p}}{2}\,\frac{\mathbf{p}}{2}\right)$$

$$-2n_0 f_0^2 \int d\mathbf{q}\left[\frac{1}{\varepsilon_{\rho}^0 - \varepsilon_{\mathbf{q}}^0 - \varepsilon_{\mathbf{k}}^0 + i\delta} + \frac{1}{4\varepsilon_{\mathbf{q}}} + \frac{1}{4\varepsilon_{\mathbf{k}}}\right].$$

The value of $\mathrm{Im}\, f_S\,(\mathbf{p}/2\ \ \mathbf{p}/2)$ can be obtained from Eq. (3.13), and the integrals not involving p^0 can be carried out exactly. In this way Eq. (5.8) becomes

$$\Sigma_{20(02)}^{(2)}(p+\mu) = \frac{1}{2}\, n_0 f_0^2 \int \frac{d\mathbf{q}}{\varepsilon_{\mathbf{q}}\varepsilon_{\mathbf{k}}} R(qk)\left[\frac{1}{p^0 - \varepsilon_{\mathbf{q}} - \varepsilon_{\mathbf{k}} + i\delta} -\right.$$

$$\left.-\frac{1}{p^0 + \varepsilon_{\mathbf{q}} + \varepsilon_{\mathbf{k}} - i\delta}\right] + \frac{1}{\pi^2}\sqrt{n_0 f_0^3}\, n_0 f_0, \qquad (5.9)$$

$$\Sigma_{11}^{(2)}(p+\mu) = \frac{1}{2}\, n_0 f_0^2 \int \frac{d\mathbf{q}}{\varepsilon_{\mathbf{q}}\varepsilon_{\mathbf{k}}}\left[\frac{Q^-(qk)}{p^0 - \varepsilon_{\mathbf{q}} - \varepsilon_{\mathbf{k}} + i\delta} -\right.$$

$$\left.-\frac{Q^+(qk)}{p^0 + \varepsilon_{\mathbf{q}} + \varepsilon_{\mathbf{k}} - i\delta} + \varepsilon_{\mathbf{q}} + \varepsilon_{\mathbf{k}}\right] + \frac{8}{3\pi^2}\sqrt{n_0 f_0^3}\, n_0 f_0, \qquad (5.10)$$

$$\mu^{(2)} = (5/3\pi^2)\sqrt{n_0 f_0^3}\cdot n_0 f_0, \qquad (5.11)$$

with

$$R(qk) = 2\varepsilon_{\mathbf{q}}^0\varepsilon_{\mathbf{k}}^0 - 2\varepsilon_{\mathbf{q}}\varepsilon_{\mathbf{k}} + n_0^2 f_0^2,$$

$$Q^{\mp}(qk) = 3\varepsilon_{\mathbf{q}}^0\varepsilon_{\mathbf{k}}^0 - \varepsilon_{\mathbf{q}}\varepsilon_{\mathbf{k}} + n_0 f_0\,(\varepsilon_{\mathbf{q}}^0 + \varepsilon_{\mathbf{k}}^0) +$$

$$+ n_0^2 f_0^2 \mp [n_0 f_0\,(\varepsilon_{\mathbf{q}} + \varepsilon_{\mathbf{k}}) - \varepsilon_{\mathbf{q}}\varepsilon_{\mathbf{k}}^0 - \varepsilon_{\mathbf{k}}\varepsilon_{\mathbf{q}}^0]. \qquad (5.12)$$

It is convenient to express the Green's function (4.5) in a form analogous to Eq. (5.4). In this approximation we find

$$G(p+\mu) = \frac{A_{\mathbf{p}} + \alpha_p}{p^0 - \varepsilon_{\mathbf{p}} - \Lambda_p^-} - \frac{B_{\mathbf{p}} + \alpha_p}{p^0 + \varepsilon_{\mathbf{p}} + \Lambda_p^+}, \qquad (5.13)$$

where $\alpha_{\mathbf{p}}$ and $\Lambda_{\mathbf{p}}^{\mp}$ are the second-order corrections

$$\alpha_p = \frac{n_0 f_0}{4\varepsilon_{\mathbf{p}}^3}\{2\varepsilon_{\mathbf{p}}^0\Sigma_{20}^{(2)} - n_0 f_0\,(\Sigma_{11}^+ + \Sigma_{11}^- - 2\mu - 2\Sigma_{20})^{(2)}\};$$

$$\Lambda_p^{\mp} = \frac{\varepsilon_{\mathbf{p}}^0}{2\varepsilon_{\mathbf{p}}}(\Sigma_{11}^+ + \Sigma_{11}^- - 2\mu)^{(2)} +$$

$$+\frac{n_0 f_0}{2\varepsilon_{\rho}}(\Sigma_{11}^+ + \Sigma_{11}^- - 2\mu - 2\Sigma_{20})^{(2)} \pm \frac{1}{2}(\Sigma_{11}^+ - \Sigma_{11}^-)^{(2)}. \qquad (5.14)$$

These $\alpha_{\mathbf{p}}$ and $\Lambda_{\mathbf{p}}^{\mp}$ are combinations of the integrals (5.9) and (5.10). In the limits of small and large momentum (compared with $\sqrt{n_0 f_0}$), explicit expressions can be obtained for the functions $\alpha_{\mathbf{p}} = \alpha(p^0;\ \mathbf{p})$ and $\Lambda_{\mathbf{p}}^{\mp} = \Lambda^{\mp}(p^0;\ \mathbf{p})$. When these are examined it is found that there are no new poles of the Green's function. We here exhibit the behavior of the Green's function near to the poles $p_0 \approx \pm\epsilon_{\mathbf{p}}$. In this region we may write $|p^0| = \epsilon_{\mathbf{p}}$ in $\alpha_{\mathbf{p}}$, and we need retain only terms of first order in the difference $(\epsilon_{\mathbf{p}} \mp p^0)$ in $\Lambda_{\mathbf{p}}^{\mp}$. For small momenta $(p \ll \sqrt{n_0 f_0})$ we then find

$$\alpha_p = \sqrt{n_0 f_0^3}\left(\frac{2}{3\pi^2}\,\frac{n_0 f_0}{\varepsilon_{\rho}} + i\,\frac{1}{64\pi}\,\frac{\varepsilon_{\rho}}{n_0 f_0}\right)$$

$$(p \ll \sqrt{n_0 f_0};\ \ \varepsilon_{\rho} \approx p\sqrt{n_0 f_0}),$$

$$\Lambda_p^{\mp} \equiv \Omega_p + \lambda_p(\varepsilon_{\mathbf{p}} \mp p^0) = \sqrt{n_0 f_0^3}\left(\frac{7}{6\pi^2}\,\varepsilon_{\mathbf{p}} - i\,\frac{3}{640\pi}\,\frac{\varepsilon_{\rho}^5}{n_0^4 f_0^4}\right)$$

$$+(\varepsilon_{\mathbf{p}} \mp p^0)\sqrt{n_0 f_0^3}\left(\frac{1}{2\pi^2} + i\,\frac{1}{32\pi}\,\frac{\varepsilon_{\rho}^2}{n_0^2 f_0^2}\right). \qquad (5.15)$$

For large momenta only the imaginary part of $\Lambda_{\mathbf{p}}^{\mp}$ is important,

$$\Lambda_p^{\mp} = \Omega_p = -\frac{i}{4\pi}\, p f_0 n_0 f_0 \quad (p \gg \sqrt{n_0 f_0}). \qquad (5.16)$$

For small momenta, in virtue of Eq. (5.13) and (5.15), the Green's function near to the poles may be written in the form

$$G(p+\mu) = (1 - \lambda_{\mathbf{p}})\left[\frac{A_{\mathbf{p}} + \alpha_p}{p^0 - \varepsilon_{\mathbf{p}} - \Omega_p} - \frac{B_{\mathbf{p}} + \alpha_p}{p^0 + \varepsilon_{\rho} + \Omega_p}\right]. \qquad (5.17)$$

For large momenta, $\alpha_{\mathbf{p}}$ and $\lambda_{\mathbf{p}}$ may be neglected in Eq. (5.17).

6. QUASI-PARTICLE SPECTRUM AND GROUND-STATE ENERGY

We have already mentioned that the energy of a quasi particle is determined by the value of $p^0(\mathbf{p})$ at a pole of $G(p+\mu)$. Only those poles are to be considered for which the imaginary part of the energy is negative, so that the damping is positive. In the range $p \ll \sqrt{n_0 f_0}$, Eq. (5.15) and (5.17) give

$$\varepsilon = p\sqrt{n_0 f_0}\left(1 + \frac{7}{6\pi^2}\sqrt{n_0 f_0^3}\right)$$

$$-i\,\frac{3}{640\pi}\sqrt{n_0 f_0^3}\,\frac{p^5}{(n_0 f_0)^{5/2}} \quad (p \ll \sqrt{n_0 f_0}), \qquad (6.1)$$

In the high-momentum range, according to Eq. (5.16), we have

$$\varepsilon = \varepsilon_p^0 + n_0 f_0 \left(1 - \frac{i}{4\pi} p f_0\right) \approx \varepsilon_p^0 + n_0 f(\mathrm{pp}) \quad (p \gg \sqrt{n_0 f_0}). \tag{6.2}$$

Equation (6.1) shows that for small p the quasi particles are phonons. The second approximation gives a correction to the sound velocity, and a damping proportional to p^5 which is connected with a process of decay of one phonon into two. In the high-momentum range, the second approximation gives a damping which is related to the imaginary part of the forward scattering amplitude, and so to the total cross section.

In Sec. (I, 7) we found connections between the Green's function and various physical properties of the system. The mean number of particles $\overline{N}_{\mathbf{p}}$ with a given momentum $\mathbf{p}$ in the ground state of the system is related to the residue of the Green's function at its upper pole,

$$\overline{N}_{\mathbf{p}} = i \int G\, dp^0 / 2\pi = (B_{\mathbf{p}} + \alpha_p)(1 - \lambda_p). \tag{6.3}$$

When $p \ll \sqrt{n_0 f_0}$, Eqs. (5.15) and (5.5) give

$$\overline{N}_p = \frac{n_0 f_0}{2\varepsilon_p} \left(1 + \frac{5}{6\pi^2} \sqrt{n_0 f_0^3}\right) \tag{6.4}$$

The imaginary parts of $\alpha_{\mathbf{p}}$ and $\lambda_{\mathbf{p}}$ here cancel, as they should. To find the total number of particles with $\mathbf{p} \neq 0$, we need to know $\overline{N}_{\mathbf{p}}$ for all momenta. We therefore use only the first approximation formula for $\overline{N}_{\mathbf{p}}$, namely $\overline{N}_{\mathbf{p}} = B_{\mathbf{p}}$. For the density of particles with $\mathbf{p} \neq 0$ we find

$$n - n_0 = i \int G\,(p + \mu)\, d^4p = \int B_{\mathbf{p}}\, d\mathbf{p} = \sqrt{n_0 f_0^3}\, n_0 / 3\pi^2. \tag{6.5}$$

Equation (6.5) gives the relation between the density n_0 of particles in the condensed phase, which appeared as a parameter in all our equations, and the total number of particles in the system.

We note here one important point. It can be seen from the way the calculations were done that the validity of the "gaseous" approximation requires that n_0 be small. It is not directly required that the total density n be small, since n does not appear explicitly in the problem. But Eq. (6.5) shows that when n_0 is small n is necessarily small, too. This means that it is not possible to decrease significantly the density of the condensed phase by increasing the interaction or the total density, so long as $n_0 \ll f_0^{-3}$. This result confirms and strengthens the assertion made in I that the condensed phase does not disappear when interactions are introduced.

We can calculate the ground-state energy from the chemical potential μ. By Eq. (4.4) and (5.11),

$$\mu = n_0 f_0 \left(1 + \frac{5}{3\pi^2} \sqrt{n_0 f_0^3}\right), \tag{6.6}$$

Expressing n_0 in terms of n by means of Eq. (6.5), we have in the same approximation

$$\mu = n f_0 \left(1 + \frac{4}{3\pi^2} \sqrt{n f_0^3}\right). \tag{6.7}$$

By definition we have $\mu = \frac{\partial}{\partial n}\left(\frac{E_0}{V}\right)$. Therefore, integrating Eq. (6.7) with respect to n, we obtain the ground-state energy

$$\frac{E_0}{V} = \frac{1}{2} n^2 f_0 \left(1 + \frac{16}{15\pi^2} \sqrt{n f_0^3}\right), \tag{6.8}$$

This coincides with the result of Lee and Yang[3] for the hard-sphere gas, if we remember that in that case $f_0 = 4\pi a$.

The condition for the system to be thermodynamically stable is $\partial P/\partial V = -\partial^2 E/\partial V^2 < 0$. This condition reduces to $f_0 > 0$. Our results are only meaningful when this condition is satisfied.

7. POSSIBILITY OF HIGHER APPROXIMATIONS

In the first two approximations, all the results can be expressed in terms of the amplitudes f. Thus the problem of many interacting particles is reducible to the problem of two particles.

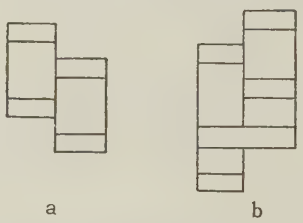

FIG. 4

In the next approximation we must consider contributions to Σ_{ik} proportional to $n_0 f_0^3$. Among other graphs, we must include the "triple ladders" illustrated in Fig. 4. The integrals arising from graphs of this type diverge at high momenta and become finite only when the momentum dependence of f is taken into account. For an estimate we may cut the integrals off at a momentum $p \sim f_0^{-1}$. We see then that an increase in the number of "rungs" does not change the order of magnitude of the integral. In fact, each rung adds a factor $f_0 G^2$ and an integration over one momentum 4-vector. For a rough estimate we take $q^0 \sim q^2$, $G \sim q^{-2}$, and find

$$\int f_0 G^2 d^4q \sim f_0 \int dq \sim 1,$$

Therefore we have to consider simultaneously all such graphs with any number of rungs. The totality of these triple ladders describes completely the interaction of three particles. Therefore the sum of contributions from such graphs can be expressed only by means of three-particle amplitudes.

In the third approximation (terms proportional to $n_0 f_0^3$) we thus require a solution of the three-particle problem (see also Ref. 4). Since the problem of three strongly interacting particles is in general insoluble, the higher approximations to the many-particle problem are physically meaningless.

8. HIGH EXCITATIONS ($pf_0 \sim 1$) IN A HARD-SPHERE GAS

For the high-energy excitations, the momentum dependence of the amplitudes becomes important. We therefore consider as an example the case of a gas of hard spheres of radius $(a/2)$. We also consider only the first approximation in the density expansion, i.e., we use Eq. (4.6). The amplitude $f(\mathbf{p}\ 0)$ can be computed exactly from Eq. (3.10). For $f_s(\mathbf{p}/2\ \mathbf{p}/2)$ we consider only s-waves. The higher waves (the symmetrized amplitude involves only even values of ℓ) add a numerically unimportant contribution. For example the d-waves at $pa \sim 1$ contribute about 10 per cent. We substitute into Eq. (4.7) the values of the amplitudes

$$f(\mathrm{p}0) = 4\pi \frac{\sin pa}{p}; \quad f_s\left(\frac{\mathbf{p}}{2}\,\frac{\mathbf{p}}{2}\right) = \frac{8\pi}{p} \sin\frac{pa}{2}\, e^{-ipa/2}, \quad (8.1)$$

and obtain for the quasi-particle energy

$$\varepsilon = \left[\left(\frac{p^2}{2} + 8\pi n_0 \frac{\sin pa}{p} - 4\pi n_0 a\right)^2 - 16\pi^2 n_0^2 \frac{\sin^2 pa}{p^2}\right]^{1/2}, \quad (8.2)$$

At high momenta this becomes

$$\varepsilon \approx \frac{p^2}{2} + 4\pi n_0 a\left(2\frac{\sin pa}{pa} - 1\right). \quad (8.3)$$

The second term in Eq. (8.3) changes sign at $pa \approx 1.9$. An oscillating component is superimposed on the usual parabolic dependence. This oscillation will not be important since the magnitude of the term is small; when $pa \sim 1$ it is of relative order $n_0 a^3$. However, if one formally allows the parameter $n_0 a^3$ to become larger in Eqs. (8.3) or (8.2), the second term of Eq. (8.3) produces an increasing departure of the dispersion law from the parabolic form, until at sufficiently high densities there appears first a point of inflection and finally a maximum and a minimum in the curve. The spectrum then resembles qualitatively the spectrum postulated by L. D. Landau[5] to explain the properties of liquid helium II. This extrapolation is certainly unwarranted. But it allows one to suppose that the difference between liquid helium and a non-ideal Bose gas is only a quantitative one, and that no qualitatively new phenomena arise in the transition from gas to liquid.

9. CONCLUSION

We summarize the main features of the approximation which we have studied.

(1) The interaction between particles is specified not by a potential but by an exact scattering amplitude. This allows us to deal with strong interactions. After the potential has been replaced by the amplitude, it is possible to make a perturbation expansion in powers of the amplitude, or more precisely in powers of $\sqrt{n_0 f_0^3}$.

(2) We make a series expansion not of the quasi-particle energy (this appears as the denominator of the Green's function), but of the effective interaction potentials Σ_{ik} and the chemical potential μ. The formula giving the Green's function in terms of Σ_{ik} and μ is exact.

From Eq. (4.7) and (4.9) we see that ϵ_p can be expanded in powers of f only for high-momentum excitations with $p \gg \sqrt{n_0 f_0}$. The low-lying excitations of the system are in principle impossible to obtain by perturbation theory. For this reason, the expression obtained by Huang and Yang[4] for the energy of the low excitations of a Bose hard-sphere gas is incorrect. They used perturbation theory with a "pseudopotential," and their result agrees with a formal expansion of Eq. (4.7) in powers of f_0.

In conclusion I wish to thank A. B. Migdal and especially V. M. Galitskii for fruitful discussions, and also L. D. Landau for criticism of the results.

[1] S. T. Beliaev, J. Exptl. Theoret. Phys. (U.S.S.R.) **34**, 417 (1958); Soviet Phys. JETP **7**, 289 (1958) (this issue).

[2] V. M. Galitskii and A. B. Migdal, J. Exptl. Theoret. Phys. (U.S.S.R.) **34**, 139 (1958); Soviet Phys. JETP **7**, 96 (1958).

[3] T. D. Lee and C. N. Yang, Phys. Rev. **105**, 1119 (1957).

[4] K. Huang and C. N. Yang, Phys. Rev. **105**, 767 (1957).

[5] E. M. Lifshitz, Usp. Fiz. Nauk **34**, 512 (1948).

Translated by F. J. Dyson
78

SCATTERING OF IONS BY ATOMS

O. B. FIRSOV

Academy of Sciences, U.S.S.R.

Submitted to JETP editor August 2, 1957

J. Exptl. Theoret. Phys. (U.S.S.R.) **34**, 447-452 (February, 1958)

The dependence of the impact parameter on energy of relative motion and scattering angle, and the transport cross section for atomic collisions are calculated using the interatomic potential previously found by the author from the Thomas-Fermi statistical theory of the atom.

INTRODUCTION

IF we treat the scattering of ions or atoms by atoms as elastic, and limit ourselves to scattering angles $\alpha > 10^{-2}$ (in the c.m. system), we find that, for energies of relative motion $E > 100$ ev/M (where M is the reduced mass in units of the mass of the hydrogen atom), the scattering is determined by the laws of classical mechanics. For very high energies, when the relative velocity of the colliding atoms exceeds $Z_1Z_2e^2/\hbar$, classical mechanics is not applicable, but the scattering is practically determined by the coulomb interaction, for which the results of quantum and classical mechanics coincide.

We may therefore assume that the scattering as calculated by the methods of classical mechanics gives the correct result for collision energies greater than 100 ev/M. The energy is limited from above only by relativistic velocities.

Actually, for energies exceeding ~ 1 kev, in addition to elastic scattering there is scattering accompanied by excitation, single or multiple ionization, and charge exchange of the colliding atoms.[1] As a result of this there is some uncertainty in the kinetic energy and interaction potential of the colliding atoms, which results in an additional smearing out of the wave packet which is not taken into account in deriving the condition for applicability of classical mechanics to elastic scattering.

However, for low collision velocities the probability of inelastic processes is small. For velocities exceeding 10^7 cm/sec the cross sections for elastic and inelastic scattering are of the same order, but appreciable scattering occurs only for strong overlapping of the electronic shells of the atoms. In this case the interaction potential is determined practically by the inner electrons alone, and they have velocities which are large compared to the velocity of the colliding atoms, and are weakly excited. Excitation of electrons in the outer shells of the atoms hardly changes the scattering potential. Finally, if the velocity of the colliding atoms is of the same order as, or greater than the velocity of the inner electrons, the scattering is practically coulombian. The change of kinetic energy in the collision process is also relatively slight,[2] not exceeding a few percent.

So, independently of the inelastic processes occurring during collision of the atoms, we can calculate approximately the dependence of the scattering angle on the impact parameter, using the potential for elastic interaction according to classical mechanics.

Such a calculation is needed for all sorts of problems; the depth of penetration of accelerated ions into matter; the disruption of the atomic lattice during penetration of ions into a solid (provided their velocity is so small that they lose energy mainly by elastic collision and not by ionization of the atoms; the determination of the energy which is given to the atoms of a gas during collisions with a beam of ions, and also the corresponding cross sections.

Here we treat only collisions with energies significantly greater than the ionization potential of the atoms (~ 1 kev or greater), where appreciable scattering is observed when there is a considerable overlap of the electronic shells of the atoms. It is only in this case that the scattering potential can be determined for any pair of colliding atoms on the basis of the statistical model.[3] When this is not the case, the interaction depends essentially on the outer electron shells of the atoms and must be determined individually for each colliding pair. In this latter case, the scattering itself is obviously isotropic (except for the region of very small angles), and has a weak energy dependence, while the cross section is of the order of gas-kinetic values.

DIMENSIONLESS ENERGY AND IMPACT PARAMETER

In a previous paper[4] it was found that, to an accuracy of 10%, the interaction potential for atoms, calculated on the basis of the statistical model for the electrons, can be represented as

$$U(r) = \frac{Z_1 Z_2 e^2}{r} \chi\left(\psi(Z_1, Z_2)\frac{r}{a}\right), \quad (1)$$

where $\chi(x)$ is the screening function in the Thomas-Fermi potential, Z_1 and Z_2 are the atomic numbers of the interacting atoms, r is the distance between the nuclei,

$$a = (9\pi^2/128)^{1/3}\hbar^2/me^2 = 4.7\cdot 10^{-9}\ \text{cm}, \quad (2)$$

$$\psi(Z_1, Z_2) = (Z_1^{1/2} + Z_2^{1/2})^{2/3} \quad (3)$$

for $0 < x < 15$, which describes the whole range of interactions, including $Z_1 = Z_2 = 100$.

The function (1) can be improved by using

$$\psi = 3[(Z_1 + Z_2)^{7/3} - Z_1^{7/3} - Z_2^{7/3}]/7Z_1Z_2, \quad (4)$$

for $0 < x < 2$, and

$$\psi = (Z_1^{2/3} + Z_2^{2/3})^{1/2}. \quad (5)$$

for $2 < x < 7$. Expressions (3), (4), and (5) coincide if Z_1/Z_2 is either large or small. For $Z_1 = Z_2$, the values of expressions (3), (4), and (5) are in the ratio 1:0.82:0.89. Possibly, such an improvement exceeds the accuracy of the theory.

The polar angle φ, which is related to the scattering angle α, is given in classical mechanics by the formula

$$\varphi = \frac{\pi - \alpha}{2} = \int_{r_0}^{\infty} \frac{p\,dr}{r^2\sqrt{1 - U(r)/E - (p/r)^2}}, \quad (6)$$

where p is the impact parameter, E is the kinetic energy of relative motion for $r \to \infty$, and

$$1 - U(r_0)/E - (p/r_0)^2 = 0. \quad (7)$$

If we introduce a new variable

$$x = \psi r/a, \quad (8)$$

then

$$U(r)/E = (Z_1Z_2\psi e^2/Ea)(\chi(x)/x) = V(x)/\mathcal{E}, \quad (9)$$

where $V(x) = \chi(x)/x$, and the dimensionless energy $\mathcal{E}$ is

$$\mathcal{E} = Ea/e^2Z_1Z_2\psi = E/30.5\,Z_1Z_2\psi, \quad (10)$$

where E is expressed in ev. If in addition we define a dimensionless impact parameter by

$$b = \psi p/a, \quad (11)$$

then (6) is expressed as

$$\alpha = \pi - 2\int_{x_0}^{\infty} \frac{b\,dx}{x^2\sqrt{1 - V(x)/\mathcal{E} - (b/x)^2}}, \quad (12)$$

where, in accordance with (7),

$$1 - V(x_0)/\mathcal{E} - (b/x_0)^2 = 0. \quad (13)$$

The solution of Eq. (12) for $b = b(\alpha, \mathcal{E})$ enables us, by calculating a single integral, to find the differential scattering cross section for any pair of colliding atoms, or for an atom and a singly charged ion:

$$\sigma(\alpha) = pdp/\sin\alpha d\alpha = a^2 b\,db/\sin\alpha d\alpha. \quad (14)$$

It is assumed that for strong interaction, when the electron shells of the atoms overlap, ionization of one of the atoms before collision is not very likely.

Frequently one is interested in the transport cross section

$$\sigma^* = \int_0^{\infty} (1 - \cos\alpha)\,2\pi p dp = \pi\int_0^{\pi} p^2 \sin\alpha\,d\alpha = a^2\sigma^{(*)}, \quad (15)$$

where

$$\sigma^{(*)} = \pi\int_0^{\pi} b^2 \sin\alpha\,d\alpha, \quad (16)$$

is the dimensionless transport cross section.

CALCULATION OF $b(\alpha, \mathcal{E})$ AND $\sigma^{(*)}(\mathcal{E})$

For the calculation of the polar angle, it is convenient to set $x = x_0/\cos\theta$ in (12), so that

$$\alpha = \pi - \frac{2b}{x_0}\int_0^{\pi/2} y(\theta)\,d\theta,$$

$$y(\theta) = \sin\theta\left[1 - \frac{V(x_0/\cos\theta)}{\mathcal{E}} - \left(\frac{b}{x_0}\right)^2\cos^2\theta\right]^{-1/2}. \quad (17)$$

The integrand in (17) has no singularities, is equal to 1 for $\theta = \pi/2$, while for $\theta \to 0$,

$$y(\theta) \to [(b/x_0)^2 - x_0V'(x_0)/2\mathcal{E}]^{-1/2}, \quad V'(x) < 0. \quad (18)$$

The derivative $y'(\theta)$ is equal to zero for $\theta = 0$ and $\theta = \pi/2$. If $V(x) \sim x^{-2}$, $y(\theta) \equiv 1$. It is also useful to introduce an "index" $n(x)$ according to the formula

$$n(x) = -xV'(x)/V(x).$$

The meaning of $n(x)$ is that, for values of x not too much greater than x_0,

$$V(x) \approx V(x_0)(x_0/x)^{n(x_0)} \quad (19)$$

$n(x)$ varies very slowly: from unity for $x = 0$ to $n \approx 3$ for $x = 15$. Using $n(x)$, the expression (18) is transformed to

$$\left[1-\left(1-\frac{1}{2}n(x_0)\right)V(x_0)/\mathcal{E}\right]^{-1/2}.$$

Since $V(x)$ is a monotonically decreasing function of x, and $V(x_0)$ is always less than $\mathcal{E}$, from our discussion, to an accuracy of 1%, the integral (17) is easily calculated for several points. However, when $\alpha = 0.3$, an error of 1% in the integral (17) gives an error of 10% in α. So for $\alpha < 0.3$, α is extrapolated using a power law: if $V(x)$ is written in the form of (19), then for small angles,

$$\alpha \approx -\frac{1}{\mathcal{E}}\int_b^\infty V'(x)\frac{b\,dx}{\sqrt{x^2-b^2}} \sim 1/\mathcal{E}b^{n(b)}. \qquad (20)$$

The results of the calculations for $\alpha \geq 0.3$ are given in the table.

The value of b for $\alpha < 0.3$ can be found by extrapolation using (20):

$$b = b(0.3; \mathcal{E})(0.3/\alpha)^{1/n}.$$

A good approximation for $\alpha \leq 1$ is

$$\alpha = V(b)\sqrt{\pi n(b)/2 - 0.57}/\mathcal{E},$$

for which $n(b)$ has the following values:

$b=$	0	0.3	0.5	1	2	3	4	6	8	12	20	∞
$n=$	1	1.3	1.5	1.7	2	2.2	2.4	2.6	2.8	2.9	3	4

where the value of b should be taken as the nearest greater value than that from $b(0.3, \mathcal{E})$.

In the interval $0.7 < x < 5$, $V(x)$ differs little from $0.45x^{-2}$. For $\alpha \geq 0.3$, there correspond to this range in x the values $0.05 < \mathcal{E} < 1$, where to sufficient accuracy we can replace $V(x)$ by $0.45x^{-2}$ and evaluate the integral (17) analytically. Finally, for $\mathcal{E} > 10$, $x \ll 1$, $\chi(x) \approx 1$, $V(x) \approx 1/x$ and

$$b = 1/2\mathcal{E}\tan\frac{\alpha}{2}. \qquad (21)$$

In intermediate cases, $b(\alpha, \mathcal{E})$ is found by standard interpolation in α and $\mathcal{E}$.

The transport cross section was also calculated using (15). The results of the calculation using the table are described to good accuracy by the formula (for $\mathcal{E} \geq 0.02$)

$$\sigma^{(*)} = (\pi/\mathcal{E})\ln(1+0.7\mathcal{E}), \qquad (22)$$

or

$$\sigma^* = \pi(Z_1Z_2e^4/E^2)\ln(1+0.7E/30.5Z_1Z_2\psi), \ (E \text{ Bev}).$$

The dependence of $p(\alpha, \mathcal{E})$ for collision of argon ions and argon atoms with relative energy 37.5 ev was determined in the work of Kaminker and Federenko[5] from the formula

$$p^2 = 2\int_\alpha^\pi \frac{d\sigma}{d\Omega}\sin\alpha\,d\alpha, \qquad (23)$$

Values of $b(\alpha, \mathcal{E})$

$\mathcal{E}$ \ α	0.3	0.5	0.7	1	1.5	2	2.5	$2.5 < \alpha < \pi$
0.02	8.8	6.7	5.6	4.2	2.8	1.8	1.0	
0.03	7.4	5.8	4.6	3.5	2.3	1.5	0.8	$1.3(\pi-\alpha)$
0.05	6.0	4.6	3.8	2.9	1.9	1.2	0.65	$1.0(\pi-\alpha)$
$0.05 < \mathcal{E} < 1$	$b \approx (\pi-\alpha)[0.45/(2\pi-\alpha)\alpha\mathcal{E}]^{1/2}$							
1	1.45	1.00	0.76	0.55	0.34	0.21	0.11	$0.18(\pi-\alpha)$
1.5	1.10	0.78	0.58	0.41	0.25	0.15	0.08	$0.12(\pi-\alpha)$
2	1.90	0.63	0.47	0.33	0.19	0.12	0.06	$0.09(\pi-\alpha)$
3	0.72	0.47	0.33	0.23	0.15	0.090	0.045	$0.07(\pi-\alpha)$
4	0.60	0.37	0.26	0.18	0.11	0.070	0.035	$0.053(\pi-\alpha)$
5	0.50	0.30	0.23	0.15	0.093	0.060	0.030	$0.045(\pi-\alpha)$
7	0.36	0.23	0.17	0.12	0.070	0.042	0.022	$0.033(\pi-\alpha)$
10	0.28	0.18	0.11	0.087	0.050	0.029	0.046	$0.024(\pi-\alpha)$

where $d\sigma/d\Omega$ is the "total differential cross section," i.e., the sum of all the differential cross sections for elastic and inelastic scattering as well as charge exchange. Actually the measurements were done only over the angular range $1° \leq \alpha \leq 22°$. The authors then extrapolated $d\sigma/d\Omega$ up to $\alpha = \pi$. So actually (23) was calculated using the formula

$$p^2 = 2\int_\alpha^{22°}\frac{d\sigma}{d\Omega}\sin\alpha d\alpha + p_0^2, \qquad (24)$$

where

$$\rho_0^2 = 2\int_{24°}^{\pi}\frac{d\sigma}{d\Omega}\sin\alpha\,d\alpha$$

was largely determined by quite arbitrary extrapolation of $d\sigma/d\Omega$. As a result of this extrapolation, they found a marked change in the behavior of $p(\alpha)$ in going from $\alpha = 16°$ to $\alpha = 24°$. We have recomputed their results, choosing p_0 so that the smooth variation of $p(\alpha)$ is not spoiled. Instead

of $p_0 = 5 \times 10^{-10}$ cm we used $p_0 = 1.26 \times 10^{-9}$ cm, after which the comparison of experimental and theoretically calculated values of $\rho(\alpha)$ looks as follows (in the lowest line, the uncorrected values of $\rho(\alpha)$ are given in parentheses):

α,°	2	4	6	8	10	12	16	20	24
$10^9 \rho_{theor.}$	5.6	4.1	3.3	2.9	2.5	2.3	1.9	1.7	1.54
$10^9 \rho_{exp.}$	7.8	5.5	4.1	3.1	2.5	2.1	1.6	1.4	1.26
	(7.7)	(5.3)	(3.9)	(2.8)	(2.3)	(1.8)	(1.2)	(0.8)	(0.5)

The calculated values of $\rho(\alpha)$ correspond approximately to a potential $\sim 1/r^2$. The experimental values for $\alpha > 6°$ are closer to a Coulomb law with $Z_1 Z_2 = 114$ (fitted at $\alpha = 10°$). Thus according to experiment[5] the scattering proceeds as if right at the start of interaction all the outer shells of both of the colliding atoms flew off, or at least were "swollen" considerably (i.e., excited), while the inner (neon-like) shells were left complete.

[1] N. V. Federenko, J. Tech. Phys. (U.S.S.R.) **24**, 769 (1954); V. M. Dukel' skii and N. V. Federenko, J. Tech. Phys. (U.S.S.R.) **25**, 2193 (1955); N. V. Federenko, J. Tech. Phys. (U.S.S.R.) **24**, 1950 (1954); V. M. Dukel' skii and E. R. Zandberg, Dokl. Akad. Nauk SSSR **82**, 33 (1952); J. Exptl. Theoret. Phys. (U.S.S.R.) **21**, 1270 (1951); D. M. Kaminker and N. V. Federenko, J. Tech. Phys. (U.S.S.R.) **25**, 1843 (1955).

[2] N. V. Federenko, J. Tech. Phys. (U.S.S.R.) **24**, 1942 (1954). V. V. Afrosimov, Dissertation, Leningrad Physics and Technology Institute, Acad. Sci. U.S.S.R., 1957.

[3] O. B. Firsov, J. Exptl. Theoret. Phys. (U.S.S.R.) **32**, 1464 (1957), Soviet Phys. JETP **5**, 1192 (1957).

[4] O. B. Firsov, J. Exptl. Theoret. Phys. (U.S.R.R.) **32**, 696 (1957).

[5] D. M. Kaminker and N. V. Federenko, J. Tech. Phys. (U.S.S.R.) **25**, 2239 (1955).

Translated by M. Hamermesh
79

APPLICATION OF DISPERSION RELATIONS TO π—N SCATTERING AT LOW ENERGIES

L. I. LAPIDUS

Joint Institute of Nuclear Studies

Submitted to JETP editor August 3, 1957

J. Exptl. Theoret. Phys. (U.S.S.R.) 34, 453-462 (February, 1958)

The consequences of the dispersion relations for $\pi - N$ scattering at low energies are studied without resort to the use of the Low equations. Relations between the scattering lengths in various states are obtained from the values of the derivatives of the dispersion relations at $k^2 = 0$.

1. In the application of the dispersion relations to the low-energy region it is common practice to go from these relations to the Chew-Low equations and then study the consequences of these equations.[1] In the present paper the consequences of the dispersion relations for $\pi - N$ scattering at low energies are studied without resorting to the use of the Low equations.

Let us consider the dispersion relations for $\pi - N$ scattering,[2] written in the form

$$D_\pm(k) - \frac{1}{2}\left(1+\frac{\omega}{\mu}\right)D_+(0) - \frac{1}{2}\left(1-\frac{\omega}{\mu}\right)D_\mp(0) = k^2 J_\pm(\omega) \pm \frac{2f^2}{\mu^2}\frac{k^2}{\omega \mp \mu^2/2M}, \quad (1)$$

where we have used the notation $J_\pm(\omega)$ to denote the dispersion integral

$$J_\pm(\omega) = \frac{1}{4\pi^2} P \int_\mu^\infty \frac{d\omega' k'}{} \left[\frac{\sigma_\pm(\omega')}{\omega' - \omega} + \frac{\sigma_\mp(\omega')}{\omega' + \omega}\right], \quad (2)$$

ω is the total energy of the meson in the laboratory system, and the other notations are obvious. We shall assume that in Eq. (1) the meson energy is low, $\omega - \mu \ll \mu$. For $\eta^2 = k^2/\mu^2 \to 0$ both sides of Eq. (1) go to zero. Therefore, wishing to obtain the consequences of the dispersion relations for $\eta^2 \to 0$, we turn to the values of the derivatives of Eq. (1) with respect to η^2 at $\eta^2 \to 0$. In calculating the derivatives we use the form of the energy dependence of the phase shifts as given by the "effective range theory"[3]

$$\eta_b^{2l+1} \cot \delta_l = 1/a_{2l+1} + P_l \eta_b^2 + Q_l \eta_b^4, \quad (3)$$

where a_{2l+1} is the scattering length in the l-state, and $k_b = \eta_b \mu$ is the momentum of the meson in the center-of-mass system, so that

$$k/k_b = \eta/\eta_b = (1 + 2\omega/M + \mu^2/M^2)^{1/2}. \quad (4)$$

The derivatives of the second and third terms in the left member of Eq. (1) will have the form

$$\tfrac{1}{2}(\omega/\mu)^{(n)}[D_\mp(0) - D_\pm(0)] = \pm \tfrac{1}{2}(\omega/\mu)^{(n)}[D_-(0) - D_+(0)].$$

Since

$$\left(\frac{\omega}{\mu}\right)' = \frac{1}{2}\left(\frac{\mu}{\omega}\right); \quad \left(\frac{\omega}{\mu}\right)'' = -\frac{1}{4}\left(\frac{\mu}{\omega}\right)^3; \quad \left(\frac{\omega}{\mu}\right)''' = \frac{3}{8}\left(\frac{\mu}{\omega}\right)^5, \ldots$$

(the prime denotes differentiation with respect to η^2), we have for $\eta^2 \to 0$

$$\pm\frac{1}{4}[D_-(0) - D_+(0)] = \pm\frac{\lambda_c}{6}\left(1+\frac{\mu}{M}\right)(a_1 - a_3); \quad \left(\lambda_c = \frac{\hbar}{\mu c}\right) \quad (5)$$

for the first derivative and

$$\mp\frac{1}{8}[D_-(0) - D_+(0)] = \mp\frac{1}{12}\lambda_c\left(1+\frac{\mu}{M}\right)(a_1 - a_3) \quad (6)$$

for the second derivative. Here, as usual, a_3 and a_1 mean the scattering lengths in the s states with isotopic spins $T = 3/2$ and $T = 1/2$, respectively.

The unobserved region gives for the first derivative

$$\pm 2f^2\lambda_c\left\{\frac{1}{\omega/\mu \mp \mu/2M} - \frac{\eta^2}{(\omega/\mu \mp \mu/2M)^2}\frac{1}{2}\frac{\mu}{\omega}\right\}_0 = \pm\frac{2f^2\lambda_c}{(1 \mp \mu/2M)} \quad (7)$$

and for the second derivative

$$\mp 2f^2\lambda_c/(1 \pm \mu/2M)^2 \quad (8)$$

The index 0 means throughout that the value of the expression is taken for $\eta^2 = 0$. If we confine ourselves to the values of only the first two derivatives at $\eta^2 = 0$, it suffices to represent $D_+(k)$, for example, in the form

$$2k_b^2 D_+(k) = k\{\sin 2\alpha_3 + \sin 2\alpha_{31} + 2(\sin 2\alpha_{33} + \sin 2\delta_{33}) + 3\sin 2\delta_{35}\}, \quad (9)$$

where δ_{33} and δ_{35} denote the phase shifts for the

states $d_{3/2}$ and $d_{5/2}$ with $T = 3/2$ and the usual notations are used for the phase shifts of the s and p states. Using Eq. (3), we write the expression (9) in the form

$$k_b D_+(k) = \lambda_c k \left\{ \frac{A_3}{A_3^2 + x} + \frac{x A_{31}}{A_{31}^2 + x^3} + 2\left[\frac{x A_{33}}{A_{33}^2 + x^3} + \frac{x^2 B_{33}}{B_{33}^2 + x^5} \right] + \frac{3x^2 B_{35}}{B_{35}^2 + x^5} \right\}, \quad (10)$$

where A_3, A_{31}, A_{33}, B_{33}, and B_{35} denote the right members of Eq. (3) for the states $s_{1/2}$, $p_{1/2}$, $p_{3/2}$, $d_{3/2}$, and $d_{5/2}$ with $T = 3/2$, and $x = \eta_b^2$.

For the value of the first derivative of the expression (10) at $x = 0$ we get

$$D'_{+0}(k) = \frac{\lambda_c}{(1 + \mu/M)} \left\{ 2a_{33} + a_{31} + \frac{\mu}{2M} a_3 - P_3 a_3^2 - a_3^3 \right\}. \quad (11)$$

Combining Eqs. (6), (7), and (11), from the value of the first derivative of Eq. (1) for $\eta^2 = 0$ we have the relation

$$\frac{\lambda_c}{(1 + \mu/M)} \left\{ 2a_{33} + a_{31} + \frac{\mu}{2M} a_3 - P_3 a_3^2 - a_3^3 \right\} + \frac{\lambda_c}{6} \left(1 + \frac{\mu}{M} \right) (a_1 - a_3) = \{k^2 J_+\}'_0 + \frac{2f^2 \lambda_c}{(1 - \mu/2M)}, \quad (12)$$

which establishes the connection between the scattering lengths for mesons in various states which follows from the dispersion relations. In what follows we shall denote $k^2 J_\pm(\omega)$ by $F_\pm(\omega)$. For the scattering of negative mesons in hydrogen, expressing $D(k)$ in terms of the amplitudes in states with definite values of the isotopic spin,

$$3D_-(k) = 2D_1(k) + D_3(k),$$

we get in a similar way

$$\frac{\lambda_c}{3(1 + \mu/M)} \left\{ \frac{\mu}{2M} (2a_1 + a_3) - (2a_1^3 + a_3^3) - (2P_1 a_1^2 + P_3 a_3^2) + 4a_{13} + 2(a_{33} + a_{11}) + a_{31} - \frac{1}{2} \left(1 + \frac{\mu}{M} \right)^2 (a_1 - a_3) \right\} = F'_{-0} - \frac{2f^2 \lambda_c}{1 + \mu/2M}. \quad (13)$$

For the half-sum of (11) and (12), representing the scattering of π^0 mesons by nucleons, we have

$$\frac{1}{3} \frac{\lambda_c}{(1 + \mu/M)} \left\{ \frac{\mu}{2M} (a_1 + 2a_3) - (a_1^3 + 2a_3^3) - (P_1 a_1^2 + P_3 a_3^2) + 2(a_{13} + a_{31}) + a_{11} + 4a_{33} \right\} = \left\{ \frac{F_{+0} + F_{-0}}{2} \right\}' + \frac{\mu}{2M} \frac{2f^2 \lambda_c}{[1 - (\mu/2M)^2]}. \quad (14)$$

Substitution of the experimental data on the phase shifts[4]

$$\alpha_3 = -(0.105 \pm 0.010)\,\eta_b, \quad P_{33} = 0.6, \quad d_{33} = 0.0035,$$

$$\alpha_1 = (0.165 \pm 0.012)\,\eta_b, \quad Q_{33} = -0.8, \quad d_{35} = -0.0035,$$

$$\alpha_{33} = 0.235$$

(the scattering lengths in the $d_{3/2}$ and $d_{5/2}$ states are denoted by d_{33} and d_{35}), with $2f^2 = 0.16$ (and $2f^2 = 0.19 \pm 0.01$[5]) and zero values of the other coefficients, gives

$$\lambda_c^{-1} D'_{+0} = 0.40, \quad \lambda_c^{-1} D'_{-0} = 0.14$$

and

$$F'_{+0} = 0.28\,(0.25)\,\lambda_c, \quad F'_{-0} = 0.24\,(0.27)\,\lambda_c,$$

where the contribution of the unobserved region [$-0.173\,(0.206)$ and $+0.149\,(0.177)$] is considerable. For the half-sum, however,

$$\{1/2\,(F_+ + F_-)'\}_0 = 0.26\,\lambda_c$$

the contribution of the term containing f^2 amounts to only $-0.01\,\lambda_c$. The calculation of $F'_{\pm 0}$ from the data on the total cross-sections is discussed in the following section.

For the second derivative of Eq. (10) we have

$$D''_{+0}(k) = \lambda_c \left(1 + \frac{\mu}{M} \right) [2a_3^3 (a_3 + 2P_3)(a_3 + P_3) - 2a_3^2 (Q_3 + a_3 P_3^2) - 3(a_{31}^2 P_{31} + 2a_{33}^2 P_{33}) + 2(2d_{33} + 3d_{35})] + \frac{\mu}{M} \frac{\lambda_c}{(1 + \mu/M)^3} [2a_{33} + a_{31} - P_3 a_3^2 - a_3^3] - \frac{\mu}{4M} \frac{\lambda_c}{(1 + \mu/M)} \left[1 + \frac{\mu}{M} \left(1 + \frac{\mu}{M} \right)^2 \right] a_3. \quad (15)$$

By means of Eqs. (10), (6), and (8) we get from the value of the second derivative of Eq. (1) the second group of relations

$$D''_{+0}(k) - \frac{\lambda_c}{12} \left(1 + \frac{\mu}{M} \right) (a_1 - a_3) = F''_{+0} - \frac{2f^2 \lambda_c}{(1 + \mu/2M)^2} \quad (16)$$

for $\pi^+ p$ scattering;

$$D''_{-0}(k) + \frac{\lambda_c}{12} \left(1 + \frac{\mu}{M} \right) (a_1 - a_3) = F''_{-0} + \frac{2f^2 \lambda_c}{(1 - \mu/2M)^2} \quad (17)$$

for the scattering of negative mesons; and

$$\frac{1}{2} (D''_+ + D'_-)_0 = \frac{1}{2} (F''_+ + F''_-)_0 - \frac{\mu}{M} \frac{2f^2 \lambda_c}{[1 - (\mu/2M)^2]}, \quad (18)$$

where D''_- is constructed in analogy with Eq. (15).

By using the data on the phase shifts given earlier we have

$$\lambda_c^{-1} D''_{+0} = \left(1 + \frac{\mu}{M} \right) [2a_3^5 - 6a_{33}^2 P_{33} + 2(2d_{33} + 3d_{35})] + \frac{\mu/M}{(1 + \mu/M)^3} (2a_{33} - a_3^3) - \frac{\mu/4M}{(1 + \mu/M)} \left[1 + \frac{\mu}{M} \left(1 + \frac{\mu}{M} \right)^2 \right] a_3; \quad (19)$$

$$3\lambda_c^{-1} D_{-0}(k)'' = \left(1+\frac{\mu}{M}\right)[2(2a_1^5+a_3^5) - 6a_{33}^2 P_{33} + 4(2d_{13}+d_{33}) + 6(2d_{15}+d_{35})] + \frac{\mu}{M}\frac{2a_{33}-(2a_1^3+a_3^3)}{(1+\mu/M)^3} - \frac{\mu/4M}{(1+\mu/M)}\left[1+\frac{\mu}{M}\left(1+\frac{\mu}{M}\right)^2\right](2a_1+a_3). \quad (20)$$

Substitution of the experimental data on the phase shifts gives

$$D''_{+0} = -0.180\,\lambda_c; \quad D''_{-0} = -0.052\,\lambda_c;$$
$$\{{}^1/_2(D''_+ + D''_-)\}_0 = -0.116\,\lambda_c;$$
$$F''_{+0} = -0.019\,\lambda_c \quad (2f^2 = 0.16);$$
$$F''_{+0} = +0.016\,\lambda_c \quad (2f^2 = 0.19);$$
$$F''_{-0} = -0.162\,\lambda_c \quad (2f^2 = 0.16);$$
$$F''_{-0} = -0.187\,\lambda_c \quad (2f^2 = 0.19);$$
$$\{{}^1/_2(F''_- + F''_+)\}_0 = -0.090\,\lambda_c \quad (2f^2 = 0.16);$$
$$\{{}^1/_2(F''_- + F''_+)\}_0 = -0.085\,\lambda_c, \quad (2f^2 = 0.19),$$

where the contribution of the unobserved region turns out to be very important for the first two values and amounts to about 35 percent for the half-sum. The value of the second derivative of F_+ consists mainly of the difference of the resonance contribution and that from the unobserved region (this latter contribution being $+0.188\lambda_C$ and $0.222\lambda_C$). For the scattering of negative mesons the resonance transition is of less importance, so that the contribution of the unobserved region, amounting to $-0.138\lambda_C$ and $-0.161\lambda_C$, is the main one.

2. In the preceding section the values of the derivatives of $F_\pm$ were obtained from the experimental data on the phase shifts. These same quantities can be calculated directly from Eq. (2) and the experimental data on the total cross-sections. This provides a more searching check on the correspondence between the experimentally determined phase shifts and the dispersion relations.

Having obtained $F_\pm$, one can calculate the values of the derivatives by direct differentiation. But the differentiation of a curve drawn from experimental data introduces large errors; therefore we shall represent the derivative in another form. For this purpose, being interested in the values of the derivatives at $\eta^2 \to 0$, we break up the dispersion integral $J_+(\omega)$ into three parts:

$$4\pi^2 J_+(\omega) = \mathrm{P}\int_\mu^z \frac{d\omega'}{k'}\frac{\sigma_+(\omega')}{\omega'-\omega} + \int_z^\infty \frac{d\omega'}{k'}\frac{\sigma_+(\omega')}{\omega'-\omega} + \int_\mu^\infty \frac{d\omega'}{k'}\frac{\sigma_-(\omega')}{\omega'+\omega}, \quad (21)$$

so that the second integral already contains no singularity ($z > \omega$). We choose the value of z so that with the limitation to s and p states and use of Eq. (3) the expression for $\sigma_+(\omega)$ can be put in the form

$$\sigma_+(\omega) = 4\pi\left\{a_3^2 + \frac{(a_{31}^2+2a_{33}^2)}{(1+\mu/M)^4}\eta^4\right\}. \quad (22)$$

Substituting Eq. (22) into the first integral in Eq. (21), we get for it

$$\pi L(\omega) = (4\pi)^{-1}\mathrm{P}\int_\mu^z \frac{d\omega'}{k'}\frac{\sigma_+(\omega')}{\omega'-\omega} = a_3^2 J_\alpha(p) + \frac{(a_{31}^2+2a_{33}^2)}{(1+\mu/M)^4} J_\beta(p), \quad (23)$$

where

$$J_\alpha(p) = -\frac{1}{p}\ln\left[1+\frac{(\omega-\mu)(z+\mu)+p\sqrt{z^2-\mu^2}}{\mu(z-\omega)}\right],$$

$$\mu^4 J_\beta(p) = \frac{1}{3}(z^2-\mu^2)^{3/2} + \frac{1}{2}(z^2-\mu^2)^{1/2}(\omega z+p^2) + p^4 J_\alpha(p) - \frac{1}{2}\mu(\mu^2-p^2)\ln\left[\frac{\sqrt{z^2-\mu^2}+z}{\mu}\right]. \quad (23')$$

For small values of p^2

$$\mu^2 J_\alpha(p) = -\sqrt{z^2-\mu^2}\left\{\frac{1}{z'-1} + \frac{p^2}{6}\frac{2-z'}{(z'-1)^2} + \frac{p^4}{40}\frac{3z'^2-9z'+8}{(z'-1)^3} + \ldots\right\} \quad \left(z' = \frac{z}{\mu}\right), \quad (23'')$$

so that (with $z = 1.43\,\mu$)

$$J_\alpha(0) = -\frac{\sqrt{z^2-\mu^2}}{\mu(z-\mu)} = -2.38\,\lambda_c,$$

$$\mu^4 J_\beta(0) = \frac{(z^2-\mu^2)^{3/2}}{3} + \frac{\mu z(z^2-\mu^2)^{1/2}}{2} - \frac{\mu^3}{2}\ln\left[\frac{\sqrt{z^2-\mu^2}+z}{\mu}\right] = 0.639\,\mu^3, \quad (24)$$

$$J_+(\mu) = \frac{a_3^2}{\pi}J_\alpha(0) + \frac{(a_{31}^2+2a_{33}^2)}{\pi(1+\mu/M)^4}J_\beta(0) + \frac{1}{4\pi^2}\int_z^\infty \frac{d\omega'}{k'}\frac{\sigma_+(\omega')}{\omega'-\mu} + \frac{1}{4\pi^2}\int_\mu^\infty \frac{d\omega'}{k'}\frac{\sigma_-(\omega')}{\omega'+\mu}.$$

The expression for $J_-(\mu)$ is obtained from Eq. (24) by the replacements

$$\sigma_+ \rightleftarrows \sigma_-, \quad 3a_3^2 \to a_3^2 + 2a_1^2; \quad 3a_{33}^2 \to a_{33}^2 + 2a_{13}^2, \quad 3a_{31}^2 \to a_{31}^2 + 2a_{11}^2. \quad (25)$$

From Eqs. (21) and (23) there follow expressions for the dispersion relations that are convenient for calculations in the range of energies $\omega - \mu \ll \mu$. Before using them to calculate the values of the de-derivatives for $\eta^2 \to 0$, we make several remarks.

In the second term of Eq. (22) (the contribution of the p waves) the change from the center-of-mass system to the laboratory system has been carried out approximately. Working more exactly,

using Eq. (4), instead of $J_\beta(p)/(1+\mu/M)^4$ we get

$$L_\beta(p) = \int_\mu^z \frac{d\omega'}{\omega'-\omega} \frac{k'^3}{(1+2\omega'/M+\mu^2/M^2)^2} = \left(1+\frac{2\omega}{M}+\frac{\mu'}{M^2}\right)^{-2} \int_{\mu-\omega}^{z-\omega} \frac{R^{3/2}dx}{x(1+\gamma x)^2},$$

where

$$\gamma = \frac{2\mu}{M}\left(1+\frac{2\omega}{M}+\frac{\mu^2}{M^2}\right)^{-2}, \quad R = p^2+2\omega x+x^2,$$

or

$$\left(1+\frac{2\omega}{M}+\frac{\mu^2}{M^2}\right)^2 L_\beta(p) = J_\beta(p) - \gamma\left\{\int_{\mu-\omega}^{z-\omega} \frac{R^{3/2}dx}{1+\gamma x} + \int_{\mu-\omega}^{z-\omega} \frac{R^{3/2}dx}{(1+\gamma x)^2}\right\} \qquad (26)$$
$$= J_\beta(p) - \gamma N_\beta(p).$$

We give the expression for $N_\beta(p)$ which is obtained when the denominators of the integrands are expanded in series up to terms in γ^2:

$$N_\beta(p) = \left[\left(\frac{N^2}{2}-\frac{3}{4}\right)zN - \frac{3}{16}\ln(\omega+2z+N)\right] - 3\gamma\left[\frac{N}{5} - z\left(\frac{\omega N^3}{4}-\frac{3}{8}N\right) - \frac{3}{8}\ln(\omega+2z+N)\right] + 4\gamma^2\left[\left(\frac{z-1}{6}-\frac{7\omega}{30}\right)N^5 + \frac{(6\omega^2+1)}{6}z\left(\frac{N^3}{4}-\frac{3N}{8}\right) + \frac{(6\omega^2+1)}{16}\ln(\omega+2z+N)\right], \qquad (27)$$

where $N = (z^2-1)^{1/2}$ $(\mu = 1)$. The last term in Eq. (27) gives less than 6.5 percent of the value of N_β at $p = 0$. The value of $\gamma N_\beta(0)$ itself is 0.085, which leads to the change from $J_\beta(0) = 0.639$ to $L_\beta(0) = 0.554$, i.e., gives a correction of about 15 percent. Use of only the first term in Eq. (27) gives $L_\beta(0) = 0.530$, from which it is clear that the remaining terms give less than 5 percent. Since the entire contribution from $J_\beta(0)$ is not large, one can just use Eq. (23′), bringing in the first term of Eq. (27) as a correction.

We shall now obtain the expressions for the derivatives of $F_\pm$. For arbitrary momenta

$$F'_+(\omega) = J_+(\omega) + \eta^2 J'_+(\omega). \qquad (28)$$

From Eqs. (21), (23), and (27) it can be seen that

$$\eta^2 J'_{+0}(\omega) = 0. \qquad (29)$$

Since Eq. (28) is also correct for $\eta^2 J'_-$, we get

$$F'_{\pm 0}(\omega) = J_\pm(\mu). \qquad (30)$$

This last equation enables us to reduce the calculation of the derivative of F to the value of the dispersion integral at the single point $\omega = \mu$. The value of the derivative is calculated from Eqs. (30), (23), and (24). For $z = 1.43$ the contribution of the first two terms in Eq. (23) gives $-0.026/\pi$ for the s wave and $+0.0350/\pi$ for the p waves, which is a very small fraction of the value $F'_{+0} = 0.28\,(0.25)\,\lambda_c$ obtained in the preceding section.

Similarly, for the interaction of negative mesons with protons we have instead of Eq. (24)

$$J_-(\mu) = \frac{(a_3^2+2a_1^2)}{3\pi} J_\alpha(0) + \frac{(a_{31}^2+2a_{11}^2+a_{33}^2+2a_{13}^2)}{3\pi(1+\mu/M)^4} L_\beta(0) + \frac{1}{4\pi^2}\int_z^\infty \frac{d\omega'}{k'}\frac{\sigma_-(\omega')}{\omega'-\mu} + \frac{1}{4\pi^2}\int_\mu^\infty \frac{d\omega'}{k'}\frac{\sigma_+(\omega')}{\omega'+\mu}. \qquad (31)$$

For the contribution of the first two terms in Eq. (31) we get

$$\pi L_- = -0.051 + 0.012 = -0.039.$$

Here also the contributions of the s and p waves, which are comparable with each other, turn out at $z = 1.43$ to be tiny in comparison with the contribution of the integral terms in Eq. (31), if we judge by the results of the preceding section. For the second derivative of F at arbitrary momenta we find

$$F''(\omega) = 2J'(\omega) + \eta^2 J''(\omega).$$

For $\eta^2 \to 0$ the second term vanishes, so that

$$F''_0(\omega) = 2J'(\mu). \qquad (32)$$

Breaking $J'_+(\omega)$ up into parts as in Eq. (21), we get from Eq. (23) for the contribution of the s and p waves

$$\pi L'_+(\mu) = -a_3^2\frac{N(2-z)}{6(z-1)^2} + \frac{a_{31}^2+2a_{33}^2}{\pi(1+\mu/M)^4} \times \left\{\frac{N}{2}\left(1+\frac{z}{2}\right)+\frac{1}{2}\ln(N+z)\right\}; \qquad (33)$$

$$J'_+(\mu) = L'_+(\mu) + \frac{1}{4\pi^2}\int_z^\infty \frac{d\omega'}{k'}\frac{\sigma_+(\omega')}{(\omega'-\mu)^2} - \frac{1}{4\pi^2}\int_\mu^\infty \frac{d\omega'}{k'}\frac{\sigma_-(\omega')}{(\omega'+\mu)^2}. \qquad (34)$$

The contribution of the terms outside the integrals is $+0.002\lambda_c$. The expression for $J'_-(\mu)$ is obtained from Eq. (34) by the replacements (25). For $\pi^- - p$ the contribution of the terms outside the integrals is $-0.002\lambda_c$.

3. The numerical values of the dispersion integrals are

$$J_+(\mu) = 6.96/4\pi^2 = 0.176, \quad J_-(\mu) = 4.99/4\pi^2 = 0.126. \qquad (35)$$

Comparison of Eqs. (35) and (30) with the previously obtained values 0.28 (0.25) and 0.24 (0.27) provides a further confirmation of the positive sign of a_{33}. Moreover, it follows from Eqs. (35) and (12) that a_{31} is a negative quantity, and

$$\begin{aligned} &\text{for } 2f^2 = 0.16: \quad D'_+(0) = 0.258\ \lambda_c, \quad a_{31} = -0.115, \\ &\text{for } 2f^2 = 0.19: \quad D_+(0) = 0.320\ \lambda_c, \quad a_{31} = -0.080. \end{aligned} \tag{36}$$

From Eqs. (35) and (13) we have as a consequence of the dispersion relations that

$$\begin{aligned} &\text{for } 2f^2 = 0.16: \quad D'_-(0) = 0.026\ \lambda_c, \\ &\qquad 2a_{13} + a_{11} = -0.139; \\ &\text{for } 2f^2 = 0.19: \quad D_-(0) = -0.00(4)\ \lambda_c, \\ &\qquad 2a_{13} + a_{11} = -0.208. \end{aligned} \tag{37}$$

On the hypothesis that $a_{13} = a_{31}$ it follows from Eq. (37) that

$$\begin{aligned} &\text{for } 2f^2 = 0.16: \quad a_{11} = 0.09, \\ &\text{for } 2f^2 = 0.19: \quad a_{11} = -0.05. \end{aligned} \tag{38}$$

It must be emphasized that it is difficult to determine the errors in the numerical values of a_{31} and a_{11}. Although the idea of a small and negative scattering length a_{31} and a small a_{11} corresponds roughly to the experimental data on $\pi - N$ scattering, the value of $D'_-(0)$ is in noticeable disagreement with the experimental data.

For the values of the derivatives of the dispersion integrals we get by numerical integration

$$2J'_+(\mu) = 0.08\ \lambda_c, \quad 2J'_-(\mu) = 0.04\ \lambda_c. \tag{39}$$

It is at present difficult to get results analogous to Eq. (36) — (38), since for this more precise data are needed.

Thus the analysis that has been given by using information about the scattering phase shifts at low energies only confirms the results of Puppi and Stanghellini.[5] For the scattering of π^+ mesons by protons the dispersion relations enable us to determine from the data on a_1, a_3, and a_{33} a value of a_{31} that agrees with the experimental data, but the consequences of the dispersion relations for $\pi^- - p$ scattering cannot be brought into agreement with experiment. The actual disagreement at low energies is not large, as it is at higher energies. It is not clear just how far it exceeds the limits of the experimental errors in the phase shifts.

The causes of the disagreement remain unclear. All kinds of isotopically noninvariant corrections are small. In connection with the important part played by isotopic invariance in the derivation of the final form of the dispersion relations, the possibility of an additional check on the isotopic invariance in the $\pi - N$ scattering is discussed in the Appendix. The contribution of the πp mesic atom calls for special examination.

In the situation that has arisen, it is very desirable that additional experiments be carried out, and also that the experimental data be processed more precisely. Experiments that could be of particular value are studies of the polarization of recoil nucleons, and also of the interference with the Coulomb scattering.

The writer is grateful to Ia. A. Smorodinskii, N. N. Bogoliubov, N. P. Klepikov, A. A. Logunov, and D. V. Shirkov for valuable discussions, and to I. V. Popova for aid with the numerical calculations.

APPENDIX

As is well known, the unitary character of the S matrix, together with invariance under time reversal, decidedly reduces the number of independent parameters occurring in the S matrix. Recently it has been shown[6] that these conditions make it possible to reconstruct the scattering amplitude in the case in which only elastic scattering takes place, unaccompanied by inelastic processes.

We shall now consider the unitary conditions for $\pi^- - p$ scattering, in which in parallel with the elastic scattering there occurs an inelastic process — the conversion of the charged meson into a neutral meson — and shall show how these conditions can aid in checking the isotopic invariance.

We introduce the S-matrix elements

$$S_{ik}^{Jl} = \rho_{ik}^{Jl} \exp\left[2i\alpha_{ik}^{Jl}\right]$$

(α_{ik} and ρ are real numbers) for a state characterized by the angular momentum J and by $l = J + 1/2$ (hereafter the indices J, l are omitted). S_{11} corresponds to the elastic scattering of the π^- meson by a proton, $\pi^- + p \to \pi^-$; $S_{12} = S_{21}$ corresponds to the exchange scattering $\pi^- + p \to \pi^0$; and S_{22}, to the elastic scattering $\pi^0 + n \to \pi^0$.

The requirement that the matrix be unitary, written in the form

$$\sum_k S_{ik}^* S_{lk} = \delta_{il}, \tag{A.1}$$

is easily seen to give three independent conditions:

$$|S_{11}|^2 + |S_{12}|^2 = 1; \tag{A.2}$$

$$|S_{22}|^2 + |S_{12}|^2 = 1; \tag{A.3}$$

$$S_{11}^* S_{12} + S_{12}^* S_{22} = 0. \tag{A.4}$$

For the $\pi^+ - p$ scattering Eq. (1) gives instead of

Eqs. (2) — (4) only a single condition, which makes it possible to introduce real phases.

From Eqs. (2) and (3) we get the relations between absolute values

$$|S_{11}|^2 = |S_{22}|^2 = \rho_{11}^2 = \rho_{22}^2 = \rho^2,$$
$$|S_{12}|^2 = \rho_{12}^2 = 1 - \rho^2, \tag{A.5}$$

and from Eqs. (4) and (5) a connection between the phases

$$4\alpha_{12} = 2(\alpha_{11} + \alpha_{22}) + n\pi. \tag{A.6}$$

Consequently in this case, in virtue of the three relations (2) — (4) the amplitudes of the three processes, including both elastic and inelastic scattering, can be expressed in terms of three real numbers, which must be determined by experiment.

We note that when one goes to a larger number of channels Eq. (6) remains an approximately true relation if the probabilities of transitions between channels are small in comparison with those for transitions within the channels (cf. Ref. 7, for example).

Relations (5) and (6) can be put in another form. The situation here recalls that which is encountered when, in considering the transitions $^3P_2 \to {}^3P_2$, $^3F_2 \to {}^3F_2$, $^3P_2 \rightleftarrows {}^3F_2$ in nucleon-nucleon scattering, one introduces real phases and mixing coefficients.[8] In analogy with this we introduce two real phases δ_J^I and δ_J^{II} and a mixing parameter ϵ_J:

$$S_{11}^{Jl} = \exp[2i\delta_J^I]\cos^2\varepsilon_J + \exp[2i\delta_J^{II}]\sin^2\varepsilon_J,$$
$$2S_{12}^{Jl} = \{\exp[2i\delta_J^I] - \exp[2i\delta_J^{II}]\}\sin 2\varepsilon_J, \tag{A.7}$$
$$S_{22}^{Jl} = \exp[2i\delta_J^I]\sin^2\varepsilon_J + \exp[2i\delta_J^{II}]\cos^2\varepsilon_J$$

(unlike the case of N — N scattering, here both $\delta_J^{I,II}$ and also ϵ_J depend on l as well as on J, and the ϵ_J do not drop out of the expressions for the integrated cross-sections). The connection between the quantities ρ, α_{11}, α_{22} and δ_J^I, δ_J^{II}, ϵ_J follows from Eqs. (5), (6), and (7). The elements of the S matrix are expressed in this way in the exact formulation when the existence of isotopic invariance is not assumed. As is well known, under this further condition one has

$$3S_{11}^{Jl} = 2b_1^{Jl} + b_3^{Jl}; \quad 3S_{12}^{Jl} = \sqrt{2}\,(b_3^{Jl} - b_1^{Jl});$$
$$3S_{22}^{Jl} = b_1^{Jl} + 2b_3^{Jl} \tag{A.8}$$

($b_{2T}^{Jl} = \exp[2i\delta_{2T}^{Jl}]$ characterizes the scattering in a state with given J and isotopic spin T). From a comparison of Eqs. (8) and (7) it can be seen that isotopic invariance corresponds to the case in which ϵ_J, not depending on J and l (there remain two real parameters) takes the constant value $\arctan 2^{1/2} \approx 55°$, if δ_J^I corresponds to δ_3 and δ_J^{II} to δ_1.

By checking these last assertions (lack of dependence of ϵ_J on J and l and definite value of ϵ_J) one has a possibility for confirming the isotopic invariance in the scattering of charged mesons. It might seem that, since the cross-section for elastic scattering of π^0 mesons appears in Heitler's relation

$$d\sigma(\pi^+ + p \to \pi^+) + d\sigma(\pi^- + p \to \pi^-)$$
$$= 2d\sigma(\pi^0 + p \to \pi^0) + d\sigma(\pi^- + p \to \pi^0)$$

the π — N scattering cannot be used for checking the isotopic invariance. Fermi has pointed out[7] that, at least when one takes into account only the s and p waves, such a check can be carried out with experiments with charged mesons. From the results of this appendix it follows that this can be done with the inclusion of an arbitrary number of states. The check proposed here goes beyond this. It makes it possible to see to what accuracy isotopic invariance is fulfilled in each state of the π — N system.

We note a generalization of the symmetry pointed out by Minami[9,10] to the case in which an inelastic process occurs in parallel with the elastic process. By direct verification one readily finds that the unpolarized cross-sections of the processes in question remain unchanged if one makes the simultaneous replacements

$$\delta_{J,\,J-1/2}^{I,\,II} \rightarrow \delta_{J,\,J+1/2}^{I,\,II}; \quad \varepsilon_{J-1/2}^{J} \rightarrow \varepsilon_{J+1/2}^{J}.$$

---

[1] F. E. Low, Phys. Rev. **97**, 1392 (1955). G. C. Wick, Revs. Mod. Phys. **27**, 339 (1955). G. F. Chew and F. E. Low, Phys. Rev. **101**, 1570 (1956). Castillejo, Dalitz, and Dyson, Phys. Rev. **101**, 453 (1956). F. J. Dyson, Phys. Rev. **106**, 157 (1957).

[2] M. L. Goldberger, Phys. Rev. **97**, 508 (1955). Goldberger, Miyazawa, and Oehme, Phys. Rev. **99**, 986 (1955). B. L. Ioffe, J. Exptl. Theoret. Phys. (U.S.S.R.) **31**, 583 (1956), Soviet Phys. JETP **4**, 534 (1957); Bogoliubov, Medvedev, and Polivanov, (Problems in the Theory of Dispersion Relations), Gostekhizdat (in press).

[3] L. Landau and Ia. Smorodinskii, J. Exptl. Theoret. Phys. (U.S.S.R.) **14**, 269 (1944). H. Bethe, Phys. Rev. **76**, 38 (1949).

[4] J. Orear, Phys. Rev. **96**, 176 (1954). A. I. Mukhin and B. M. Pontecorvo, J. Exptl. Theoret. Phys. (U.S.S.R.) **31**, 550 (1956), Soviet Phys. JETP **4**, 373 (1957).

[5] G. Puppi and A. Stanghellini, Nuovo cimento **5**, 1305 (1957).

[6] Puzikov, Ryndin, and Smorodinskii, J. Exptl. Theoret. Phys. (U.S.S.R.) 32, 592 (1957), Soviet Phys. JETP 5, 489 (1957).
[7] E. Fermi, Suppl. Nuovo cimento 2, 17 (1955).
[8] J. M. Blatt and L. C. Biedenharn, Revs. Mod. Phys. 24, 258 (1952).
[9] S. Minami, Prog. Theor. Phys. 11, 213 (1954).
[10] R. Ryndin and Ia. Smorodinskii, Dokl. Akad. Nauk SSSR 103, 69 (1955).

Translated by W. H. Furry.
80

SOVIET PHYSICS JETP VOLUME 34 (7), NUMBER 2 AUGUST, 1958

TRANSITION BETWEEN HYPERFINE STRUCTURE LEVELS IN MU-MESIC HYDROGEN

S. S. GERSHTEIN

Institute for Physical Problems, Academy of Sciences, U.S.S.R.

Submitted to JETP editor August 12, 1957

J. Exptl. Theoret. Phys. (U.S.S.R.) 34, 463-468 (February, 1958)

It is shown that, through the mechanism of "jumping" of the μ^- meson from one proton to another, which was proposed by Ia. B. Zel'dovich, mesic hydrogen atoms convert completely to the ground state of the hyperfine structure during the lifetime of the μ meson. As a result, there is complete depolarization of μ mesons in hydrogen, and the neutrons which are formed from capture of μ^- mesons by protons via $\mu^- + p = n + \nu$ will be completely polarized along their direction of motion.

THE separation between the upper ($F = 1$, where F is the total spin of the mesic atom) and lower ($F = 0$) levels of the hyperfine structure for a μ meson in the K orbit of a mesic hydrogen atom, is[1]

$$\Delta\varepsilon = \frac{16\pi}{3}\beta_\mu\beta_N g_i |\psi(0)|^2 = 0.25 \text{ ev} \qquad (1)$$

(β_μ is the μ-mesonic and β_N the nuclear Bohr magneton, $g_i = 2 \times 2.79$ is the gyromagnetic ratio of the proton).

Because of the smallness of this separation, the radiative transition to the lower state is extremely improbable ($\tau_{rad} \sim 10^6$ sec). However, because of the neutrality of mesic hydrogen there is a very effective mechanism via which there is a complete transition into the lower hyperfine structure state during the lifetime of the μ meson. This mechanism is the "jump" of the μ meson from one proton to another with simultaneous transition into the lower state of the hyperfine structure.* Since the hyperfine splitting is much greater than the thermal energy in collisions of a proton and a mesic atom, the process is irreversible. In the present paper we give an estimate of the cross section for this transition.

In mesic units ($e = 1$, $\hbar = 1$, $m_\mu = 1$), the Hamiltonian for the interaction of a meson with a pair of protons, including the interaction of the spins of the meson and the protons is

$$\hat{H} = -\frac{1}{2M}\Delta_{R_1} - \frac{1}{2M}\Delta_{R_2} - \frac{1}{2}\Delta_r - \frac{1}{r_1} - \frac{1}{r_2} + \frac{1}{R} + \frac{4}{3}g_i\beta_\mu\beta_N\left(\frac{\delta(r_1)}{r_1^2}\mathbf{si}_1 + \frac{\delta(r_2)}{r_2^2}\mathbf{si}_2\right) \qquad (2)$$

($\mathbf{R}_1$, $\mathbf{R}_2$, $\mathbf{r}$ are the coordinates and $\mathbf{i}_1$, $\mathbf{i}_2$, $\mathbf{s}$ are the spins of the protons and the meson, $R = |\mathbf{R}_1 - \mathbf{R}_2|$ is the distance between the protons, while $r_1 = |\mathbf{r} - \mathbf{R}_1|$ and $r_2 = |\mathbf{r} - \mathbf{R}_2|$ are the distances of the meson from the two protons). We are neglecting the spin-spin interaction between the protons and between the meson and the second proton when the meson is at the position of the first proton.

At the velocities we are considering, the relative motion of the protons is described by an s wave, so that the total spin is conserved. The spin of the system consisting of two protons and a μ

*This was called to the attention of the author by Ia. B. Zel'dovich.

meson can take on the values $3/2$ and $1/2$. However, transitions to the lower hyperfine structure state are possible only for the state with spin $1/2$. The wave function for such a state, antisymmetric under interchange of the protons, is expressible as

$$\Psi = G(R)\,\Sigma_g(R,\ \mathbf{r})\,S^0_{1/2,\,1/2}(1,\ 2;\ \mu) + H(R)\,\Sigma_u(R,\ \mathbf{r})\,S^1_{1/2,\,1/2}(1,\ 2;\ \mu). \tag{3}$$

(where, to be specific, we consider a state with projection of the total spin on the arbitrary z axis equal to $+1/2$). Σ_g and Σ_u are the wave functions of the μ meson in the field of the two fixed protons; they contain the distance between the protons as a parameter and are, respectively, symmetric and antisymmetric under interchange of the protons:

$$\left(-\frac{1}{2}\Delta_r - \frac{1}{r_1} - \frac{1}{r_2} + \frac{1}{R}\right)\Sigma_{g,\,u} = E_{g,\,u}(R)\,\Sigma_{g,\,u}. \tag{4}$$

$S^0_{1/2,1/2}(1,\ 2;\ \mu)$ and $S^1_{1/2,1/2}(1,\ 2;\ \mu)$ are spin functions corresponding to total spin of 0 and 1 for the particles whose indices are separated off by the semicolon; the total spin of the system is $1/2$ and the total spin projection on the z axis is $+1/2$. Introducing the usual spin functions $\alpha = \begin{pmatrix}1\\0\end{pmatrix}$ and $\beta = \begin{pmatrix}0\\1\end{pmatrix}$ for the two protons and the μ meson, we can write

$$S^0_{1/2,\,1/2}(1,2;\ \mu) = \frac{1}{\sqrt{2}}\,[\alpha(1)\,\beta(2) - \beta(1)\,\alpha(2)]\,\alpha(\mu),$$

$$S^1_{1/2,\,1/2}(1,2;\ \mu) = \frac{1}{\sqrt{6}}\,[\alpha(1)\,\beta(2) + \beta(1)\,\alpha(2)]\,\alpha(\mu) - \sqrt{\frac{2}{3}}\,\alpha(1)\,\alpha(2)\,\beta(\mu). \tag{5}$$

On the other hand, for sufficiently large distance between the protons, the wave function of the system with total spin $1/2$ and spin projection $+1/2$, for the lower hyperfine structure state ($F = 0$) is

$$\Psi^0 = K(R)\,\psi(r_1)\,S^0_{1/2,\,1/2}(1,\ \mu;\ 2) - K(R)\,\psi(r_2)\,S^0_{1/2,\,1/2}(2,\ \mu;\ 1), \tag{6}$$

and for the upper state ($F = 1$)

$$\Psi^1 = L(R)\,\psi(r_1)\,S^1_{1/2,\,1/2}(1,\ \mu;\ 2) - L(R)\,\psi(r_2)\,S^1_{1/2,\,1/2}(2,\ \mu;\ 1), \tag{7}$$

where $\psi(\mathbf{r}_1)$ and $\psi(\mathbf{r}_2)$ are the wave functions of the μ meson at the first and second protons, respectively.

At large distances between the protons

$$\Sigma_{g,\,u} \approx (\psi(r_1) \pm \psi(r_2))/\sqrt{2}, \tag{8}$$

and the wave function (3) of the system must be a linear combination of (6) and (7), so we easily find the relations between the functions $G(R)$, $H(R)$ and $K(R)$, $L(R)$:

$$\begin{aligned} G(R) &= (K - \sqrt{3}\,L)/\sqrt{2},\\ K(R) &= (G - \sqrt{3}\,H)/2\sqrt{2},\\ H(R) &= (-\sqrt{3}\,K - L)/\sqrt{2},\\ L(R) &= (-\sqrt{3}\,G - H)/2\sqrt{2}. \end{aligned} \tag{9}$$

Substituting the wave function (3) in the Schrödinger equation $\hat{H}\Psi = E\Psi$ with the Hamiltonian (3) and using (4), we find, after multiplying the equations for the functions $G(R)$ and $H(R)$ by $\Sigma_g S^0_{1/2,1/2}(1,\ 2;\ \mu)$ and $\Sigma_u S^1_{1/2,1/2}(1,\ 2;\ \mu)$, respectively, and integrating over the μ-meson coordinates:

$$\begin{aligned} &-\frac{1}{M}\Delta_R G + E_g G - \frac{1}{2M}K_{gg}G + \frac{4\pi}{3}g_i\beta_\mu\beta_N\sqrt{3}\,|\psi(0)|^2 H = EG,\\ &-\frac{1}{M}\Delta_R H + E_u H - \frac{1}{2M}K_{uu}H + \frac{4\pi}{3}g_i\beta_\mu\beta_N\,|\psi(0)|^2(\sqrt{3}\,G - 2H) = EH, \end{aligned} \tag{10}$$

where

$$K_{gg} = \int \Sigma_g(\Delta_{\mathbf{R}_1} + \Delta_{\mathbf{R}_2})\,\Sigma_g\,d\mathbf{r},$$

$$K_{uu} = \int \Sigma_u(\Delta_{\mathbf{R}_1} + \Delta_{\mathbf{R}_2})\,\Sigma_u\,d\mathbf{r}. \tag{11}$$

For sufficiently large distance between the protons (neglecting exponentially small terms and terms of order R^{-4}),

$$K_{gg} = 2\int \Sigma_g\,\Delta_{\mathbf{R}_1}\Sigma_g\,d\mathbf{r} \approx \int \psi(r_1)\Delta_{r_1}\Psi(r_1)\,d\mathbf{r} = -1.$$

In this same approximation, $K_{uu} \approx K_{gg}$. The expressions $-K_{gg}/2M$ and $-K_{uu}/2M$ are thus the correction to the kinetic energy of motion of the proton in the mesic atom, which is usually taken into account by introducing the reduced mass. The equations for $K(R)$ and $L(R)$ follow from (9) and (10):

$$\begin{aligned} &\frac{1}{M}\Delta_R L + \varepsilon L - {}^1/_4(3E_g + E_u + 2)\,L + \frac{\sqrt{3}}{4}(E_g - E_u)\,K = 0,\\ &\frac{1}{M}\Delta_R K + (\varepsilon + \Delta\varepsilon)\,K - {}^1/_4(3E_u + E_g + 2)\,K + \frac{\sqrt{3}}{4}(E_g - E_u)\,L = 0, \end{aligned} \tag{12}$$

where

$$\varepsilon = E + \frac{1}{2} - \frac{1}{2M} - \frac{1}{4}\Delta\varepsilon,$$

and $\Delta\epsilon$ is the hyperfine structure energy (1).

The relative motion of the mesic atom and the proton is described by the function $L(R)$ in the upper hyperfine structure state, and by $K(R)$ in the lower state. Equation (12) thus describes the transfer of hyperfine structure energy into energy of relative motion (ϵ and $\epsilon + \Delta\epsilon$, for $R \to \infty$, are equal to the kinetic energy of relative motion in the upper and lower hyperfine structure states, respectively).

Finding the cross section for "jumping" of the μ meson is essentially a problem of inelastic scattering of slow particles.[2] Because of the smallness of the quantity $k_0 = \sqrt{M\Delta\epsilon} = 0.02$ (mesic units), there is a quite large region of free motion ($1 \ll R \ll 1/k_0$) in which we can neglect both the energies E_g and E_u as well as the energies ϵ and $(\epsilon + \Delta\epsilon)$. The cross section for the transition into the lower hyperfine structure state will be determined by the asymptotic form of the functions $L(R)$ and $K(R)$ in this region.

For sufficiently small R we can neglect ϵ and $(\epsilon + \Delta\epsilon)$ compared to E_g and E_u. In this region, Eqs. (10) for the radial functions $g(R) = RG(R)$ and $h(R) = RH(R)$ have the form

$$\frac{1}{M}\frac{d^2g}{dR^2} - \left(E_g + \frac{1}{2}\right)g = 0, \tag{13}$$

$$\frac{1}{M}\frac{d^2h}{dR^2} - \left(E_u + \frac{1}{2}\right)h = 0. \tag{14}$$

In the neighborhood of the minimum ($R_0 = 2$), the function E_g is well approximated by the Morse potential[3]

$$E_g = -1/2 + A[e^{-2\alpha(R-R_0)} - 2e^{-\alpha(R-R_0)}].$$

The parameters A (the depth of the well $E_g + \frac{1}{2}$ at the minimum) and α are determined from the exact values of $E_g(R)$, which are found by numerical integration:[4]

$$A = 0.1027;\ 2\alpha^2 A = d^2E_g/dR^2 = 0.0976;\ \alpha \approx 0.69.$$

For energy $\epsilon > 0$, the Schrödinger equation with the Morse potential has the exact solution

$$g = e^{-\xi/2}[\xi^{is}e^{-is\varphi_0}F(-n,\ 1+2is,\ \xi) - \xi^{-is}e^{is\varphi_0}F(-n^*, 1-2is,\ \xi)],$$

where

$$\xi = (2\sqrt{MA}/\alpha)\,e^{-\alpha(R-R_0)};\quad is = \sqrt{-M\varepsilon}/\alpha;$$

$$n = \sqrt{MA}/\alpha - 1/2 - is;$$

$$e^{2is\varphi_0} = \Gamma(1+2is)\,\Gamma(-n^*)/\Gamma(1-2is)\,\Gamma(-n).$$

In the region $1 \ll R - R_0 \ll 1/s$, for $\epsilon \to 0$, the solution becomes

$$g \sim R + \vartheta, \tag{15}$$

where

$$\vartheta = \frac{\varphi_0}{\alpha} - R_0 - \frac{1}{\alpha}\ln\frac{2\sqrt{MA}}{\alpha},$$

$$\varphi_0 = 2\psi(1) - \psi\left(1/2 - \frac{\sqrt{MA}}{\alpha}\right);$$

$\psi(x)$ is the logarithmic derivative of the Γ-function and has poles at the points $0, -1, -2, \ldots$. In addition, the quantity $(\frac{1}{2} - \sqrt{MA}/\alpha) \approx -0.88$ is near to -1, which leads to a quite large value of $\varphi_0 \approx 11$. This is related to the fact that there is a virtual level of the mesic molecule near to zero energy, which results in resonance.[5]

To find the asymptotic form of $h(R)$, we note that at sufficiently large distances [for which, however, Eq. (14) is still valid]

$$E_{g,u} \approx -\frac{1}{2} \mp \frac{2}{e}Re^{-R}$$

[The solution of Eq. (4) in the approximation (9) gives $E_{g,u} \approx 1/2 \mp 2/3\,Re^{-R}$.]

At distances R for which the expression $(2M/e)Re^{-R}$ ($M = 8.87$) is still important, it can be approximated well by the function

$$(2M/e)Re^{-R} \approx e^{-\alpha'(R-R_1)};\quad R_1 \approx 3;$$

$$\alpha' = 1 - 1/R_1 \approx 0.7.$$

In this case, Eq. (14) is reduced to the Bessel equation by the substitution $\xi = \exp\{-\alpha'(R-R_1)/2\}$. Since for a repulsive state there should be no solution for which $h(R)$ increases exponentially with decreasing R, we find

$$h(K) = K_0\left(\frac{2}{\alpha'}e^{-\alpha'(R-R_1)/2}\right),$$

where $K_0(x)$ is a Bessel function of imaginary argument.

Since $K_0(x) \to \ln(2/x)$ for $x \to 0$, we have, for $R - R_1 \gg 1$,

$$h(R) \sim R + \omega;\quad \omega = -R_1 - (2/\alpha')\ln(1/\alpha'). \tag{16}$$

Using (9), (15), and (16) we easily find the asymptotic form of the radial functions $p(R) = R \times K(R)$ and $q(R) = RL(R)$:

$$p = (\lambda - \sqrt{3}\,\nu)R + (\lambda\vartheta - \sqrt{3}\,\nu\omega),$$

$$q = -(\lambda\sqrt{3} + \nu)R - (\lambda\sqrt{3}\,\vartheta + \nu\omega).$$

The constants λ and ν are to be fixed by using the condition that $p(R)$ contain only an outgoing wave e^{ik_0R} for $R \to \infty$, and from the normalization to unity of the probability density

in the incoming wave q(R).

Thus

$$p \approx \frac{\sqrt{3}\,(\vartheta-\omega)}{4-ik_0(3\omega+\vartheta)}(1+ik_0R),$$
$$q \approx R + \frac{(3\vartheta+\omega)-4ik_0R}{4-ik_0(3\omega+\vartheta)}. \qquad (17)$$

The cross section for transition to the lower hyperfine structure state is

$$\sigma = 4\pi\frac{k_0}{k}\frac{3(\vartheta-\omega)^2}{16+k_0^2(3\omega+\vartheta)^2}, \qquad (18)$$

or, inserting the numerical values of the parameters,

$$\sigma \approx \frac{3}{4}\frac{\varphi_0^2}{\alpha^2}\pi\frac{k_0}{k} \approx 150\pi\frac{k_0}{k}. \qquad (19)$$

The statistical weight of the spin ½ state of the system consisting of a μ meson and two protons is equal to ⅓. The probability of transition per unit time to the lower hyperfine structure state is

$$W = {}^1/_3\,\sigma v N \approx 50\pi a_\mu^2 v_0 N \approx 2\cdot 10^9\ \text{sec}^{-1} \qquad (20)$$

$(N = 4\cdot 10^{22}\ \text{cm}^{-3};\ v_0 = \sqrt{\Delta\varepsilon/M} \approx 5\cdot 10^5\ \text{cm/sec};$

$a_\mu = \hbar^2/m_\mu e^2 = 2.55\cdot 10^{-11}\ \text{cm}).$

This value may be somewhat high. Inclusion of terms $\sim m_\mu/M$ in the interaction potential energy and deviations E_g from the Morse function may cause a shift from resonance, and consequently, reduce the value of σ. However, since the transition probability (20) is at least three orders of magnitude greater than the probability of decay of the μ meson ($W_{dec} = 0.5\times 10^6\ \text{sec}^{-1}$), the conclusion that there is an almost complete transfer of the μ-mesic atom into the lower hyperfine structure state undoubtedly remains valid.*

This result has two unusual consequences.

First, μ^- mesons entering hydrogen should be completely depolarized.

Second, neutrons produced from μ^- capture by protons in the reaction $\mu^- + p = n + \nu$ should be completely polarized in the direction of their motion. For, since the capture of the μ meson occurs from the lower hyperfine structure state (the total angular momentum of the $\mu + p$ system is zero), and the neutrino is polarized along its direction of motion, our statement follows from the conservation laws.*

In conclusion, I express my deep gratitude to L. D. Landau and Ia. B. Zel'dovich for interest in the work and valuable remarks.

[1] E. Fermi, Z. Physik **60**, 320 (1930).

[2] L. D. Landau and E. M. Lifshitz, Квантовая механика (Quantum Mechanics), Gostekhizdat, 1948.

[3] G. Hertzberg, Molecular Spectra and Molecular Structure, New York, Prentice-Hall, 1939.

[4] H. A. Bethe, Handbuch der Physik, vol. 24-1, Berlin, Springer, 1933.

[5] Ia. B. Zel'dovich, Dokl. Akad. Nauk SSSR **95**, 493 (1954).

Translated by M. Hamermesh
81

*Since the wavelength of the μ meson is comparable to the dimensions of the H_2 molecule, it is necessary to treat the scattering of the μ meson by the H_2 molecule, and not by a free proton. This treatment leads to a difference in the cross sections for the process in para- and orthohydrogen, but does not change the basic conclusions of the present paper.

*For capture of the μ meson from both hyperfine structure levels, the polarization of the neutrons along their direction of motion would be a relativistic effect $\sim v_n/c$.

SOME REMARKS ON A COMPOUND MODEL OF ELEMENTARY PARTICLES

L. B. OKUN'

Submitted to JETP editor August 14, 1957; resubmitted October 31, 1957

J. Exptl. Theoret. Phys. (U.S.S.R.) **34**, 469-476 (February, 1958)

An examination is made of some properties of a compound model of elementary particles, in which Λ particles and nucleons are assumed as the primary particles.

1. INTRODUCTION

THE number of strongly interacting elementary particles is very large: already known at the present time are seven kinds of mesons, eight kinds of baryons (including Ξ^0), and eight kinds of antibaryons; two of these last ($\bar{p}$ and $\bar{n}$) have already been found, and scarcely anyone doubts that the others will be found in the very near future. This very abundance of strongly interacting particles makes one doubt their elementary nature. It is therefore quite natural that many papers have recently appeared in which attempts are made to reduce somehow the number of "elementary" particles by regarding them as compound systems constructed from a small number of "truly elementary" particles. The first step in this direction was made by Fermi and Yang,[1] who suggested that the π meson may be a bound state of a nucleon and an antinucleon. The compound models of the elementary particles that are being discussed at the present time can be divided into two groups.

The first group incldues schemes in which the basic particles are taken to be K mesons and nucleons (KN scheme), K mesons and Ξ hyperons (KΞ scheme), or K mesons and Λ hyperons (KΛ scheme). The KN scheme has been considered by Goldhaber,[2] Gyorgyi (D'erdi),[3] and Zel'dovich,[4] and the KΞ scheme has been discussed by Neganov.[5]

In our opinion these schemes have a number of shortcomings. In the first place, the construction of compound baryons and π mesons (if the latter are not also assumed to be elementary particles) requires two different types of forces: baryon-boson forces are used for the construction of the compound baryons, and baryon-antibaryon forces for the construction of π mesons. Secondly, the KN, KΛ, and KΞ schemes postulate the existence of two types of weak interactions: lepton-fermion, of type (np)(eν), and letpon-boson, of type K($\mu\nu$), since other wise one cannot explain all the various letpon decays of mesons and baryons. Thirdly, to explain the existence of the decays $K_{\mu 3}$ and K_{e3} in these schemes one must either introduce one more additional weak interaction with the leptons, or else introduce a strong interaction gKKπ, which is possible only if there is a parity doublet of K mesons (in this connection see Ref. 6). All this to a considerable extent deprives the KN, KΞ, and KΛ schemes of the economy which is the main motive for their construction.

The other group of schemes is essentially a generalization of the Fermi-Yang model. In Markov's model[7] all the hyperons were included along with nucleons as primary particles (NY scheme). In Sakata's model,[8] considered subsequently by King and Peaslee,[9] nucleons and Λ particles are taken as the elementary particles (NΛ scheme).

In this paper we make a number of remarks about the NΛ scheme, which obviously makes it possible to describe in a unified way both the structure and also the interactions of the various particles. Following Sakata we shall assume three particles to be the primary ones: the Λ hyperon, the proton, and the neutron. These primary particles have the same parity, spin, charge, and strangeness as the actual physical Λ, p, and n, but, generally speaking, the masses of the physical and primary particles can be different. In particular, we can assume that for the primary particles $m_\Lambda = m_N$. The values of the charge Q, the strangeness S, the isotopic spin T, the isotopic spin component T_3, the spin I, the parity P,* and the baryon number $\mathfrak{N}$ for the primary particles and antiparticles are shown below (a

*Since the weak interactions do not conserve parity and strong interactions conserve strangeness, the parity of the Λ particle, and also of other particles with $S = \pm 1$, is not a physically observable quantity. Therefore the choice of the parity of the Λ particle which we have made is purely conventional. As a physically observable quantity one has, for example, the product of the parities of Λ particle, K meson, and nucleon, $P_\Lambda P_K P_N$ (see below).

bar over a letter denotes the antiparticle).

	Q	S	T	T_3	I	P	$\mathfrak{N}$
p	+1	0	1/2	+1/2	1/2	+1	+1
$\bar{p}$	−1	0	1/2	−1/2	1/2	−1	−1
n	0	0	1/2	−1/2	1/2	+1	+1
$\bar{n}$	0	0	1/2	+1/2	1/2	−1	−1
Λ	0	−1	0	0	1/2	+1*	+1
$\bar{\Lambda}$	0	+1	0	0	1/2	−1*	−1

2. THE ISOTOPIC SCHEME

The isotopic scheme set forth in this section essentially repeats the contents of the paper of Sakata.[8]

The Mesons. The mesons are bound states of the primary particles and antiparticles with $\mathfrak{N} = 0$. Thus the π meson, having $T = 1$, is a bound state of a nucleon and an antinucleon:

$$T_3 = +1,\ \pi^+ = p\bar{n};\quad T_3 = -1,$$

$$\pi^- = \bar{p}n;\ T_3 = 0,\ \pi^0 = (p\bar{p} + n\bar{n})/\sqrt{2},$$

The K and $\bar{K}$ mesons, having $T = \frac{1}{2}$, are the bound states $N + \bar{\Lambda}$ and $\bar{N} + \Lambda$, respectively:

$$K^+ = p\bar{\Lambda},\quad T_3 = {}^1/_2;\quad K^0 = n\bar{\Lambda},\quad T_3 = -{}^1/_2;$$
$$K^- = \bar{p}\Lambda,\quad T_3 = -{}^1/_2;\quad \bar{K}^0 = \bar{n}\Lambda,\quad T_3 = {}^1/_2.$$

Thus the strangeness of the K meson is $S = +1$, and for the $\bar{K}$ meson $S = -1$.

In the framework of this scheme there is the possibility of two additional neutral mesons, which have not so far been observed:

$$\rho_1^0 = \Lambda\bar{\Lambda},\quad \rho_2^0 = (p\bar{p} - n\bar{n})/\sqrt{2}.$$

The isotopic spin of the ρ mesons is zero. Their other properties are considered briefly in Sec. 3.

The Hyperons. In the present scheme the hyperons are bound states of two particles and one antiparticle with $\mathfrak{N} = 1$.

Thus the Σ particle with $T = 1$ can be represented in the form

$$\Sigma^+ = p\bar{n}\Lambda,\quad T_3 = +1;\quad \Sigma^- = \bar{p}n\Lambda,\quad T_3 = -1;$$
$$\Sigma^0 = (p\bar{p}\Lambda + n\bar{n}\Lambda)/\sqrt{2},\quad T_3 = 0.$$

In an equally natural way one gets the isotopic doublet of the cascade particle:

$$\Xi^- = \Lambda\Lambda\bar{p},\ T_3 = -{}^1/_2;\quad \Xi^0 = \Lambda\Lambda\bar{n},\quad T_3 = +{}^1/_2.$$

The isotopic multiplets of the antihyperons are obtained from the hyperon multiplets by the interchange $\Lambda \longleftrightarrow \bar{\Lambda}$, $n \longleftrightarrow \bar{n}$, $p \longleftrightarrow \bar{p}$.

3. SPIN AND PARITY

The data on the spins and parities of the Λ particle, the proton, and the neutron are shown in the table.

It is well known that the π meson has spin $I = 0$ and parity $P = -1$. This means that the primary nucleon and antinucleon forming the π meson are in a $^1S_0$ state. It is natural to assume that the particles forming the K meson are also in a $^1S_0$ state. Then we find that, like the π meson, the K meson has $I = 0$ and $P = -1$. The entire body of experimental data relating to the weak interactions of K mesons (decays), and also to the strong interactions, indicates that the spin of the K meson is zero. As regards the parity of the K meson, it is as yet unknown. In our present model $P_K P_N P_\Lambda = -1$. In the KN scheme, in the form considered by Zel'dovich,[4] for example, $P_K P_N P_\Lambda = +1$. In this connection the measurement of the quantity $P_K P_N P_\Lambda$ is of great importance as a test of the correctness of our present scheme.

Assuming that the particles forming the ρ^0 meson are also in a $^1S_0$ state, we find that in this case $I = 0$, $P = -1$. The masses of ρ^0 mesons must obviously be considerably larger than those of π mesons, since otherwise a number of effects would occur which could not have remained unobserved. In particular, the existence of ρ^0 mesons would manifest itself in the phase-shift analysis of the scattering of π mesons by nucleons, since in addition to the process $\pi^- + p \to \pi^0 + n$ the process $\pi^- + p \to \rho^0 + n$ would also occur. Another example of a possible manifestation of the ρ^0 meson is the decay of the K meson. For example, besides the decay $K^+ \to \pi^+ + \pi^0$ there would have to occur the decay $K^+ \to \pi^+ + \rho^0$. We note that for this decay one does not have the forbidden character arising from the selection rule $\Delta T = \frac{1}{2}$, which decreases the probability of the decay $K^+ \to \pi^+ + \pi^0$ by a factor of several hundred. This is readily understood if we note that for the system $\pi^+ + \pi^0$ with $I = 0$ the state with $T = 1$ is forbidden, while for the system $\pi^+ + \rho^0$ it is allowed.

It is possible that the presence of a maximum at $E = 900$ Mev in the scattering of π^- mesons is due to the ρ^0 meson. In this case the mass of the ρ^0 meson must be of the order of the nucleonic mass. Such a ρ^0 meson should decay into three π mesons (the decay into two π mesons is forbidden by parity) in a time of the order of 10^{-23} sec.

If we make no additional assumptions, nothing can be said about the spins and parities of the Σ and Ξ particles within the framework of our present model.

4. THE STRONG INTERACTIONS

The interactions leading to the formation of bound baryon-antibaryon systems must be stronger than ordinary nuclear forces by several orders of magnitude. It is known that the depth of the potential well in nuclei is on the order of 30 Mev. The estimate made by Fermi and Yang[1] of the depth of the "well" containing the nucleon and antinucleon forming a π meson gave a value on the order of 30 Bev (on the assumption that the radius of the well is $r \sim \hbar/M_N c$). The presence of such a strong interaction between nucleons and antinucleons is confirmed by the measurements recently made of the interaction cross-sections between antinucleons and nucleons. Fermi and Yang assumed further that also between two nucleons, in addition to the usual interaction, there is a strong interaction comparable in magnitude and range with that between nucleon and antinucleon, but that this nucleon-nucleon interaction is a repulsive one.

As a generalization of the idea of Fermi and Yang it is natural to postulate that there is a strong interaction between any two baryons, attractive in the case of particle interacting with antiparticle, and repulsive in the case of two particles or two antiparticles. In our present model there are three types of vertex parts, corresponding to:

(a) the interaction of nucleon with nucleon (interaction constant g_1);

(b) the interaction of a nucleon with a Λ particle (constant g_2);

(c) the interaction of two Λ particles (constant g_3) (see Fig. 1).

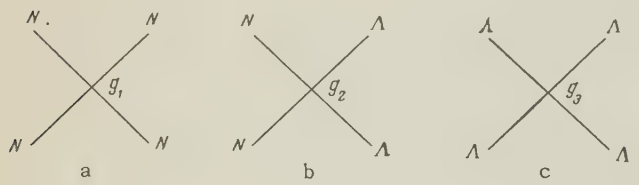

FIG. 1

The interaction characterized by the constant g_1 is responsible for the formation of a bound state of a nucleon and an antinucleon — the π meson. This same interaction is responsible for the production of nucleon-antinucleon pairs, the production of π mesons, and so on. The processes caused by the interaction g_1 are well described by a statistical theory.

The interaction characterized by the constant g_2 is responsible for the formation of a bound state of a nucleon and an antihyperon — the K meson. This same interaction is responsible for the production of hyperon-antihyperon pairs, the production of K mesons, and so on. Indeed, any process in which strange particles appear from collisions of ordinary particles must include at least one vertex of the type g_2, corresponding to the production of a pair $\Lambda + \bar{\Lambda}$. The fact that the mass of the K meson is considerably larger than π meson masses suggests that the interaction g_2 is weaker than the interaction g_1. The same thing is indicated by numerous experiments such as those reported at the 1957 Rochester conference, according to which the cross-sections for the production of K mesons by the action of γ rays, π mesons, and nucleons are about an order of magnitude smaller than the corresponding π-meson cross-sections and the cross-sections obtained on the basis of statistical calculations.

If we proceed on the assumption that $g_2 < g_1$, it must be expected that the cross-section for the production of a real hyperon-antihyperon pair in a beam of π mesons or nucleons must be smaller by about an order of magnitude than the cross-section for the production of a nucleon-antinucleon pair, if we consider both processes sufficiently far from their thresholds. On the other hand, the cross-section for the production of an antihyperon-nucleon pair in collisions of K^+ mesons with nucleons may not turn out to be small, since in this case there will occur a reaction analogous to the disintegration of the deuteron and not involving the relatively weak interaction g_2:

$$K^+ + p = (\bar{\Lambda} + p) + p \xrightarrow{g_1} \bar{\Lambda} + p + p.$$

The same also applies to the cross-section for scattering of $K^{\pm}$ mesons, which, as is well known, is not small. This process can go through the vertex g_1 alone. Another cross-section which turns out not to be small is that for absorption of K^- mesons (reactions of the type $K^- + p \to \Sigma^- + \pi^+$), which can also go through the strong interaction g_1 alone.

Thus in our present scheme the smallness of the cross-section for production of strange particles does not necessarily bring with it smallness of the cross-sections for their scattering and their conversion into other strange particles, since basically different interactions are responsible for these processes. This conclusion is in qualitative agreement with a large body of experimental data, according to which strange particles have small cross-sections for production, but large cross-sections for absorption and scattering.

We note that this peculiarity of strange particles does not find its reflection in the model recently proposed by Gell-Mann.[10] According to this model all interactions of baryons with π mesons

are equally strong, and the interaction of baryons with K mesons is relatively weak. The conclusions obtained from this are directly contradictory to those at which we arrived above. In particular, according to Gell-Mann's model the cross-sections for scattering of $K^{\pm}$ mesons and that for absorption of K^- mesons must be small. The cross-section for production of a hyperon-antihyperon pair in a beam of π mesons or nucleons must be larger than the cross-section for production of a nucleon-antihyperon pair in a beam of K mesons.

At the present time one cannot draw any conclusions about the strength of the interaction of two Λ particles at small distances (about the quantity g_3). If $g_3 \sim g_1$, then the ratio of the probability of production of four strange particles to that for production of two strange particles must be determined by just the statistical weights. If $g_3 \sim g_2$, it must be an order of magnitude smaller than this. These considerations are also entirely applicable to the production of a cascade particle: if $g_3 \sim g_1$, the production of a Ξ particle in collisions of nucleons must have a probability comparable with that for the production of the other hyperons (Λ and Σ). If, on the other hand, $g_3 \sim g_2$, the probability for Ξ production must be smaller than that for production of Λ or Σ by about an order of magnitude.

5. THE WEAK INTERACTIONS

Two types of decays of baryons and mesons are known: lepton decays and non-lepton decays, the latter being characteristic of strange particles only. A feature that these two types of decay have in common is that the interactions causing them have coupling constants of the same order of magnitude ($F^2 \sim f^2 \sim 10^{-13}$ in units $\hbar = c = \mu_\pi = 1$) and do not conserve spatial and charge-conservation parity. We shall consider first the non-lepton decays, assuming the simplest type of weak interaction between the "primary" particles.

Non-lepton Decays. Examples of these are such as $K \to 2\pi$, $K \to 3\pi$, $\Lambda \to N + \pi$, $\Sigma \to N + \pi$, $\Xi \to \Lambda + \pi$, the decays of hyperfragments, and so on. Any one of the non-lepton decays known at present can be described as a process in which one of the links in the slow transition $\Lambda \longleftrightarrow N$ and all of the other links are fast transitions that conserve strangeness. The simplest assumption would seem to be that the $\Lambda \longleftrightarrow N$ transition is a single-particle process, i.e., can be described by the diagram of Fig. 2. But, as can easily be seen, such

FIG. 2

an interaction would lead* to the strict (apart from electromagnetic corrections) selection rule $\Delta T = \frac{1}{2}$ for all non-lepton decays of strange particles (and hyperfragments). Since cases occur in which the rule $\Delta T = \frac{1}{2}$ is known to be violated, we are forced to resort to a more complicated class of slow interactions — two-particle interactions described by the diagrams of Fig. 3.†

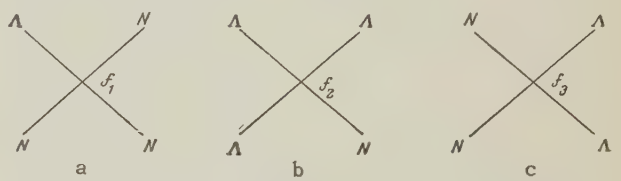

FIG. 3

The interactions described by the constant f_3 (transition of two nucleons into two Λ particles) has not been observed so far. If f_3 were to turn out to be comparable with f_1 and f_2, processes with $\Delta S = \pm 2$ would have probabilities comparable with those of processes with $\Delta S = \pm 1$, to which the first two diagrams of Fig. 3 correspond. In particular, the decay $\Xi^- \to n + \pi^-$ would have to occur, and the mass difference of the K_1^0 and K_2^0 mesons would be of the order $\Delta m \sim f_3 \mu_\pi \sim 10 - 100$ ev, where f_3 is the dimensionless constant of the weak interaction ($f_3 \sim 10^{-6} - 10^{-7}$) and μ_π is the mass of the π meson. (If $f_3 = 0$ the mass difference of K_1^0 and K_2^0 is $\Delta m \sim f_1^2 \times \mu_\pi \sim f_2^2 \mu_\pi \sim 10^{-5}$ ev). We shall not go further into the discussion of this question, since it has been dealt with in detail in a paper by Pontecorvo and the writer.[11] As for the vertices f_1 and f_2, it is easy to see that for them $\Delta S = \pm 1$; for f_1, $\Delta T = \frac{1}{2}, \frac{3}{2}$, and for f_2, $\Delta T = \frac{1}{2}$. If the rule $\Delta T = \frac{1}{2}$ holds approximately, this means that $f_1 \ll f_2$. None of the vertices of Fig. 3 gives transitions with $\Delta T = \frac{5}{2}$, so that such transitions are forbidden. Recently Gell-Mann[12] called attention to the fact that the experimental ratio of the probabilities for the decays $K^0 \to 2\pi^0$ and $K^0 \to \pi^+ + \pi^-$ indicates that transitions with $\Delta T = \frac{5}{2}$ occur. If the experimental data in question are correct, this means that in the framework of our present scheme

*An essential assumption in this proof is that all strong interactions are isotopically invariant.

†We do not distinguish in the diagrams between particles and antiparticles. The vertex f_3 (Fig. 3) differs from the vertex g_2 (Fig. 1) by the fact that for the former $\Delta S = 2$, while for the latter $\Delta S = 0$.

it becomes necessary to introduce three-particle weak interactions of the type shown in Fig. 4, since they alone can give $\Delta T = 5/2$. It seems undesirable to resort to such three-particle weak interactions, and therefore if the presence in the weak interactions of an amplitude with $\Delta T = 5/2$ were proved this would, in our opinion, be a strong argument against the scheme discussed here.

FIG. 4

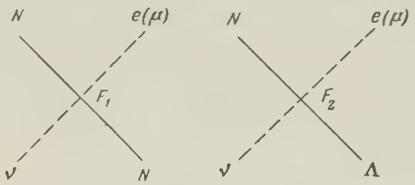

FIG. 5

Lepton Decays. Examples of lepton decays of ordinary particles are the decays $\pi \to \mu + \nu$ and $n \to p + e + \nu$; examples of lepton decays of strange particles are the decays $K \to \mu + \nu$, $K \to \mu + \nu + \pi$, and $K \to e + \nu + \pi$. Lepton decays of hyperons have so far not been observed. In the NΛ scheme two types of interactions of the primary baryons with leptons are possible (see Fig. 5). The interaction F_1 causes lepton processes in which π mesons and nucleons are involved. The interaction F_2 causes lepton processes involving K mesons and hyperons. Moreover, it is easy to see that decays

$$\Lambda \to p + e^-(\mu^-) + \bar{\nu},$$

should occur, which have not been observed so far, and that decays of Λ to $e^+(\mu^+)$ are forbidden, since there is no negative primary baryon. Similarly there should be decays

$$\bar{\Lambda} \to \bar{p} + e^+(\mu^+) + \nu$$

and decays of $\bar{\Lambda}$ to $e^-(\mu^-)$ are forbidden. Since in our present scheme all lepton decays in which the strangeness of strongly interacting particles changes have to go by way of the lepton decay F_2 of the Λ ($\bar{\Lambda}$) particle, it follows that in decays with $\Delta S = -1$ and $e^+(\mu^+)$ must appear.

The result is that the decays $K^0 \to e^+(\mu^+) + \nu + \pi^-$ and $\bar{K}^0 \to e^-(\mu^-) + \bar{\nu} + \pi^+$ turn out to be allowed, and the decays $K^0 \to e^-(\mu^-) + \bar{\nu} + \pi^+$ and $\bar{K}^0 \to e^+(\mu^+) + \nu + \pi^-$ are forbidden. As is shown in Ref. 6, this leads to a quite definite time dependence of the ratio of the numbers of $e^+(\mu^+)$ and $e^-(\mu^-)$ decays in a beam of neutral K mesons, namely:

$$\frac{n_{e^+}}{n_{e^-}} = \frac{n_{\mu^+}}{n_{\mu^-}} = \frac{e^{-t/\tau_1} + e^{-t/\tau_2} + 2e^{-t/2\tau_1 - t/2\tau_2}\cos(\Delta m t)}{e^{-t/\tau_1} + e^{-t/\tau_2} - 2e^{-t/2\tau_1 - t/2\tau_2}\cos(\Delta m t)}.$$

Here n is the number of the decays in question per unit time and τ_1 and τ_2 are the lifetimes of the K_1^0 and K_2^0 mesons, the former of which has time (combined) parity +1 and the latter, −1. (We assume that the time parity is conserved in the slow decays.) Δm is the difference of the masses of the K_1^0 and K_2^0 mesons.

Another example is that of the decays $\Sigma^+ \to n + e^+(\mu^+) + \nu$; according to the above statements, these decays are forbidden, while the decays $\Sigma^- \to n + e^-(\mu^-) + \bar{\nu}$ are allowed. Similarly, the decays $\Xi^0 \to \Sigma^- + e^+(\mu^+) + \nu$ are forbidden, and the decays $\Xi^0 \to \Sigma^+ + e^-(\mu^-) + \bar{\nu}$ are allowed. We note that the decays $\Sigma^+ \to \Lambda + e^+ + \nu$ and $\Sigma^- \to \Lambda + e^- + \bar{\nu}$, which go through the vertex F_1, are allowed in our present scheme.

Since all lepton decays with change of strangeness go by way of the decay of Λ ($\bar{\Lambda}$), it is easy to see that for these decays the rule $\Delta S = \pm 1$ must hold, where S is the strangeness of the strongly interacting particles. From this it follows that the decays

$$\Xi^- \to n + e^-(\mu^-) + \bar{\nu} \text{ and } \Xi^0 \to p + e^-(\mu^-) + \bar{\nu}$$

must be forbidden, while the decays $\Xi^- \to \Lambda + e^-(\mu^-) + \bar{\nu}$ are allowed.

Since in the transition $\Lambda \to p + e^-(\mu^-) + \bar{\nu}$ the isotopic spin of the strongly interacting particles changes by $\Delta T = \frac{1}{2}$, it follows that in all lepton decays of strange particles the isotopic spin of the strongly interacting particles changes by $\Delta T = \frac{1}{2}$.* This makes it possible to obtain a relation between the probabilities of the decays

$$K^+ \to e^+(\mu^+) + \nu + \pi^0 \text{ and } K^0 \to e^+(\mu^+) + \nu + \pi^-.$$

Here it turns out that[6]

$$w(K^0) = 2w(K^+).$$

All these conclusions are obtained if we assume that the interactions of strange particles with leptons are represented by the diagram F_2. If we admit the possibility of the existence of more complicated interactions (see, for example, Fig. 6), the rules of forbiddenness and the ratios obtained above disappear. But the consideration of such interactions seems to us extremely artificial.

6. CONCLUSIONS

It can be seen from the above that the NΛ scheme makes it possible to give a more or less satisfactory qualitative description of the existing

*In decays of particles with S = 0 (π mesons and nucleons), $\Delta T = 0.1$.

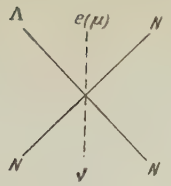

FIG. 6

experimental data and to make a number of predictions which can be tested experimentally. These predictions relate to both the strong and the weak interactions of strange particles. It must be emphasized, however, that many of these conclusions, in particular those relating to the strong interactions, are of an extremely qualitative nature and cannot be considered completely convincing.

As for experimental tests of the NΛ model, it is quite obvious that the experimental confirmation of any particular conclusions among those drawn above cannot by any measure serve as a demonstration of the correctness of the NΛ model, since one could have arrived at these very same conclusions on the basis of an entirely different physical picture (cf. in this connection Ref. 6). A disagreement between the conclusions drawn above and experiment will mean that the assumptions which we have made within the framework of the model, and which appear extremely plausible, are incorrect.

In conclusion we remark that the model that has been considered may take on considerably greater interest if the study of the possibility of constructing a theory of strongly interacting Fermi fields[5] has a successful outcome.

The writer is grateful to I. Ia. Pomeranchuk and Ia. B. Zel'dovich for their interest in this work and for discussions.

[1] E. Fermi and C. N. Yang, Phys. Rev. **76**, 1739 (1949).

[2] M. Goldhaber, Phys. Rev. **101**, 433 (1956).

[3] Geza D'erdi (Gyorgyi), J. Exptl. Theoret. Phys. (U.S.S.R.) **32**, 152 (1957), Soviet Phys. JETP **5**, 152 (1957).

[4] Ia. B. Zel'dovich, J. Exptl. Theoret. Phys. (U.S.S.R.) **33**, 829 (1957), Soviet Phys. JETP **6**, 641 (1958).

[5] B. Neganov, J. Exptl. Theoret. Phys. (U.S.S.R.) **33**, 260 (1957), Soviet Phys. JETP **6**, 200 (1958).

[6] L. B. Okun', J. Exptl. Theoret. Phys. (U.S.S.R.) **32**, 400 (1957), Soviet Phys. JETP **5**, 334 (1957).

[7] M. A. Markov, О систематике элементарных частиц (On Systematics of the Elementary Particles), Acad. Sci. Press, 1955.

[8] S. Sakata, Prog. Theor. Phys. **16**, 686 (1956).

[9] R. W. King and D. C. Peaslee, Phys. Rev. **106**, 360 (1957).

[10] M. Gell-Mann, Phys. Rev. **106**, 1296 (1957).

[11] L. Okun' and B. Pontecorvo, J. Exptl. Theoret. Phys. (U.S.S.R.) **32**, 1587 (1957), Soviet Phys. JETP **5**, 1297 (1957).

[12] M. Gell-Mann, Nuovo cimento **5**, 758 (1957).

Translated by W. H. Furry
82

ON THE POLARIZATION OF THE CERENKOV RADIATION FROM A FAST PARTICLE CARRYING A MAGNETIC MOMENT

Iu. M. LOSKUTOV and A. B. KUBANOV

Moscow State University

Submitted to JETP editor August 21, 1957

J. Exptl. Theoret. Phys. (U.S.S.R.) **34**, 477-482 (February, 1958)

The problem of the polarization of the Cerenkov radiation from a magnetic moment moving in a ferrodielectric material is treated by the methods of quantum electrodynamics. Calculations are made of both the part of the radiated intensity accompanied by flip of the spin ($ss' = -1$) and the part of the intensity emitted without spin-flip ($ss' = +1$). It is shown that the radiation is composed of a polarized part (which vanishes at the threshold, $\cos\theta = 1$) and an unpolarized part (which does not vanish at the threshold). The unpolarized part of the radiation is accompanied by spin-flip.

The energy losses are treated by classical methods, and the separation of the losses into Cerenkov loss and ionization loss is indicated.

THE problem of the polarization of the Cerenkov radiation of a charge in a dielectric has been dealt with by Sokolov and Loskutov,[1] who have shown that the radiation is partially polarized and does not vanish at the threshold; this last fact is due to the presence of the spin of the electron. It is not hard to show that in the case of the motion of a charge through a ferrodielectric material one gets for the intensity radiated per unit length the formulas

$$W_3 = \frac{e^2}{c^2}\int_0^{\omega_{max}} \mu(\omega)\,\omega\left\{\frac{n^2\omega^2\hbar^2}{4c^2p^2}(1-n^{-2}) + (1-\cos^2\theta)\right\}d\omega, \quad (1)$$

$$W_2 = \frac{e^2}{c^2}\int_0^{\omega_{max}} \mu(\omega)\,\omega\frac{n^2\omega^2\hbar^2}{4c^2p^2}(1-n^{-2})\,d\omega, \quad (2)$$

where W_3 and W_2 are the intensities respectively in and perpendicular to the plane $(\kappa\mathbf{k})$ and $n = (\epsilon\mu)^{1/2}$.

Comparing Eqs. (10) and (11) of Ref. 1 with Eqs. (1) and (2), we see that inclusion of the effect of the magnetic susceptibility of the medium does not change the nature of the polarization of the radiation in the dielectric.

1. POLARIZATION OF THE CERENKOV RADIATION OF A MAGNETIC MOMENT

(a) As is well known, the operator for the interaction energy of a magnetic moment μ_0 and the electromagnetic field in a medium is given by

$$W = \mu_0\rho_3(\sigma\mathbf{B}) + \mu_0\rho_2(\sigma\mathbf{E}), \quad (3)$$

where ρ_3, ρ_2, and σ are Dirac matrices.

The expression for the vector potential $\mathbf{A}$ of the quantized transverse electromagnetic field in a medium characterized by the constants $\epsilon(\omega)$ and $\mu(\omega)$ can be written in the form (cf. Ref. 2)

$$\mathbf{A} = L^{-3/2}\sum_{\varkappa}(2\pi c''\hbar/\varkappa)^{1/2}[\mathbf{a}\exp(-ic'\varkappa t + i\varkappa\mathbf{r}) + \mathbf{a}^+\exp(ic'\varkappa t - i\varkappa\mathbf{r})], \quad (4)$$

where $c' = c/(\epsilon\mu)^{1/2}$, $c'' = c'\mu$; $\hbar\varkappa$ is the momentum of a photon; and the amplitudes $\mathbf{a}$ and $\mathbf{a}^+$ obey the commutation relations

$$a_n a'^+_{n'} - a'^+_{n'}a_n = \delta_{\varkappa\varkappa'}(\delta_{nn'} - \varkappa^{-2}\varkappa_n\varkappa_{n'}). \quad (5)$$

In particular, when there are no photons in the initial state (as we shall assume in what follows) we can set

$$a'^+_{n'}a_n = 0,\quad a_n a'^+_{n'} = \delta_{\varkappa\varkappa'}(\delta_{nn'} - \varkappa^{-2}\varkappa_n\varkappa_{n'}). \quad (6)$$

To study the polarization of the radiation we resolve the amplitude $\mathbf{A}$ of the vector potential into components (cf. Ref. 3) which characterize definite states of polarization:

$$\mathbf{a} = \mathbf{a}_2 + \mathbf{a}_3 = \beta_2 q_2 + \beta_3 q_3,$$
$$\beta_2 = [\varkappa^0\mathbf{k}^0]/\sqrt{1-(\varkappa^0\mathbf{k}^0)^2},\quad \beta_3 = [\varkappa^0\beta_2] \quad (7)$$

in the case of linear polarization, and

$$\mathbf{a} = \mathbf{a}_1 + \mathbf{a}_{-1} = \beta_1 q_1 + \beta_{-1} q_{-1},$$
$$\sqrt{2}\,\beta_\lambda = \beta_2 + i\lambda\beta_3, \quad \lambda = 1, \ -1 \tag{8}$$

in the case of circular polarization. Here $\boldsymbol{\kappa}^0$ is a unit vector in the direction of $\boldsymbol{\kappa}$ and $\mathbf{k}^0$ is a unit vector along the direction of motion of the magnetic moment. In Eqs. (7) and (8) the quantum part of the amplitudes satisfies the relations

$$q_{j'}^+ q_j = 0, \ q_j q_{j'}^+ = \delta_{jj'}; \quad j, \ j' = 2, \ 3, \ 1, \ -1. \tag{9}$$

Using the fact that

$$\mathbf{B} = \operatorname{curl} \mathbf{A}, \quad \mathbf{E} = -\frac{1}{c}\frac{\partial \mathbf{A}}{\partial t},$$

and also recalling the absence of photons in the initial state, we find for the interaction energy operator W^+ (cf. Ref. 3)

$$W_j^+ = -i\mu_0 L^{-3/2} \sum_{\varkappa} (2\pi c''\hbar/\varkappa)^{1/2} \exp\{i(c'\varkappa t - \varkappa \mathbf{r})\}$$
$$\times \left\{\rho_3 (\sigma [\varkappa \mathbf{a}_j^+]) + \frac{c'}{c} \varkappa \rho_2 (\sigma \mathbf{a}_j^+)\right\}. \tag{10}$$

By the use of the methods of perturbation theory it is not hard to find (cf. Ref. 4) the probability of emission of radiation by the magnetic moment:

$$W_j = \frac{2\pi}{c\hbar^2} \sum_{\mathbf{k}', \varkappa} R_j^+ R_j \delta_{\mathbf{k}, \mathbf{k}'+\varkappa} \delta(K' + \varkappa/n - K), \tag{11}$$

where

$$R_j = -i\mu_0 L^{-3/2} (2\pi c''\hbar/\varkappa)^{1/2} b'^+ \left\{\rho_3 (\sigma [\varkappa \mathbf{a}_j^+]) + \frac{c'}{c} \varkappa \rho_2 (\sigma \mathbf{a}_j^+)\right\} b,$$

k, $K = (k^2 + k_0^2)^{1/2}$ and k', $K' = (k'^2 + k_0^2)^{1/2}$ correspond to the magnitudes of the momenta ($\hbar k$, $\hbar k'$) and energies ($c\hbar K$, $c\hbar K'$) of the magnetic moment respectively before and after the act of emission. Calculating out the required matrix elements (cf. Ref. 5, Sec. 21) to find W_j by Eq. (11), we get the expression

$$W_j = \frac{c\mu_0^2}{16\pi} \int \frac{\varkappa^2}{n^2} \delta(K' + \varkappa/n - K)\, d^3\varkappa$$
$$\times \sum_{s, s'} \left\{\left(1 - ss' \frac{kk'}{KK'} + \frac{k_0^2}{KK'}\right)\left[\left(1 - ss' \frac{(\mathbf{kk'})}{kk'}\right)\right.\right.$$
$$\left. + 2ss' \frac{(\mathbf{k}[\varkappa^0 \mathbf{a}_j])(\mathbf{k}'[\varkappa^0 \mathbf{a}_j^+])}{kk'}\right]$$
$$+ \frac{c'^2}{c^2}\left(1 - ss' \frac{kk'}{KK'} - \frac{k_0^2}{KK'}\right)\left[\left(1 - ss' \frac{(\mathbf{kk'})}{kk'}\right) + 2ss' \frac{(\mathbf{ka}_j)(\mathbf{k'a}_j^+)}{kk'}\right]$$
$$\left. + 2\frac{c'}{c}\left(s\frac{k}{K} - s'\frac{k'}{K'}\right)\left(\frac{1}{kk'}(sk'\mathbf{k} - s'k\mathbf{k}')\left[[\varkappa^0 \mathbf{a}_j]\ \mathbf{a}_j^+\right]\right)\right\},$$
$$(j = 2, \ 3), \tag{12}$$

where s and s' are the spins of the magnetic-moment particle respectively before and after the emission of the photon.

(b) For the intensity of the radiation per unit length we find after averaging over the spin states

$$W_j = \mu_0^2 \int_0^{\omega_{\max}} \frac{n^2\omega^3}{\beta^2 c^4} \mu(\omega) \{(j-2)\beta^2 (1 - \cos^2\theta)$$
$$+ (1 - \beta^2)\}(1 - n^{-2})\, d\omega, \tag{13}$$

$$(j = 2, 3); \quad W_1 = W_{-1} = {}^1/_2 (W_2 + W_3), \tag{14}$$

θ is the angle between the directions of travel of the emitted photon and of the magnetic moment.

(c) For the intensities of the radiation per unit length in the cases of spin-flip ($ss' = -1$, upper sign) and of absence of spin-flip ($ss' = +1$, lower sign) we get

$$W_j(\mp) = \frac{1}{4}\mu_0^2 \int_0^{\omega_{\max}} \frac{n^2\omega^3}{\beta c^4} \mu(\omega) \left[\frac{2}{\beta}\left\{(j-2)\beta^2 (1 - \cos^2\theta)\right.\right.$$
$$\left. + (1 - \beta^2)\right\}(1 - n^{-2}) \pm \Gamma\left\{\beta(1 + n^{-2}) - \frac{2}{n}\cos\theta\right\}$$
$$\pm \Gamma^{-1}\left\{\left(1 + (j-3)\,2\sin^2\theta - \frac{n\omega\hbar}{cp}\cos\theta\right)(2/\beta - \beta - \omega\hbar/cp)\right.$$
$$+ \frac{1}{n^2}\left(1 - (j-2)\,2\sin^2\theta - \frac{n\omega\hbar}{cp}\cos\theta\right)(\beta - \omega\hbar/cp) \tag{15}$$
$$\left.\left. - \frac{2}{n}(\cos\theta - n\omega\hbar/cp)\left(1 - \beta\frac{\omega\hbar}{cp}\right)\right\}\right] d\omega, \quad (j = 2, \ 3),$$

$$W_1(\mp) = W_{-1}(\mp) = {}^1/_2 (W_2(\mp) + W_3(\mp)), \tag{16}$$

where

$$\Gamma = (1 - (2n\omega\hbar/cp)\cos\theta + n^2\omega^2\hbar^2/c^2p^2)^{1/2}.$$

According to Eq. (15) we get for the radiation at the threshold

$$W_j(+) = 0, \tag{17}$$

$$W_j(-) = \mu_0^2 \int_0^{\omega_{\max}} \frac{n^2\omega^3}{\beta^2 c^4} \mu(\omega)(1 - \beta^2)(1 - n^{-2})\, d\omega. \tag{18}$$

It can be seen from Eqs. (13) and (14) that the radiation is partially polarized and is nonvanishing at the threshold; Eqs. (17) and (18) show that this last fact is due to the spin-flip, i.e., is a purely quantum effect. Also not without importance is the fact that the polarized and unpolarized parts of the radiation are of the same order of magnitude, and for $1/n < \beta < ({}^2/_3 + 1/n^2)^{1/2}$ the unpolarized part even exceeds the polarized. We note in passing that the threshold radiation vanishes in the ultrarelativistic approximation, just as in the classical approximation. The result of Eq. (18), that the radiation at the threshold is finite, is a consequence of the fact that, as is shown by calculation [by means of Eq. (12)], in the case

of absence of spin-flip the probability of emission of radiation at threshold is zero, but with spin-flip it remains finite.

The fact that the threshold radiation of a magnetic electron described by the Pauli equation is nonvanishing has been pointed by Ginzburg.[6]

2. ENERGY LOSS OF A MAGNETIC MOMENT MOVING THROUGH A FERRODIELECTRIC MEDIUM

In dealing with the energy loss in a ferrodielectric medium we shall assume that the direction of the magnetic moment coincides with the direction of motion. In this case the electric moment $\mathbf{p}$ appearing because of the motion of the magnetic moment is zero. The equations for the potentials must here be written in the form

$$\Delta \mathbf{A} - (\varepsilon\mu/c^2)\,\partial^2\mathbf{A}/\partial t^2 = -4\pi\mu \operatorname{curl}\mathbf{M},$$
$$\Delta\varphi - (\varepsilon\mu/c^2)\,\partial^2\varphi/\partial t^2 = 0, \tag{19}$$

where $\mathbf{M} = \mu_0\delta(\mathbf{r} - \mathbf{r}_\xi)$ and $\mathbf{r}_\xi(t)$ specifies the position of the magnetic moment.

Setting $\varphi \equiv 0$, we have for the intensities of the electric and magnetic fields

$$\mathbf{E} = -\frac{1}{c}\frac{\partial \mathbf{A}}{\partial t}, \quad \mathbf{H} = \frac{1}{\mu}\operatorname{curl}\mathbf{A}, \tag{20}$$

and setting $\mathbf{A} = \operatorname{curl}\boldsymbol{\Pi}$, where $\boldsymbol{\Pi}$ is the magnetic polarization potential, we get the equation

$$\Delta\boldsymbol{\Pi} - \frac{\varepsilon\mu}{c^2}\frac{\partial^2\boldsymbol{\Pi}}{\partial t^2} = -4\pi\mu\mu_0\,\delta(\mathbf{r} - \mathbf{r}_\xi). \tag{21}$$

In the case of uniform motion of the magnetic moment along the z axis (for method of solution of such equations see, for example, Ref. 7 or Ref. 8) we find

$$\boldsymbol{\Pi} = \frac{\mu_0}{\pi}\int \mu K_0(\zeta r)\exp\{i\varkappa(z - vt)\}\,d\varkappa, \tag{22}$$

where $K_0 = (\pi i/2)H_0^{(1)}(i\zeta r)$ and $\kappa = \omega/c$. Here

$$\zeta = \varkappa(1 - \varepsilon\mu\beta^2)^{1/2}\operatorname{sign}\operatorname{Re}\varkappa(1 - \varepsilon\mu\beta^2)^{1/2},$$

and $H_0^{(1)}$ is the Hankel function.

For the energy loss W_b in collisions with impact parameter larger than b we compute the flux of the Umov-Poynting vector through the lateral surface of a cylinder of radius b surrounding the z axis:

$$W_b = \frac{c}{4\pi v}\int_{\tilde{c}} \mathbf{E}\times\mathbf{H}\,d\mathbf{S}$$
$$= \frac{b\mu_0^2}{\pi v^2}\operatorname{Re}\int_{-\infty}^{+\infty} i\omega\mu^*(\omega)\,\zeta^*\zeta^2\,K_0(\zeta b)\,K_1(\zeta^* b)\,d\omega, \tag{23}$$

where $d\mathbf{S}$ is a surface element of the cylinder.

In the derivation of Eq. (23) we have used the relations (20) and (22), and also the formulas

$$K_{n+1}(\xi) - K_{n-1}(\xi) = 2nK_n(\xi)/\xi,$$
$$dK_n(\xi)/d\xi = -K_{n-1}(\xi) - \frac{n}{\xi}K_n(\xi).$$

In proceeding to the consideration of small values of the parameter b (of the order of interatomic distances), regarding the extinction coefficients in the actual expressions for ϵ and μ as finite, we can confine ourselves to the first terms of the expansions of the Bessel functions $K_0(\xi)$ and $K_1(\xi)$ (since $|\zeta b| \ll 1$):

$$K_1 = 1/\zeta^* b,\ K_0(\zeta b) = \frac{1}{2}\ln(4/3.17\,\zeta^2 b^2).$$

Consequently, at small impact parameters we have for W_b

$$W_b = \frac{\mu_0^2}{2\pi v^2}\operatorname{Re}\int_{-\infty}^{+\infty} i\omega\mu^*(\omega)\,\zeta^2\ln\frac{4}{3.17\zeta^2 b^2}\,d\omega. \tag{23a}$$

From this we get

$$W_b = \frac{\mu_0^2}{\pi v^4}\int_0^\infty \omega^3\{[\operatorname{Im}\mu + \beta^2|\mu|^2\operatorname{Im}\varepsilon]\ln\frac{4v^2}{3.17b^2\omega^2|1 - \varepsilon\mu\beta^2|}$$
$$+ \varphi[\operatorname{Re}\mu - \beta^2|\mu|^2\operatorname{Re}\varepsilon]\}\,d\omega, \tag{24}$$

where

$$\varphi = \tan^{-1}\frac{-\beta^2\operatorname{Im}\varepsilon\mu}{1 - \beta^2\operatorname{Re}\varepsilon\mu}$$

for the Bohr frequencies $(1 - \beta^2\operatorname{Re}\epsilon\mu > 0)$ and

$$\varphi = -\pi + \tan^{-1}\frac{\beta^2\operatorname{Im}\varepsilon\mu}{-1 + \beta^2\operatorname{Re}\varepsilon\mu}$$

for the Cerenkov frequencies $(1 - \beta^2\operatorname{Re}\epsilon\mu < 0)$.

In making the separation of the losses into Cerenkov and ionization losses we use the fact that the frequency at which the Cerenkov radiation breaks off $(\omega = \omega_{max})$ is not a characteristic frequency for the ionization losses. Consequently, the mathematical formula for the latter losses must not change on passage through this frequency. Thus we can write

$$W_b^{cer} = -\frac{\mu_0^2}{v^4}\int_{\operatorname{Re}\varepsilon\mu\beta^2>1} \omega^3(\operatorname{Re}\mu - \beta^2|\mu|^2\operatorname{Re}\varepsilon)\,d\omega \tag{25}$$

for the Cerenkov loss and

$$W_b^{ion} = \frac{\mu_0^2}{\pi v^4}\int_0^\infty \omega^3\left\{(\operatorname{Im}\mu + \beta^2|\mu|^2\operatorname{Im}\varepsilon)\ln\frac{4v^2}{3.17b^2\omega^2|1 - \varepsilon\mu\beta^2|}\right.$$
$$\left. - (\operatorname{Re}\mu - \beta^2|\mu|^2\operatorname{Re}\varepsilon)\tan^{-1}\frac{\beta^2\operatorname{Im}\varepsilon\mu}{1 - \beta^2\operatorname{Re}\varepsilon\mu}\right. \tag{26}$$

for the ionization loss. For $\mu = 1$, Eq. (25) gives the result of Eq. (16) in Ref. 6.

In conclusion we thank Professor A. A. Sokolov for suggesting this topic and for a discussion of our results.

[1] A. A. Sokolov and Iu. M. Loskutov, J. Exptl. Theoret. Phys. (U.S.S.R.) **32**, 630 (1957), Soviet Phys. JETP **5**, 523 (1957).

[2] A. A. Sokolov and V. N. Tsytovich, J. Exptl. Theoret. Phys. (U.S.S.R.) **30**, 136 (1956), Soviet Phys. JETP **3**, 94 (1956).

[3] A. A. Sokolov and I. M. Ternov, J. Exptl. Theoret. Phys. (U.S.S.R.) **31**, 473 (1956), Soviet Phys. JETP **4**, 396 (1957).

[4] A. A. Sokolov, Dokl. Akad. Nauk SSSR **28**, 415 (1940).

[5] A. A. Sokolov and D. D. Ivanenko, Квантовая теория поля (Quantum Field Theory), M.-L., 1952.

[6] V. L. Ginzburg, J. Exptl. Theoret. Phys. (U.S.S.R.) **10**, 589 (1940).

[7] D. D. Ivanenko and A. A. Sokolov, Классическая теория поля (Classical Field Theory), M.-L., 1951.

[8] D. D. Ivanenko and V. N. Tsytovich, J. Exptl. Theoret. Phys. (U.S.S.R.) **28**, 291 (1955), Soviet Phys. JETP **1**, 135 (1955).

Translated by W. H. Furry
83

SOVIET PHYSICS JETP VOLUME 34 (7), NUMBER 2 AUGUST, 1958

GLOW OF AIR DURING A STRONG EXPLOSION, AND THE MINIMUM BRIGHTNESS OF A FIREBALL *

Iu. P. RAIZER

Academy of Sciences, U.S.S.R.

Submitted to JETP editor August 26, 1957

J. Exptl. Theoret. Phys. (U.S.S.R.) **34**, 483-493 (February, 1958)

The optical properties of air at temperatures below 6,000° are considered. It is shown that the radiation and absorption of visible light at temperatures between 6,000° and 2,000° is due to the nitrogen dioxide that is formed in the air at these temperatures. This affords an explanation for several optical phenomena observed in strong explosions: the glow of air in a shock wave at low temperatures (down to 2,000°), the separation of the shock-wave front from the boundary of the fireball when the temperature of the front is close to 2,000°, and the peculiar effect of minimum brightness of the fireball.

A general description of the optical effects observed during strong (atomic) explosions in air is given in an American survey.[2]

A shock wave propagates from the center of the explosion along a trajectory which was shown by Sedov[3] to satisfy, with good approximation, the self-similar law $R \sim t^{2/5}$.

So long as the amplitude of the wave is sufficiently large, the surface of the front of the shock wave (SWF) glows brightly, forming the so-called fireball (FB). The brightness or the effective temperature of the FB, taken to mean the absolute temperature of a black body producing an identical radiation flux as the FB, diminishes with time as the true temperature behind the SWF decreases. At a certain instant of time, t_{min}, which is on the order of 10^{-2} sec for an explosion with energy $E \sim 10^{21}$ ergs, the SWF stops glowing and the boundary of the glowing body separates from the wave front. The brightness of the FB now goes through a minimum, after which it increases again — the FB, so to speak, flares up again. Now the dimensions of the FB increase much slower, while

*The work was performed in 1954. For a brief communication of the results see the review, Ref. 1.

the front of the shock wave moves far ahead. The brightness of the FB rises to a maximum at an instant $T_{max} \sim 10^{-1}$ sec, after which it dies down slowly, within approximately one second.

Figures 1 and 2 show schematically the dependence of the effective FB temperature on the time and on the trajectory of the SWF, and also the time dependences of the SWF trajectory, $R_f(t)$, and of the FB boundary trajectory, $R_0(t)$. The scales are based on an explosion energy $E \sim 10^{21}$ ergs.

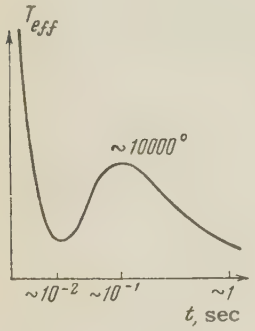

FIG. 1

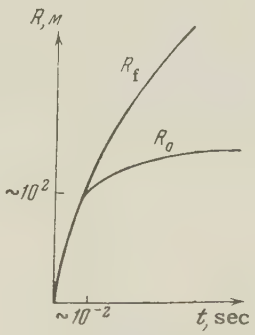

FIG. 2

The energy radiated during the explosion amounts to approximately one third of the explosion energy, and the fraction of the light radiated prior to the minimum, a time interval of one-hundredths of the total glow time, is on the order of 1%.

At temperatures above approximately 10,000°, the air absorbs a continuous spectrum in the visible region, principally by photoionization of the highly excited nitrogen and oxygen atoms (and molecules). The light is radiated as the result of the inverse process, photorecombination of free electrons with the ions.

Quanta of frequency ν can be absorbed only by atoms excited to an energy $I - h\nu$ (I is the ionization potential). The number of these atoms is proportional to the Boltzmann factor $\exp[-(I - h\nu)k/T]$, with $I - h\nu \gg kT$ at $T \sim 10{,}000°$. The coefficient of continuous absorption, κ_ν, therefore diminishes very rapidly with decreasing temperature. Although the range of the light amounts to tens of centimeters at $T \sim 9{,}000°$, it is on the order of meters at $T \sim 8{,}000°$, and on the order of kilometers at approximately 6,000°.

At temperatures above ~ 9,000°, the range of the light is less than the distances at which the temperature behind the SWF changes noticeably, on the order of meters. Therefore, when the SWF temperature is above 9,000°, the front radiates like an absolutely black body, and the effective temperature coincides with the true temperature behind the SWF.*

Cold air, as is known, is quite transparent to visible radiation, since the molecules of the nitrogen and oxygen absorb light only in the ultraviolet portion of the spectrum. Let us assume that the only light-absorption mechanism during heating is the photoionization process of the highly-excited nitrogen and oxygen atoms and molecules, a mechanism that is effective in practice above approximately 9,000°. This would, first, stop the SWF from glowing as soon as its temperature drops to ~ 9,000°, for even at $T \sim 5{,}000°$ the light-emissionability would become negligible. Second, at SWF temperature below ~ 9,000°, the layer of air between the front and the surface of ~ 9,000° would be practically transparent to the visible light and the hotter region of air with $T \sim 9{,}000°$ would glow across this layer (the temperature in the explosion wave rises from the periphery to the center[3]). The effective temperature of the FB would therefore not fall below ~ 9,000°.

Experience has shown that the air in the shock wave actually glows at temperatures down to ~ 2,000°, for it is exactly at this temperature that the front becomes invisible and the boundary of the FB becomes separated from the SWF. In addition, the effective temperature of the FB diminishes to values below ~ 9,000°. This is evidence that, in the temperature interval from ~ 9,000° to 2,000°, another mechanism exists in the air for continuous absorption and radiation of visible light.

We shall discuss in this article the optical properties of the air at temperatures below ~ 9,000°. It turns out that these properties are determined by the nitrogen oxides NO and NO_2 that are formed in the heated air.

This will lead to an explanation for the following experimentally-observed phenomena: glow of a shock wave at temperatures considerably below

*This is true only up to $T_f \approx 90{,}000°$ behind the SWF. With further increase in the amplitude of the shock wave, the effective temperature diminishes rapidly to a limiting value $T_{eff} \approx 18{,}000°$ and is no longer dependent on the amplitude. The cause of this phenomenon, examined in detail in Ref. 4, lies in the self-screening of the SWF at high T_f, when the SWF expands through radiant heat exchange.

It must be noted that the maximum and limiting brightness temperatures observed experimentally may turn out to be lower than the values mentioned above, owing to partial absorption of light by the non-equilibrium nitrogen dioxide, which should appear in the cold air ahead of the SWF under the influence of the neutrons and the γ quanta.

9,000°, abrupt cessation of glow at $T_f \sim 2{,}000°$ and the separation of the SWF from the boundary of the FB, and the very peculiar effect of the minimum brightness and subsequent "flareup" of the FB. The kinetics of the formation of the oxides of nitrogen in the air during strong explosions, and the concentration of these oxides, were considered in an earlier work.[5]

1. METHOD OF COMPUTING THE EFFECTIVE RADIATION TEMPERATURE

We are interested in the region of minimum brightness, i.e., that stage of the explosion, in which the temperature of the SWF is still sufficiently high, above ~ 1,500°, and the shock wave is strong. Only a small fraction of the total explosion energy is radiated at this stage, and therefore the hydrodynamics of the shock wave can be described with sufficient accuracy by the self-similar solution of Sedov[3] with a certain effective adiabatic exponent γ (Ref. 5).

In the center, when the temperatures are very high, on the order of 100,000°, the self-similar solution naturally no longer conforms to reality, for in this region the temperature profile becomes equalized by radiant heat exchange. Nevertheless, this does not affect in practice the distribution of the hydrodynamic quantities in the external layers of the wave, the only distribution of importance when considering the brightness of the FB.

The thickness of the radiating layer near the surface of the FB is considerably smaller than the radius of the FB, which is on the order of hundreds of meters, and the radiating layer can therefore be considered plane.

It is easy to derive a general formula for the radiation flux from the surface of a heated body, at a frequency ν, by integrating the sources of light along the ray at a certain angle to the normal, with allowance for the absorption along the path, and then integrating the resultant expression over the angles. This gives the well-known expression for the spectral brightness[6]

$$S_\nu = 2\int_0^\infty B_\nu(T)\, E_2(\tau_\nu)\, d\tau_\nu, \tag{1}$$

where

$$E_2(\tau_\nu) = \int_1^\infty e^{-\tau_\nu z}\frac{dz}{z^2}; \tag{2}$$

$B_\nu(T)$ is the Planck radiation flux at frequency ν, emitted from the surface of an absolutely black body,

$$B_\nu(T) = \frac{2\pi h}{c^2}\frac{\nu^3}{e^{h\nu/kT}-1}; \tag{3}$$

τ_ν is the optical thickness for radiation at a frequency ν, measured inward from the surface of the SWF

$$\tau_\nu = \int_0^x \varkappa_\nu\, dx, \tag{4}$$

x is the radial distance, also measured inward from the surface of the SWF, and κ_ν is the absorption coefficient, corrected for the forced emission, and equal to the reciprocal of the range of the light, $\kappa_\nu = 1/\ell_\nu$. The effective temperature of radiation at a frequency ν is determined from the obvious formula

$$B_\nu(T_{\text{eff}}) = 2\int_0^\infty B_\nu(T)\, E_2(\tau_\nu)\, d\tau_\nu. \tag{5}$$

Knowing the temperature profile T(x) behind the SWF and the light absorption coefficient $\kappa_\nu(x)$ at any point, it is possible to calculate the effective temperature of radiation from Eqs. (5), (3), and (4).

To be specific, all further calculations will be referred to the red line $\lambda = 6500$ A ($h\nu = 1.91$ ev).

The temperature and density distributions behind the SWF will be taken from Sedov's self-similar solution with effective adiabatic exponents $\gamma = 1.23$ at $T_f > 3{,}000°$ and $\gamma = 1.27$ at $T_f < 3{,}000°$ (see Ref. 5). If the temperature changes little in the radiating layer behind the SWF, i.e., in the layer that gives the principal contribution to the integral (5) (its optical thickness is on the order of unity), then we can put in (5) $B_\nu(T) \approx B_\nu(T_f) = \text{const}$. This yields, as expected, $T_{\text{eff}} \approx T_f$.

2. TYPICAL PROPERTIES OF AIR ABOVE 6,000°

To calculate the coefficient of absorption of red light by photoionization of the highly-excited atoms and molecules, let us employ the well-known Kramers formula for hydrogenlike atoms.[6] This formula takes also into account the absorption by free electrons in the field of the ions (which is considerably less than the photoionization at ~ 10,000°). After inserting the constants, the Kramers formula becomes (for the red line)

$$\varkappa_\nu = 1.48\, T^{\circ}\eta\,(e^{h\nu/kT}-1)\sum_i c_i e^{-I_i/kT}\ \text{cm}^{-1}. \tag{6}$$

Here η is the compression, i.e., the ratio of the

air density ρ to the normal density $\rho_0 = 1.25 \times 10^{-3}$ g/cm^3, $c_i = n_i/n_0\eta$ is the concentration of particles of the i-th kind (n_i is the number of particles per cm^3 and $n_0 = 2.67 \times 10^{19}$ cm^{-3} is the number of molecules per cm^3 of air under standard conditions), I_i are the ionization potentials ($I_O = 13.6$ ev, $I_N = 14.5$ ev, $I_{O_2} = 12.5$ ev, $I_{N_2} = 15.5$ ev). The effective charge of the atomic remnant, which is proportional to $\sqrt{\kappa_\nu}$, is taken to be 2.5 (Ref. 6).

Some doubt may be raised by the application of the Kramers formula to nonhydrogenlike atoms, and particularly to molecules. One must bear in mind, however, that red light with $h\nu = 1.91$ ev is absorbed only by electrons that are at very high levels, moving in a field close to the Coulomb field. In addition, as will be shown below, the quantities that are of interest from the point of view of calculating the effective temperature depend only logarithmically on the factor of the exponential in formula (6). On the other hand, the fundamental (Boltzmann) temperature dependence of the absorption is unconditionally correct also for nonhydrogenlike atoms and for molecules.

At temperatures below ~ 12,000° and at high compressions, such as prevail near the SWF, the nitrous oxide NO, which is formed in heated air, makes a substantial contribution to the sum (6). In spite of its small concentration (on the order of several percent, see Ref. 5), the absorption of the oxide is large, for it has a considerably lower ionization potential, $I_{NO} = 9.4$ ev.*

Table I gives the values of κ_ν for different temperatures and for two values of compression, $\eta = 10$ and $\eta = 1$. The table lists also the partial absorption coefficient $\kappa_{\nu NO}$. At temperatures below ~ 9,000°, practically the entire absorption is due to the nitrous oxide.

The limiting temperature, for the mechanism of light absorption considered here, must be taken to mean that temperature at which the range becomes on the order of a meter, i.e., on the order of the characteristic dimensions, at which the temperature changes noticeably in the shock wave. The nitrous oxide reduces this limit from ~ 9,000° to ~ 6,000°. It is to this temperature, $T_f \approx 6{,}000°$, that the SWF radiates as a black body, $T_{eff} \approx T_f$.

If, when calculating the effective temperature of the FB for the instants of time when the temperature of the SWF is considerably lower than 6,000°, we break up the integral (5) into two parts, one for outer colder layer of air, $0 < \tau_\nu < \tau_\nu^*$ ($0 < x < x^*$) with a temperature $T_f < T < 6{,}000°$, and one for the inner, hotter region with $T > 6{,}000°$, then the integral can be written

$$B_\nu(T_{eff}) = 2\int_0^{\tau_\nu^*} B_\nu(T)\,E_2(\tau_\nu)\,d\tau_\nu + B_\nu(T^*)\,E_3(\tau_\nu^*), \qquad (7)$$

where T^* is certain effective temperature of the radiation leaving the surface that bounds the inner, hotter region. This temperature, thanks to the exponential dependence of κ_ν on T, depends only logarithmically on the density and on the value of the factor ahead of the exponent in the Kramers formula (as already noted above, this circumstance indeed makes possible the use of this formula).

The temperature T^* has a rather narrow range from ~ 7,000 to ~ 9,000°, increasing somewhat with decreasing density.

TABLE I

T°	$\eta = 1$		$\eta = 10$	
	κ_ν, cm^{-1}	$\kappa_{\nu NO}$, cm^{-1}	κ_ν, cm^{-1}	$\kappa_{\nu NO}$, cm^{-1}
5000			$2.64 \cdot 10^{-4}$	$2.64 \cdot 10^{-4}$
6000	$2.65 \cdot 10^{-4}$	$2.65 \cdot 10^{-4}$	$5.74 \cdot 10^{-3}$	$5.7 \cdot 10^{-3}$
8000	$6.5 \cdot 10^{-3}$	$6 \cdot 10^{-3}$	0.17	0.17
10000	$4.6 \cdot 10^{-2}$	$2.7 \cdot 10^{-2}$	1.19	1.0
12000	0.31	$5 \cdot 10^{-2}$	5.4	2.6

*The values of the coefficient of absorption of red light behind the SWF in air, measured by Model' (Ref. 7) at two values of T_f, can be viewed as experimental evidence that absorption of light is essentially due to precisely the nitrous oxide. The oxygen and the nitrogen would give a considerably greater difference in the values of κ_ν than was obtained experimentally. A quantitative comparison of the experimental values of κ_ν with the theoretical ones is difficult, owing to the fact that the temperature is not known accurately. Apparently, the value $\kappa_\nu = 3.7$ cm^{-1} must pertain not to the temperature of 10,900° as measured by the brightness, but to the temperature $T_f = 11{,}500°$, calculated from the wave velocity 8.05 km/sec with the aid of the shock adiabatic.

3. OPTICAL PROPERTIES OF THE AIR BELOW 6,000°

Let us formulate the fundamental requirements that must be satisfied by the sought mechanism of light absorption, in order that it be usable for the

explanation of the following experimental facts:

(1) The absorption (and radiation) spectrum should be practically continuous in the visible region.

(2) The absorption and radiation should cease abruptly at a temperature of ~ 2,000°.

(3) In the temperature range from ~ 6,000 to 2,000°, the absorption should lead to a range of light on the order of meters. In fact, if l_ν is much less than a meter, then a layer with temperature ~ 6,000 — 2,000° will not shield to a sufficient extent the low-temperature radiation T*. If, on the other hand, l_ν is much less than a meter, then the layer will be quite opaque, and the effective temperature, reaching a minimum, cannot increase noticeably.

(4) For the same reason, the temperature dependence of the absorption cannot be greater than the Boltzmann value $\kappa_\nu \sim \exp(-W/kT)$ with $W \gg kT$, since the range would change very strongly in the above temperature range.

Let us consider the possible mechanisms for the absorption of light at temperatures below 6,000°.

At low temperatures, the negative oxygen ions formed are either atomic, with binding energy $\epsilon \approx 2.2$ ev, or molecular, with $\epsilon \approx 1$ ev. These ions are due essentially to the transfer of electrons from the NO molecules to the oxygen, since NO has the very lowest ionization potential. The oxygen ions absorb the visible light, causing detachment of an additional electron. Calculation of the ion concentration in accordance with the Sach formula from known[5] concentrations of O, O_2, and NO shows that the ion concentration depends on the temperature in accordance with the Boltzmann equation, with the high energy $W \approx 3.6$ ev.

In addition, an estimate of the absolute value of the absorption coefficient, with the aid of known data on the absorption cross-section[8] $\sigma_0^- \approx 2.5 \times 10^{-18}$ cm^2, shows that the ions can produce a noticeable effect only at high temperatures, above 5,000°.

Being transparent to the visible light, the oxygen, nitrogen, and nitrous-oxide molecules that remain in the electronic ground state at ordinary temperatures absorb, as is known, only the ultraviolet radiation. At high temperatures, the absorption spectra of the molecules shift towards the red side, since the smaller quanta can be absorbed by the molecules in which oscillations are excited.

A detailed investigation of the possible transitions, using the potential-curve schemes of various electronic states of the O_2, N_2, and NO molecules of Refs. 9 and 10, shows noticeable absorption of the red light calls for high excitation, i.e., the coefficient of absorption is proportional to the Boltzmann factor with a high energy W.

An estimate of the absorption cross-section is evidence that, as in the case of negative oxygen ions, this mechanism gives a certain effect only at temperatures above ~ 5,000°.*

The most probable is the hypothesis that the light is absorbed by the nitrogen dioxide, which forms in air at temperatures ~ 6,000 — 2,000° in quantities on the order of 10^{-2}% (Ref. 5).

Deferring the experimental confirmation of this hypothesis to the next section, let us consider the optical properties of nitrogen dioxide.

Cold nitrogen dioxide is an opaque gas, whose brownish-red color is due primarily to the absorption of light in the blue portion of the spectrum. The molecular bands, which form a complex system, are so closely adjacent, that they give a practically continuous absorption spectrum. The dependence of the absorption cross-section on the frequency in the visible portion of the spectrum was investigated by many authors; the most complete data were obtained by Dixon[12] who measured the absorption from $\lambda \approx 4{,}000$ A ($h\nu \approx 3.1$ ev) to $\lambda \approx 7{,}000$ A ($h\nu \approx 1.78$ ev).

The cross-section diminishes monotonically in this interval from $\sigma \approx 6.5 \times 10^{-19}$ cm^2 to $\sigma \approx 10^{-20}$ cm^2. According to Harris and King,[13] the absorption in the infrared region is very small — $\sigma < 4.5 \times 10^{-23}$ cm^2 at $\lambda \approx 10^{-4}$ A. From the Dixon curve it is seen that the cross-section approaches a maximum at $\lambda \sim 4{,}000$ A. This is also confirmed by the indication that the cross-section passes through a minimum at $\lambda \approx 3020$ A (Ref. 14).

*Note (November 25, 1957). A recently published article by Kivel, Mayer, and Bethe[11] contains a detailed examination of the molecular radiation (and absorption) of light by nitrous oxide at high temperatures. Upon substitution of numerical values, the approximate formula given by these authors for the coefficient of absorption becomes (for red light)

$$\varkappa_\nu = \frac{8.4 \times 10^4 c_{NO} \eta}{T} e^{-43000/T} \text{ cm}^{-1}.$$

At $T = 5{,}000°$ and at standard density ($\eta = 1$), we get $\varkappa_\nu = 2.3 \times 10^{-4}$ cm^{-1} and $l = 43$ m; at lower temperatures the range is even greater, this confirming that the above mechanism cannot give a substantial effect below ~ 5,000°.

It must be noted that below 6200° the molecular absorption by the nitrous oxide becomes greater than the photoelectric absorption (each of these mechanisms yields $\varkappa_\nu = 6 \times 10^{-4}$ cm^{-1} at $\nu = 1$). As the temperature rises, the relative role of this mechanism diminishes: thus, if $T = 8{,}000°$ it amounts to 17% of the photoelectric one.

It is very important to have an idea of the temperature variation of the cross-section in the red portion of the spectrum (there are no reliable experimental data). For this purpose it would be necessary, at least, to know the potential-surface scheme of the NO_2 molecule. There are no indications to this effect in the literature. We must therefore confine ourselves to semi-quantitative estimates.

It is natural to assume that the entire absorption spectrum in the visible region is due to a transition to the next nearest electron level. Judging from the fact that σ drops abruptly to a negligible value at $h\nu \approx 1.7$ ev, one might think that the energy of the level amounts to $\epsilon \approx 1.7$ ev. The maximum of the cross-section at $h\nu \approx 3.1$ ev can be explained by the fact that the transition from such an energy satisfies the Frank-Condon law in the best manner. Starting from these considerations, one can imagine a certain section of potential surfaces in the form shown in Fig. 3. As the

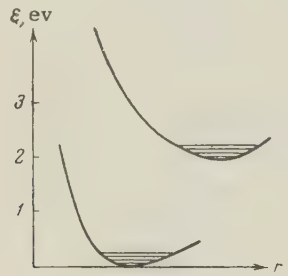

FIG. 3

temperature rises, vibrational levels are excited in the NO_2 molecules and, as seen from Fig. 3, the maximum of the cross-section, corresponding to the transition that satisfies the Frank-Condon law in the best manner, shifts towards the red side together with the entire $\sigma(\nu)$ curve. Since the electron level in the NO_2 molecule lies very low, even a relatively small increase in temperature can excite to a sufficient degree vibrational levels whose energy (in ev) is $\epsilon = 0.079v_1 + 0.169v_2 + 0.199v_3$ (v_1, v_2, and v_3 are the quantum numbers). Thus, for example, at a temperature on the order of 2,500°, 65% of the molecules are at levels not lower than $\epsilon_{111} = 0.45$ ev, from which the transition with absorption of a red quantum $h\nu = 1.91$ ev becomes quite probable.

Thus, we can assume that the cross-section for the absorption of red light by nitrogen dioxide increases monotonically (to a certain limit) with the temperature, and already at relatively small temperatures, on the order of several thousands of degrees, it reaches a value on the order of the maximum cross-section of the cold dioxide.

Unfortunately, there are no sufficient experimental information on the NO_2 molecule,* with which to carry out the very complicated temperature dependence of the absorption. Therefore, to calculate the effective temperature of the FB, we shall use the following likely values for the cross-section of absorption of red light:

$T°$	5000	4000	3000	2600	2000
$\sigma_{NO_2} \cdot 10^{19}$ cm^2	3.6	3.0	2.15	1.8	0.84

4. MINIMUM BRIGHTNESS OF FIREBALL

The hypothesis concerning the absorption of light by nitrogen dioxide leads to an easy and natural explanation of the characteristic features of the observed phenomena. It becomes quite clear why at a SWF temperature $T_f \approx 2{,}000°$ the SWF stops glowing and detaches itself from the boundary of the FB.

As shown in Ref. 5, the exceedingly abrupt reduction in the rate of nitrogen oxidation with diminishing temperature, at the very temperature $\approx 2{,}000°$, results in practice in a cessation of the formation of the oxide, and consequently, also of the dioxide of nitrogen in the layers of the air included in the SWF.

After the separation, at $T_f \approx 2{,}000°$, the boundary of the glowing region is at first that layer of air behind the SWF, which was heated by the SWF to a temperature $\approx 2{,}000°$ and which bounds the region of the existence of the dioxide. This layer moves forward, and stops gradually as the pressure in it drops to atmospheric (see the trajectory of the FB on Fig. 2). In the case of adiabatic expansion, the temperature in the layer diminishes slowly from the initial value of ~ 2,000 to ~ 800°.† Probably, the boundary of the FB will penetrate with time somewhat deeper, into layers in which temperatures are closer to 2,000°, since the radiating ability, which is proportional to $\exp(-h\nu/kT)$ ($h\nu \gg kT$) diminishes very sharply with decreasing temperature. More accurately speaking, the boundary of the FB is determined by the sensitivity of the recording instrument. This naturally explains also the effect of the minimum brightness of the FB near the instant when the SWF breaks away from the FB.

Let us note first that the absorption of light by the nitrogen dioxide is of the required order of

*The probabilities of transition between the various vibrational levels were calculated only for certain diatomic molecules.

†The initial pressure in the layer is $p_f \approx 50$ atmos; $T \sim p^{(\gamma-1)/\gamma} \sim p^{1/4}$, for in this temperature region $\gamma \approx 1.35$.

magnitude. For example, at $T = 3{,}000°$ and a compression $\eta = 5$, the concentration of NO_2, according to calculations of Ref. 5, is 1.58×10^{-4}. With an absorption cross-section $\sigma_{NO_2} = 2.15 \times 10^{-19}$ cm^2, this gives a range $\ell = 2.2$ m.

The temperature dependence of the concentration c_{NO_2} and of the cross-section σ_{NO_2}, and consequently, of the coefficient of absorption is quite weak in the interval from ~ 6,000 to ~ 2,000°.

Consider a layer of air behind the SWF at any one instant of time, say when the temperature of the SWF is $T_f = 3{,}000°$. The temperature behind the SWF rises, and the density decreases. Accordingly, the concentration of the dioxide diminishes rather rapidly with the distance from the SWF. Using the method discussed in Ref. 5 to calculate the concentration $c_{NO_2}(x)$ at each point x, with the known temperature and density known from the self-similar solution, and employing also the absorption cross-sections $\sigma_{NO_2}(T)$ given above, it is possible to plot the distribution of the absorption coefficient behind the SWF, $\kappa_\nu(x)$.

At the point where the temperature reaches ~ 6,000 — 7,000°, the concentration of the NO_2 and the absorption becomes very small. However, starting with temperatures of the same order of magnitude, the absorption of light by the nitric oxide comes into play, as does also the absorption by the oxygen and nitrogen, considered in Sec. 2; this absorption increases very sharply with increasing temperature, i.e., with increasing distance from the SWF.

Figure 4 shows the distribution $\kappa_\nu(x)$ for the instant $t = 1.5 \times 10^{-2}$ sec for a SWF radius $R_f = 107$ m (explosion energy $E = 10^{21}$ erg), at which the SWF temperature becomes $T_f = 3{,}000°$. The same diagram shows the values of the temperatures and density at several points x. Another typical distribution of $\kappa_\nu(x)$ is obtained when the SWF temperature is below ~ 2,000° (see Fig.

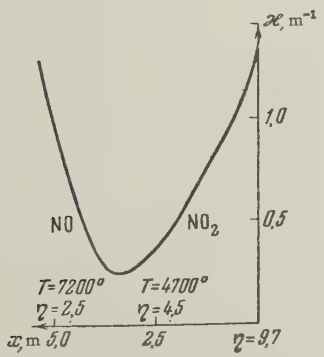

FIG. 4

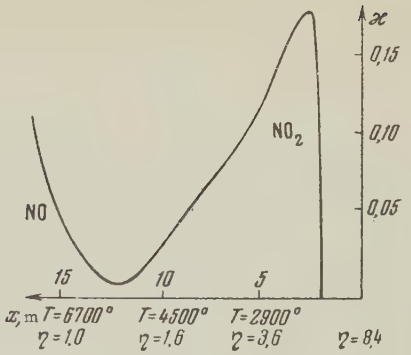

FIG. 5

5, which pertains to $t = 2.64 \times 10^{-2}$ sec, $R_f = 138$ m, $T_f = 1{,}600°$). In this case the absorption begins not immediately behind the SWF, but somewhat away from its surface, in the particles that were heated by the passage of the SWF to a temperature ~ 2,000°. No dioxide was formed in the outer layer, in which $\kappa_\nu = 0$.

The layer of air between the surface of the SWF and the surface where the temperature has an order of 6,000°, containing the nitrogen dioxide and having an optical thickness τ^*_ν, plays a double role. On the one hand, it absorbs the radiation of temperature $T^* \sim 7{,}000 - 9{,}000°$, which is generated in the internal region with $T > 6{,}000°$ [the screening factor $E_3(\tau^*)$ in the formula (7)]. On the other hand, it radiates light on its own [first term of (7)].

As the temperature of the SWF diminishes, starting with $T_f \approx 6{,}000°$, the actual and optical thicknesses of the air layer containing the dioxide increase, and the effective temperature T_{eff} drops. Since the optical thickness τ^*_ν is on the order of unity, the effective temperature exceeds the temperature of the SWF substantially. The ratio of the first term to the second in formula (7) diminishes, and when $T_f \approx 2{,}000°$ it becomes very small: the role of the dioxide layer reduces, essentially, to screening the internal hot region, and the layer itself radiates little.

When the temperature of the SWF reaches ~ 2,000° no more dioxide is formed in the layers of air newly captured by the front. Even if the total amount of the dioxide transformed by that instant of time were to remain constant, the optical thickness of the screening layer would diminish with time. In fact, as a consequence of the scattering of the air in the explosion wave, the same number of molecules N_{NO_2} would be distributed over a spherical layer of an ever increasing radius

$$\tau^*_\nu = \int_0^{R_f} n_{NO_2} \sigma_{NO_2} \, dr$$

and diminishes with constant

$$N_{NO_2} = \int_0^{R_f} 4\pi r^2 n_{NO_2} dr,$$

roughly speaking in proportion to $\sim R_f^{-2}$.

Actually, the total amount of the dioxide, after it stops being produced in the air layers newly captured by the SWF, diminishes within a certain length of time,[5] which leads to an even faster reduction of τ_ν^*. Thus, at $T_f < 2{,}000°$, the screening by the dioxide layer diminishes and the internal hot region gradually "becomes bare;" the effective temperature in this case increases — the FB, so to speak, flares up again.

The above qualitative considerations concerning the nature of the minimum brightness are illustrated in Table II, which lists the effective temperatures calculated in accordance with formula (5) for an explosion with energy $E = 10^{21}$ erg. The effective temperature passes through a minimum, and the optical thickness τ_ν^* passes through a maximum, at $T_f \approx 2{,}600°$, close to the breakaway temperature $T_f \approx 2{,}000°$.

TABLE II

$E = 10^{21}$ erg

$t \cdot 10^3$ sec	R_f, m	T_f°	T_{eff}°	τ_ν^*
0.75	82	5000	5930	1.06
1.05	93	4000	4810	1.96
1.50	107	3000	4110	2.42
1.81	109	2600	3600	3.23
1.95	112	2300	4150	2.16
2.25	128	2000	4520	1.80
2.39	132	1800	4810	1.61
2.64	138	1600	5400	1.15
2.94	143	1400	5600	1.11

It is interesting to trace what happens to the minimum brightness of the FB with changing explosion energy. All the values of the time and all the dimensions remain proportional in a like manner to $E^{1/3}$ (thanks to the approximate correctness of the self-similar hydrodynamic solution). The concentration of the dioxide in the principal region is in an equilibrium state, i.e., it depends only on the temperature and density of the particles, and not on its lifetime in the heated state, and therefore, roughly speaking, the optical thicknesses during the corresponding instants of time (for a definite SWF temperature) are proportional to the dimensions, i.e., also to $\sim E^{1/3}$. It follows therefore that the screening by the dioxide diminishes with diminishing explosion energy, and the excess of T_{eff} over T_f increases. By way of an example, Table III lists the results of the calculations for an energy $E = 10^{20}$ erg.

TABLE III

$E = 10^{20}$ erg

$t \cdot 10^3$ sec	R_f, m	T_f°	T_{eff}°	τ_ν^*
0.43	49	5000	6380	0.61
0.61	53	4000	5560	1.16
0.72	58	3000	5060	1.42
0.82	60	2600	4800	1.77
0.95	65	2300	5380	1.18
1.01	66	2000	5850	0.96
1.16	70	1800	6050	0.88
1.38	73	1600	6510	0.71
1.41	75	1400	6980	0.54

The position of the minimum is practically unchanged ($T_f \approx 2{,}600°$), and T_{eff} at the minimum is higher. In the limiting case of very small energies, the screening by the dioxide tends to zero and the minimum brightness should degenerate.

In the case of very high energies, the excess of T_{eff} over T_f diminishes, the minimum becomes deeper (the dioxide layer, which is placed directly behind the SWF, radiates on its own).

The effective temperature at the minimum can never become less than the temperature limit for the formation of nitric oxide, which remains close to 2,000° for observable energies. Thus, at $E = 10^{24}$ erg the characteristic times increase merely ten-fold compared with $E = 10^{21}$ erg. This affects quite negligibly the temperature limit, owing to the exceedingly sharp temperature dependence of the reaction velocity for the oxidation of nitrogen.

Assuming that the brightness of the FB reaches a minimum during an instant when the temperature on the SWF has a definite value, and that the distribution of the NO_2 concentration, together with the profiles of the temperature and the density, changes in a similar manner, we arrive at an approximation $t_{min} \sim E^{1/3}$. Inasmuch as all these conditions are satisfied only approximately, the dependence of t_{min} on E may be somewhat different. We restrict ourselves here to an examination of the stage of the minimum brightness of the FB. Other sections of the $T_{eff}(t)$ curve (the maximum and the subsequent decrease), are more affected by radiation processes in which the nitrogen dioxide does not play such an important role.

We take advantage of the opportunity to express deep gratitude to D. I. Blokhintsev, M. A. El'iashevich, Ia. B. Zel'dovich, and A. S. Kompaneets for interest in the work and for valuable discussions.

[1] Ia. B. Zel'dovich and Iu. P. Raizer, Usp. Fiz. Nauk **63**, 613 (1957).
[2] The Effects of Atomic Weapons, New York-Toronto-London, 1950.
[3] L. I. Sedov, Методы подобия и размерности в механике (Similitude and Dimensionality Methods in Mechanics), 3rd Ed., GTTL, 1954.
[4] Ia. B. Zel'dovich, J. Exptl. Theoret. Phys. (U.S.S.R.) **32**, 1126 (1957), Soviet Phys. JETP **5**, 919 (1957). Iu. P. Raizer, J. Exptl. Theoret. Phys. (U.S.S.R.) **32**, 1528 (1957); **33**, 101 (1957), Soviet Phys. JETP **5**, 1242 (1957), **6**, 77 (1958).
[5] Iu. P. Raizer, Журнал физической химии (J. of Phys. Chem.) **32** (1958).
[6] A. Unsold, Physics of Stellar Atmospheres, IIL, 1949.
[7] I. Sh. Model', J. Exptl. Theoret. Phys. (U.S.S.R.) **32**, 714 (1957), Soviet Phys. JETP **5**, 589 (1957).
[8] D. R. Bates and H. S. W. Massey, Phil. Trans. Roy. Soc. **A239**, 269 (1943).
[9] G. Hertzberg, Molecular Spectra and Molecular Structure, Vol. I, Prentice-Hall, 1939.
[10] A. G. Gaydon, Dissociation and Spectra of Diatomic Molecules, Dover, 1950
[11] Kivel, Mayer, and Bethe, Annales of Physics **2**, 57 (1957).
[12] J. K. Dixon, J. Chem. Phys. **8**, 157 (1940).
[13] L. Harris and G. W. King, J. Chem. Phys. **2**, 51 (1934).
[14] Lambrey, Compt. rend. **188**, 251 (1922).

Translated by J. G. Adashko
84

SOVIET PHYSICS JETP VOLUME 34 (7), NUMBER 2 AUGUST, 1958

SOME OPTICAL EFFECTS OF PLASMA OSCILLATIONS IN A SOLID

I. I. SOBEL'MAN and E. L. FEINBERG

P. N. Lebedev Physics Institute, Academy of Sciences, U.S.S.R.

Submitted to JETP editor August 27, 1957

J. Exptl. Theoret. Phys. (U.S.S.R.) **34**, 494-500 (February, 1958)

Three optical effects involving "plasmons" (collective oscillations of electrons in a solid) are considered: (a) excitation of a plasmon by absorption of an x-ray quantum and its effect on the structure of the x-ray absorption edge, (b) Raman scattering by a plasmon, (c) absorption of light of the plasmon frequency. The cross sections for all three processes are large.

ALTHOUGH data on characteristic energy losses by fast electrons in a solid may be explained semiquantitatively on the basis of the concept of collective electron oscillations,[1,2] the question of the reality of these oscillations cannot be considered to have been completely cleared up. It therefore seems useful to consider other effects, and in particular optical ones. Two types of collective oscillations are possible in a "plasma" of free electrons in a solid — optically active ones capable of absorbing and emitting light, and optically inactive ones. However, indirect interaction with light is possible for oscillations of both types. In this article we shall consider the following processes:

1. Excitation of a plasmon by the absorption of an x-ray quantum (this process is important for the structure of the absorption edge).

2. Excitation of a plasmon by inelastic scattering of a photon (Raman scattering).

3. Absorption of light of frequency of an optically-inactive plasma oscillation due to the virtual excitation of one of the inner electrons.

All these processes are due to the Coulomb interaction of a plasmon with the inner electrons. As will be shown below their probabilities are quite appreciable.

The effects in which we are interested are not associated with plasma inhomogeneity; therefore, in order to make rough estimates, we can consider that the plasma oscillation has the form of a plane wave

$$\rho(\mathbf{r}, t) = \rho e^{i(\mathbf{kr}-\omega t)};\ \rho = (\hbar k^2 \rho_0/2\omega m V)^{1/2};$$
$$\omega^2 = \omega_p^2 + \langle v^2\rangle k^2;\ \omega_p^2 = 4\pi\rho_0 e^2/m, \qquad (1)$$

where V is the normalization volume; ρ_0 and $\langle v^2\rangle$ are the density and the mean-squared velocity of plasma electrons. The wave number k is bounded from above by the condition $k \lesssim k_c$, and we shall assume that $\langle v^2\rangle k_c^2 \ll \omega_p^2$, although in actual fact the inequality is satisfied with but a small margin. As a rule $\hbar\omega_p \lesssim me^4/\hbar^2$. The energy of the inner electrons which is of order of magntidue $Z_{eff}^2 me^4/\hbar^2$ already at $Z_{eff} \gtrsim 3$ is large compared to $\hbar\omega$. Thus, during the time $\hbar/Z_{eff}^2 me^4$ (period of motion of an inner electron) $\rho(\mathbf{r}, t)$ practically does not change. This allows us to treat the motion of the inner electrons keeping the configuration of the outer electrons fixed, and to treat the excitation of a plasmon by introducing the perturbing potential*

$$U(\mathbf{r}, t) = U(\mathbf{r})\, e^{-i\omega t} = e\int \frac{\rho e^{i(\mathbf{kr}'-\omega t)}}{|\mathbf{r}-\mathbf{r}'|} d\mathbf{r}' = \frac{4\pi e\rho}{k^2} e^{i(\mathbf{kr}-\omega t)}. \qquad (2)$$

For the sake of definiteness we shall assume that the inner electron is in the K-shell (it is, of course, not difficult to generalize this). In making rough estimates, it is sufficient simply to replace Z by Z_{eff}.

1. THE EDGE OF THE X-RAY ABSORPTION BAND

Let us consider an electron in the K shell which, as a result of absorbing a photon $\hbar\omega_0$, goes over into a state in the continuum (propagation-vector $\mathbf{k}_f$), while a plasmon $\hbar\omega$ is excited (propagation-vector $\mathbf{k}$). The effective cross section of such a process is equal to

$$\sigma = \frac{2\pi V}{\hbar c}\int |M|^2 \delta(E - E_0)\frac{V d\mathbf{k}_f}{(2\pi)^3}\frac{V d\mathbf{k}}{(2\pi)^3}; \qquad (3)$$

$$M = \sum_n \left\{\frac{W_{fn}^* V_{n0}}{(\varepsilon_0 + \hbar\omega_0 - \varepsilon_n)} + \frac{V_{fn} W_{n0}^*}{(\varepsilon_0 - \hbar\omega - \varepsilon_n)}\right\}. \qquad (4)$$

Here V is the operator for the interaction of the electron with radiation, W = eU is the operator for the interaction with the plasmon; ϵ_0, ϵ_n are the energies of the electron in the initial and the intermediate states. The summation in (4) is carried out over the discrete states and the states of the continuum lying beyond the Fermi boundary. The principal contribution comes from the states in the continuum, and therefore only these states are taken into account below. Of particular importance are the states with $\epsilon_n \approx \epsilon_0 + \hbar\omega$ for which the denominator of the first term in (4) is small. One may neglect the second term in (4) since $|\epsilon_0| = (me^4/2\hbar^2)Z^2 \gg \hbar\omega$ and the denominator $(\epsilon_0 - \hbar\omega - \epsilon_n)$ is large for all ϵ_n. The matrix element V_{n0} differs from zero only if in the intermediate state $\ell = 1$, i.e.,

$$V_{n0} = V_{100}^{\varkappa 1m} = ie\omega_{\varkappa 1;10}\sqrt{\frac{2\pi\hbar}{\omega_0 V}}\frac{\sqrt{4\pi}}{3} Y_{1m}^*(\theta_e, \varphi_e)\int R_{\varkappa 1} r^3 R_{10} dr, \qquad (5)$$

where **e** is the polarization vector of the photon. The radial function of the initial state R_{10} differs from zero only near the nucleus for $r \lesssim \hbar^2/me^2 Z = a_0/Z$. Therefore one can take for the radial function $R_{\kappa 1}$ for the state of wave number κ a function from the continuum of the motion of an electron in the Coulomb field due to a charge Ze. It is in this approximation that the same integral is evaluated in the theory of the photo-effect:[3]

$$\int R_{\varkappa 1} r^3 R_{10} dr = \frac{2^4 Z^3 \exp\left(-2\frac{Z}{\varkappa'}\operatorname{arc\,tan}\frac{\varkappa'}{Z}\right)}{(Z^2+\varkappa'^2)^{3/2}[1-\exp(-2\pi Z/\varkappa')]^{1/2}}\sqrt{\varkappa} a_0^2. \qquad (6)$$

Here κ' is the dimensionless wave number (in atomic units). For small values of κ' which are of interest to us, $\kappa'/Z \ll 1$ and

$$V_{100}^{\varkappa 1m} = i\left(\frac{4}{e}\right)^2\frac{\sqrt{4\pi}}{3} Y_{1m}^*(\theta_e, \varphi_e)\, e\left(\frac{2\pi\hbar\omega_0\varkappa}{V}\right)^{1/2}\frac{a_0^2}{Z^2}. \qquad (7)$$

Here we have set

$$\omega_{\varkappa 1';10} = \hbar^{-1}(\hbar^2\varkappa^2/2m - \varepsilon_0) = \omega_0.$$

For the evaluation of $W_{fn}^* = W_{\mathbf{k}_f;\kappa 1m}^*$ we can take for the functions $\psi_{\mathbf{k}_f}$ and $\psi_{\kappa 1m}$ the free electron wave functions since the inner region in which it is necessary to take into account the field of the nucleus is not of great importance here. On setting $\psi_{\mathbf{k}_f} = V^{-1/2}\exp(i\mathbf{k}_f\cdot\mathbf{r})$, we obtain from (2)

*In the original Hamiltonian one may neglect the terms $p^2/2m$ corresponding to the outer electrons. In this case the coordinates of the outer electrons will appear as parameters in the Schrödinger equation for the inner electrons. It is this fact which allows one to treat the excitation of a plasmon by introducing the potential (2) (see Bethe,[3] § 15). It is interesting to note that the effects under discussion are analogous to the interaction with light of molecular vibrations. Thus, process 1 corresponds to the vibrational structure of the absorption band, process 2 to Raman scattering, and process 3 to infra-red absorption.

$$W_{\mathbf{k}_f;\varkappa 1m} = \frac{4\pi\rho}{k^2}\frac{e^2}{V\sqrt{V}}\int \exp(-i\,\mathbf{k}_f\mathbf{r} - i\,\mathbf{kr})\,R_{\varkappa 1}(r)\,Y_{1m}(\theta,\varphi)\,d\mathbf{r}. \tag{8}$$

In the expansion of the factor $\exp(-i\mathbf{p}\cdot\mathbf{r})$ with $\mathbf{p} = \mathbf{k} + \mathbf{k}_f$ into spherical waves, the term with $\ell = 1$ is important, and is given by

$$-i\frac{4\pi}{p}\sqrt{\frac{\pi}{2}}\,R_{p1}\sum_{m'} Y^*_{1m'}(\theta,\varphi)\,Y_{1m'}(\theta_p,\varphi_p);$$

$$R_{p1} = -\sqrt{\frac{2}{\pi}}\frac{d}{dr}\frac{\sin pr}{pr}. \tag{9}$$

Substituting (9) into (8) we obtain

$$W^*_{\mathbf{k}_f;\varkappa 1m} = -i\frac{4\pi\rho e^2}{k^2}\left(\frac{8\pi^3}{V}\right)^{1/2}\frac{\delta(p-\varkappa)}{p}\,Y_{1m}(\theta_p,\varphi_p). \tag{10}$$

Thus, according to (1), (4), and (10)

$$M \sim \sum_m Y^*_{1m}(\theta_e,\varphi_e)\,Y_{1m}(\theta_p,\varphi_p)\int\frac{\delta(\varkappa-p)\sqrt{\varkappa}\,d\varkappa}{p\,(\varepsilon_0+\hbar\omega_0-\hbar^2\varkappa^2/2m)}$$
$$= \frac{3}{4\pi}\frac{ep}{p}\frac{1}{\sqrt{p}\,(\varepsilon_0+\hbar\omega_0-\hbar^2p^2/2m)}; \tag{11}$$

$$\sigma = \left(\frac{4}{e}\right)^4 e^2\hbar\omega\omega_0\frac{e^2}{\hbar c}\frac{a_0^4}{4\pi Z^4}$$
$$\times\int\frac{\cos^2\theta_{\mathbf{k}+\mathbf{k}_f,\mathbf{e}}\,\delta(E-E_0)\,d\,\mathbf{k}_f d\,\mathbf{k}}{k^2\,|\,\mathbf{k}+\mathbf{k}_f\,|\,\{\varepsilon_0+\hbar\omega_0-\hbar^2(\mathbf{k}+\mathbf{k}_f)^2/2m\}^2}. \tag{12}$$

From the law of conservation of energy it follows that

$$\varepsilon_0+\hbar\omega_0 = \hbar\omega+\hbar^2k_f^{02}/2m,\quad \delta(E-E_0) = (m/\hbar^2k_f)\,\delta(k_f-k_f^0).$$

Moreover, the approximation employed by us requires that $\hbar^2k_f^{02}/2m \gg \hbar\omega$ should hold, so that $k_f^0 \gg k_c$. Therefore we can put in (12)

$$\cos^2\theta_{\mathbf{k}+\mathbf{k}_f,\mathbf{e}} \approx \cos^2\theta_{\mathbf{k}_f,\mathbf{e}},\quad |\,\mathbf{k}_f+\mathbf{k}\,| \approx k_f,$$

$$\varepsilon_0+\hbar\omega_0-\hbar^2(\mathbf{k}+\mathbf{k}_f)^2/2m \approx \hbar\omega.$$

On setting also $\hbar\omega_0 \approx Z^2me^4/2\hbar^2$ we obtain

$$\sigma = \frac{2\pi}{3}\left(\frac{4}{e}\right)^4\frac{e^2}{\hbar c}\left(\frac{me^4}{\hbar^3\omega}\right)\frac{a_0^2}{Z^2}(a_0k_c). \tag{13}$$

Let us compare (13) with the cross section for the ordinary photo-effect evaluated in the same approximation (cf. Bethe[3]):

$$\sigma_0 = \frac{2\pi^2}{3}\left(\frac{4}{e}\right)^4\frac{e^2}{\hbar c}\frac{a_0^2}{Z^2}. \tag{14}$$

Since $a_0k_c \sim 1$ we have $\sigma \sim \sigma_0$.

It is easy to generalize formulas (13) and (14) to the case when the level density of final states dk_f/dE is an arbitrary function (it is customary to explain the structure of the absorption edge just by such a non-uniformity of the level density[4]):

$$\sigma = \frac{2\pi}{3}\left(\frac{4}{e}\right)^4\left(\frac{e^2}{\hbar c}\right)^2\left(\frac{me^4}{\hbar^3\omega}\right)\frac{a_0^2}{Z^2}\,a_0k_c\hbar c\alpha(E')\left(\frac{2E'\hbar^2}{me^4}\right)^{1/2};$$

$$E' = \hbar\omega_0-\hbar\omega-\frac{Z^2me^4}{2\hbar^2}; \tag{15}$$

$$\sigma_0 = \frac{2\pi^2}{3}\left(\frac{4}{e}\right)^4\left(\frac{e^2}{\hbar c}\right)^2\frac{a_0^2}{Z^2}\,\hbar c\alpha(E)\left(\frac{2E\hbar^2}{me^4}\right)^{1/2};$$

$$E = \hbar\omega_0-\frac{Z^2me^4}{2\hbar^2}. \tag{16}$$

2. RAMAN SCATTERING

Let ω_0 and $\mathbf{e}_0$ be the frequency and the polarization vector of the incident photon, and ω', $\mathbf{e}'$ those of the scattered photon. The matrix element which determines the probability of excitation of a plasma oscillation by the scattering of the photon is equal to (we have here omitted the terms whose denominators are large)

$$M = \sum_{n,k}\frac{V^*_{0k}W^*_{kn}V_{n0}}{(\varepsilon_0+\hbar\omega_0-\varepsilon_n)(\varepsilon_0+\hbar\omega_0-\varepsilon_k-\hbar\omega)}. \tag{17}$$

We assume that $\hbar\omega_0$ is close to $|\,\epsilon_0\,|$. In this case, as before, the main role is played by the states of the continuum with energies $\hbar^2\kappa_1^2/2m$, $\hbar\kappa_2^2/2m \ll Z^2me^4/\hbar^2$. Therefore $V_{n\theta}$ and V^*_{0n} are evaluated in exactly the same way as in the preceding section. For W^*_{kn} we shall obtain instead of (8)

$$W^*_{kn} = W^*_{\varkappa_1 1m'} = \frac{4\pi\rho e^2}{k^2}\int R_{\varkappa_1 1}(r)\,R_{\varkappa_1 1}(r)$$
$$\times\,Y^*_{1m'}(\theta,\varphi)\,Y_{1m'}(\theta,\varphi)\,e^{-i\mathbf{kr}}\,d\mathbf{r}. \tag{18}$$

We expand the function $R_{\kappa 1}Y_{1m} = \psi_{\kappa 1m}$ into plane waves:

$$\psi_{\varkappa 1m} = \int a_p e^{i\mathbf{rp}}d\,\mathbf{p};$$

$$a_p = -\frac{4\pi i}{(2\pi)^3 p}\sqrt{\frac{\pi}{2}}\,\delta(\varkappa-p)\,V_{1m}(\theta_p,\varphi_p). \tag{19}$$

Then

$$W^*_{kn} = \frac{\rho e^2}{8\pi^2k^2}\int\frac{\delta(\varkappa_1-p_1)\,\delta(\varkappa_2-p_2)}{p_1p_2}\,Y_{1m}(\theta_{p_1},\varphi_{p_1})$$
$$\times\,Y_{1m'}(\theta_{p_2},\varphi_{p_2})\,e^{i(\mathbf{p}_1-\mathbf{p}_2-\mathbf{k})\mathbf{r}}\,d\mathbf{p}_1\,d\mathbf{p}_2 d\mathbf{r}; \tag{20}$$

$$M \sim \sum_{mm'}\int Y_{1m}(\theta_{p_1},\varphi_{p_1})\,Y_{1m'}(\theta_{p_2},\varphi_{p_2})\,Y^*_{1m}(\theta_{e_s},\varphi_{e_s})\,Y^*_{1m'}(\theta_e,\varphi_e)$$
$$\times\frac{\delta(\varkappa_1-p_1)\,\delta(\varkappa_2-p_2)\,\delta(\mathbf{p}_1-\mathbf{p}_2-\mathbf{k})\sqrt{\varkappa_1\varkappa_2}\,dp_1\,dp_2\,d\varkappa_1\,d\varkappa_2}{p_1p_2\{\varepsilon_0+\hbar\omega_0-\hbar^2\varkappa_1^2/2m\}\{\varepsilon_0+\hbar\omega_0-\hbar\omega-\hbar^2\varkappa_2^2/2m\}}. \tag{21}$$

Summing over m, m' and integrating over $d\kappa_1$ we shall obtain

$$M = -\left(\frac{4}{e}\right)^4 \frac{\pi}{2} \frac{\rho e^4 \hbar}{k^2} \frac{V\overline{\omega'\omega_0}}{V} \times \int \frac{\cos\theta_{p_2+k,\,e_0} \cos\theta_{p_2 e'}\, d\,p_2}{V\overline{p_2 |\,p_2+k|}\,\{\varepsilon_0 + \hbar\omega_0 - \hbar^2(p_2+k)^2/2m\}\,\{\varepsilon_0+\hbar\omega_0-\hbar\omega-\hbar^2 p_2^2/2m\}} \quad (22)$$

Leaving out of consideration, as usual, the special resonance case $\hbar\omega_0 + \epsilon_0 = \hbar^2k^2/2m$ and $\hbar\omega_0 + \epsilon_0 - \hbar\omega = \hbar^2k^2/2m$ we can neglect in (22) the small region $p \approx k$ and consider that $p \gg k$. Finally, integration yields

$$M = -\left(\frac{4}{e}\right)^4 \frac{4\pi^2}{6} \frac{\rho e^4}{k^2} \frac{V\overline{\omega_0\omega'}}{\omega V} \frac{a_0^4}{Z^4} \frac{m}{\hbar^2} \ln \frac{\varepsilon_0 + \hbar\omega_0 - \hbar\omega}{\varepsilon_0 + \hbar\omega_0} \cos\theta_{e_0 e'}. \quad (23)$$

Expression (23) must be multiplied by the number ξ of electrons in the shell (for the K-shell $\xi = 2$). The effective cross section for the process is equal to (q is the propagation vector of the scattered photon; moreover, we have set $\sqrt{\omega_0\omega'} = \omega_0 = Z^2 m \times e^4/2\hbar^3$)

$$\sigma = \frac{2\pi V}{\hbar c} \int |M|^2 \delta(E - E_0) \frac{V d\,k}{(2\pi)^3} \frac{V d\,q}{(2\pi)^3} = \left(\frac{2}{e}\right)^8 \left(\frac{2}{3}\right)^3 \left(\frac{me^4}{\hbar^3\omega}\right) \left(\frac{e^2\xi}{mc^2}\right)^2 a_0 k_c \left\{\ln \frac{\varepsilon_0 + \hbar\omega_0 - \hbar\omega}{\varepsilon_0 + \hbar\omega_0}\right\}^2. \quad (24)$$

Let us compare (24) with the effective cross section for coherent scattering. In order to estimate the order of magnitude of the latter we can take the classical expression

$$\sigma_0 = (8\pi/3)(Ze^2/mc^2)^2. \quad (24a)$$

The ratio of the cross sections for incoherent and coherent scattering is thus equal in order of magnitude to

$$\frac{\sigma}{\sigma_0} = \frac{1}{9\pi} \left(\frac{2}{e}\right)^8 \left(\frac{me^4/\hbar^2}{\varepsilon_0 + \hbar\omega_0}\right) \left(\frac{\hbar\omega}{\varepsilon_0 + \hbar\omega_0}\right) a_0 k_c \frac{\xi^2}{Z^2}. \quad (24b)$$

Here we have set

$$\ln \frac{\varepsilon_0 + \hbar\omega_0 - \hbar\omega}{\varepsilon_0 + \hbar\omega_0} \approx \frac{\hbar\omega}{\varepsilon_0 + \hbar\omega_0}.$$

3. ABSORPTION AT THE PLASMA OSCILLATION FREQUENCY

The probability of excitation of an "optically-inactive" plasma oscillation by the absorption of a photon of frequency $\omega_0 = \omega$ and propagation vector q is determined by the matrix element

$$M = \sum_n \left\{ \frac{W^*_{0n} V_{n0}}{\varepsilon_0 + \hbar\omega_0 - \varepsilon_n} + \frac{V_{0n} W^*_{n0}}{\varepsilon_0 + \hbar\omega - \varepsilon_n} \right\}. \quad (25)$$

The small terms $\hbar\omega_0$ and $\hbar\omega$ in the denominators may be neglected so that therefore both terms in (25) are of the same order of magnitude. In this case there is no longer any justification for assuming that ϵ_n is small, and therefore V_{n0} and V_{0n} will be determined by relations (5) and (6). In $W^*_{n0} = W^{*\kappa 1 m}_{100}$, just as in V_{n0}, the principal contribution comes from the small region $r \lesssim a_0/Z$. It is therefore convenient to expand W into spherical waves:

$$W(\mathbf{r}) = \rho e^2 \int \frac{e^{i\mathbf{k}\mathbf{r}'}}{|\mathbf{r} - \mathbf{r}'|} d\,\mathbf{r}' \approx \rho e^2 \sum_{l,m} \frac{4\pi}{2l+1} \int \frac{r^l}{r'^{l+1}} e^{i\mathbf{k}\mathbf{r}'} Y^*_{lm}(\theta, \varphi)\, Y_{lm}(\theta', \varphi')\, d\,\mathbf{r}'. \quad (26)$$

We shall then obtain

$$W(\mathbf{r}) = \sum_{l,m} r^l Y^*_{lm}(\theta, \varphi)\, \eta_{lm}, \qquad \eta_{lm} = \frac{4\pi\rho e^2}{2l+1} \int \frac{e^{i\mathbf{k}\mathbf{r}}}{r^{l+1}} Y_{lm}(\theta, \varphi)\, d\,\mathbf{r}. \quad (27)$$

Only the term with $l = 1$ is important for $W^{*\kappa 10}_{100}$ in (27). Expansion of $\exp(i\mathbf{k}\cdot\mathbf{r})$ into spherical waves (9) yields:

$$\eta_{1m} = i \frac{16\pi^2}{3} \frac{\rho e^2}{k} Y_{1m}(\theta_k, \varphi_k),$$

$$W(\mathbf{r}) = i \frac{16\pi^2}{3} \frac{\rho e^2}{k} \mathbf{r} Y^*_{1m}(\theta, \varphi)\, Y_{1m}(\theta_k, \varphi_k); \quad (28)$$

$$W^{*\varkappa 1 m}_{100} = -i \frac{(4\pi)^{3/2}}{3} \frac{\rho e^2}{k} Y^*_{1m}(\theta_k, \varphi_k) \int R_{\varkappa 1} r^3 R_{10}\, dr. \quad (29)$$

For the radial integral in (29) we have Eq. (6). Taking into account the fact that $\omega_{\kappa 1;\,10} = \hbar^{-1} \times (\hbar^2k^2/2m - \epsilon_0)$ we shall obtain

$$M \sim \sum_m \{Y^*_{1m}(\theta_e, \varphi_e)\, Y_{1m}(\theta_k, \varphi_k) + Y_{1m}(\theta_e, \varphi_e)\, Y^*_{1m}(\theta_k, \varphi_k)\} \times \int \frac{Z^6 \exp\left\{-4\frac{Z}{\varkappa'} \tan^{-1}\frac{\varkappa'}{Z}\right\} \varkappa' d\varkappa'}{(Z^2 + \varkappa'^2)^5 \{1 - \exp(-2\pi Z/\varkappa')\}} \approx \frac{3\cos\theta_{ek}}{16\pi e^4 Z^3}, \quad (30)$$

and finally

$$M = -\left(\frac{2}{e}\right)^4 \frac{16}{9} (2\pi)^{3/2} \frac{\rho e^3}{k\hbar} \sqrt{\frac{\hbar}{\omega_0 V}} \frac{a_0^2}{Z^2} \cos\theta_{ek}. \quad (31)$$

Therefore the transition probability is equal to

$$dW = \frac{2\pi}{\hbar} \int |M|^2 \delta(E - E_0) \frac{V d\,q}{(2\pi)^3} = 4\left(\frac{2}{e}\right)^8 \left(\frac{2}{3}\right)^4 \left(\frac{e^2}{\hbar c}\right)^2 \frac{\omega^2}{c} \frac{a_0^4}{Z^4 V} \cos^2\theta_{ek}\, do. \quad (32)$$

In order to obtain the energy S absorbed per second it is necessary to multiply (32) by $\hbar\omega$, and also, since the plasma oscillation is normalized over the volume V, by the total number of electrons in a given shell equal to $\xi V/V_0$ where V_0 is the atomic volume. If the incident beam has an intensity $I_0(\omega)\,d\omega\,do$ erg/cm^2-sec then on averaging S over the directions of the polarization vector e we shall obtain [cf. the derivation of formula (17.19) of Heitler[5]]

$$S=\frac{1}{9}\left(\frac{2}{e}\right)^8\left(\frac{8\pi}{3}\right)^3\left(\frac{e^2}{\hbar c}\right)^2\frac{a_0^2\xi}{V_0}\frac{ca_0I_0}{Z^4}\,do. \qquad (33)$$

The energy absorbed by an ordinary single electron excitation is equal to[5]

$$S=\frac{4\pi^2}{3}\frac{e^2}{\hbar c}\omega|x_{ab}|^2 I_0(\omega)\,do;\quad |x_{ab}|^2=\frac{1}{2}f\left(\frac{me^4}{\hbar^3\omega}\right)a_0^2, \qquad (34)$$

where f is the strength of the transition oscillator.

Thus (33) corresponds to absorption with an effective value of the square of the matrix element equal to

$$|x_{ab}|^2_{\text{eff}}=\left(\frac{2}{e}\right)^8\left(\frac{4}{3}\right)^4\frac{a_0^3\xi}{V_0}\left(\frac{me^4}{\hbar^3\omega}\right)\frac{a_0^2}{Z^4}, \qquad (35)$$

and differing from (34) essentially only by the factor Z_{eff}^{-4}.

4. DISCUSSION OF THE RESULTS

It follows from (13) and (14) that the mechanism discussed above for the excitation of plasmons by the absorption of x-ray quanta is a very effective one. Let us investigate in what way can this process have an effect on the structure of the absorption edge. The formulas obtained above are valid at distances from the absorption boundary which exceed ω by several fold, so that consequently it is not possible to draw unambiguous conclusions with respect to the shape of the curve in the region $\hbar\omega_0+\epsilon_0\approx\hbar\omega$. According to (13), σ does not depend on k_f^0; it therefore seems probable that there is no additional maximum at a distance $\hbar\omega$ from the boundary. From (15) and (16) it follows that if the function $\alpha(E)$, and consequently σ_0, have a maximum, then σ also has a similar maximum but shifted by an amount $\hbar\omega$. This fact may turn out to be important for the intepretation of the structure of the absorption edge. It was noted earlier[2] that in a number of cases the values of the discrete losses coincide with the distances between the maxima of the structures of the K and L x-ray absorption edges, and the opinion was expressed that this coincidence should be related to the concept of plasmons.

This process is also sufficiently effective with respect to Raman scattering. Therefore in the reflected (scattered) light one can expect the appearance of long wave satellites $\omega_0-\omega$.

Generally speaking, all electrons — both the inner ones, and also those close to the periphery — take part in the absorption of light of frequency of an "optically-inactive" plasma oscillation. According to (35), the principal role is played by the latter ($Z_{\text{eff}}\approx 1$). The approximation used above is not suitable in this case. Nevertheless it is obvious that the effectiveness of the mechanism considered above increases as $Z_{\text{eff}}\to 1$. One is here dealing essentially with the same mechanism which is used to explain the large width of plasmon levels — the exchange of energy between the plasmon and the individual electron which undergoes transitions between conduction bands.[6-8] Since this mechanism leads to a considerable broadening of the plasmon levels, it is not surprising that the probability of excitation of the plasmon due to the virtual excitation of the electron is large (for $Z_{\text{eff}}\to 1$).

Because of this effect, the division of plasma oscillations into "optically-inactive" and "inactive" ones becomes quite arbitrary, and signifies only the separation of the mechanism of the process.

In addition to the optical effects investigated above, which are associated with excitation of plasmons, a number of other effects can also take place, for example, the emission of an x-ray quantum in the transition n's → n"s (without the excitation of a plasmon such a transition is evidently impossible). It may be shown that the probability of such a transition is proportional to $(Z'_{\text{eff}}Z''_{\text{eff}})^{-2}$.

In conclusion it must be noted that, in principle, all the processes considered above are possible also in the case that a second electron participates in them in place of a plasmon. However, for a plasmon, in the case that it involves several peripheral electrons, the corresponding transition probabilities should be greater [cf., for example, (24b) where σ/σ_0 is proportional to ω, i.e., to $\sqrt{\rho_0}$]. Apparently the most promising method of identifying plasma effects is to make use of the dependence of ω on the effective number of electrons taking part in a plasma oscillation.

[1] D. Pines, Revs. Mod. Phys. **28**, 184 (1956).

[2] L. Marton, Revs. Mod. Phys. **28**, 172 (1956).

[3] H. Bethe, The Quantum Mechanics of the Simplest Systems, (Russ. Transl.) ONTI, 1935.

[4] M. Blokhin, Физика рентгеновских лучей (The Physics of X-Rays), GITTL, 1953.

[5] W. Heitler, The Quantum Theory of Radiation, Oxford, 1954.

[6] P. Wolff, Phys. Rev. **92**, 18 (1953).

[7] H. Kanazawa, Prog. Theoret. Phys. **13**, 227 (1955).

[8] P. Nozieres and D. Pines, In press (see Ref. 1).

Translated by G. Volkoff
85

Letters to the Editor

THE MEASUREMENT OF THE SPECTRA OF FISSION NEUTRONS FROM U^{233}, U^{235}, AND Pu^{239} IN THE 50 — 700 kev RANGE

V. P. KOVALEV

Submitted to JETP editor September 28, 1957

J. Exptl. Theoret. Phys. (U.S.S.R.) **34**, 501-502 (February, 1958)

THE spectra of fission neutrons have been measured by means of a cloud chamber, filled with water vapor and hydrogen to a pressure of 210 mm of mercury. The sources of fission neutrons were samples of mixed oxides of uranium and plutonium dioxide, prepared in the form of disks 60 mm in diameter and 2.5 mm thick, and irradiated by a beam of thermal neutrons from a reactor.

The cloud chamber was placed out of the beam at a distance of 16.5 cm from the sample. The chamber of 20 cm diameter and of 6 cm depth was constructed so as to have a minimum of neutron scattering material. The beam of thermal neutrons was interrupted by a fast-acting mechanical screen of boron carbide. The screen was opened in synchronization with the expansion of the chamber. Experimentally, on the average, there were approximately 10 proton recoil tracks per expansion. The background of fast neutrons from the reactor was less than 2%. Approximately 30,000 proton recoil tracks were obtained for each sample.

The lengths of the proton recoil tracks making an angle < 15° with the neutron direction were measured during the analysis of the results. The pictures were analyzed by stereoscopic projection. The region covered had a diameter of 17 cm and a height of 4.5 cm.

The distribution of the recoil protons, terminating in the gas of the chamber, by energy intervals, is given in the table. The lower limit of the measured energy is 50 kev which corresponds to a track length of 0.8 cm. Tracks shorter than 0.8 cm were easily observed on photographs, but it was difficult to measure them with sufficient accuracy.

In converting from a spectrum of proton recoils to a spectrum of neutrons, it is necessary to take into account the dependence of the neutron-proton scattering cross section on energy, and the geometric correction, in the probability P that tracks of varying lengths will terminate in the chamber. The scattering cross section and the term 1/P by which the number of tracks must be multiplied are displayed in the table.

ΔE, kev	Track length in cm	Number of tracks			σ, bn	$\frac{1}{P}$
		U^{233}	U^{235}	Pu^{239}		
50—100	0.8— 1.3	59	62	51	14.0	1.10
100—200	1.3— 2.5	111	118	124	11.5	1.15
200—300	2.5— 4.5	103	109	102	9.1	1.37
300—400	4.5— 6.9	60	61	67	7.6	1.81
400—500	6.9— 9.6	49	39	41	6.5	2.62
500—700	9.6—16.2	32	30	27	5.6	6.74

The fission neutron spectra are presented in the figure.

Comparing the experimental data in the table and in the figure, one can see that the fission neutron spectra from U^{233}, U^{235}, and Pu^{239} in the measured region coincide within the experimental errors (10 to 20%), and satisfactorily approximate Watt's formula[1]

$$F(E) \sim e^{-E/T} \sinh (2\sqrt{\omega E/T}) \qquad (1)$$

for values of the parameters $\omega = 0.5$ Mev and $T = 1$ Mev.

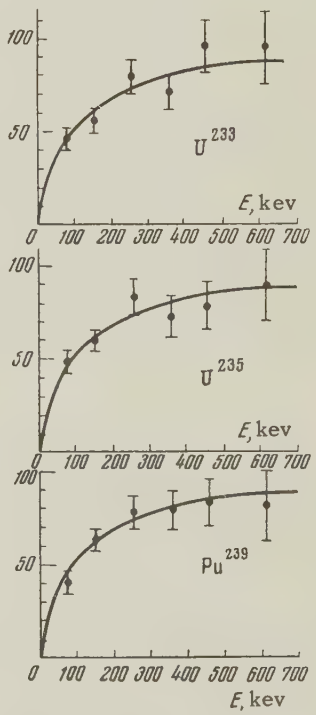

Spectra of the fission neutrons from U^{233}, U^{235}, and Pu^{239}. The experimental points are given in the form of relative number of neutrons per 100-kev energy interval. The full lines correspond to formula (1).

The low energy region of the U^{235} fission spectrum was measured earlier with a cloud chamber by Bonner et al.[2] and by Barton.[3] Within the limits

of error (15 to 20%), these authors also obtained agreement between the form of the spectrum and curve (1).

In our earlier work,[4] estimates were obtained of the temperatures of fragments from U^{233} and Pu^{239} relative to U^{235}, equal to (1.04 ± 0.01) and (1.05 ± 0.01) Mev. The value of the function F(E) for parameters $\omega = 0.5$ Mev, $T_0 = 1$ Mev, $T_1 = 1.03$ Mev, $T_2 = 1.06$ Mev in the spectrum energy region 0 — 1 Mev differ from each other by not more than 4%, which is less than the accuracy of our measurements.

In this work, we also determined the ratio of the number of recoil protons in the interval 0.05 — 0.6 Mev to their number with energies > 0.6 Mev was also determined. The experimental values of the ratios for U^{233}, U^{235}, and Pu^{239} are respectively equal to 0.49 ± 0.04, 0.53 ± 0.04, and 0.48 ± 0.04. A calculation using formula (1) and the parameter values given above gave for these values the numbers 0.5, 0.52, and 0.495.

Thus, the measurements of fission neutron spectra in the region of low energies are in agreement with the results of Ref. 4, confirming the conclusion that the previously noted difference in the fission neutron spectra of U^{233}, U^{235}, and Pu^{239} lies in the high energy region.

In conclusion I express my gratitude to I. I. Bondarenko and O. D. Kazachkovski for suggestions and discussion of the results and to A. I. Leipunskii for his continued interest in this work.

[1] B. Watt, Phys. Rev. **87**, 1037 (1952).

[2] Bonner, Ferrell, and Rinehart, Phys. Rev. **87**, 1032 (1952).

[3] R. Leachman, Paper at the International Conference on the Peaceful Uses of Atomic Energy, Geneva (1955).

[4] Kovalev, Andreev, Nikolaev, and Guseinov, J. Exptl. Theoret. Phys. (U.S.S.R.) **33**, 1069 (1957), Soviet Phys. JETP **6**, 825 (1958).

Translated by Fay Ajzenberg-Selove
86

SYSTEMATICS OF THE AVERAGE NUMBER ν OF PROMPT FISSION NEUTRONS

B. D. KUZ'MINOV and G. N. SMIRENKIN

Submitted to JETP editor September 30, 1957

J. Exptl. Theoret. Phys. (U.S.S.R.) **34**, 503-504 (February, 1958)

THE number ν of prompt neutrons emitted during fission, is determined by the energy balance equation

$$E_f = E_k + E_x = E_k + \nu E_n + E_\gamma, \qquad (1)$$

in which E_f is the fission energy, E_k and E_x are the kinetic and the excitation energies of the pair of fragments, and νE_n and E_γ are the energies carried by the prompt neutrons and γ rays respectively. In this work we compare the experimental values of ν (Refs. 1 — 8) with the results of calculations based on the assumptions that will be discussed below.

We considered the masses of only two fragments, a light one M_ℓ and a heavy one M_h, corresponding to the most probable method of fission. When calculating the fission energy, the mass of the fissioning nucleus M(A, Z) was determined from the Green[9] semi-empirical formula, and the masses of the fission fragments $M(A_\ell, Z_\ell)$, $M(A_h, Z_h)$ were calculated by the Fermi formula with the Fong correction factors,[10] which take into account the shell structure of the nuclei. Since the mass of the heavy fragment varies slightly[11] over the wide range $232 < A < 252$, owing to the shell effect, and has an average value 139 ± 3, we assumed for simplicity $A_h = 140$ (prior to the neutron emission). The values of Z_ℓ and Z_h, the initial charges of the fission fragments, are calculated subject to the hypothesis of equal β-decay chains.

The kinetic energy E_k of the fission fragments was calculated from the formula

$$E_k = c_1 Z^2 A^{-1/3} (1 - c_2 Z^2/A), \qquad (2)$$

obtained by representing E_k as the Coulomb repulsion energy of two charged deformed spheres.[10] The constants c_1 and c_2 are chosen to obtain the best fit between Eq. (2) and the experimental values of ν in Eq. (1).

The average energy E_n carried by a prompt neutron consists of the binding energy E_b of the last neutron in the fragment and its mean kinetic energy 2T with respect to the fragment at rest. The temperature T of the fragment, after the emission of the neutron, was estimated from data on the neutron spectra of the fission of U^{233}, U^{235}, and Pu^{239} by thermal neutrons[12] and the spontaneous fission of Cf^{252} (Ref. 13). The values of E_b were calculated from the mass formula of Fermi-Fong.[10] The value $\nu_\ell/\nu_h = 1.3$, obtained by Fra-

ser[14] for the fission U^{235} by thermal neutrons, was extended to include the entire nucleus under consideration. The calculated values of E_n were found to be in good agreement with measured values of $d\nu/dE_x = 1/E_n$ (Refs. 15 – 17).

The mean energy E_γ of the instantaneous γ rays was assumed constant, 8 Mev, in the calculations, as confirmed by experiments on the study of the prompt-fission γ rays from U^{235} (n, f) and Cf^{252} (Refs. 15, 18).

For comparison with the calculations, all the experimental values of γ, for the fission induced by neutrons, were reduced to values of ν for spontaneous fission of the corresponding compound nuclei, using the formula $d\nu/dE_x = 1/E_n$. The validity of this operation was confirmed by direct comparison of ν for the processes Pu^{235} (n, f) and Pu^{241} (n, f) (Ref. 5) with ν for spontaneous fission of Pu^{240} and Pu^{242} (Refs. 1 – 3).

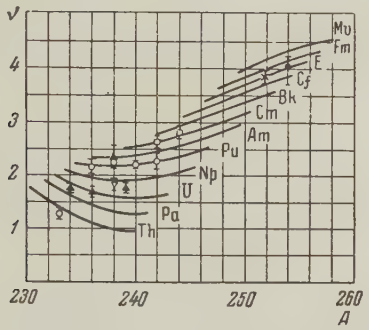

Fig. 1. Dependence of the average number of prompt fission neutrons on A, for various Z. Lower point ○ – Th, ▲ – U, ▽ – Np, ○ – Pu, □ – Cn, × – Cf, ● – Fm.

The diagram shows a family of curves of ν as functions of A for various Z. Most experimental data are in satisfactory agreement with the calculations. An exception is the value of ν for the spontaneous fission of U^{238} (Ref. 7). The value of ν for the spontaneous fission of Th^{232} was not compared with the results of these calculations, for, according to the latest measurements for the period of spontaneous fission of Th^{232} (Ref. 19), there is a certain doubt concerning the value $\nu_{Th}/\nu_U = 1.07 \pm 0.1$ (Ref. 6).

The non-monotonic course of $\nu(A)$ is due to the shell structure of the fragments. Without taking the shells into account, $d\nu/dA > 0$. On nuclei with $A < 240$, i.e., with $A\ell < 100$, the nearness of a shell with 50 neutrons manifests itself – the excitation energy increases with diminishing A, and the sign of $d\nu/dA$ is reversed.

The authors express deep gratitude to Professor A. I. Leipunskii and I. I. Bondarenko for valuable advice and remarks.

[1] Crane, Higgins, and Bowman, Phys. Rev. **101**, 1804 (1956).

[2] Diven, Martin, Taschek, and Terrell, Phys. Rev. **101**, 1012 (1956).

[3] Hicks, Ise, and Pyle, Phys. Rev. **101**, 1016 (1956).

[4] Kuz'minov, Kutsaeva, and Bondarenko, Атомная энергия (Atomic Energy) **4**, No. 2 (1958).

[5] D. J. Hughes and R. B. Schwartz, Neutron Cross Sections, Suppl. 1957.

[6] Barclay, Galbraith, and Whitehouse, Proc. Phys. Soc. **A65**, 73 (1952).

[7] D. J. Littler, Proc. Phys. Soc. **A65**, 203 (1952).

[8] Choppin, Harvey, Hicks, Ise, and Pyle, Phys. Rev. **102**, 766 (1956).

[9] A. E. S. Green, Phys. Rev. **95**, 1006 (1954).

[10] P. Fong, Phys. Rev. **102**, 434 (1956).

[11] W. J. Swiatecki, Phys. Rev. **100**, 936 (1955).

[12] Kovalev, Andreev, Niklaev, and Guseinov, J. Exptl. Theoret. Phys. (U.S.S.R.) **33**, 1069 (1957), Soviet Phys. JETP **6**, 825, (1958).

[13] Hjalmar, Slatis, and Tompson, Ark. Fyzik. **10**, 357 (1956).

[14] J. S. Fraser, Phys. Rev. **88**, 536 (1952).

[15] R. B. Leachman, Phys. Rev. **101**, 1005 (1956).

[16] Smirenkin, Bondarenko, Kutsaeva, Mishchenko, Prokhorova, and Shemetenko, Атомная энергия (Atomic Energy) **4**, No. 2 (1958).

[17] Kalashnikova, Lebedev, and Spivak, Атомная энергия (Atomic Energy) **2**, 18 (1957).

[18] Smith, Fields, and Friedman, Phys. Rev. **104**, 699 (1956).

[19] Podgurskaia, Kalashnikova, Stoliarov, Vorob'ev, and Flerov, J. Exptl. Theoret. Phys. (U.S.S.R.) **28**, 503 (1955), Soviet Phys. JETP **1**, 392 (1955).

Translated by J. G. Adashko
87

ON THE DOUBLE BETA-DECAY OF Ca^{48}

V. B. BELIAEV and B. N. ZAKHAR'EV

Joint Institute of Nuclear Studies

Submitted to JETP editor November 8, 1957

J. Exptl. Theoret. Phys. (U.S.S.R.) **34**, 505-506 (February, 1958)

A number of experimental researches have shown[1,2] that the period of double β-decay is greater than 10^{18} years. In this connection, the necessity has arisen of re-examining the esti-

mates that have been given in the literature for the probability of β-decay with the emission of two neutrinos. Goeppert-Mayer[3] estimated the probability of two-neutrino decay, but did not calculate the nuclear matrix element, which led to disagreement with experiment. We have carried out this calculation in the approximation of the shell model.

We consider the case most convenient for calculation, the decay $Ca^{48} - Ti^{48}$. The maximum decay energy, the identical structures of the parent and product nuclei, and the fully occupied shells of definite spins J distinguish this reaction among all the cases for which double β-decay is energetically possible.

It is assumed that the transition occurs by way of the virtual intermediate state Sc^{48}. All three of the nuclei in question (Ca^{48}, Sc^{48}, Ti^{48}) have the same core Ca^{40}, which plays no part in the process. Therefore we shall be interested in only 8 nucleons in each nucleus. We note further that the radial functions of the nuclei in question are identical, and the corresponding integrals are not involved in our considerations. The construction of the functions is facilitated by the convenient structure of the nuclei chosen. Their filled shells and almost filled shells do not require the rather complicated apparatus of fractional parentage coefficients.

The functions for the initial and final states have been given by Maksimov and Smorodinskii.[4] The function for the intermediate state is constructed analogously. Its spin-orbit corresponds to the Young schemes [2111111] for T = 3 and [11111111] for T = 4. In the first case the intermediate function reduces, from the point of view of spatial symmetry, to a function of s = 2 nucleons. Thus we have

$$\Phi_p^M = \frac{1}{\sqrt{8}} \sum \pm \chi(i)\, \Psi_p^M(i),$$

where, for example, for the case in which the first nucleon is a proton

$$\Psi_p^M(1) = \frac{r}{8!\,27\cdot 7}\, \hat{A}_7 \left[\begin{matrix}3\\4\end{matrix}\right]\left(\left[\begin{matrix}5\\6\end{matrix}\right]\left[\begin{matrix}7\\8\end{matrix}\right] - \left[\begin{matrix}5\\7\end{matrix}\right]\left[\begin{matrix}6\\8\end{matrix}\right] - \left[\begin{matrix}5\\8\end{matrix}\right]\left[\begin{matrix}6\\7\end{matrix}\right]\right) \sum_m ({}^7/_2\, {}^7/_2\, M - mm \,|\, {}^7/_2\, {}^7/_2\, 1M)\, \varphi^{(1)}_{M-m} \varphi^{(2)}_m$$

Here $(j_1 j_2 m_1 m_2 \,|\, j_1 j_2 JM)$ is a Clebsch-Gordan coefficient, M is the z component of the angular momentum J, and $\hat{A}_7$ denotes antisymmetrization with respect to seven particles (without the first). The square of the matrix element (with tensor interaction) for the transition $Ca^{48} - Sc^{48}$ (T = 3) $- Ti^{48}$ is $M^2 = 0.006$ (for the transition through Sc^{48} with T = 4 it is an order of magnitude smaller). The half-value period is

$$T = \frac{0.693 \cdot 6 \cdot 7 \cdot 15\, |\Gamma(3+2s)|\, {}^4\hbar^{13}}{4^6\pi^8 \gamma^2 m^{11} c^{10} g^4} \times \left(\frac{4\pi mc\rho}{h}\right)^{-4s} \frac{m^2c^4}{M^2} \cdot 10^{-9} \text{ years (Ref. 3).}$$

Taking it into account that the decay can also go through excited intermediate states, we get for the half-life a value of about 10^{19} years. As has been shown by Bohr and Mottelson,[5] a correction factor must be applied to the probability of decay calculated by the shell model; we take it from the data for nuclei in the neighborhood of Ca^{48}; $\lambda \sim 0.01$. In our case, however, the transition is between even-even nuclei, and therefore it can be hoped that less of a correction to the shell model may turn out to be needed ($\lambda > 0.01$). It would therefore be interesting to check how reliable the shell model is for Ca^{48}.

We take occasion to express our gratitude to Professor Ia. A. Smorodinskii and to L. A. Maksimov for valuable advice.

[1] M. Awschalom, Phys. Rev. **101**, 1041 (1956).

[2] Dobrokhotov, Lazarenko, and Luk'ianov, Dokl. Akad. Nauk SSSR **110**, 966 (1956), Soviet Phys. "Doklady" **1**, 600 (1956).

[3] M. Goeppert-Mayer, Phys. Rev. **48**, 512 (1935).

[4] L. A. Maksimov and Ia. A. Smorodinskii, Izv. Akad. Nauk SSSR, ser. fiz. **19**, 365 (1955).

[5] A. Bohr and B. R. Mottelson, Danske Mat.-Fys. Medd. **27**, No. 16 (1953).

Translated by W. H. Furry
88

METHOD OF MEASURING PARTICLE ENERGIES ABOVE 10^{11} ev

N. L. GRIGOROV, V. S. NURZIN, and I. D. RAPOPORT

Moscow State University

Submitted to JETP editor October 25, 1957

J. Exptl. Theoret. Phys. (U.S.S.R.) **34**, 506-507 (February, 1958)

MORE than two years ago one of us (Grigorov) proposed a method for determining the energy of a separate nuclear-active particle, based on the measurement of the total energy liberated in dense matter by all the secondary particles produced

when the primary particle passes through a thick layer of matter.

If we know the ionization $I(x)$ produced by the "primary" particle and all its descendents at each point x of the absorber, then the energy E_0 of the "primary" particle will be

$$E_0 = \varepsilon \int_0^\infty I(x)\,dx,$$

disregarding the decay processes involving neutrino production (in dense matter this process can be neglected); ϵ is the mean energy for the production of one pair of ions in the material of the absorber.

We recently constructed an instrument based on the above principle, and obtained experimental results at 3860 m above sea level.

The instrument is a truncated pyramid 170 cm high, the upper cross-section of which is approximately 0.6 m^2, and the lower one approximately 0.8 m^2 (Fig. 1). The pyramid contains eight layers of iron with a total thickness of 85 cm.

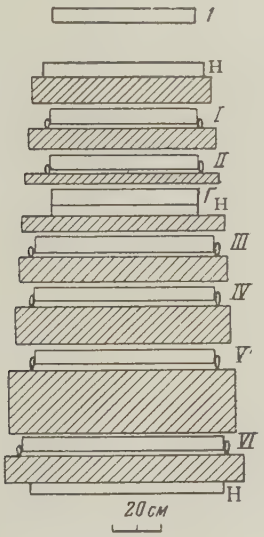

Fig. 1. Schematic cross-section through the setup. I–VI – rows of ionization chambers; 1, 2 – rows of telescopic counters; H – boxes with hodoscopic counters.

When chosing the absorber material it was necessary to compromise between the following requirements: (a) the range of the electron-photon cascade should be greater than the range for the nuclear interaction; (b) the absorber matter should be sufficiently dense to absorb all the primary and all the secondary particles at sufficiently small thickness, ~ 1 m.

The ionization was measured in our instrument by means of cylindrical pulse ionization chambers, made of iron and brass (to eliminate transient effects), with walls 1 mm thick. The chambers cover an area 0.36 m^2 in the upper section of the pyramid and 0.6 m^2 in the lower one. The diameter of each chamber is 4 cm, and the length fluctuates from 65 to 75 cm. The chambers are filled with pure argon to a pressure of 5.5 atmos.

The ionization chambers are placed in the instrument between layers of iron in six rows (I – VI in Fig. 1). The upper row contains 15 chambers, the lower 21. The total number of chambers in the instrument is 105. Each three chambers is connected to one amplifier with a dynamic range of approximately 800, whose output is connected with an individual cathode ray tube 8 cm in diameter. The electric pulses produced in the ionization chambers are recorded by photographing the screens of all tubes, which are mounted in a single block. This block, which we call a multi-channel oscillograph, contains 49 cathode ray tubes. In addition to ionization chambers, the instrument contains a counter telescope (row 1 and 2) that restricts the solid angle for "primary" particles, and several boxes with hodoscopic counters.

The instrument is controlled as follows. The ionization pulse from each row of chambers, regardless of the chamber in which the pulse originates is received by a special selector, which operates if the pulse exceeds a certain threshold value V_{thr} simultaneously in any n rows of chambers (both n and V_{thr} can be varied over a wide range). If the selector operates simultaneously with the discharges in the telescopic counters, the resultant electric pulse triggers the beams of all the multi-channel oscillograph tubes and the amplitude of the pulses from the ionization chambers are photographed. The minimum recordable ionization corresponds to a simultaneous passage of 5 – 10 relativistic particles through the center line of the chamber.

The fact that our instrument records ionization with the aid of a large number of independently-operating chambers, makes it possible to trace

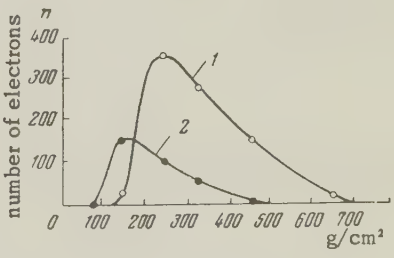

Fig. 2. Examples of events of electron-nuclear cascades: 1 – energy of "primary" particle 1.5×10^{11} ev, 2 – energy of "primary" particle 0.4×10^{11} ev.

the energy losses of an individual high-energy particle in a dense substance.

Certain examples of recorded events are shown in Fig. 2. In the future we plan to place a cloud chamber over the energy detector to permit study of an elementary interaction event between nuclear-active particles of known energy and nuclei of specified atomic numbers.

A detailed description of the experimental data obtained with the above instrument will be published.

Translated by J. G. Adashko
89

COLLECTIVE MOTIONS IN A SYSTEM OF QUASI-PARTICLES

P. S. ZYRIANOV

Ural' Polytechnic Institute

Submitted to JETP editor October 26, 1957

J. Exptl. Theoret. Phys. (U.S.S.R.) **34**, 508-509 (February, 1958)

In the self-consistent field approximation the consideration of a strong interaction between particles leads to a dependence of the energy of a separate particle (which is considered as a quasi particle) on the state of motion of the other particles in the system. Even in the case of a spatially uniform distribution of the particles in the system, a consideration of the interaction leads to a complicated dependence of the particle energy on its momentum.*

The Hamiltonian function of a quasi particle in the case of a non-uniform distribution in space can be taken in the form

$$\varepsilon_j(\mathbf{p}) + \int G(|\mathbf{r}-\mathbf{r}'|) \sum_i |\psi_i(\mathbf{r}')|^2 d\mathbf{r}', \qquad (1)$$

where the first term takes into account correlations at small distances apart and the kinetic energy, while the second term refers to long-range interactions (Hartree field). The equation of motion for ψ_j is of the form

$$\varepsilon_j(\hat{\mathbf{p}})\varphi_j + \int G(|\mathbf{r}-\mathbf{r}'|) \sum_i |\psi_i(\mathbf{r}')|^2 d\mathbf{r}' \psi_j = \varepsilon_j \psi_j. \qquad (2)$$

We shall restrict our considerations to those states of the system which are close to a spatially uniform distribution of the quasi particles as far as the coordinates are concerned, and to a random distribution as far as the velocities are concerned, i.e., to states near the ground state. In that case the momenta of the collective motions (motions of a hydrodynamical character) will be small and the operator $\epsilon_j(\hat{\mathbf{p}})$ can be written in the form $\epsilon_j(\hat{\mathbf{p}}_0 + \hat{\mathbf{p}})$, where $\hat{\mathbf{p}}$ is the operator of the momentum of the collective motion (a small quantity) and $\hat{\mathbf{p}}_0$ the operator of the momentum of the random motion. Expanding ϵ_j in powers of $\hat{\mathbf{p}}$ and limiting ourselves to terms quadratic in $\hat{\mathbf{p}}$, we obtain

$$\varepsilon_j(\hat{\mathbf{p}}_0 + \hat{\mathbf{p}}) = \varepsilon_j(\hat{\mathbf{p}}_0) + \frac{1}{2}[\nabla_{\mathbf{p}_0}\varepsilon_j(\hat{\mathbf{p}}_0), \mathbf{p}]_+ + \frac{1}{4}[\Delta_{\mathbf{p}_0}\varepsilon_j(\hat{\mathbf{p}}_0), \hat{\mathbf{p}}^2]_+ + \cdots, \qquad (3)$$

where $[,]_+$ denotes an anticommutator.

We introduce into the wave function the new variable $\mathbf{r}_0$, canonically conjugate to $\hat{\mathbf{p}}_0$. If we assume that the commutator $[\hat{\mathbf{p}}_0, \hat{\mathbf{p}}]_- = 0$, then $\psi_j = \psi_{0j}(\mathbf{r}_0)\Phi_j(\mathbf{r})$. Substituting (3) into (2) and averaging over the functions $\psi_{0j}(\mathbf{r}_0)$ which satisfy the equation

$$\varepsilon_j(\hat{\mathbf{p}}_0)\psi_{0j} = \varepsilon_{0j}\psi_{0j}, \qquad (4)$$

we obtain the equation

$$-\frac{\hbar^2}{2m_j^*}\Delta\Phi_j - i\hbar(\mathbf{v}_j^0\nabla)\Phi_j + \int G(|\mathbf{r}-\mathbf{r}'|) \sum_i |\Phi_i(\mathbf{r}')|^2 d\mathbf{r}'\Phi_j = (\varepsilon_j - \varepsilon_{0j})\Phi_j, \qquad (5)$$

in which we have used the notation

$$1/m_j^* = \int \psi_{0j}^* \Delta_{\mathbf{p}_0}\varepsilon_j(\hat{\mathbf{p}}_0)\psi_{0j}d\mathbf{r}',$$

$$\mathbf{v}_j^0 = \int \psi_{0j}^* \nabla_{\mathbf{p}_0}\varepsilon_j(\hat{\mathbf{p}}_0)\psi_{0j}d\mathbf{r}', \quad \varepsilon_{0j} = \int \psi_{0j}^* \varepsilon_j(\hat{\mathbf{p}}_0)\psi_{0j}d\mathbf{r}'.$$

Equation (5) obtained in this way describes only the collective motions in a system of quasi particles, but its coefficients depend on the characteristics of the random motion of the quasi particles in the ground state determined by Eq. (4).

Substituting into (5)

$$(\varepsilon_j - \varepsilon_{0j}) \to i\hbar\partial/\partial t, \quad \Phi_j = (1+\rho_j)^{1/2} e^{iS_j/\hbar}$$

(Φ_j is normalized in a unit volume), and retain-

---

*Taking exchange interaction into account gives, for instance, in the case of Coulomb forces,

$$\varepsilon(p) = \frac{e^2}{\pi\hbar} p_0 \left(2 + \frac{p_0 - p}{p_0 p} \ln \frac{p_0 + p}{p_0 - p}\right)$$

(p_0 is the momentum at the Fermi surface); taking force correlations into account leads to a more complicated dependence $\varepsilon(p)$.

ing in the equations for ρ_j and S_j the terms linear in S_j and ρ_j, we get

$$S_j + (\mathbf{v}_j^0 \nabla) S_j + \int G(|\mathbf{r} - \mathbf{r}'|) \sum_i \rho_i(\mathbf{r}')\, d\mathbf{r}' - (\hbar^2/4m_j^*)\,\Delta\rho_j = 0, \quad (6)$$

$$\rho_j + (\mathbf{v}_j^0 \nabla)\rho_j + (1/m_j^*)\,\Delta S_j = 0.$$

For solutions of ρ_j and S_j of the form $\sim \exp[i(\mathbf{k}\cdot\mathbf{r}) - i\omega t]$ these equations lead to the following dispersion relation

$$1 = k^2 G(k) \sum_j \frac{1}{m_j^*} \left\{ (\omega - \mathbf{v}_j^0 \cdot \mathbf{k})^2 - \frac{\hbar^2 k^4}{4m_j^{*2}} \right\}^{-1}. \quad (7)$$

From (7) it follows that in the limit as $\mathbf{k} \to 0$ the frequency ω_0^* depends on the effective mass of the quasi particles which, generally speaking, differs from the ordinary mass of the particles.

In the case where $\epsilon(p) = p^2/2m$, (7) goes over into the well-known dispersion law.[1] To evaluate m_j^* it is sufficient to know the dependence of the total energy (kinetic Fermi, exchange, and correlation energy) of one particle on its momentum. In the case of a dense electron gas $\epsilon(p)$ can be evaluated by the method given in Ref. 2.

The method proposed here is suitable to find the spectrum of the plasma oscillations of electrons in a periodic field, for the case of one band.† If we understand by $\epsilon_{0j}(p_0)$ the energy of an electron in a periodic field, then Eq. (7) is equivalent to the corresponding equation in the paper by Wolff.[3]

[1] D. Pines, Phys. Rev. **92**, 626 (1953).

[2] M. Gell-Mann and K. A. Brueckner, Phys. Rev. **106**, 364 (1957); M. Gell-Mann, Phys. Rev. **106**, 369 (1957).

[3] P. A. Wolff, Phys. Rev. **92**, 18 (1953).

Translated by D. ter Haar
90

CREATION OF POSITIVE PIONS BY NEGATIVE PIONS

Iu. P. DOBRETSOV and B. A. NIKOL'SKII

Academy of Sciences, U.S.S.R.

Submitted to JETP editor October 29, 1957

J. Exptl. Theoret. Phys. (U.S.S.R.) **34**, 510-511 (February, 1958)

THE creation of pions by pions has been studied by a number of authors.[1-6] All these analyses refer to the creation of pions in the nucleus as a whole; one may assume, however, that at these incident energies, the pions are created on the individual nucleons of the nucleus. The effect of the nucleus manifests itself in this case through a second-order interaction between pions of the final state and the nucleons of the nucleus. This circumstance considerably complicates the interpretation of experimental data, and therefore we can only obtain from it the qualitative character of the creation of pions by pions.

In the present article we consider the creation of positive pions in nuclear emulsion under the action of negative pions having an energy of 340 ± 30 Mev.

The emulsion stack consisting of 60 layers of NIKFI type R emulsion, of 23 mm total thickness and 100 mm diameter was placed in the 370-Mev negative pion beam of the synchrocyclotron of the Joint Institute for Nuclear Research. In passing through the emulsion, the incident pions lost up to 60 Mev by ionization. Thus the present results describe the creation of pions under the influence of negative pions having an energy $E_0 = 340 \pm 30$ Mev. The method chosen to find cases of positive pion production consists in area scanning the emulsion and counting $\pi^+ \to \mu^+ \to e^+$ decays. Then the positive pions were followed to their creation point. This search method effectively allowed us to count the production of pions leaving a path of up to 6 cm, i.e., an energy up to 70 Mev.

In following positive pion tracks, 56 stars caused by negative pions were found. In 21 of these stars the emission of the positive pions was accompanied by the emission of a second meson identified by the grain density gradient along the track. It is evident that these events must be attributed to the formation of the positive pion. The emission of a second pion was not found in the remaining stars, but these events can again be attributed to the formation of positive pion followed by the absorption of the negative pion by the nucleus, or the emission of a neutral pion. This conclusion is supported by data on the absorption of pions by nuclei at these energies.[7]

*The method developed to find the dispersion equation is easily generalized to cover the case of many bands.

The energy of the created positive pions was determined from their range in the emulsion; the energy of the negative pions (in stars with two pions) was determined from the grain density.

The method chosen for counting positive pions in order to determine the production cross section and the angular and energy distribution of created pions, requires the introduction of a correction for edge effect, depending upon the finite size of the emulsion stack. In order to include the edge effect, every counted event of positive pion formation was assigned a statistical weight $\kappa_i = 1/p_i$, where p_i is the probability for finding a pion track of the given length and distributed in a certain way in the emulsion stack. The computation of κ_i is described in detail in Ref. 8.

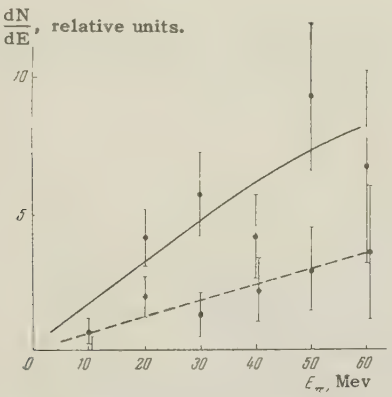

Fig. 1. Energy distribution for the creation of positive pions. The dotted curve indicates the distribution of positive pions emitted from stars in which the emission of a second pion was noted.

Figures 1 and 2 show the energy and angular distribution for the creation of positive pions. It may be seen from these figures that the distribution of positive pions accompanied and not accompanied by the emission of a second meson from the nucleus are similar. This is an additional argument for believing that almost all the observed positive pions are created.

Determinations of the relative momentum of the two pions emitted from the same nucleus, disclose no visible correlation between the two final state pions. This is only a qualitative conclusion however. A reliable determination of the momentum distribution function for the pions requires a considerably more accurate experiment.

The cross section for creation of slow positive pions ($E_{\pi^+} = 0 - 60$ Mev) by negative pions of 340 ± 30 Mev in photoemulsion nuclei was found to be

$$\sigma = (2.1 \pm 0.8) \cdot 10^{-27} \text{cm}^2.$$

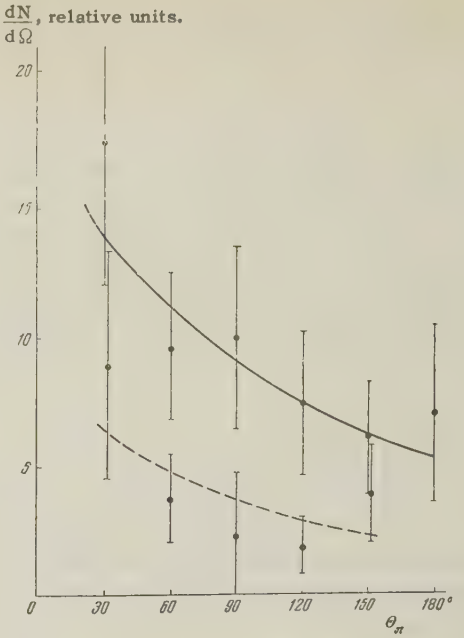

Fig. 2. Angular distribution for the creation of positive pions. The dotted curve indicates the distribution of positive pions emitted from stars in which the emission of a second pion was noted.

In conclusion the authors would like to express their gratitude to Professor I. I. Gurevich for discussing the results, to S. A. Ali-Zade, L. V. Sukrov, A. P. Mishakov, and L. A. Smirnov for helping with the experiment, to D. M. Samoilovich for developing the emulsion.

[1] V. V. Krivitskii and A. A. Reut, Paper delivered at the All-Union Conference on Physics of High-Energy Particles, Moscow, May, 1956.

[2] M. Blau and M. Kaulton, Phys. Rev. **96**, 150 (1954).

[3] M. Blau and A. Oliver, Phys. Rev. **102**, 489 (1956).

[4] W. F. Fry, Phys. Rev. **91**, 1576 (1953).

[5] Blau, Caulton, and Smith, Phys. Rev. **92**, 516 (1953).

[6] N. A. Mitin and E. L. Grigor'ev, Dokl. Akad. Nauk SSSR **103**, 219 (1955).

[7] B. A. Nikol'skii and L. M. Barkov, Usp. Fiz. Nauk **61**, 341 (1957).

[8] Alpers, Barkov, et al., J. Exptl. Theoret. Phys. (U.S.S.R.) **30**, 1025 (1956), Soviet Phys. JETP **3**, 914 (1957).

Translated by M. A. Melkanoff
91

ROTATION OF A PLASMA

V. G. STEPANOV, V. F. ZAKHARCHENKO, and V. S. BEZEL'

Submitted to JETP editor November 4, 1957

J. Exptl. Theoret. Phys. (U.S.S.R.) **34**, 512-513 (February, 1958)

IN a gaseous discharge which takes place in a magnetic field the magnetic lines of forces are "frozen" in the plasma.[1-3] This phenomenon offers the possibility of producing rotational motion of a plasma through the use of a rotating magnetic field.

In the magneto-hydrodynamic approximation, the distribution of particles in an isothermal ideal gas follows the usual centrifugal law. As in the case of mechanical rotation, a rotating conducting gas may be used as an electromagnetic centrifuge. In this connection it is interesting to note that the velocity of rotation is not limited by mechanical considerations.

In the present experiment the plasma was produced in a glass chamber 380 mm high and 60 mm in diameter. The anode, of tantalum, was in the upper part of the chamber. The cathode was liquid mercury. The chamber contained a rotor consisting of four mica vanes fastened to a quartz shaft which was mounted along the axis of the chamber in jewel bearings. The partial pressure of the mercury vapor in the chamber ranged from 10^{-1} to 10^{-3} mm Hg. The rotating magnetic field was set up by two pairs of mutually perpendicular iron-core coils. The current in one pair of coils was shifted in phase by 90° with respect to the current in the other pair. The average field in the neighborhood of the rotor was approximately 325 gauss. At the outset it was established that (1) with the magnetic field on but with no discharge the rotor remained motionless, and (2) when the discharge was excited without the magnetic field the rotor also remained motionless. When the rotating magnetic field was switched on while there was a discharge in the chamber rotation of the rotor was observed. When the magnetic field was reversed, strong deceleration of the rotor was observed; this was followed by acceleration to the maximum velocity.

The discharge current was maintained at 12 amps throughout these experiments. Using a stroboscope it was established that the steady-state speed of the rotor was of the order of 50 rps when the speed of the magnetic field was 50 rps.

Using these results it is possible to estimate the magnitude of the forces which act on the rotor by virtue of the ionized gas which revolves in the rotating magnetic field. The equation of motion of the rotor is $I\,d\omega/dt = M_d - M_f$, where I is the moment of inertia of the rotor with respect to the axis of rotation, $d\omega/dt$ is the angular acceleration, M_d is the moment of the driving force with respect to the axis, and M_f is the moment of the friction forces. It turns out that the friction forces can be neglected in the present case. The moment of inertia of the rotor was calculated and found to be 0.7 g-cm^2. To estimate the moment of the driving forces we assume that $d\omega/dt$ is constant and equal to the mean experimental value. The rotor is accelerated to the steady-state velocity in 0.7 sec at a pressure of 10^{-1} mm Hg; an angular velocity of 50 rps is achieved. Consequently the mean acceleration is of the order of 7 rev/sec^2 or 45 rad/sec^2. Thus $M_d = 31.5$ dyne-cm. Knowing the moment of the forces which act on the rotor we can determine the mean dynamic pressure:

$$P = M_d / 4sr_{av} \approx 1.57 \text{ dynes/cm}^2$$

Since $P = Nmv^2$, $N = P/m\omega^2 r_{av} \approx 2.5 \times 10^{17}$.

The density of charged particles under the present experimental conditions is $10^{11} - 10^{12}$; an estimate of the forces indicates that the rotor is acted on by a gas with a density of 10^{17}, which is approximately equal to the density of the mercury vapor.

In Refs. 4 and 5 a rotating plasma was obtained by exciting a discharge between two coaxial cylinders (electrodes) in a fixed magnetic field. In these experiments plasma rotation arises as a result of the drift velocity $v_\varphi = cE/H$ and the particle distribution is given by $n = AR^\alpha$ where R is the distance from the axis of rotation to the point of observations and $\alpha = \mu c^2 E^2/kTH^2$. It is apparent that this method of producing plasma rotation can also be used to make an electromagnetic centrifuge.

[1] H. Alfven, Cosmical Electrodynamics, London, 1950.

[2] P. E. Kolpakov and Ia. P. Terletskii, Dokl. Akad. Nauk SSSR **76**, 185 (1951).

[3] Ia. P. Terletskii, J. Exptl. Theoret. Phys. (U.S.S.R.) **32**, 927 (1957), Soviet Phys. JETP **5**, 755 (1957).

[4] H. C. Early and W. G. Dow, Phys. Rev. **79**, 186 (1950).

[5] Batten, Smith, and Early, J. Franklin Inst. **262**, 17 (1956).

Translated by H. Lashinsky
92

FINE STRUCTURE AND HYPERFINE STRUCTURE OF PARAMAGNETIC RESONANCE OF Cr^{+++} IN SYNTHETIC RUBY

G. M. ZVEREV and A. M. PROKHOROV

Moscow State University

Submitted to JETP editor November 13, 1957

J. Exptl. Theoret. Phys. (U.S.S.R.) **34**, 513-514 (February, 1958)

THE electronic paramagnetic resonance spectrum for the Cr^{+++} ion in synthetic ruby (Al_2O_3) has been investigated earlier at 9000 and 12000 Mcs.[1-3] We have carried out a more complete investigation of this spectrum at 37,860 Mcs.

In the synthetic ruby crystal the Cr^{+++} ion (ground state ^4F, and spin $S = 3/2$) is in an electric field of trigonal symmetry. This field splits the lowest electrical level of the ion into two sublevels which are separated by 0.38 cm^{-1}. The behavior of the electrical levels in the presence of an external magnetic field is given by the spin Hamiltonian[4]

$$\mathcal{H} = D[S_z^2 - 1/3 S(S+1)] + g_{\parallel}\beta H_z S_z + g_{\perp}\beta(H_x S_x + H_y S_y) + A S_z I_z + B(S_x I_x + S_y I_y).$$

The fine structure was studied in a synthetic-ruby single crystal with a chromium dilution of 1:1,000. The lines were measured at two orientations of the crystal in the external magnetic field: (1) with the trigonal axis $Z \parallel H$, and (2) with the trigonal axis $Z \perp H$.

In the first case three absorption lines were observed; these correspond to transitions between levels with the following values of M_Z:

$$1) -3/2 \leftrightarrow -1/2, \quad 2) -1/2 \leftrightarrow +1/2, \quad 3) +1/2 \leftrightarrow +3/2.$$

In the second case the energy states ϵ_1, ϵ_2, ϵ_3, and ϵ_4 are a mixture of states with different M_Z. In all, six absorption lines were observed; the first three lines have intensities two orders of magnitude smaller than the other three.

The constants in the spin Hamiltonian determined from the lines were as follows:

$$D = -0.1912 \pm 0.0010\,cm^{-1}; \quad g_{\parallel} = 1.982 \pm 0.002; \quad g_{\perp} = 1.979 \pm 0.009.$$

The positions of all lines were calculated using these values. The agreement between the experimental values and the calculated values is good (cf. table). The sign of D is determined from a measurement of the relative line intensities at T = 4.2° K. We may note that at this temperature it is easy to saturate the lines. An estimate of the spin-lattice relaxation time T_1 indicates that this quantity is of the order of 10^{-2} sec.

Transition	H_{exp}, Oersted	H_{cal}, Oersted
Parallel orientation		
$-3/2 \longleftrightarrow -1/2$	9510	9510
$-1/2 \longleftrightarrow +1/2$	13650	13650
$+1/2 \longleftrightarrow +3/2$	—	17790
Perpendicular orientation		
$\epsilon_1 \longleftrightarrow \epsilon_4$	4293	4296
$\epsilon_3 \longleftrightarrow \epsilon_4$	5553	5557
$\epsilon_1 \longleftrightarrow \epsilon_2$	7620	7627
$\epsilon_2 \longleftrightarrow \epsilon_4$	11595	11595
$\epsilon_3 \longleftrightarrow \epsilon_2$	13400	13398
$\epsilon_1 \longleftrightarrow \epsilon_3$	15710	15697

The hyperfine structure was investigated in a sample containing 95 per cent of the Cr^{53} isotope; the dilution was 1:10,000. The hyperfine structure was resolved only for the $-\frac{1}{2} \longleftrightarrow +\frac{1}{2}$ line in the parallel orientation and the $\epsilon_2 \longleftrightarrow \epsilon_3$ line in the perpendicular orientation. There are four components, corresponding to the different projections of the nuclear spin ($I = 3/2$). The components are not equally spaced; the distance between the two inner lines is less than one-third of the distance between the outer lines. The unequal spacing may be attributed to a weak line at the center of the spectrum, due to the even chromium isotope in the sample.

The fine-structure splitting constants A and B were determined:

$$|A| = (16.8 \pm 0.04) \cdot 10^{-4}\,cm^{-1};$$

$$|B| = (16.8 \pm 0.06) \cdot 10^{-4}\,cm^{-1}$$

The fact that these values are the same indicates that the hyperfine structure is essentially isotropic.

The values found in the present work for the constants in the spin Hamiltonian for Cr^{+++} in a synthetic ruby single-crystal are in good agreement with the values reported in Refs. 1—3.

The authors are indebted to Professor A. I. Shal'nikov for help in carrying out the low temperature experiments.

[1] A. A. Manenkov and A. M. Prokhorov, J. Exptl. Theoret. Phys. (U.S.S.R.) **28**, 762 (1955), Soviet Phys. JETP **1**, 611 (1955).

[2] M. M. Zaripov and Iu. A. Shamonin, J. Exptl. Theoret. Phys. (U.S.S.R.) **30**, 291 (1956), Soviet Phys. JETP **3**, 171 (1956).

[3] A. A. Manenkov and A. M. Prokhorov, J. Exptl. Theoret. Phys. (U.S.S.R.) **31**, 346 (1956), Soviet Phys. JETP **4**, 288 (1957).

[4] B. Bleaney and K. W. H. Stevens, Rep. Prog. Phys. **16**, 108 (1953).

Translated by H. Lashinsky
93

ENERGY SPECTRUM OF ELECTRONS IN OPEN PERIODIC TRAJECTORIES

G. E. ZIL' BERMAN

Submitted to JETP editor November 13, 1957

J. Exptl. Theoret. Phys. (U.S.S.R.) **34**, 515-516 (February, 1958)

IN Ref. 1 we have given the equation of motion for an electron which obeys the dispersion relation $E(\mathbf{k}) = \Sigma A_n e^{i\mathbf{kn}}$ in a magnetic field ($H = H_z$):

$$\sum_n A_n \exp\left\{i\,(k_2 n_2 + k_3 n_3) - i\frac{n_1 n_2}{2\alpha_0^2}\right\} f\left(k_2 - \frac{n_1}{\alpha_0^2}\right) = Ef(k_2). \tag{1}$$

It is assumed that $\epsilon = \sqrt{a_1 a_2}/\alpha_0 \ll 1$ ($\alpha_0^2 = \hbar \times c/eH$; the a_i are the lattice constants). In Ref. 2 solutions of this equation were investigated for open periodic trajectories. In the present note we verify the assertion made in Ref. 2 concerning the exponential smallness of the breaks in the continuous energy spectrum in the case in which the function $\kappa_1 = \kappa_1(k_2)$ (the equation of the trajectory, i.e., the intersections of the surface $E(\mathbf{k}) = \text{const.}$ with the plane $k_3 = \text{const.}$) is analytic.

It will be assumed that κ_1 is large enough everywhere (the other cases are considered in Ref. 2) so that the quasi-classical approximation can be used, that is, we write

$$f(k_2) = \exp\left\{\frac{i}{\varepsilon^2}\varphi_1 + \varphi_2 + \frac{\varepsilon^2}{i}\varphi_3 + \left(\frac{\varepsilon^2}{i}\right)^2 \varphi_4 + \cdots\right\}. \tag{2}$$

Solution of this equation is much more difficult than solution of the Schrödinger equation because Eq. (1) is a difference rather than a differential equation. However, the general properties of the solution are the same in both cases. The following expressions are obtained in the first four approximations:

$$\varphi_1 = -\int \kappa_1 dx; \quad \varphi_2 = -\tfrac{1}{2}\ln P;$$

$$\varphi_3 = \int\left\{-\left(\frac{P'Q}{P}\right)'\frac{1}{4P} + \frac{QP'^2}{8P^3} + \frac{Q''}{8P} + \frac{R\kappa_1''}{24P}\right\}dx;$$

$$\varphi_4 = \frac{\varphi_3' Q}{2P} - \frac{1}{24P}\left\{6R(\varphi_2'^2 + \varphi_2'') + 3R'\varphi_2' + 3RP'\varphi_2' P^{-1} - 3R\varphi_2'' + \frac{1}{2}R'' + \frac{1}{2}\frac{R'P'}{P} + \frac{RP'^2}{P^2} - \frac{RP''}{2P}\right\}. \tag{3}$$

Here we have introduced the notation

$$P = \partial E/\partial\kappa_1, \quad Q = \partial^2 E/\partial\kappa_1^2, \quad R = \partial^3 E/\partial\kappa_1^3, \tag{4}$$

where κ_1 and k_2 are measured in dimensionless units (by κ_1 we are to understand $\kappa_1 a_1$ and by x we are to understand $k_2 a_2$).

Just as in the Schrödinger equation, the quantities φ_{2n}' are total derivatives and since P, Q, R, are periodic in k_2, this same property is characteristic of the even approximations $\varphi_2, \varphi_4, \ldots$. Consequently, if Eq. (2) is written in the form

$$f(k_2) = \rho e^{i\varphi}, \tag{5}$$

the modulus ρ will be a periodic function of k_2 (while the phase φ is an integral of a periodic function and does not change sign).

When displaced by one period, (5) should be multiplied by e^{ip}, where e^{ip} is ± 1 at the boundary of the allowed energy intervals. This locates the discontinuity at once. Keeping the first two approximations φ_1 and φ_2 (corresponding to the usual quasi-classical analysis), we have:

$$f(k_2) = P^{-1/2}\exp\left\{-i\varepsilon^{-2}\int_0^x \kappa_1 dx\right\}.$$

The condition $e^{ip} = \pm 1 = e^{i\pi n}$ obviously means:

$$S = 2\pi\alpha_0^{-2} n \tag{6}$$

[S is the area bounded by the curve $\kappa_1(k_2)$ in one cell]. Thus the center of the allowed interval is determined from the same relation that applies for the discrete levels in the case of closed trajectories:

$$S = 2\pi\alpha_0^{-2}(n + 1/2). \tag{7}$$

The width of the discontinuities can be determined from the usual dispersion equation:

$$\cos p = \frac{f(2\pi/a_2) + f(-2\pi/a_2)}{2f(0)}, \tag{8}$$

which follows from the relation $f(k_2 \pm 2\pi/a_2) = e^{ip} f(k_2)$. Since ρ the modulus of the function in Eq. (5) is periodic, Eq. (8) is of the form

$$\cos p = \cos\{\varepsilon^{-2}\varphi_1(2\pi/a_2) - \varepsilon^2\varphi_3(2\pi/a_2) + \varepsilon^6\varphi_5(2\pi/a_2) - \ldots\}. \tag{9}$$

This equation can always be solved. It shows that the discontinuities fall off with ϵ faster than any finite power of ϵ. The results of Ref. 2 and the well-known fact that in the discontinuities in the

Mathieu equation fall off exponentially indicate that the reduction of the discontinuities with ϵ for the case of an analytic function $\kappa_1(k_2)$ is exponential.

The author wishes to take this opportunity to thank I. M. Lifshitz for a discussion of the results and A. Ia. Povzner for illuminating remarks concerning the mathematical aspects of the problem considered herein.

[1] G. E. Zil'berman, J. Exptl. Theoret. Phys. (U.S.S.R.) **32**, 296 (1957), Soviet Phys. JETP **5**, 208 (1957).

[2] G. E. Zil'berman, J. Exptl. Theoret. Phys. (U.S.S.R.) **33**, 387 (1957), Soviet Phys. JETP **6**, 299 (1958).

Translated by H. Lashinsky
94

LATERAL DISTRIBUTION OF PHOTONS NEAR THE AXIS OF EXTENSIVE ATMOSPHERIC SHOWERS

A. A. EMEL'IANOV

P. N. Lebedev Physics Institute, Academy of Sciences, U.S.S.R.

Submitted to JETP editor November 20, 1957

J. Exptl. Theoret. Phys. (U.S.S.R.) **34**, 516-518 (February, 1958)

IT is known that it is very difficult to calculate the lateral-distribution function of the soft component of extensive atmospheric showers with allowance for the cascade processes and for the ionization losses. However, at small values of r, the principal role is played by high-energy particles, for which the ionization losses can be neglected. In the works by Pomeranchuk[1] and Migdal[2] the lateral distribution function of electrons with energies greater than a given value has been calculated for small r, with the ionization losses neglected*

$$N(t,\ E,\ r) \sim 1/r^{2-s}, \tag{1}$$

and with the parameter s determined from the condition

$$-\lambda_1'(s)\,t = \ln(E_0/\beta) - \ln(R/r)$$

(the same result was obtained by Nishimura and Kamata[4]).

Let us determine the photon density corresponding to such an electron distribution. For this purpose we use one of the Landau equations (see Ref. 5):

$$\partial\Gamma(t,\ E,\ \mathbf{r},\ \theta)/\partial t + \theta\partial\Gamma(t,\ E,\ \mathbf{r},\ \theta)/\partial\mathbf{r}$$

$$= -\sigma_0\Gamma(t,E,\mathbf{r},\theta) + \int_E^\infty P(t,\ E',\ \mathbf{r},\ \theta)\,\varphi_{\mathrm{rad}}(E',\ E)\,dE', \tag{2}$$

where $\varphi_{\mathrm{rad}}(E', E)$ is the probability that an electron with energy E' will radiate a photon with energy E, r is the radius vector in the transverse plane, and θ is the projection of the direction of motion of the particles on this plane.

To solve our problem it is quite enough to put $\varphi_{\mathrm{rad}}(E', E) = 1/E$. Then, integrating over all θ, and also over the azimuth in the plane perpendicular to the axis of the shower (taking account of the symmetry of the problem in the last equation), Eq. (2) can be rewritten†

$$\partial N_\Gamma(t,\ E,\ r)/\partial t = -\sigma_0 N_\Gamma(t,\ E,\ r) + N(t,\ E,\ r)/E. \tag{3}$$

We assume for N(t, E, r) the expression given in Ref. 3

$$N(t,\ E,\ r) \approx e^{\lambda_1(s)t} E_k^{-s}\,[1 - (rE/E_k)^{2-s}]/r^{2-s}(2-s).$$

A solution of Eq. (3), with boundary conditions at $t = 0$, $N_B = 0$, is

$$N_\Gamma(t,\ E,\ r) \approx \frac{e^{\lambda_1(s)t} - e^{-\sigma_0 t}}{\lambda_1(s) + \sigma_0}\,\frac{E_k^{-s}[1 - (rE/E_k)^{2-s}]}{r^{2-s}(2-s)E}.$$

This expression is correct for $E_k/E_0 < r < E/E_k$.

Let us now determine the ratio $\dfrac{N_1(t, > E, r)}{N(t, E, r)}$, where $N_1(t, > E, r)$ is the number of photons with energies greater than the given value. Taking it into account that at a fixed value of r the particle energy E cannot be greater than E_k/r (see Ref. 3), we obtain the following value for N_1:

$$N_1 \sim \ln(E_k/rE)/r^{2-s}. \tag{4}$$

Let us note that in the derivation of Eq. (3) we used the condition $rE/E_k \ll 1$, which determines the boundary of applicability of formula (1). Thus, we obtain

$$N_1/N \sim \ln(E_k/rE). \tag{5}$$

*The symbols used here are the same as in the book by Belen'kii.(Ref. 3).

†It can be shown that for our problem it is possible to neglect the term containing the derivative with respect to r.

This result is in good agreement with the data given by Moliere[6] for $rE/E_k \ll 1$.

By way of an example it is easy to calculate that for $E = 10^8$ ev, at a distance of 1 m from the axis of the shower and at a primary-electron energy of $E_0 = 10^{14}$ ev, we have $N_1/N \approx 7-8$. This effect can be explained by the fact that the high-energy electrons located near the shower axis are accompanied by a greater number of photons. For distances $r \geq E_k/E$ it is necessary to take ionization losses into account.

In conclusion I express my gratitude to I. L. Rozental' for advice and aid in this work, and also to I. P. Ivanenko for useful discussions.

[1] I. Ia. Pomeranchuk, J. Exptl. Theoret. Phys. (U.S.S.R.) **14**, 1252 (1944).

[2] A. B. Migdal, J. Exptl. Theoret. Phys. (U.S.S.R.) **15**, 313 (1945).

[3] S. Z. Belen'kii, Лавинные процессы в космических лучах (Cascade Processes in Cosmic Rays), Gostekhizdat, 1948.

[4] J. Nishimura and K. Kamata, Progr. Theor. Phys. **5**, 899 (1950).

[5] L. D. Landau, J. of Phys. (U.S.S.R.) **3**, 235 (1940).

[6] G. Moliere, Phys. Rev. **77**, 715 (1950).

Translated by J. G. Adashko
95

CONTRIBUTIONS TO THE THEORY OF DISPERSION RELATIONS

S. M. BILEN'KII

Joint Institute for Nuclear Research

Submitted to JETP editor November 19, 1957

J. Exptl. Theoret. Phys. (U.S.S.R.) **34**, 518-519 (February, 1958)

IT was shown by Bogoliubov, Logunov, and the author[1] that for those processes in which μ, e, and ν particles participate on par with strongly interacting particles, the anti-Hermitian part of the amplitudes expressed through the action of such weakly-interacting particles is equal to zero to first order in the weak-interaction constant C. This simplifies considerably the consequences of the dispersion relations as well as their form. Namely, the dispersion relations lead in this case to the statement that the amplitude for the process depends polynomially upon the sum of the 4-momenta of the weakly interacting particles (for decay, upon the difference), while the polynomial coefficients depend only upon the momenta of the strong-interacting particles. If as usual, the interaction Lagrangian does not contain derivatives of the fields, then the amplitudes are independent of the momenta of the weakly-interacting particles. It is easy to consider similarly processes in which only weakly-interacting particles participate (for example, the decay of the μ meson). The causality principle leads in this case to a Lagrangian which is local in all the fields, and the dispersion relations lead to the statement that the amplitude depends only polynomially upon the momenta.

It is worth noting that the weak interaction cases allow simple analyses on the basis of dispersion theory. For example, the wide spread opinion that in order to obtain the dispersion relations it suffices to apply the principle of causality formulated through the vanishing of the probability current commutator of space-like points, is easily seen to be incorrect.

Indded, to first order in C, the probability current commutator for weakly-interacting particles is zero over all space for any Lagrangian including a non-local one. Generally, non-local Lagrangians do not lead to polynomial dependence. Consider, for example, the Lagrangian:

$$L(x) = \int K(\xi^2)\,\varphi(x+\xi)\,\varphi(x-\xi)\,\psi(x+\xi)\,\psi(x-\xi)\,d\xi.$$

Applying to it perturbation theory, we obtain the following expression for the scattering amplitude:

$$S(p,q;\,p',q') = \delta(p+q-p'-q')\,\bar{K}((q+p)^2),$$

where q, q′ are the momenta of the scattered particles, and p, p′ are the momenta of the scatterers.

In this fashion, the dependence of the amplitude upon the momenta is determined from the kernel of the interaction Lagrangian and, in general, is not polynomial. Note that in deriving the dispersion relations, Goldberger et al.[2] also make use of time-ordered operators, in addition to the causality principle in the form of a commutator. These two conditions are combined in the generalized formulation of the principle of causality, and the formulation now proves sufficient to obtain the dispersion relations. From the example of weak interactions, it is easy to verify that the dispersion relations may similarly arise in certain non-local interactions. Consider for example the

process indicated on the figure.

The shaded area refers to strongly interacting particles. The momentum transfer is $q' - q = p - p'$, and therefore the amplitude depends only upon the squares of the momentum transfer $(p - p')^2$ (relativistic invariance), even though the interaction of scattered particles is non-local.

Thus if the scattering amplitude satisfies the dispersion relations, it still does not generally follow that the causality principle is satisfied.

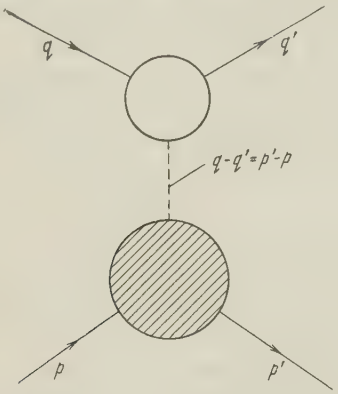

One can only assert that if the dispersion relations are violated, then so is the principle of causality. A similar example was suggested by Lehmann.[4]

In conclusion I consider it my pleasant duty to thank N. N. Bogoliubov for his guidance and A. A. Logunov for discussion of the subjects presented here.

[1] Bogoliubov, Bilen'kii, and Logunov, Dokl. Akad. Nauk SSSR **115**, 891 (1957), Soviet Phys. "Doklady" **2**, 381 (1957).

[2] Проблемы современной физики (Probl. of Contemp. Physics) **2** (1957), Dispersion relations.

[3] N. N. Bogoliubov, Izv. Akad. Nauk SSSR, ser. fiz. **19**, 237 (1955).

[4] Proceedings of Seventh Rochester Conference, IV, 33 (1957).

Translated by M. A. Melkanoff
96

ADHESION OF SLOW ELECTRONS TO SF_6 *AND* CCl_4 *MOLECULES*

N. S. BUCHEL'NIKOVA

Institute of Chemical Physics, Academy of Sciences, U.S.S.R.

Submitted to JETP editor November 21, 1957

J. Exptl. Theoret. Phys. (U.S.S.R.) **34**, 519-521 (February, 1958)

FOX[1] has shown recently that the process $SF_6 + e \rightarrow SF_6^-$ has a resonant character and occurs in an energy range on the order of 0.05 ev at electron energies less than 0.1 ev. Carbon tetrachloride also captures electrons with energies close to zero, dissociating thereby into CCl_3 and Cl^- (Refs. 2—4), but in this case the energy and width of the capture region were determined with low accuracy.

We determined the energy and resonant capture cross-section of slow electrons in SF_6 and CCl_4.

The measurements were carried out in a setup similar to that of Lozier.[5] The electron beam was collimated by a cellular diaphragm and a magnetic field (15—20 oersted), and was passed through a diaphragm with variable potential and a screening grid into an equipotential region, and then to a collector. The ions produced in the equipotential region were gathered on a cylindrical collector, screened by the grid. Equality of the potential was insured by thorough compensation for the contact potentials.

To obtain monochromatic electrons, use was made of the so-called "quasi-monochromatization,"[6] which consists of passing a beam of electrons through a diaphragm that transmit only electrons with energies exceeding the diaphragm potential. The diaphragm potential was periodically varied by ΔV, and the increment in ion current due to this variation was measured. Obviously this increment is due to electrons with a distribution of width ΔV. It was possible to obtain by this method electrons with an exponential energy distribution 0.2 — 0.3 ev wide (the vertical and the right-hand solid curves of Figs. 1 and 2). The

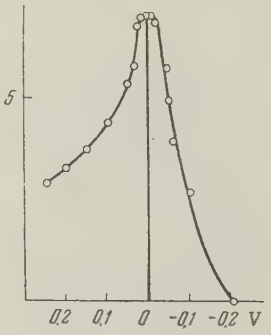

Fig. 1. o — ion current in SF_6.

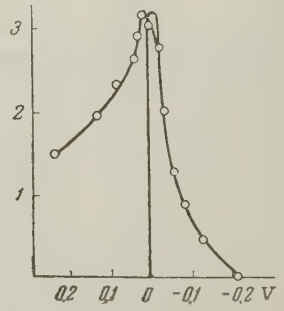

Fig. 2. o — ion current in CCl_4.

sharp boundary of the distribution makes it possible to set the energy scale reliably.

If capture took place in an energy interval that was narrow compared with the width of the electron distribution, the shape of the ion peak duplicates the shape of the distribution, and the shift of the maximum ion current relative to the maximum distribution determines the capture energy. Figures 1 and 2 show the electron distributions in the ion-current curves for SF_6 and CCl_4 (the ion and electron currents are given in arbitrary units, and a common scale is used). The correspondence in the shapes of the ion peaks and of the electron distribution in the region of the maxima is evidence that resonant electron capture in a narrow energy interval takes place for SF_6 and CCl_4. From the shifts of the maxima it was determined that the capture takes place at 0 ± 0.01 ev in SF_6 and 0.02 ± 0.01 ev in CCl_4 (in both cases the values are obtained by averaging eight measurements).

The resonant capture cross-section of SF_6 and CCl_4 was found under the assumption that the capture takes place in an energy interval of 0.05 ev. The cross-section was determined from the maximum ion current and from the electron current in the interval from 0 to 0.05 ev, and calculated from the formula

$$\sigma = (I_{max}/\eta\xi) / (\Delta I_{el}/\beta)\, 3{,}55 \cdot 10^{16} \cdot 273\,(p/T)\,\lambda L.$$

Here I_{max} is the maximum ion current, ΔI_{el} is the current of the electrons with energies from 0 to 0.05 ev, p the pressure of the investigated gas, T the temperature of the working region, equal to room temperature, L the length of the working region, η the correction for recapture of ions by the grids that screen the ion collector, ξ the correction for the ion escape, β the correction for the recapture of electrons by the grid that screens the collector, and λ the correction for the elongation of the electron path in the magnetic field.

It was determined as a result that $\sigma = (1.2 \pm 0.4) \times 10^{-15}$ cm^2 for SF_6 and $\sigma = (1.7 \pm 0.4) \times 10^{-16}$ cm^2 for CCl_4 (both values were obtained by averaging six measurements).

I thank V. L. Tal'roze for continuous interest in the work and for valuable advice.

[1] W. M. Hickam and R. E. Fox, J. Chem. Phys. **25**, 642 (1956).

[2] Marriott, Thorburn, and Craggs, Proc. Phys. Soc. B67, 437 (1954).

[3] J. Marriott and J. D. Craggs, Electr. Res. Assoc. Report L/T, 308 (1954).

[4] Reese, Dibeler, and Mohler, J. Research Natl. Bur. Standards **57**, 367 (1956).

[5] W. W. Lozier, Phys. Rev. **46**, 268 (1934).

[6] Fox, Hickam, Grove, and Kjeldaas, Rev. Sci. Instr. **26**, 1101 (1955).

Translated by J. G. Adashko
97

QUANTUM YIELD OF INTERNAL PHOTOEFFECT IN GERMANIUM

V. S. VAVILOV and K. I. BRITSYN

Moscow State University

Submitted to JETP editor November 21, 1957

J. Exptl. Theoret. Phys. (U.S.S.R.) **34**, 521-523 (February, 1958)

IT is known that at photon energies near the threshold of the internal photoeffect, corresponding to approximately 0.7 ev for pure germanium, the quantum yield is constant and equal to unity.[1,2] This is in agreement with the usual concept of the creation of one electron-hole pair upon absorption of a photon.

If the photon has a sufficient excess energy above threshold, additional electrons can be liberated in the crystal as a result of impact ionization. The possibility of a quantum yield of photoluminescence in excess of unity, upon excitation by quanta with energies more than double the energy of the luminescence quantum, was indicated by S. I. Vavilov[3] in 1947. This phenomenon was observed experimentally by Butaeva and Fabrikant[4] in short-wave excitation of luminophors and by Koc in an investigation of the internal photoeffect in germanium. Experimental data on the increase in quantum yield by impact ionization with photo electrons or holes are important from the point of view of the theory of scattering of carriers in a crystal and the theory of impact ionization, developed by Chuenkov[6] and others.

We measured the quantum yield of the internal photoeffect in N-type germanium in the wavelength range from 1.5 to 0.254μ. The quantum yield Q was determined as the ratio of the number of excess free carriers to the number of absorbed photons. Single germanium crystals with a specific resistivity ρ ranging from 10 to 20 ohm-cm and with initial diffusion length L of approximately 1.5 mm were used in the experiments. Crystals in the shape of platelets 0.3 — 0.6 mm thick and approximately 1 cm^2 in area were illuminated on one side by

monochromatic light. On the opposite side, indium was fused into the platelets[2] to produce an N-P junction. Light of the required wavelength was separated by a monochromator with a quartz prism. The light sources were a SVDSh lamp for the infrared and visible regions, and a PRK-4 mercury quartz lamp for the ultraviolet region. The energy flux of the incident beam was measured with a compensated thermopile calibrated against a Hefner lamp.

The receiver for the 366, 313, 289, and 254μ lines in the ultraviolet region comprised the luminescent compound "lumogen," which has a constant glow yield, and a FEU-25 photomultiplier. Calibration was by direct comparison with the readings of the thermopile at a wavelength of 365μ.

The quantum yield was calculated from the formula

$$Q = Ihc/\alpha e\lambda P_i (1 - R), \qquad (1)$$

where A is the short-circuit current between the N and P regions, corresponding to a hole current from the N region, where the photons are absorbed, into the P region of the crystal; P_i is the power of the incident radiation; α is the coefficient of carrier collection, which in this case can be calculated from

$$2/\alpha = (1 + SL/D)\, e^{d/L} + (1 - SL/D)\, e^{-d/L}. \qquad (2)$$

Here L is the diffusion length of the excess carriers in the N-region, d the thickness of the crystal, D the bipolar diffusion constant, and S the speed of the surface recombination.

The total coefficient of reflection R, as was already indiciated,[7] depends on the method of treating the germanium surface, which is etched to reduce the speed of surface recombination. R was measured with an integrating photometric sphere that permitted determination of the ratio of the coefficient of reflection from the investigated germanium crystals to that from the surface of a thick layer of magnesium oxide, whose coefficient of reflection is known. The radiation receiver used in the ultraviolet region, as in the measurement of the energy flux, was a layer of "lumogen" and a photomultiplier.

The diagram shows the curve $R(h\nu)$ and the values of the quantum yield in the energy range of photons from 0.83 to 4.9 ev, calculated from formula (1). The quantum yield vs. photon energy curve shows clearly the considerable increase in Q, which, however, begins not with the energy of the liberated electron ($\approx$ 1.4 ev), but at higher energies. This was to be expected on the basis of the work by Chuenkov,[6] according to which the probability of impact ionization is negligibly small

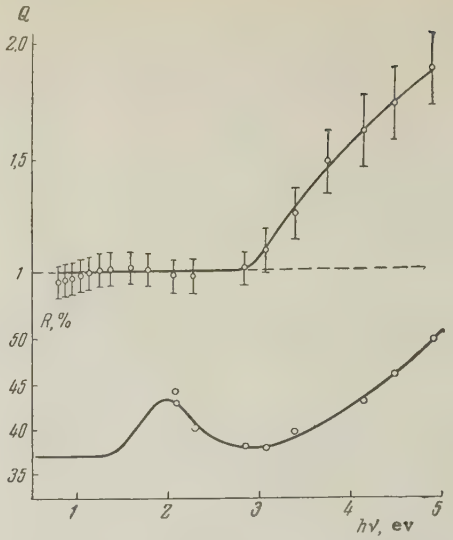

compared with the probability of energy transfer at carrier energies only slightly above the width of the forbidden band. According to Chuenkov's calculations, the probability of impact ionization reaches a value of $\frac{1}{2}$ at a carrier energy of approximately 2 ev. At large values of $h\nu$ the rise in the quantum yield slows down, i.e., the mean energy ϵ, expanded on the production of the electron-hole pair, increases. It was observed in experimental investigations of the "multiplication" of fast electrons in germanium, that increasing the electron energy W leads also to a certain increase in ϵ, whose value is 3.7 $\pm$ 0.4 ev at W = 5 — 15 kev and to 4.5 — 5 ev at W = 500 — 1,000 kev.[8]

The authors express deep gratitude to M. N. Alentsev, B. M. Vul, and V. A. Chuenkov for criticism and advice.

[1] P. S. Goucher, Phys. Rev. **78**, 816 (1950).

[2] V. S. Vavilov and L. S. Smirnov, Радиотехника и электроника (Radio Engineering and Electronics) **1**, 8, 1147 (1956).

[3] S. I. Vavilov, "Luminescence and its Duration," 1947. Collected Works, Vol. 2, Acad. of Sciences Press, 1952, p. 293.

[4] F. A. Butaeva and V. A. Fabrikant, Ivz. Akad. Nauk SSSR, ser. fiz. **21**, 541 (1957); **18**, 2 (1954).

[5] S. Koc, Ceskoslov. Casopis pro fisiku **6**, 668 (1956).

[6] V. A. Chuenko, Izv. Akad. Nauk SSSR, sef. fiz. **20**, 1550 (1956).

[7] Vavilov, Gippius, and Gorshkov, J. Tech. Phys. (U.S.S.R.) (1957) (in press).

[8] Vavilov, Smirnov, and Patskevich, Dokl. Akad. Nauk SSSR **112**, 1020 (1957), Soviet Phys. "Doklady" **2**, 93 (1957).

Translated by J. G. Adashko
98

ON THE QUANTUM-KINETIC EQUATION FOR A SYSTEM OF CHARGED PARTICLES OF MANY KINDS

S. V. TEMKO

Submitted to JETP editor November 26, 1957

J. Exptl. Theoret. Phys. (U.S.S.R.) **34**, 523-524 (February, 1958)

BY the method of Bogoliubov[1,2] one can obtain a natural generalization of the quantum-kinetic equation for the description of stochastic processes in a system of charged particles in which the particles belong to an arbitrary number $M \geq 2$ of different kinds. If in the spatially homogeneous case (cf. Ref. 3) one substitutes into the quantum equation for the distribution function $F_a(p; t)$ of any single chosen particle of type a the solution of the system of quantum equations for the quantum correlation-deviation functions g_{ab}, then one can obtain the quantum-kinetic equation for the plasma of many kinds of particles. Since, however, the determination of the exact solution for the functions g_{ab} is a difficult task, it is expedient to introduce the simplifying assumption that the Coulomb and exchange interactions are weak and that the chosen particle exerts only a small reaction influence on the behavior of the large number of charged particles surrounding it. With these assumptions, since an exchange interaction is possible only between particles of the same kind, we find

$$\frac{\partial w_a(p;\ t)}{\partial t} = \sum_{(1\leqslant b\leqslant M)} \frac{2\pi n_b}{(2\pi\hbar)^6\hbar} \int \left\{ \frac{\nu_{ab}(|p-p'|/\hbar)\,\nu_{ab}(|p'-p|/\hbar)}{1+B_{ab}((p'-p)/\hbar;\ (p+p')/2)} \right.$$

$$\left. \pm \frac{\nu_{ab}(|p-p_1'|/\hbar)\,\nu_{ab}(|p'-p_1|/\hbar)}{1+B_{ab}((p-p_1')/\hbar;\ (p_1'+p)/2)} \right\} \delta(p+p_1-p'-p_1')$$

$$\times \delta(E_a+E_{1,b}-E_a'-E_{1,b}') \qquad (1)$$

$$\times [(1\pm n_a w_a(p;t))(1\pm n_b w_b(p_1;\ t))\, w_a(p';\ t)\, w_b(p_1';\ t)$$

$$-(1\pm n_a w_a(p';\ t))(1\pm n_b w_b(p_1';\ t))$$

$$\times w_a(p;\ t)\, w_b(p_1;\ t)]\, dp_1 dp' dp_1' + \delta R_a.$$

Here

$$w_a(p;t) = \frac{(2\pi)^3}{v} F_a(p;t);\quad E_a = \frac{p^2}{2\mu_a};$$

$$\nu_{ab}(|k|) = \int e^{ikq}\,\Phi_{ab}(|q|)\,dq; \qquad (2)$$

$$B_{ab}(k,\ p) = |\operatorname{Re} i \sum_c n_c \frac{\nu_{cc}(|k|)}{(2\pi)^9\hbar^4} \int_0^\infty \int [e^{i\hbar k\tau/2} - e^{-i\hbar k\tau/2}]$$

$$\times \exp\{i\vartheta k(p'/\mu_b - p/\mu_a) + i\tau(\eta - p')\}\, w_b(\eta)\, d\vartheta\, d\tau\, d\eta\, dp' |;$$

n_c, μ_c are the concentration and particle mass of the particles of type c in the plasma, $c = 1, 2, \ldots, M$; v is the average volume per particle; and δR_a, a term taking into account the actions on each other of the set of neighboring particles, can be approximately evaluated by a method analogous to that used in Ref. 4.

For heterogeneous systems of large numbers of charged particles obeying the Fermi statistics, under conditions of complete degeneracy the approximate expression for the screening coefficient B_{ab} takes the form

$$B_{ab}(k,\ p) = \frac{1}{r_D^2 k^2} + \frac{1}{2r_D^2 k^2}\left(\frac{\mu_b kp}{\mu_a kp_0}\right) \ln \left| \frac{1-\mu_b kp/\mu_a kp_0}{1+\mu_b kp/\mu_a kp_0} \right|. \qquad (3)$$

Here $r_D = (p_0^2 v/12\pi\mu_b \sum_c n_c e_c^2)^{1/2}$ is the Debye radius for the distribution of the Fermi particles of type b, p_0 is the average upper limit momentum for the system of many kinds of particles, and e_c is the charge of a particle of type c in the plasma.

I express my deep gratitude to Academician N. N. Bogoliubov for directing this work.

[1] N. N. Bogoliubov, Проблемы динамической теории в статистической физике (Problems of Dynamical Theory in Statistical Physics), Gostekhizdat, 1946.

[2] N. N. Bogoliubov and K. P. Gurov, J. Exptl. Theoret. Phys. (U.S.S.R.) **17**, 614 (1947).

[3] Iu. L. Klimontovich and S. V. Temko, J. Exptl. Theoret. Phys. (U.S.S.R.) **33**, 132 (1957), Soviet Phys. JETP **6**, 102 (1958).

[4] S. V. Temko, J. Exptl. Theoret. Phys. (U.S.S.R.) **31**, 1021 (1956), Soviet Phys. JETP **4**, 898 (1957).

Translated by W. H. Furry
99

THE MAGNETIC SUSCEPTIBILITY OF A UNIAXIAL ANTIFERROMAGNETIC

M. I. KAGANOV and V. M. TSUKERNIK

Submitted to JETP editor November 26, 1957

J. Exptl. Theoret. Phys. (U.S.S.R.) **34**, 524-525 (February, 1958)

IN a large number of papers,[1] the high frequency magnetic susceptibility of an antiferromagnetic is found by using the concept of the precession of the

magnetic moments of the sublattices. These authors do not take into account relaxation processes. Our problem is to take relaxation processes into account, in the spirit of the equations of Landau and Lifshitz,[2] and to connect the constants entering into the phenomenological equations of motion of the magnetic moments with the experimentally-observed quantities (static magnetic susceptibility, resonance frequency, and antiferromagnetic resonance line width).

We consider for the sake of simplicity a uniaxial ferromagnetic (we take the chosen axis along the z axis). The equation of motion of the magnetic moments of each of the two sublattices has the form

$$\partial \mathbf{M}_j / \partial t = g \mathbf{M}_j \times \mathbf{H}_j^{\text{eff}} - \gamma M^{-2} \mathbf{M}_j [\mathbf{M}_j \times \mathbf{H}_j^{\text{eff}}], \quad (j = 1, 2). \quad (1)$$

Here

$$\mathbf{H}_1^{\text{eff}} = \mathbf{H} - \alpha \mathbf{M}_2 - \lambda (\mathbf{M}_1 - \mathbf{M}),$$
$$\mathbf{H}_2^{\text{eff}} = \mathbf{H} - \alpha \mathbf{M}_1 - \lambda (\mathbf{M}_2 + \mathbf{M}); \quad (2)$$

α is a constant describing the exchange interaction between the sublattices (the order of magnitude of α is determined by the ratio $\Theta_C/\mu M \sim 10^2$, where $\mu = g\hbar$ is the Bohr magneton, Θ_C the Curie temperature, and M the magnetic moment of each of the sublattices), λ is the anisotropy constant ($\lambda \sim 10^{-2}\alpha$, since the anisotropy energy is not determined by the large isotropic exchange interaction but by a relativistic interaction of the spin-orbit coupling type), while the constant γ describes relaxation processes. In the absence of an external field, which we assume here to be applied at right angles to the z axis, the magnetic moments of the sublattices are respectively equal to $\mathbf{M}_1 = \mathbf{M}$, $\mathbf{M}_2 = -\mathbf{M}$.

Assuming the variable magnetic field $\mathbf{H} = \mathbf{H}' e^{-i\omega t}$ to be small we linearize (2)

$$\partial \boldsymbol{\mu}_1 / \partial t = -g [\mathbf{M}, \alpha (\boldsymbol{\mu}_1 + \boldsymbol{\mu}_2) + \lambda \boldsymbol{\mu}_1]$$
$$+ \alpha\gamma (\boldsymbol{\mu}_1 + \boldsymbol{\mu}_2) + \lambda\gamma \boldsymbol{\mu}_1 + g [\mathbf{M} \times \mathbf{H}] + \gamma \mathbf{H},$$
$$\partial \boldsymbol{\mu}_2 / \partial t = g [\mathbf{M}, \alpha (\boldsymbol{\mu}_1 + \boldsymbol{\mu}_2) + \lambda \boldsymbol{\mu}_2]$$
$$+ \alpha\gamma (\boldsymbol{\mu}_1 + \boldsymbol{\mu}_2) + \lambda\gamma \boldsymbol{\mu}_2 - g [\mathbf{M} \times \mathbf{H}] + \gamma \mathbf{H}. \quad (3)$$

Taking into account the fact that μ_1 and μ_2 are proportional to $e^{-i\omega t}$ we find (we use the fact that $\lambda \ll \alpha$, $gM \gg \gamma$)

$$\boldsymbol{\mu} = \boldsymbol{\mu}_1 + \boldsymbol{\mu}_2 = 2 \frac{\lambda (gM)^2 + i\omega\gamma}{2\alpha\lambda g^2 M^2 - \omega^2 - 2i\omega\alpha\gamma} \mathbf{H}. \quad (4)$$

Hence

$$\chi_\perp = 2 \frac{\lambda (gM)^2 + i\omega\gamma}{2\alpha\lambda (gM)^2 - \omega^2 - 2i\omega\alpha\gamma}$$

Or, since $1/\alpha = \chi_\perp (\omega = 0) \equiv \chi_\perp (0)$,

$$\chi_\perp (\omega) = \chi_\perp (0) \frac{\omega_0^2 (\omega_0^2 - \omega^2) + 2i\omega\Gamma (2\omega_0^2 - \omega^2)}{(\omega_0^2 - \omega^2)^2 + 4\omega^2\Gamma^2}, \quad (5)$$

where

$$\omega_0 = gM\sqrt{2\alpha\lambda}, \quad \Gamma = \alpha\gamma. \quad (6)$$

For $\omega \ll \omega_0$

$$\chi (\omega) = \chi_\perp (0) (1 + 4i\omega\Gamma / \omega_0^2),$$

and for $\omega \sim \omega_0$ (near the resonance frequency)

$$\chi_\perp (\omega) = \chi_\perp (0) \frac{2i\omega_0^3\Gamma}{(\omega_0^2 - \omega^2)^2 + 4\omega_0^2\Gamma^2}.$$

Let us note some facts:

1. $\chi_\perp (\omega)$ does not contain gyrotropy: the rotation of the moments of the sublattices proceeds in such a manner that the total magnetic moment is directed along the magnetic field. This will not be the case in a strong magnetic field, applied along the specimen axis, since $\mathbf{M}_1 (\mathbf{H}_0) \neq -\mathbf{M}_2 (\mathbf{H}_0)$.

2. The line width Γ is determined not only by relativistic effects as a ferromagnetic (γ), but also by the exchange interaction energy (α).

3. If the antiferromagnetic is a metal, the exchange interaction will lead to an additional line broadening, produced by the effect of the inhomogeneity of the magnetic moments (see Refs. 3 – 5).

[1] C. Kittel, Phys. Rev. **82**, 565 (1951); T. Nagamiya, Progr. Theor. Phys. **6**, 350 (1951).

[2] L. D. Landau and E. M. Lifshitz, Physik. Z. Sowietunion **8**, 153 (1935).

[3] C. Kittle and C. Herring, Phys. Rev. **77**, 725 (1950).

[4] S. S. Ament and G. T. Rado, Phys. Rev. **97**, 1558 (1955).

[5] Akhiezer, Bar'iakhtar, and Kaganov, Физика металлов и металловедение (Physics of Metals and Metal Research) (in press).

Translated by D. ter Haar
100

PHASE INDETERMINACIES IN NUCLEON-NUCLEON SCATTERING

L. G. ZASTAVENKO, R. M. RYNDIN, and CHOU GUAN-CHAO

Joint Institute for Nuclear Research

Submitted to JETP editor November 26, 1957

J. Exptl. Theoret. Phys. (U.S.S.R.) **34**, 526-527 (February, 1958)

THE cross section for scattering of mesons by nucleons remains invariant under the phase substitution indicated by Minami.[1] The two sets of phase shifts, obtained from one another through this substitution, can only be distinguished either by means of polarization experiments,[2-3] or by analyzing the energy dependence of the cross section at low energies. We obtain below a similar transformation for the case of nucleon-nucleon scattering.

The elastic scattering of nucleons against nucleons is completely described by the scattering matrix $M(\mathbf{k}, \mathbf{k}_0; \sigma_1, \sigma_2)$, which determines the amplitude χ_f of the scattered wave in terms of the initial spin state χ_i:

$$\chi_f = M(\mathbf{k}, \mathbf{k}_0; \sigma_1, \sigma_2)\chi_i. \tag{1}$$

Here σ_1 and σ_2 are the Pauli matrices for the two nucleons, and $\mathbf{k}_0$ and $\mathbf{k}$ denote unit vectors along the incident and scattered nucleon directions.

In order to obtain the transformation of interest, note that the scattering cross section for unpolarized nucleons $\sigma_0 = \frac{1}{4}\mathrm{Sp}\, MM^+$, is invariant to an exchange of $M(\mathbf{k}, \mathbf{k}_0; \sigma_1, \sigma_2)$ with one of the following matrices

$$M_1 = (\sigma_1\mathbf{k})M(\sigma_1\mathbf{k}_0), \quad M_2 = (\sigma_2\mathbf{k})M(\sigma_2\mathbf{k}_0),$$
$$M_3 = (\sigma_1\mathbf{k})(\sigma_2\mathbf{k})M(\sigma_1\mathbf{k}_0)(\sigma_2\mathbf{k}_0). \tag{2}$$

We expand now the matrix M in terms of the spherical function $Y^{jm}_{\ell s}(\mathbf{k})$ describing a state of given total angular momentum j, its z-component m, orbital angular momentum ℓ and spin s. Then

$$M(\mathbf{k}, \mathbf{k}_0; \sigma_1, \sigma_2) = \sum_{j,m}\frac{2\pi}{ik}\sum_{l,s;\,l',s'} Y^{jm}_{ls}(\mathbf{k})\, Y^{jm+}_{l's'}(\mathbf{k}_0)\, R^{j}_{ls;\,l's'}. \tag{3}$$

The values of s and ℓ are determined from the rule for adding angular momenta, and are as follows: for s = 0 (singlet) $\ell = j$; for s = 1 (triplet) $\ell = j, j \pm 1$. For a given value of j, the quantities $R^{j}_{\ell s, \ell' s'}$ form a symmetric (reversibility of the motion) four-rowed matrix R^j satisfying the condition

$$R^{j+}R^j = -R^j - R^{j+}, \tag{4}$$

which arises from the unitarity of the S-matrix.

Consider, for example, the first of the transformations (2). Since the operator $(\sigma_1\mathbf{k})$ commutes with the total angular momentum operator,

$$(\sigma_1\mathbf{k})\, Y^{jm}_{ls}(\mathbf{k}) = L^{(1)j}_{l_1 s_1, ls}\, Y^{jm}_{l_1 s_1}(\mathbf{k}). \tag{5}$$

Thus

$$M_1(\mathbf{k}, \mathbf{k}_0; \sigma_1, \sigma_2) = \sum_{j,m}\frac{2\pi}{ik}\sum_{l,s;\,l',s'} Y^{jm}_{ls}(\mathbf{k})\, Y^{jm+}_{l's'}(\mathbf{k}_0)\, R^{(1)j}_{ls,\,l's'}, \tag{6}$$

where

$$R^{(1)j} = L^{(1)j}R^jL^{(1)j+} \tag{7}$$

The matrix $L^{(1)j}$ is a unitary, antisymmetric, Hermitian matrix. Therefore $R^{(1)j}$ satisfies Eq. (4) and has the same symmetry properties as R^j. Therefore the elements of $R^{(1)j}$ may be considered as the elements of a new scattering matrix which leads to the same cross section as M. All this applies as well to the matrices $R^{(2)j} = L^{(2)j} \times R^jL^{(2)j+}$ and $R^{(3)j} = L^{(3)j}R^jL^{(3)j+}$, corresponding to the second and third transformation of (2).

The matrix $L^{(i)j}$ has the form

$$L^{(1,2)j} = \frac{i}{\sqrt{2j+1}}\begin{pmatrix} 0 & 0 & \mp\sqrt{j+1} & \mp\sqrt{j} \\ 0 & 0 & \sqrt{j} & -\sqrt{j+1} \\ \pm\sqrt{j+1} & -\sqrt{j} & 0 & 0 \\ \pm\sqrt{j} & \sqrt{j+1} & 0 & 0 \end{pmatrix},$$

$$L^{(3)j} = \begin{pmatrix} -1 & 0 & 0 & 0 \\ 0 & 1 & 0 & 0 \\ 0 & 0 & -\frac{1}{2j+1} & -\frac{2\sqrt{j(j+1)}}{2j+1} \\ 0 & 0 & -\frac{2\sqrt{j(j+1)}}{2j+1} & \frac{1}{2j+1} \end{pmatrix}. \tag{8}$$

The first columns (row) correspond to singlet states, the remaining to triplet states in the following ordering of ℓ: j, j + 1, j − 1. The upper sign corresponds to superscript 1, and the lower sign to superscript 2.

Inasmuch as the operators $(\sigma_{1,2}\mathbf{k})$ in contradistinction to $(\sigma_1\mathbf{k})(\sigma_2\mathbf{k})$ do not commute with the square of the total spin operator $\frac{1}{4}(\sigma_1 + \sigma_2)^2$, the matrices M_1 and M_2 lead to singlet-triplet transitions. Therefore the first two transformations cannot take place in the case of identical nucleon collisions where singlet-triplet transitions are forbidden by the Pauli principle. This also is true for n − p scattering if isotopic invariance holds.

The operators $(\sigma_i\mathbf{q})$ represent operators which

rotate the spin of the i-th nucleon by an angle π about the direction **q**. This allows to determine the transformation properties of various spin characteristics when R^j is replaced by $R^{(3)j}$. For example, this exchange leads to a change in the sign of the polarization P which takes place in the collision of unpolarized nucleons.

We finally remark that changing the sign of all the phase shifts (taking the complex conjugate of R^j) leaves the cross section unchanged, and changes the sign of $\mathbf{P}_0$. Thus a simultaneous application of this transformation with the transformation R^j into $R^{(3)j}$ leaves unchanged the cross section as well as the polarization. Therefore the two sets of elements of R obtained from one another by means of the indicated transformation, cannot be distinguished through the simplest polarization experiments (double scattering).

[1] S. Minami, Progr. Theor. Phys. **11**, 213 (1954).

[2] Hayakwa, Kawaguchi, and Minami, Progr. Theor. Phys. **12**, 355 (1954).

[3] R. Ryndin and Ia. Smorodinskii, Dokl. Akad. Nauk SSSR **103**, 69 (1955).

Translated by M. A. Melkanoff
101

RESONANCE ABSORPTION OF ELECTROMAGNETIC WAVES BY AN INHOMOGENEOUS PLASMA

N. G. DENISOV

Gor'kii State University

Submitted to JETP editor November 28, 1957

J. Exptl. Theoret. Phys. (U.S.S.R.) **34**, 528-529 (February, 1958)

THE phenomenological description of the propagation of electromagnetic waves in a plasma is based on the possibility of introducing an index of refraction for the medium. A magneto-active plasma is usually characterized by two indices of refraction. It is well known that at certain values of the electron concentration one of these indices becomes infinite (neglecting the collisions of electrons with heavy particles). This may be called a resonance effect since the singularity in the index of refraction is related to the resonance properties of the plasma.[1,2]

In the resonance region, an electromagnetic wave incident on an inhomogeneous layer is partially or totally absorbed. The first of these effects has been discussed by Ginzburg (cf. Ref. 1, §79, and Ref. 2) for the case of quasi-longitudinal propagation. A calculation of absorption in the region of the singularity in the index of refraction has been carried out by Budden[3] using a simplified model of an inhomogeneous layer. The complete solution of the problem can be obtained in the case in which the plasma is not highly inhomogeneous. The results of an analysis of this kind are given below.

In a weakly inhomogeneous medium, except for one case which is discussed below, the interaction between the ordinary and extraordinary waves can be neglected. For simplicity, we consider transverse propagation although the final results can be generalized quite easily. In transverse propagation the index of refraction for the extraordinary wave has a singularity, the dependence of which on electron concentration is given by the following:

$$n^2(v) = 1 - \frac{v(1-v)}{1-u-v} \qquad \left(v(z) = \frac{4\pi e^2 N(z)}{m\omega^2};\quad u = \frac{\omega_H^2}{\omega^2}\right) \tag{1}$$

(the wave propagates along the z axis, and the electron concentration N depends on z). The function $n^2(v)$ has two zeros, $v_1(z_1) = 1 - \sqrt{u}$ and $v_2(z_2) = 1 + \sqrt{u}$, and a pole at $v_3(z_3) = 1 - u$. We consider the case $u < 1$, in which the resonance region ($v = v_3$) lies between the zeros of the function $n^2(v)$. The solution for the reflection of waves from such a layer by the "standard-equation" method[4] shows[5] that the reflection coefficient for the region ($v_1 v_2$) is

$$|R|^2 = 1 - 4e^{-\delta}(1 - e^{-\delta})\sin^2 s, \tag{2}$$

where δ and s are defined by the expressions

$$\delta = 2ik_0\int_{z_1}^{z_3}\sqrt{n}\,dz; \qquad s = k_0\int_{z_3}^{z_2}\sqrt{n}\,dz; \qquad \left(k_0 = \frac{\omega}{c}\right). \tag{3}$$

Equation (2) indicates that the maximum value of the absorption coefficient ($1 - |R|^2$) is approximately 35 per cent.

In calculating absorption in the resonance region it is necessary to take account of the interaction between the different waves only in the case of quasi-longitudinal propagation. In this case, in the region $v \sim 1$ (in the vicinity of which the resonance is found) the index of refraction for the ordinary wave $n_1(\epsilon)$ and for the extraordinary wave $n_2(\epsilon)$ ($\epsilon = 1 - v$) assume values which are approximately the same and two waves exhibit a strong interaction effect.[2]

If an ordinary wave is incident on the interac-

tion region from below, it produces a reflected wave of the same type, characterized by a reflection coefficient $|R_1| = (1 - e^{-2\delta_0})$. The transmission of the wave is characterized by a transmission coefficient $|D_2| = e^{-\delta_0}$ (cf. Ref. 6). In this case the mean absorbed energy is

$$1 - |R_1|^2 - |D_2|^2 = e^{-2\delta_0}(1 - e^{-2\delta_0}). \quad (4)$$

The real quantity δ_0 is defined by the integral

$$\delta_0 = -\frac{1}{4} ik_0 \oint (n_2 - n_1)\, dz. \quad (5)$$

The integral is taken over a path which encloses the two singularities of the integrand at which $n_1 = n_2$. If, however, an extraordinary wave is incident on the interaction region from above, it is not reflected but is scattered into two waves in the interaction region. The amplitudes of these two waves are (cf. Ref. 5)

$$d_1 = e^{-\delta_0}; \quad d_2 = (1 - e^{-2\delta_0})^{1/2}. \quad (6)$$

The factor d_1 characterizes the transmission of the ordinary wave. The factor d_2 characterizes the extraordinary wave which is produced in the interaction region and holds in the direction of the pole of the functions $n_2^2(\epsilon)$. This wave is then completely absorbed. The absorption ($|d_2|^2$) is small only when δ_0 is small. When $\delta_0 \gg 1$, $d_2 \sim 1$ and the wave which is incident from above is almost completely absorbed in the region of high $n_2^2(\epsilon)$.

Because of the thermal motion of the electrons,[2] a wave traveling in the direction of the pole of the function $n_2^2(\epsilon)$ is converted into a plasma wave, the energy of which, in the final analysis, is dissipated in heating the plasma. Thus the absorption effect being discussed is related to the conversion of electromagnetic waves into plasma waves.

Finally we may note that in experiments in which the ionosphere is "sounded" by pulses the interaction mechanism being considered here may explain the fact that only three pulses are observed. The incident wave is presumably split into an extraordinary wave and an ordinary wave. The extraordinary wave is reflected at a level corresponding to $\epsilon = \sqrt{u}$ (first signal); the ordinary wave is reflected in the interaction region ($\epsilon = 0$) (second signal) and partially penetrates as an extraordinary wave into the region $\epsilon < 0$. The extraordinary wave reflected from the point corresponding to $\epsilon = -\sqrt{u}$ passes through the interaction region without reflection and reaches the point of observation as an ordinary wave (third signal). Thus, multiple-reflection effects are impossible.

The author is indebted to V. L. Ginzburg for discussion of the results of this work.

[1] Al'pert, Ginzburg, and Feinberg, Распространение радиоволн (Propagation of Radio Waves), GITTL, 1953.

[2] Gershman, Ginzburg, and Denisov, Usp. Fiz. Nauk **61**, 561 (1957).

[3] K. G. Budden, "Physics of the Ionosphere," Reports on the Physical Society Conference, 320 (1955).

[4] S. C. Miller and R. G. Good, Phys. Rev. **91**, 174 (1953).

[5] N. G. Denisov, Радиотехника и электроника (Radio Engineering and Electronics) (in press).

[6] N. G. Denisov, Труды Физ.-техн. ин-та и mm радиофакультета Горьковского ун-та, серия физич. (Trans. Phys. Tech. Inst. and Radio Faculty, Gor'kii State University, Phys. Series) **35**, 3 (1957).

Translated by H. Lashinsky
102

RECOMBINATION CAPTURE OF MINORITY CARRIERS IN N-TYPE GERMANIUM BY LATTICE DEFECTS FORMED UPON IRRADIATION BY FAST NEUTRONS

A. V. SPITSYN and V. S. VAVILOV

P. N. Lebedev Physics Institute, Academy of Sciences, U.S.S.R.

Submitted to JETP editor November 29, 1957

J. Exptl. Theoret. Phys. (U.S.S.R.) **34**, 530-531 (February, 1958)

In an earlier work[1] an estimate was made of the cross-section for recombination capture of minority carriers by radiation defects in the crystal structure of N-type germanium, produced by irradiation with fast neutrons. The following relations were used in the calculations

$$1/\tau - 1/\tau_0 = n_d v_p \theta, \quad (1)$$

$$n_d = n_{Ge} N_n \bar{N}_d \sigma. \quad (2)$$

Here τ is the lifetime of the minority carriers after irradiation, τ_0 the lifetime of the minority carriers before irradiation, n_α the concentration of the radiation lattice defects, v_p the thermal velocity of the minority carriers (holes), n_{Ge} the number of germanium atoms per cm^3, N_n the integral dose of neutrons (expressed in neutrons per

$N_n \left(\frac{\text{neutrons}}{\text{cm}^2}\right)$	$0.7 \cdot 10^{11}$	$5 \cdot 10^{11}$	$5 \cdot 10^{11}$	$4 \cdot 10^{11}$	$3 \cdot 10^{12}$	$3 \cdot 10^{12}$	$3 \cdot 10^{12}$	$3 \cdot 10^{12}$	$3 \cdot 10^{13}$
					Specimens irradiated in reactor				
E_n (Mev)	14	14	14	14					
ρ_0 (Ω cm)	37	20.5	9.5	4.7	20	9.6	3.7	1.7	0.35
ρ (Ω cm)	42.5	24.0	10.5	5.3	24.5	11.0	3.9	~1.7	~0.35
τ_0 (micron/sec)	450	170	230	29	300	160	130	60	30
τ (micron/sec)	70	20	18	8	23	19	10	7	8
Δn (10^{13} cm^{-3})	1.8	1.6	1.8	3.0	2.0	2.1	2.4	—	—
n_d (10^{13} cm^{-3})	1.4	1.2	1.2	1.2	1.4	1.3	1.3	(1.3)	(1.3)
N_d	260±50	280±30	290±20	(350±100)	—	—	—	—	—
θ (10^{-16} cm^2)	0.8	3.2	3.8	6	2.7	3.3	6.5	8.5	~7

cm^2), $\overline{N}_d$ the average number of displaced germanium atoms per single neutron scattering, and σ the scattering cross-section of the neutrons by germanium nuclei.

To estimate the value of θ, we used values of $\overline{N}_d$ calculated with the formula given by Fan and Lark-Horovitz.[2] To check the correctness of the method employed to calculate $\overline{N}_d$, we set up additional experiments on the irradiation of N-germanium with neutrons. By increasing the doses of neutron irradiation, we obtained measurable values of the change in specific resistivity, $\rho - \rho_0 = \Delta\rho$, which were compared with the lifetime changes in the same specimens. At the doses of neutron irradiation employed, the mobility can be assumed constant, and the change of carrier concentration Δn for given $\Delta\rho$ can be determined from the theoretical relation $\rho = f(n)$ given by Prince,[3] which is found to be well satisfied in the employed germanium single crystals.

Reference 4 gives the experimental values of the number of conduction electrons ($-\Delta n/n_d$) captured by a single radiation defect when n-type germanium specimens of different specific resistivity are bombarded by neutrons. On the basis of these data, the values of Δn were used to estimate the defect concentration n_d for all the irradiated specimens. Relation (2) was used to determine the value of $\overline{N}_d$ for specimens irradiated by monoenergetic neutrons. The values of the latter quantity are close to 260, in accordance with the formula by Kinchin and Pease.[5]

The data obtained are listed in the table.

The values of θ obtained are one order of magnitude greater than the cross-sections for the capture of carriers by singel Frenkel' defects produced by electron irradiation.[6]

What is interesting is the regular increase in values of θ with diminishing ρ_0, i.e., with displacement of the Fermi level upward from the center of the forbidden band. The value of θ which we introduced into relation (1) is the product of the effective "geometric" cross-section of the defect, as the capture center, by the degree of filling of the corresponding energy level. The increase in θ is therefore obviously due to the fact one of the recombination levels lies in the upper half of the forbidden band.

The authors express their gratitude to B. M. Vul for evaluating the results and to I. A. Arkhipova, who participated in the measurements of the lifetime of non-equilibrium carriers in germanium.

[1] Vavilov, Spitsyn, Smirnov, and Chukichev, J. Exptl. Theoret. Phys. (U.S.S.R.) **32**, 702 (1957), Soviet Phys. JETP **5**, 579 (1957).

[2] H. Fan and K. Lark-Horovitz, Paper delivered at the International Conference on Semiconductors and Crystal Phosphors, Munich, 1956; Проблемы современной физики (Problems of Contemporary Physics) **8**, 156 (1957).

[3] M. Prince, Phys. Rev. **92**, 680 (1953); Проблемы современной физики (Problems of Contemporary Physics) **2**, 40 (1955).

[4] Cleland, Crawford, and Pigg, Phys. Rev. **98**, 1742 (1955).

[5] G. Kinchin and R. Pease, Reports on Progress in Physics **18**, 1 (1955); Usp. Fiz. Nauk **60**, 590 (1956).

[6] L. S. Smirnov and V. S. Vavilov, J. Tech. Phys. (U.S.S.R.) **27**, 427 (1957), Soviet Phys. JTP **2**, 387 (1957).

Translated by J. G. Adashko
103

ANGULAR DISTRIBUTION OF μ^+ MESONS FROM $\pi-\mu$ DECAY

N. P. BOGACHEV, A. K. MIKHUL, M. G. PETRASHKU, and V. M. SIDOROV

Joint Institute for Nuclear Research

Submitted to JETP editor December 4, 1957

J. Exptl. Theoret. Phys. (U.S.S.R.) **34**, 531-532 (February, 1958)

AT the Varenna (Italy) conference in 1957, Lattes reported on certain experimental data on angular distribution of μ^+ mesons from $\pi-\mu$ decay, and the possibility of asymmetry in such an angular distribution was discussed. In further experiments[1-4] it was found that the asymmetry parameter $b = 2(N_F - N_B)/(N_F + N_B)$ lies between the limits $b = -0.447 \pm 0.082$ and $b = 0.052 \pm 0.058$; here N_F and N_B are the numbers of μ^+ mesons emitted forwards and backwards, respectively, relative to the direction of the π^+-meson beam. At the Venice[5] conference it was noted that despite the wide scatter of values of b obtained by different authors there is, apparently, no asymmetry in the $\pi-\mu$ decay and the various values of b are caused by one or another systematic error.

In the present work we report on the results of an analysis of 10,000 cases of $\pi-\mu$ decays of π^+ mesons stopped in NIKFI type R emulsion. The emulsion layers were irradiated by the π^+-meson beam from the Laboratory for Nuclear Problems synchrocyclotron and were placed, during the exposure time, inside a steel screen which shielded them from the external magnetic fields.

Observation of $\pi-\mu$-decay events was carried out by aerial scanning with the MBI-3 microscope at an amplification of about 100. The identification of the $\pi-\mu$-decay events was carried out visually. Measurements were made of the projections onto the emulsion plane of the angles between the initial direction of the μ^+ meson and the direction of the collimator of the π^+-meson beam. The error in the measurement of the angular projections did not exceed ± 3°. The angular distribution obtained directly from scanning is shown in Fig. 1a; the asymmetry coefficient for this angular distribution is $b = -0.048 \pm 0.020$.

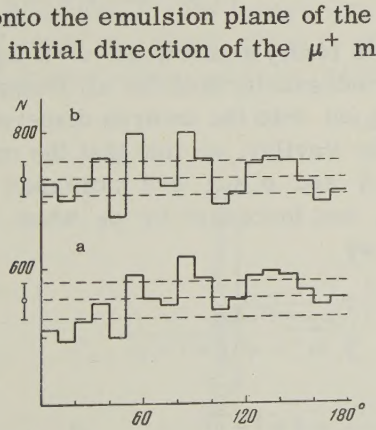

FIG. 1

In order to estimate systematic errors that could have been introduced in the process of emulsion scanning, we carried out two identical scannings of the same area at the suggestion of L. L. Gurevich. We measured the projection θ^* of the angle between the final direction of the π^+ meson and the initial direction of the μ^+ meson. The $\pi-\mu$-decay events found twice were identified, and the probability of observation of such a decay event was computed as a function of θ^*. It can be seen from Fig. 2 that the probability of observing a $\pi-\mu$-decay event decreases for small values of θ^*.

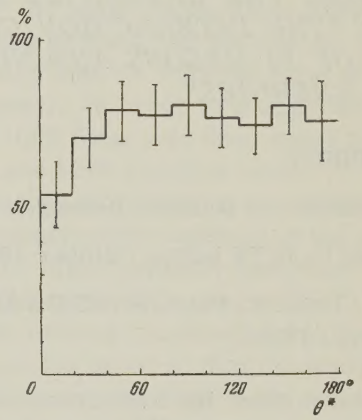

FIG. 2

The "direct" distribution of Fig. 1a was corrected by taking into account the scanning efficiency (Fig. 2) and the distribution found experimentally, of the angles between the initial and final π^+-meson directions. Figure 1b shows the projected angular distribution of the μ^+ mesons. Here the asymmetry coefficient is $b = +0.009 \pm 0.018$. It therefore follows that the angular distribution of μ^+ mesons from $\pi-\mu$ decays of stopped π^+ mesons is isotropic.

It appears probable that the cause of asymmetry observed by some authors can, at least partially, be related to the systematic error studied in this work.

The authors consider it their pleasant duty to express gratitude to Professor M. Danysz and Professor V. P. Dzhelepov for interest in this work and discussion of results, as well as to V. F. Poenko for scanning of emulsions and to V. V. Chistiakova for aid in computations.

[1] F. Bruin and M. Bruin, Physica **23**, 551 (1957).
[2] J. I. Friedman and V. L. Telegdi, Phys. Rev. **106**, 1290 (1957).
[3] Hulubei, Ausländer, Balea, Friedländer, Titeica, and Visky, Compt. rend. **245**, 1037 (1957).
[4] Alston, Evans, Morgan, Newport, Williams, and Kirk, Phil. Mag. **2**, 1143 (1957).
[5] Bhowmik, Evans, Prowse, Garwin, Gidal, Lederman, and Weinrich, International Conference of Mesons and Recently Discovered Particles (riassunti delle communicazioni), Padova-Venezia, 22 — 28 Settembre, 1957.

Translated by A. Bincer
104

CONCERNING THE LETTER BY P. V. VAVILOV, "THE INTERACTION CROSS SECTION OF PI MESONS AND NUCLEONS AT HIGH ENERGIES"

N. P. KLEPIKOV

Joint Institute for Nuclear Research

Submitted to JETP editor October 29, 1957

J. Exptl. Theoret. Phys. (U.S.S.R.) **34**, 533-534 (February, 1958)

In the articles cited[1] the total cross section for the interaction of pions with nucleons at infinitely large energies are calculated with the aid of a dispersion relation, usually called the inverse relation, which expresses the imaginary part of the forward-scattering amplitude in terms of the real part of this amplitude. The real part of the amplitude, on the other hand, is calculated in the work of Cool et al.,[2] which Vavilov uses, from experimental data on the total cross sections for the interaction of pions with nucleons, and the dispersion relation employed is direct with respect to the above-mentioned inverse relation.

Since experimental data on the total cross sections are available only up to 1770 Mev for positive pions and to 4500 Mev for negative ones, total interaction cross sections, extrapolated for infinite energies at a constant level of approximately 30 millibarns, are used in Ref. 2 to calculate the real part of the amplitude of the elastic forward scattering. No wonder therefore that the cross section obtained in Ref. 1 is $\sigma_\infty = 30$ millibarns. The result of such a calculation is not the prediction of a quantity not yet measured experimentally, but a verification of the compatibility of the employed direct and inverse dispersion relations. Such an agreement should obtain for any extrapolation of the total cross section, and is independent of the accuracy of the experimental quantities.

The contents of the note referred to can also be represented as a calculation of the sections $\sigma_\pm(\omega)$ with the aid of relations of the form

$$\sigma_\pm(\omega) = F_\pm(\omega) + \int_0^\infty \{K_{\pm,+}(\omega, \omega')\,\sigma_+(\omega') + K_{\pm,-}(\omega, \omega')\,\sigma_-(\omega')\}\,d\omega', \tag{1}$$

which are obtained when the real parts of the forward scattering amplitudes $D_\pm(\omega)$ are eliminated from the direct and inverse dispersion relations. But such an elimination, if one considers that

$$\int_{-\infty}^{\infty} dx/(x-a)(x-b) = \pi^2\delta(a-b), \tag{2}$$

yields

$$F_\pm(\omega) = K_{+,-}(\omega, \omega') = K_{-,+}(\omega, \omega') = 0,$$
$$K_{+,+}(\omega, \omega') = K_{-,-}(\omega, \omega') = \delta(\omega - \omega'),$$

and relation (1) turns into the identity $\sigma_\pm(\omega) = \sigma_\pm(\omega)$, which would be meaningless to verify experimentally.

To refute the widely held opinion that the dispersion relation yields results that are totally insensitive to the behavior of the cross sections at $\sigma \to \infty$, let us consider a simple example. Let us add to cross sections $\sigma_+(\omega)$ and $\sigma_-(\omega)$ a constant cross section σ_0 in the frequency interval $\omega > \omega_0$. Then, as can be readily verified, the real parts of the amplitudes $D_+(\omega)$ and $D_-(\omega)$ are increased by

$$\Delta D_\pm(\omega) = \sigma_0 \frac{\sqrt{\omega^2-\mu^2}}{4\pi^2} \ln \frac{\sqrt{\omega_0^2-\mu^2} + \sqrt{\omega^2-\mu^2}}{|\sqrt{\omega_0^2-\mu^2} - \sqrt{\omega^2-\mu^2}|}. \tag{3}$$

This quantity is really small when $\omega \ll \omega_0$, but this does not necessarily hold for all frequencies. Inserting $\Delta D_\pm(\omega)$ into the inverse dispersion relation quoted by Vavilov, we find that the cross sections $\sigma_+(\omega)$ and $\sigma_-(\omega)$ are increased by zero when $\omega < \omega_0$, and increased by σ_0 when $\omega > \omega_0$, since at $\omega > \omega_0$

$$\int_0^\infty \frac{d\omega'}{(\omega'^2-\omega^2)\sqrt{\omega'^2-\mu^2}} \times \ln \frac{|\sqrt{\omega_0^2-\mu^2} - \sqrt{\omega'^2-\mu^2}|}{\sqrt{\omega_0^2-\mu^2} + \sqrt{\omega'^2-\mu^2}} = \frac{\pi^2}{2\omega\sqrt{\omega^2-\mu^2}} \tag{4}$$

and the integral (4) vanishes when $\omega < \omega_0$. This result can be readily checked by integrating in the complex plane of the variable ω', provided we take into account that a singular integral with a parameter, lying on the path of integration, is equal in the limit to half the sum of the integrals with complex parameters, lying on opposite sides of the path of integration. Thus, no matter how high the frequency ω_0, the cross section σ_∞, obtained by successive employment of the direct and inverse dispersion relations, will be determined by that level, to which the experimental cross sections are extrapolated.

[1] P. V. Vavilov, J. Exptl. Theoret. Phys. (U.S.S.R.) **32**, 940 (1957), Soviet Phys. JETP **5**, 768 (1957).

[2] Cool, Piccioni, and Clark, Phys. Rev. **103**, 1082 (1956).

Translated by J. G. Adashko
105

MEASUREMENT OF THE VELOCITY OF SOUND IN LIQUIDS UNDER PRESSURES UP TO 2500 ATMOSPHERES BY AN OPTICAL METHOD

L. F. VERESHCHAGIN and N. A. IUZEFOVICH

Laboratory of Physics of Ultra High Pressures, Academy of Sciences, U.S.S.R.

Submitted to JETP editor November 11, 1957

J. Exptl. Theoret. Phys. (U.S.S.R.) **34**, 534-536 (February, 1958)

SEVERAL different methods of measurement have been employed for the measurement of the velocity of sound in a liquid which is under pressure. The most widespread is an optical method which utilizes the diffraction of light on ultrasonic waves which are propagated perpendicular to the beam of light in the liquid. This method, proposed by Debye and Sears,[1] has found wide use in measurements of the velocity of sound in liquids and compressed gases.

Biquard[2,3] measured the velocity of sound in several liquids under pressures up to 600 atmospheres, at temperatures in the range of room temperature. It seems of interest to measure the velocity of sound in liquids at still higher pressures, where one might already expect compression of the very molecules.

The optical scheme of the apparatus which we employed[4] is shown in Fig. 1. A SVDSh mercury lamp served as the source of light S. A slit A_1 was set in the path of the light beam. Condenser K produced a parallel beam of light. A second slit A_2, perpendicular to the first, cut out a narrow pencil of the beam which, after going through the liquid being studied, was focused by the long-focus collecting lens O onto the plate of a microphoto attachment. In order to get narrow diffraction lines, a light filter was used which transmitted the 5770 and 5790 A yellow lines.

The ultrasonic vibrations were excited by an X-cut piezo-quartz plate inserted in the oscillating circuit of a high frequency generator wired in push-pull. This generator used a GU-29 tube. The range of working frequencies was 3 — 4 Mcs. The generator was tuned so that the quartz plate operated at a frequency close to its natural frequency of oscillation. The frequency of the generator was measured by means of a heterodyne wavemeter; with this, the accuracy of the frequency measurements could be regarded as within 400 cycles at working frequencies of 3 — 4 Mcs. The ultrasonic waves passed into the vessel and the liquid being studied through a steel wall, inasmuch as the piezo-quartz plate was placed outside the vessel and was pressed against its ground surface by a light spring. This considerably simplified the construction of the high-pressure ves-

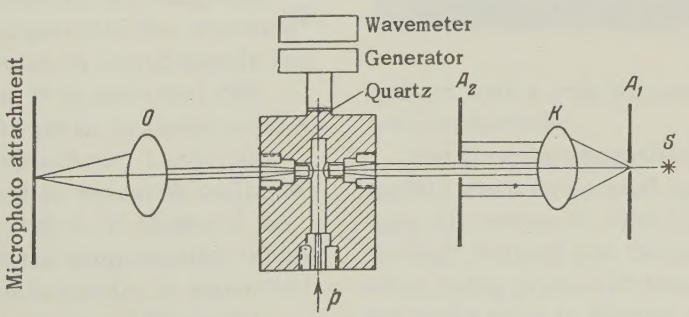

FIG. 1

sel, obviating the use of high-pressure electrical leads.

Two little glass windows were made for passing the light through the investigated liquid in the high-pressure vessel (Fig. 1). The pressure was fed into the vessel by means of a hydraulic compressor.[5] To separate the liquid compressed in the hydro-compressor from that investigated, a device was placed in the passage which assured separation of the liquids by means of a "floating" piston. The pressure was measured by means of a pointer manometer of first class accuracy. The experiments were carried out at a temperature between 19 and 20° C.

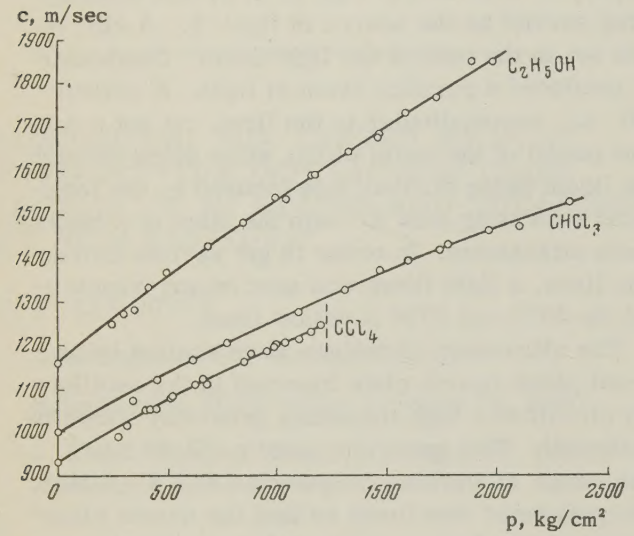

FIG. 2

The dependence of the velocity of sound c on pressure p for the three liquids investigated by us is shown in Fig. 2. As is seen from the figure, the curves are slightly concave towards the pressure axis. Measurement of the velocity of sound above a pressure of 1200 atmos was not possible for carbon tetrachloride, since above this pressure, apparently, crystallization occurs and the liquid becomes practically opaque.

The absolute ethyl alcohol, chloroform, and carbon tetrachloride of high purity were prepared by A. M. Poliakova and kindly furnished for our experiments. We take this opportunity to express our thanks to her.

[1] P. Debye and F. W. Sears, Proc. Nat. Acad. Sci (U.S.) **18**, 409 (1932).

[2] P. Biquard, Compt. rend. **206**, 897 (1938).

[3] P. Biquard, Rev. d'Acoustique **8**, 130 (1939).

[4] L. F. Vereshchagin and I. V. Brandt, Приборы и техника эксперимента (Instruments and Instrum. Engg.) (in press).

[5] L. F. Vereshchagin, J. Tech. Phys. (U.S.S.R.) **16**, 669 (1946).

Translated by R. Eisner
106

---

*CORRECTION TO ARTICLE, "FLUCTUATIONS IN COLLISION OF HIGH ENERGY PARTICLES" [J. Exptl. Theoret. Phys. (U.S.S.R.) **29**, 296 (1955)]*

M I. PODGORETSKII, I. L. ROSENTAL', and D. S. CHERNAVSKII

J. Exptl. Theoret. Phys. (U.S.S.R.) **34**, 536 (February, 1958)

IN the paper cited, an error has been admitted in the calculation of the quantity $\overline{(n-\bar{n})(E-\bar{E})}$.

The right-hand sides in Eqs. (5) and (7) must be replaced by 7.21 bkT (instead of 7.65 bkT) and 5.49 bkT (instead of 5.68 bkT). As a consequence, the right sides of Eqs. (13) and (14) are replaced by 1.29 b and 0.31 b (respectively, in place of 1.03 b and 0.22 b). Furthermore, the quantity α in the adiabatic case comes to 0.54 for Bose particles and 0.17 for Fermi particles (instead of 0.43 and 0.12).

We thank A. I. Nikishov for having pointed out the error.

Translated by R. Eisner
107